UNIVERSITY OF LONDON THESIS

Degree PhD Year 2006 Name of Author WHITWELL Jennifer Louise

MR-BASED VOLUMETRIC MEASUREMENTS IN FRONTOTEMPORAL LOBAR DEGENERATION: APPLICATION TO DIAGNOSIS AND MEASUREMENT OF PROGRESSION

THESIS SUBMITTED FOR THE DEGREE OF DOCTOR OF PHILOSOPHY

JENNIFER LOUISE WHITWELL

INSTITUTE OF NEUROLOGY

UNIVERSITY COLLEGE LONDON

2005

ProQuest LLC
789 East Eisenhower Parkway
P.O. Box 1346
Ann Arbor, MI 48106-1346

Abstract

This thesis investigates the role of volumetric MRI in the diagnosis and measurement of progression in patients with frontotemporal lobar degeneration (FTLD). Patterns of regional atrophy were assessed cross-sectionally using both visual ratings and the automated unbiased technique of voxel-based morphometry (VBM). Both techniques identified characteristic patterns of atrophy in FTLD, and its syndromic variants. In addition, a network of structures was identified that may contribute to the behavioural abnormalities observed in FTLD patients.

Detailed regional volumetric measurements of temporal lobe structures were performed in both clinically and pathologically diagnosed patients with FTLD and Alzheimer's disease (AD). Characteristic patterns of atrophy were identified in both groups that may be useful in the differential diagnosis of FTLD and AD. Patterns of atrophy in the different pathological subtypes of FTLD were also assessed using VBM. Significant differences were observed between groups suggesting that imaging may also be useful in predicting the underlying pathological substrate of FTLD.

Longitudinal analyses were performed in subjects with serial volumetric MRI scans. Techniques for ensuring stability in voxel dimension over time were assessed. The positional matching of serial scans using registration provided the best correction for drift in voxel dimension. Registration was then utilised to assess rates of whole brain atrophy over time in FTLD subjects. Rates of atrophy were approximately 2% per year in all three syndromic groups. The registration of multiple serial MRI then

demonstrated that rates of atrophy remained relatively constant throughout the disease. Longitudinal changes in the patterns of regional atrophy were investigated using a combination of fluid registration and VBM. The syndromic variants of FTLD displayed different patterns of regional longitudinal change, giving complementary information to that provided by the cross-sectional analysis.

Table of Contents

Abstract **2**

Background **22**

Aims **24**

1. Background to Dementia **25**

1.1. Dementia 25

1.2. Frontotemporal lobar degeneration (FTLD) 25

1.2.1. History and terminology 26

1.2.2. Epidemiology 29

1.2.3. Frontal-variant frontotemporal dementia (fvFTD) 30

1.2.4. Semantic dementia (SD) 32

1.2.5. Progressive non-fluent aphasia (PNFA) 33

1.2.6. Other FTLD syndromes 34

1.2.7. Histopathology 35

1.3. Alzheimer's disease (AD) 42

1.4. Differential diagnosis 44

1.4.1. Neuropsychology 45

1.4.2. Behavioural and personality assessments 48

1.4.3. Other investigations 50

2. Neuroimaging **52**

2.1. Imaging modalities 53

2.2. Analysis techniques 57

2.3. Patterns of atrophy in FTLD 59

2.4. Differential diagnosis of FTLD 67

2.5. Measurement of progression in FTLD 71

3. Methods Overview **72**

3.1. Image Analysis 72

3.1.1. Image Acquisition 72

3.1.2. Image quality 72

3.1.3. MIDAS 78

3.1.4. Image Registration 79

3.1.5. Voxel-based morphometry 91

3.2. Subjects 104
3.2.1. The Specialist Cognitive Disorders Clinic 105
3.2.2. Prospective Longitudinal FTLD Study 106
3.2.3. MIRIAD 107
3.2.4. Normal Control Study 108
3.3. Statistics 109
4. Visual assessments of regional atrophy in FTLD 110
4.1. Introduction 110
4.2. Methods 111
4.2.1. Subjects 111
4.2.2. Analysis 113
4.2.3. Statistics 115
4.3. Results 115
4.3.1. Intra-rater reliability 115
4.3.2. Patterns of atrophy on MRI 115
4.3.3. Patterns of atrophy in the syndromic variants of FTLD 117
4.4. Discussion 128
4.5. Conclusion 131
5. Cross-sectional pattern of atrophy in the syndromic variants of FTLD ..132
5.1. Introduction 132
5.2. Methods 135
5.2.1. Subjects 135
5.2.2. Neuropsychological assessments 136
5.2.3. Behavioural assessments 136
5.2.4. Imaging 137
5.2.5. Statistics 138
5.3. Results 139
5.3.1. Patient characteristics 139
5.3.2. Neuropsychological assessment 140
5.3.3. Behavioural assessment 143
5.3.4. VBM analysis 145
5.4. Discussion 166
5.5. Conclusion 173

6. Imaging correlates of 'sweet tooth' in FTLD 174
6.1. Introduction 174
6.2. Methods 175
6.2.1. Subjects 175
6.2.2. Image analysis 177
6.3. Results 178
6.4. Discussion 182
6.5. Conclusion 184
7. Amygdala measurements in the differential diagnosis of FTLD and AD. 185
7.1. Introduction 185
7.2. Methods 187
7.2.1. Subjects 187
7.2.2. Image analysis 188
7.2.3. Statistics 188
7.3. Results 189
7.4. Discussion 198
7.5. Conclusion 201
8. Amygdala and hippocampus measurements in pathologically confirmed FTLD and AD 202
8.1. Introduction 202
8.2. Methods 203
8.2.1. Subjects 203
8.2.2. Neuropathological procedure 204
8.2.3. Manual Segmentation 205
8.2.4. Statistical Analysis 206
8.3. Results 208
8.3.1. Syndromic variants of FTLD 215
8.4. Discussion 217
8.5. Conclusion 221
9. MRI correlates of FTLD pathology 222
9.1. Introduction 222
9.2. Correlates of tau immunohistochemistry 223
9.2.1. Introduction 223

9.2.2. Methods 224
9.2.3. Results 227
9.2.4. Discussion 230
9.3. Correlates of specific tissue pathology in FTLD 233
9.3.1. Introduction 233
9.3.2. Methods 234
9.3.3. Results 237
9.3.4. Discussion 251
9.4. Conclusion 255
10. Stability in Longitudinal Scanning 256
10.1. Introduction 256
10.2. Intracranial volume normalisation 258
10.2.1. Introduction 258
10.2.2. Methods 259
10.2.3. Results 266
10.2.4. Discussion 275
10.2.5. Conclusion 277
10.3. Nine degrees-of-freedom registration 278
10.3.1. Introduction 278
10.3.2. Methods 279
10.3.3. Results 283
10.3.4. Discussion 290
10.3.5. Conclusion 292
11. Rates of whole brain atrophy in FTLD 294
11.1. Introduction 294
11.2. Methods 296
11.2.1. Subjects 296
11.2.2. Image analysis 296
11.2.3. Statistics 296
11.3. Results 297
11.3.1. Patient characteristics 297
11.3.2. Image analysis 300
11.3.3. Regression analysis 309

11.3.4. Discriminate analysis 312
11.4. Discussion 314
11.5. Conclusion 317
12. Change in rates of brain atrophy over time in FTLD 318
12.1. Introduction 318
12.2. Methods 321
12.2.1. Subjects 321
12.2.2. Image analysis 321
12.3. Results 322
12.4. Discussion 326
12.5. Conclusion 328
13. Longitudinal patterns of regional atrophy in FTLD 329
13.1. Introduction 329
13.2. Methods 330
13.2.1. Subjects 330
13.2.2. MRI Acquisition and MIDAS pre-processing 332
13.2.3. SPM pre-processing 333
13.2.4. Statistical analysis 333
13.3. Results 335
13.3.1. Controls 335
13.3.2. FTLD 335
13.3.3. fvFTD 343
13.3.4. SD 350
13.3.5. PNFA 357
13.4. Discussion 364
13.5. Conclusion 368
Overall Discussion 370
Acknowledgements 383
Publications 385
Appendix 1: Diagnostic criteria for FTLD 389
Appendix 2: Diagnostic criteria for AD 398
Appendix 3: Clinical assessment scales 402
Appendix 4: Image Acquisition protocols 414

Appendix 5: Regional segmentation protocols **415**

Appendix 6: Chapter 4 radiology questionnaire **419**

Appendix 7: Patterns of temporal lobe atrophy in SD and AD (study by Chan et al 2001) **421**

Glossary **450**

Reference List **454**

Figures

Figure 1.1: Slice through the brain of a patient with FTLD (Pick's disease) showing atrophy of the frontal and temporal lobes. Note the very prominent loss of inferior temporal lobe tissue with relative preservation of the superior temporal gyrus. ..26

Figure 1.2: Intracellular inclusions from the dentate gyrus of the hippocampus in FTLD: A) tau-positive inclusions (Pick bodies) in PiD, and B) ubiquitin-positive inclusions in FTLD-U. 39

Figure 1.3: Associations between the clinical syndromes of FTLD and the underlying histopathology based on cases reported in a number of large case series (Galton et al., 2000; Josephs et al., 2003; Hodges et al., 2004; Paviour et al., 2004; Davies et al., 2005; Kertesz et al., 2005; Josephs et al., 2006b; Knibb et al., 2006). 41

Figure 2.1: Axial slices through A) T1-weighted, B) T2-weighted and C) PD image from a healthy control 56

Figure 2.2: Coronal and axial T1-weighted images of a subject with fvFTD. Note the severe atrophy of the frontal lobes bilaterally and also the involvement of the temporal lobes, specifically in inferior and medial temporal regions. 61

Figure 2.3: Coronal and axial T1-weighted images of a subject with SD. 64

Figure 2.4: T1-weighted images of a subject with PNFA. Atrophy involves the left perisylvian region, including both left superior temporal and left inferior frontal regions. Note that the left frontal lobe appears more generally atrophic (damage beyond the inferior frontal regions).....66

Figure 2.5: T1-weighted images of a subject with predominant right temporal lobe atrophy. Note the similarity with figure 2.2 (SD). Here the right anterior temporal lobe is more affected that the posterior structures. Again the inferior temporal gyri are more atrophic than the superior temporal gyrus. 67

Figure 3.1: Examples of common image quality problems: A) patient movement, B) poor contrast, and C) intensity inhomogeneity. 76

Figure 3.2: Coronal slices through two T1-weighted images from the same individual performed on different scanners 9 months apart. Note the difference in grey-white matter contrast and the susceptibility artefacts in the temporal lobe on scanner 1. 77

Figure 3.3: Coronal T1-weighted images from A) a healthy control and B) a subject with FTLD showing the baseline image (Base), rigidly-registered repeat image (RR) and the difference image for the registered pair. Note the increase in the left temporal horn is obvious on the difference image. 84
Figure 3.4: A representation of an intensity profile through a boundary of the brain on both a baseline and registered repeat scan. During the interval between the scans the boundary has shifted by ΔW, which is determined as the area A divided by the intensity window (I_1-I_2) (modified from Fox et al 1997) 85
Figure 3.5: BBSI colour overlay showing regions of atrophy over a one-year interval in a healthy control and a subject with FTLD (fvFTD). 86
Figure 3.6: Coronal T1-weighted images from a patient with FTLD showing A) the baseline image, B) the fluid-registered repeat image, C) the difference image from the rigid-registration, and D) the difference image from the fluid registration.....88
Figure 3.7: Voxel-compression maps showing regions of expansion and contraction over a one-year interval in a healthy control and subject with FTLD (fvFTD). ...90
Figure 3.8: VBM pre-processing steps 92
Figure 3.9: Normalised T1-weighted images from A) healthy controls, B) AD subjects, and C) FTLD subjects. All images have been normalised to the same template image using the default SPM parameters. 95
Figure 3.10: An example of tissue segmentation. The T1-weighted image has been segmented into grey matter, white matter and CSF. 96
Figure 3.11: Grey matter segmentations of a subject with FTLD using A) default and B) customised prior probability maps. The default results in little value being added by the priors; this is improved with customised maps. Note also the partial volume misclassification around the ventricles....98
Figure 3.12: Grey matter segmentations A) before and B) after masking with a MIDAS brain mask....99
Figure 3.13: Grey matter, white matter and CSF images before (A-C) and after smoothing (D-F) with an 8mm smoothing kernel 102
Figure 4.1: Examples of temporal lobes that were visually rated as normal (0), mild (1), moderate (2) or severely (3) atrophic 114
Figure 4.2: Mean atrophy scores plotted for each cortical region for the non-FTLD and FTLD groups. Frontal regions have been colour coded in blue, temporal

regions in red, parietal in yellow and occipital in green. Left hemisphere = solid colour, right hemipshere = hatched. Error bars represent standard error. 121
Figure 4.3: Prevalence of asymmetry in the non-FTLD and FTLD groups (%) 122
Figure 4.4: Prevalence of anterior-posterior gradient of atrophy in the non-FTLD and FTLD groups 123
Figure 4.5: Mean atrophy scores plotted for each cortical region for the fvFTD, SD and PNFA subgroups. Frontal regions have been colour coded in blue, temporal regions in red, parietal in yellow and occipital in green. Left hemisphere = solid colour, right hemipshere = hatched. Error bars represent standard error. 125
Figure 4.6: Prevalence of asymmetry in the fvFTD, SD and PNFA subgroups 126
Figure 4.7: Prevalence of anterior-posterior gradient of atrophy in the fvFTD, SD and PNFA subgroups 127
Figure 5.1: Statistical parametric map showing regions of grey matter loss in FTLD compared with controls (uncorrected, $p<0.001$) 146
Figure 5.2: Statistical parametric map showing regions of white matter loss in FTLD compared with controls (uncorrected, $p<0.001$) 147
Figure 5.3: Statistical parametric map showing regions of CSF increase in FTLD compared with controls (uncorrected, $p<0.001$) 148
Figure 5.4: Statistical parametric map showing regions of grey matter loss in fvFTD compared with controls (uncorrected, $p<0.001$) 150
Figure 5.5: Statistical parametric map showing regions of white matter loss in fvFTD compared with controls (uncorrected, $p<0.001$) 151
Figure 5.6: Statistical parametric map showing regions of CSF increase in fvFTD compared with controls (uncorrected, $p<0.001$) 152
Figure 5.7: Statistical parametric map showing regions of grey matter loss in SD compared with controls (uncorrected, $p<0.001$) 155
Figure 5.8: Statistical parametric map showing regions of white matter loss in SD compared with controls (uncorrected, $p<0.001$) 156
Figure 5.9: Statistical parametric map showing regions of CSF increase in SD compared with controls (uncorrected, $p<0.001$) 157
Figure 5.10: Statistical parametric map showing regions of grey matter loss in two groups of SD patients split according to severity of naming deficit, compared with

controls (uncorrected, p<0.001). Group 1 = Oldfield ≥ 7 (n=6), Group 2 = Oldfield < 7 (n=9)....158
Figure 5.11: Statistical parametric map showing regions of grey matter loss in PNFA compared with controls (uncorrected, p<0.001)....160
Figure 5.12: Statistical parametric map showing regions of white matter loss in PNFA compared with controls (uncorrected, p<0.001)....161
Figure 5.13: Statistical parametric map showing regions of CSF increase in PNFA compared with controls (uncorrected, p<0.001)....162
Figure 5.14: Statistical parametric map showing regions of grey matter loss in A) fvFTD compared with both SD and PNFA, and B) SD compared with both fvFTD and PNFA (uncorrected, p<0.001)....164
Figure 5.15: Statistical parametric map showing regions of grey matter loss present in all three groups (fvFTD, SD and PNFA) when compared with controls (uncorrected, p<0.001)....165
Figure 6.1: Statistical parametric maps showing patterns of grey matter loss in the FTLDn and FTLDs groups compared to controls (p<0.001)....180
Figure 6.2: Statistical parametric maps showing regions of grey matter loss specific to the FTLDs group. The left panel shows the regions showing greater loss in the FTLDs compared to controls comparison, than in the FTLDn compared to control comparison (using masking). The right panel shows the patterns of loss in the FTLDs group compared directly to the FTLDn group (FTLDn v FTLDs, uncorrected p<0.001)....181
Figure 7.1: Average amygdala volume against amygdala asymmetry score in controls (C), AD and either A) FTLD or B) SD groups....195
Figure 7.2: Coronal sections through the temporal lobes in a control subject (1), a patient with AD (2), and a patient with SD (3). Both left and right amygdalae have been outlined. L= Left, R = Right....197
Figure 8.1: Left (A) and right (B) amygdala and hippocampal volume in controls, AD and FTLD patients....213
Figure 8.2: ROC curves showing the discrimination of AD from A) controls, B) FTLD from controls and C) FTLD from AD....214
Figure 8.3: Left (A) and right (B) amygdala and hippocampal volumes in fvFTD, SD and PNFA patients....216

Figure 9.1: Patterns of grey matter atrophy in the tau-positive and tau-negative groups of FTLD ($p<0.0001$, uncorrected) 228

Figure 9.2: Statistical parametric maps of grey matter atrophy in FTLD pathological subgroups compared to controls ($p<0.0001$, uncorrected). 241

Figure 9.3: Statistical parametric maps of white matter loss in FTLD pathological subgroups (FTLD-U and PiD) compared to controls ($p<0.0001$, uncorrected). No regions of white matter atrophy reached statistical significance in the tau exon^{10+16} group (images not shown). 242

Figure 9.4: Statistical parametric maps of CSF expansion in FTLD pathological subgroups compared to controls ($p<0.0001$, uncorrected). 243

Figure 9.5: Statistical parametric maps of grey matter atrophy in FTLD pathological subgroups compared to controls. Regions involved only in a particular subgroup and regions involved in all subgroups are shown on coronal sections of the mean customized template brain (MNI stereotactic y coordinate in mm) through the anterior commissure (y = 0), the temporo-parietal junction (y = -40), and the anterior temporal and frontal lobes (y = 15) ($p<0.0001$ uncorrected) 245

Figure 9.6: Statistical parametric maps of grey matter atrophy in PiD compared to both FTLD-U and tau exon10+16 groups ($p<0.001$, uncorrected). 246

Figure 9.7: Statistical parametric maps of grey matter atrophy in tau exon10+16 compared to both FTLD-U and PiD groups ($p<0.001$, uncorrected). 247

Figure 9.8: Histograms showing mean (standard error) corrected scores for visual assessments of atrophy in FTLD patients. † FTLD-U > PiD ($p<0.04$); ‡ PiD > FTLD-U ($p<0.03$); * tau exon 10^{+16} > PiD and FTLD-U (all significant at $p<0.04$) 249

Figure 10.1: Total intracranial region shown on a T2-weighted image 263

Figure 10.2: TIV shown on a T1-weighted image. The intensity windowing is as used for segmentation. (A) The total intracranial area is shown on one example axial slice. (B) The axial slices used to sample the total intracranial volume are marked on the sagittal view. 264

Figure 10.3: The relationship between (a) TIV and age, (b) brain volume and age, and (c) normalised brain volume and age, in normal controls. 267

Figure 10.4: Brain volumes and normalised brain volumes in male (M) and female (F) controls with group averages marked, demonstrating a reduction in gender differences after TIV normalisation. 268
Figure 10.5: Comparison of TIV measurements from T1 and T2-weighted MRI in five controls and five AD patients. 269
Figure 10.6: Serial T1-weighted TIV measurements in five controls and five AD patients 273
Figure 10.7: Serial TIV and brain volumes in (a) an at-risk patient who remained well, and (b) an at-risk patient who became clinically affected with AD, compared with, (c) normalised brain volumes from serial scans in both the at-risk patients. 274
Figure 10.8: The volume scaling factor (xyz) generated from each of the 9dof registrations, for each of the ten control subjects, is plotted against the known (artificial) scaling factor. 284
Figure 10.9: The volume scaling factors for both TIV correction (TIV2/TIV1) and 9dof registration (xyz) on ten control scans after an artificial scaling change of 4.6% (1.5% in each dimension) are shown. The known (artificial) volume scaling factor is indicated by a dashed line. 286
Figure 10.10: The relationship between the 9dof registration volume scaling factor (xyz) and the TIV ratio (the ratio of the TIV of the serial scans to baseline TIV, i.e. TIV2/TIV1) for each scan pair (n=49). 287
Figure 10.11: Correction factors from the scanner QA (upper panel) and the volume scaling factors from the 9dof registration (lower panel) are plotted against time. Correction factors are plotted for the x (x), y (•) and z dimensions (○) and represent the degree (%) of geometric distortion required to normalise the image dimensions to a reference scan. Each scan pair (n=49) is associated with a scaling; both time points (baseline and repeat) are assigned this value and plotted with a line joining them. 289
Figure 11.1: Scatter-plot showing the relationship between brain volume loss measured from the BBSI and the manual difference in brain volume between baseline and repeat scans for the FTLD subjects (n=56) 302

Figure 11.2: Scatter-plots showing rates of whole brain atrophy (measured from BBSI) in the FTLD subgroups and healthy controls. The twelve fvFTD patients with low rates of atrophy have been highlighted in red on figure 11.2B. 304
Figure 11.3: BBSI colour overlay showing regions of atrophy in two patients with fvFTD. The subject on the left showed almost no brain atrophy over time. In contrast, the patient on the right shows significant expansion of the ventricles and tissue loss around both temporal lobes and the orbitofrontal region.....306
Figure 11.4: BBSI colour overlay showing regions of atrophy in two patients with SD. Both subjects show expansion of the ventricles and asymmetric tissue loss affecting predominantly the right temporal lobe and left frontal gyri between the baseline and repeat scan. The left temporal lobe is already highly atrophic at baseline in both subjects.....307
Figure 11.5: BBSI colour overlay showing regions of atrophy in two patients with PNFA. The subject on the right shows a severe pattern of left-ward asymmetric atrophy, involving the frontal and temporal lobes. The subject on the left has a shorter interval but still demonstrates expansion of the ventricles and atrophy of the frontal and temporal lobes. 308
Figure 11.6: Rate of atrophy (%/yr) calculated from the BBSI plotted against brain volume for A) the FTLD group, and B) the fvFTD group. The subjects identified as having particularly low rates of atrophy are marked in red on B. 310
Figure 11.7: Rate of atrophy (%/yr) calculated from the BBSI plotted against MMSE for A) the FTLD group, and B) the fvFTD group. The subjects identified as having particularly low rates of atrophy are marked in red on B.....311
Figure 11.8: Receiver operator characteristic (ROC) curves illustrating the ability of rates of atrophy to discriminate between healthy controls and A) FTLD, B) fvFTD, C) SD and D) PNFA (NB clinically diagnosed) 313
Figure 12.1: Change in rates of brain atrophy over time, as determined by serial measurements of total brain volume in 12 patients with AD, represented as a proportion of TIV. Patients are individually colour-coded. Time is plotted relative to the time (t=0) when a score of 23 out of 30 was obtained on MMSE. The y-axis scale is logarithmic (Chan et al., 2003). 320
Figure 12.2: Change in rates of brain atrophy over time in 21 subjects with FTLD. 324

Figure 13.1: Statistical parametric maps showing regions of grey matter, white matter and CSF change at repeat assessment compared to baseline in healthy controls (uncorrected, p<0.001). 338

Figure 13.2: Statistical parametric maps showing regions of grey matter atrophy in FTLD compared to controls at baseline (C-B) and repeat (C-R) assessments, and regions of grey matter atrophy in FTLD at repeat assessment compared to baseline (B-R) (uncorrected, p<0.001). 339

Figure 13.3: Statistical parametric maps showing regions of white matter loss in FTLD compared to controls at baseline (C-B) and repeat (C-R) assessments, and regions of white matter atrophy at repeat assessment compared to baseline (B-R) (uncorrected, p<0.001). 340

Figure 13.4: Statistical parametric maps showing regions of CSF increase in FTLD compared to controls at baseline (C-B) and repeat (C-R) assessments, and regions of CSF increase at repeat assessment compared to baseline (B-R) (uncorrected, p<0.001). 341

Figure 13.5: Statistical parametric maps showing regions of significant fluid contraction and expansion in FTLD compared to controls (uncorrected, p<0.001). 342

Figure 13.6: Statistical parametric maps showing regions of grey matter atrophy in fvFTD compared to controls at baseline (C-B) and repeat (C-R) assessments, and regions of grey matter atrophy at repeat assessment compared to baseline (B-R) (uncorrected, p<0.001). 345

Figure 13.7: Statistical parametric maps showing regions of white matter loss in fvFTD compared to controls at baseline (C-B) and repeat (C-R) assessments, and regions of white matter atrophy at repeat assessment compared to baseline (B-R) (uncorrected, p<0.001). 346

Figure 13.8: Statistical parametric maps showing regions of CSF increase in fvFTD compared to controls at baseline (C-B) and repeat (C-R) assessments, and regions of CSF increase at repeat assessment compared to baseline (B-R) (uncorrected, p<0.001). 347

Figure 13.9: Statistical parametric maps showing regions of significant fluid contraction and expansion in fvFTD compared to controls (uncorrected, p<0.001). 348

Figure 13.10: Voxel-compression maps showing change over approximately 12 months in two patients with fvFTD. 349
Figure 13.11: Statistical parametric maps showing regions of grey matter atrophy in SD compared to controls at baseline (C-B) and repeat (C-R) assessments, and regions of grey matter atrophy at repeat assessment compared to baseline (B-R) (uncorrected, $p<0.001$). 352
Figure 13.12: Statistical parametric maps showing regions of white matter loss in SD compared to controls at baseline (C-B) and repeat (C-R) assessments, and regions of white matter atrophy at repeat assessment compared to baseline (B-R) (uncorrected, $p<0.001$). 353
Figure 13.13: Statistical parametric maps showing regions of CSF increase in SD compared to controls at baseline (C-B) and repeat (C-R) assessments, and regions of CSF increase at repeat assessment compared to baseline (B-R) (uncorrected, $p<0.001$). 354
Figure 13.14: Statistical parametric maps showing regions of significant fluid contraction and expansion in SD compared to controls (uncorrected, $p<0.001$). 355
Figure 13.15: Voxel-compression maps showing change over approximately 20 months in two patients with SD. 356
Figure 13.16: Statistical parametric maps showing regions of grey matter atrophy in PNFA compared to controls at baseline (C-B) and repeat (C-R) assessments, and regions of grey matter atrophy at repeat assessment compared to baseline (B-R) (uncorrected, $p<0.001$). 359
Figure 13.17: Statistical parametric maps showing regions of white matter loss in PNFA compared to controls at baseline (C-B) and repeat (C-R) assessments, and regions of white matter atrophy at repeat assessment compared to baseline (B-R) (uncorrected, $p<0.001$). 360
Figure 13.18: Statistical parametric maps showing regions of CSF increase in PNFA compared to controls at baseline (C-B) and repeat (C-R) assessments, and regions of CSF increase at repeat assessment compared to baseline (B-R) (uncorrected, $p<0.001$). 361

Figure 13.19: Statistical parametric maps showing regions of significant fluid contraction and expansion in PNFA compared to controls (uncorrected, $p<0.001$). 362

Figure 13.20: Voxel-compression maps showing change over approximately 15 months in two patients with PNFA 363

Tables

Table 4-1: Patient characteristics 112
Table 4-2: Regional atrophy on MRI across disease groups 119
Table 4-3: Regional atrophy on MRI across disease groups (results are given for both the left and right hemisphere) 120
Table 4-4: Associations between asymmetries in different MRI regions in all patients 124
Table 5-1: Patient characteristics 139
Table 5-2: Neuropsychological data for each patient. The scores for naming, RMW, RMF and HMG are given in percentiles. NT = not performed. 142
Table 5-3: Behavioural data 144
Table 6-1: Patient characteristics. 176
Table 7-1: Patient characteristics 192
Table 7-2: Volumetric results 193
Table 7-3: Screening performance by disease type according to cut-off of average amygdala volume (average of left and right volumes). Sensitivity = percentage of patients with average amygdala measurement at or below the specified cut-off level; Specificity = percentage of patients with average amygdala measurement above the specified cut-off level. 194
Table 8-1: Patient characteristics 209
Table 8-2: Mean volumes and standard deviations (StDev) of TIV adjusted hippocampus and amygdala in controls, AD and FTLD subjects. 212
Table 9-1: Characteristics of tau-positive and tau-negative groups 225
Table 9-2: Locations of maximal volume loss in tau-positive and tau-negative groups. Data are derived from comparisons of each of the two FTLD subgroups with the healthy control subjects. Voxel coordinates are in mm after transformation into standard MNI stereotactic space. Only those local maxima exceeding a stringent statistical threshold of $p<0.001$ corrected for multiple comparisons across the entire brain volume are shown. 229
Table 9-3: Patient characteristics of control subjects and patients at MRI 238
Table 9-4: Regions of grey matter atrophy in FTLD-U, PiD and tau exon 10^{+16} relative to controls. Voxel coordinates are in mm after transformation into

standard MNI stereotactic space. Only local maxima exceeding a stringent statistical threshold ($p < 0.001$ corrected for multiple comparisons across the entire brain volume) are presented. The uncus includes the amygdala and medial temporal cortex overlying the amygdala. 244
Table 9-5: The positive predictive value (PPV), sensitivity, and specificity of VBM signatures of pathology were estimated from the individual visual assessment scores for each pathological subgroup with respect to the other subgroups. 250
Table 10-1: Reproducibilities and operator times 271
Table 11-1: Patient characteristics. 299
Table 11-2: TIV-corrected brain volumes and rates of atrophy (calculated from BBSI) 301
Table 11-3: Clinical characteristics and brain volume data for the fvFTD patients. The cohort has been divided into those patients identified with a low rate of atrophy, and then the rest of the fvFTD cohort that had 'higher' rates of atrophy. 305
Table 12-1: Estimated mean (95% CI) annual rates according to time (relative to the time when the MMSE score was 23/30) and according to method of measurement of atrophy (Chan et al., 2003) 319
Table 12-2: Patient characteristics for subjects showing a low rate of atrophy versus the rest of the cohort. 325
Table 13-1: Patient characteristics 331

Background

Degenerative dementia is one of the most pressing public health problems facing the developed world. Over 500,000 individuals in the UK are estimated to be affected; Alzheimer's disease (AD) is the most common cause but over the last decade other dementias have been increasingly recognised. Frontotemporal lobar degeneration (FTLD) is the second most common dementia in the under 65 age group (Neary et al., 1998). Diagnostic criteria have recently been refined; however diagnosis is still very difficult in the early stages of the disease, particularly in those cases where behavioural features dominate the clinical presentation. In these subjects there is often little insight into their problems, and the cognitive deficits can be subtle. There is a need to improve diagnosis in these individuals, particularly with the development of therapies for the treatment of AD. The advent of the cholinesterase inhibitors (AChEI) means it is more important than previously to correctly differentiate FTLD from AD: in FTLD the AChEI can worsen behavioural problems without bringing the cognitive benefits seen in AD. As a result there has been interest in using MRI to improve diagnosis. Regional atrophy is a characteristic finding at least in moderately advanced cases of FTLD.

Characteristic early features of FTLD include alterations in personality, social disinhibition, aggression, stereotypic behaviour, and changes in dietary preference (Neary et al., 1998). It has been postulated that such abnormal behaviour may reflect dysfunction in a network of limbic structures including for example the orbitofrontal cortex and amygdala (Boccardi et al., 2005). However, very few studies have

systematically investigated the structural correlates of these behavioural features in FTLD.

There is also a need to more clearly define the natural history of the different variants of FTLD in terms of structural progression. This has been a relatively neglected area of research with very few studies utilising accurate serial measurements of relevant structures. The importance of understanding progression in the degenerative dementias has been highlighted in AD where there has been a recognition that serial MR-based measurements may be useful as surrogate markers of disease progression (Black, 1999). The molecular genetic deficits underlying some of the familial FTLD cases have recently been elucidated (Heutink, 2000). The hope is that this will accelerate drug discovery in FTLD. When these therapies become available potential surrogate markers of progression will be very valuable. MRI may prove useful as an outcome measure in FTLD although much more research is required to assess its potential and define its roles.

Aims

To use quantitative MRI analysis in FTLD, and related dementias, to investigate a) potential biomarkers for in vivo diagnosis and disease progression, and b) the structural correlates of clinical and behavioural deficits in these disorders, by:

- Identifying particular structures of interest using unbiased assessments of the patterns of regional atrophy throughout the whole brain in FTLD
- Correlating patterns of grey matter atrophy to cognitive and behavioural deficits in FTLD
- Providing detailed information on the structural differences between patients with FTLD and AD, and investigating the diagnostic value of regional volumetric measurements
- Assessing rates of whole brain atrophy and patterns of regional progression in FTLD

1. Background to Dementia

1.1. Dementia

Dementia is a clinical state defined as an acquired, usually progressive impairment of multiple domains of cognition including memory, sufficient to interfere with activities of daily living, and in the presence of normal consciousness. It is often accompanied by disturbances of mood, behaviour, and personality. It is an increasingly common syndrome with a prevalence that increases with age; affecting 7% of the general population older than 65 years, and 30% of those aged over 80 years (McKeith et al., 2004). In order for the diagnosis of dementia to be made patients should fulfil standard criteria such as those in the Diagnostic and Statistical Manual of Mental Disorders, 4th Edition (DSM-IV) (American Pyschiatric Association, 1994). Dementia is a clinical syndrome and there are many diseases that can cause, or be associated with dementia. Degenerative and vascular causes are the most common, with Alzheimer's disease (AD), dementia with Lewy Bodies, vascular dementia and frontotemporal lobar degeneration being the most prevalent causes in the UK.

1.2. Frontotemporal lobar degeneration (FTLD)

Frontotemporal lobar degeneration (FTLD) is a progressive degenerative disorder associated with atrophy of the temporal and frontal lobes (figure 1.1). It is characterised by the insidious onset of behavioural and language deficits. Memory loss is usually mild at early stages, and patients often have relatively preserved orientation in their local environment.

Figure 1.1: Slice through the brain of a patient with FTLD (Pick's disease) showing atrophy of the frontal and temporal lobes. Note the very prominent loss of inferior temporal lobe tissue with relative preservation of the superior temporal gyrus.

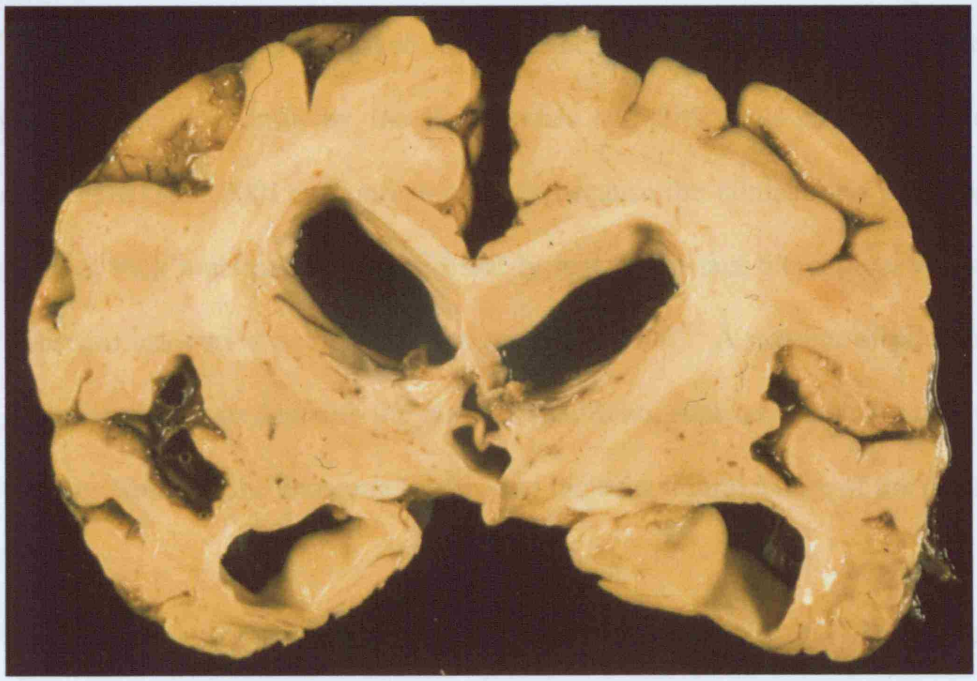

1.2.1. History and terminology

Many different terms have been used to describe FTLD in the literature, both for the clinical and pathological variants of the disease. This can lead to considerable confusion. The history of FTLD has involved a number of changes in terminology over the last 100 years. The clinical syndrome associated with FTLD was first described by Arnold Pick in 1892 (Pick, 1892). He later reported six cases presenting with language and personality change that showed frontal and temporal lobe atrophy at autopsy (Pick, 1906). The histopathology was described by Alzheimer in 1911 (Alzheimer, 1911). He commented on the absence of the senile plaques and tangles that characterise AD, and described the key features of what we know today as Pick bodies and Pick cells (see pathology section). The term Pick's disease was first

adopted to describe cases with circumscribed atrophy without plaques and tangles (Onari and Spatz, 1926), but was then employed more widely to encompass all those cases with frontotemporal lobar atrophy and the associated clinical features. However, more detailed pathological studies have since been performed and the term Pick's disease has been employed to describe a specific pathological variant, characterised predominantly by the Pick bodies and Pick cells first identified by Alzheimer (Dickson, 2001). Confusion arises because the clinical and pathological diagnoses of Pick's disease do not necessarily match. In fact the clinical variant of Pick's disease has varied pathology (Hodges et al., 2004). A number of other terms have been employed to describe the clinical syndrome, such as 'dementia of frontal lobe type' or 'frontal lobe dementia', reflecting the behavioural nature of the disease.

The confusion over terminology and the renewed interest in FTLD led to the description of detailed diagnostic criteria. The Lund-Manchester group adopted the term 'frontotemporal dementia' (FTD) in recognition of the finding that the behavioural disorder is invariably associated with atrophy of the temporal poles as well as the frontal lobes (Brun, 1994). They describe the core diagnostic features of FTD, including behavioural, affective and speech symptoms, as well as physical signs and useful investigations including brain imaging and neuropsychology (See Appendix 1). These criteria were further refined by Neary and colleagues in 1998 (Neary et al., 1998). They used the term frontotemporal lobar degeneration (FTLD) and detailed three common cannonical presentations of FTLD: frontotemporal dementia (FTD), which is characterised by predominant behavioural changes; and semantic dementia (SD) and progressive non-fluent aphasia (PNFA), that both involve early language deficits (see Appendix 1). However, the term used to describe

the behavioural variant (FTD) in the Neary criteria is easily confused with the term 'FTD' defined by the Lund-Manchester group. Therefore, various other terms have been used for this behavioural variant, including frontal-variant FTD (fvFTD) (Hodges et al., 2003).

The study of primary progressive aphasia (PPA) has also been important in the research and history of FTLD. PPA was first described by Mesulam in 1982 and is characterized by a gradual and isolated impairment of word usage and comprehension (Mesulam and Weintraub, 1992; Mesulam, 2001). This clinical diagnosis can be made when the principal signs and symptoms are confined to language for at least 2 years, although language dysfunction may be noted in isolation for as many as 10-14 years (Mesulam, 2001). The aphasia can be fluent, showing normal articulation, rate of utterance and phrase length, or non-fluent. Semantic dementia is typically referred to as a fluent variant of PPA, and PNFA as a non-fluent variant. Therefore, SD and PNFA are considered by different authors as variants of PPA, as well as of FTLD. Various research groups have also recognized that other conditions affect the frontal lobes and display similar behavioural features to FTLD. Kertesz has proposed the term 'Pick Complex' to cover a family of related conditions that all share common clinical patterns (Kertesz et al., 1994; Kertesz, 2003; Kertesz et al., 2003). The Pick's complex includes fvFTD, SD, PNFA, corticobasal degeneration (CBD) and Progressive Supranuclear Palsy (PSP). More detail on each of these disorders is provided below.

This thesis will adopt the terminology described by Neary et al 1998 (Neary et al., 1998). The term FTLD will be used to describe patients with a progressive dementia

with prominent behavioural and/or language deficits and relative preservation of posterior cognitive function accompanied by supportive imaging and other investigations. The language variants of FTLD will be referred to as SD and PNFA according to consensus criteria (Neary et al., 1998), and the term fvFTD will be used to describe those patients with predominant behavioural changes.

1.2.2. Epidemiology

Diagnostic criteria have improved the recognition of FTLD and allowed detailed epidemiology studies to be performed. The onset of FTLD typically occurs between the ages of 45 and 65. In the United Kingdom FTLD is probably the second most common dementia in the under 65-age group (Harvey et al., 2003). A couple of studies have shown a prevalence of FTLD of approximately 15 per 100,000 in the 45 to 64 year age range (Ratnavalli et al., 2002; Harvey et al., 2003). However, the prevalence appears to vary depending on the region or method of study, for example a lower prevalence of 4.0 per 100,000 was found in a study from the Netherlands (Rosso et al., 2003). FTLD accounts for a lower proportion of cases in more elderly populations; approximately 22% of FTLD patients have an onset over the age of 65 (Rosso et al., 2003). The fvFTD syndromic variant has been reported to be the most common, accounting for between approximately 60-80% of FTLD cases, with SD and PNFA only accounting for between 10-40% of cases (Hodges, 2001; Snowden et al., 2002; Johnson et al., 2005).

A positive family history has been reported to be present in approximately one half of patients with FTLD (Chow et al., 1999; Ratnavalli et al., 2002; Rosso et al., 2003). Of these, approximately 10 to 30% of cases have a recognised pathogenic mutation in

the tau gene (Bird et al., 2003). The tau protein is a microtubule binding protein involved in the assembly and stabilisation of microtubules. Six different isoforms of tau are produced in the healthy brain by alternative splicing from a gene on chromosome 17q21. Mutations in the tau gene on chromosome 17 have been discovered in many families with FTLD (Reed et al., 2001). Individuals in these families often develop Parkinsonian features, and so were originally described as having FTD with Parkinsonism that is chromosome 17-linked (FTDP-17) (Foster et al., 1997). Tau mutations in FTDP-17 may be missense, deletion, or silent mutations in the coding region or intronic mutations located close to the splice donor site of the intron following exon 10. Some common examples include the P301L and exon^{10+16} mutations (Bird et al., 1999; Poorkaj et al., 2001; Janssen et al., 2002; Bird et al., 2003). A mutation in the endosomal ESCRTIII-complex subunit CHMP2B on chromosome 3 has also recently been identified in a large Danish family (Brown et al., 1995; Skibinski et al., 2005), although another study has failed to find the CHMP2B mutation in 141 familial FTLD probands suggesting that this mutation may be specific to the Danish family (Cannon et al., 2006). Linkage to chromosome 9 has also been identified in familial FTLD (Hosler et al., 2000; Morita et al., 2006; Vance et al., 2006). Familial cases appear to have similar age of onset, disease duration and clinical symptoms to sporadic forms of the disease (Piguet et al., 2004; Godbolt et al., 2005).

1.2.3. Frontal-variant frontotemporal dementia (fvFTD)

The frontal variant of FTLD (fvFTD) has also been described as the behavioural variant, due to the early alteration in personality and social conduct. Some authors have suggested that the behavioural changes can be split into broad but overlapping

types (Hodges, 2001; Snowden et al., 2002). Patients can often be disinhibited, overactive, socially inappropriate and show a lack of concern. On the other hand, they can be bland, apathetic, inert, lacking volition and mental effort and often mentally rigid. Patients showing disinhibition are often less apathetic than those without (Levy et al., 1996), however both disinhibited and apathetic behavioural features may be observed in the same patient at different stages of the disease (Perry and Miller, 2001). Patients also often show stereotypic and ritualistic behaviours (Snowden et al., 2002). Other common behavioural features include changes in eating behaviour, sexual behaviour, and personal hygiene (Snowden et al., 2001). Emotional blunting, involving the inability to express emotion, and loss of insight into their condition, are also common. Authors have suggested that these complex behavioural deficits may be due to damage of an integrated circuit of structures, including the orbitofrontal cortex, amygdala and insula (Ames et al., 1994; Hodges and Miller, 2001). It has also been speculated that damage to the striatum may contribute to the genesis of stereotypical behaviours (Ames et al., 1994; Neary et al., 2000; Nyatsanza et al., 2003). Studies with rats have shown that stereotypic behaviours result from imbalanced activity along the processing pathways of the basal ganglia (Presti and Lewis, 2005). These striking behavioural and personality changes are a particular problem for carers. Studies have shown that FTLD patients account for approximately 1.9% of the primary dementia population in psychiatric hospitals in Germany, and that the admission circumstances were mainly behavioural disturbances (Ibach et al., 2003). Marriage guidance counsellors are commonly consulted, particularly due to changes in sexual behaviour and personality. There is some evidence that serotonergic deficits contribute to the behavioural features in FTLD and that treatment with serotonin reuptake inhibitors may improve the behavioural

symptoms (Pasquier et al., 2003), although studies have found conflicting results (Deakin et al., 2004).

Memory function is relatively spared in fvFTD, however results from a recent study has challenged this thinking by demonstrating severe amnesia at presentation in patients with a pathological diagnosis of FTLD (Graham et al., 2005). Visuospatial function is also relatively preserved early in the disease and they are typically oriented and negotiate their local environment without getting lost. Speech output is typically economical, ultimately leading to mutism. Increasing deficits in planning, organization and other aspects of executive function occur as the disease progresses (Hodges and Miller, 2001).

1.2.4. Semantic dementia (SD)

Patients with SD present with early impairments in semantic memory (Warrington, 1975; Hodges, 2001). This is the component of long-term memory which contains the representation of knowledge about things in the world and their inter-relationships i.e. facts, concepts, words, meanings (Hodges et al., 1992; Garrard et al., 1997). Patients often initially present complaining of loss of memory for words. They show impaired naming, word comprehension and visual object recognition. Complex low frequency words are often lost first and replaced by superordinate words or broad general approximations. They are often aware of their reduced vocabulary but less aware of their impaired comprehension. Their speech is fluent, except for word-finding pauses, although it eventually becomes empty, paraphasic (patients use the incorrect words) and circumlocutious (patients use complex phrases to compensate for missing vocabulary) as they are unable to find the correct words to express

thoughts. Patients may also present with difficulty recognizing and naming faces, which is associated with predominantly right-sided temporal atrophy (Thompson et al., 2003). In clinical practice the term SD has also been used to diagnose patients with a fluent aphasia and word comprehension deficits, in the absence of deficits in visual object recognition. There is considerable disagreement concerning whether visual object recognition deficits should be required for a diagnosis of SD. In fact, visual object recognition deficits are not always formally assessed in FTLD patients.

Episodic memory is initially relatively well preserved in SD patients, although they have been reported to show poor recall of distant memories (Nestor et al., 2002), and their orientation is also relatively intact. Behavioural changes similar to those observed in fvFTD often develop over the course of the disease (Snowden et al., 2001). Changes in eating behaviour, repetitive behaviours, compulsive behaviours, depression, sleep disturbances disinhibition and aggression are common in SD (Snowden et al., 2001; Liu et al., 2004). In addition, they are often described as becoming selfish and lacking sympathy and empathy (Snowden et al., 2001).

1.2.5. Progressive non-fluent aphasia (PNFA)

Patients with PNFA present with complaints of speech dysfluency (Green et al., 1990; Weintraub et al., 1990). They have distorted hesitant speech characterized by reduced phrase length and diminished use of grammatical elements. Phonologic errors are common, for example they might say 'efelant' rather than 'elephant'. Word comprehension is relatively well preserved, especially in the early stages of the disease. In late stages patients become mute, or limited to one or two syllables or grunts, and effectively word deaf (Hodges, 2001). Memory and visuospatial function

are typically less affected (much less so than in AD) and patients can cope with many aspects of everyday life. Behavioural and personality changes often develop as the disease progresses (Kertesz et al., 1994) although few studies have systematically assessed the behavioural deficits in PNFA. It is worth noting that some cases also present with mixed aphasia, showing clinical features of both SD and PNFA (Grossman, 2002).

1.2.6. Other FTLD syndromes

There are a number of other disorders that display similar frontal type presentations to FTLD subjects and are considered by some to be part of the FTLD spectrum. Corticobasal degeneration (CBD) is a mixed movement and cognitive disorder, characterized by progressive asymmetric rigidity, cortical sensory loss and apraxia (Rebeiz et al., 1968; Gibb et al., 1989; Riley et al., 1990). Behavioural, cognitive and language disturbances are also frequent features suggesting the presence of frontal and temporal lobe dysfunction (Kertesz et al., 2000a; Boeve et al., 2003). Aphasia (usually non-fluent) is common in CBD, whereas memory is relatively spared (Kertesz et al., 2000a; Boeve et al., 2003). The term corticobasal syndrome (CBDs or CBS) is often used in order to differentiate it from the pathological diagnosis of corticobasal degeneration (CBD). Progressive supranuclear palsy (PSP) presents with features such as bradykinesia, falls, rigidity, and vertical supranuclear gaze palsy (Litvan et al., 1996), however there is an overlap with CBD (Kertesz and Munoz, 2004) and patients often show some frontal behavioural features (Aarsland et al., 2001).

Motor-neuron disease (MND) has also been associated with FTLD. MND is characterized by wasting, weakness, fasiculations, and bulbar features such as dysarthria and dysphagia. Personality and behaviour change, and frontal cognitive features are also frequently observed (Bak and Hodges, 1999; Bak and Hodges, 2001). A significant number of patients with FTLD also develop features of MND. Patients with both FTLD and MND features tend to have a rapidly progressive course, with early death from dysphagia (Kertesz and Munoz, 1998). Amyotrophic lateral sclerosis (ALS) is considered a subtype of MND, although the terms ALS and MND are also often used interchangeably (Bak and Hodges, 2001). The incidence of FTLD in ALS is approximately 48% (Portet et al., 2001), conversely a study by Lomen-Hoerth 2002 looked at a group of 36 patients with clinically diagnosed FTLD and found that 14% met criteria for definite ALS, and 36% showed features of ALS (Lomen-Hoerth et al., 2002).

1.2.7. Histopathology

The definitive diagnosis of FTLD requires pathological confirmation. However, even the pathological diagnosis which is currently the gold standard is in an evolving state. Some clinicians and neuropathologists argue to include certain diagnoses under the rubric of FTLD, for example, progressive supranuclear palsy (PSP), yet others are resistant to such inclusions.

The pathologic diagnosis of FTLD is heterogeneous, including a number of conditions characterized by the presence of intracellular inclusions formed by abnormal cytoskeletal components both in neurons and glial cells (McKhann et al., 2001). Tau proteins appear to play an important role in several neurodegenerative

disorders, therefore current classification of FTLD divides FTLD into tau-positive and tau-negative diseases (Hodges et al., 2003; Josephs et al., 2006b). The tau positive group includes four forms of tauopathy: Pick's disease (PiD), progressive supranuclear palsy (PSP), corticobasal degeneration (CBD), and FTDP-17. The tau negative group includes one form with tau-negative, ubiquitin positive inclusions without motor neuron disease (FTLD-U), one form with tau-negative, ubiquitin positive inclusions with motor neuron disease (FTLD-MND) and one form with neither tau-positive nor ubiquitin-positive inclusions (dementia lacking distinctive histology, or DLDH (Knopman et al., 1990)). In addition to these three tau negative diseases, an additional form associated with intermediate filaments is recognized (Josephs et al., 2003). These neuropathological subtypes of FTLD are described in greater detail below.

1.2.7.1. Tau positive

Pick's disease is diagnosed when on histological examination there are intracytoplasmic, rounded inclusions that are stained positive with tau, ubiquitin and silver stains (Pick bodies, see figure 1.2A, (Dickson, 2001)). These inclusions are found predominately in the frontal and temporal cortices including the dentate granular cell layer of the hippocampus. Inclusions can also occur elsewhere however including other cortical regions, the striatum and even in brainstem areas.

PSP is defined by the presence of tau positive inclusions affecting mainly subcortical grey and brainstem structures especially the globus pallidum and the subthalamic nucleus. Unlike in Pick's disease where the morphology of the inclusions are rounded, PSP is defined by four different lesions including globose neurofibrillary

tangles, and glial inclusions known as oligodendroglial coiled bodies, threads and the tufted astrocyte (Dickson, 1999).

The histological diagnosis of CBD is dependent on the findings of specific lesions as well as a relatively specific distribution of the pathological findings. In CBD, the posterior frontal and superior parietal cortices are most commonly affected as well as the striatum. Histopathologically, there are numerous swollen (balloon) neurons in conjunction with three other pleomorphic inclusions. Some resemble Pick bodies, some are more granular and are called pre-tangles, while others may mimic the globose neurofibrillar tangles of PSP and are called corticobasal bodies. In CBD however, unlike PSP, there is a predominance of threads and a relatively specific lesion known as the astrocytic plaque (Dickson et al., 2002).

The diagnosis of FTLD-17 is mainly a genetic one with confirmation of the presence of intracellular tau pathology on histology. The intracellular tau pathology has no signature pattern *per se* and can mimic PiD, PSP and CBD. This diagnosis however is usually suspected if the intracellular pathology and distribution of the pathology is more widespread than what is typically encountered in PSP, CBD or Pick's disease.

1.2.7.2. Tau Negative

Even though there are more variants within the tau positive groups, the majority of cases of FTLD (60%) are tau negative (Josephs et al., 2004b). Frontotemporal lobar degeneration with ubiquitin only immunoreactive changes (FTLD-U) is the most common subtype (Josephs et al., 2004b). In this disease the pathological finding are more specific in terms of distribution and tend to mainly affect the frontotemporal

cortex and the dentate granular cells. Unlike the tau positive group, tau immunohistochemistry is negative in this disease. Inclusions can only be visualized with ubiquitin immunohistochemistry. FTLD-U is possibly the more recognized terminology for this disease however others have referred to this disease as dementia with ubiquitin positive inclusions (DUI) (Rossor et al., 2000), and as motor neuron disease – inclusion dementia (MNDID) (Jackson et al., 1996). The second variant within the tau negative group is similar to FTLD-U with the exception that motor neurons in the brainstem nuclei or spinal cord are also affected in which case the disease is referred to as frontotemporal lobar degeneration with motor neuron disease (FTLD-MND). This disease behaves more like typical motor neuron disease with a very short duration of illness (Josephs et al., 2005). When no inclusions are found with extensive immunohistochemical analysis yet there is evidence of neuronal loss in the frontal and temporal cortex, the disease is designated as dementia lacking distinctive histology (DLDH) (Knopman et al., 1990).

A final disease recently described and included under the rubric of tau negative disease is neurofilament inclusion body disease (NIBD) (Cairns et al., 2003; Josephs et al., 2003). Unlike all the diseases described above, NIBD is defined by the presence of neurofilament positive inclusions. These inclusions are not highlighted with tau staining and are very lightly stained with ubiquitin. Recently, alpha-internexin, an intermediate filament, was shown to be a component of the inclusions of NIBD but not of other variants of FTLD (Cairns et al., 2004), making this disease different from all the above.

Figure 1.2: Intracellular inclusions from the dentate gyrus of the hippocampus in FTLD: A) tau-positive inclusions (Pick bodies) in PiD, and B) ubiquitin-positive inclusions in FTLD-U.

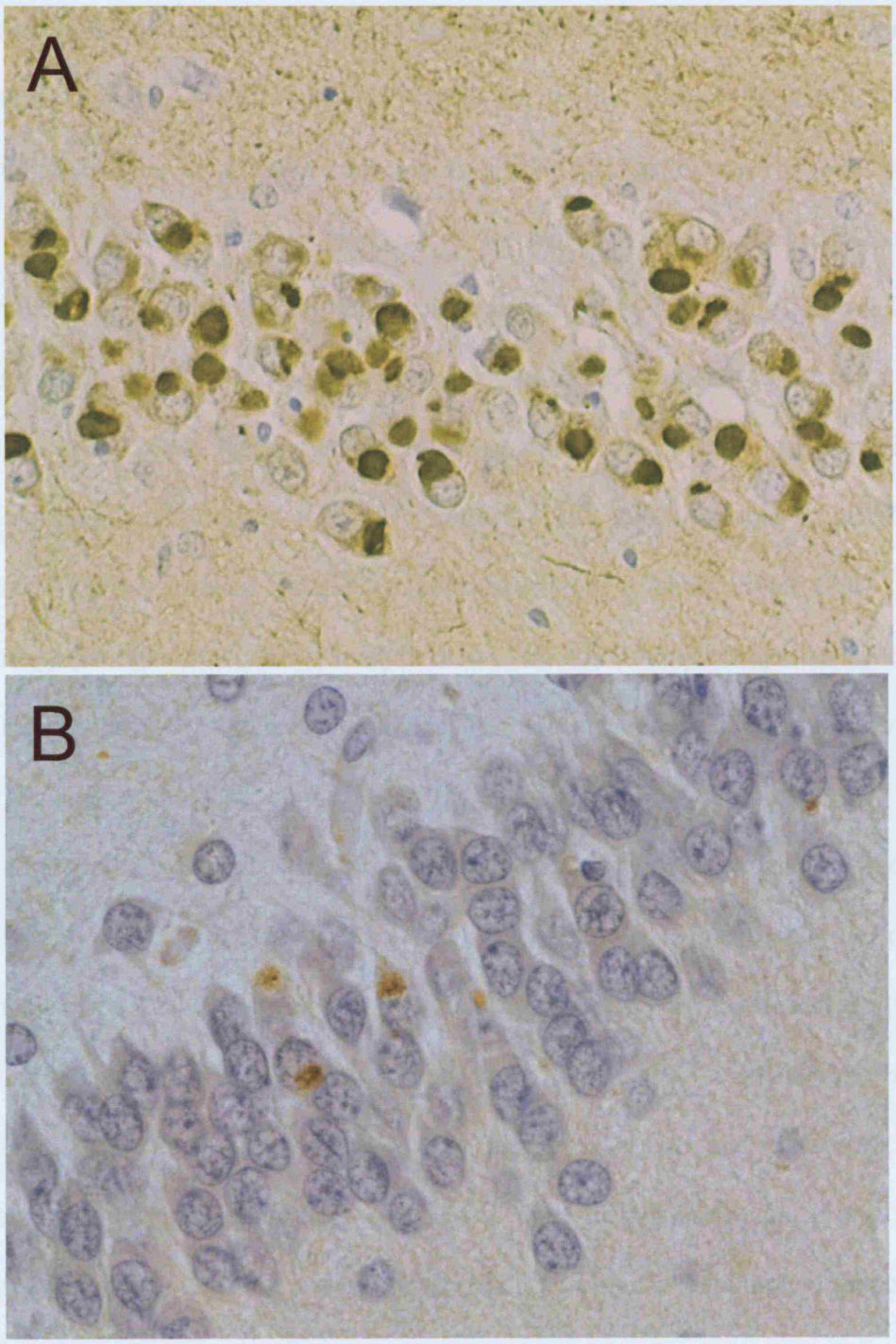

These pathological subtypes of FTLD do not map neatly onto the clinical syndromes, making it difficult to predict FTLD pathology during life. There is considerable overlap between the clinical and pathological diagnoses of FTLD. However, recent clinicopathological studies have suggested that prediction may be possible in certain diagnostic groups: patients with FTD-MND are highly likely to have FTLD-MND pathology (Hodges et al., 2004; Josephs et al., 2006b), patients with PNFA tend to have a tau positive pathology (Kertesz et al., 2005), which is often CBD or PSP (Josephs et al., 2006b), and the most common pathology to underlie SD is FTLD-U (Davies et al., 2005). The pathology underlying fvFTD appears to be more varied (Hodges et al., 2004; Josephs et al., 2006b), although there is a suggestion that the most common pathology is FTLD-U (Kertesz et al., 2005; Josephs et al., 2006b). Patients fulfilling clinical criteria for CBD are likely to show either CBD or PSP pathology (Hodges et al., 2004; Josephs et al., 2006b), although subjects with clinical PSP are highly likely to have pathological PSP (Josephs et al., 2006b) but have been reported to have FTLD-U and FTLD-MND (Paviour et al., 2004). Subjects with a pathological diagnosis of NIBD have been reported with a clinical diagnosis of fvFTD and CBD (Josephs et al., 2003). Interestingly, subjects with a clinical diagnosis of fvFTD, PNFA or SD have also been reported with AD pathology (Galton et al., 2000; Kertesz et al., 2005; Knibb et al., 2006). Figure 1-3 summarises the results of the clinicopathological studies discussed above and illustrates which pathological substrates have been reported to underlie which clinical group. Please note that the figure does not attempt to represent all clinical-pathological associations ever published but merely illustrates the complexity that has arisen from these few recent studies.

Figure 1.3: Associations between the clinical syndromes of FTLD and the underlying histopathology based on cases reported in a number of large case series (Galton et al., 2000; Josephs et al., 2003; Hodges et al., 2004; Paviour et al., 2004; Davies et al., 2005; Kertesz et al., 2005; Josephs et al., 2006b; Knibb et al., 2006).

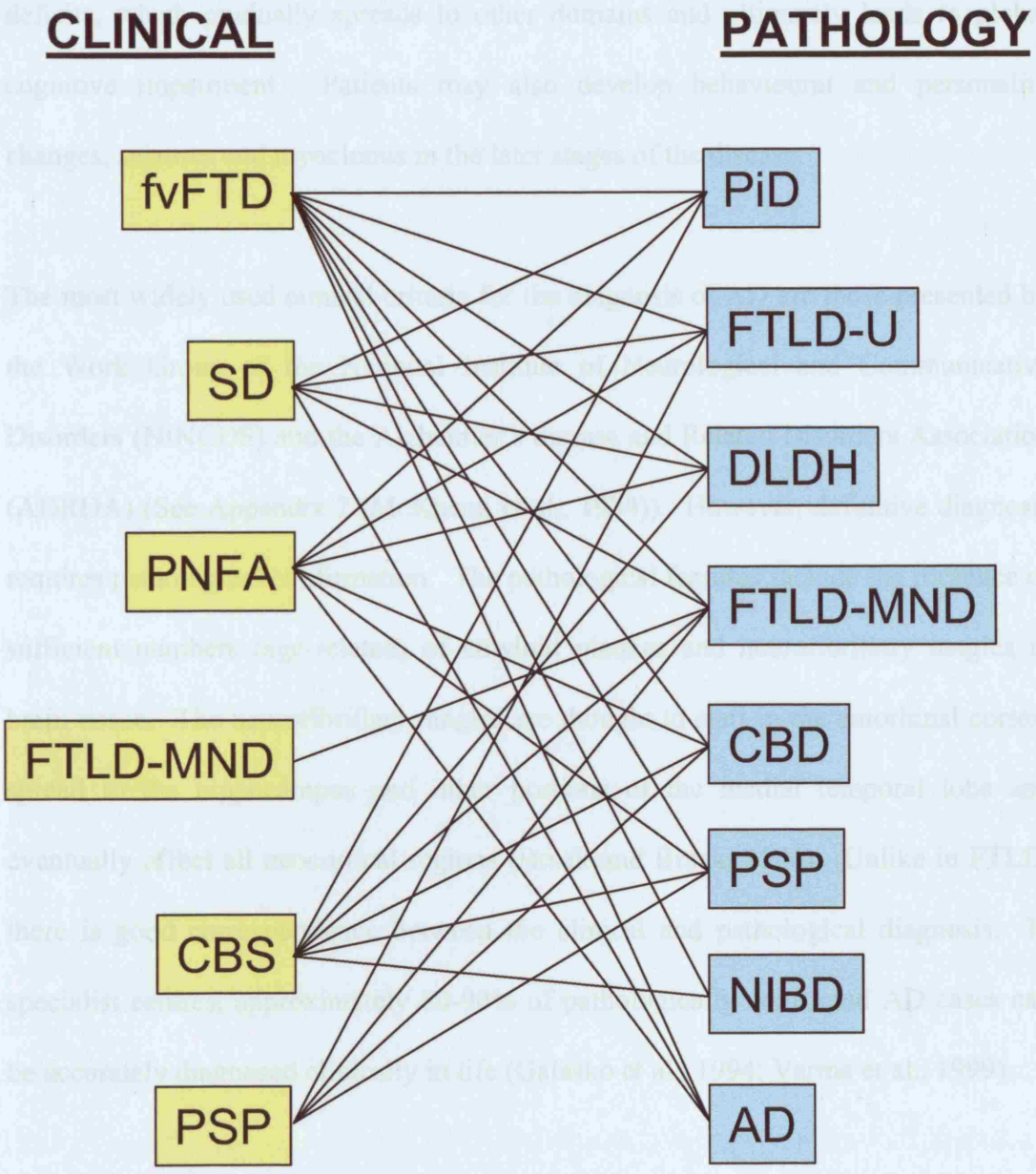

1.3. Alzheimer's disease (AD)

Alzheimer's disease (AD) is the most common cause of dementia. The prevalence increases exponentially with age, increasing from 0.05% in the under-sixties, to 20% in the over-eighties. It is characterised by the insidious onset of episodic memory deficits, which gradually spreads to other domains and ultimately leads to global cognitive impairment. Patients may also develop behavioural and personality changes, seizures and myoclonus in the later stages of the disease.

The most widely used clinical criteria for the diagnosis of AD are those presented by the Work Group of the National Institute of Neurological and Communicative Disorders (NINCDS) and the Alzheimer's disease and Related Disorders Association (ADRDA) (See Appendix 2 (McKhann et al., 1984)). However, definitive diagnosis requires pathological confirmation. The pathological features include the presence of sufficient numbers (age-related) of amyloid plaques and neurofibrillary tangles in brain tissue. The neurofibrillary tangles are thought to start in the entorhinal cortex, spread to the hippocampus and other portions of the medial temporal lobe and eventually affect all neocortical regions (Braak and Braak, 1996). Unlike in FTLD, there is good correspondence between the clinical and pathological diagnosis. In specialist centres, approximately 80-90% of pathologically confirmed AD cases can be accurately diagnosed clinically in life (Galasko et al., 1994; Varma et al., 1999).

The most common form of AD is late-onset sporadic AD (SAD), which accounts for over 95% of cases (Holmes, 2002). Although a family history of AD is a risk factor in SAD there is no clear pattern of autosomal dominant inheritance in these cases. The combination of genetic and environmental factors that may contribute to the

disease are still unclear (Schott et al., 2002). One established risk factor is the ε4 allele of the apolipoprotein (APOE) gene. A small number of subjects have autosomal dominant familial AD (FAD). These individuals generally have an early age of onset, typically under the age of 60 years (Wisniewski et al., 1998). Causative mutations have been identified in three genes: amyloid precursor protein (APP), Presenilin 1 (PS1) and PS2 (Goate et al., 1991; Rogaev et al., 1995; Sherrington et al., 1995). These three mutations account for 50% of all autosomal dominant cases, therefore a number of FAD cases do not possess any identified genetic mutation (Holmes, 2002). A few cases of PS1 mutations however have shown FTLD pathology (Dermaut et al., 2004).

Symptomatic treatments for AD are available and are routinely prescribed. There are two main treatment categories: cholinesterase inhibitors (e.g. Donepezil, Rivastigmine, Galantamine) and NMDA-antagonists (e.g. Memantine) (O'Brien and Ballard, 2001; Ballard, 2002). Vitamin E was also commonly prescribed but recently has lost favour as studies show increasing mortality in patients with cardiac disease on vitamin E (Miller et al., 2005). A recent trial of vaccination with aggregated Aβ amyloid was implemented after the observation that immunization with Aβ reduces the pathological signs of AD in transgenic mice (Schenk et al., 1999). The trial was interrupted when encephalitis developed in 6% of the subjects. Although primary clinical outcome measures were all negative, analysis of those subjects who generated a high titre of Aβ antibodies showed a significantly lower decline on a composite measure of a battery of neuropsychological tests (Gilman et al., 2005). Additionally serial MRI results showed an extra 1% of brain loss in the same subject group. This has lead to speculation that the vaccination led to amyloid removal in some subjects

(Fox et al., 2005). Future trials may focus on passive immunization techniques (Wilcock et al., 2004).

1.4. Differential diagnosis

The clinical diagnosis of FTLD can be difficult. Several other disorders present with frontotemporal symptoms, such as frontal lobe tumours, alcohol-associated dementia, Huntington's disease, AD, VaD and Creutzfeldt Jacob disease (CJD). One study suggested that only approximately 14% of pathologically confirmed FTLD cases are accurately diagnosed during life (Mendez et al., 1993). The most difficult differential diagnosis can be the differentiation of FTLD from AD. Both are common in patients under 65 years old, have an insidious onset and produce a progressive dementia syndrome that can include executive dysfunction, language impairment, and can cause alterations in behaviour. Many patients with pathologically confirmed FTLD meet the NINCDS-ADRDA criteria for probable AD during life (Varma et al., 1999). The development of detailed diagnostic criteria has improved the recognition of FTLD. Recent studies from specialist centres suggest that between 63 and 79% of pathologically confirmed FTLD cases are correctly classified as FTLD on their first assessment (Rosen et al., 2002b; Knopman et al., 2005). Differentiating FTLD and AD is increasingly important since new treatments are being developed for both diseases. Attempts to improve diagnosis have looked for biomarkers as well as clinical features with a focus on neuropsychological testing and behavioural assessments.

1.4.1. Neuropsychology

Detailed neuropsychological testing may be very helpful in characterising the cognitive profile.

The mini-mental state examination (MMSE) is routinely assessed in all dementia patients and provides a crude overall index of neuropsychological impairment (See Appendix 3 (Folstein et al., 1975)). Although the MMSE has been useful as a quick measure of disease severity in AD (Fox et al., 1999a), it is insensitive to the behavioural dysfunction, and much influenced by language dysfunction, in FTLD. It therefore provides a poor measure of disease severity in FTLD and has limited value in differentiating FTLD and AD. The Addenbrooke's Cognitive Examination (ACE) has been developed as a modification to the MMSE with particular focus on the language and verbal fluency deficits present in FTLD (Mathuranath et al., 2000). It is more sensitive to FTLD than the MMSE, and provides better discrimination between FTLD and AD. The Clinical Dementia Rating (CDR) is another measure of disease severity again largely developed for AD. It assesses aspects of cognitive functioning in daily living (See Appendix 3 (Hughes et al., 1982)), although it is still particularly influenced by memory impairment.

Many studies have examined differences in the detailed neuropsychological profile between FTLD and AD. However, some early neuropsychological studies were inconclusive and showed contradictory results. This is most likely due to the small subject numbers and grouping together the different variants of FTLD, thereby masking important group differences. Recent studies have differentiated between the different syndromic variants of FTLD and have demonstrated different patterns of

deficit in each group. Individuals with fvFTD usually show poor performance on frontal executive tasks, such as the Wisconsin card sorting test, Stroop test and verbal fluency test (Hodges and Miller, 2001), but have relatively preserved semantic (Hodges et al., 1999) and episodic memory. Generally AD subjects perform better than fvFTD individuals (although differences in matching for disease severity undermine these statements) on tests of executive function, although cases of fvFTD have been reported with no dysexecutive features (Lough et al., 2001) and executive deficits have been reported in AD (Johnson et al., 1999). Executive tests are often complex making it likely that they will be performed poorly by both groups and so limiting their diagnostic value. These tasks are thought to be particularly affected by dorsolateral frontal deficits. Tests for the orbitofrontal functions have been suggested as including decision-making and risk taking tests. Subjects with fvFTD often have a poor ability to make judgements that involve assessing relative reward values and to make inferences about the mental state of others. These features are thought to be associated with orbitofrontal atrophy.

Individuals with SD (by definition) show marked impairment on semantic memory tasks, especially if they require verbal output, such as the category fluency tests and picture naming, but have relative preservation of executive tasks (Hodges and Miller, 2001). They also show deficits in single-word comprehension, as assessed by word-picture matching, and reading and spelling irregular words. In contrast, PNFA patients perform well on tests of semantic memory but poorly on tests of phonologic competence, such as being asked to repeat multisyllabic words (Hodges, 2001). Patients with PNFA perform worse on tests of letter fluency, and make more paraphasic errors than AD patients (Mendez et al., 2003). Memory is relatively

spared and orientation and recall of personal events is relatively good in all three FTLD variants in the early stages.

Individuals with AD typically present with early loss of episodic memory (Perry and Hodges, 2000). They perform significantly worse on tests of episodic memory (including recall memory and recognition memory for words) than both fvFTD and SD patients (Perry and Hodges, 2000). Some studies have shown that AD subjects perform worse on tests for visuoperceptual and calculation than FTLD subjects (Mendez et al., 1996; Rascovsky et al., 2002); although these features have been suggested by some authors as not being useful for differential diagnosis (Pachana et al., 1996; Lindau et al., 1998). A wide variety of neuropsychological changes may be observed in VaD. Small vessel disease VaD often is characterised by executive deficits (Pasquier, 1999). Deficits tend to reflect sub-cortical and frontal dysfunction and cognitive domains are affected in a patchy manner.

Increasingly it is recognised that the profile of deficits is most useful. Studies have shown that combinations of different neuropsychological tests can help in the differentiation of FTLD and AD. For example, Kramer et al 2003 found that a combination of 5 neuropsychological variables (including tests of naming, category fluency and executive function) could correctly classify 89% of fvFTD, SD and AD cases (Kramer et al., 2003). Similarly, Rascovsky et al (2002) used a combination of verbal fluency, memory and visuospatial tests to correctly classify 86% of pathologically confirmed FTLD and AD subjects (Rascovsky et al., 2002). A recent study by Knopman et al (2005) found that 62% of pathologically confirmed FTLD cases had psychometric test scores consistent with a diagnosis of FTLD (Knopman et

al., 2005). However, results from different studies are often contradictory; depending critically on the severity of the patients and on the specific tests administered. FTLD subjects may also perform disproportionately badly on tests due to deficits in attention and language. Neuropsychological tests that are dependent on verbal instructions and responses may lead to the incorrect conclusion that non-language domains are impaired. Despite the undoubted value of clinical assessment and neuropsychological testing there is still a need for biomarkers that can support or refine the clinical diagnosis especially in early cases.

1.4.2. Behavioural and personality assessments

A number of studies have assessed and compared the behavioural profiles in FTLD and AD. They typically use caregiver-based questionnaires such as the Neuropsychiatric Inventory (NPI) (Cummings et al., 1994) and Manchester and Oxford Universities Scale for the Psychopathological Assessment of Dementia (MOUSEPAD) (see Appendix 3 (Allen et al., 1996)). The NPI rates the severity and frequency of a number of behaviors, including delusions, hallucinations, agitation, depression, anxiety, apathy, disinhibition, irritability and aberrant motor behaviour. The carer is asked to assess a 'behavioral symptom' as a feature that reflects a notable change from the patient's premorbid state.

Behavioural features are a common early feature of FTLD, but are also present in AD. An early study by Levy et al (1996) showed disinhibition, euphoria, apathy and aberrant motor behaviours were all more common in FTLD than AD (Levy et al., 1996). Features such as delusions, hallucinations, agitation, depression, anxiety and irritability were less useful in differentiating FTLD and AD. A discriminate analysis

showed that disinhibition, apathy, and depression could accurately diagnose 77% of FTLD subjects and 77% of AD subjects (Levy et al., 1996). A number of studies have emphasised that stereotypic behaviours, changes in eating behaviour and loss of social awareness can most strongly discriminate between FTLD and AD (Miller et al., 1997; Bozeat et al., 2000; Bathgate et al., 2001). Complex ritualised behaviours, such as clock watching, repetitive eating of the same food, rigid adherence to routine, are more common in both fvFTD and SD, than AD; whereas, more simple verbal repetitive behaviours, such as use of stock phrases and echolalia, are common in all three groups (Nyatsanza et al., 2003). Bathgate et al (2001) also found that those behavioural features that can differentiate FTLD from AD, can also discriminate between FTLD and VaD (Bathgate et al., 2001). Generally behavioural assessments have been shown to be able to classify between approximately 70% and 95% of patients (Levy et al., 1996; Bozeat et al., 2000; Bathgate et al., 2001). However, studies do not always agree, for example in contrast to the results by Levy et al (1996), a study by Bozeat et al found no significant differences between FTLD and AD in aberrant motor behaviour and apathy (Bozeat et al., 2000). This may be due to the different behavioural questionnaires employed or different patient groups studied. A combination of both behavioural assessments and neuropsychological tests may be the most diagnostically useful.

Studies have also investigated other changes in personality and social cognition in FTLD. A recent study using the interpersonal adjectives scale questionnaire has shown that both patients with FTLD and AD show changes in personality (Rankin et al., 2003). Subjects with FTLD tend to become pathologically rigid and exaggerated, whereas AD subjects became increasingly introverted with a decrease in assuredness.

In addition, patients with SD become more "cold-hearted" while at a group level the fvFTD subjects tend to become more docile and submissive. There is also some suggestion that FTLD subjects show deficits in theory of mind, whereas AD subjects do not. Theory of mind refers to the individuals' awareness about the mental state of others (Gregory et al., 2002). Therefore, assessments of behaviour, personality and social cognition may all help in the differential diagnosis of FTLD. Although many of the scales applied are not used during a clinical exam but are mainly for research purposes.

1.4.3. Other investigations

The EEG is often performed as part of the clinical workup in FTLD and AD. Some studies have suggested that the EEG may be helpful in differentiating AD and FTLD (Yener et al., 1996). The EEG often shows generalised slowing (loss of alpha) in AD subjects, and was often considered to be normal in FTLD. A recent study has however found a lack of significant difference in the severity of EEG abnormality between FTLD and AD patient groups (Chan et al., 2004).

Studies have also investigated the diagnostic utility of CSF biochemical markers in FTLD (Pasquier et al., 2003). Phosphorylated tau protein concentrations have been reported to be elevated in the CSF of fvFTD and SD patients (Arai et al., 1997), although other studies have shown low total tau (Grossman et al., 2005) or normal levels of phosporylated (Grossman et al., 2005) and total tau (Sjogren et al., 2000b). There is some suggestion that a combination of both CSF tau and Aβ42 may help to differentiate AD and FTLD: Tau is elevated in FTLD, but not as much as in AD, and Aβ42 levels are lower than normal controls, but higher than AD (Riemenschneider et

al., 2002). However, due to discrepancies between studies the role of tau biochemical markers remains uncertain. Further work needs to be carried out before CSF markers could be considered as sensitive and specific diagnostic markers for FTLD.

The lack of definitive laboratory tests (blood, CSF, EEG) has led to interest in using neuroimaging to improve diagnosis in FTLD.

2. Neuroimaging

As discussed in chapter 1 a definitive diagnosis of FTLD requires pathological confirmation, and there is still uncertainty in the clinical diagnosis, even with established diagnostic criteria. Imaging is increasingly recognised as an important tool in the diagnosis of degenerative dementias. Histopathological changes arising from neurodegenerative conditions are associated with atrophy, with brain weights significantly reduced. Atrophy can be visualised and quantified with imaging and has been taken to have a direct relationship to the underlying disease process in FTLD and AD. The most widely used neuroimaging modalities are structural; namely X-ray computed tomography (CT) and magnetic resonance imaging (MRI). Both are widely available and non-invasive. There is also increasing recognition of the value of functional imaging (especially Positron Emission Tomography (PET)) in differentiating FTLD from AD. Indeed in the US reimbursement for PET scans for this specific indication was approved for the first time in 2004. This thesis will however focus on MRI and functional imaging will not be discussed in any detail.

Historically the role of neuroimaging in dementia was to exclude structural and potentially reversible causes. The most important of these are cerebral tumours, hydrocephalus and subdural haematoma; both CT and MRI scanning will detect most of these pathologies. More recently a CT or MRI has become a routine part of the clinical workup to aid differential diagnosis. In fact, recommendations from the American Academy of Neurology suggest that at least one structural scan should be performed in all cases of dementia.

2.1. Imaging modalities

Structural imaging techniques provide an image of the brain that allows differentiation of tissue types and the identification of different cerebral structures. CT involves the reconstruction of a cross-sectional image of the brain from X-ray attenuation data. In contrast, MR utilises the fact that hydrogen nuclei emit a radio signal following excitation by a radiofrequency (RF) pulse at their resonant frequency. In order to provide spatial information the magnetic field has a different strength at each point through the cross-section; therefore the MRI signal frequency depends upon position in this field. Once the RF pulse is switched off the protons relax and return to their normal state. Different tissues then relax at a different rate, dependent upon the tissue composition, structure and surroundings.

CT scans are widely available, cheap and relatively rapid. However, in evaluating and quantifying brain structures MRI has a number of advantages. Firstly, MR has better tissue contrast and resolution. Partial volume effects produce practical problems for the delineation of structures in CT. MR imaging sequences can be chosen to maximise the contrasts that most clearly delineate the structural detail of the tissue of interest allowing the sensitive differentiation of tissue types and the detection of inhomogeneities within tissues. Second, MR is not subject to the presence of beam hardening artefacts that often obscure the temporal lobes on CT, hence MR has been shown to be more sensitive to focal temporal lobe abnormalities (Sinnatamby et al., 1996). Third, MR avoids the risks associated with ionising radiation, and therefore serial studies involving repeated measures over time are possible. However, longer scanning times are required with MR, and the scans are therefore more sensitive to

movement artefact (see chapter 3). This is a particular problem in patients with dementia; they may forget instructions and have difficulty keeping still.

In MRI, the time between RF pulses and the time between the pulse and the collection of the signal can be varied in order to create different types of image. Three of the most common types of MR image are the T1-weighted image, in which tissue appears brighter than CSF (see figure 2.1A), the T2-weighted image in which CSF has a higher signal intensity than tissue (see figure 2.1B), and the proton density (PD) image which have darker CSF than the T2-weighted images (see figure 2.1C). Image analysis techniques generally use T1-weighted images due to the better resolution and brain-CSF contrast. However, the high CSF signal on T2-weighted images makes them especially useful for the measurement and identification of vascular lesions and for measuring total intracranial volume (see chapter 12).

Functional imaging techniques are also often applied in patients with dementia. In the United Kingdom this is more often as a research tool rather than a diagnostic aid. These techniques measure neural activity indirectly using glucose metabolism or cerebral blood flow as surrogate markers. The three main functional imaging modalities include Positron Emission Tomography (PET), Single Photon Emission Computed Tomography (SPECT) and functional MRI (fMRI). Both PET and SPECT involve the detection of gamma rays produced by radioactive tracers. Brain areas that are active take up the tracer. In contrast, fMRI does not require a tracer. It utilises the magnetic properties of oxygenated and deoxygenated blood to estimate cerebral blood flow. High signal intensity indicates a high level of blood oxygenation. Functional imaging provides different, yet complementary information

to structural imaging. In many instances brain anatomy appears normal even though clinical examinations are impaired, in these situations functional imaging can be informative.

This thesis is particularly interested in the role of structural MRI in FTLD, both in the assessment of regional patterns of atrophy and measurement of progression. As mentioned above functional imaging will not be considered in this thesis. However, CT and functional studies have been important in the characterisation of FTLD, and therefore will be referred to where appropriate.

Figure 2.1: Axial slices through A) T1-weighted, B) T2-weighted and C) PD image from a healthy control

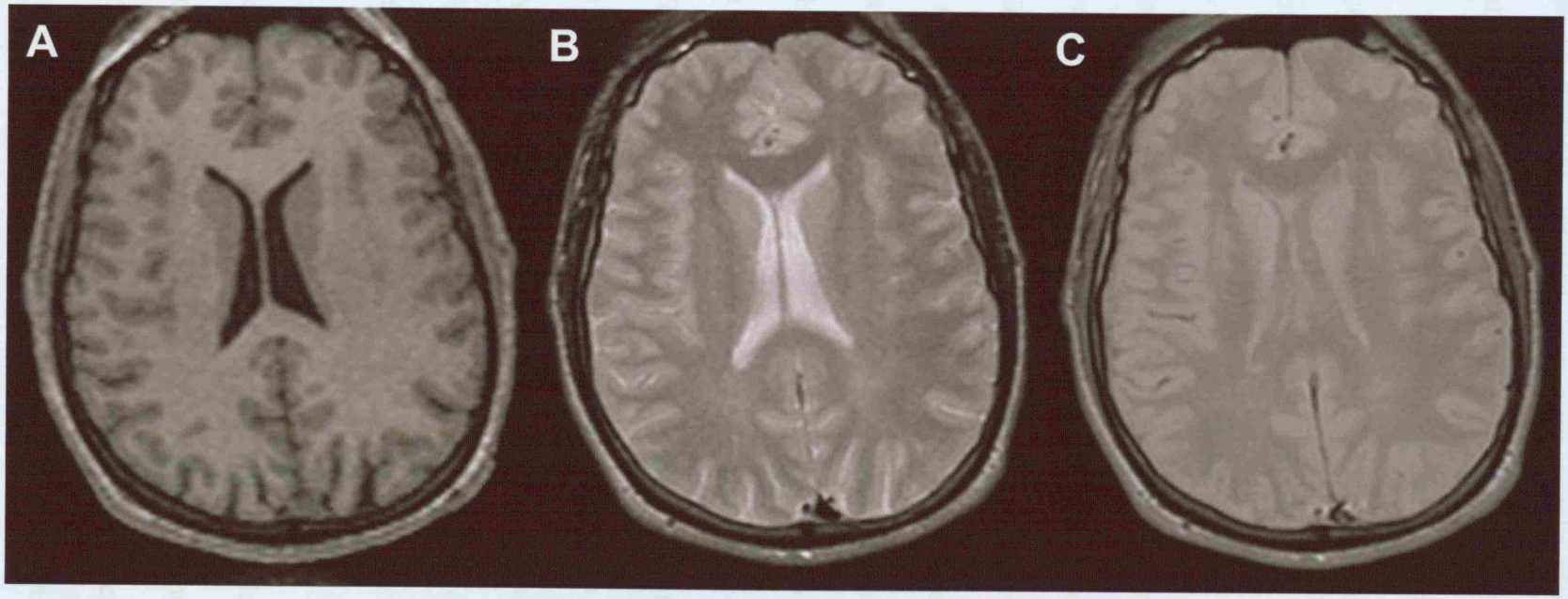

2.2. Analysis techniques

A number of methods, ranging from very simple visual assessments to more sophisticated techniques, have been developed to assess structural brain changes on imaging. Visual inspection of CT or MRI scans is the only method of assessment routinely used by radiologists and neurologists to aid diagnosis and identify non-degenerative pathologies. It is particularly important in the diagnosis of vascular dementia, which has characteristic signal changes in basal ganglia and white matter on MR, but may be difficult to differentiate clinically from AD, DLB or FTLD. Qualitative ratings of atrophy can be produced using a scoring system. These typically focus on the size of the ventricles or degree of cortical atrophy (Scheltens et al., 1995; Galton et al., 2001b). Although there is evidence that these techniques aid in diagnosis there is also considerable overlap between disease groups and controls. These techniques are critically dependent on the skill and experience of the raters, and may have poor inter-observer reliability. In fact, the consortium to Establish a Registry for Alzheimer's disease (CERAD) concluded that inter-rater agreement on MR scans was unsatisfactory and that 'eyeball' inspection of MR scans was highly subjective, and that more objective techniques were required (Davis et al., 1992). This thesis will apply visual assessments to analyse the regional patterns of atrophy in FTLD in chapter 4.

Several quantitative measurements of atrophy have been developed in an attempt to produce greater objectivity. These include linear measurements of structures, such as the medial temporal lobe, hippocampus and frontal lobes (Frisoni et al., 1996a; Frisoni et al., 1996b), as well as cross-sectional area (Ikeda et al., 1994) and volume measurements (Jack et al., 1997; Chan et al., 2001b). Linear measurements have the

advantage of speed and simplicity; however, they depend on the slice selected and the identification of two recognisable landmarks. Area measurements similarly depend upon accurate slice selection. Estimating volumes of cerebral structures should be less subjective and provide information on the whole of the structure. It usually involves defining a region of interest (ROI) on a number of slices and then summing the area measurements and multiplying by the distance between slices (Cavalieri's principle). Most studies measure volumes manually using a mouse-driven cursor, and often employ intensity thresholds to help in the identification of CSF from brain tissue. However, these techniques are very labour intensive and limited by rater error. Automated techniques have been developed which are more reproducible and less time-consuming, although anatomical accuracy may be compromised. Both manual and automated volume measurements may be helpful in the diagnosis of dementia, although anatomical definitions vary making it difficult to compare between studies.

ROI measurements require a priori decisions concerning which structures to assess; whereas visual assessment is not limited in this way. Unbiased measurement techniques have been developed to assess cross-sectional patterns of atrophy throughout the whole brain. One of the most widely used techniques is voxel-based morphometry (VBM) (Ashburner and Friston, 2000). This technique involves a number of pre-processing steps including normalising all the subject images into the same space, segmenting grey, white matter and cerebrospinal fluid (CSF) and smoothing. VBM then applies robust statistics at each point within an image to highlight regions of significant difference between groups. More details on VBM are provided in chapter 3. This technique has been applied to highlight reductions in grey matter in normal ageing (Good et al., 2001a), temporal lobe epilepsy (Keller et al.,

2002), Huntingtons disease (Thieben et al., 2002), AD (Rombouts et al., 2000; Baron et al., 2001) and in FTLD (as will be discussed in the next section). A number of other automated techniques have been developed, such as deformation-based morphometry (DFM) and tensor-based morphometry (TBM), which provide information about differences in brain shape (Good et al., 2001b).

The techniques discussed so far have all been cross-sectional, therefore involving the assessment of atrophy at one time-point. This has the disadvantage that small brain changes tend to be masked by large variation between individuals. Longitudinal studies use serial scans to measure changes in cerebral structure over time in a single individual. Rates of atrophy have been shown to be diagnostically useful in AD (Jack et al., 1998). However, even with longitudinal studies, detection of small changes remains difficult (see chapter 12). To avoid the problems associated with manual measurements automated image registration and subtraction algorithms have been developed (Fox et al., 1996b; Fox and Freeborough, 1997). Non-linear registration techniques have also been developed to allow unbiased assessments of regional patterns of change between serial scans. Further details of these registration techniques are provided in chapter 3.

2.3. Patterns of atrophy in FTLD

Structural and functional imaging techniques have been critical to the characterisation of the FTLD syndromes. Early studies identified patterns of frontal and anterior temporal atrophy in FTLD cases; consistent with patterns of gross atrophy identified at post-mortem (Dickson, 2001). This frontotemporal involvement has since been shown both as hypometabolism in PET and SPECT studies (Starkstein et al., 1994;

Miller and Gearhart, 1999; Varma et al., 2002a; Varrone et al., 2002), and atrophy in MRI/CT studies (Kitagaki et al., 1998; Varma et al., 2002a; Grossman et al., 2004; Larsson et al., 2004; Williams et al., 2005). Involvement of parietal and subcortical structures has also been reported (Kitagaki et al., 1998; Garraux et al., 1999; Sjogren et al., 2000a; Varma et al., 2002a). In fact, the presence of frontal and anterior temporal lobe abnormalities on brain imaging forms part of the diagnostic criteria for FTLD (Neary et al., 1998). However, frontotemporal atrophy may not always be present. A recent study by Knopman et al (2005) found that only 50% of cases with pathologically confirmed FTLD showed a characteristic frontotemporal pattern of atrophy on MRI (on visual assessment) (Knopman et al., 2005).

Characteristic patterns of atrophy have been suggested in each of the syndromic variants of FTLD. Clinical criteria state that fvFTD is associated with 'frontal and/or temporal' degeneration (Neary et al., 1998), although structural and functional studies have suggested that the frontal lobes are the main focus of damage (see figure 2.2) (Starkstein et al., 1994; Jauss et al., 2001; Rosen et al., 2002c; Diehl et al., 2004; Boccardi et al., 2005). Frontal lobe atrophy is usually symmetrical, although asymmetric right-sided atrophy has been reported (Fukui and Kertesz, 2000; Rosen et al., 2002c). These changes would be consistent with the role of the frontal lobes in executive function and behaviour. VBM studies have also shown atrophy in a network of limbic areas that are likely to be involved in the fine tuning of behaviour, including the ventromedial cortex, anterior cingulate and amygdala (Rosen et al., 2002c; Boccardi et al., 2005). Atrophy of temporal lobe regions, such as the hippocampus and parahippocampal gyrus, has also been reported in fvFTD patients (Galton et al., 2001b; Grossman et al., 2004).

Figure 2.2: Coronal and axial T1-weighted images of a subject with fvFTD. Note the severe atrophy of the frontal lobes bilaterally and also the involvement of the temporal lobes, specifically in inferior and medial temporal regions.

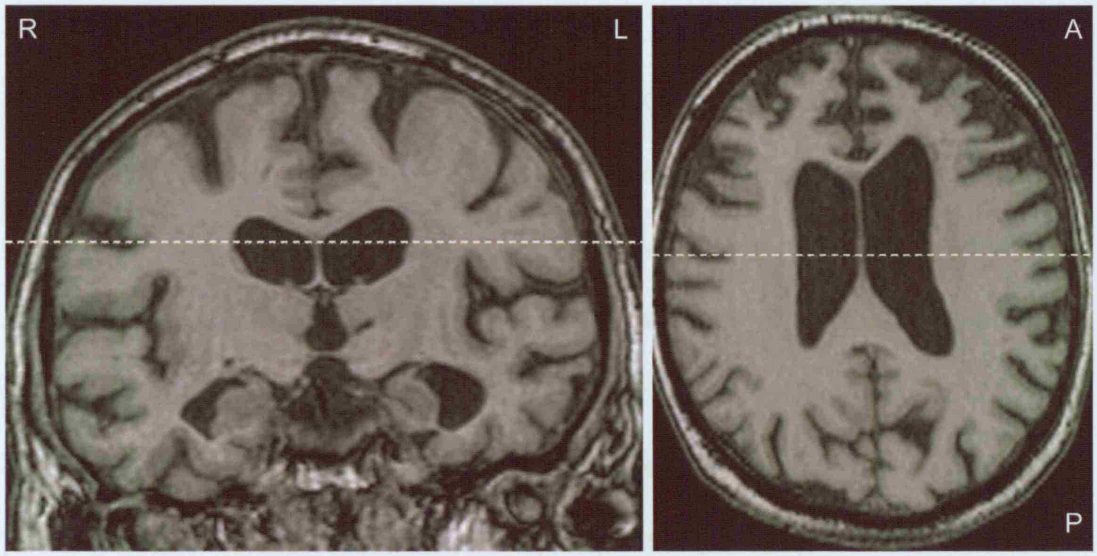

In contrast, the language variants of FTLD (SD and PNFA) show atrophy and metabolic change predominantly in the left (or dominant) hemisphere (Snowden et al., 1992; Sinnatamby et al., 1996; Westbury and Bub, 1997). Early studies tended to group together the language variants of FTLD under the diagnosis of 'slowly progressive aphasia', they found that the patterns of atrophy were highly variable, often depending on the specific language disturbance (Chawluk et al., 1986; Kempler et al., 1990; Snowden et al., 1992; Sinnatamby et al., 1996). Recent studies have therefore attempted to distinguish between the different language variants of FTLD (SD and PNFA) using consensus criteria (Neary et al., 1998).

It is well recognised that SD is associated with an asymmetric pattern of left temporal lobe atrophy, with varying involvement of the right temporal lobe. At post mortem the atrophy appears either asymmetric (Graff-Radford et al., 1990; Rossor et al., 2000), or symmetric (Harasty et al., 1996; Rossor et al., 2000), with marked involvement of the temporal lobes (Graff-Radford et al., 1990; Harasty et al., 1996; Rossor et al., 2000). Practically all left temporal lobe regions can be involved, with particularly severe atrophy often found in inferior temporal regions, including the fusiform and inferior temporal gyrus, with relative sparing of the superior temporal gyrus (Abe et al., 1997; Mummery et al., 1999; Mummery et al., 2000; Chan et al., 2001b; Galton et al., 2001b; Galton et al., 2001a; Good et al., 2002; Rosen et al., 2002c; Gorno-Tempini et al., 2004a; Grossman et al., 2004; Studholme et al., 2004). The anterior regions of the temporal lobe are generally more severely affected than posterior regions (Mummery et al., 2000; Chan et al., 2001b). Studies have shown inconsistent results concerning involvement of the hippocampus; a few found no hippocampal atrophy and concluded that this correlates to a relatively preserved episodic memory in SD patients (Mummery et al., 2000). However, a large number of other studies have shown significant involvement of the hippocampus, especially in anterior portions (see chapter 7) (Chan et al., 2001b; Galton et al., 2001b; Galton et al., 2001a; Good et al., 2002). The lack of hippocampal loss in the study by Mummery et al (2000) is likely to be artefactual for technical VBM related reasons. Figure 2.3 demonstrates this asymmetric temporal lobe atrophy in a patient with SD. Although the brunt of the atrophy lies in the left temporal lobe, these structures often show a similar pattern of atrophy to a lesser degree on the right (Thompson et al., 2003). These temporal regions have been shown to be critically involved in language production and will be discussed in greater detail later.

As well as these temporal lobe regions, MR studies have shown atrophy in ventromedial and superior frontal regions in SD (Mummery et al., 2000; Gorno-Tempini et al., 2004a; Studholme et al., 2004). Atrophy of the frontal lobes is consistent with the fact that SD patients often develop behavioural deficits as the disease progresses (see chapter 1). Posterior changes have also been reported in SD, although less severe than the more anterior temporal and frontal lobe changes (Studholme et al., 2004).

Figure 2.3: Coronal and axial T1-weighted images of a subject with SD. This case shows severe atrophy of the left temporal lobe, with milder involvement of the right temporal lobe and frontal regions. Note the very severe loss of the anterior temporal lobes (on the axial projection) and in the coronal view the loss of inferior temporal lobe with almost no fusiform gyrus identifiable, very major destruction of the parahippocampal gyrus, loss of all inferior and medial temporal gyri, with hippocampus and superior temporal gyrus relatively less destroyed.

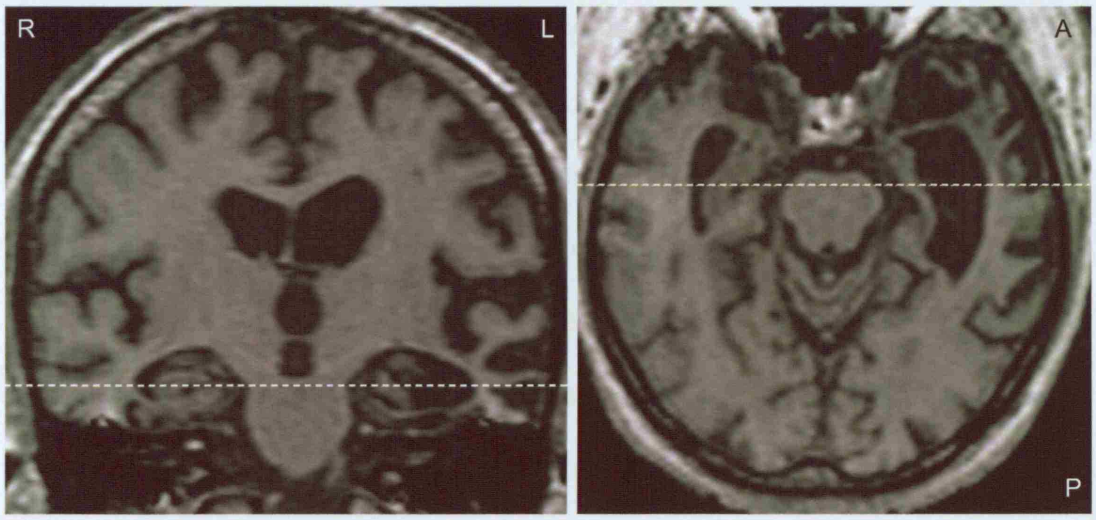

Cases of PNFA have most consistently been reported to show left frontal and perisylvian atrophy on MRI (Figure 2.4; (Turner et al., 1996; Abe et al., 1997; Fukui and Kertesz, 2000; Nestor et al., 2003a; Sonty et al., 2003; Gorno-Tempini et al., 2004a; Grossman et al., 2004) and at post-mortem (Turner et al., 1996). However, the patterns of atrophy are highly variable, ranging from no atrophy, to left hemisphere atrophy, left frontotemporal atrophy (Caselli et al., 1992; Turner et al., 1996), bifrontal atrophy (Caselli et al., 1992) and generalised atrophy (Caselli et al., 1992; Rosen et al., 2002d; Sonty et al., 2003). Differences in disease duration and the extent of additional cognitive deficits may contribute to this variability. For example, Caselli et al 1992 described two patients with PNFA; one displayed pure nonfluency

and had a focal pattern of frontal opercular atrophy, while another was not only nonfluent but also had impaired comprehension, naming and behavioural change, and showed a more widespread pattern of atrophy affecting bifrontal and left temporoparietal regions (Caselli et al., 1992). Widespread cognitive and behavioural deficits often occur in PNFA patients as the disease progresses (see chapters 1 and 5). VBM studies have allowed group comparisons and have provided more anatomical detail but at a group level. Regions involved include the left anterior and ventral temporal lobe, Broca's area, inferior and middle frontal gyri, inferior prefrontal regions, insula, caudate nucleus, putamen and premotor regions (Nestor et al., 2003a; Gorno-Tempini et al., 2004a; Grossman et al., 2004). Studies have suggested that some of these regions play a role in motor speech and syntax processing, for example the premotor and supplemental motor cortices (Josephs et al., 2006a), and the left precentral gyrus of the insula (Dronkers, 1996) have been associated with apraxia of speech, a motor speech disorder characterised by slow speaking rate, abnormal prosody, and distorted sound substitutions, additions, repetitions, and prolongations (Josephs et al., 2006a).

Figure 2.4: T1-weighted images of a subject with PNFA. Atrophy involves the left perisylvian region, including both left superior temporal and left inferior frontal regions. Note that the left frontal lobe appears more generally atrophic (damage beyond the inferior frontal regions).

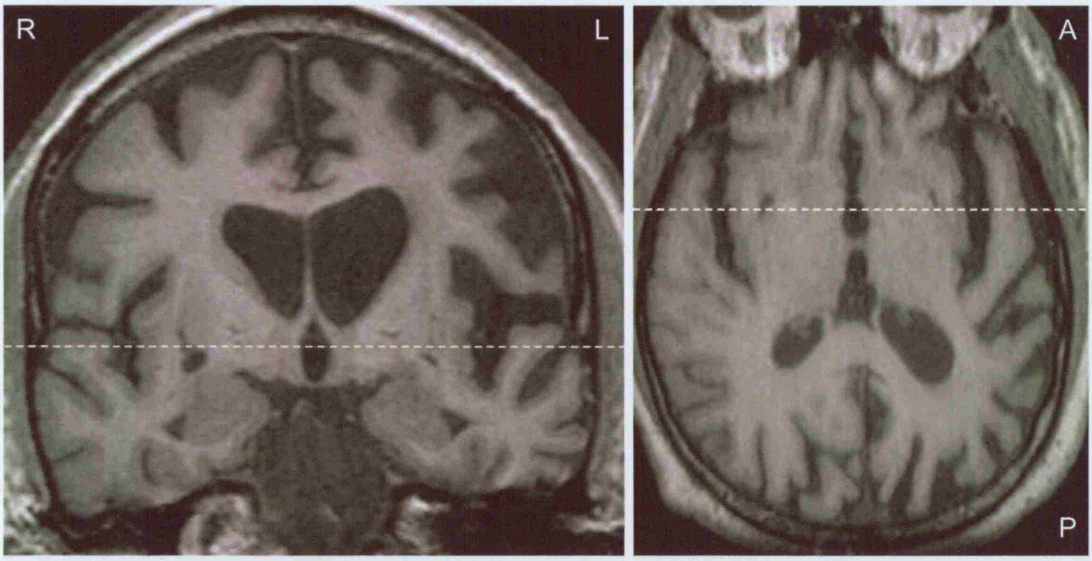

Neuroimaging has also allowed the identification of a further subcategory of 'right temporal variant' FTLD. These patients show very severe and focal patterns of right temporal atrophy, providing almost the mirror image of the patterns observed in SD (figure 2.5). The earliest descriptions involved case reports of subjects showing decreased facial expression, deficits in the recognition of familiar faces (Tyrrell et al., 1990; Evans et al., 1995) and in the recognition of emotion from faces (Perry et al., 2001). More recently studies have selected subjects based on this right temporal pattern of atrophy, or hypoperfusion, and described the associated clinical phenotype. These studies have tended to show severe behavioural abnormalities (Thompson et al., 2003), common features include irritability, impulsiveness, obsessive behaviour, bizarre alterations in dress and aggression (Edwards-Lee et al., 1997). These right

temporal variants tend to be more socially inappropriate than the left temporal variants of FTLD (Miller et al., 1993; Edwards-Lee et al., 1997).

Figure 2.5: T1-weighted images of a subject with predominant right temporal lobe atrophy. Note the similarity with figure 2.2 (SD). Here the right anterior temporal lobe is more affected that the posterior structures. Again the inferior temporal gyri are more atrophic than the superior temporal gyrus.

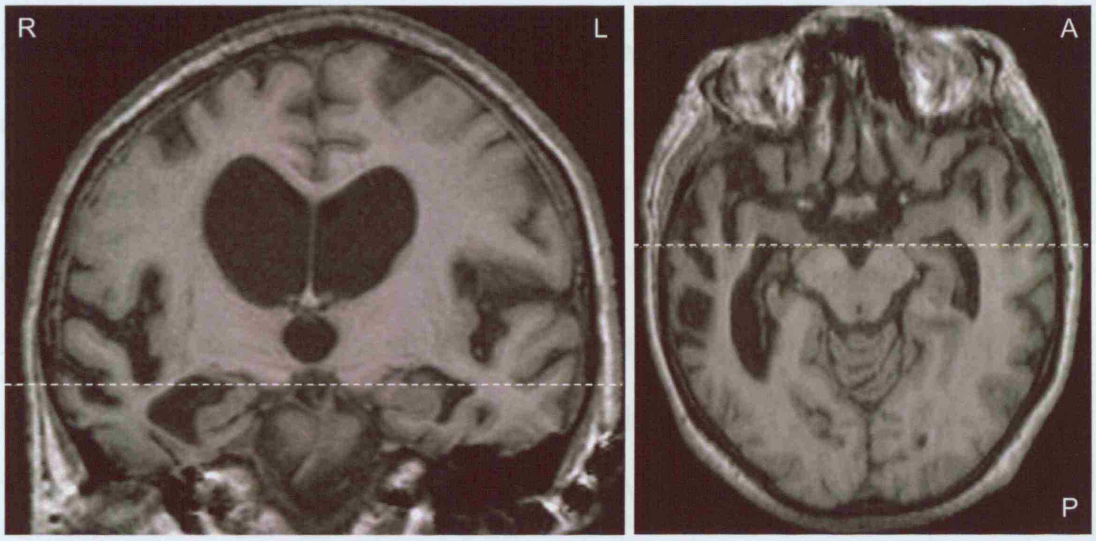

2.4. Differential diagnosis of FTLD

Many studies have looked at the diagnostic utility of these patterns of atrophy in differentiating between the different syndromic variants of FTLD, and also in differentiating FTLD from other neurodegenerative diseases. As discussed in chapter 1, the diagnosis of FTLD can be difficult, particularly in differentiating it from AD. There is considerable overlap in the clinical features of AD and FTLD and they may be confused with vascular dementia, depression, as well as each other, especially in the early stages.

Alzheimer's disease is associated initially with a pattern of medial temporal atrophy that progresses to involve more generalised cortical atrophy (Scahill et al., 2003). Studies have shown hippocampal atrophy in presymptomatic AD cases (Fox et al., 1996a; Convit et al., 1997), and reductions of approximately 20-40% in hippocampal volume in advanced AD subjects compared to controls (Kesslak et al., 1991; Jack et al., 1997). Various studies have demonstrated that for the same amount of global atrophy FTLD has relatively greater atrophy of anterior temporal and frontal regions than AD, with AD showing more posterior patterns of temporoparietal atrophy (Frisoni et al., 1996c; Kitagaki et al., 1998; Chan et al., 2001b; Galton et al., 2001a; Grossman et al., 2004). Fukui et al 2000 showed that fvFTD has greater right frontal atrophy, and PPA greater left frontotemporal atrophy, than AD (Fukui and Kertesz, 2000). They concluded, as have many others, that asymmetry is diagnostically important (Kitagaki et al., 1998; Miller and Gearhart, 1999; Fukui and Kertesz, 2000; Varma et al., 2002a; Boccardi et al., 2003). Asymmetry is a common feature of FTLD (Miller and Gearhart, 1999; Rosso et al., 2003), whereas AD shows a more symmetric pattern (Varma et al., 2002a). The prevalence of asymmetry in FTLD will be discussed further in chapter 4. The anterior-posterior gradient of atrophy found in FTLD patients may also be diagnostically useful since it is rarely found in AD patients (Chan et al., 2001b). Sjogren et al (1999) found that a ratio of frontal to temporal regional cerebral blood flow as measured by SPET, representing (to some extent) an anterior-posterior gradient, had a sensitivity of 87.5% for fvFTD and specificity of 80% for AD (Sjogren et al., 2000a).

Studies have also compared the different syndromic variants of FTLD. They have shown that SD has relatively more atrophy in anterior temporal gyri, anterior hippocampus and ventromedial cortex than fvFTD (Rosen et al., 2002c). PNFA shows more right dorsolateral prefrontal and inferior frontal atrophy than SD (Grossman et al., 2004), and fvFTD shows more atrophy of the anterior cingulate, insula and frontal regions than SD (Rosen et al., 2002c; Grossman et al., 2004). However, significant overlap is observed between groups, with many structures being involved across all three syndromic groups (Rosen et al., 2002c).

A number of ROI studies have examined the diagnostic utility of single structures. Due to their prominent pathological involvement in AD, there has been particular focus on the hippocampus and other medial temporal structures. Studies have shown inconsistent results; whilst some have found smaller hippocampi and medial temporal lobes in AD than FTLD (Frisoni et al., 1999), others have found no difference between the groups (Frisoni et al., 1996c; Varma et al., 2002a). There is some suggestion that the anterior-posterior profile of the hippocampus differs between FTLD and AD; with the anterior portions most affected in FTLD and the posterior portions most affected in AD (see chapter 7). Similar patterns of anterior-posterior gradients of atrophy have been shown in the corpus callosum (Kaufer et al., 1997; Yamauchi et al., 2000). Studies have shown that SD patients have significantly smaller volumes of nearly all left temporal structures than AD, with the temporal pole and inferolateral regions giving the best discrimination between SD and AD (Galton et al., 2001b; Galton et al., 2001a). In addition, studies have shown that fvFTD patients have significantly smaller frontal lobes than AD patients (Boccardi et al., 2002).

However, many of these studies have found poor discriminative power, possibly limited by intrinsic variability present in the FTLD cohorts. Some studies have suggested that a pattern of atrophy may be more informative than looking at specific structures. Boccardi et al 2003 found that a combination of measures from both the frontal and temporal lobes were able to discriminate FTD from AD with a specificity of 93% and sensitivity of 90% (Boccardi et al., 2003). Similarly, in another study a combination of right posterior cingulate, left parietal lobe, right amygdala and right anterior temporal lobe were best able to discriminate between AD, SD and controls, correctly classifying 96% of patients (Boxer et al., 2003).

Studies have also looked at the role of neuroimaging in the differential diagnosis of FTLD from VaD. Studies have shown that measures of frontal atrophy and asymmetry are useful in the differentiation of FTLD from VaD (Sjogren et al., 2000a; Varma et al., 2002a). The presence of high signal abnormalities is less diagnostically useful; although they are most severe in VaD, they are also present in both FTLD and AD (Kitagaki et al., 1997; Larsson et al., 2000; Varma et al., 2002b), and can only correctly classify 42% of subjects (Varma et al., 2002b). Studies have also compared FTLD with other tauopathies. Grossman et al 2004 showed that FTLD has more left anterior temporal and left anterior cingulate atrophy than CBD (Grossman et al., 2004). CBD shows a more posterior pattern of atrophy involving parietal regions, although temporal and frontal regions may also be atrophic. Results have also suggested that FTLD has more prefrontal involvement than PSP (Garraux et al., 1999; Yamauchi et al., 2000).

2.5. Measurement of progression in FTLD

A number of studies have examined the longitudinal patterns of atrophy in AD. Rates of whole brain and hippocampal atrophy have been shown to be significantly greater in AD than controls (Fox and Freeborough, 1997; Fox et al., 2000), and to correlate with cognitive decline (Fox et al., 1999a). Furthermore, studies have shown hippocampal atrophy to be a risk factor for conversion from MCI to AD (Jack et al., 2000; Grundman et al., 2002). However, the majority of neuroimaging studies in FTLD have been cross-sectional. Only a few have reported serial MRI results in FTLD patients, showing varying degrees and patterns of progression (Graff-Radford et al., 1990; Rosen et al., 2002d; Janssen et al., 2005). Very little work has systematically examined longitudinal patterns of change in FTLD, although there is some suggestion that rates of whole brain atrophy are greater in FTLD subjects than controls and that the regional atrophy rates may vary between different syndromic variants of FTLD (Chan et al., 2001a). This thesis will look at the longitudinal rates of atrophy in large groups of FTLD subjects, and include the use of automated techniques to examine the regional patterns of atrophy in chapters 12 – 14.

3. Methods Overview

3.1. Image Analysis

A number of image analysis techniques have been used in this thesis to investigate the patterns of atrophy in FTLD. This chapter provides some background to each of these techniques and details on how each method was implemented.

3.1.1. Image Acquisition

All images in this thesis were acquired on an MRI scanner with a magnetic field strength of 1.5 Tesla (T). A spoiled gradient echo technique was used. Scans generally included a sagittal T1-weighted scout sequence, an axial dual-echo sequence (T2-weighted and PD image), and a T1-weighted volumetric image. The imaging parameters used in this thesis are listed in Appendix 4. The scanning protocol took approximately 20 minutes. T1-weighted images had approximately 124 contiguous 1.5mm thick coronal slices.

3.1.2. Image quality

Many of the image analysis techniques described in this chapter rely on the detection of differences in voxel intensity between for example brain and CSF, and grey and white matter. Therefore good image resolution and quality is critically important. The quality of all images was assessed before inclusion in this thesis. There are a number of common image quality problems, originating either from the subject or from the acquisition process.

The most common problem is the subject moving within the scanner causing the scans to appear blurry or have a characteristic 'movement striping affect' (see figure 3.1A). This is a particular problem in severely affected patients, especially if the scanning time is increased. The problem can be reduced by a variety of methods, including using padding around the head, head straps or bite devices. Unfortunately even with such measures severely affected subjects are still unable to remain still in the scanner. A review of scan-pair quality performed in chapter 14 revealed that 13% of FTLD patients had to be excluded due to excessive movement artefact on their scans. The presence of metallic implants can also cause distortion of the scan, generally showing as a signal void.

A number of problems are introduced during scan acquisition. Poor scan contrast can be a particular problem for image analysis techniques, reducing the resolution of the grey to white matter, or the brain to CSF boundaries (see figure 3.1B). Contrast can be optimised by adjusting the time between pulses (TR), and between pulses and collection of the signal (TE) in the scanning protocol. Intensity inhomogeneity is another common problem caused by non-uniformity in the magnetic field or gradient driven eddy currents. This can be seen as a slowly varying intensity gradient though the image, often resulting in intensity variations of up to 20% and signal loss in the inferior or superior regions of the scan (see figure 3.1C). A number of post-acquisition techniques have been developed to correct this inhomogeneity. One of the most commonly employed is the N3 method developed by Sled et al in 1998 (Sled et al., 1998). This technique models the inhomogeneity as a smooth, slowly varying multiplicative field. The measured signal of an image is made up of the true signal emitted by a tissue, multiplied by the inhomogeneity field with the addition of

independent white Gaussian noise. The algorithm aims to maximise the high frequency content of the signal emitted from the tissue. The technique has been shown to perform well compared to other correction methods (Arnold et al., 2001), although it may not always significantly improve image analysis results (Gunter et al., 2003). The N3 correction technique was applied to all scans that were judged on visual inspection to show a significant intensity gradient. Chemical shift can also cause a significant problem for image analysis techniques. Simply put this is when the fat surrounding the skull shifts down so that it is very close to the brain surface. This shift occurs because of the chemical composition of fat. In the reconstruction of the image the position of a signal in space is calculated by its frequency; fat has a different resonant frequency to water and its position is effectively shifted in space relative to brain tissue.

Changes in scan quality over time cause a particular problem for longitudinal studies that aim to investigate subtle differences in brain atrophy. Performing serial scans on different scanners and across scanner upgrades can cause dramatic differences in image quality. Figure 3.2 shows two scans from the same subject performed on two different scanners. The dramatic difference in contrast between the two scans would affect the reliability of brain atrophy measurements. Therefore, serial MRI scans that cross a scanner upgrade or were performed on different scanners were excluded from analysis in this thesis. Fluctuations in performance can also occur within the same scanner. For example, drifts in scanner calibration or fluctuation in the performance of scanner gradients can cause variations in voxel dimension over time. Chapter 11 discusses this problem in more detail and investigates two correction methods. Differences in intensity inhomogeneity between two serial scans can also confound

the reliability of brain atrophy measurements, since they typically rely on voxel intensity to identify tissue boundaries. A technique has recently been developed that aims to correct this differential bias (Lewis and Fox, 2004). It identifies the differential bias field between two serial scans from the same patient using the difference image, which can be considered to be made up of noise, atrophy, and the differential bias field, and the application of simple filters. The serial scan pair can then be corrected for this differential bias field. The technique (termed 'differential bias correction' (DBC)) has been validated using serial scans from patients with AD and was shown to improve the reliability of serial measures of brain loss using the brain boundary shift integral.

Figure 3.1: Examples of common image quality problems: A) patient movement, B) poor contrast, and C) intensity inhomogeneity.

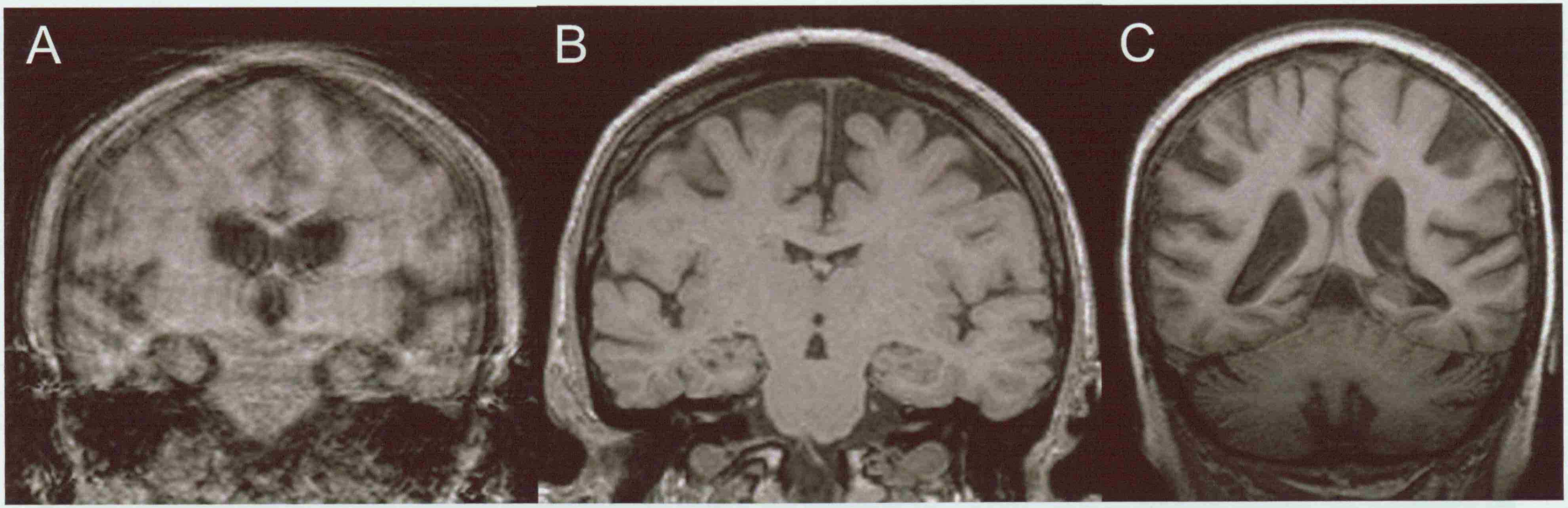

Figure 3.2: Coronal slices through two T1-weighted images from the same individual performed on different scanners 9 months apart. Note the difference in grey-white matter contrast and the susceptibility artefacts in the temporal lobe on scanner 1.

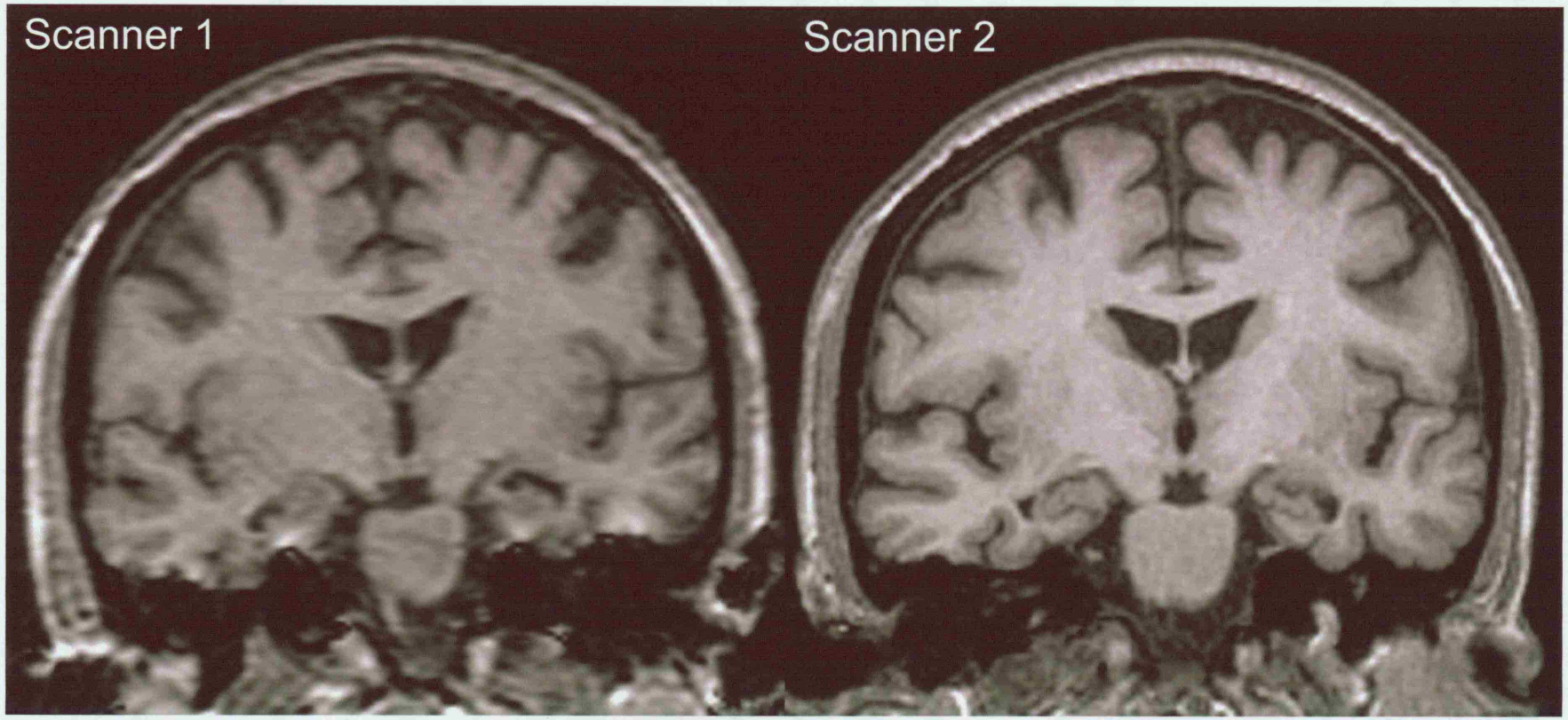

3.1.3. MIDAS

All volumetric image analysis was performed using the MIDAS image analysis software (Freeborough et al., 1997) on a UNIX operating system. This software allows simultaneous image viewing and outlining of regions in coronal, sagittal and axial orientations. Structures can be outlined using both semi-automated and manual techniques.

Whole brain segmentation was performed using a semi-automated technique. Intensity thresholds were used to separate brain tissue from CSF, and a series of erosions and dilations were performed to remove all non-brain structures such as dura and scalp (see Appendix 5 for protocol). Some degree of manual editing of the brain region was often required; especially in cases with poor scan quality. Smaller structures, such as the amygdala and hippocampus, were segmented manually using a mouse-driven cursor (see protocols in Appendix 5). Intensity thresholds were often used as a guide to segmentation and to increase the reproducibility of the measurements.

All measurements were performed blind to patient details and diagnosis. Scans were loaded into MIDAS in a blinded and randomised fashion. In order to allow unbiased measurement of regional structures in the left and right hemisphere, scans were flipped about the mid-sagittal plane ensuring that the rater was blinded to left/right orientation.

3.1.4. Image Registration

The aim of registration is to match scans positionally so that they are in the same spatial framework. This alignment aims to ensure approximate morphological correspondence and allow meaningful comparisons between scans, either within subject or between different subjects. A typical approach is as follows. One image remains stationary (the reference image), and then the other (the source image) is spatially transformed to match it (Ashburner and Good, 2003). The registration first calculates the parameters necessary to transform the source image onto the reference image, and then performs these transformations by re-sampling the source image to create a new image that is spatially aligned with the reference image.

The transformation parameters are determined by successive iterations that aim to incrementally improve the match between the two images. The accuracy of the match could be determined using points within the image, such as the skull, internal markers within the brain, or voxel intensities. Optimising differences between voxel intensities within the scan is commonly used and has been shown to be the most accurate (Strother et al., 1994; Freeborough et al., 1996). Optimising based on points in the skull may lead to inaccuracies within the brain itself. The iterations will be performed until the registration is terminated, usually determined by a cost function. This cost function is a measure either of similarity or difference between the two scans, which will be maximised or minimised respectively. Some examples include the sum of squared intensity differences (SSD), or ratio image uniformity (RIU), which minimises the standard deviation of a ratio image, created from the source and reference image. A multi-resolution approach is often applied, firstly finding a coarse

match and then refining this to an increasingly local level, which reduces the likelihood of finding false minima.

In order to re-sample (re-slice) the source image it is necessary to determine for each voxel in the transformed image, the corresponding intensity in the original image. This requires estimating intensities at positions that are 'in between' those of the voxels in the original image, i.e. interpolation. The simplest approach is to take the intensity value of the nearest neighbouring voxel. However, although this approach is quick it results in a degraded, 'blocky', appearance of the resultant image. Trilinear interpolation improves the appearance of the resulting images by calculating a weighted average of the neighbouring voxels. More complex techniques include sinc interpolation, which uses a weighted average of neighbouring voxels determined by a Gaussian kernel.

Registration can be applied in a number of different situations, depending on the question being asked. Intra-subject registration aims to match serial scans from the same individual, whereas inter-subject registration matches scans from different individuals. Inter-subject registration represents a far greater challenge due to the large variation in head size and brain shape within the normal population. Registration can be used to match scans from different modalities (i.e. MRI to PET), or different sequences within the same modality (e.g. T1 to T2 weighted MRI). Registration algorithms can also be linear or non-linear. Linear registration generally refers to an algorithm that applies exactly the same set of parameters to all image voxels in order to transform the source image onto the reference image. In contrast, non-linear registration techniques provide more accurate matching of gyral anatomy

by providing more freedom to warp one image onto the other. Non-linear techniques are generally more computationally expensive and may not be appropriate for inter-individual registration. Examples include elastic registration, B-splines, and the fluid registration technique that will be discussed briefly below.

The following sections describe the specific registration techniques that have been applied in this thesis.

3.1.4.1. Rigid-body registration

Rigid-body registration is generally used for registering images of the same subject. It uses six transformation parameters (three translations and three rotations), in each of the x, y and z dimensions. It is therefore referred to as having six degrees of freedom (6dof). Scaling factors can be included in the registration in order to correct for changes in voxel dimension, thus increasing the degrees of freedom to nine (9dof). The accuracy of the scaling correction is analysed in chapter 11. In addition, shears can be included in the registration increasing the degrees of freedom to twelve (12dof) for a full affine registration.

A 9dof registration technique was employed in this thesis in order to register serial scans from the same individual. The algorithm was based upon of the techniques of Freeborough and colleagues (Freeborough et al., 1996), and the Automated Image Registration (AIR) algorithm developed by Woods and colleagues (Woods et al., 1998b; Woods et al., 1998a). A multi-resolution approach was adopted; matching images using an RIU cost function calculated over a defined brain region, rather than over the whole image. Brain segmentations were performed both on the baseline and

repeat images prior to the registration. This intensity-matching algorithm allows for the fact that the brain may move within the skull. It improves the match and allows intra-subject registration to sub-voxel accuracy (Freeborough et al., 1996) (Freeborough 1996). For the reslice, a Chirp-Z interpolation was employed which performs a Fourier transform and simultaneously implements discrete sinc interpolation (Tong and Cox, 1999). This method is fast but accurate; it can reslice an image in about a quarter of the time of a standard sinc interpolation.

This technique is able to register scans to sub-voxel accuracy, visualise intra-individual changes over time, and demonstrate significant differences between individuals with AD and healthy controls (Fox et al., 1996b; Freeborough et al., 1996). Registration accuracy can be checked either by examining the difference images or by loading both the baseline and registered repeat scans on top of each other in MIDAS and flicking back and forth. Figure 3.3 shows the difference image for a healthy control and a subject with AD, showing accurate registration and enlargement of the ventricles in AD.

Atrophy can be quantified from a registered scan pair using the brain boundary shift integral (BBSI) (Freeborough and Fox, 1997). The BBSI determines the total volume through which the boundaries of a given structure have moved, and hence, the volume change, directly from voxel intensities. The boundaries of a brain will have a characteristic intensity profile, with brighter voxels in brain to dark voxels in CSF (figure 3.4). The BBSI compares the intensity profile of the baseline brain to the corresponding intensity profile on a registered repeat scan. If the boundaries have shifted then the profiles may be depicted as in figure 3.4. The BBSI calculates the

difference in the two boundaries over a specific intensity window (I_1-I_2), determined as the area labelled "A" divided by (I_1-I_2). This simple theory is then applied in three-dimensions throughout the whole brain boundary. The segmented brain region on both the baseline and registered repeat scan defines these boundaries: the boundary region is the union of baseline and registered repeat regions minus the intersection of the baseline and registered repeat regions (eroded by one voxel). Intensity normalisation is also performed to minimize any differences in the level of voxel intensities between the two scans. This technique has been validated using simulated brain atrophy and against large numbers of manual measurements and is highly reproducible. Rates of atrophy based on the BBSI allow accurate discrimination of healthy controls from subjects with AD (Fox and Freeborough, 1997; Freeborough and Fox, 1997; Gunter et al., 2003; Jack et al., 2004), and have been used increasingly as outcome measures in clinical trials (Fox et al., 2005). Figure 3.5 shows the BBSI overlay in a healthy control and a subject with FTLD.

Figure 3.3: Coronal T1-weighted images from A) a healthy control and B) a subject with FTLD showing the baseline image (Base), rigidly-registered repeat image (RR) and the difference image for the registered pair. Note the increase in the left temporal horn is obvious on the difference image.

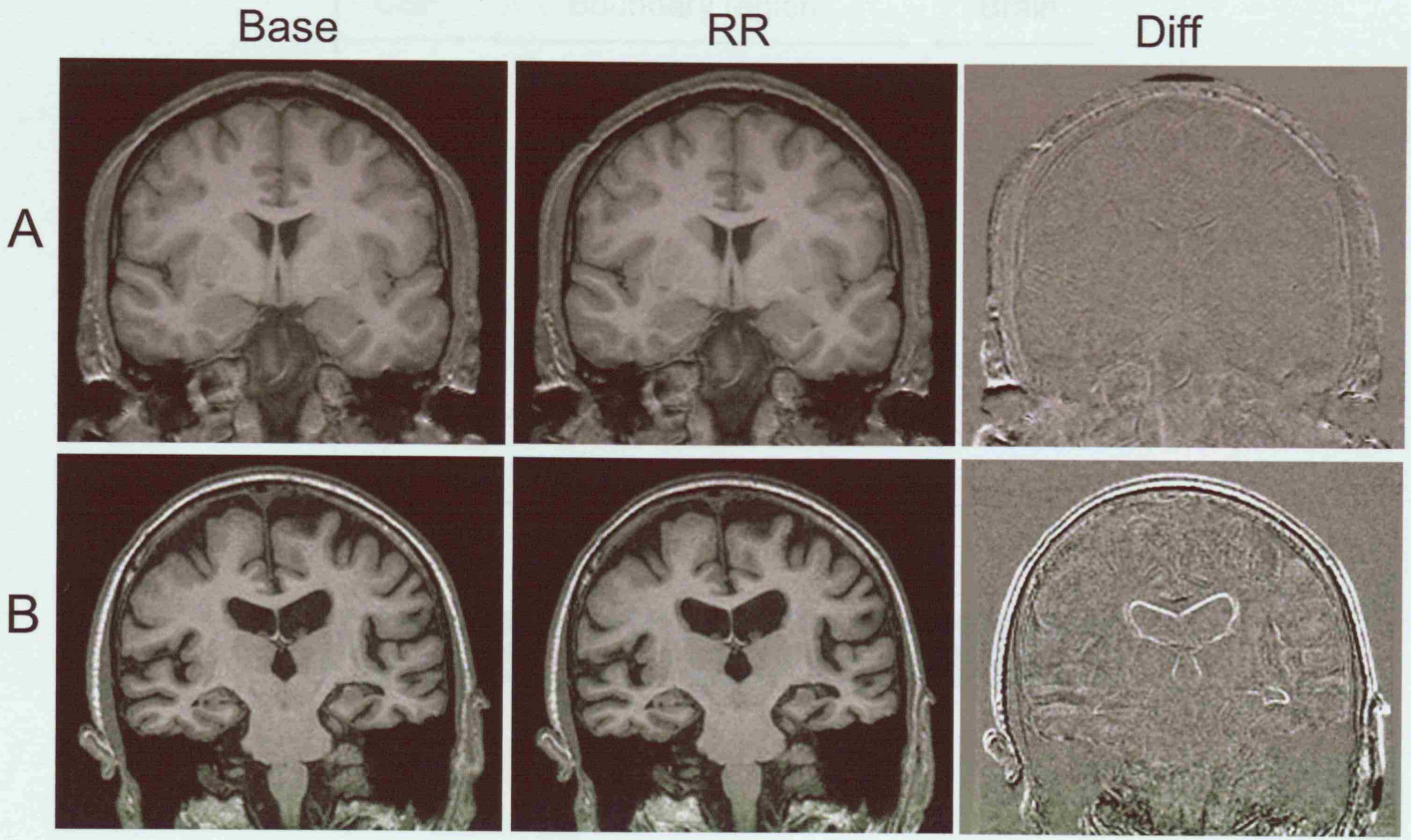

Figure 3.4: A representation of an intensity profile through a boundary of the brain on both a baseline and registered repeat scan. During the interval between the scans the boundary has shifted by ΔW, which is determined as the area A divided by the intensity window (I_1-I_2) (modified from Fox et al 1997)

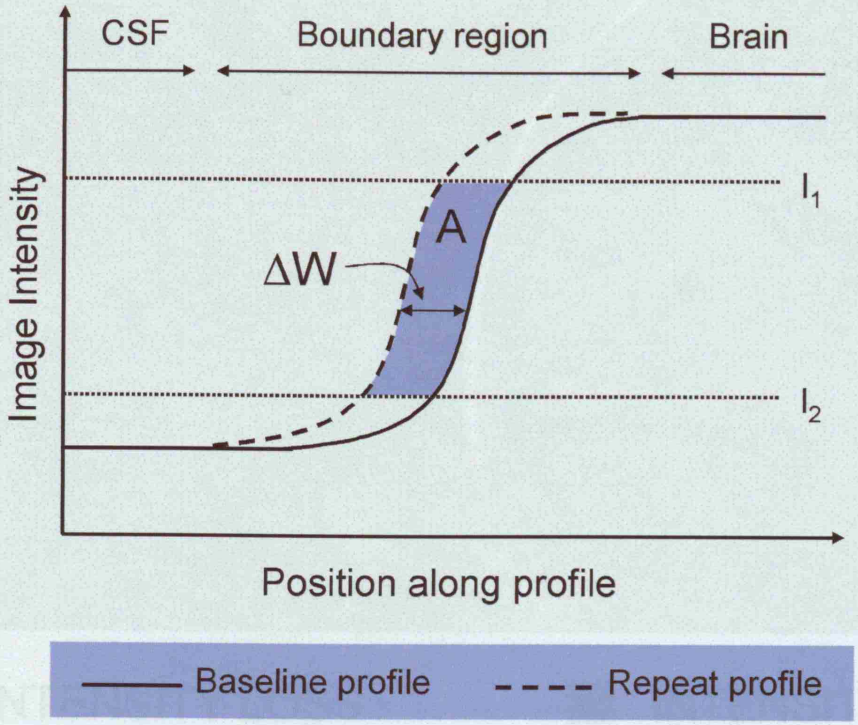

Figure 3.5: BBSI colour overlay showing regions of atrophy over a one-year interval in a healthy control and a subject with FTLD (fvFTD).

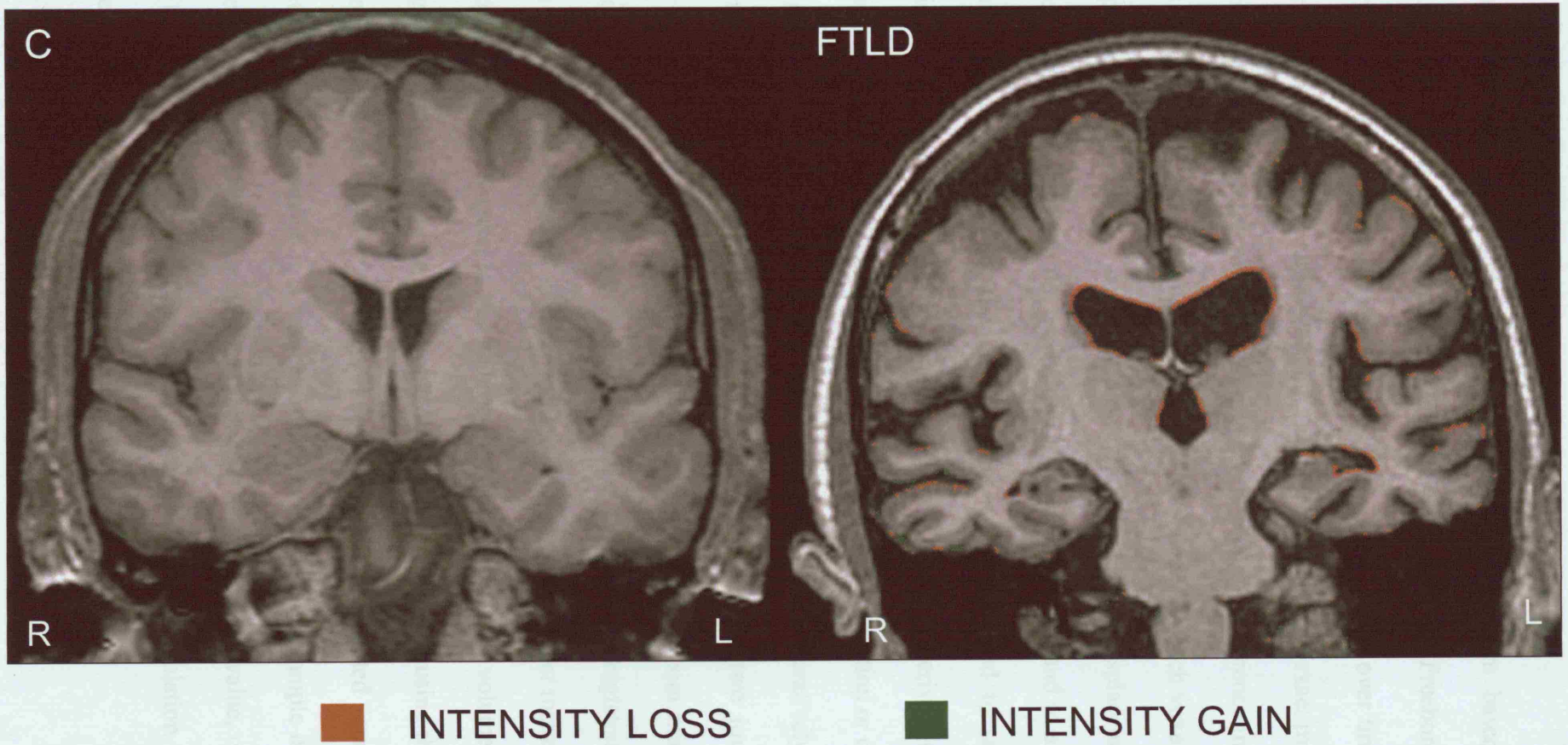

3.1.4.2. Fluid registration

The fluid registration is a high-dimensional non-linear algorithm based on the constraints of a compressible viscous fluid (Christensen et al., 1996; Freeborough and Fox, 1998). It has been used to assess patterns of regional change over time within subjects. The model aims to deform the source image to provide an exact match with the reference image, thereby producing an effectively 'empty' difference image (see figure 3.6). The deformation field represents the displacement of each voxel from its initial position. In order to prevent biologically implausible displacements (for example, a voxel moving from the cerebellum to the frontal lobe) and to ensure the smoothness of the final deformation the movements are confined to satisfy the properties of a viscous fluid. The determinants of the partial derivatives of the deformation field, i.e. the Jacobian values, give a measure of contraction or expansion at each point (voxel). Following a 9dof registration, the algorithm iteratively seeks to maximise the cross-correlation between voxel intensities in the two images. A number of parameters can be varied to help determine this optimum match. For example, the viscosity term can be reduced in order to reduce the registration time, and the time step can be varied in order to limit how far a voxel can move within a single time frame. If a voxel in the volume of interest reduces in volume by more than a given factor, a regridding step propagates the image forward using the current deformation field and restarts the registration using the propagated image. The registration can be terminated in a number of different ways, for example it could be set to terminate if the change in the cost function is less than a set value, or it could simply be set to run for a limited number of iterations. Sinc interpolation is used in both the regridding step and the final transformation.

Figure 3.6: Coronal T1-weighted images from a patient with FTLD showing A) the baseline image, B) the fluid-registered repeat image, C) the difference image from the rigid-registration, and D) the difference image from the fluid registration.

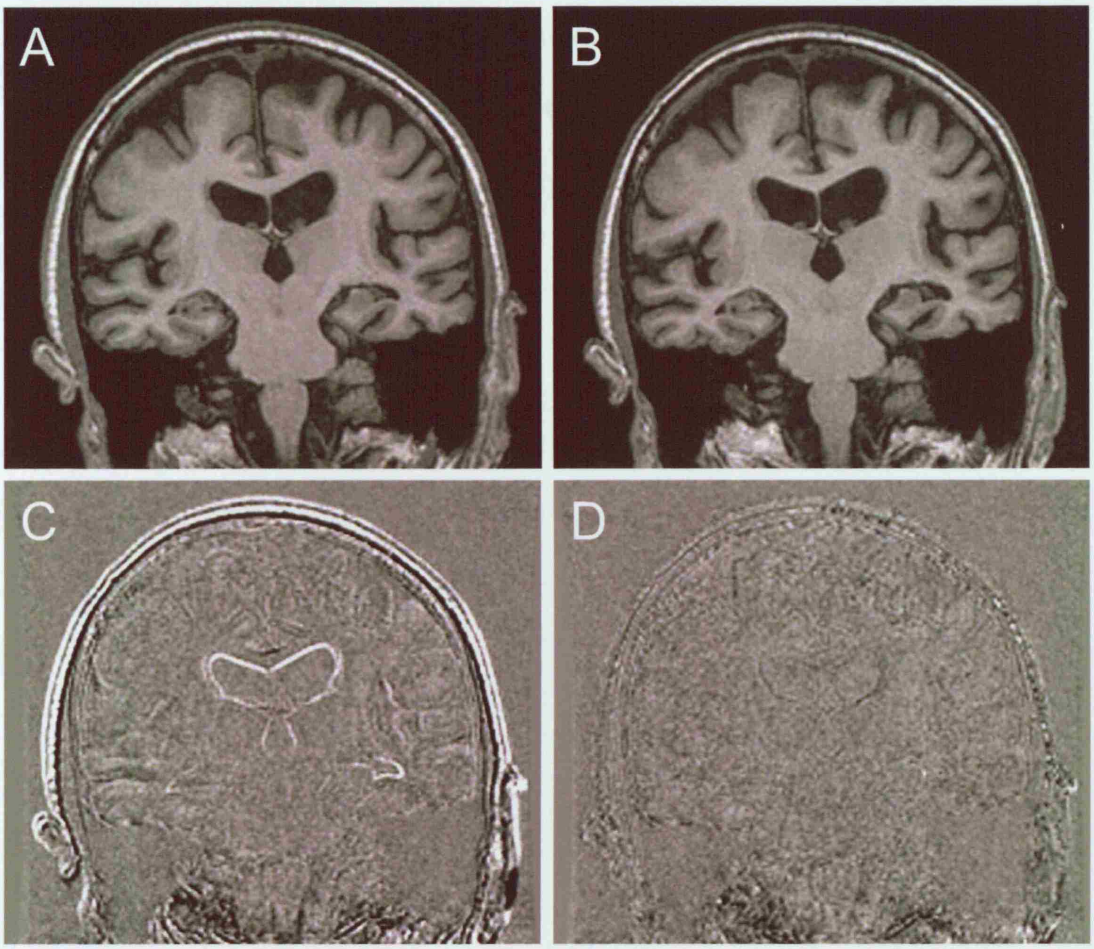

Voxel-compression maps can be derived from the deformation field by calculating the determinant of the matrix of partial derivatives at each point. These maps can be represented as a colour overlay to highlight regions of structural contraction and expansion occurring between the baseline and repeat scan. This technique has been applied to identify longitudinal patterns of regional change in disease such as AD (Freeborough and Fox, 1998; Fox et al., 2001; Scahill et al., 2003) and FTLD

(Janssen et al., 2005). Figure 3.7 shows the colour overlays from a patient with FTLD and a healthy control. Volume change can also be quantified from the fluid registration by calculating the integral of the Jacobians over a defined region (Crum et al., 2001). However, it is possible that the accuracy of the fluid registration could be limited by factors such as poor scan resolution, large signal-to-noise ratio, or lesions or artefacts appearing on the image. For this reason it is always important to check the accuracy of the fluid image before interpreting the fluid overlay.

Figure 3.7: Voxel-compression maps showing regions of expansion and contraction over a one-year interval in a healthy control and subject with FTLD (fvFTD).

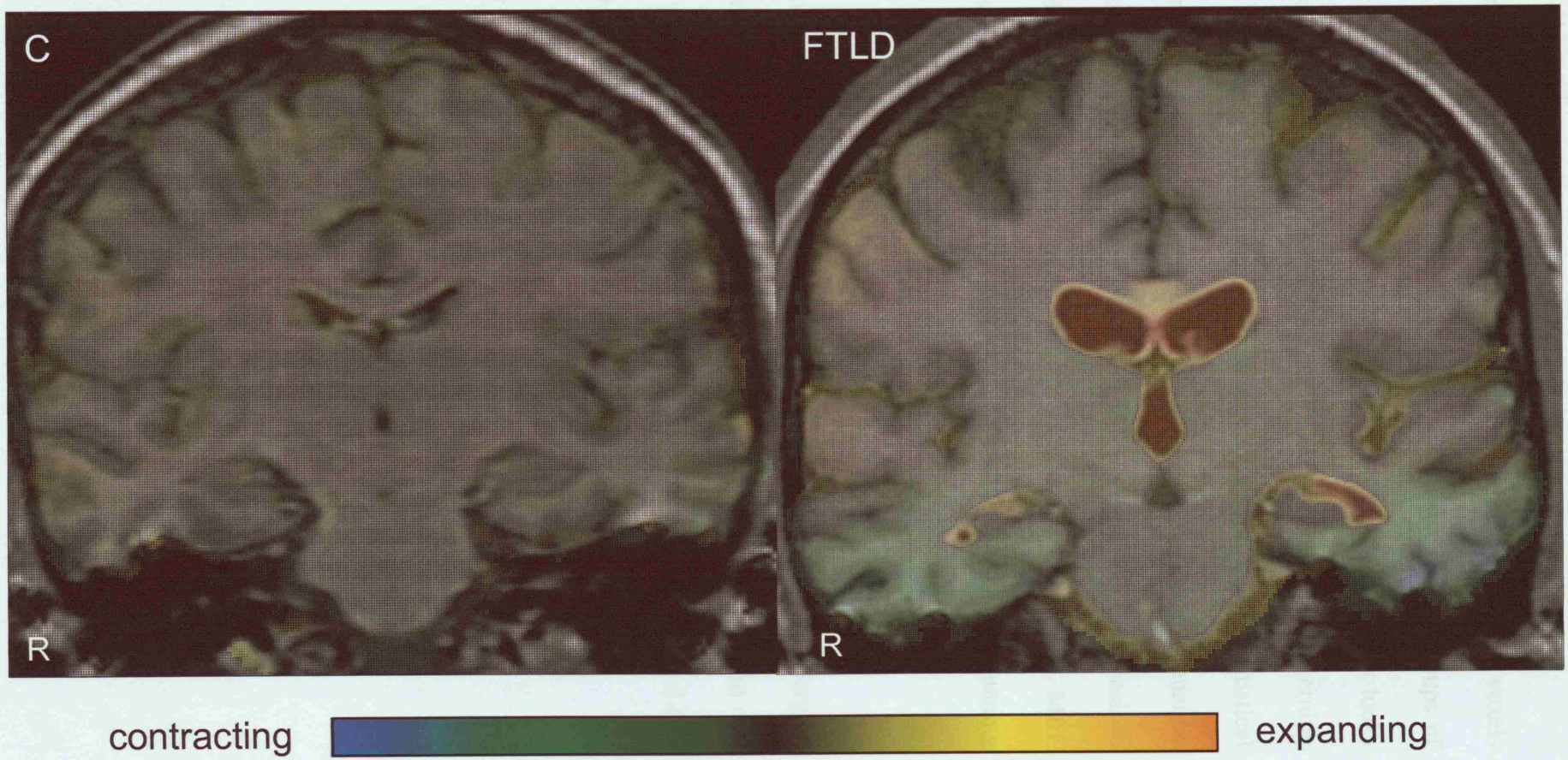

3.1.5. Voxel-based morphometry

Voxel-based morphometry (VBM) is an automated technique that involves a voxel-wise comparison of the local concentration of grey matter between two groups of subjects (Ashburner and Friston, 2000). It is an unbiased technique in that it looks throughout the whole brain and does not require any a priori assumptions concerning which structures to assess. It was developed as a modification of the Statistical Parametric Mapping (SPM) methodology that was originally developed to analyse functional imaging data (Friston et al., 1995). VBM has been applied in this thesis to analyse group differences in patterns of regional atrophy on volumetric MRI. Analysis was performed using SPM99 (http://www.fil.ion.ucl.ac.uk/spm) running under MATLAB 6® (http://www.mathworks.com).

In order to perform accurate statistical analyses the images need to first undergo a series of pre-processing steps, including spatial normalisation, segmentation and smoothing. The pre-processing steps applied in this thesis are shown in figure 3.8. I will discuss each of these steps in turn:

Figure 3.8: VBM pre-processing steps

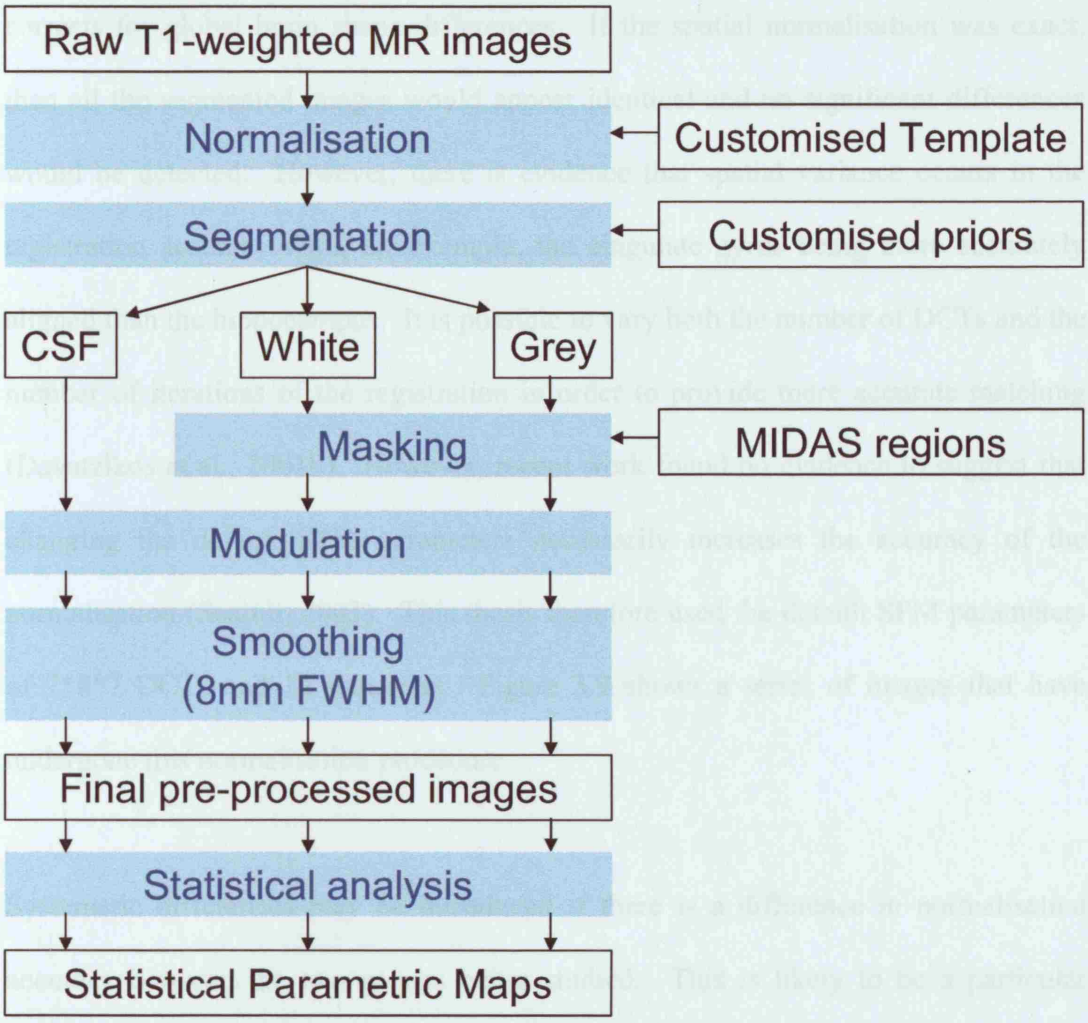

3.1.5.1. Spatial Normalisation

The aim of spatial normalisation is to transform all the subjects' data into the same stereotactic space. It is generally achieved by registering each image onto the MNI template image (Mazziotta et al., 1995), which is in approximate Talairach space (Talairach and Tournoux, 1988). An initial affine 12-parameter transformation, matching the whole head, including scalp, is followed by a non-linear transformation. The nonlinear registration relies on a series of discrete cosine transforms (DCTs) and aims to minimise the cost function, which is based on a sum of squared differences between image intensities, while maximising the smoothness of the deformations.

This method does not attempt to match every cortical feature exactly, but merely corrects for global brain shape differences. If the spatial normalisation was exact, then all the segmented images would appear identical and no significant differences would be detected. However, there is evidence that spatial variance occurs in the registration accuracy with, for example, the cingulate gyrus being more accurately aligned than the hippocampus. It is possible to vary both the number of DCTs and the number of iterations of the registration in order to provide more accurate matching (Davatzikos et al., 2001b). However, recent work found no evidence to suggest that changing the default SPM parameters necessarily increases the accuracy of the normalisation (Scahill, 2003). This thesis therefore used the default SPM parameters of 7*8*7 DCTs and 12 iterations. Figure 3.9 shows a series of images that have undergone this normalisation procedure.

Systematic differences may be introduced if there is a difference in normalisation accuracy between the two groups being studied. This is likely to be a particular problem when there is extensive atrophy due to neurodegeneration, and may affect subsequent processes such as the accuracy of grey matter segmentation. Systematic differences have been demonstrated in the normalisation of controls and patient groups (Muzik et al., 2000; Gitelman et al., 2001) with the patient groups showing a greater level of mismatch to the template image (which is based on healthy controls) (Scahill, 2003). The use of a customised template, created using images from both controls and the patient group, reduces this systematic bias (Scahill, 2003). Therefore it is important to use customised templates when attempting to highlight differences between controls and disease states, so that change can be attributed to the disease process rather than registration accuracy. The customised template would ideally

consist of subjects that are not included in the study. Customised templates were used throughout this thesis. Details on how the customised templates were created are described in section 3.1.5.6.

Figure 3.9: Normalised T1-weighted images from A) healthy controls, B) AD subjects, and C) FTLD subjects. All images have been normalised to the same template image using the default SPM parameters.

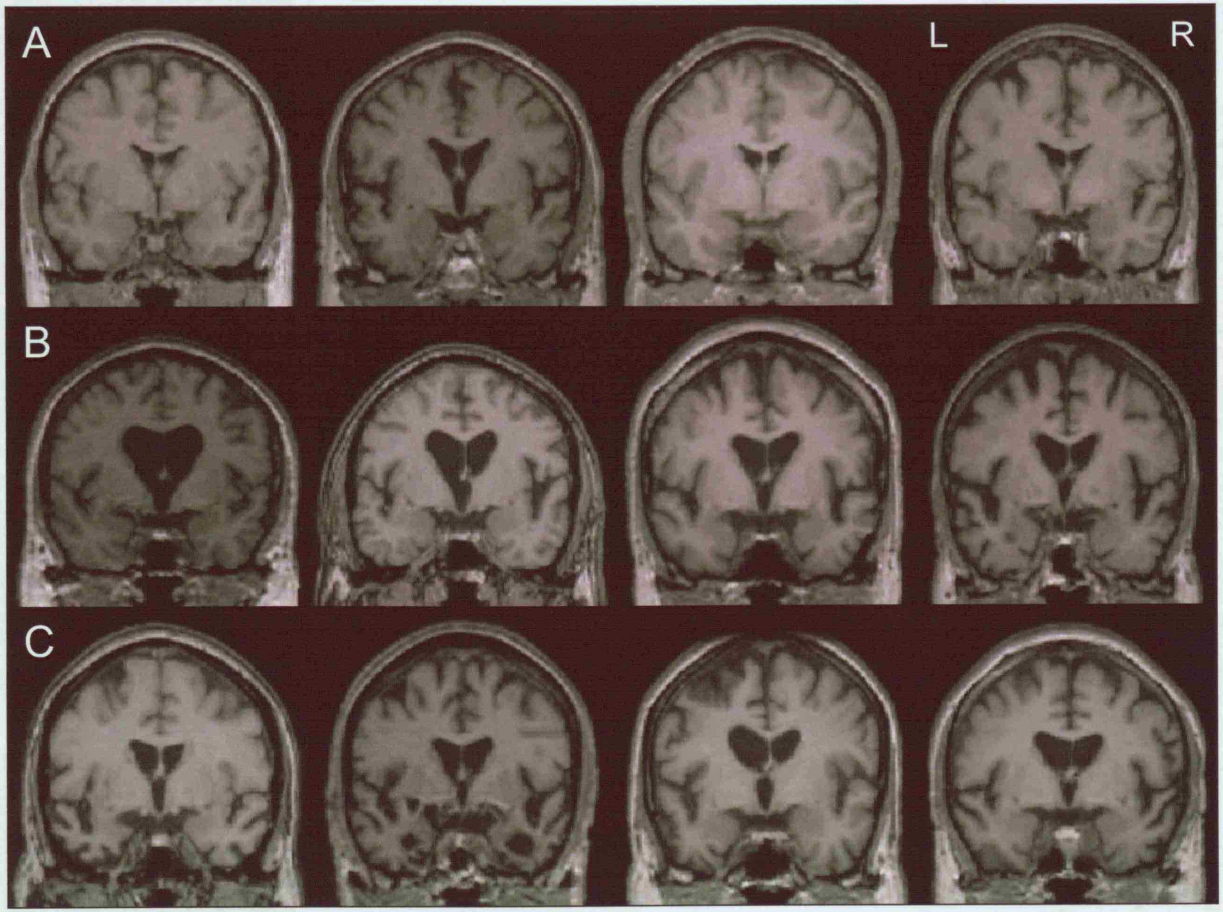

3.1.5.2. Segmentation

After normalisation the scans are segmented into grey matter, white matter and CSF (see figure 3.10). The SPM algorithm uses a Bayesian approach where tissue classification is based upon both the voxel intensity within the image and a priori knowledge of the spatial distribution of these tissues in normal subjects, derived from prior probability maps (Ashburner and Friston, 2000). The segmentation also incorporates an image intensity non-uniformity correction that appears to improve tissue classification (Ashburner and Friston, 2000).

Figure 3.10: An example of tissue segmentation. The T1-weighted image has been segmented into grey matter, white matter and CSF.

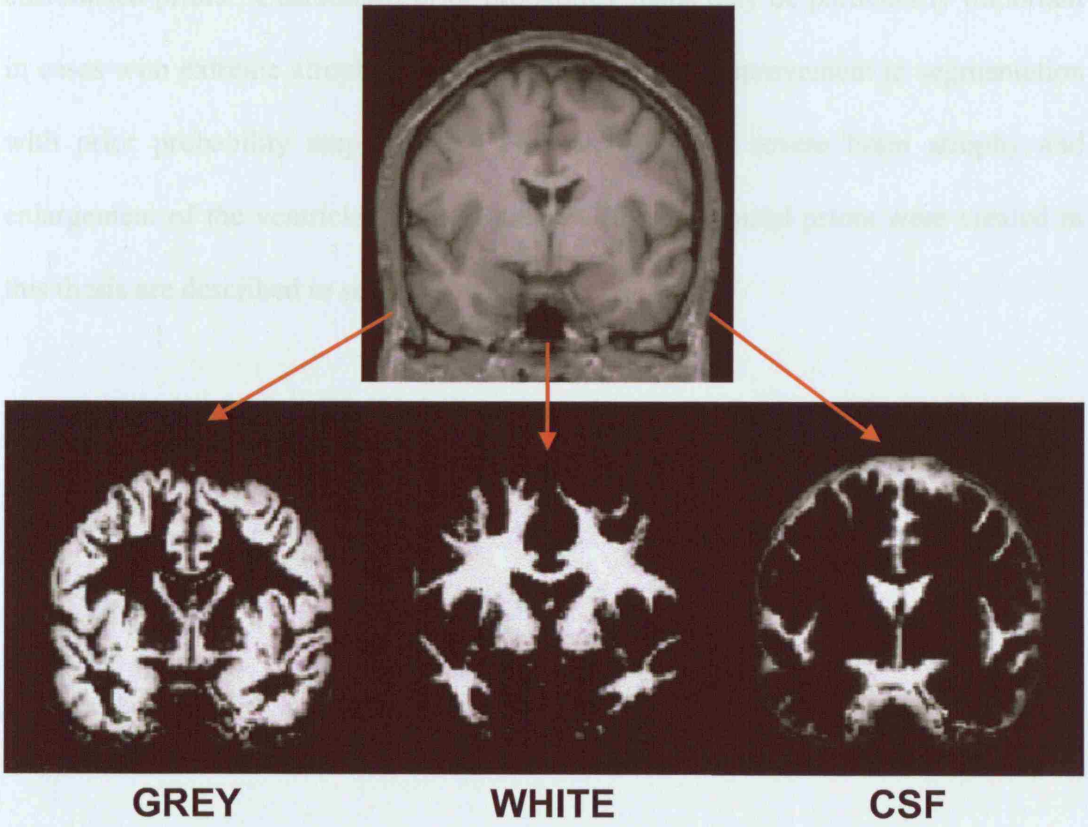

The segmentation requires good contrast between tissue types. Therefore, structures such as those in the central grey matter that have intensities less distinguishable from white matter will be poorly segmented. Partial volume also causes problems for the segmentation. For example, those voxels at the interface between white matter and ventricular spaces often appear as grey matter (see figures 3.10 and 3.11). Errors in segmentation are introduced when there is mis-match in the registration with the prior probability maps (Ashburner and Friston, 2000). Ventricular enlargement may alter the value of the a priori knowledge of tissue distribution (priors). There is some evidence to suggest that the use of customised prior probability maps, based on controls and the patient group, could improve segmentation (Burton et al., 2002; Scahill, 2003), although segmentation errors still occur with both the default and customised priors. Customised prior probability maps may be particularly important in cases with extreme atrophy. Figure 3.11 shows the improvement in segmentation with prior probability maps in an FTLD subject with severe brain atrophy and enlargement of the ventricles. Details on how the customised priors were created in this thesis are described in section 3.1.5.6.

Figure 3.11: Grey matter segmentations of a subject with FTLD using A) default and B) customised prior probability maps. The default results in little value being added by the priors; this is improved with customised maps. Note also the partial volume misclassification around the ventricles.

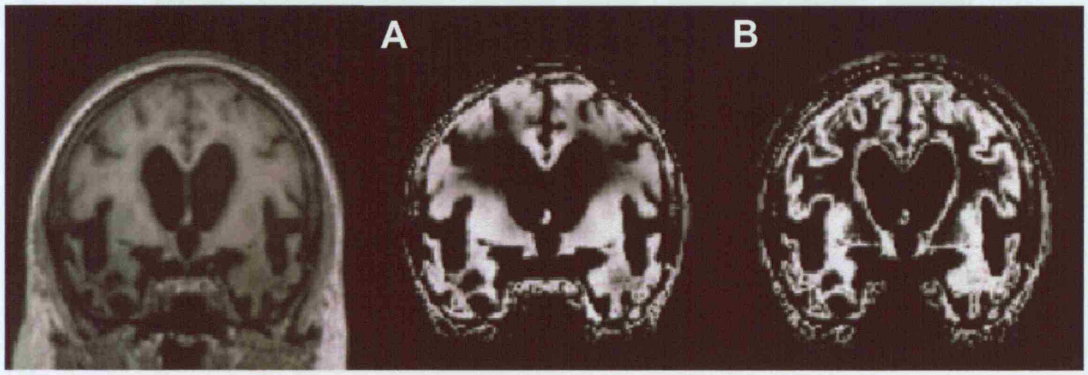

3.1.5.4. Masking

The grey and white matter images for each subject are masked with the MIDAS brain segmentation to exclude non-brain voxels. Figure 3.12 shows grey matter segmentations before and after masking, showing significant improvement in the segmentation. Recent work has shown that using a MIDAS brain region provides better results than using an extraction step based on the SPM brain segmentation (created by adding the grey and white matter segmentations (Good et al., 2001a)) (Scahill, 2003).

Figure 3.12: Grey matter segmentations A) before and B) after masking with a MIDAS brain mask

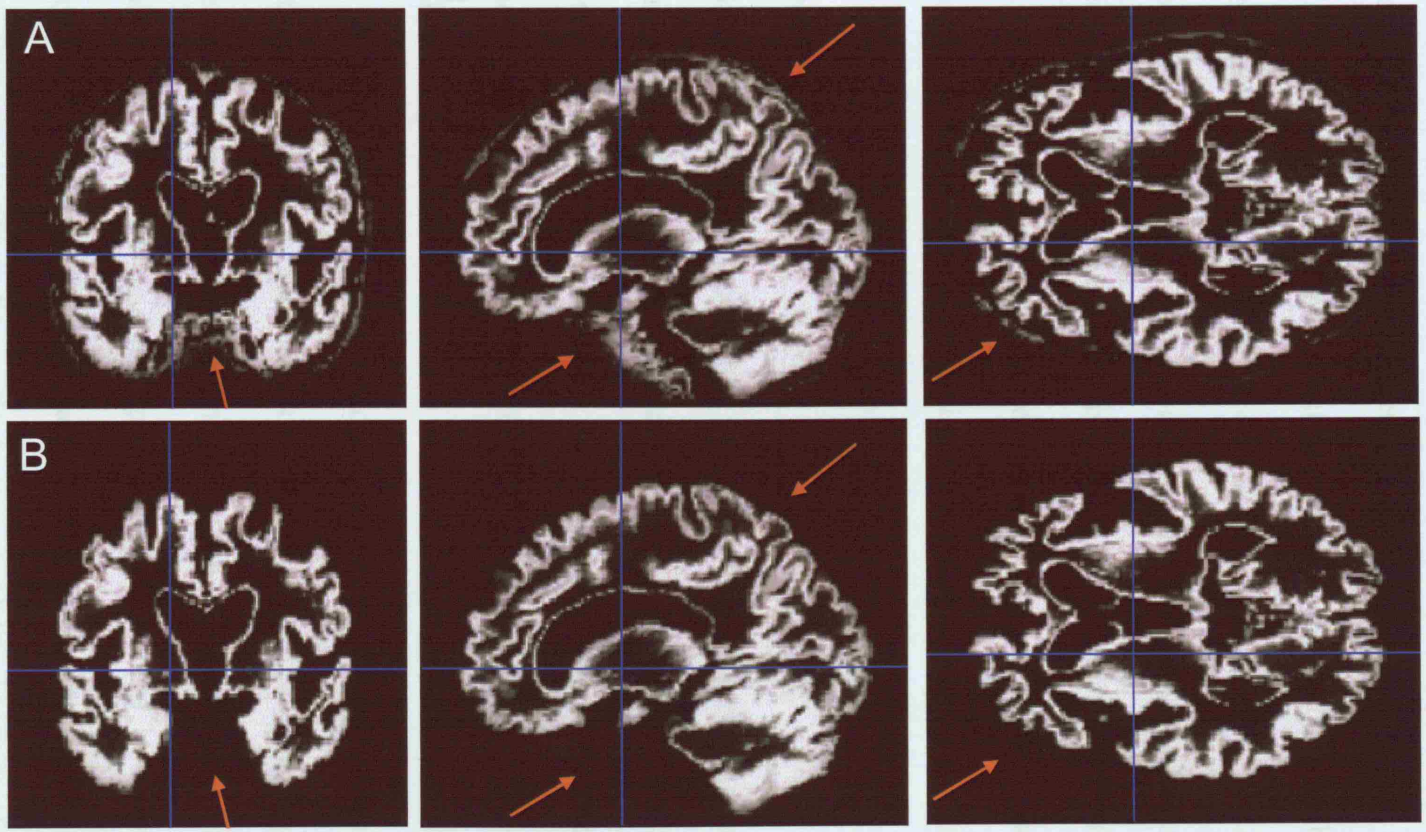

3.1.5.5. Modulation

Modulation aims to correct for volume change during the spatial normalisation step (Good et al., 2001a). For example, volume differences due to disease may be lost when an individual is matched onto a larger, non-atrophic template image. Without modulation a brain which had atrophy affecting grey and white matter equally would appear to be identical to a normal brain after spatial normalisation. In order to recover atrophy and preserve the volume of a particular tissue (grey or white matter or CSF), intensities within the image are divided by the Jacobian values from the registration. Regions that have undergone extensive expansion will consequently show reduced intensities, reflecting a reduction in density of tissue.

3.1.5.6. Smoothing

The normalised, segmented and modulated images are then smoothed by convolving with an isotropic Gaussian kernel (Ashburner and Friston, 2000; Good et al., 2001a). The intensity of each voxel is replaced by the weighted average of the surrounding voxels. The size of this region is defined by the size of the smoothing kernel. This makes the data conform more closely to the Gaussian field model that is an important assumption of SPM, renders the data more normally distributed, increasing the validity of the parametric tests, and reduces inter-subject variability. It also helps to compensate for the inexact nature of the normalisation. High levels of smoothing increase the ability of VBM to detect grey matter differences by reducing the variance, however the ability to localise change is then compromised. The optimum kernel size is likely to vary depending on the imaging modality, image resolution and the normalisation method. Generally the size of the smoothing kernel should be equivalent to the size of the expected regional differences between the groups of

brains. Previous VBM studies have used kernel sizes ranging from 4 to 12mm (Maguire et al., 2000; Mummery et al., 2000; Baron et al., 2001). Davatizkos et al (Davatzikos et al., 2001a) examined simulated atrophy and found that the optimal smoothing kernel was 13mm for the default SPM resolution, but 9mm when high-dimensional matching was used. However recent work performed using simulated atrophy suggested an optimum smoothing kernel of 8 mm full width at half maximum (FWHM) (Scahill, 2003). Increased areas of atrophy were detected with increasing kernel size. Analysis using a kernel of less than 8mm failed to detect all simulated atrophy, whereas kernel sizes over 8mm detected changes outside brain, including scalp. This work was performed using scans acquired identically to those used in this thesis, therefore a smoothing kernel of 8mm FWHM has been applied in all VBM studies. Figure 3.13 shows grey matter, white matter and CSF images after smoothing with an 8mm kernel.

Figure 3.13: Grey matter, white matter and CSF images before (A-C) and after smoothing (D-F) with an 8mm smoothing kernel

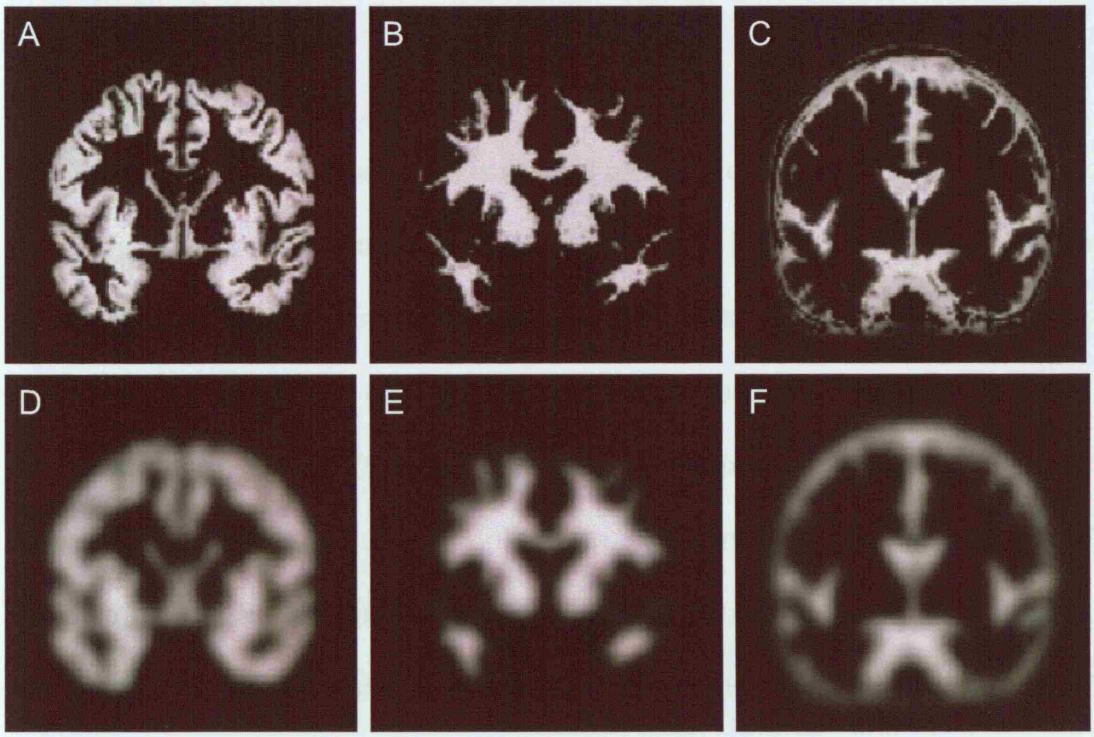

3.1.5.7. Creating customised templates and prior probability maps

Customised templates and prior probability maps were created from groups of control and disease subjects that were age and gender matched to the study cohort. Therefore the specific make-up of the group will vary in each chapter dependent upon the study population. In order to generate the customised template all selected scans were normalised (i.e. registered) to the MNI template image. A mean image is then created from these normalised images and smoothed at 8mm FWHM. This smoothed mean forms the customised template that can be used in the main analysis. In order to create the customised priors the selected scans are normalised to the MNI template, segmented into grey matter, white matter and CSF, masked, modulated and smoothed at 8mm FWHM. A mean image is created of the smoothed grey matter images, as

well as the smoothed white matter and CSF images. These smoothed images are then used as the priors for segmentation in the main analysis.

3.1.5.8. Statistical analysis

The smoothed data is analysed using statistical parametric mapping (SPM) (Friston et al., 1995). This uses the general linear model (GLM) to identify differences in tissue density between subject groups. The analysis generates statistical parametric maps (SPMs) showing regions of significant difference between groups. Standard parametric statistical tests (t-tests and F-tests) are performed at every voxel in the image. The significance of any differences is ascertained using the theory of Gaussian random fields. Since a large number of statistical tests are preformed it is important to correct for multiple comparisons in order to prevent the occurrence of false positives. The traditional multiple comparison correction within SPM is a modification of a Bonferroni correction, controlling the chance of any false positives (Family-wise Error rate (FWE)). However, this is a very harsh statistical test. It was originally developed for functional imaging studies in which each individual has many scans and may not be appropriate for structural data. A more lenient approach recently developed is the false discovery rate (FDR) correction that controls the expected proportion of false positives among suprathreshold voxels (www.fil.ion.ucl.ac.uk). In other words it requires that the p value survive threshold only in the activated voxels, rather than all voxels in the image.

It is important to eliminate any potential confounding effects. For example, it is not appropriate to compare two different groups if the images are acquired on different scanners. If this is the case then any group differences may be due to differences in

scanner rather than to the subjects themselves. In order to prevent such confounders all group comparisons in this thesis were matched for scanner. Age and gender were also included in the models as nuisance variables.

VBM is a widely used technique, and has been applied to highlight reductions in grey matter in normal ageing (Good et al., 2001a), temporal lobe epilepsy (Keller et al., 2002), AD (Rombouts et al., 2000; Baron et al., 2001), FTLD (Janssen et al., 2005), Huntingtons disease (Thieben et al., 2002), and progressive supranuclear palsy (Price et al., 2004). Studies have also attempted to validate VBM against the current 'gold standard' of manual measurement (Vargha-Khadem et al., 1998; Maguire et al., 2000; Good et al., 2002). Differences between the two techniques are likely to be due to inaccuracies in the segmentation step and reduced ability to localise change due to smoothing in VBM. The sensitivity of VBM to detect differences is also greatly reduced in areas of high variability. Chapter 10 investigates this issue further by comparing the results of VBM to visual assessments of patterns of regional atrophy in pathologically confirmed cases of FTLD.

3.2. Subjects

This thesis uses patients recruited from a number of sources that have been outlined below. Ethics approval for the project was obtained from the 'The National Hospital for Neurology and Neurosurgery and the Institute of Neurology' joint ethics committee, and the 'UCL Hospitals NHS Trust' approved the study.

3.2.1. The Specialist Cognitive Disorders Clinic

This clinic is based at the National Hospital for Neurology and Neurosurgery, Queen Square, London. It is a tertiary referral centre, with patients referred from GPs and secondary level services such as Old Age Psychiatrists and Neurologists throughout the United Kingdom. Patients tend to be younger than a typical elderly population and usually show diagnostic uncertainty. Each patient undergoes a full clinical assessment, including a full history taken together with a close informant, and a comprehensive general medical and neurological examination. In addition, patients are investigated with detailed neuropsychological testing (including the MMSE); standard screening blood tests to exclude other treatable causes of cognitive problems such as renal or liver failure, B12 and thyroid function; EEG to exclude seizures, or identify patterns indicative of particular types of dementia; and neuroimaging using MRI to exclude treatable causes such as tumours and subdural haemotomas.

All patients included in this thesis had initially been recruited through the Specialist Cognitive Disorders Clinic. Cases were identified by performing a search of the clinic database. Clinical records were then reviewed retrospectively by Professor Martin Rossor or Professor Nick Fox. Patients were diagnosed according to standard criteria (as described in chapter 1) without reference to imaging findings. The information available to the clinician included a detailed clinical history and the results of a detailed medical and neurological examination.

Genetic testing may be performed for those individuals in a family with a known genetic mutation. This is supported by a full genetic counselling service. In addition, the issue of brain donation is discussed with the patients and their families. If the

patient provides consent then, on death, the brains will be collected by the Queen Square Brain Bank and processed for post-mortem at the Institute of Neurology, London. Brain donations before 1996 were collected and processed at the Institute of Psychiatry, King's College London. A brain biopsy may be performed during life in order to provide a pathological diagnosis. This is usually only performed in cases of extreme diagnostic uncertainty.

3.2.2. Prospective Longitudinal FTLD Study

The aims of this study were to explore the longitudinal course of FTLD by documenting change in clinical and behavioural features, and caregiving experiences. The outcomes of the disease were assessed in terms of disease progression, caregiver burden and health service utilisation. Thirty-seven FTLD subjects were recruited from the Specialist Cognitive disorders clinic. Each subject had undergone full clinical assessments in the clinic before recruitment (see above). Inclusion criteria included a clinical diagnosis of FTLD according to the Lund and Manchester criteria; and the presence of a caregiver or informant willing to participate in the study and who is in regular contact with the patient (must have seen them at least twice weekly). Patients were excluded if they had already been placed in long-term residential care or if they had a diagnosis of PNFA. Clinical review was performed by Dr Elizabeth Sampson and Dr Richard Harvey. All carers and patients gave informed written consent to participate in the study. If the patient was unable to consent due to memory impairment, behavioural disturbance or loss of language the next of kin was asked to sign their assent for their relative to be included in the study. Ethics approval was obtained from both The National Hospital Joint Ethics Committee and St Mary's local Research Ethics Committee.

Each patient attended a comprehensive assessment at baseline and then again a year later. Neuropsychiatric and behavioural assessments were performed using the Manchester and Oxford University Scale for the assessment of Psychopathology in Dementia (MOUSEPAD) (see Appendix 3 (Allen et al., 1996)). This is a caregiver-based questionnaire that measures the presence, severity and frequency of a number of behavioural features, including delusions, hallucinations, aggression, walking, sleep, sexual behaviour and changes in eating behaviour. Neuropsychological assessments were also performed using a battery designed to probe areas of frontal, language and semantic function. In addition, each patient was assessed using the MMSE and CDR (see Appendix 3), and underwent a volumetric MRI at both visits (see Appendix 4 for acquisition parameters). The carer was interviewed separately to complete measures of carer burden and resource utilisation.

3.2.3. MIRIAD

The Minimal Interval Resonance Imaging in Alzheimer's disease and normal ageing (MIRIAD) study aimed to determine the shortest interval required to detect differences between AD subjects and healthy controls using measures from serial volumetric MRI (Schott, 2004). Forty-six individuals with sporadic AD and 23 control subjects were recruited from the Specialist Cognitive disorders clinic. Inclusion criteria for the patients included: age over 55; diagnosis of probable AD according to the NINCDS-ADRDA criteria; patient and carer willing to participate and able to give informed consent; MMSE score >12 (range 0 – 30), and CDR <3 (range 0.5 – 3). Clinical review was performed by Dr Jonathon Schott, Professor Martin Rossor and Professor Nick Fox. The control subjects were age, sex and

education matched to the patient group and had an MMSE >26. In many cases the control subjects were the spouses of the patients. All subjects gave written informed consent. Ethics approval was obtained from the local research ethics committee at The National Hospital for Neurology and Neurosurgery, London.

Each subject had undergone a full clinical assessment in the Specialist Cognitive disorders clinic before recruitment (see above). Then, as part of the study, subjects were assessed at baseline, and at 2, 6, 14, 26, 38 and 52 weeks. A small number of subjects also returned for a 2-year visit. At baseline and 52 weeks all subjects underwent a full history, neurological examination, MMSE and detailed neuropsychology. APOE genotyping and EEGs were performed on the AD patients. A volumetric MRI was performed at each visit (see Appendix 4 for acquisition parameters). In addition, at baseline, 6 weeks and 38 weeks two scans were acquired on the same day.

3.2.4. Normal Control Study

Neurologically healthy individuals are routinely recruited to act as normal controls. Exclusion criteria included a history of stroke or dementia. These are often spouses of affected or at-risk study members and a number of normal volunteers. All subjects have a detailed history taken and undergo a neurological examination, MMSE and an MRI scan. The spouses of study subjects are usually scanned on the same day as their partners and therefore have as closely comparable MR acquisitions as possible.

3.3. Statistics

Statistical analysis was performed using SPSS version 8 (SPSS Inc., Chiacgo, Illinois, USA) and STATA version 8 (Stata Corporation, College Station, Texas, 1999). More details are provided in each chapter.

4. Visual assessments of regional atrophy in FTLD

4.1. Introduction

The visual assessment of brain MRI is routinely used by radiologists and neurologists in order to aid diagnosis. Increasingly there is interest in assessing the presence of pathological atrophy to distinguish normal ageing from a degenerative process and using the pattern of atrophy to differentiate the different causes of dementia. Rating scales have been developed which allow a quantitative assessment of the pattern of regional atrophy (Scheltens et al., 1995; Galton et al., 2001b). They have the advantage that they are quick and simple to apply and therefore can be performed on large numbers of scans and do not require any specialised software. The disadvantage is that there may be a loss of sensitivity or specificity compared to more detailed volumetric studies. However, studies have shown rating scales to be both reliable and comparable to other measures of atrophy, including both stereological assessments (Wahlund et al., 1999; Wahlund et al., 2000) and volumetric measurements (Galton et al., 2001b). Visual ratings on MRI have also been shown to be as good, or better, at detecting focal abnormalities than visual ratings from both CT (Sinnatamby et al., 1996) and SPECT (Miller and Gearhart, 1999; Varma et al., 2002a).

A number of visual rating studies have focused on the temporal lobe. This is predominantly because of the interest in medial temporal lobe atrophy as a sensitive diagnostic marker for AD. Studies have shown that visual ratings of medial temporal lobe atrophy are good as discriminating AD from controls (Wahlund et al., 1999; Wahlund et al., 2000), however they are not as good at discriminating AD from FTLD and other dementias (Wahlund et al., 2000; Galton et al., 2001b; Varma et al., 2002a);

medial temporal lobe atrophy is present in both AD and FTLD. It is possible that non-temporal lobe regions may be more useful in the differential diagnosis of FTLD (for example frontal lobe atrophy). Few studies have used visual ratings to assess regions over the whole brain. Assessment of brain asymmetry is also extremely important in the diagnosis of FTLD. Asymmetric patterns of atrophy are common, and relatively specific to FTLD (Sinnatamby et al., 1996; Miller and Gearhart, 1999; Varma et al., 2002a; Likeman et al., 2005). Both volumetric and visual rating studies have shown that asymmetry on MRI may be useful in distinguishing FTLD from AD (Varma et al., 2002a; Boccardi et al., 2003; Likeman et al., 2005).

This chapter aims to use visual assessments to characterise and quantify the patterns of regional atrophy present throughout the whole brain in FTLD subjects. These patterns will be compared to the patterns of atrophy in a range of other dementias and neurological conditions found in a typical cognitive disorders clinic. The patterns of atrophy will also be assessed in all three syndromic variants of FTLD (fvFTD, PNFA, and SD).

4.2. Methods

4.2.1. Subjects

All subjects were recruited from the specialist cognitive disorders clinic (see chapter 3) and were fully investigated including a detailed history, neurological and general examination, screening blood tests, neuropsychometry (including the MMSE), and MR imaging. All MR scans were acquired using the standard protocol in Appendix 4. Fifty patients fulfilling consensus criteria for FTLD were included in the study (28 fvFTD, 10 PNFA, 12 SD (Neary et al., 1998)). This FTLD cohort was age and

gender-matched to a group of 48 patients with a neurological disorder other than FTLD. This group included 31 patients that fulfilled the NINCDS-ADRDA criteria for "probable" AD (McKhann et al., 1984), five with vascular dementia, three with corticobasal degeneration, two with multiple sclerosis, two with CJD, and single cases of PSP, Lafora body disease, epilepsy, Lewy Body disease and mixed dementia. Eight of the FTLD and 11 of the 'other' cases had post mortem, biopsy or genetic confirmation. All subjects had an MRI scan within 3 months of a detailed neuropsychological assessment. When multiple scans were available the scan closest to the time of diagnosis was used.

Table 4-1: Patient characteristics

	Non-FTLD (n=48)	FTLD (n=50)	fvFTD (n=28)	PNFA (n=10)	SD (n=12)
Gender (M:F)	29:19	30:20	16:12	8:2	6:6
Age (yrs)	61.6 (9.9)	61.0 (7.6)	60.1 (8.1)	60.7 (7.5)	64.2 (6.5)
Handedness R:L:A	N/A	25:2:1*	12:2:0*	7:0:0*	6:0:1*
MMSE	20.3 (6.0)	20.6 (7.9)	20.6 (8.0)	19.9 (9.6)	21.0 (7.0)
Duration (yrs)	3.5 (2.3)	4.7 (3.0)	5.5 (3.5)	3.3 (1.4)	3.8 (1.9)

* Handedness information was not available in all cases, R = right, L = left, A = ambidextrous; N/A = not available. Age, MMSE and duration expressed as mean (standard deviation)

4.2.2. Analysis

Each T1-weighted volumetric MRI scan was assessed and graded by an experienced neuroradiologist in terms of regional atrophy. Images were presented randomly in groups of approximately 30. The raters were blinded to clinical diagnosis and all other clinical information other than age at time of scan. They were also blinded to the number of FTLD and non-FTLD cases in any given group. Ten of the images randomly appeared twice in the series in order to assess intra-rater reliability.

The questionnaire completed by the radiologist is shown in Appendix 6. Individual regions throughout the brain were graded as normal (score = 0), mildly atrophic (score = 1), moderately atrophic (score = 2) or severely atrophic (score = 3). Regions included the frontal (FL), temporal (TL), parietal (PL) and occipital lobes (OL). The left and right hemispheres were assessed separately in each case. The frontal lobes were assessed as a whole and then separate assessments were made for the orbitofrontal cortex (OFC) and dorsolateral frontal cortex (DLC). Similarly, the temporal lobes were assessed as a whole and then separate assessments were made for the superior temporal gyrus (STG), inferior temporal gyrus (ITG), fusiform gyrus (FG), parahippocampal gyrus (PHG), hippocampus (HIP) and amygdala (AMY). Further assessments were made to grade the level of cerebellum atrophy, ventricular dilation and vascular load, again using the scale normal, mild, moderate or severe. Figure 4.1 shows examples of the temporal lobe ratings.

An assessment of asymmetry of atrophy on MRI scans was made for all regions. Regions were graded as either having no asymmetry, having more atrophy on the left than right (L > R), or more atrophy on the right than left (R > L). Ventricular dilation

was graded as either having no asymmetry, left ventricle larger than right (L > R) or right ventricle larger than left (R > L), and vascular load was graded as either having no asymmetry, greater vascular load on the left than right (L > R), or greater vascular load on the right than left (R > L). In addition an assessment of the gradient of anterior-posterior atrophy throughout the whole brain was made and rated either as no gradient, anterior atrophy greater than posterior (A > P), or posterior atrophy greater than anterior atrophy (P >A).

Figure 4.1: Examples of temporal lobes that were visually rated as normal (0), mild (1), moderate (2) or severely (3) atrophic

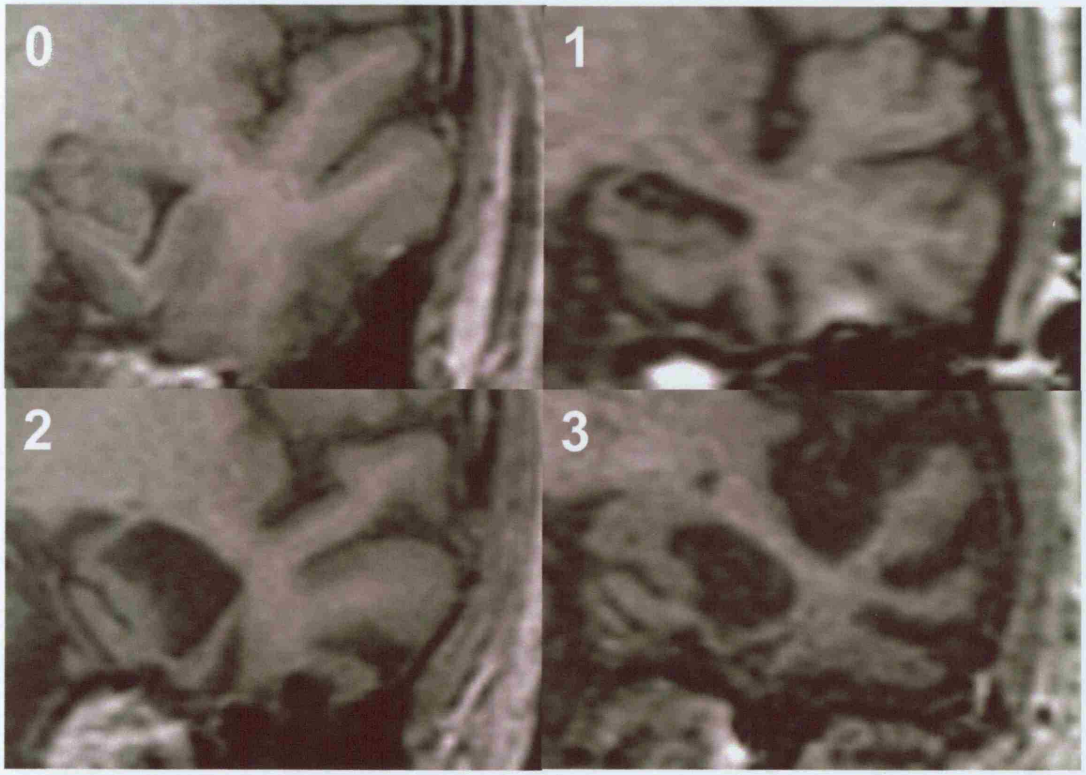

4.2.3. Statistics

All analysis was performed using STATA. Mean atrophy scores were calculated for each region, and each patient group. Differences in the mean atrophy scores were assessed firstly using ANOVA and then two sample T-tests to investigate specific group differences.

Intra-rater reliability was assessed for the radiological symmetry assessments using ten patients who had repeat assessments. The kappa statistic was reported, which gives the excess proportion of agreement, above that which would be expected by random chance, in the absence of any associations. Only the first assessment of these ten cases was included in the main analysis. The relationship between asymmetry in the different MRI regions was also assessed using the Kappa statistic.

4.3. Results

4.3.1. Intra-rater reliability

Good agreement was found between the first and second assessments with an average kappa (representing the proportion of agreement between assessments, above that expected by chance) of 0.83 ± 0.19 (mean $\pm$ StDev).

4.3.2. Patterns of atrophy on MRI

The results from the visual assessments of MRI are shown in tables 4-2 and 4-3. In addition the mean atrophy score in each group, for each region, is plotted in figure 4.2. Cerebral atrophy was thought to be present in 82% (41/50) of the FTLD subjects and 71% (34/48) of the non-FTLD subjects (table 4-2).

The FTLD group had more atrophy than the non-FTLD group across all frontal and temporal regions (figure 4.2). However only regions in the left temporal lobe had a significantly higher atrophy score; including the STG, ITG, FG, PHG, hippocampus and amygdala ($p<0.001$ in all). There were no significant differences in the right temporal lobe or the frontal lobes. Conversely the non-FTLD group seemed to show more parietal lobe atrophy than the FTLD group ($p=0.05$), although parietal lobe atrophy was still present in approximately 30% of the FTLD subjects.

The FTLD group showed a more asymmetric pattern of atrophy than the non-FTLD subjects, with the scores in the left hemisphere significantly greater than the right in the frontal ($p<0.002$), temporal ($p<0.0001$), and parietal lobes ($p<0.05$). Only the frontal lobes showed significantly greater left than right sided atrophy in the non-FTLD group ($p<0.05$). Figure 4.3 illustrates the proportion of patients assessed as having asymmetries in each of the specified regions in the non-FTLD and FTLD groups. The FTLD subjects had a greater proportion of left-sided asymmetries than the non-FTLD group: 48% of the FTLD subjects showed greater atrophy on the left, than the right, in the temporal lobe on MRI compared to only 10% in the non-FTLD subjects. Right greater than left asymmetries were present in the temporal lobes in approximately 10% of the FTLD subjects. The non-FTLD group were rarely asymmetric.

Highly significant associations existed between assessments of asymmetry in the frontal, temporal and parietal lobes on MRI in the whole group (table 4-4). For example, temporal lobe asymmetry was associated with asymmetry in the hippocampus ($k=0.70$, $p<0.001$), amygdala ($k=0.74$, $p<0.001$), ventricles ($k=0.28$,

$p<0.001$), parietal lobe ($k=0.26$, $p<0.001$) and frontal lobes ($k=0.75$, $p<0.001$). A similar pattern of associations was observed when looking in both the FTLD and non-FTLD subjects separately.

Fifty-two percent of FTLD subjects also had an anterior-posterior gradient of atrophy (figure 4.4), with more severe atrophy in anterior than posterior regions. Almost none of the FTLD subjects showed a posterior-anterior gradient of atrophy (2%). In contrast, an anterior-posterior gradient was rare in the non-FTLD subjects (13%), whereas a posterior-anterior gradient was present in 23% of subjects (figure 4.4).

4.3.3. Patterns of atrophy in the syndromic variants of FTLD

The FTLD group can be divided into the three syndromic variants: fvFTD, PNFA and SD (see table 4-3 and figure 4.5). Global atrophy was present in 100% of the SD patients, 75% of the fvFTD patients and 80% of the PNFA patients.

Frontal lobe atrophy was present in all three syndromic variants (present in 46% of fvFTD, 70% of PNFA and 58% of SD patients, table 4-3). Whilst, there were no significant differences between the FTLD subgroups in the frontal lobe atrophy scores, severe (score = 3) frontal lobe atrophy, particularly of the dorsolateral frontal and orbitofrontal cortex, was only found in the fvFTD patients. The SD group had a significantly higher mean atrophy score in the left temporal lobe than the fvFTD ($p=0.006$) and PNFA groups ($p=0.03$). This included all regions except the left superior temporal gyrus which was not significantly different from the PNFA group (STG atrophy was present in 70% of the PNFA patients). The most severe temporal lobe atrophy in the SD group was found in the left fusiform gyrus; over 80% of the

SD subjects had moderate or severe atrophy compared to 10% of the PNFA subjects and 25% of the fvFTD subjects. The parahippocampal gyrus was also severely affected in the SD group with 59% showing moderate or severe atrophy. The right parietal lobe was significantly more atrophied in the fvFTD and PNFA groups than the SD group and the left parietal lobe was significantly more atrophied in the PNFA group than the SD group. There were no significant differences in occipital lobe atrophy.

Both the SD and PNFA groups showed an asymmetric pattern of temporal lobe atrophy, with the left temporal lobe significantly more atrophied than the right (SD $p<0.003$, PNFA $p<0.03$). In addition, the left frontal lobe ($p<0.03$) and orbitofrontal cortex ($p<0.02$) were significantly more atrophic than the right in the SD group. Figure 4.6 illustrates the high proportion of left-sided asymmetries present in both the SD and PNFA group. In comparison, the fvFTD group were rarely asymmetric. In addition, 85% of the SD patients had an anterior-posterior gradient of atrophy, with more severe atrophy in anterior than posterior regions, compared to approximately 40% in both the fvFTD and PNFA groups (figure 4.7).

Table 4-2: Regional atrophy on MRI across disease groups

	Score	NON-FTLD (n=48)		FTLD (n=50)		fvFTD (n=28)		PNFA (n=10)		SD (n=12)	
		N	%	N	%	N	%	N	%	N	%
Global atrophy	0	14	29	9	18	7	25	2	20	0	0
	1	34	71	41	82	21	75	8	80	12	100
Ventricles	0	24	50	16	32	9	32	4	40	3	25
	1	10	21	17	34	11	39	2	20	4	33
	2	11	23	17	34	8	29	4	40	5	42
	3	3	6	0	0	0	0	0	0	0	0
Cerebellum	0	47	98	49	98	27	96	10	100	12	100
	1	1	2	1	2	1	4	0	0	0	0
	2	0	0	0	0	0	0	0	0	0	0
	3	0	0	0	0	0	0	0	0	0	0
Vascular load	0	29	60	33	66	17	61	5	50	11	92
	1	6	13	9	18	6	21	2	20	1	8
	2	11	23	7	14	4	14	3	30	0	0
	3	2	4	1	2	1	4	0	0	0	0

Table 4-3: Regional atrophy on MRI across disease groups (results are given for both the left and right hemisphere)

Region	Score	NON-FTLD (n=48)				FTLD (n=50)				fvFTD (n=28)				PNFA (n=10)				SD (n=12)			
		LEFT		RIGHT		LEFT		RIGHT		LEFT		RIGHT		LEFT		RIGHT		LEFT		RIGHT	
		N	%	N	%	N	%	N	%	N	%	N	%	N	%	N	%	N	%	N	%
Frontal lobe	0	28	58	30	63	23	46	31	62	15	54	17	61	3	30	5	50	5	42	9	75
	1	16	33	16	33	18	36	14	28	6	21	6	21	6	60	5	50	6	50	3	25
	2	4	8	2	4	7	14	4	8	5	18	4	14	1	10	0	0	1	8	0	0
	3	0	0	0	0	2	4	1	2	2	7	1	4	0	0	0	0	0	0	0	0
OFC	0	28	58	30	63	24	48	32	64	16	57	18	64	3	30	5	50	5	42	9	75
	1	16	33	16	33	14	28	13	26	5	18	5	18	5	50	5	50	4	33	3	25
	2	4	8	2	4	10	20	4	8	5	18	4	14	2	20	0	0	3	25	0	0
	3	0	0	0	0	2	4	1	2	2	7	1	4	0	0	0	0	0	0	0	0
DLC	0	29	60	30	63	28	56	34	68	17	61	18	64	4	40	6	60	7	58	10	83
	1	17	35	16	33	13	26	11	22	4	14	5	18	4	40	4	40	5	42	2	17
	2	2	4	2	4	7	14	4	8	5	18	4	14	2	20	0	0	0	0	0	0
	3	0	0	0	0	2	4	1	2	2	7	1	4	0	0	0	0	0	0	0	0
Temporal lobe	0	26	54	30	63	14	28	27	54	12	43	15	54	2	20	6	60	0	0	6	50
	1	19	40	15	31	20	40	16	32	9	32	8	29	6	60	4	40	5	42	4	33
	2	3	6	3	6	11	22	6	12	5	18	4	14	2	20	0	0	4	33	2	17
	3	0	0	0	0	5	10	1	2	2	7	1	4	0	0	0	0	3	25	0	0
STG	0	27	56	33	69	17	34	29	58	15	54	16	57	2	20	6	60	0	0	7	58
	1	19	40	13	27	18	36	14	28	7	25	7	25	5	50	4	40	6	50	3	25
	2	2	4	2	4	13	26	6	12	4	14	4	14	3	30	0	0	6	50	2	17
	3	0	0	0	0	2	4	1	2	2	7	1	4	0	0	0	0	0	0	0	0
ITG	0	27	56	33	69	20	40	30	60	17	61	17	61	3	30	6	60	0	0	7	58
	1	19	40	13	27	14	28	13	26	5	18	6	21	6	60	4	40	3	25	3	25
	2	2	4	2	4	12	24	7	14	3	11	5	18	1	10	0	0	8	67	2	17
	3	0	0	0	0	4	8	0	0	3	11	0	0	0	0	0	0	1	8	0	0
FG	0	27	56	32	67	18	36	29	58	15	54	16	57	3	30	6	60	0	0	7	58
	1	19	40	14	29	14	28	13	26	6	21	7	25	6	60	4	40	2	17	2	17
	2	2	4	2	4	7	14	8	16	3	11	5	18	1	10	0	0	3	25	3	25
	3	0	0	0	0	11	22	0	0	4	14	0	0	0	0	0	0	7	58	0	0
PG	0	25	52	30	63	19	38	27	54	14	50	15	54	4	40	6	60	1	8	6	50
	1	20	42	16	33	17	34	15	30	7	25	8	29	6	60	4	40	4	33	3	25
	2	3	6	2	4	5	10	8	16	3	11	5	18	0	0	0	0	2	17	3	25
	3	0	0	0	0	9	18	0	0	4	14	0	0	0	0	0	0	5	42	0	0
Amygdala	0	25	52	25	52	16	32	22	44	11	39	11	39	4	40	6	60	1	8	5	42
	1	19	40	17	35	20	40	12	24	9	32	6	21	4	40	2	20	7	58	4	33
	2	3	6	5	10	8	16	15	30	4	14	10	36	2	20	2	20	2	17	3	25
	3	1	2	1	2	6	12	1	2	4	14	1	4	0	0	0	0	2	17	0	0
Hippocampus	0	20	42	21	44	14	28	19	38	10	36	9	32	4	40	5	50	0	0	5	42
	1	21	44	20	42	20	40	16	32	10	36	8	29	4	40	4	40	6	50	4	33
	2	6	13	6	13	12	24	14	28	7	25	11	39	1	10	0	0	4	33	3	25
	3	1	2	1	2	4	8	1	2	1	4	0	0	1	10	1	10	2	17	0	0
Parietal lobe	0	25	52	27	56	32	64	36	72	18	64	18	64	4	40	6	60	10	83	12	100
	1	14	29	12	25	15	30	12	24	8	29	8	29	5	50	4	40	2	17	0	0
	2	8	17	8	17	3	6	2	4	2	7	2	7	1	10	0	0	0	0	0	0
	3	1	2	1	2	0	0	0	0	0	0	0	0	0	0	0	0	0	0	0	0
Occipital lobe	0	36	75	36	75	44	88	44	88	23	82	23	82	9	90	9	90	12	100	12	100
	1	11	23	11	23	4	8	4	8	3	11	3	11	1	10	1	10	0	0	0	0
	2	1	2	1	2	2	4	2	4	2	7	2	7	0	0	0	0	0	0	0	0
	3	0	0	0	0	0	0	0	0	0	0	0	0	0	0	0	0	0	0	0	0

Figure 4.2: Mean atrophy scores plotted for each cortical region for the non-FTLD and FTLD groups. Frontal regions have been colour coded in blue, temporal regions in red, parietal in yellow and occipital in green. Left hemisphere = solid colour, right hemipshere = hatched. Error bars represent standard error.

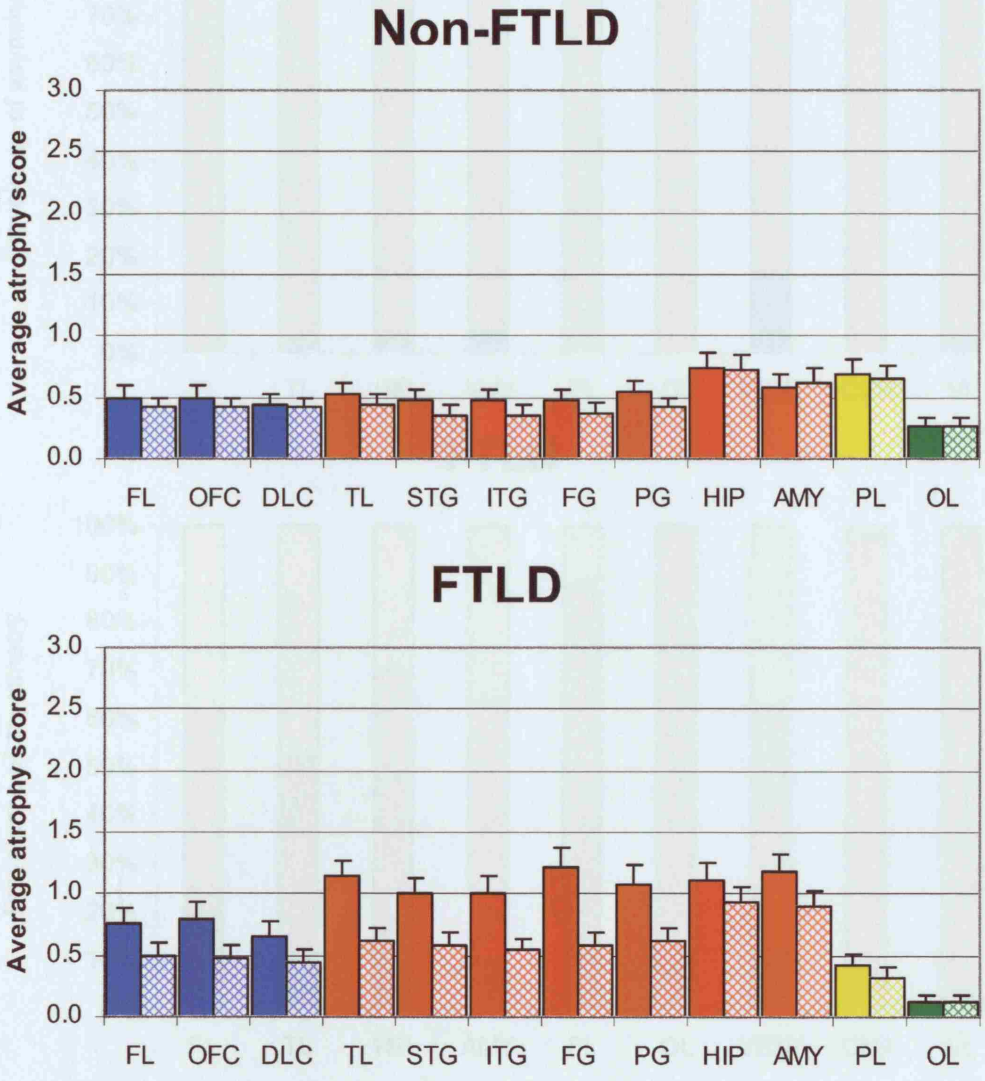

Figure 4.3: Prevalence of asymmetry in the non-FTLD and FTLD groups (%)

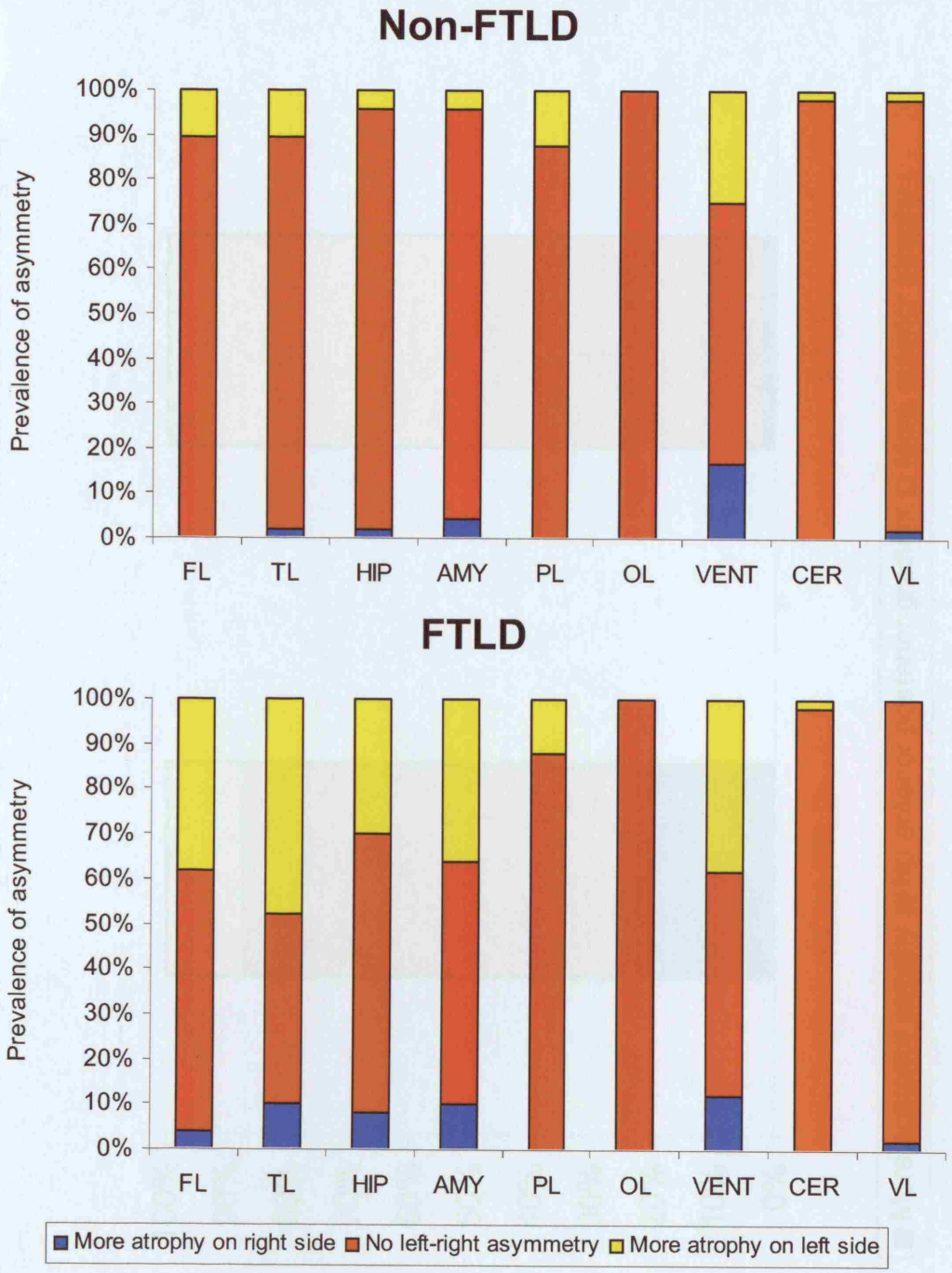

Figure 4.4: Prevalence of anterior-posterior gradient of atrophy in the non-FTLD and FTLD groups

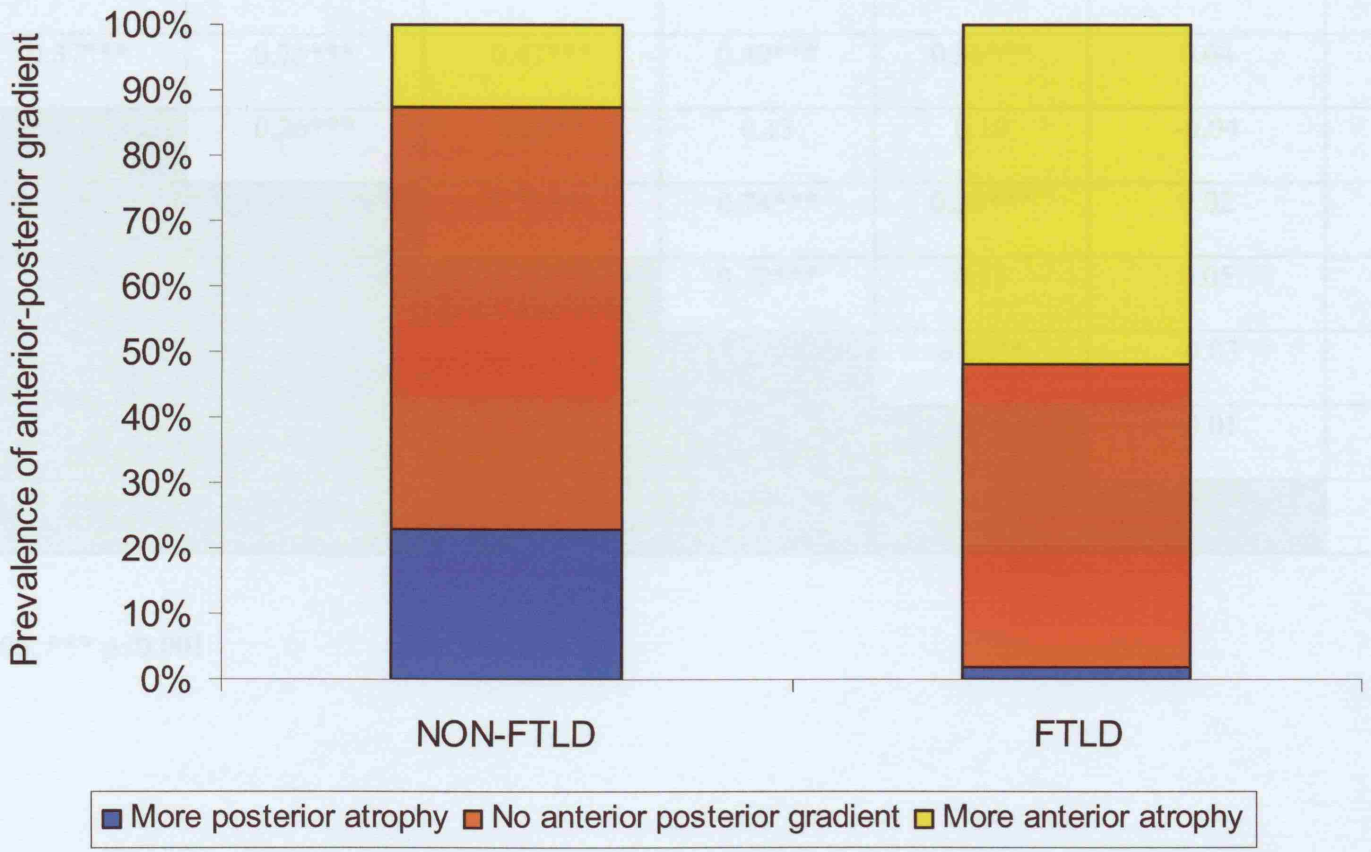

Table 4-4: Associations between asymmetries in different MRI regions in all patients

	Parietal lobe	Temporal lobe	Hippocampus	Amygdala	Ventricles	Cerebellum	Vascular load
Frontal lobe	0.37***	0.75***	0.47***	0.49***	0.36***	0.04	0.03
Parietal lobe		0.26***	0.25**	0.13	0.10	-0.04	0.10*
Temporal lobe			0.70***	0.74***	0.28***	0.02	0.01
Hippocampus				0.72***	0.11	0.05	0.04
Amygdala					0.22**	-0.03	0.03
Ventricles						-0.01	0.00
Cerebellum							-0.02

* $p<0.05$, ** $p<0.005$, *** $p<0.001$

Figure 4.5: Mean atrophy scores plotted for each cortical region for the fvFTD, SD and PNFA subgroups. Frontal regions have been colour coded in blue, temporal regions in red, parietal in yellow and occipital in green. Left hemisphere = solid colour, right hemipshere = hatched. Error bars represent standard error.

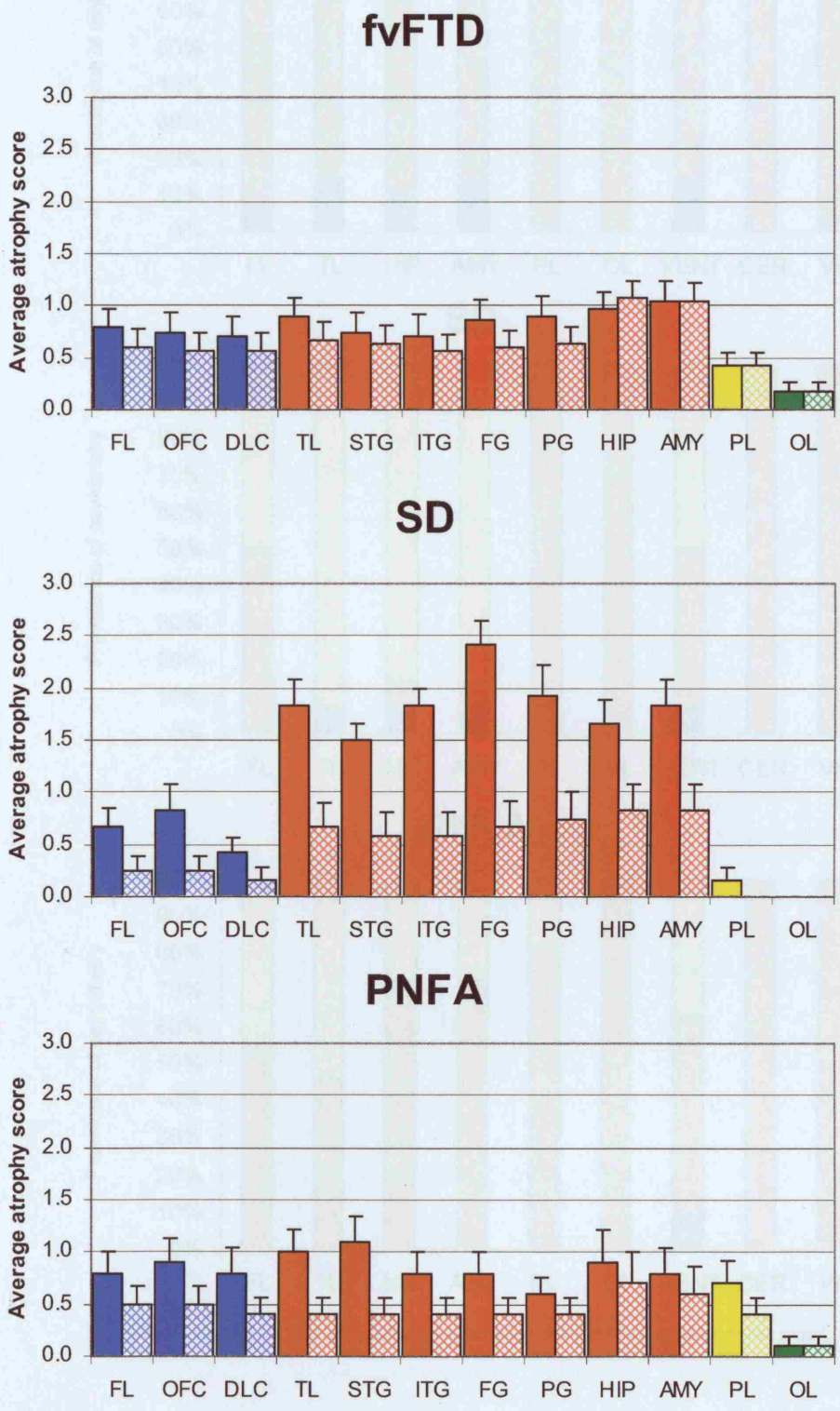

Figure 4.6: Prevalence of asymmetry in the fvFTD, SD and PNFA subgroups

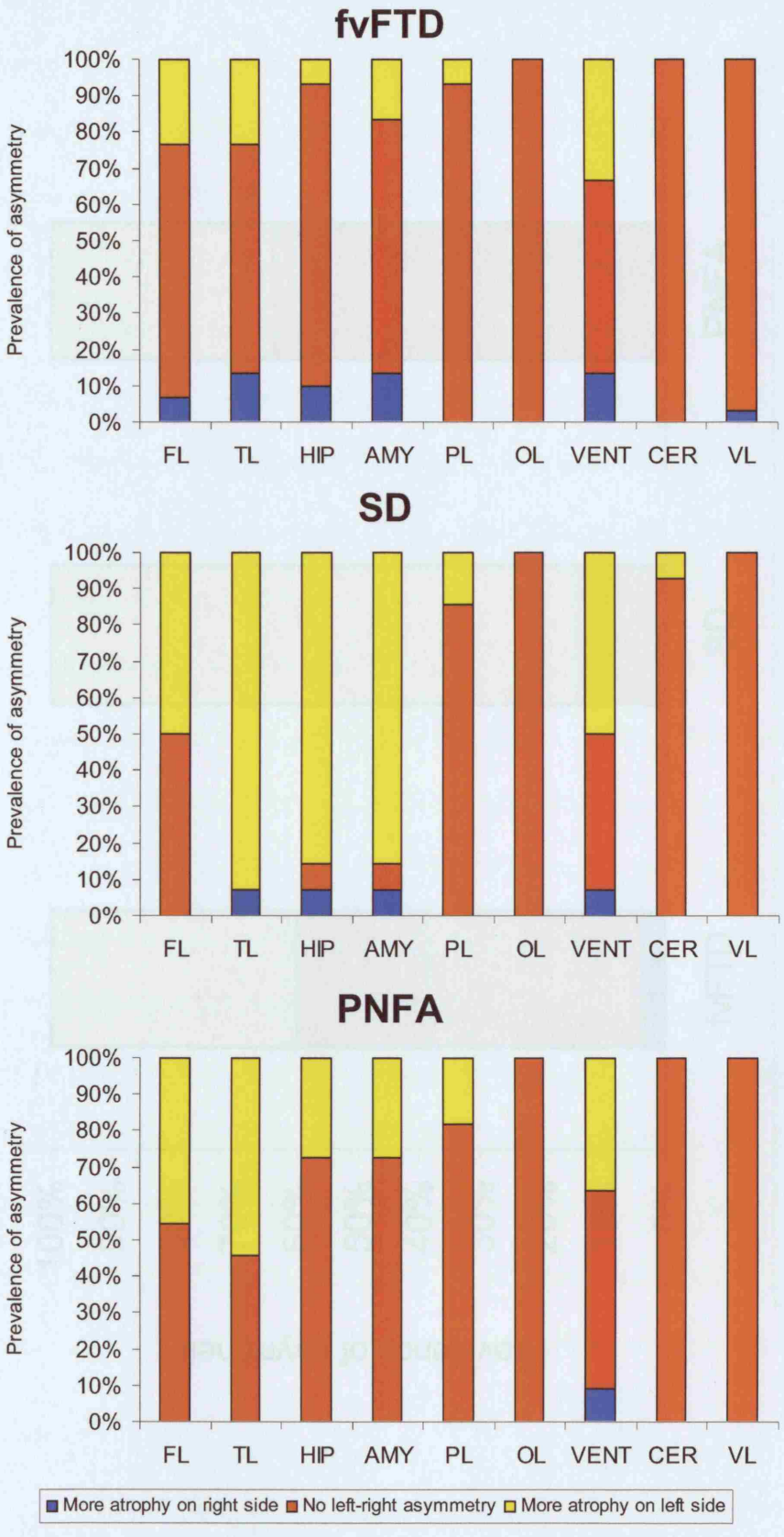

Figure 4.7: Prevalence of anterior-posterior gradient of atrophy in the fvFTD, SD and PNFA subgroups

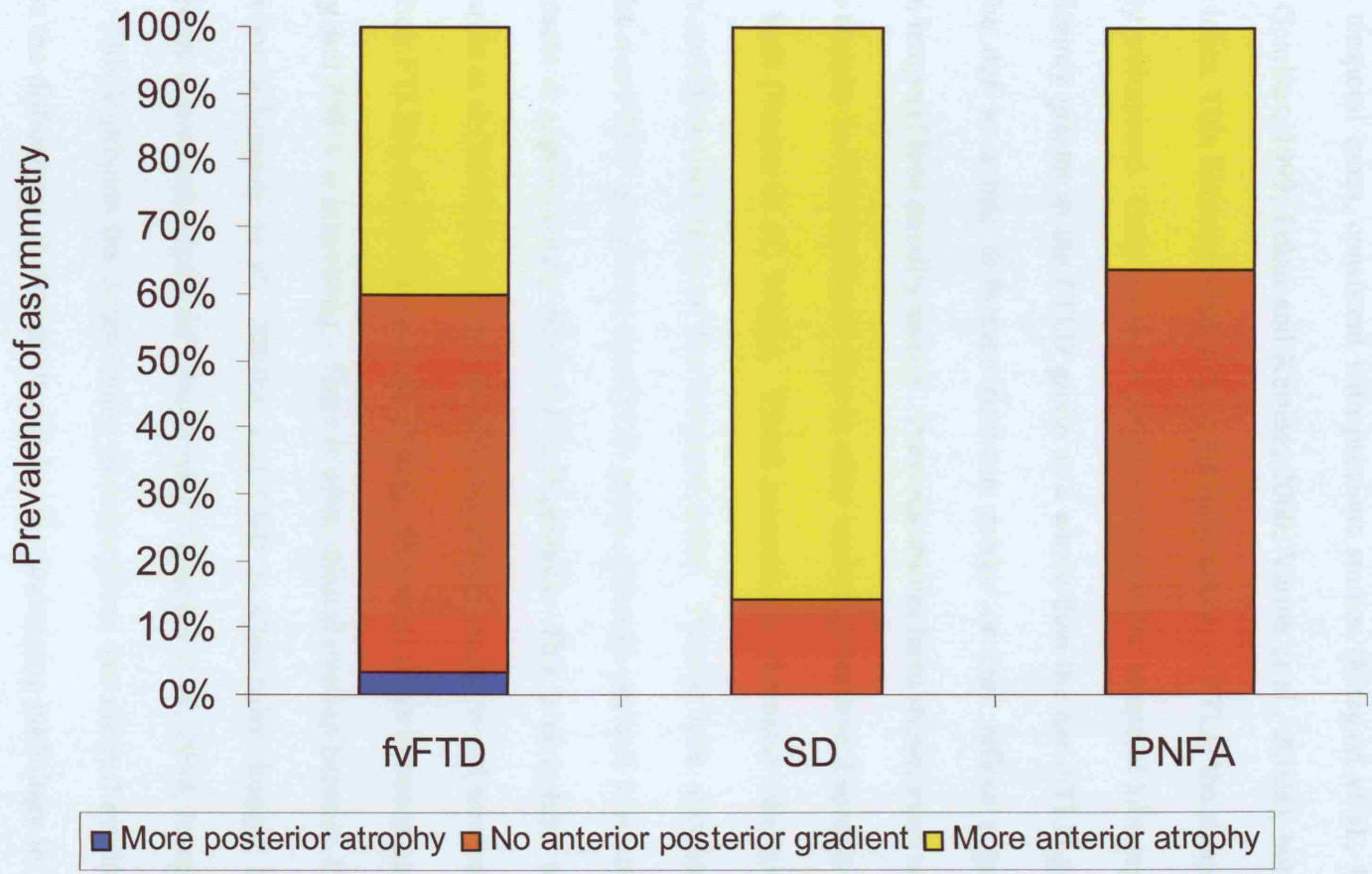

4.4. Discussion

This chapter used visual ratings to characterise the patterns of regional atrophy in FTLD. The FTLD group showed patterns of atrophy affecting predominantly the frontal and temporal lobes, consistent with previous studies (Kitagaki et al., 1998; Miller and Gearhart, 1999; Fukui and Kertesz, 2000; Varma et al., 2002a), but also the parietal lobes. This illustrates that despite the focal nature of FTLD the atrophy is actually very widespread. Only the mean atrophy scores in the temporal lobe regions were significantly greater in the FTLD group as a whole than the non-FTLD group. This may be due to a true difference between groups or may reflect a greater reliability in temporal lobe atrophy ratings. Previous studies have shown more severe frontal lobe atrophy in FTLD patients than in other neurodegenerative disorders such as AD and VaD (Varma et al., 2002a). Visual assessments of frontal lobe atrophy may be less sensitive than those of the temporal lobes. Parietal lobe atrophy was greater in the non-FTLD group than the FTLD group, although parietal lobe atrophy was still present in approximately 30% of FTLD patients. This is consistent with a study by Varma et al (2002) that found parietal lobe atrophy using visual assessments in 52% of their FTLD cohort (Varma et al., 2002a). The association between parietal lobe atrophy and PNFA is interesting. There is often clinical overlap between PNFA and CBD (Gorno-Tempini et al., 2004b), and CBD is classically thought to be characterised by asymmetrical parietal lobe atrophy (Groschel et al., 2004; Josephs et al., 2004a). This highlights the commonality between these two clinical syndromes and explains the difficulty in distinguishing in life the underlying pathology in these cases.

Frontal and temporal lobe atrophy was present across all three syndromic groups of FTLD. The SD patients showed the most severe pattern of atrophy affecting the left temporal lobe, especially the fusiform and parahippocampal gyri with a relative sparing of the superior temporal gyrus. These patterns of atrophy in the SD group are consistent with a number of previous MRI studies (Chan et al., 2001b; Galton et al., 2001a). Galton et al (2001) performed visual assessments of temporal lobe atrophy and similarly found significantly more atrophy in the parahippocampal gyrus in SD patients than in fvFTD patients (Galton et al., 2001b). The fvFTD and PNFA groups showed less severe temporal lobe atrophy than the SD patients. The bilateral medial temporal lobes were the most severely affected temporal structures in fvFTD, while the left superior temporal gyrus was the most severely affected in PNFA. There were no significant differences in frontal lobe atrophy score between the syndromic groups, however, severe frontal lobe atrophy was most common in the fvFTD patients. There was also a suggestion that the frontal atrophy in SD mainly involved the left orbitofrontal cortex. Indeed, orbitofrontal atrophy has previously been reported in SD patients in studies using VBM (Rosen et al., 2002c).

Asymmetric patterns of atrophy were common in the FTLD group. Fifty-eight percent of the FTLD patients showed asymmetry in the temporal lobes, and 42% in the frontal lobes. Asymmetry in the parietal lobes was rare (12%), and no asymmetry was observed in the occipital lobes. The left hemisphere typically showed more atrophy than the right, although right greater than left asymmetries were present in the temporal lobes in 10% of FTLD subjects. Miller and Gearhart (1999) similarly found asymmetry on MRI in over 50% of FTLD patients (Miller and Gearhart, 1999). In contrast, the non-FTLD patients were rarely asymmetric. This difference has been

noted by previous studies (Varma et al., 2002a), and asymmetry has been shown to be useful in the differential diagnosis of FTLD from AD (Boccardi et al., 2003; Likeman et al., 2005). However, it is clear from the analysis of the different subgroups of FTLD that the asymmetry comes predominantly from the SD and PNFA patients, the fvFTD group were relatively symmetrical.

An anterior-posterior gradient of atrophy was also common in the FTLD patients. Fifty-two percent had greater atrophy in anterior than posterior regions; whereas a posterior-anterior gradient was rare (2%). The non-FTLD patients showed the opposite pattern with an anterior-posterior gradient only present in 13% of patients, and a posterior-anterior gradient relatively more common and present in 23% of patients. This is perhaps unsurprising given that the non-FTLD group consisted predominantly of AD patients which have been reported to show a posterior pattern of atrophy (Rombouts et al., 2000; Baron et al., 2001; Boxer et al., 2003; Bonte et al., 2004; Likeman et al., 2005). The presence of an anterior-posterior gradient of atrophy on MRI could therefore be useful diagnostically. In fact, Sjogren et al found that an anterior-posterior gradient of cerebral blood flow could distinguish FTLD patients from both AD and subcortical white matter dementia patients (Sjogren et al., 2000a), and a recent study by Likeman et al showed that presence of an anterior-posterior gradient and asymmetry of atrophy on MRI were 85% specific for FTLD, when compared to AD and other neurodegenerative disorders (Likeman et al., 2005). The present study has extended these previous results by demonstrating that while the anterior-posterior gradient of atrophy does occur in all three syndromic variants of FTLD; it is significantly more common in the SD variants reflecting the severe anterior temporal and frontal lobe atrophy present in these subjects.

This study has the advantage that it used a large group of subjects (n=98) and all the assessments were performed in a blinded and randomised fashion. However, the subjects in this study were diagnosed clinically. Post mortem provides the only true 'gold standard' diagnosis. Pathological confirmation was however available in approximately 20% of cases.

4.5. Conclusion

This chapter used visual assessments to investigate the patterns of regional atrophy in FTLD. It showed that FTLD is associated with an asymmetric pattern of atrophy affecting predominantly the frontal and temporal lobes, often with an anterior > posterior gradient of atrophy, and that each of the syndromic variants of FTLD have a different pattern of atrophy at least at the group level. However, visual assessments of atrophy are subjective and may have varying levels of reliability throughout the brain. Assessments of parietal lobe asymmetry were particularly difficult. Although visual assessments are not perfect they do give a good overview of the patterns of atrophy in these disorders, and serve as a guide for future chapters that apply more automated methods.

5. Cross-sectional pattern of atrophy in the syndromic variants of FTLD

5.1. Introduction

As discussed in chapter 2, MRI has become increasingly recognised as a useful tool in FTLD. It has contributed to the identification of different patterns of atrophy in the different syndromic variants of FTLD (chapter 4). The pattern of atrophy in the SD variant has perhaps been most studied and results are relatively consistent across studies. The most severely affected structures are found in the temporal lobes, especially in the left, or dominant, hemisphere (Mummery et al., 2000; Chan et al., 2001b; Galton et al., 2001a; Rosen et al., 2002c). However, the fvFTD and PNFA groups appear to show more variability. The behavioural or frontal-variant (fvFTD) group is generally associated with atrophy involving the frontal and anterior temporal lobes bilaterally, although the reported focus of atrophy often varies in different studies (Boccardi et al., 2002; Rosen et al., 2002c; Boccardi et al., 2005). In PNFA atrophy is generally found to be greatest in the left (dominant) hemisphere, and the focus is in the perislyivan region, although various different distributions have been reported (Abe et al., 1997; Nestor et al., 2003a; Gorno-Tempini et al., 2004a; Grossman et al., 2004). Whilst each clinical group has distinctive diagnostic features, all three show considerable overlap in clinical, language and behavioural deficits, and can be difficult to diagnose from each other. Therefore, the careful characterisation of differences in the patterns of atrophy between groups on MRI may help in the diagnosis of the clinical groups.

A number of studies have used detailed regional measurements to assess patterns of atrophy in the syndromic variants of FTLD (Frisoni et al., 1999; Fukui and Kertesz, 2000; Chan et al., 2001b; Galton et al., 2001a). However, regional measures are laborious and time-consuming, neuroanatomical boundaries and definitions vary between studies, and are subject to wide inter-rater and intra-rater variability. Visual assessments of patterns of atrophy (as discussed in chapter 4) are subjective and may lack sensitivity. In addition, these techniques also require a priori decisions concerning which structures to measure/rate. The technique of VBM provides an automated unbiased alternative. It allows the assessment of patterns of atrophy throughout the whole brain without a priori decisions concerning which structures to assess. It incorporates a number of pre-processing steps (see chapter 3); scans are spatially normalised into a standard space, segmented into grey matter, white matter and CSF, and smoothed in order to conform to the assumptions of VBM. Voxel-wise statistical tests are then performed throughout the data. This technique has been used in the past to document structural brain abnormalities in a number of diseases, including AD (Rombouts et al., 2000; Baron et al., 2001) and Huntingdon's disease (Thieben et al., 2002).

VBM has also been applied to analyse the patterns of atrophy in the different syndromic variants of FTLD (Mummery et al., 2000; Good et al., 2002; Rosen et al., 2002c; Boxer et al., 2003; Nestor et al., 2003a; Sonty et al., 2003; Gorno-Tempini et al., 2004a; Grossman et al., 2004). Whilst these VBM studies have provided detailed and useful assessments of patterns of atrophy, the patient groups have been relatively small, and the results are variable and difficult to compare between studies. Subjects tend to vary in age and disease severity, patient groups are often diagnosed using

slightly different clinical criteria, and different studies use different variations of the VBM pre-processing steps. For example, some studies modulate the data in order to compensate for volume change during normalisation, while others do not. The large number of pre-processing steps, and the available modifications of each step, can potentially complicate the interpretation of regional volume loss. In addition, previous studies have not always customised the normalisation templates or the segmentation prior probability maps to the study population. Chapter 3 discussed the importance of using customised templates and prior probability maps created from both control and disease subjects. This reduces the differential bias in normalisation accuracy between patients and healthy controls, and improves the segmentation of severely atrophic subjects. Several previous studies have used a 12mm FWHM smoothing kernel, whereas recent work has suggested that an 8mm FWHM smoothing kernel may provide a more accurate assessment of brain volume loss based on T1-weighted volumetric scans (see chapter 3).

The aim of this chapter was to investigate the cross-sectional patterns of regional atrophy in large groups of fvFTD, SD and PNFA patients, and to identify regions specific to each group and common across all three groups. The analysis was performed using VBM to provide an unbiased assessment of atrophy across the whole brain. The traditional method (Ashburner and Friston, 2000) was optimised by using customised templates and prior probability maps, and an 8mm FWHM smoothing kernel. Detailed assessments of neuropsychological and behavioural data were performed in order to relate the patterns of atrophy to specific functional deficits in each syndromic group.

5.2. Methods

5.2.1. Subjects

Patients were recruited from the Specialist Cognitive Disorders Clinic (chapter 3). A detailed history, neurological and general examination, screening blood tests, neuropsychometry (including the MMSE), and MR imaging had been performed for all subjects. Disease duration was defined as the time from first symptom onset to MRI. Fifty-three patients fulfilling consensus criteria for FTLD were included (Neary et al., 1998). Twenty of these patients were diagnosed with fvFTD, 17 with SD, and 16 with PNFA. The FTLD subgroups were matched for age, gender, scanner and disease duration. Post-mortem confirmation was obtained in nine FTLD subjects (three PiD, three FTLD-U, two tau positive with a tau exon^{10+16} mutation, and one CBD). The case with CBD pathology was included in the study since they met criteria for the clinical diagnosis of FTLD at the time of scan. CBD has been increasingly considered part of the pathological spectrum of FTLD (see chapter 1). The distribution of the pathological diagnoses within the clinical subgroups is shown in table 5-1. The majority of patients were followed-up over time. Three cases of PNFA went on to develop clinical features of CBD (including gait disturbances, myoclonic jerks, extrapyramidal signs, cogwheeling and hesitant walk) later in the disease course (not including the case with CBD pathology).

The cohort was also age, gender and scanner matched to 15 healthy controls. The control subjects were typical of normal ageing and had no complaints of cognitive impairment or behavioural problems. Exclusion criteria included a history of stroke or dementia.

5.2.2. Neuropsychological assessments

Comprehensive neuropsychological evaluations were performed near the time of the MRI scan as part of the clinic work-up. The standard test battery included measures of current intelligence, verbal and visual memory, naming, and perception and arithmetic. However, the specific tests performed on each subject varied to some extent. The tests administered on most (over 80%) subjects included the Wechsler Adult Inventory Scale (Wechsler, 1981), Recognition Memory Test for faces (RMF) and words (RMF) (Warrington, 1984) and either the Graded Naming Test (GNT) (McKenna and Warrington, 1983) or the Oldfield naming test (Oldfield and Wingfield, 1965). The homophone meaning generation (HMG) test was performed on the fvFTD patients only. Neuropsychological data was unavailable for five subjects (one fvFTD, two SD and two PNFA).

5.2.3. Behavioural assessments

Behavioural abnormalities were assessed from the medical records of each patient. Features were graded as either present or absent and grouped into a number of categories, based on those used in two widely used behavioural scales (the NPI (Cummings et al., 1994) and MOUSPAD assessment scales (Allen et al., 1996)). The study evaluated the following aspects of behaviour:

1. *Social and personal*: disinhibition or inappropriate behaviours, impaired insight and loss of empathy.
2. *Affect*: dysphoria, euphoria, anxiety, agitiation, apathy and irritability
3. *Eating and oral behaviours*: overeating, cramming, altered food preference, food fads, weight gain and the carer limiting food intake.

4. *Obsessions and rituals*: simple motor stereotypies, perseveration, repetitive speech, mental rigidity, hoarding, counting/ordering, fixed route wandering, and compulsive symptoms such as clock watching.
5. *Psychiatric disturbances*: hallucinations and delusions.
6. *Function*: driving and poor self care.
7. *Other*: aggression was assessed as a separate feature.

Detailed behavioural data was unavailable for two subjects (both SD).

5.2.4. Imaging

The standard imaging protocol described in Appendix 4 was used for acquisition of T1-weighted images. Analysis was performed using SPM99 running under MATLAB 6®. VBM analysis was performed using the procedures outlined in chapter 3. In order to optimize normalization, a customized template was based on MR brain images from a group of 10 healthy controls and 10 patients with FTLD, age- and gender-matched to the study cohort and acquired on the same scanner; these template images were normalized to the Montreal Neurologic Institute (MNI) standard brain, and the mean template image was smoothed with an isotropic Gaussian kernel of 8mm FWHM. All study images were normalized to this customized template and each normalized image was segmented into grey matter, white matter and cerebrospinal fluid using customized prior probability maps. Each grey matter and whiter matter image was masked with a brain region to exclude all non-brain voxels; brain masks were created using a semi-automated technique based on MIDAS image analysis software as described previously. All images were modulated and smoothed with an isotropic Gaussian kernel of 8mm FWHM. The

smoothed images were analysed using a single subject condition and covariate model that incorporated age and gender as nuisance variables. MMSE score was also included as a nuisance variable to correct for differences in disease severity between the clinical subgroups. Grey and white matter analysis was performed using the average MIDAS-derived whole brain mask, and CSF analysis was performed over the whole brain image using the SPM default mask (i.e. including CSF).

Regional grey matter, white matter and CSF images were compared between each clinical subgroup and controls. Differences were assessed both at an uncorrected statistical threshold ($p<0.001$) and after correction for multiple comparisons over the whole brain volume (Family wise error) ($p<0.05$). Inclusive masking was used to identify voxels at which grey matter volume loss occurred in every FTLD subgroup relative to controls. To identify regions of atrophy specific to each group direct comparisons were performed between each group and the other two groups, i.e. the fvFTD group was compared directly to the SD and PNFA groups, the SD group was compared directly to the fvFTD and PNFA groups, and the PNFA group was compared directly to the fvFTD and SD groups.

5.2.5. Statistics

Statistical analysis was performed in STATA version 8. Age, MMSE and disease were compared between groups using the Mann Whitney U test. Gender ratios were compared using the Fisher's exact test. The proportion of abnormal behavioural features in each FTLD subgroup was compared using the Fisher's exact test.

5.3. Results

5.3.1. Patient characteristics

There was no significant difference in age or gender distribution between the controls and the FTLD group, or any of the clinical FTLD subgroups (table 5-1). The FTLD group had a significantly lower MMSE score than the controls ($p<0.0001$), and the SD ($p=0.02$) and PNFA ($p=0.02$) groups had a significantly lower MMSE score than the fvFTD group. There was no significant difference in disease duration between any of the three clinical subgroups of FTLD. Post-mortem confirmation was available in five fvFTD patients, two SD patients and two PNFA patients (table 5-1).

Table 5-1: Patient characteristics

	C (n=15)	FTLD (n=53)	FvFTD (n=20)	SD (n=17)	PNFA (n=16)
Gender (M:F)	8:7	36:17	16:4	9:8	11:5
Age (yrs)	62.6 (28.9)	63.2 (7.0)	62.3 (6.9)	64.4 (18.2)	63.0 (8.1)
MMSE (/30)	28.9 (1.0)	20.6 (8.4)*	25.0 (4.0)*	18.2 (9.9)*‡	18.2 (9.4)*‡
Duration (yrs)	NA	4.6 (2.0)	4.9 (2.2)	4.3 (1.7)	4.5 (2.0)
Pathology (No. cases)					
PiD	NA	3	1	1	1
FTLD-U	NA	3	2	1	0
tau exon^{10+16}	NA	2	2	0	0
CBD	NA	1	0	0	1

*Age, MMSE and duration are expressed as mean (standard deviation); * Significantly different from controls ($p<0.05$); ‡ Significantly different from fvFTD ($p<0.05$); NA = not applicable; F = female, M = male*

5.3.2. Neuropsychological assessment

The mean absolute time between neuropsychological assessment and MR scan was 4.4 ± 4.8 (mean ± standard deviation) months. The neuropsychological results are shown in table 5-2. The fvFTD patients had IQ scores a little below published population averages (Wechsler, 1981), with a mean verbal IQ of 91.6 ± 18.0, and a mean performance IQ of 92.1 ± 21.0; the SD and PNFA patients also had below average IQ scores, and showed worse verbal IQ (SD 79.4 ± 16.5, PNFA 75.3 ± 12.0) than performance IQ (SD 94.2 ± 12.2, PNFA 89.0 ± 20.3). These mean scores do not include a small number of patients who were unable to be tested (severely affected language skills) in the PNFA and SD groups. Although all groups were poor at naming, this was much more pronounced in the SD group. A wide inter-individual variation in performance on the naming tests was observed in the fvFTD and PNFA patients, although the fvFTD patients did perform better on the GNT (fvFTD 16.2 ± 8.8, PNFA 12.1 ± 8.3). The majority of the SD patients could not score on the GNT and even scored poorly on the easier Oldfield. Similarly, a wide variation in performance was observed in the recognition memory test scores (for both words and faces). The SD patients appeared to perform worse on word recognition than the fvFTD and PNFA patients. All SD patients scored below the 25th percentile, compared to 55% of the PNFA patients and 65% of the fvFTD patients. The homophone meaning generation (HMG) test, a 'frontal' test, was only used in the fvFTD patients. They all performed below or severely below average, with the

majority of subjects scoring below the fifth percentile suggesting a loss of 'executive function' skills.

There is a degree of correlation between MMSE and neuropsychological scores in all groups. The average MMSE was highest in the fvFTD group. As discussed in chapter 1, the MMSE is not a reliable test of severity in FTLD. It is particularly sensitive to language deficits and therefore the language variants are likely to perform disproportionately badly.

Table 5-2: Neuropsychological data for each patient. The scores for naming, RMW, RMF and HMG are given in percentiles. NT = not performed.

				WAIS		Naming GNT or *easier Oldfield	RMW (/50) or *(/25)	RMF (/50), or *(/25)	HMG
Patient	Group	Age	MMSE	VIQ	PIQ				
1	fvFTD	62	30	130	136	<1	>75	>75	25-50
2	fvFTD	73	29	NT	NT	NT	NT	NT	NT
3	fvFTD	56	29	98	101	50-75	25-50	10-25	NT
4	fvFTD	68	28	131	105	>75	>75	50-75	5-10
5	fvFTD	47	28	84	85	1-5	<1	<1	NT
6	fvFTD	64	27	94	83	>75	10-25	1-5	<5
7	fvFTD	57	27	61	66	<1	<1	<1	NT
8	fvFTD	54	26	75	76	25-50	25-50	25-50	<5
9	fvFTD	69	25	87	102	<5*	<5*	<5*	NT
10	fvFTD	67	25	86	90	5-10	50-75	1-5	<5
11	fvFTD	65	24	99	79	50-75	5-10	10-25	5
12	fvFTD	54	24	91	96	<5*	<1	<1	NT
13	fvFTD	67	23	84	72	10-25	1-5	<1	NT
14	fvFTD	66	23	88	112	50-75	25-50	<1	<5
15	fvFTD	66	23	105	87	>75	<1	<1	<5
16	fvFTD	53	23	87	144	>75	<1	50-75	<5
17	fvFTD	74	22	75	75	1-5	NT	NT	<5
18	fvFTD	57	22	81	86	25-50	<1	<1	<5
19	fvFTD	62	17	74	67	<5*	NT	NT	NT
20	fvFTD	63	15	84	76	>75	<1	<1	<5
21	SD	60	28	NT	NT	NT	NT	NT	NT
22	SD	67	26	102	111	<5*	10-25	<1	NT
23	SD	55	26	Unable	Unable	<5*	NT	NT	NT
24	SD	64	25	78	98	<5*	<5*	10*	NT
25	SD	60	24	100	92	<5*	1-5	<1	NT
26	SD	59	24	76	104	<5*	<5*	50*	NT
27	SD	70	23	73	99	<5*	10-25*	5-10*	NT
28	SD	70	22	91	90	<5*	<5*	5*	NT
29	SD	57	19	76	87	<5*	<1	50-75	NT
30	SD	77	18	60	93	<5*	5*	10*	NT
31	SD	59	17	63	95	<5*	<5*	10-25	NT
32	SD	58	3	Unable	Unable	NT	NT	NT	NT
33	SD	68	0	53	60	<5*	NT	NT	NT
34	SD	72	0	NT	NT	NT	NT	NT	NT
35	SD	66	NT	68	92	<1	5*	1-5	NT
36	SD	66	NT	103	103	<5*	10-25	<1	NT
37	SD	57	NT	89	101	<1	10-25	50-75	NT
38	PNFA	67	30	NT	NT	NT	NT	NT	NT
39	PNFA	68	27	85	113	1-5	>75	25-50	NT
40	PNFA	53	27	96	83	50-75	5*	25*	NT
41	PNFA	61	25	73	117	25-50	25-50	50-75	NT
42	PNFA	65	24	NT	NT	NT	NT	NT	NT
43	PNFA	75	21	66	91	<5*	50*	25-50*	NT
44	PNFA	66	21	94	114	1-5	1-5	<1	NT
45	PNFA	56	20	75	72	50-75	1-5	50-75	NT
46	PNFA	63	16	60	76	<5*	NT	NT	NT
47	PNFA	63	15	76	85	1-5	5-10*	<5*	NT
48	PNFA	62	11	72	64	<1	<1	<1	NT
49	PNFA	54	5	57	74	<1	<1	<1	NT
50	PNFA	55	4	Unable	Unable	NT	NT	NT	NT
51	PNFA	65	NT	Unable	71	<5*	NT	NT	NT
52	PNFA	53	NT	79	122	50-75	>75	10-25	NT
53	PNFA	51	NT	71	75	5*	50-75	5-10	NT

5.3.3. Behavioural assessment

The most common behavioural features in the FTLD group were abnormal social behaviour or personality changes, eating behaviours, changes in affect and the presence of obsessive and ritualistic behaviours (table 5-3). Unsurprisingly, these four behavioural categories were most prevalent in the fvFTD group, with a frequency of over 70% in each category. Changes in eating and oral behaviours were the most common behaviours in the fvFTD group (95%), and were significantly more frequent than in both the SD ($p<0.001$) and PNFA ($p<0.002$) groups. Forty-two percent of the fvFTD patients displayed either poor self-care or problems driving. Approximately half of the SD patients showed abnormalities in social behaviour (47%), affect (47%), eating behaviour (47%) and obsessive and ritualistic behaviours (47%). The PNFA group generally had a low frequency of behavioural features, although obsessive and ritualistic behaviour was the most common feature, present in 50% of the cohort. Psychiatric disturbances were the least common feature in all three syndromic groups, only present in 15% of the fvFTD patients, 7% of the SD patients and 6% of the PNFA patients. Aggression was more prevalent in the fvFTD group (40%) than in the other subgroups (20% in SD, 13% in PNFA).

Table 5-3: Behavioural data

Behavioural category	FvFTD (n=20)	SD (n=15)	PNFA (n=16)	Total (n=51)
Social and personality	75‡	47	25	55
Affect	70	47	38	57
Eating / oral	95*‡	47	31	66
Obsessions and rituals	70	47	50	62
Psychiatric	15	7	6	11
Function	45	27	13	32
Aggression	40	20	13	28

*Data is expressed as % of patients with each behavioural feature; * Significantly different from SD ($p < 0.05$); ‡ Significantly different from PNFA ($p < 0.05$)*

5.3.4. VBM analysis

5.3.4.1. FTLD v controls

The FTLD group as a whole showed a widespread pattern of grey matter loss involving the frontal and temporal lobes, also with involvement of the parietal lobes, when compared with controls (figure 5.1). The losses were most marked in the left hemisphere, reflecting the large number of language variant cases included. Regions that survived the correction for multiple comparisons were found in the left insula and anterior temporal lobe ($p<0.05$). Significant white matter atrophy was found in the left temporal and frontal lobes, and around the lateral ventricles (figure 5.2). Significant CSF increases were observed around the temporal and frontal lobes, predominantly on the left, and throughout the lateral and third ventricles (figure 5.3).

Figure 5.1: Statistical parametric map showing regions of grey matter loss in FTLD compared with controls (uncorrected, p<0.001)

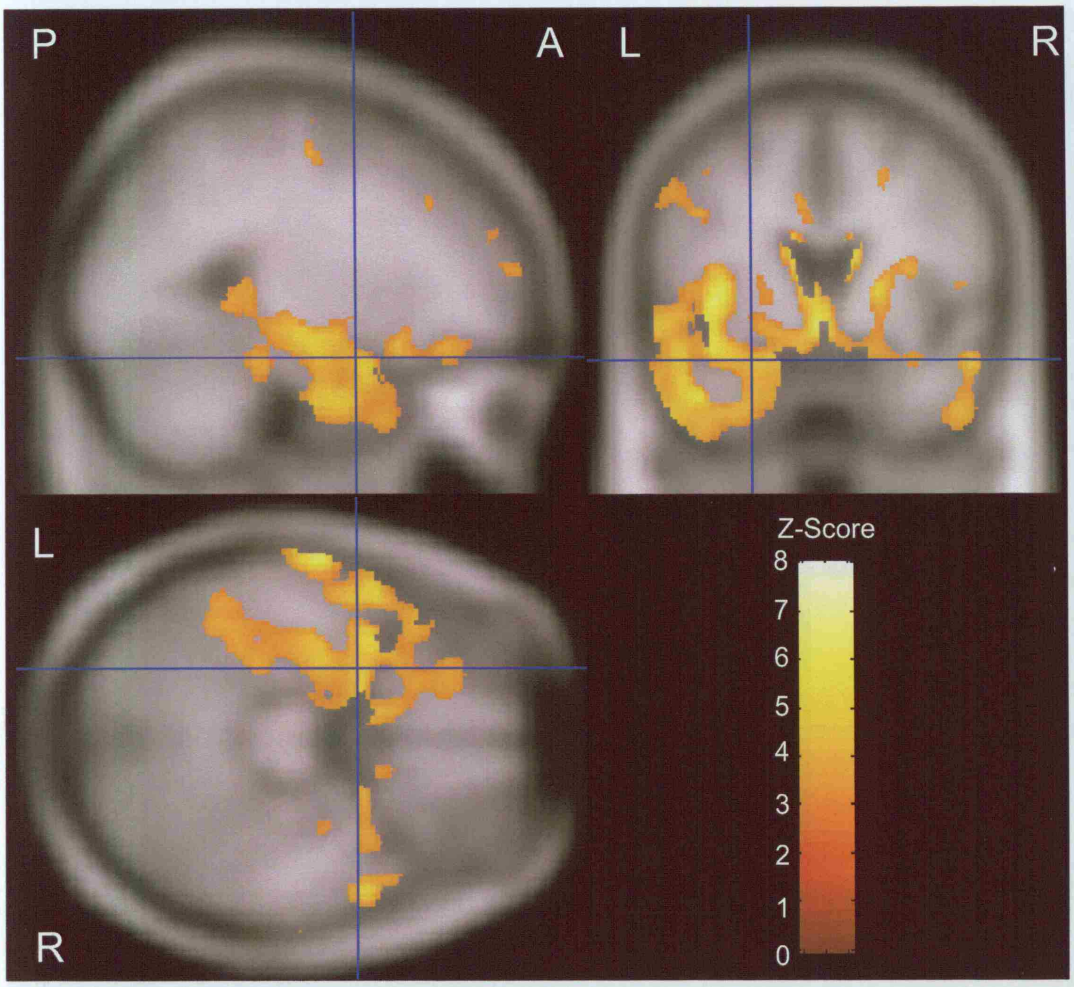

Figure 5.2: Statistical parametric map showing regions of white matter loss in FTLD compared with controls (uncorrected, p<0.001)

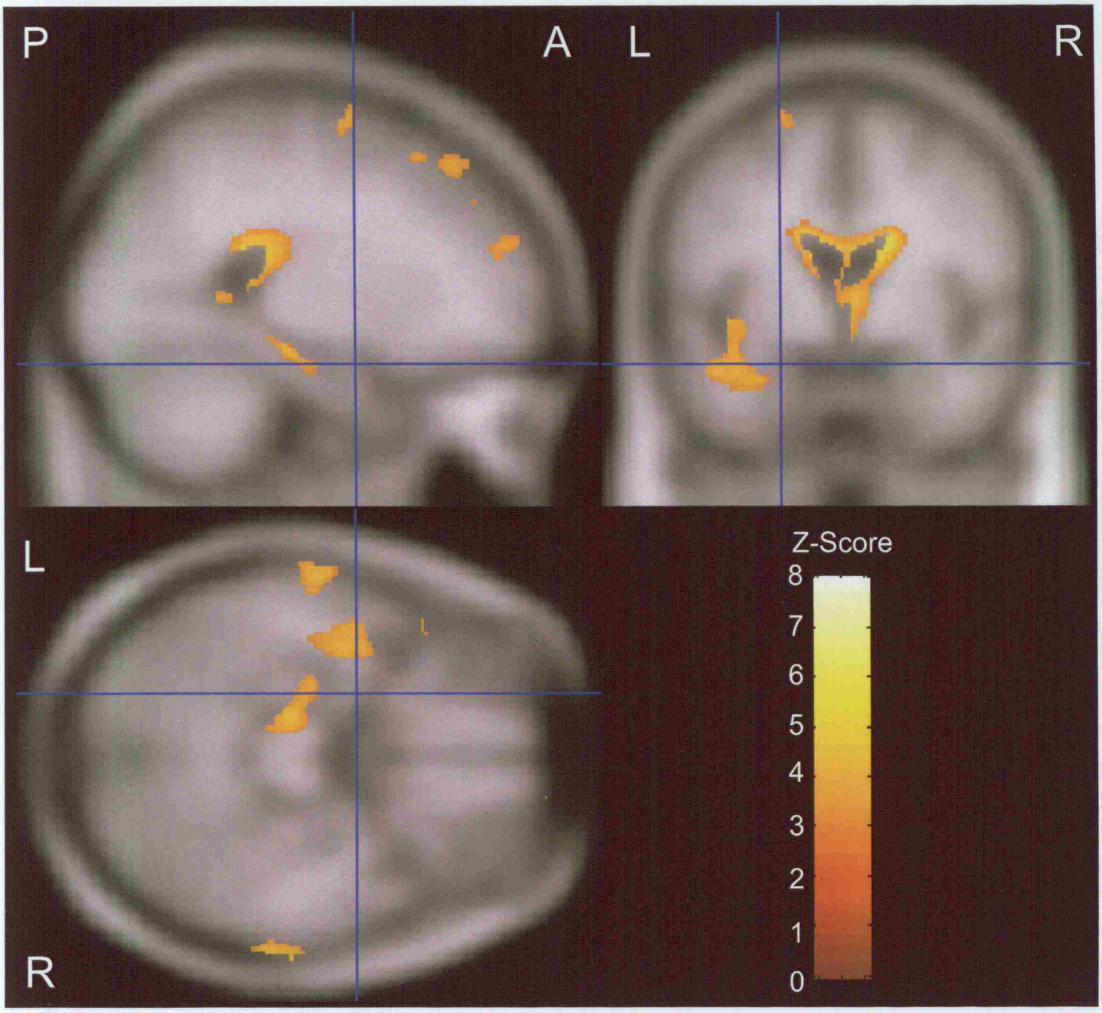

Figure 5.3: Statistical parametric map showing regions of CSF increase in FTLD compared with controls (uncorrected, p<0.001)

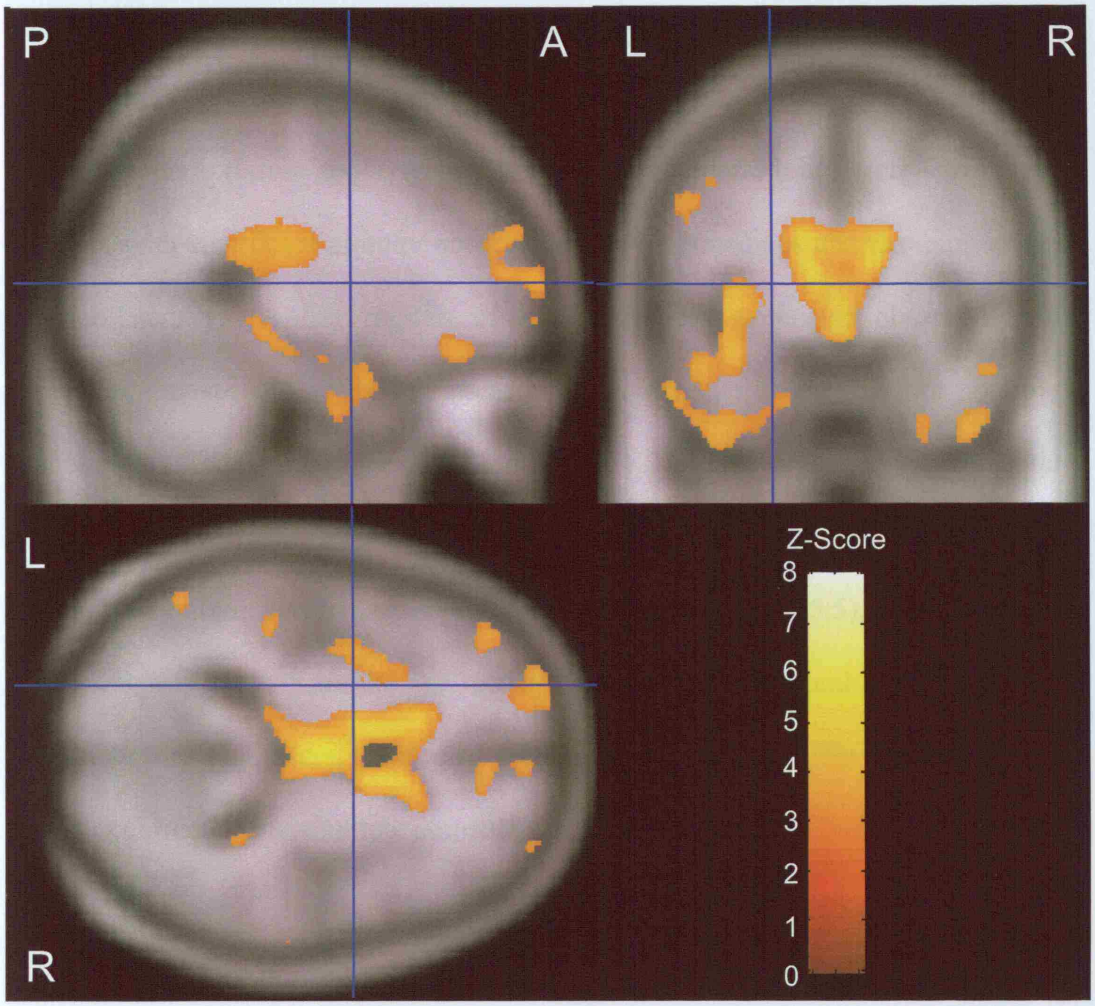

5.3.4.2. fvFTD v controls

The fvFTD group showed a widespread bilateral pattern of frontal lobe grey matter atrophy, with severe involvement of the frontal pole, compared to controls (figure 5.4). There was also involvement of the anterior cingulate, and apparent loss in the interhemispheric fissure and sylvian fissures. The temporal lobes were less severely affected, with significant atrophy observed in the hippocampus and parahippocampal gyrus bilaterally. A few regions of significant loss were also observed in the cerebellum, most likely reflecting intensity inhomogeneity on the scans or possibly a spatial normalisation bias due to frontal atrophy. There was no evidence for any left/right asymmetry in the patterns of grey matter atrophy. Significant white matter atrophy was only observed around the lateral ventricles (figure 5.5). Significant CSF expansion was present around the medial frontal lobes, temporal lobes, and in the sylvian fissure and lateral ventricles bilaterally (figure 5.6). No regions survived stringent correction for multiple comparisons (FWE) at $p<0.05$.

Figure 5.4: Statistical parametric map showing regions of grey matter loss in fvFTD compared with controls (uncorrected, p<0.001)

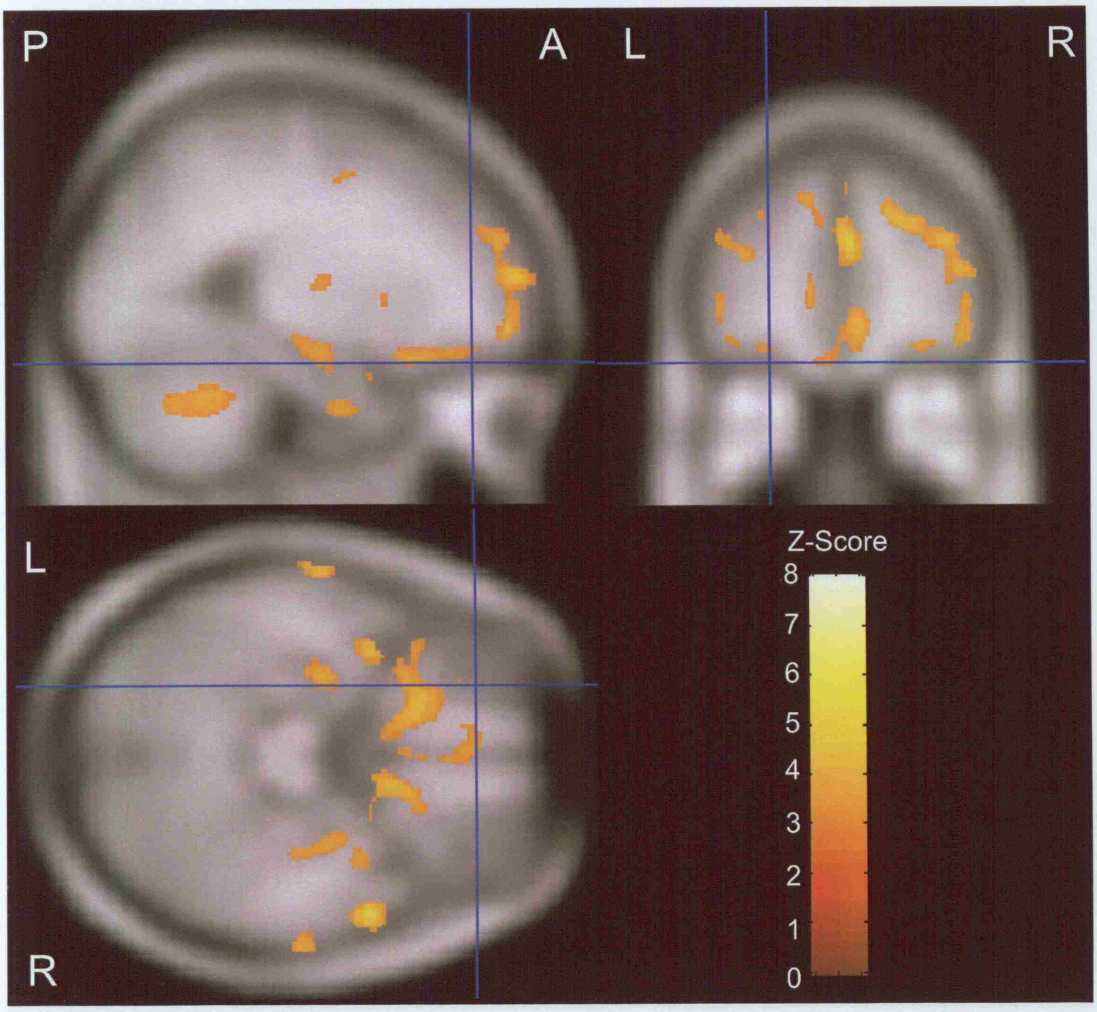

Figure 5.5: Statistical parametric map showing regions of white matter loss in fvFTD compared with controls (uncorrected, p<0.001)

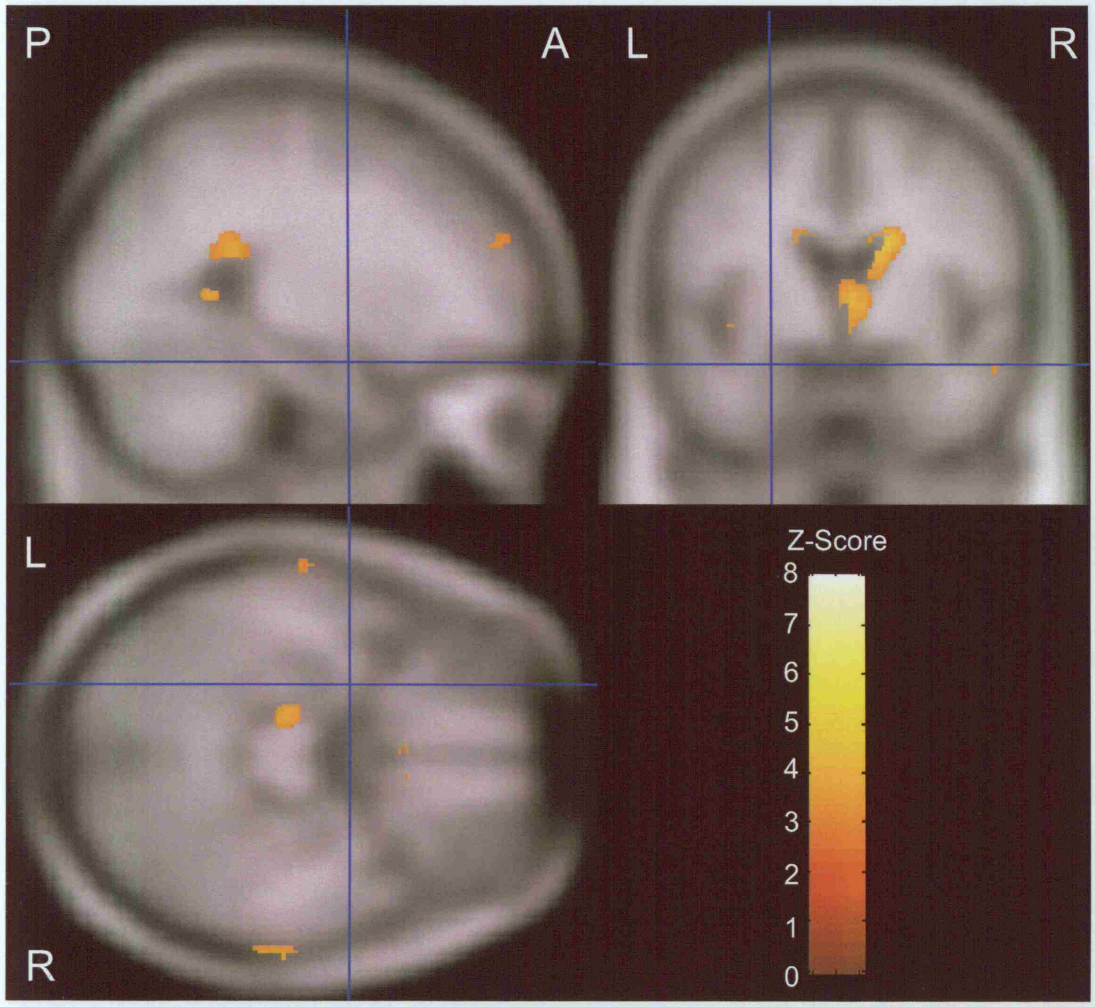

Figure 5.6: Statistical parametric map showing regions of CSF increase in fvFTD compared with controls (uncorrected, p<0.001)

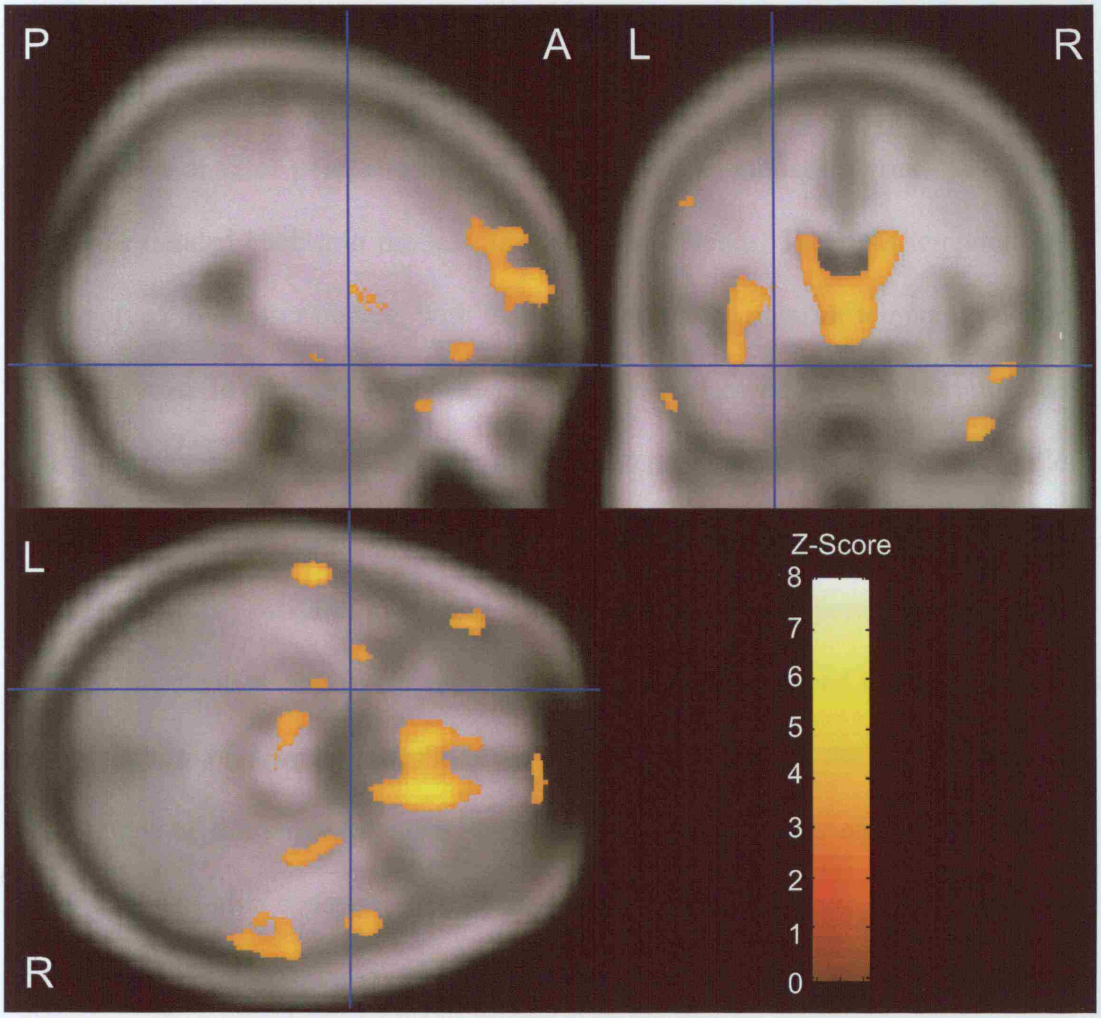

5.3.4.3. SD v controls

Severe grey matter atrophy was observed bilaterally in the temporal lobes of the SD group compared to controls (figure 5.7). The left temporal lobe was more severely affected than the right, with marked loss throughout all areas of grey matter, especially the anterior pole, and the inferior and middle temporal gyrus. Regions of loss also extended back into the left inferior parietal lobe. The right temporal lobe was involved to a lesser degree, with loss focussed on the anterior temporal pole and fusiform gyrus. In addition, grey matter atrophy was observed in the left orbitofrontal cortex, left anterior cingulate, and the insula bilaterally. Changes throughout the left temporal lobe survived the correction for multiple comparisons (FWE) with severe involvement of the fusiform gyrus and relative sparing of the superior temporal gyrus ($p<0.05$). A small region in the right temporal pole also survived the correction. A similar pattern of loss was observed in the white matter in the SD group, with involvement of the temporal lobes bilaterally, but more severe on the left. White matter loss was also observed around the lateral ventricles (figure 5.8). Significant CSF expansion was shown in the CSF spaces around the temporal lobes, but greater on left, and in the left sylvian fissure and the lateral ventricles (figure 5.9).

In an attempt to examine the progression of atrophy in the SD patients the group was split into two according to severity of naming impairment (based on the Oldfield). Group one included patients with an Oldfield score greater than or equal to seven (n=6), and group two included patients with an Oldfield score of less than seven (n=9). All subjects scored below the 5th percentile but the patients with a higher Oldfield show slightly less severe naming deficits. The patterns of grey matter atrophy in each group compared to controls are shown in figure 5.10. Group one

shows predominantly left temporal lobe atrophy, with a small region of loss in the right fusiform gyrus. Group two shows a more severe pattern of left temporal lobe atrophy with greater involvement of the right temporal lobe and the inferior frontal lobe.

Figure 5.7: Statistical parametric map showing regions of grey matter loss in SD compared with controls (uncorrected, p<0.001)

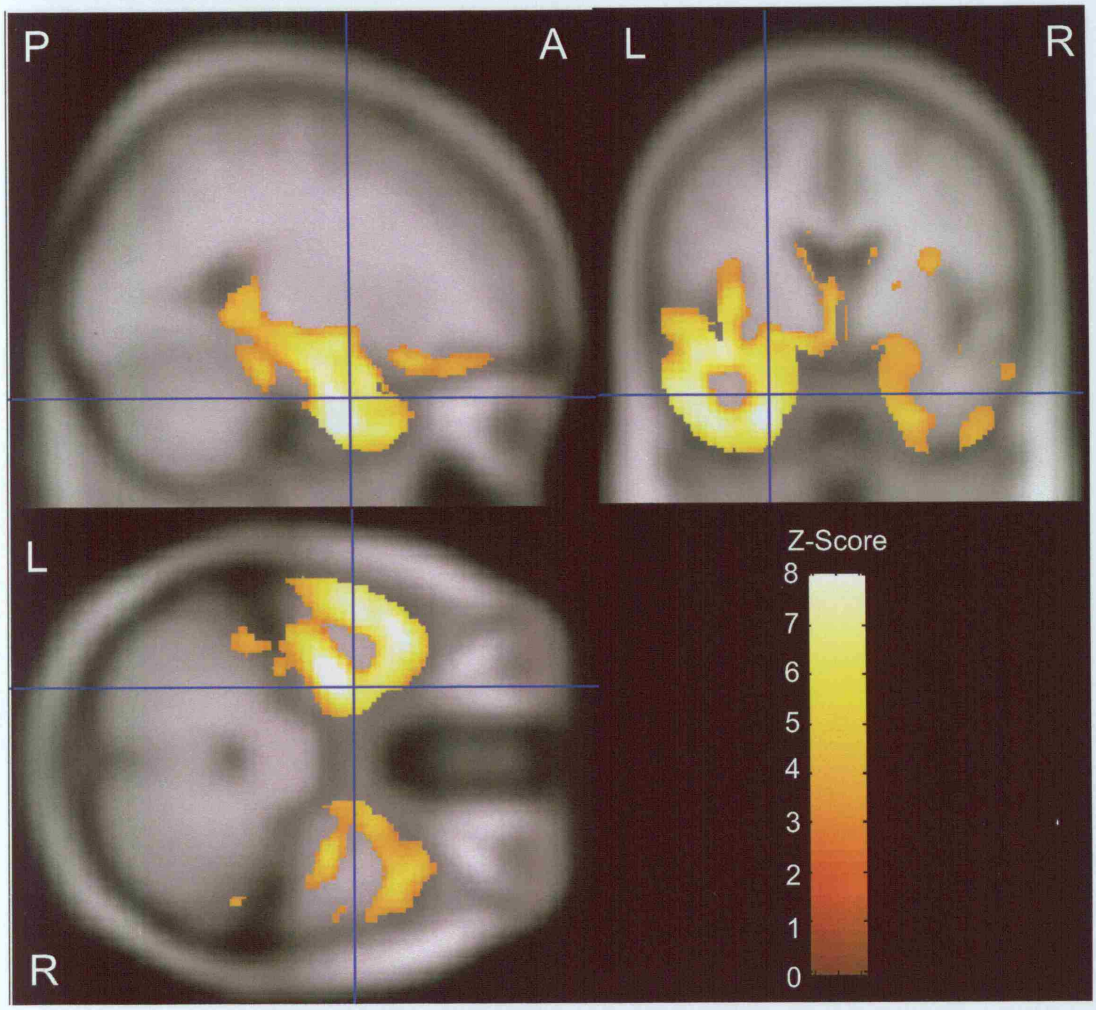

Figure 5.8: Statistical parametric map showing regions of white matter loss in SD compared with controls (uncorrected, p<0.001)

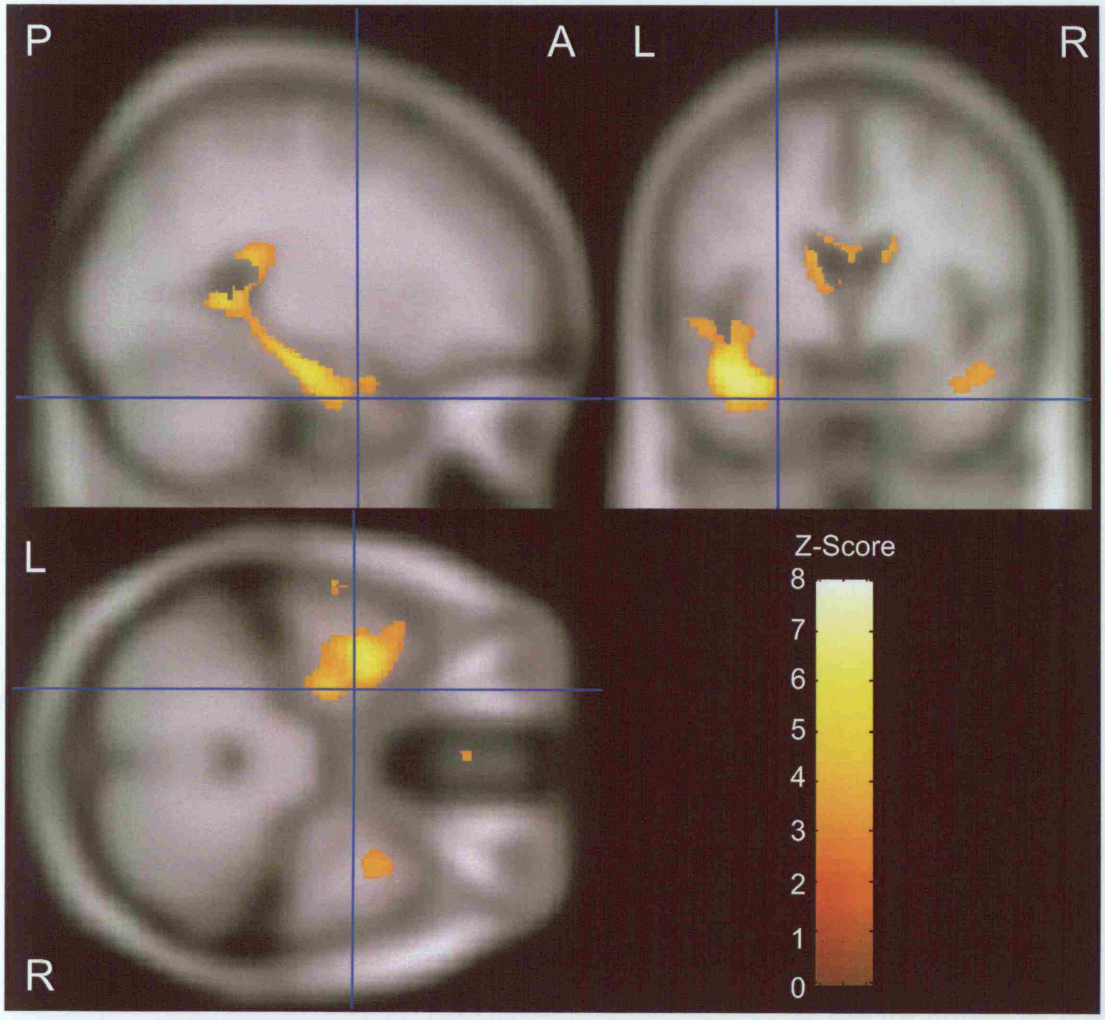

Figure 5.9: Statistical parametric map showing regions of CSF increase in SD compared with controls (uncorrected, p<0.001)

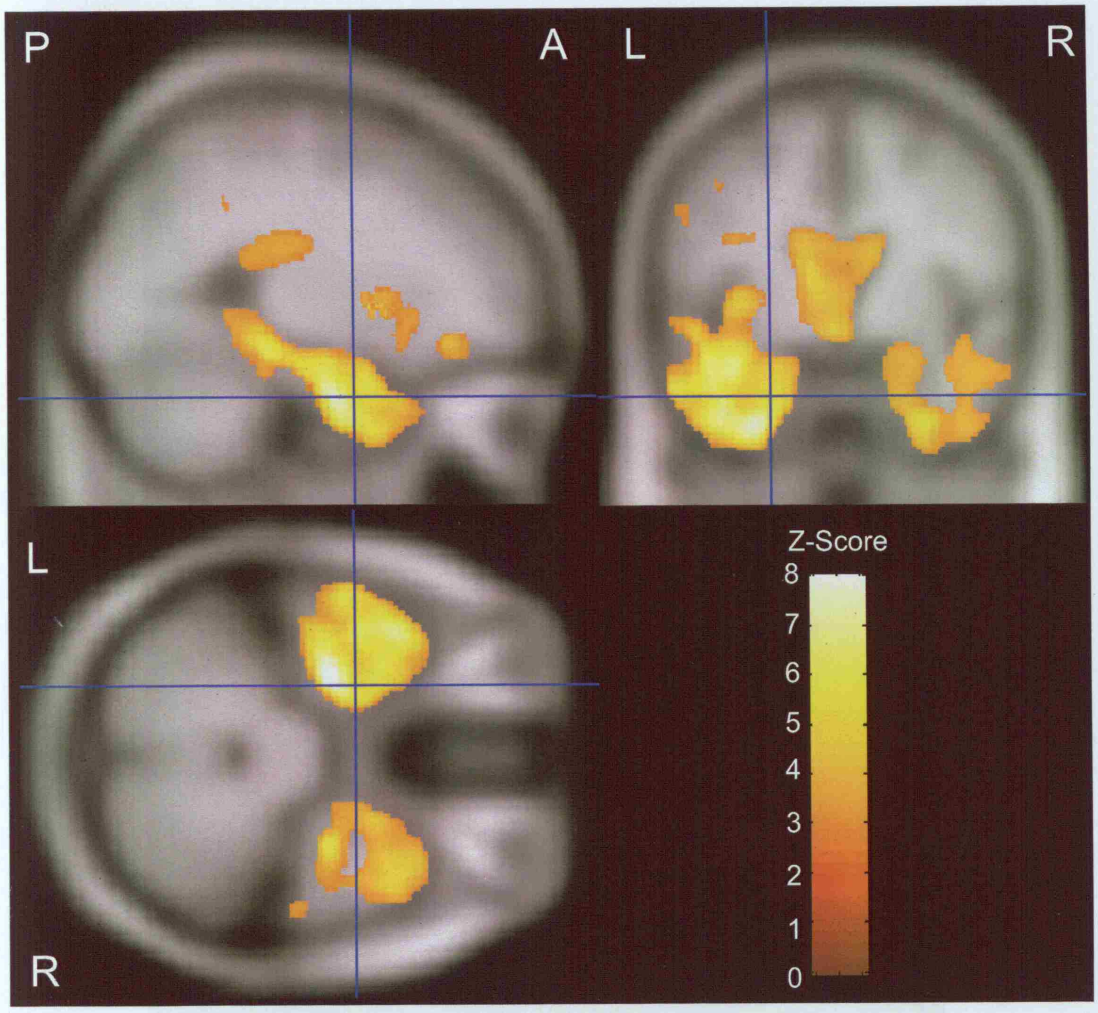

Figure 5.10: Statistical parametric map showing regions of grey matter loss in two groups of SD patients split according to severity of naming deficit, compared with controls (uncorrected, p<0.001). Group 1 = Oldfield ≥ 7 (n=6), Group 2 = Oldfield < 7 (n=9)

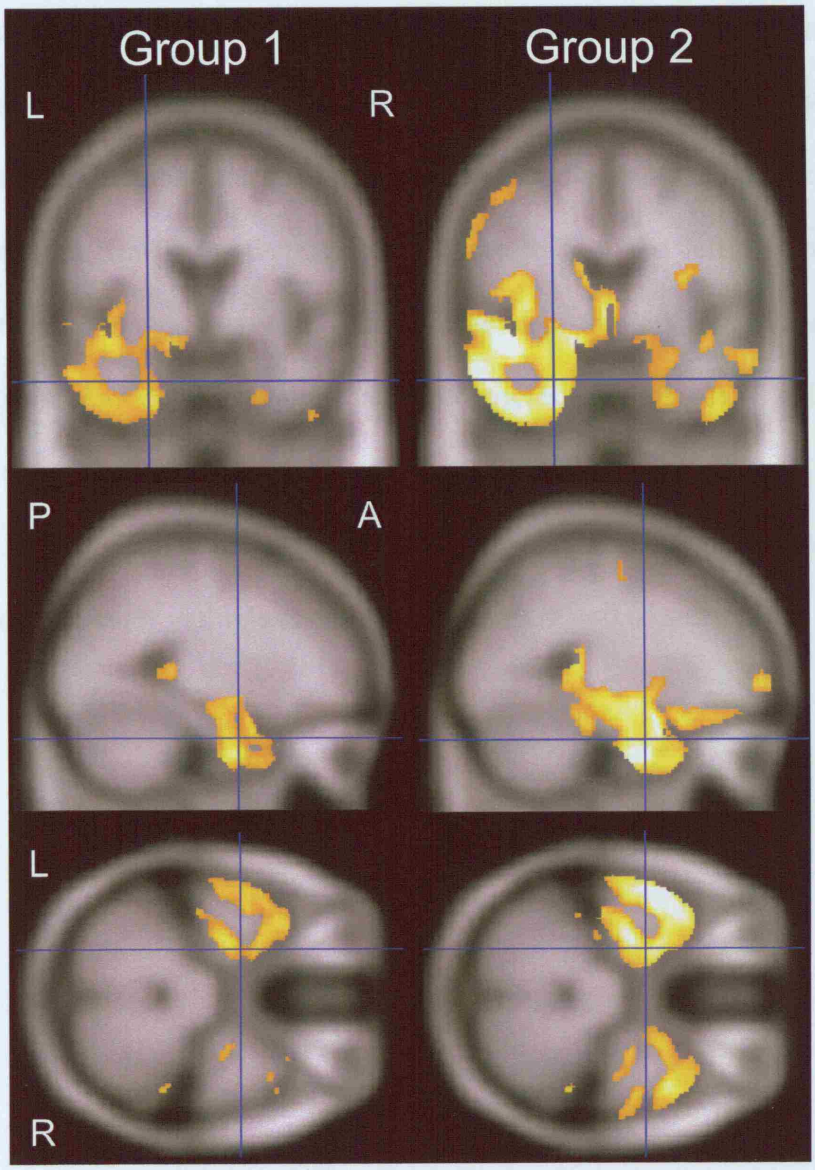

5.3.4.4. PNFA v controls

The PNFA group showed a left sided asymmetric pattern of grey matter atrophy involving the inferior frontal lobe, temporal lobe and insula compared to controls (figure 5.11). Apparent grey matter loss in the anterior interhemispheric fissure provided evidence of widespread frontal lobe atrophy. Significant grey matter atrophy was also observed in the left orbitofrontal cortex, the left anterior cingulate and the putamen. Regions that survived the correction for multiple comparisons were found along the frontal interhemispheric fissure and in the left insula ($p<0.05$). Regions of white matter loss were found scattered in the left frontal and temporal lobes, and were also found around the lateral ventricles (figure 5.12). Significant CSF increases were observed in the frontal interhemispheric fissure and the lateral ventricles (figure 5.13). No regions of white matter or CSF difference survived stringent correction for multiple comparisons (FWE) at $p<0.05$.

Figure 5.11: Statistical parametric map showing regions of grey matter loss in PNFA compared with controls (uncorrected, p<0.001)

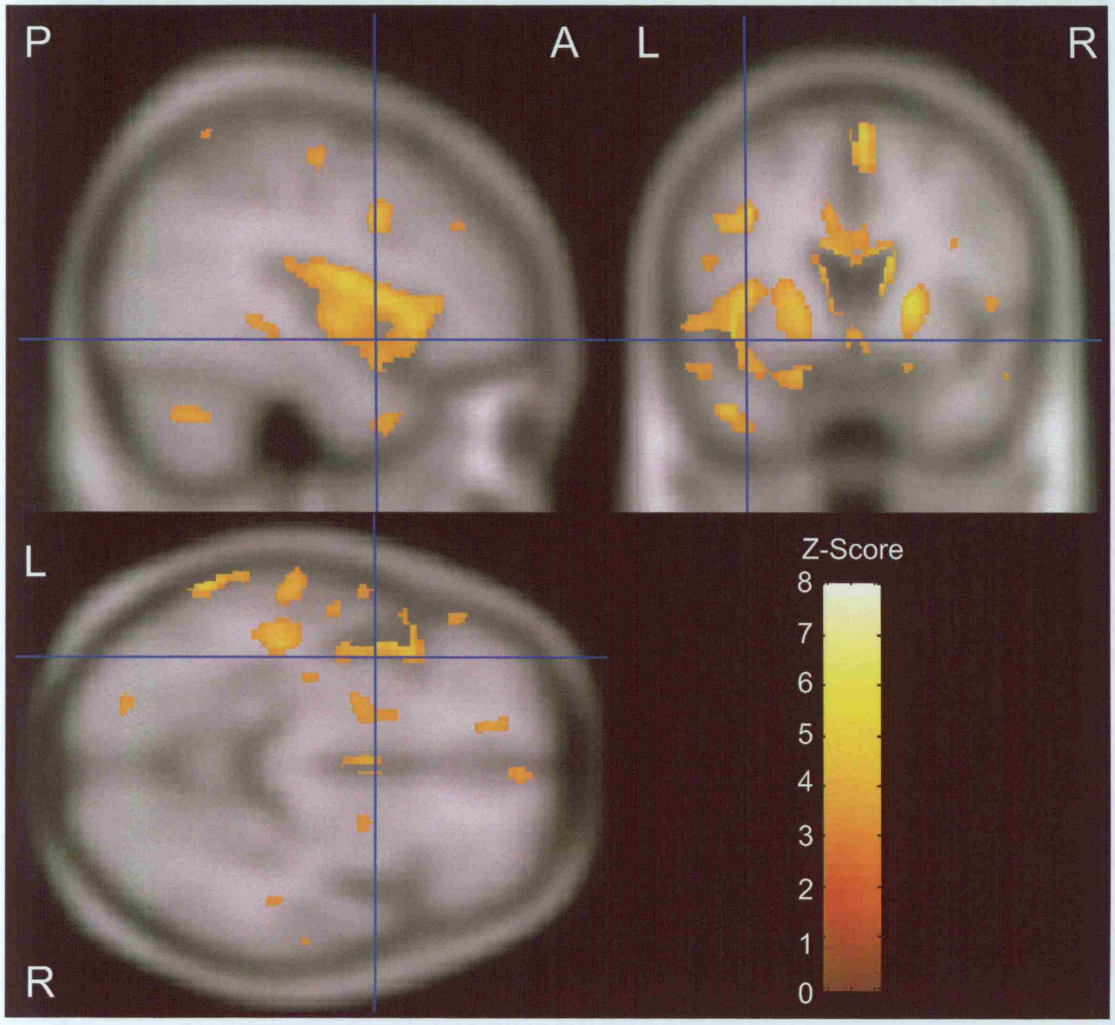

Figure 5.12: Statistical parametric map showing regions of white matter loss in PNFA compared with controls (uncorrected, p<0.001)

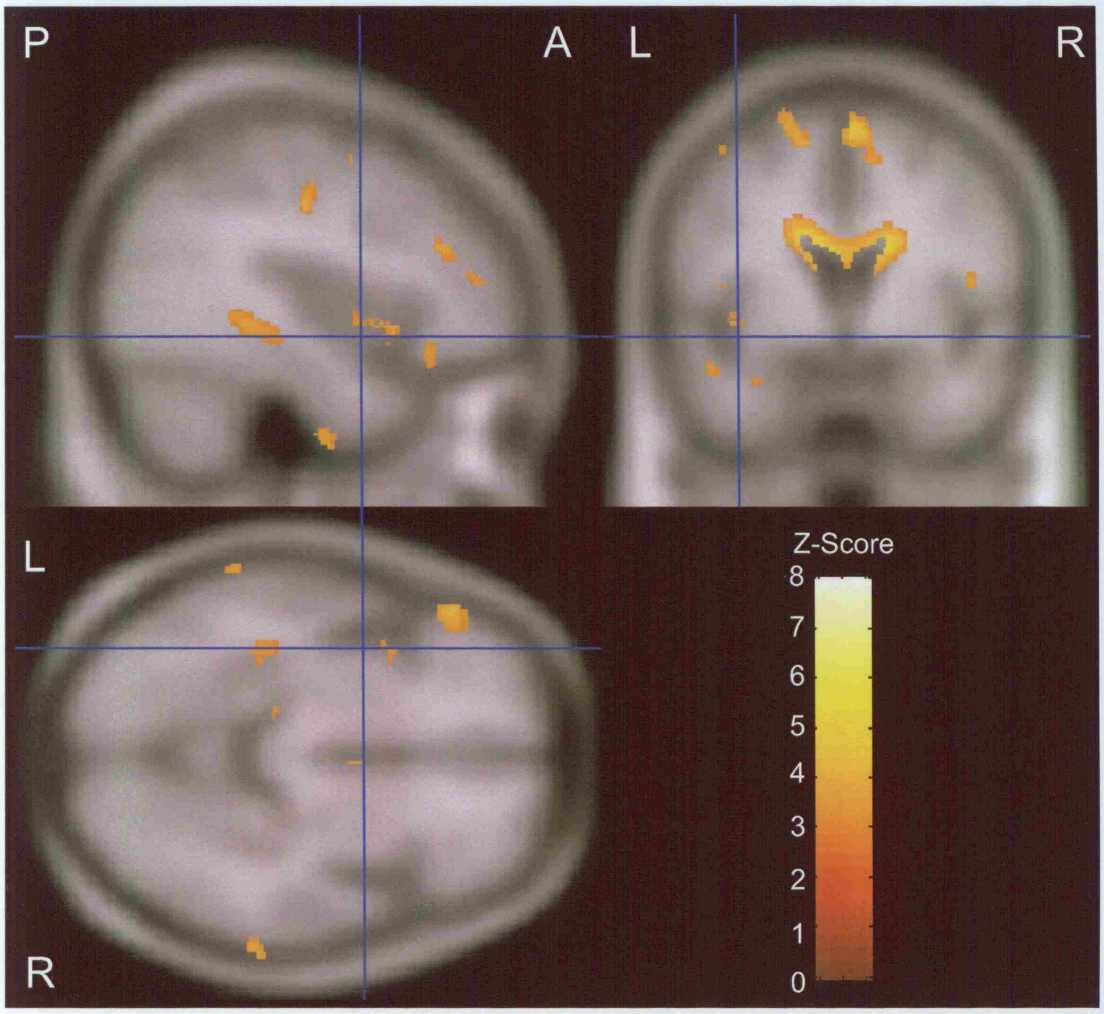

Figure 5.13: Statistical parametric map showing regions of CSF increase in PNFA compared with controls (uncorrected, p<0.001)

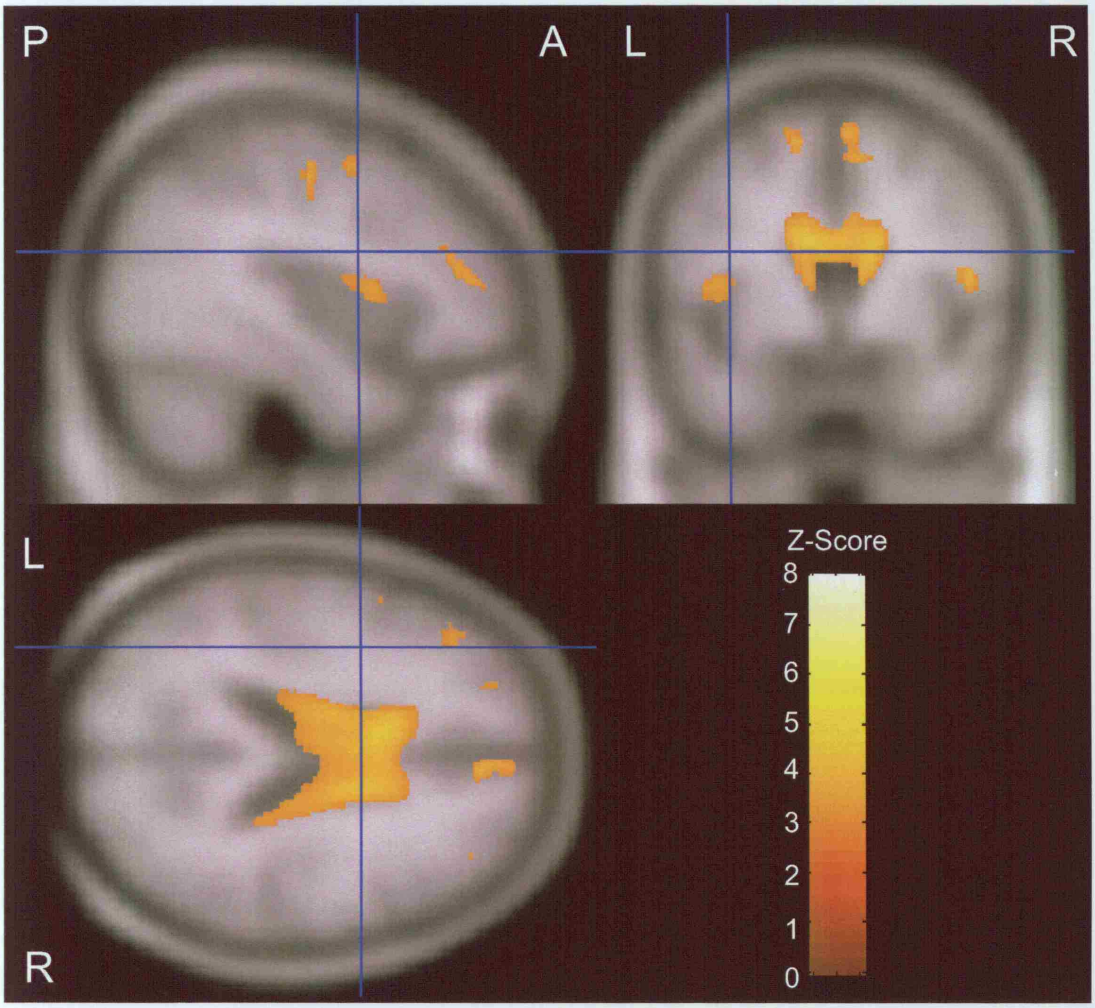

5.3.4.5. FvFTD v (SD and PNFA)

This comparison identified regions where significant grey matter loss was present in the fvFTD group compared to both the SD and PNFA groups (figure 5.14). Losses were found predominantly in the right frontal lobe, although apparent losses were also identified in the posterior cingulate and around the ventricles ($p<0.001$, uncorrected).

5.3.4.6. SD v (fvFTD and PNFA)

Regions of grey matter loss present in the SD group, compared with the fvFTD and PNFA groups, were found exclusively in the temporal lobes (figure 5.14). The left temporal lobe was the most severely affected with relative sparing of the superior temporal gyrus. The right temporal lobe was involved to a lesser degree, with loss found in the anterior temporal pole, medial temporal lobe and fusiform gyrus ($p<0.001$, uncorrected).

5.3.4.7. PNFA v (fvFTD and SD)

Very little significant atrophy was present in the PNFA group, compared with both the fvFTD and SD groups ($p<0.001$, uncorrected).

5.3.4.8. All groups v controls

This comparison identified regions of significant grey matter atrophy present in all three of the clinical subgroups when compared to controls (figure 5.15). Losses common to all groups were focused on the left insula. However, small regions of loss were also observed in the anterior cingulate, the orbitofrontal cortex and the left temporal lobe ($p<0.001$, uncorrected).

Figure 5.14: Statistical parametric map showing regions of grey matter loss in A) fvFTD compared with both SD and PNFA, and B) SD compared with both fvFTD and PNFA (uncorrected, p<0.001)

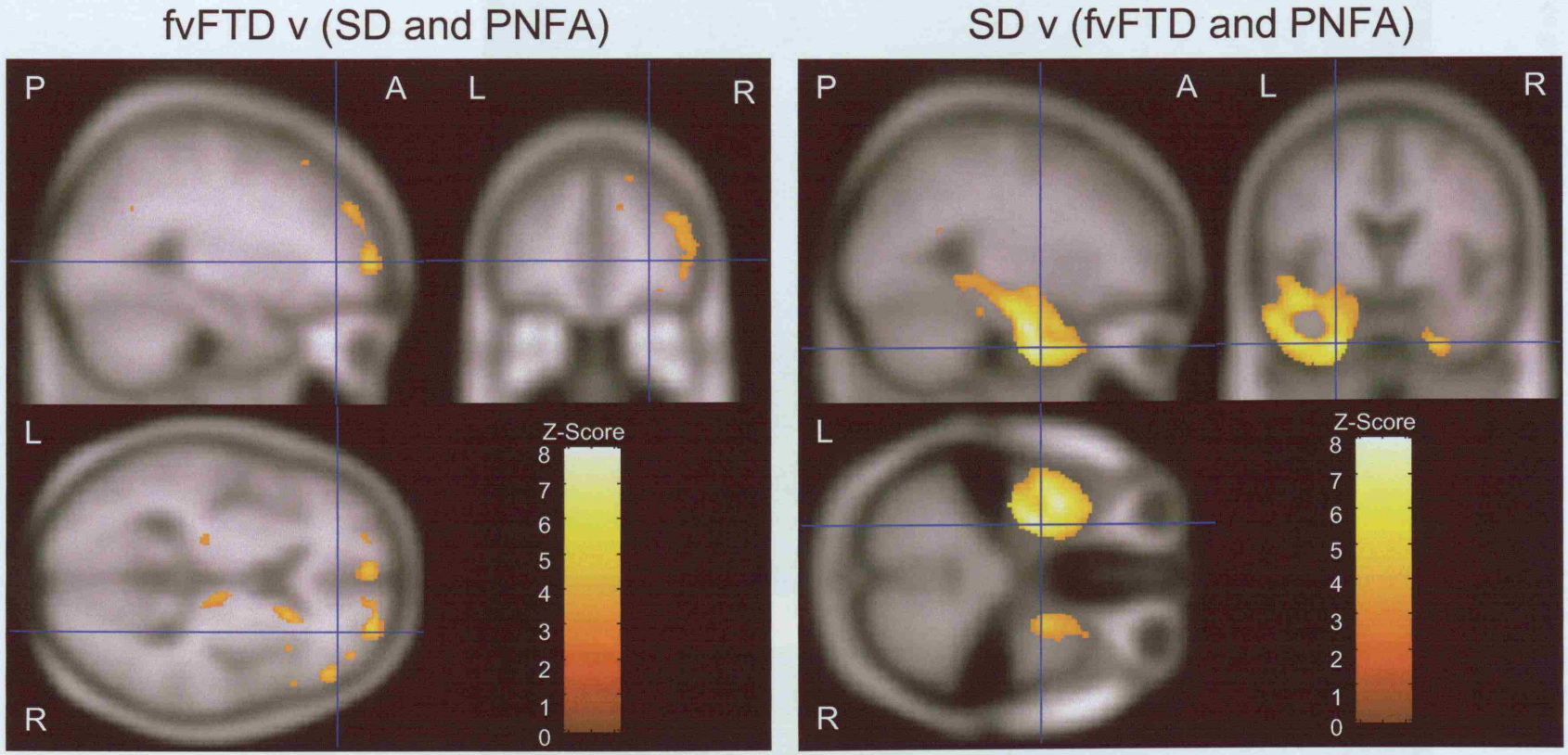

Figure 5.15: Statistical parametric map showing regions of grey matter loss present in all three groups (fvFTD, SD and PNFA) when compared with controls (uncorrected, p<0.001)

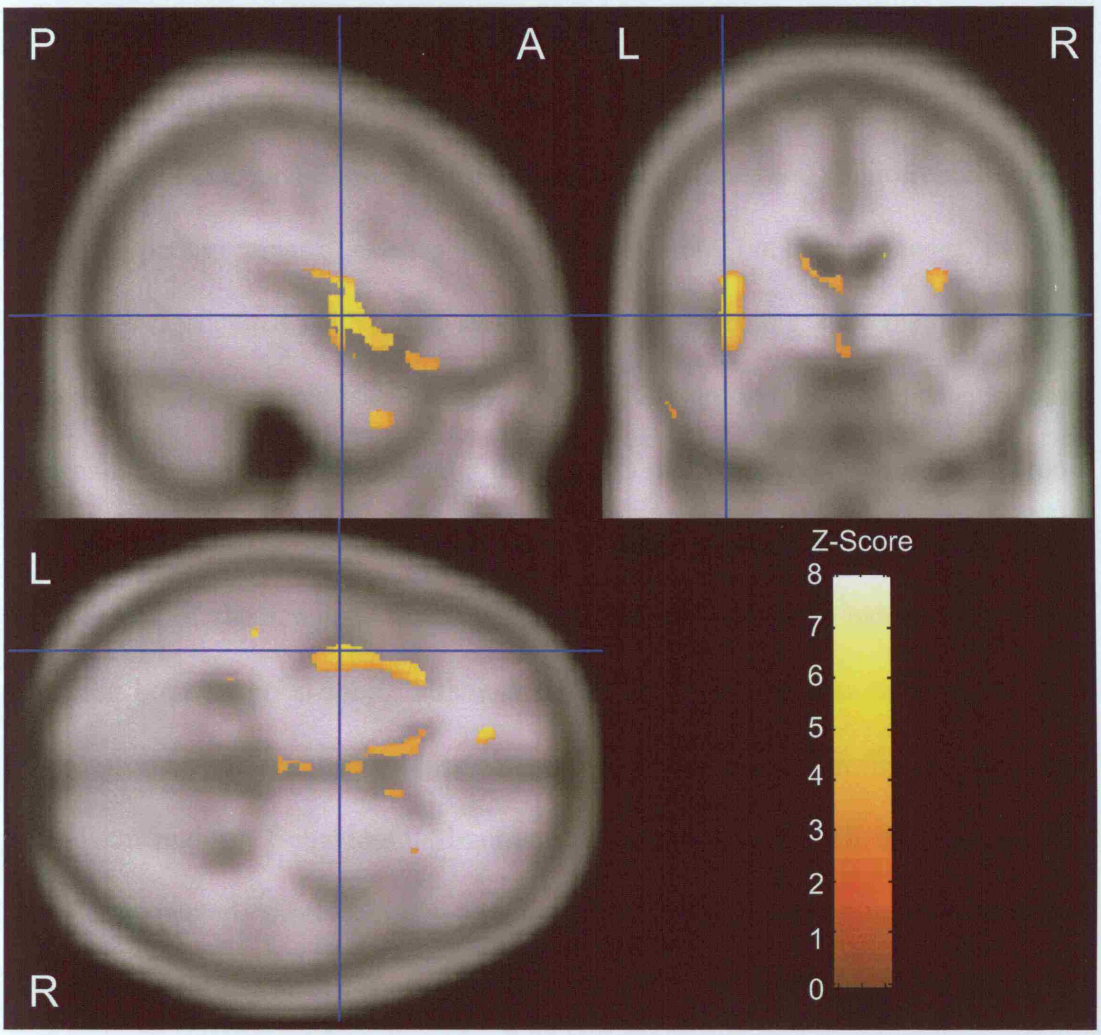

5.4. Discussion

This study analysed MRI patterns of brain atrophy in clinically defined FTLD subgroups using the unbiased technique of VBM. As expected, the FTLD group as a whole showed patterns of atrophy that preferentially involved the frontal and temporal lobes. Certain brain regions were consistently involved in all three syndromic variants of FTLD, including the insula, anterior cingulate, and orbitofrontal cortex. Reflecting perhaps areas of overlap between the different (but heterogeneous) patterns of atrophy associated with each syndrome and confirming that the patterns of neuronal loss, like the clinical features, are definitely not mutually exclusive in these subgroups. In addition, differences in the patterns of atrophy between each subgroup were identified. The fvFTD group showed severe frontal atrophy, with milder involvement of the temporal lobes. The SD group showed a pattern of atrophy involving both temporal lobes, although with a much greater loss on the left. The PNFA group showed atrophy predominantly involving the left frontal lobe and perisylvian region. Behavioural abnormalities were present in all three groups but were, as expected, most common in the fvFTD group. Obsessive and ritualistic behaviours were the most common behaviours in SD and PNFA, but were also very prevalent in fvFTD. It is likely that the regions involved across all three subgroups may contribute to these behavioural features which are inevitably very heterogeneous. This clinical heterogeneity is difficult to capture with rating scales or clinical reporting.

Atrophy of the insula, especially on the left, was found in all three syndromic variants. This may reflect sensitivity to detection of loss using VBM in this region: a grey matter region which because of its position may be more consistently registered

across subjects than other peripheral cortical regions. It is also possible that apparent insula atrophy may simply reflect widening of the perisylvian fissure due to gross and widespread atrophy in the inferior frontal and temporal lobes. The anatomical complexity of this region also makes it difficult for VBM to accurately localise change. Alternatively these findings may reflect a consistent and particular vulnerability of this region in FTLD. The insula has been associated with control of the autonomic nervous system (Augustine, 1996; Critchley et al., 2000), emotion perception (Wright et al., 2004), and has been suggested to play a role in the modulation of stimulus-reward associations (Small et al., 2001). FTLD patients commonly show deficits in emotion recognition (Rosen et al., 2004). Damage to the insula may therefore play a role in the social and behavioural abnormalities in FTLD patients. However, it is also well known to be involved in language. A recent PET study has demonstrated hypometabolism of the insula in patients with PNFA (Nestor et al., 2003a). It appears to play a role in motor articulatory planning and syntactic processing, and it may contribute to the non-fluent speech deficits present in the PNFA patients (Dronkers, 1996; Nestor et al., 2003a; Gorno-Tempini et al., 2004a); although this study shows that insula atrophy is present in all FTLD subgroups, and is not specific to PNFA. PET studies have similarly demonstrated hypometabolism of the insula in FTLD subjects (Jeong 2005).

There was also evidence that the orbitofrontal cortex was involved in all three FTLD subgroups. Human and animal lesion studies have provided strong evidence that the orbitofrontal cortex is linked to social behaviour (Eslinger and Damasio, 1985; Berlin et al., 2004; Seguin, 2004). Patients with damage to the orbitofrontal cortex are typically described as disinhibited, socially inappropriate, obsessive, impulsive

(Berlin et al., 2004), and aggressive, and they often misinterpret moods and have poor insight (Rolls et al., 1994; Seguin, 2004). Investigators have proposed that behavioural deficits after orbitofrontal cortex damage may be due to impairments in decision making (Damasio, 1996; Bechara et al., 2000), the representation of the mental states of others (Stone et al., 1998), or inappropriate alteration of behaviour in response to environmental cues (Rolls et al., 1994). Abnormalities in the orbitofrontal cortex have also been directly linked to obsessive-compulsive behaviours (Evans et al., 2004; Kang et al., 2004; Mataix-Cols et al., 2004; Pujol et al., 2004; Ogai et al., 2005); features which were common in all three of the syndromic variants of FTLD in this study.

A small region in the anterior cingulate was also affected in all three FTLD subgroups. It has been suggested that anterior cingulate damage may be related to apathetic behaviour (Rosen et al., 2002c), and may interact with the orbitofrontal cortex in the selection of action based on stimulus-reward associations. However, it is possible that anterior cingulate atrophy may simply be an artefact created by the misclassification of tissue due to ventricular expansion. A couple of previous VBM studies have similarly demonstrated atrophy of the orbitofrontal cortex, insula and the anterior cingulate in both SD and fvFTD patients and concluded that these regions may contribute to the behavioural deficits (Rosen et al., 2002c; Boccardi et al., 2005). This study supports this hypothesis and strengthens it with the inclusion of PNFA patients, with the caveat again of possible artefactual effects of VBM. In addition, functional imaging studies using PET and SPECT have similarly demonstrated involvement of these regions in subjects with FTLD (Kempler et al., 1990; Starkstein et al., 1994; Varrone et al., 2002; Nestor et al., 2003a; Jeong et al., 2005).

Significant differences in the patterns of atrophy were observed in the different subgroups of FTLD. The fvFTD group showed a severe pattern of frontal lobe atrophy, and had significantly more right frontal atrophy than either of the other two groups. A volumetric analysis by Fukui et al (2000) similarly showed greater right frontal atrophy in fvFTD compared to PNFA (Fukui and Kertesz, 2000) and VBM studies have shown more right frontal atrophy in fvFTD compared to SD (Rosen et al., 2002c; Grossman et al., 2004). A right sided pattern of frontal lobe hypometabolism has also been reported in PET studies of fvFTD (Diehl et al., 2004). The fvFTD group showed reduced function on executive tests and displayed a wide range of behavioural features, including both disinhibited and apathetic features. A recent study has shown that aberrant behaviour (as measured by the NPI) correlates to loss of grey matter volume in the dorso-medial frontal lobe in FTLD (Williams et al., 2005). The most common behavioural feature was a change in eating behaviours, including eating more, eating more quickly and a preference for sweet foods. Correlations between changes in eating behaviour and structural brain changes will be discussed further in chapter 6.

The left temporal lobe was the most severely affected structure in SD patients, consistent with many previous MRI and PET studies (Kempler et al., 1990; Mummery et al., 1999; Mummery et al., 2000; Chan et al., 2001b; Galton et al., 2001a; Rosen et al., 2002c; Boxer et al., 2003; Diehl et al., 2004; Grossman et al., 2004) and chapter 4. The right temporal lobe was also atrophied, but to a lesser degree than the left. Regions in the left temporal lobe have been shown to be critically involved in language production, including the formulation of language, and semantic processing.

In fact, the degree of left temporal atrophy on MRI has been shown to correlate significantly with semantic performance in FTLD patients (Mummery et al., 2000; Short et al., 2005; Williams et al., 2005). The subjects in this study all showed severe naming deficits, failing to score on the GNT and performing below average on the easier Oldfield naming test. In order to attempt to assess the progression of atrophy over time the SD patients were divided into two groups according to the severity of their naming deficits. The results from this analysis suggest that the disease starts in the left temporal lobe, and then as the patients' progress clinically it spreads across to the right temporal lobe, starting in the fusiform gyrus and anterior temporal pole. This is however a crude analysis since the data collected was cross-sectional. In addition, all the subjects scored below the 5th percentile on the Oldfield and therefore were all clinically severe and showed a limited range of severity. There were also fewer subjects in the milder group and so this comparison may have had less statistical power. The progression of regional atrophy will be investigated further using longitudinal data and is discussed in chapter 14.

The PNFA group showed a pattern of left frontal and temporal atrophy. There was evidence of loss in the left superior temporal gyrus in agreement with the visual assessment results presented in chapter 4. In contrast to the study by Fukui et al (2000) that found more left frontal atrophy in PNFA than fvFTD patients (Fukui and Kertesz, 2000), this study showed that very few regions were involved in PNFA over and above that seen in the other FTLD subgroups. Previous VBM studies in PNFA have found varying degrees of grey matter atrophy, ranging from a single cluster in the left perisylvian region (Nestor et al., 2003a), to more widespread patterns of frontal and temporal atrophy (Gorno-Tempini et al., 2004a; Grossman et al., 2004).

Functional imaging studies have also shown varied results, although the left inferior frontal and temporal lobes, including the superior temporal gyrus, have been implicated (Kempler et al., 1990; Nestor et al., 2003a; Zahn et al., 2005). As mentioned above, hypometabolism of the insula has been demonstrated in one study of PNFA (Nestor et al., 2003a), although this has not been replicated in other PET studies (Zahn et al., 2005), and while insula atrophy was observed in PNFA in this chapter it was also found in both fvFTD and SD patients suggesting that it would not be diagnostically useful. This variablility across studies may reflect differences in inclusion criteria and disease severity between studies. The PNFA cohort in this study showed significant behavioural and cognitive deficits perhaps reflecting the widespread pattern of atrophy.

Regions of grey matter atrophy were also found in the putamen in PNFA, as has been reported in a previous VBM study (Gorno-Tempini et al., 2004a). Hypometabolism of the putamen has also been reported in cases of PNFA on SPECT and PET (Caselli et al., 1992; Zahn et al., 2005). A proportion of PNFA cases turn out to have CBD at post-mortem (Hodges et al., 2004; Josephs et al., 2006b). Therefore it is perhaps not surprising that PNFA cases show atrophy in the putamen, as pathological changes occur in this region in CBD (Dickson et al., 2002). In fact one PNFA case from this study had CBD on post-mortem, and three patients went on to develop features of Parkinsonism suggestive of CBD pathology. However, these results should be interpreted with caution. Structures in the central grey matter have intensities that are difficult to distinguish from white matter and are therefore subject to segmentation errors (especially template-based segmentation) in the presence of atrophy, making it difficult to localise change within this region.

This study has a number of clinical limitations. The clinical diagnosis was only confirmed pathologically in nine cases and it was difficult to ensure that the groups were matched for clinical severity. In the absence of any better alternative, the MMSE was included in the analysis as a nuisance variable in order to attempt to correct for differences in clinical severity. However, as discussed in chapter 1, the MMSE is particularly sensitive to language deficits, and therefore will be disproportionately low in the language variants and may have contributed to an underestimation of the VBM findings. Due to the retrospective nature of the study detailed neuropsychological reports were not available for every subject at the time of scan, and even in those subjects with reports the data was patchy and not all tests were performed on all subjects. Many tests also rely to some degree on comprehension and verbal output, and therefore may produce misleadingly low scores in the language variants of FTLD. Behavioural assessments were made retrospectively from the patient records. This information is likely to be biased towards behavioural features that were a particular problem for the carers, or that were particularly striking. The carer may not mention more subtle behaviours unless specifically asked by the clinician. The technique of VBM also has a number of limitations. Small sample sizes and variability among individuals within each group reduce sensitivity for the detection of group differences. The segmentation step provides an additional potential source of error: the misclassification of tissue is especially likely in atrophic brains, both because there is greater potential for partial volume effects between grey matter and CSF, and because tissue pathology may be associated with reduced grey/white matter contrast (Good et al., 2002). Errors in segmentation can also occur due to displacement of tissues. If the interfaces between compartments move due to

mass effect or volume loss, the changes can be reflected in both compartments (Good et al., 2002). This is a particular problem in cases with ventricular enlargement, where VBM often shows changes in the CSF and white matter compartments. This may have contributed to the white matter atrophy observed around the ventricles in this study. However, customised prior probability maps were used in an attempt to improve the segmentation of the FTLD patients. In addition, spatial smoothing reduces anatomical resolution, involving a trade-off between the sensitivity to detect atrophy and the specificity of region localization.

5.5. Conclusion

This chapter has demonstrated that each of the clinical syndromes of FTLD is associated with a different pattern of regional atrophy but that patterns of atrophy are not mutually exclusive and overlap at least when moderately severely affected subjects are compared. These patterns of loss are likely to contribute to the behavioural and cognitive deficits observed in the FTLD patients. The insula, orbitofrontal cortex and anterior cingulate were involved across all three groups, and are therefore likely to play a role in the common behavioural deficits, especially obsessive and ritualistic behaviours. The results also suggest that in SD the disease spreads over time from a focus in the left temporal lobe to the right temporal lobe, particularly the inferior temporal gyrus, and the left inferior frontal lobe. The finding has important implications for the study of progression in SD and warrants further study. The patterns of atrophy identified in this chapter are likely to be useful in the differential diagnosis of the different variants of FTLD.

6. Imaging correlates of 'sweet tooth' in FTLD

6.1. Introduction

The neuroanatomical basis of specific human behaviours is poorly understood. Behavioural abnormalities are an early and prominent feature in FTLD; therefore these individuals present a unique opportunity to identify critical brain substrates for the regulation of specific human behaviours. The results from the previous chapter, as well as those from other studies (Rosen et al., 2002c; Boccardi et al., 2005; Williams et al., 2005), suggest that atrophy of the frontal lobes and limbic system may underlie the predominant behavioural dysfunction in FTLD.

Changes in eating behaviour are one of the most common behavioural problems in FTLD and are reported more frequently than in other dementias (Miller et al., 1995; Bozeat et al., 2000; Snowden et al., 2001; Ikeda et al., 2002; Liu et al., 2004). Indeed the previous chapter found abnormal eating behaviours in 95% of fvFTD subjects. Patients may exhibit hyperphagia, compulsive food seeking and food fads. In addition, the craving of carbohydrates or sweet foods, often referred to as 'sweet tooth', is common (Miller et al., 1995; Cullen et al., 1997; Ikeda et al., 2002). Patients may develop an intense desire to eat a single food (or several foods); in fact they may eat nothing but sweet foods. Typical behaviours may include buying a packet of 50 chocolates, eating them all within an hour and then hiding the wrappers from their spouse, or waking up during the night and leaving the house to specifically go and buy sweets.

A recent study has suggested that changes in eating behaviour are associated with atrophy in the right frontal cortex and ventromedial frontal cortex in FTLD (Liu et al., 2004). However, the authors made no attempt to examine correlations with specific eating abnormalities. The aim of this chapter was to investigate the grey matter correlates of pathological sweet tooth in patients with FTLD.

6.2. Methods

6.2.1. Subjects

Twenty-six patients fulfilling consensus criteria for FTLD were recruited from the cognitive disorders clinic. All subjects were assessed as part of the Prospective Longitudinal FTLD Study described in chapter 3. Therefore all behavioural data was collected prospectively and systematically. Eating behaviour was assessed using the MOUSEPAD (Allen et al., 1996): this scale rates the presence/absence of eating more food, eating food more quickly, and the development of a preference for sweet foods, where this behaviour represents a substantive change from the individual's premorbid state. MOUSEPAD assessments were also performed to assess the presence/absence of other behavioural features, including disinhibition and obsessional and ritualistic behaviours. Subjects were divided into two groups based on the presence (FTLDs) or absence (FTLDn) of newly developed pathological sweet tooth. The patient characteristics of both groups are shown in table 6-1. There was no significant difference in age, MMSE or CDR between the FTLDs and FTLDn groups. The majority of patients were male in both groups. In addition, the majority of subjects had a clinical diagnosis of fvFTD, with only three SD subjects in each group. Abnormal behaviours were most common in the FTLDs group.

Table 6-1: Patient characteristics.

Characteristics	Controls (n=15)	FTLDs (n=13)	FTLDn (n=12)
Gender (M:F)	9:6	9:4	11:1
Age (yrs)	63.2 (13.6)	64.2 (7.6)	64.5 (6.0)
MMSE (/30)	28.9 (0.9)	19.0 (11.3)*	18.0 (9.6)*
CDR	N/A	1.4 (0.8)	1.1 (0.5)
Abnormal behaviours			
Disinhibition	N/A	6/13 (46%)	0/12 (0%)
Obsessionality, mental rigidity or rituals	N/A	12/13 (92%)	8/12 (67%)
Other abnormal eating behaviours			
Increased speed of eating	N/A	7/13 (54%)	4/12 (33%)
Increased quantity of food consumed	N/A	7/13 (54%)	2/12 (17%)
Clinical syndrome			
fvFTD	N/A	10	9
SD	N/A	3	3

*FTLDn, frontotemporal dementia without pathological sweet tooth; FTLDs, frontotemporal dementia with pathological sweet tooth; N/A, not applicable; Age, gender, MMSE and CDR are expressed as mean (standard deviation); Behaviours are expressed as No. patients/Total (percentage); * significantly different from controls* $p<0.001$

6.2.2. Image analysis

All subjects underwent volumetric brain magnetic resonance imaging (see standard imaging protocol in Appendix 4) within six months of the MOUSEPAD assessment (and usually on the same day). Volumetric brain MRI was also performed using the same scanner in 15 age-matched healthy control subjects. Brain images were analyzed using VBM. In order to optimize normalisation, a customized template was based on MR brain images from a group of 10 healthy controls and 10 patients with FTLD, age- and gender-matched to the study cohort and acquired on the same scanner. Template images were normalized to the MNI template brain, and the mean template image was smoothed with an isotropic Gaussian kernel of 8mm FWHM. All study images were normalized to this customized template and each normalized image was segmented into grey matter, white matter and cerebrospinal fluid based on customized prior probability maps (see chapter 3). Each grey matter image was masked with a brain region to exclude all non-brain voxels. Grey matter images were modulated and smoothed with an isotropic Gaussian kernel of 8mm FWHM. In order to assess the specificity of any correlation between grey matter changes and the development of sweet tooth, indices of other abnormal behaviors (disinhibition, mental rigidity and/or obsessionality), disease severity, age and gender were incorporated in the analysis as variables of no interest. Grey matter differences between the FTLDs group and controls and between the FTLDn group and controls were assessed at an uncorrected statistical threshold of $p<0.001$. The thresholded statistical parametric maps for each contrast were compared using an exclusive masking procedure based on Boolean algebra criteria in order to identify voxels at which grey matter loss occurred only in the FTLDs group and only in the FTLDn group relative to controls. In addition, grey

matter intensity differences between the FTLDs and FTLDn groups were assessed directly at an uncorrected statistical threshold of $p<0.001$.

6.3. Results

Compared with controls, both the FTLDs and FTLDn groups had bilateral grey matter loss predominantly involving the temporal lobes, insula, and inferior frontal lobes (figure 6.1): the FTLDs group had additional grey matter loss involving bilateral orbitofrontal cortex (OFC), anterior and inferior temporal lobe, amygdala and insula (Figure 6.2, FTLDn – FTLDs). While the pattern of temporal lobe loss was bilateral in the FTLDs group, the pattern in the FTLDn group involved almost exclusively the left hemisphere, therefore the FTLDs group showed comparatively greater loss in the right temporal lobe than the FTLDn group. No brain regions were involved in the FTLDn group which were not also involved in the FTLDs group. When the two disease groups were compared directly, the FTLDs group had significantly more severe grey matter loss in the OFC bilaterally (Figure 6.2, FTLDn v FTLDs); no regions were identified in which grey matter loss was significantly more severe in the FTLDn group. The most marked grey matter differences between the FTLDs and FTLDn groups involved lateral OFC in each hemisphere: in the left hemisphere, grey matter loss was maximal within postero-lateral OFC (MNI stereotactic coordinates -45, 42, -14; Z score 5.04), and in the right hemisphere, grey matter loss was maximal in left inferior frontal gyrus (coordinates 54, 32, 6; Z score 4.93) and extended inferiorly into lateral OFC.

As an additional analysis VBM was used to assess the patterns of atrophy in patients that ate more food, and ate food more quickly (as assessed from the MOUSEPAD).

There were no significant differences in the patterns of atrophy between patients with these behaviours and those without ($p<0.001$).

Figure 6.1: Statistical parametric maps showing patterns of grey matter loss in the FTLDn and FTLDs groups compared to controls ($p<0.001$).

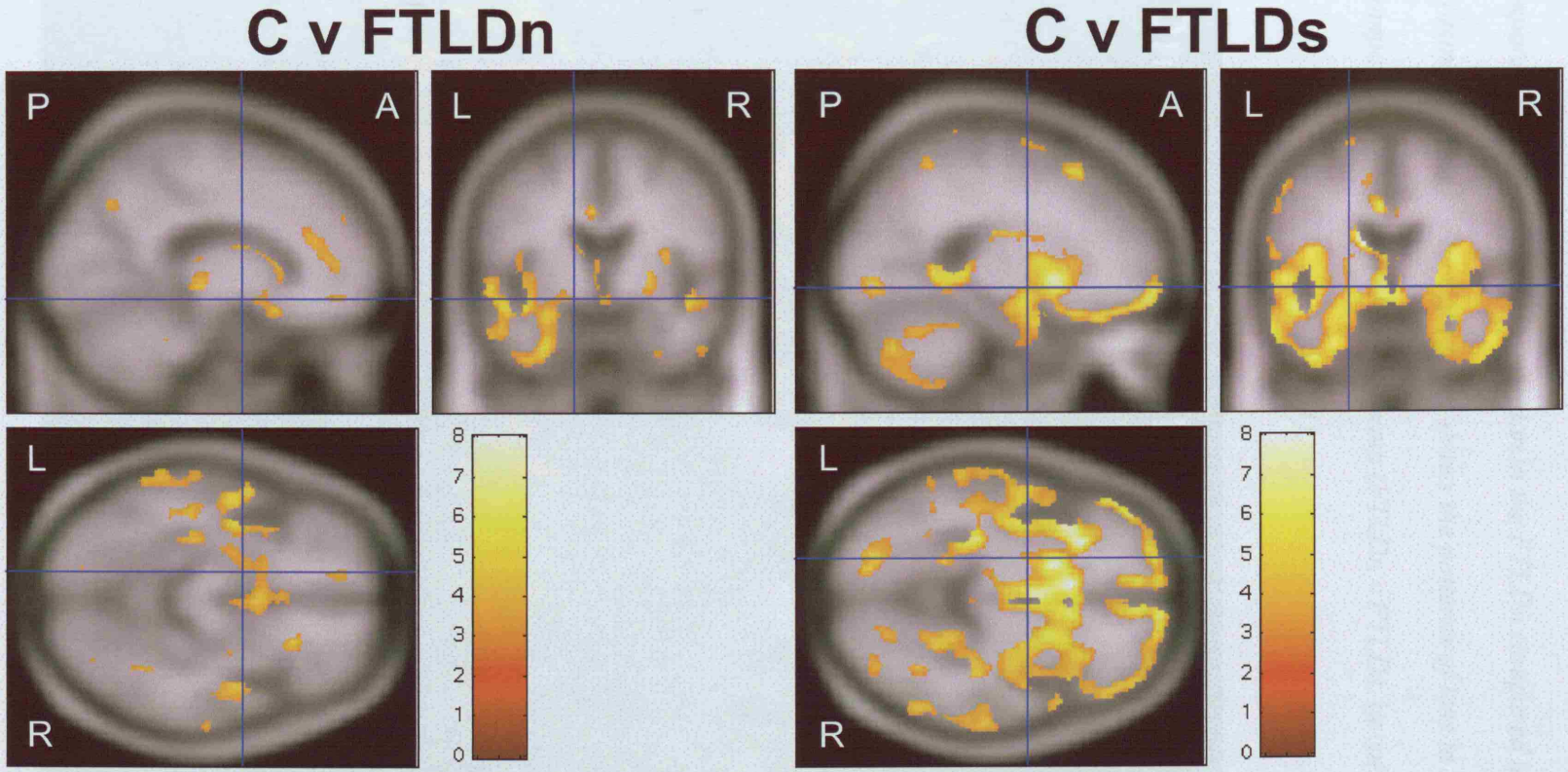

Figure 6.2: Statistical parametric maps showing regions of grey matter loss specific to the FTLDs group. The left panel shows the regions showing greater loss in the FTLDs compared to controls comparison, than in the FTLDn compared to control comparison (using masking). The right panel shows the patterns of loss in the FTLDs group compared directly to the FTLDn group (FTLDn v FTLDs, uncorrected $p<0.001$).

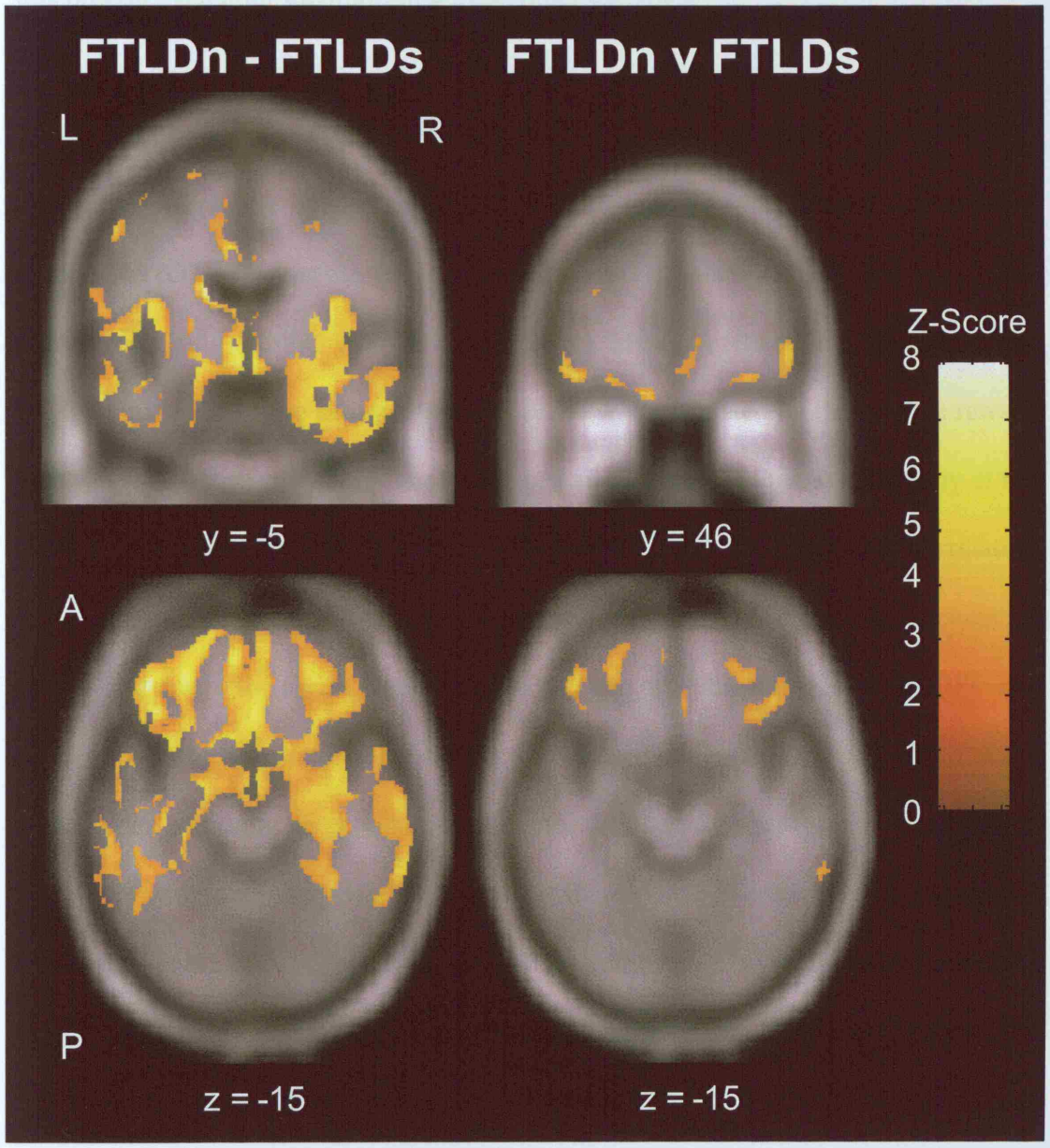

6.4. Discussion

This chapter suggests that damage involving a frontotemporal brain network gives rise to abnormal carbohydrate seeking behaviour in FTLD. Within this network, damage involving the OFC is directly and specifically correlated with the development of pathological sweet tooth. This correlation is unlikely to be a non-specific accompaniment of disease progression or behavioural dysregulation, since it was present even after incorporating these other variables.

These findings are consistent with evidence in humans and other species for the important role played by postero-lateral OFC in food seeking, hunger and feeding termination (O'Doherty et al., 2001; Small et al., 2001; Tataranni and DelParigi, 2003; Kringelbach and Rolls, 2004; Rolls, 2004). Human functional imaging and behavioural studies have shown that OFC activity is modulated by the relative reward value and subjective pleasantness of olfactory and gustatory signals (O'Doherty et al., 2001; Small et al., 2001; Tataranni and DelParigi, 2003). A significant correlation has been found between activation in the orbitofrontal cortex and self-reports of hunger and desire for food (Wang et al., 2004). In addition, damage to the OFC has been shown to interrupt the ability to reverse or extinguish stimulus-reward associations, resulting in persistent preference for the stimulus (Small et al., 2001). Both the insula and amygdala are activated in response to taste stimuli in humans (O'Doherty et al., 2001; Small et al., 2001; Tataranni and DelParigi, 2003): while the insula may control autonomic responses in preparation for food consumption, the amygdala may encode the emotional valence of the food stimulus. Both these structures have extensive reciprocal connections with the OFC, providing a substrate for the coordinated control of eating behaviour in response to both exogenous and

endogenous cues. A disease process such as FTLD that disrupts the normal interaction between postero-lateral OFC, amygdala and insula may interfere with the normal satiety response, leading to a persistent sweet preference. Interestingly, disruption in this circuit of structures has also been implicated in drug addiction (Volkow and Fowler, 2000; Lingford-Hughes et al., 2003).

This study is limited by the behavioural data available. The MOUSEPAD provided only crude present/absent information; therefore it was impossible to do any more statistically powerful correlations or regressions between grey matter loss and severity of eating behaviour. Correlational analyses have proved useful in previous studies (Mummery et al., 2000; Williams et al., 2005). In addition, the data did not allow for any measure of severity or persistence of the behavioural abnormality. The MOUSEPAD assessment does allow the calculation of a severity score; however it is heavily reliant on the assessment of symptom duration which was felt to be unreliable. The finding of no correlations with eating more and eating more quickly are not surprising, given that these features are relatively unspecific. The questions posed through the MOUSEPAD can also be ambiguous. For example, rating a subject as 'eating more' does not distinguish between eating more during the meal, eating more between meals or eating more sweet foods. The study was also limited by the small number of subjects. The results should be validated in a larger cohort with detailed behavioural data. The small number of subjects with MOUSEPAD assessments also prevented the assessment of other forms of behaviour in this thesis.

6.5. Conclusion

This chapter has shown for the first time that a persistent preference for sweet foods in patients with FTLD may be due to the disruption of a circuit of structures involving the orbitofrontal cortex, amygdala and insula. This provides important information concerning the neuroanatomical basis of eating behaviours in humans and highlights the importance of studying behavioural dysfunction in patients with FTLD.

7. Amygdala measurements in the differential diagnosis of FTLD and AD

7.1. Introduction

Previous chapters have used VBM to demonstrate that patients with the different syndromic variants of FTLD show different patterns of atrophy on MRI. Whilst VBM techniques have the advantage that they are automated and do not require any a priori hypotheses concerning which structures to assess, they have the disadvantage of limited anatomical resolution. This is due to the fact that the data is spatially smoothed prior to analysis. In addition, accuracy of the normalization procedure depends upon the size, complexity and position of the structure, and small sample sizes and variability among individuals reduces sensitivity for the detection of group differences. It is therefore difficult to draw definitive conclusions concerning specific regional involvement using VBM. Regional volumetric measurements, although time consuming, do allow a more detailed examination of the involvement of specific structures. The study presented in Appendix 7 highlights the utility of volumetric measurements (Chan et al., 2001b). The study performed detailed volumetric measurements of a number of temporal lobe structures and demonstrated substantial differences between SD and AD patients that may help in the differential diagnosis of these two diseases. These results have also been confirmed by another volumetric study (Galton et al., 2001a).

However, it is also important to be able to differentiate AD from the other syndromic variants of FTLD. Differentiating FTLD from AD can be difficult and although AD is characterised by early memory decline there may be considerable overlap in

clinical features between AD and FTLD, especially in the early stages. Accurate diagnosis is important since each has a different clinical course and specific treatments for AD are now available.

Previous studies have shown that the amygdala is one of the most severely affected structures in SD patients (Chan et al., 2001b; Galton et al., 2001a) (see Appendix 7). Animal and human studies have shown that damage to the amygdala is associated with prominent behavioural changes, including altered dietary habits, prominent oral tendencies and hypersexuality (Cummings and Duchen, 1981; Tranel and Hyman, 1990). Indeed, chapter 6 correlates atrophy of the amygdala to abnormal eating behaviours in FTLD, and emotional agnosia is a common feature of FTLD (Snowden et al., 2001) and has been associated with amygdala damage (Rosen et al., 2002a). Patients with fvFTD typically present with early and prominent behavioural problems. Although PNFA and SD are both characterised by early language deficits, behavioural features often develop with progression of the syndrome (see chapter 5) (Neary et al., 1998). Amygdala atrophy has been reported in patients with SD and fvFTD (Boccardi et al., 2002; Boccardi et al., 2005). No studies have measured the amygdala in PNFA patients, although pathological studies have shown that the amygdala is one of the most severely affected structures in Pick's disease (Cummings and Duchen, 1981; Dickson, 2001), one of the pathological substrates of PNFA (Hodges et al., 2004). Behavioural features are also common in AD, although are usually less severe than those observed in FTLD (Burns et al., 1990). While amygdala atrophy has been demonstrated on MRI in AD (Cuenod et al., 1993), it is unclear if it is useful in the differential diagnosis of AD (Laakso et al., 1995a), and

there are no volumetric MRI studies comparing amygdala atrophy in all three variants of FTLD to AD.

The aim of this study was to investigate amygdala atrophy in all three syndromic variants of FTLD, and to determine whether amygdala atrophy may be useful in the differential diagnosis of FTLD and AD.

7.2. Methods

7.2.1. Subjects

All subjects were recruited retrospectively from the specialist cognitive disorders clinic. A detailed history, neurological and general examination, screening blood tests, neuropsychometry (including the MMSE), and MR imaging had been performed for all subjects. Disease duration was defined as the time from first symptom onset to MRI scan. Forty-six patients fulfilling consensus criteria for FTLD (Neary et al., 1998) were included. Twenty-two of these patients were diagnosed with fvFTD, fourteen with SD, and ten with PNFA. Post-mortem confirmation was available in four cases. The cohort was age and gender-matched to 20 patients with AD that fulfilled the NINCDS-ADRDA criteria for "probable" AD (McKhann et al., 1984) (8 familial, 12 sporadic), and 17 healthy controls. The control subjects were typical of normal ageing and had no complaints of cognitive impairment or behavioural problems. Exclusion criteria included a history of stroke or dementia. MRI was used to exclude space occupying lesions, vascular disease, and other pathologic conditions, but the diagnosis of FTLD and AD was made on clinical grounds without further reference to MRI.

7.2.2. Image analysis

T1-weighted volumetric MR images were acquired using the standard protocol described in Appendix 4. All measurements were performed using MIDAS image analysis software and all measurements were performed blind to subject details and the results of any other measurements.

Brain volumes were obtained using a semi-automated iterative 3D morphological technique that has been described in Appendix 5. The left and right amygdalae were outlined using the protocol described in Appendix 5. Scans were flipped about the mid-sagittal plane ensuring that the rater was blinded to left/right orientation. The same rater performed all amygdala measurements; their intra-rater ICC (intra-class correlation coefficient) on repeating 12 measurements was 0.98 (95%CI 0.97-1.00); this relates to an average 4% difference between the repeated measurements of volume.

7.2.3. Statistics

All volumes were normalised to total intracranial volume (TIV) to reduce the effect of inter-individual variation in head size (Whitwell et al., 2001). Both the amygdala and brain volumes were regressed against TIV in the control group to establish the slope of the relationship with TIV. All volumes in the FTLD, AD and control groups were then standardised to TIV volume using the following equation:

$$sbv = bv - \beta(TIV - meanTIV)$$

sbv = standardised volume, bv = crude volume, β = regression coefficient of volume on TIV in controls, meanTIV = mean TIV in the control group.

Amygdala asymmetry score was calculated as follows:

$$\text{Asymmetry score} = \frac{(\text{left} - \text{right})*2}{\text{Left} + \text{right}}$$

Age, MMSE and volume measurements were compared between groups using the Mann Whitney U test; average percentage volume changes were reported based on analysis of log volumes. Proportions were compared using the Fisher's exact test. The Wilcoxon signed rank test was used to compare left and right amygdala volumes. Sensitivity and specificity were calculated from logistic regression and used to determine whether amygdala volume and asymmetry could distinguish between patients with FTLD (and its subgroups) from controls, and secondly, from AD.

7.3. Results

There were no significant differences in gender or age distribution between the disease groups and controls, or between the different FTLD diagnostic subgroups (table 7-1). There was no significant difference in disease duration between FTLD and AD or between the different FTLD diagnostic subgroups. AD and FTLD groups had similar mean MMSE scores.

TIV-adjusted brain volumes were similarly significantly reduced by 6% (95% CI 3-10%) in AD and 7% (4-11%) in FTLD compared with controls ($p<0.001$ for both). No significant difference was found between FTLD and AD groups ($p=0.51$, table 7-2).

Compared with controls TIV-adjusted amygdala volumes were significantly reduced by 41% (29 – 51%) on the left and 33% (22 – 43%) on the right in the FTLD group, and by 22% (13-31%) on the left and 19% (8-29%) on the right in the AD group.

Both left and right amygdala volumes were significantly smaller in the FTLD group than the AD group (left p=0.001, right p=0.01), even when brain volume was accounted for (left p=0.001, right p=0.02). Significant amygdala asymmetry was present only in the FTLD group, with left amygdala volumes on average 13% (6-18%) smaller than right ($p<0.001$, figure 7.1A). The absolute amygdala asymmetry score in FTLD was 0.20 ± 0.18 (mean ± standard deviation), which was significantly greater than the score for the AD group, 0.11 ± 0.07 (p=0.04), and the control group, 0.10 ± 0.07 (p=0.04).

In each of the FTLD subgroups the mean left and right amygdala volumes were significantly smaller than control volumes ($p<0.007$ for all, table 7-2). The SD group had the smallest amygdala volumes, significantly smaller than the AD, fvFTD and PNFA groups ($p<0.02$ for all, left and right). The left amygdala in the SD group was reduced to less than half the mean control volume, this 59% (51 – 65%) reduction on the left was significantly greater than the right amygdala volume reduction of 45% (33 – 54%) of mean control volume ($p<0.001$). The PNFA group also had asymmetrical amygdala volumes, with greater left sided atrophy, although this was not significant (p=0.07). Symmetrical atrophy was observed in the frontal variant fvFTD group.

Figure 7.2 shows examples of representative amygdalae from each group. Note the amygdala appear reduced in both the AD and SD patients compared to controls. In addition, the left amygdala appears smaller than the right in the SD patient. Average (mean of left and right) amygdala volumes discriminated between FTLD and controls with a specificity of 88% and a sensitivity of 63% (table 7-3, cut-off = 1260ml).

Discrimination of FTLD from AD was achieved with a specificity of 60% and sensitivity of 63% (cut-off = 1260ml). Amygdala volumes could discriminate SD from AD with a specificity of 85% and sensitivity of 86% (cut-off = 1055ml); when amygdala asymmetry was included in this regression analysis, sensitivity increased to 100% whilst keeping the specificity constant.

Table 7-1: Patient characteristics

	Disease groups			**FTLD groups**		
	Controls (n=17)	AD (n=20)	FTLD (n=46)	fvFTD (n=22)	PNFA (n=10)	SD (n=14)
Gender (M:F) (% of total)	9:8 (52.9)	12:8 (60.0)	32:14 (69.6)	18:4 (81.8)	6:4 (60.0)	8:6 (57.1)
Age (yrs)	63.6 (10.5)	63.8 (9.1)	64.0 (6.6)	64.0 (6.0)	62.5 (8.7)	65.2 (6.3)
MMSE (/30)	28.9 (1.3)	20.3 ** (5.1)	19.8 ** (9.2)	24.0 ** † (6.5)	20.1 ** (8.3)	12.2 ** † (10.2)
Disease duration (yrs)	N/A	4.5 (2.4)	5.3 (2.7)	5.7 (3.1)	4.7 (2.6)	5.1 (2.2)

Expressed as mean (stdev), N/A = Not applicable. *Significant difference from C using Mann-Whitney U, or Fisher's exact test (* $p<0.05$, ** $p<0.01$); † Significant difference from AD using the Mann-Whitney U, or Fisher's exact test († $p<0.05$, †† $p<0.01$).

Table 7-2: Volumetric results

	Disease groups			**FTLD groups**		
	Controls (n=17)	AD (n=20)	FTLD (n=46)	fvFTD (n=22)	PNFA (n=10)	SD (n=14)
Brain	1179 (74)	1102 ** (46)	1092 ** (70)	1124 * (68)	1050 ** † (40)	1071 ** (70)
Left amygdala	1.64 (0.21)	1.29 ** (0.24)	1.02 ** †† (0.33)	1.18 ** (0.31)	1.11 ** † (0.21)	0.70 ** †† (0.21)
Right amygdala	1.68 (0.31)	1.35 ** (0.26)	1.15 ** † (0.32)	1.21 ** (0.35)	1.28 ** (0.30)	0.97 ** †† (0.22)
Absolute asymmetry	0.10 (0.07)	0.11 (0.07)	0.20* † (0.18)	0.12 (0.10)	0.17 (0.17)	0.35 ** †† (0.21)

All volumes are normalised by TIV and expressed in ml (mean (standard deviation)). * Significant difference from controls using the Mann-Whitney U test (* $p<0.05$, ** $p<0.01$); † Significant difference from AD using the Mann-Whitney U test († $p<0.05$, †† $p<0.01$).

Table 7-3: Screening performance by disease type according to cut-off of average amygdala volume (average of left and right volumes). Sensitivity = percentage of patients with average amygdala measurement at or below the specified cut-off level; Specificity = percentage of patients with average amygdala measurement above the specified cut-off level.

Cut-off level used on average amygdala volume (ml)	1000	1055	1200	1260
Sensitivity (%) in FTLD (n=46)	35	41	57	63
Sensitivity (%) in FTD (n=22)	18	27	45	55
Sensitivity (%) in PNFA (n=10)	10	10	30	40
Sensitivity (%) in SD (n=14)	79	86	93	93
Specificity (%) in Controls (n=17)	100	100	94	88
Specificity (%) in AD (n=20)	85	85	60	60

Figure 7.1: Average amygdala volume against amygdala asymmetry score in controls (C), AD and either A) FTLD or B) SD groups.

A

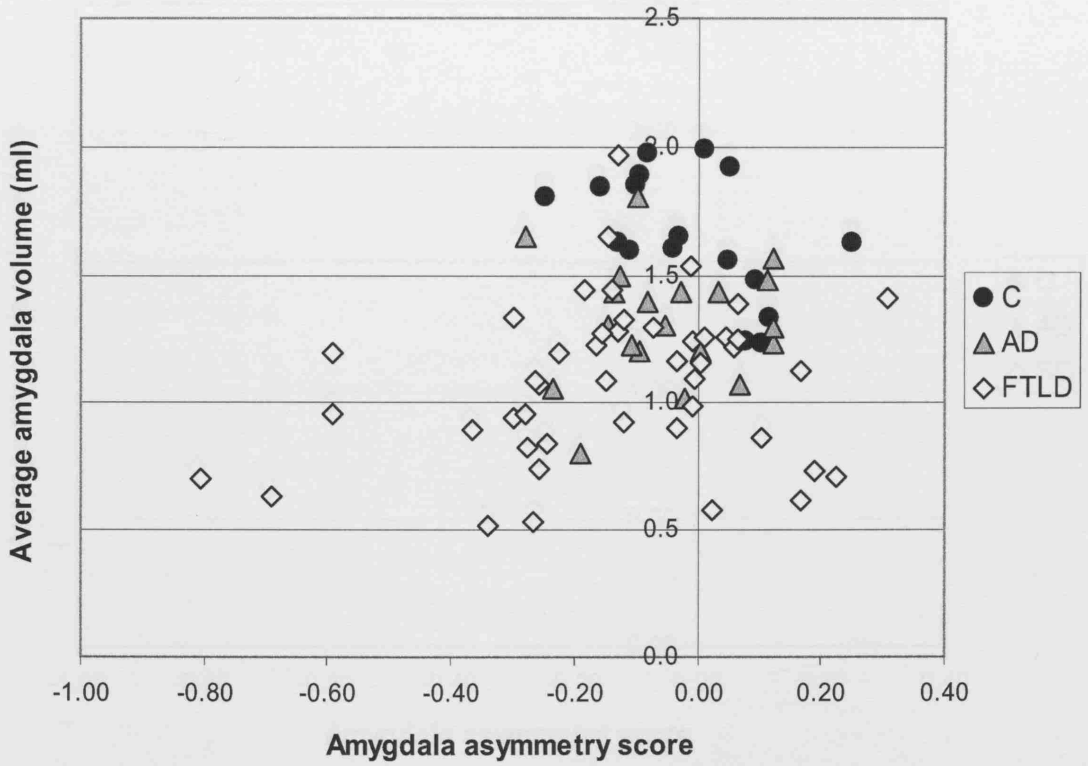

Continued...

B

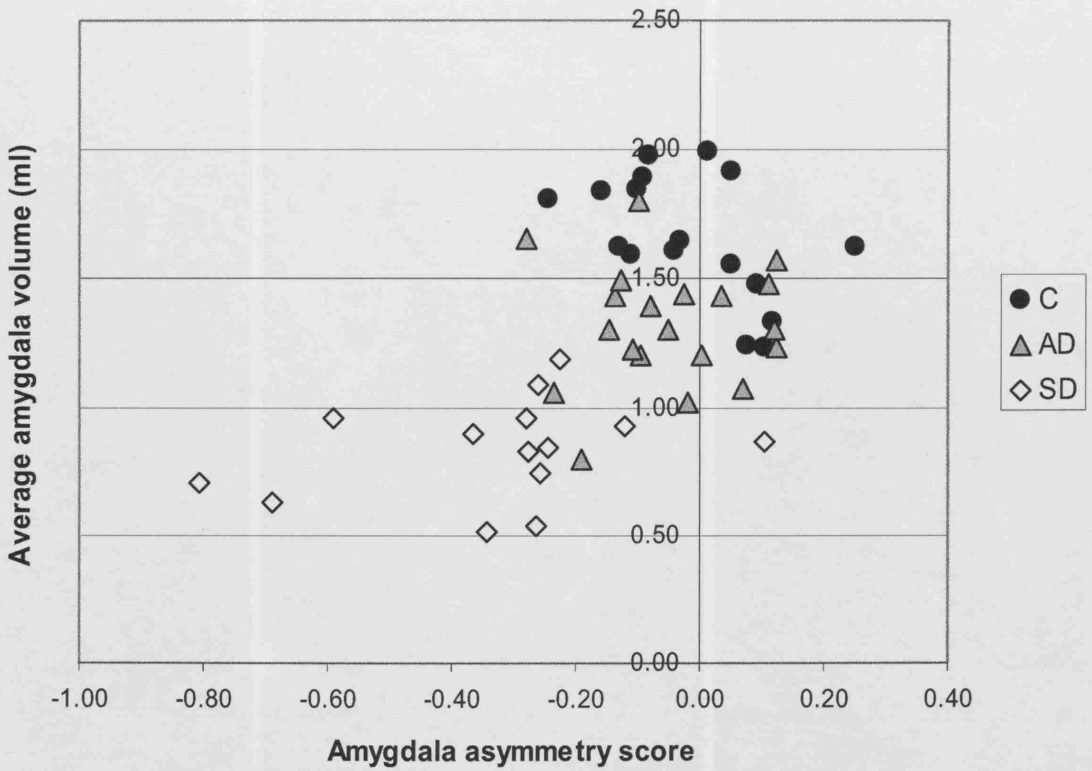
2.50
2.00
1.50
1.00
0.50
0.00
-1.00
-0.80
-0.60
-0.40
-0.20
0.00
0.20
0.40
Average amygdala volume (ml)
Amygdala asymmetry score
C
AD
SD

Figure 7.2: Coronal sections through the temporal lobes in a control subject (1), a patient with AD (2), and a patient with SD (3). Both left and right amygdalae have been outlined. L= Left, R = Right.

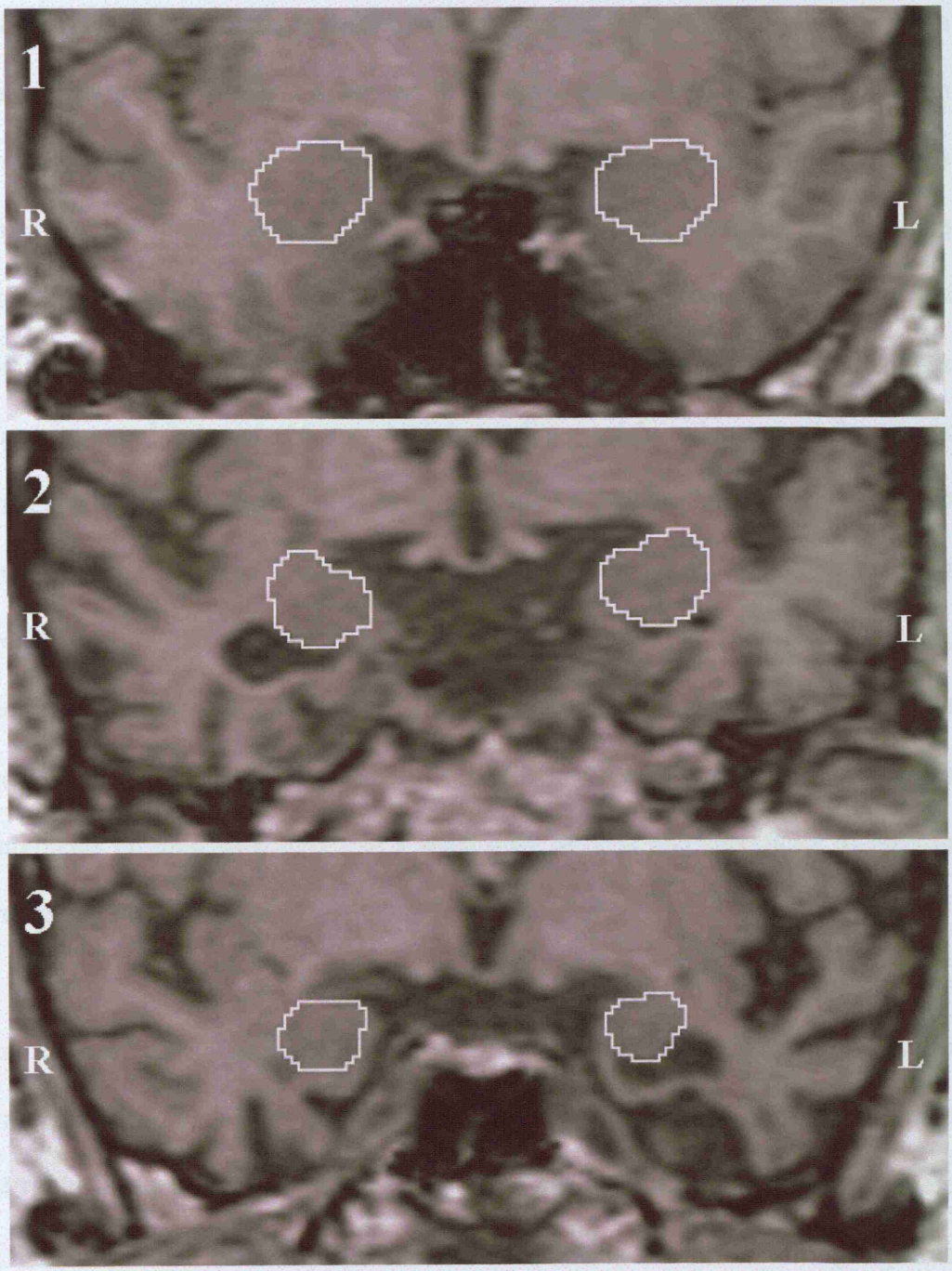

7.4. Discussion

Previous studies have shown that the amygdala is severely atrophied in the SD variant of FTLD (Chan et al., 2001b; Galton et al., 2001a) (see Appendix 7). However, the aim of this chapter was to extend these findings to the other variants of FTLD, especially fvFTD which is more difficult to diagnose than SD. Indeed, this study has demonstrated that very marked amygdala atrophy occurs in all three syndromic variants of FTLD, as well as in AD. The amygdala volumes and asymmetry scores demonstrated significant differences between FTLD, AD and control groups. In the AD patients both left and right amygdala volumes were similarly reduced by approximately 20% of mean control volume. This is consistent with previous studies that have reported between 14 and 44% loss of amygdala volume in AD patients (Cuenod et al., 1993; Laakso et al., 1995a; Laakso et al., 1995b). However, the FTLD patients, even when taken together as a group, showed an asymmetric pattern of amygdala atrophy with a striking 41% loss of volume in the left amygdala, substantially and significantly more than in the AD patients. Atrophy of the right amygdala was also greater in FTLD than AD. Overall, taking the amygdala measurements on their own they had a sensitivity of 63% and specificity of 60% in differentiating FTLD and AD.

The most severe amygdala atrophy was seen in the patients with SD, with the mean left amygdala volume being almost 60% lower than that of the control group, and over 40% lower in the right amygdala. When amygdala atrophy and asymmetry were taken into account complete separation of the SD patients from the control group was achieved in our sample and more importantly almost complete separation of SD from AD was possible (sensitivity of 100%; specificity of 85%). Our findings are in

keeping with previous studies demonstrating severe left temporal lobe (Mummery et al., 2000; Rosen et al., 2002c) and amygdala atrophy in SD(Galton et al., 2001a). Amygdala atrophy was also present in the PNFA and fvFTD groups, although not greater overall than in the AD group. Unlike the AD patients, the PNFA group appeared to display asymmetry with an estimated 12% greater left-sided damage. These findings are also in keeping with previous MRI studies that reported asymmetric left frontal and temporal lobe atrophy in PNFA (Abe et al., 1997; Rosen et al., 2002d) and one report of amygdala atrophy at autopsy in PNFA (Turner et al., 1996), however this is the first MRI study to have looked specifically at the amygdala in PNFA. Amygdala atrophy has previously been reported in fvFTD, but to a lesser degree than in AD (Boccardi et al., 2002). However in that study the AD patients were significantly (11 years) older and had longer mean disease duration than the fvFTD patients.

Damage to the amygdala has been associated with deficits in social behaviour, eating behaviours (chapter 6), and in the recognition of emotion from facial expressions (especially fear) (Cummings and Duchen, 1981; Adolphs et al., 1994). In this study amygdala atrophy was present in all syndromic variants of FTLD, but the SD group were the most severely affected. Diagnostic criteria implies that fvFTD patients have earlier and more profound behavioural change than SD patients, however there is increasing evidence that patients with SD can have significant behavioural dyscontrol, and may be commonly misdiagnosed as fvFTD (Bozeat et al., 2000; Thompson et al., 2003). Behavioural deficits such as changes in eating behaviour, repetitive behaviours, compulsive behaviours and aggression for example are common in SD (Snowden et al., 2001; Liu et al., 2004). Furthermore, deficits in the recognition of

emotion from facial expressions have been observed in patients with SD (Rosen et al., 2002a), loss of empathy is a major presenting feature of FTLD (especially SD (Snowden et al., 2001)) and the emotional reaction of fear is commonly lost in SD patients (Snowden et al., 2001), suggesting a link to amygdala damage. In fact, an association has been found between the processing of emotions and volume of the amygdala in the temporal variant of FTLD (Rosen et al., 2002a). It is likely that the behavioural as well as cognitive deficits commonly found in FTLD, especially in the fvFTD and SD variants, may involve a complex distributed network of limbic and paralimbic structures, including the amygdala.

This study assesses amygdala atrophy in a large number of FTLD patients (n=42), allowing the assessment of atrophy in all three of the syndromic variants of FTLD. Although the numbers of patients were greater than previously reported volumetric MRI studies in FTLD the syndromic groups were still relatively small. The different clinical presentations seen in FTLD make it difficult to match disease severity accurately to the AD group. MMSE score is particularly reduced in patients with language difficulties. Nevertheless, the AD and FTLD subgroups were well matched for disease duration, the patients included in this study were typical in severity to those presenting to cognitive disorders clinics, and the scans chosen for this study were the first MRIs obtained after the initial presentation at our clinic. Finally, the amygdala is a difficult structure to define and measure accurately due to poor grey-white matter boundary definition and may be associated with relatively large measurement errors. However, in this study the same observer (JW) very carefully delineated each amygdala (reproducibility error was 4% which compares well with

previous studies) and the severity of atrophy was such that very significant differences were found despite potential measurement insensitivity.

7.5. Conclusion

This study emphasises that different patterns of amygdala atrophy underlie not just differences between AD and FTLD but also the different clinical presentations of FTLD. Whilst amygdala measurements provide high sensitivity and specificity for the diagnosis of SD; the variability in amygdala volumes may limit the value of amygdala measurements in the differential diagnosis of FTLD and AD. Patterns of atrophy are usually more informative and discriminatory than measurements of single structures (Boccardi et al., 2003; Boxer et al., 2003). In contrast to the symmetric involvement of the hippocampus and medial temporal lobes seen in AD, disproportionate asymmetric atrophy of the amygdala may indicate FTLD, with left greater than right atrophy suggestive of one of the language variants. Therefore, although amygdala atrophy on its own does not provide complete discriminatory power, disproportionate amygdala atrophy should be considered diagnostically important as part of the general assessment of the pattern of atrophy in patients with cognitive impairment.

8. Amygdala and hippocampus measurements in pathologically confirmed FTLD and AD

8.1. Introduction

As discussed in the previous chapter differentiating FTLD from AD is important, but can be difficult. It has been common practice to make a diagnosis of AD if episodic memory is a prominent feature of the disease, while prominent behavioural and language dysfunction suggests a diagnosis of FTLD. This simplistic differentiation holds true for some, but not all cases. Recent clinicopathological studies have identified cases of FTLD with prominent episodic memory loss (Graham et al., 2005), while others have suggested the existence of a frontal variant of AD (Johnson et al., 1999). This overlap in syndromic features means it would be useful to have biomarkers to aid in the differentiation of these two syndromes. While previous MRI studies have examined the ability of volumetric measures to differentiate clinically diagnosed FTLD from AD (Frisoni et al., 1999; Chan et al., 2001b; Galton et al., 2001a) there is uncertainty in clinical diagnostic accuracy. Pathology remains the only gold standard in the diagnosis of AD and FTLD. Assessment of atrophy patterns against a clinical diagnosis may be circular: a regional loss/dysfunction reflects a structure/function correlation rather than specific histopathology.

The previous chapters have shown that amygdala atrophy occurs in FTLD and may be useful in the differential diagnosis of FTLD and AD. In addition, hippocampal atrophy has been demonstrated to be the signature pattern of atrophy on MRI in AD (Convit et al., 1993; Lehericy et al., 1994; Jack et al., 1997; Callen et al., 2001). These findings accord with the clinical presentation since hippocampal damage is linked to

loss of episodic memory (Vargha-Khadem et al., 1998), a prominent feature of AD, and amygdala damage has been associated with emotional and behavioral dyscontrol, prominent features of FTLD (Rosen et al., 2002a; Boccardi et al., 2005). It is therefore possible that both structures may be helpful in differentiating FTLD from AD. However, with recent reports of FTLD cases presenting with episodic memory loss and the existence of a frontal variant of AD, it is reasonable to question whether these so-called signature patterns are really helpful in identifying pathologies. Furthermore, significant hippocampal atrophy has been demonstrated in FTLD cases presenting with language impairment, or SD (see Appendix 7(Chan et al., 2001b)).

The aim of this chapter was to examine the patterns of hippocampal and amygdala atrophy in pathologically confirmed cases of FTLD and AD, and to determine whether either the hippocampus or amygdala was superior in separating AD and FTLD from controls and from one another, or whether a combination of both regions would prove significantly better. In addition we aimed to establish whether differential patterns of hippocampal and amygdala atrophy were occurring in the clinical and pathological subgroups of FTLD.

8.2. Methods

8.2.1. Subjects

A group of 17 pathologically confirmed FTLD patients (five PiD, eight FTLD-U, three tau exon 10^{+16}, and one DLDH), 10 pathologically confirmed AD patients, and 10 age and gender matched healthy controls were included in this study. All patients had been seen through the Specialist Cognitive Disorders Clinic during life. Two FTLD cases and four AD cases were diagnosed from biopsy rather than post mortem.

Medical records were reviewed and the clinical presentation, disease duration and mini mental state examination (MMSE) score at the time of the MRI study were noted. A family history of dementia was present in all tau exon 10^{+16} cases, two FTLD-U cases and one AD case. The FTLD patients were classified using established clinical criteria into fvFTD (n=12), SD (n=4) and PNFA (n=1) (Neary et al., 1998). None of the FTLD patients had any clinical evidence of motor neuron disease.

8.2.2. Neuropathological procedure

In the post-mortem cases, half of each brain was fixed in 10% buffered formalin for at least four weeks. Each fixed half brain was then cut in 0.5cm thick slices in the coronal plane and tissue blocks were selected from representative areas. After processing and paraffin wax embedding, sections were examined using routine techniques including haematoxylin and eosin, luxol fast blue, cresyl violet, and modified Bielschowsky's silver. Immunohistochemical staining was performed with the following antibodies: neurofilament proteins (RT97 and BF10) (courtesy of Prof. B. H. Anderton, Department of Neuroscience, Institute of Psychiatry, King's College London); Aβ (DAKO, Carpintera, CA); ubiquitin (DAKO); tau 12E8 (Elan Pharmaceuticals); AT8 (Autogen Bioclear), αβ-crystallin (Novacastra); α-synuclein (Courtesy of Dr. Diane Hanger, Department of Neuroscience, Institute of Psychiatry), prion protein (12F10; courtesy of Prof G. Hunsmann, German Primate Center, Göttingen, Germany or KG9, Institute of Animal Health, Compton, UK and 3F4, from Senetek, UK). In six cases (two FTLD and four AD) tissue was obtained from a full thickness right frontal biopsy, fixed in 10% formalin and processed in paraffin wax using standard procedures. Sections were cut and stained as described above.

Pathological diagnosis was based upon consensus criteria (McKhann et al., 2001). The diagnosis of FTLD-U was based on the presence of ubiquitin positive, tau and alpha-synuclein negative, abnormal neurites and neuronal, intra-cytoplasmic inclusions in frontotemporal cortices or the hippocampal dentate fascia. None of the cases classified as FTLD-U in this series had clinical or pathological characteristics of motor neuron disease. The diagnosis of PiD was based upon the findings of silver, tau and ubiquitin positive, intraneuronal Pick bodies in frontal and temporal cortices and subcortical grey matter structures including the amygdala, basal ganglia and brainstem nuclei. Cases in the tau exon 10^{+16} group all had a positive family history and tau exon 10^{+16} C-T (cytosine to thymine) splice site mutations (OMIM 157140.0006 [MAPT, IVS10, G-A, +1]). These cases were included in a previously published clinicopathological series[16]. Cases with frontotemporal lobar degeneration but without tau or ubiquitin positive inclusions were given a diagnosis of DLDH.

8.2.3. Manual Segmentation

T1-weighted MRI were obtained using the standard protocol described in Appendix 4. The software package MIDAS was used for all manual segmentation (Freeborough et al., 1997). If an individual had more than one diagnostic scan, the earliest was chosen for inclusion in the study. The operator traced around all the boundaries of the structure with two orthogonal views available.

Amygdala and hippocampal segmentations were performed using the protocols described in Appendix 5. Prior to ROI measurement, all scans were rigidly registered (six degrees of freedom) to a standard template (Mazziotta et al., 1995) to ensure all

scans were in a similar orientation. Subsequently, each scan was reflected across the mid-sagittal plane, producing two scans, each a mirror image of the other. This enabled the ROIs to be consistently measured on the right hand side of the presented image, whether the ROI was left or right. ROIs were then manually edited in both coronal and sagittal views. The investigators were blinded to the subject's name, diagnosis, and the left-right orientation of the scan. Mean intra-rater variability (calculated from the ratio of the absolute difference in measurements to the mean in each person) was 3% in the hippocampus and 4% in the amygdala, and the intra-class correlation coefficient was 0.98 for both measures. This measure of variability was based upon repeated measurements of 20 hippocampi and 12 amygdalae. No time limits were imposed, and the average segmentation time per structure was approximately 45 minutes.

8.2.4. Statistical Analysis

Data were analysed using STATA version 8 (Stata Corporation, College Station, Texas), and SAS (SAS Institute Inc., Cary, NC, USA). In order to facilitate comparisons of percentage reductions in the different ROIs left and right ROI volumes were analysed following logarithmic transformation. Volumes were also TIV corrected by standardising to mean TIV with TIV derived according to a previously described protocol (Whitwell et al., 2001). Standardisation was carried out separately for the amygdala and hippocampus. For both structures the standardisation was carried out assuming a linear relationship between log transformed values and log TIV with the slopes of the associations estimated from left and right measurements in an expanded control group to improve precision.

Linear mixed models were used to make comparisons between geometric mean volumes by i) disease group (FTLD vs. AD vs. controls in the primary analysis), ii) amygdala vs. hippocampus and iii) left vs. right side. The models incorporated interactions between each of these three factors together with the three-way interaction. Disease group-specific unstructured covariance matrices were used. Contrasts of mean levels were used to estimate effect sizes and likelihood ratio tests used to test the statistical significance of the interaction terms and main effects. The same family of linear mixed models were used to make comparisons between the FTLD subtypes, with subtypes with only a single subject omitted from the formal analysis.

The unstructured covariance models used in the comparison of mean levels lack power to compare variances of volumes between disease groups and regions. For this reason direct product unstructured covariance matrices (amygdala/hippocampus $\otimes$ left/right side) were used to compare variances between i) disease groups, ii) amydgala and hippocampus and iii) left and right sides. Likelihood ratio tests were used to compare amygdala and hippocampal variances (combining results over disease groups and left/right sides) and left and right sided variances (combining results over disease groups and regions). In comparison of variances by disease groups left and right side variances were assumed to be the same, again in order to increase statistical power.

ROC curves were used to investigate the ability of amygdala and hippocampal volume measured on the same side of the brain to differentiate between groups (AD vs. controls, FTLD vs. controls, and AD vs. FTLD). Their discriminatory ability was

compared using logistic regression models relating them individually and together to odds of disease.

8.3. Results

Table 8-1 shows the patient characteristics. There was no significant difference in age or gender distributions between the FTLD, AD and control groups. The MMSE scores were significantly higher in the control group than both the AD ($p<0.001$) and FTLD groups ($p=0.003$), and significantly higher in the FTLD group than the AD group ($p=0.03$). However, there was no significant difference in disease duration and time to death between the FTLD and AD groups.

Table 8-1: Patient characteristics

Subject characteristics	**Controls (n=10)**	**AD (n=10)**	**FTLD (n=17)**
Gender (M:F)	6:4	7:3	11:6
Age (yrs)	55.9 (11.1)	57.0 (8.8)	56.4 (10.2)
Sporadic: Familial	NA	9:1	12:5
MMSE (/30)	28.5 (1.4)	14.7 (5.4) *	21.6 (6.5)*
Mean disease duration (onset – scan) (yrs)	NA	3.1 (0.7)†	3.5 (2.0) †
Mean time to death (scan – death) (yrs)	NA	3.7 (2.3) ‡	4.5 (2.1) ‡

*Age, MMSE, duration and time to death are expressed as mean (standard deviation); † data available in 9 AD subjects and all FTLD cases; ‡ data available only in post-mortem cases; * Significantly different from controls ($p<0.003$)*

Hippocampal and amygdala volumes from the three subject groups are shown in table 8.2 and displayed as scatter-plots in figures 8.1A and 8.1B. Averaging over the hippocampus and amygdala in all subject groups the mean volumes were 5.5% greater (95% CI 0.1%, 11.2%) on the right than the left. This right left difference was more marked in the two patient groups than in controls but this tendency was not statistically significant.

When averaging over left and right regions the mean amygdala volumes were reduced by 15.0 % (95% CI 4.2%, 24.5%) and hippocampal volumes by 16.4 % (95% CI 5.9%, 25.6%) in AD patients compared with controls (calculated using log transformed geometric means). In FTLD patients the corresponding reductions were 43.1% (95% CI 31.9%, 52.6%) for the amygdala and 36.1% (95% CI 27.5%, 43.7%) for the hippocampus. The percentage reductions in the FTLD patients were significantly greater than for those of the AD patients ($P < 0.01$ in both regions).

Variability in hippocampus and amygdala volumes relative to mean levels was greater in FTLD patients than AD patients, and greater in patients than controls ($p<0.001$ for all cases vs. controls, $p=0.02$ for AD vs. FTLD pooling over structures). There was no evidence of differences in variability between amygdala and hippocampal volumes (pooling over left and right and disease groups) or between structures on the left and right (pooling over disease groups and structures).

The ROC curves presented in figures 8.2A-C show the utility of hippocampal and amygdala volumes to differentiate between AD and controls (A), FTLD and controls (B), and AD and FTLD (C) respectively. As expected from the comparison of means

and standard deviations, all four volumes (left and right hippocampus, and left and right amygdala) could significantly discriminate between AD (vs. controls), and FTLD (vs. controls and vs. AD) in logistic regression models ($p< 0.05$). When the specificity was set at 80%, the sensitivity for detection of AD subjects from controls ranged from 65% in the left amygdala to 80% in the right amygdala with both hippocampal measures between. In comparison the sensitivity for detection of FTLD from controls was over 90% in all structures and reached 100% in the right hippocampus. In addition, for a specificity of 80% the right amygdala could discriminate FTLD and AD subjects with a sensitivity of 88% whereas the other three structures ranged from 50 to 71%. There was no statistically significant evidence from multiple regression models that combinations of volumes (including ratios of amygdala and hippocampus on the same side of the scan) were better able to discriminate between groups than single volumes. However, the pair-wise comparison of different structures' discriminatory ability provided some evidence ($p=0.028$) that the right amygdala was superior to the right hippocampus in distinguishing between AD and FTLD. However since this was the only statistically significant result from six such comparisons this result should be interpreted cautiously.

Table 8-2: Mean volumes and standard deviations (StDev) of TIV adjusted hippocampus and amygdala in controls, AD and FTLD subjects.

Volume mm^3	**Controls**		**AD**		**FTLD**	
	Left	Right	Left	Right	Left	Right
Amygdala Mean (95% CI)	1555 (1491, 1619)	1618 (1515, 1721)	1314 (1128, 1500)	1415 (1257, 1573)	940 (806, 1074)	976 (830, 1122)
StDev	89	144	260	221	260	283
Hippocampus Mean (95% CI)	2898 (2723, 3073)	2967 (2457, 2937)	2410 (2088, 2732)	2534 (2276, 2792)	1883 (1643, 2123)	1962 (1721, 2203)
StDev	245	336	450	361	466	468

Figure 8.1: Left (A) and right (B) amygdala and hippocampal volume in controls, AD and FTLD patients

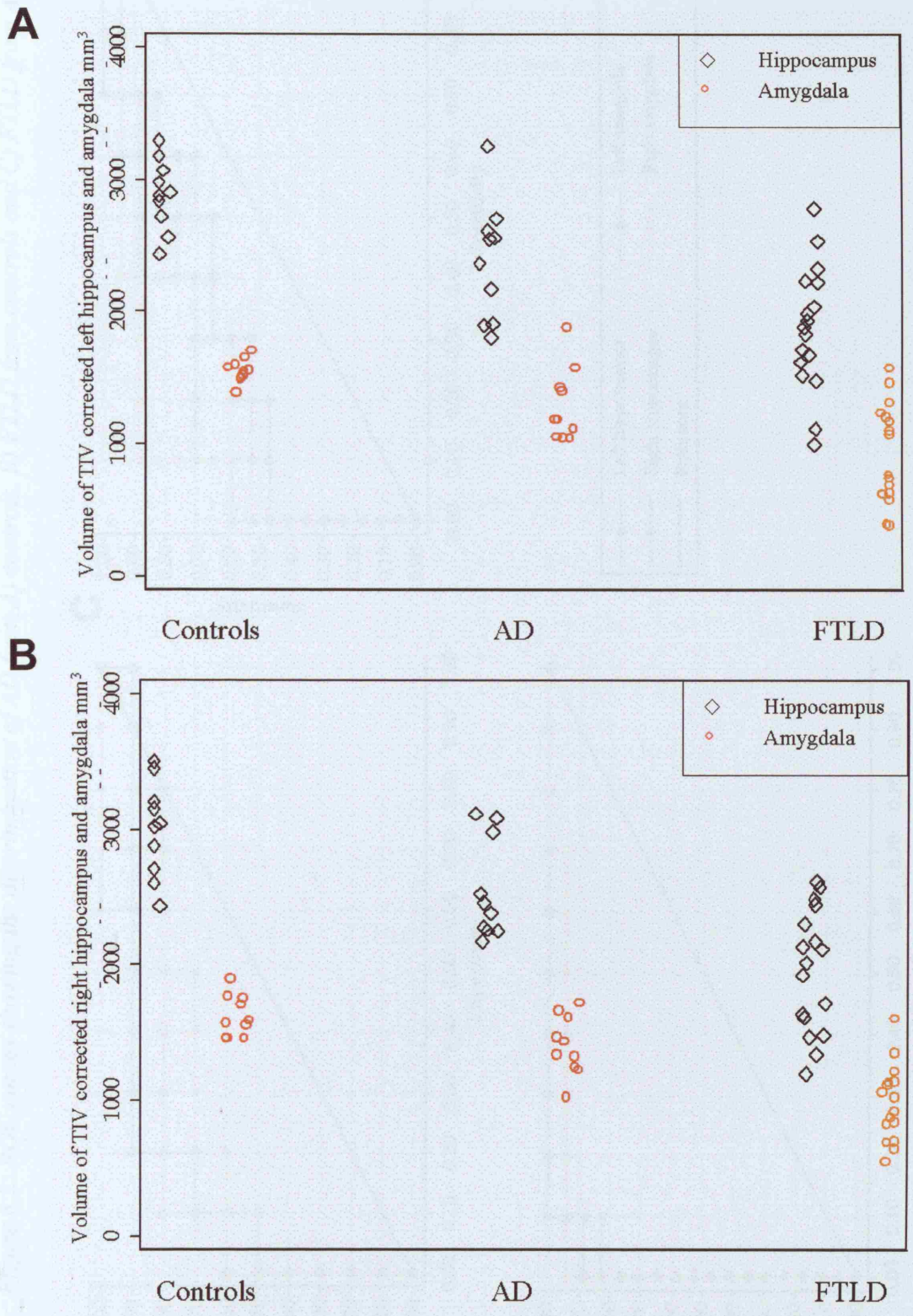

Figure 8.2: ROC curves showing the discrimination of AD from A) controls, B) FTLD from controls and C) FTLD from AD

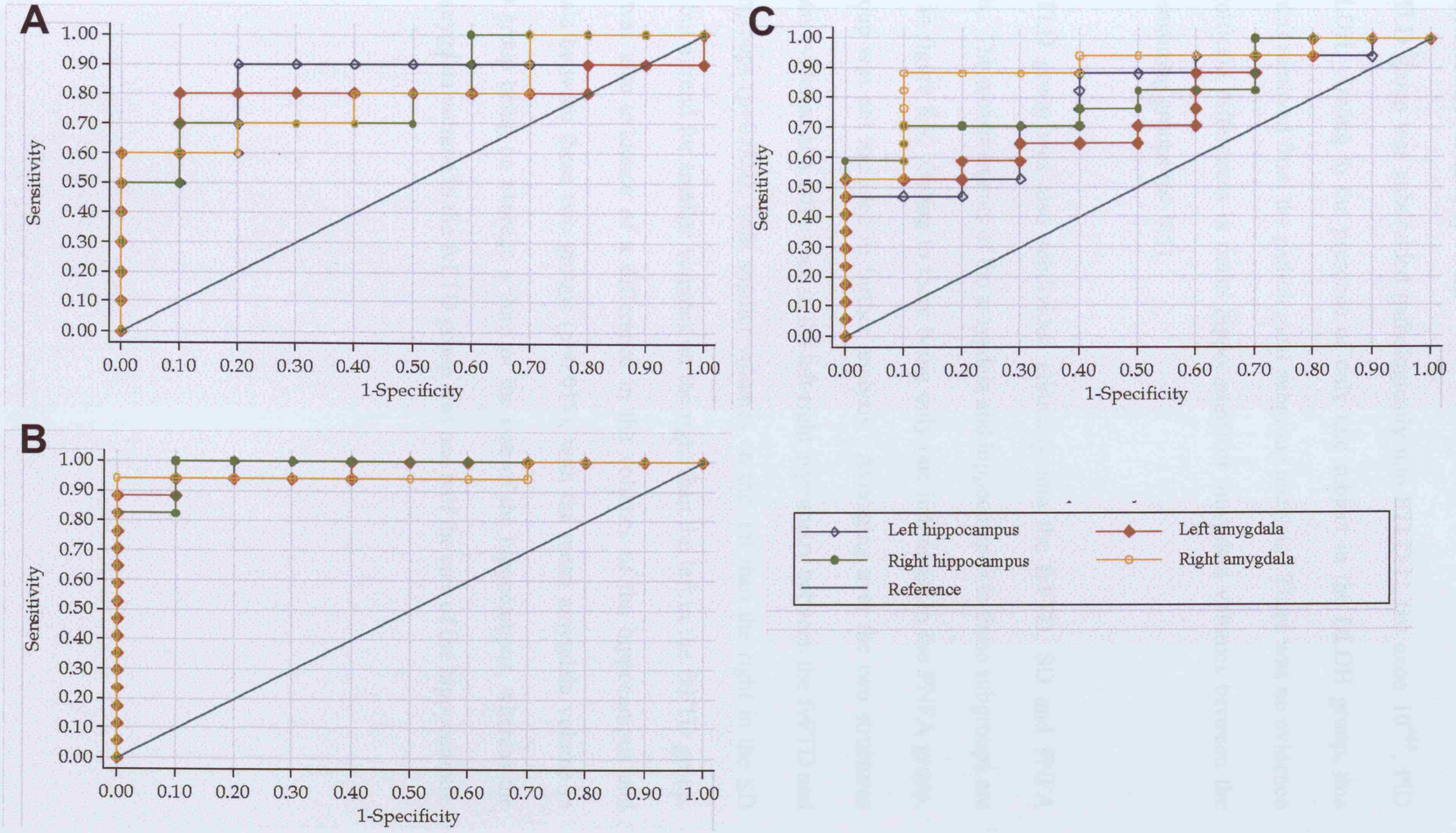

8.3.1. Syndromic variants of FTLD

The FTLD group was subdivided pathologically into FTLD-U, tau exon 10^{+16}, PiD and DLDH. Owing to the presence of only one subject in the DLDH group, this group was removed from the pathological subgroup analysis. There was no evidence for significant differences in mean hippocampal or amygdala volumes between the three remaining groups ($p > 0.5$).

The FTLD group was also subdivided clinically into the fvFTD, SD and PNFA variants. The measurements of the amygdala and hippocampus in these subgroups are shown in figure 8.3. Owing to there being only one individual in the PNFA group, this group was not included in further analysis. Averaging over the two structures there was evidence of a difference in the left-right asymmetry between the fvFTD and SD subgroups (p=0.004), with smaller volumes on the left than the right in the SD group, but a trend for smaller volumes on the right than the left in the fvFTD group. There was also evidence of a difference in the volumes of the hippocampus and amygdala between these two groups (p=0.018), with the mean amygdala volume in the SD group being on average a third of the size of the hippocampus, whereas the mean amygdala volume in the fvFTD group was one half the size of the hippocampus.

Figure 8.3: Left (A) and right (B) amygdala and hippocampal volumes in fvFTD, SD and PNFA patients

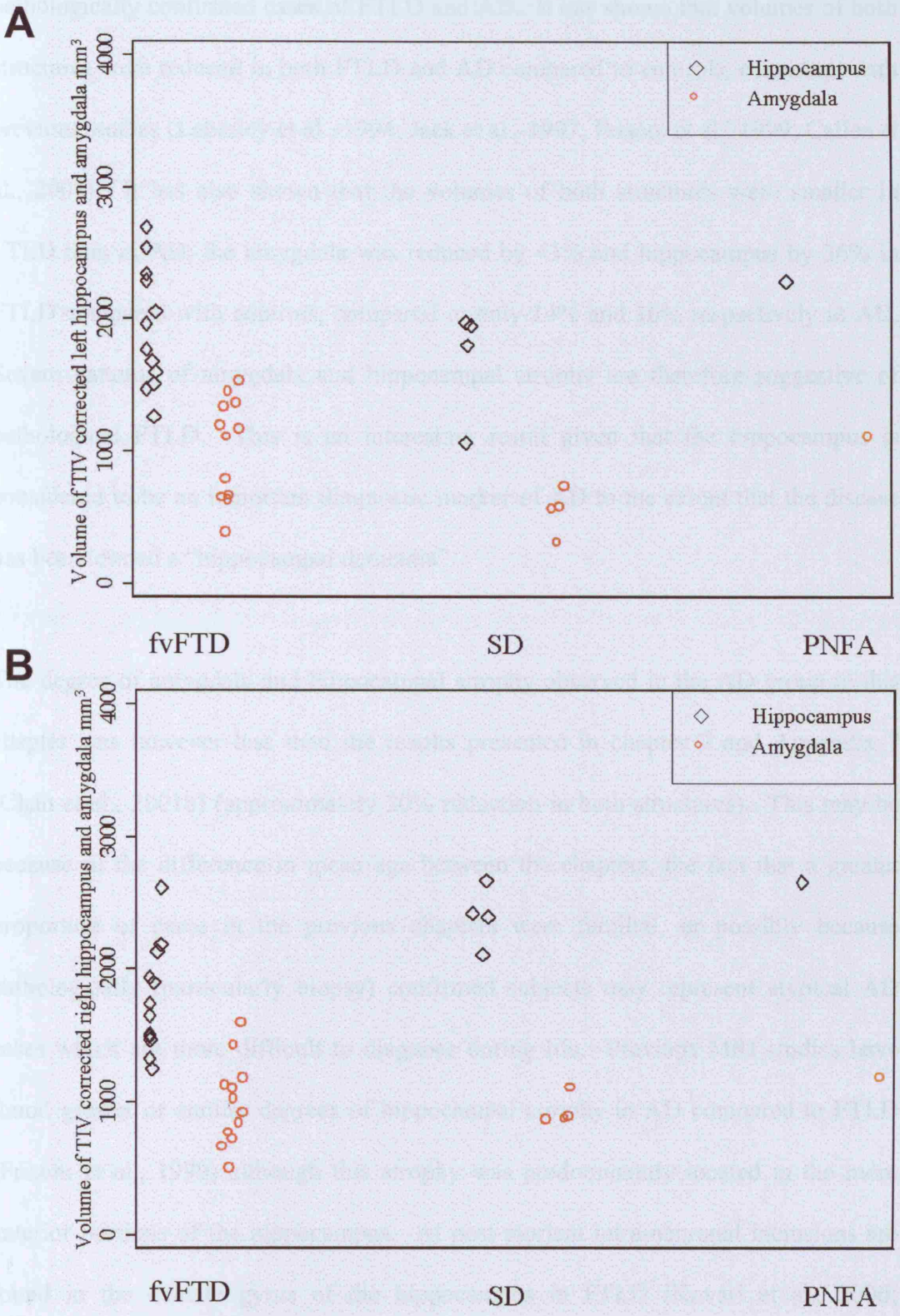

8.4. Discussion

This chapter examined the patterns of amygdala and hippocampal atrophy in pathologically confirmed cases of FTLD and AD. It has shown that volumes of both structures were reduced in both FTLD and AD compared to controls, consistent with previous studies (Lehericy et al., 1994; Jack et al., 1997; Frisoni et al., 1999; Callen et al., 2001). It has also shown that the volumes of both structures were smaller in FTLD than in AD; the amygdala was reduced by 43% and hippocampus by 36% in FTLD compared with controls, compared to only 14% and 16% respectively in AD. Severe patterns of amygdala and hippocampal atrophy are therefore suggestive of pathological FTLD. This is an interesting result given that the hippocampus is considered to be an important diagnostic marker of AD to the extent that the disease has been termed a "hippocampal dementia".

The degree of amygdala and hippocampal atrophy observed in the AD group in this chapter was however less than the results presented in chapter 7 and Appendix 7 (Chan et al., 2001b) (approximately 20% reduction in both structures). This may be because of the difference in mean age between the chapters, the fact that a greater proportion of cases in the previous chapters were familial, or possibly because pathologically (particularly biopsy) confirmed subjects may represent atypical AD cases which are more difficult to diagnose during life. Previous MRI studies have found greater or similar degrees of hippocampal atrophy in AD compared to FTLD (Frisoni et al., 1999) although this atrophy was predominantly located in the more anterior portions of the hippocampus. At post-mortem intra-neuronal inclusions are found in the dentate gyrus of the hippocampus in FTLD (Kovari et al., 2000; McKhann et al., 2001) and hippocampal sclerosis is common (Josephs et al., 2004c).

Severe patterns of focal lobar atrophy are also reported in FTLD at post-mortem; gyri are often so thin that they have a "knife-blade" appearance (Gustafson et al., 1992; Dickson, 2001). So it is perhaps unsurprising that adjacent regions of the temporal lobe such as the amygdala and hippocampus would be affected to a similar degree. It is possible that a pattern of disproportionate medial temporal lobe atrophy is a signature of AD, whereas a pattern of more widespread severe temporal lobe atrophy suggests FTLD. The finding of smaller amygdala volumes in FTLD than AD is consistent with the results from chapter 7, although three subjects were included in both chapters which may partly explain the similarity of results. Disruption of the amygdala as well as other components of the rostral limbic system may contribute to the behavioural deficits observed in FTLD patients (Boccardi et al., 2005).

Measurements of both the hippocampus and amygdala provided good discrimination of FTLD and AD subjects from controls. The specificity of 70% and sensitivity of 90% for discrimination of AD from controls using the left hippocampus is similar to previous hippocampal studies (Xu et al., 2000). The discrimination of FTLD subjects from controls was achieved with a specificity of 80% and sensitivity greater than 90% for all structures, which is superior to the results found in some other studies (Frisoni et al., 1999). Comparisons between studies are difficult because of the difference between subject groups (especially if pathological confirmation is lacking) and differences in severity of disease at the time of the scan. In addition, previous studies have found poor discrimination between AD and FTLD using single volumetric measures (Frisoni et al., 1996c; Frisoni et al., 1999). This study however suggested that for a specificity of 90% both the hippocampus and amygdala could differentiate FTLD from AD with sensitivities over 70%. This improved discrimination is likely

to be because all cases in this study had been pathologically confirmed, whereas all previous studies have used clinically defined groups. Recent studies suggest that only between 63 and 79% of pathologically confirmed FTLD cases are correctly classified clinically on their first assessment (Rosen et al., 2002b; Knopman et al., 2005). As a result, some patients may not be accurately assigned to a patient group which will adversely affect the accuracies of any sensitivities and specificities quoted in such papers. This study found no suggestion that any one structure was significantly superior to any other in the discrimination of AD or FTLD from controls. The right amygdala was significantly superior in the discrimination of the AD and FTLD groups; however this was one significant result following six pair-wise comparisons so caution must be taken with interpretation of this result.

In our FTLD subgroup analysis we were unable to show differential patterns of amygdala and hippocampal atrophy by pathological subtype. However, when dividing our FTLD group by clinical subtype we found differences in the patterns of atrophy. Firstly, the SD patients showed a more asymmetrical pattern of atrophy than the fvFTD group, and second, the SD group had a disproportionately smaller amygdala compared to the hippocampus than the fvFTD group. This is consistent with the previous chapters in this thesis and with other volumetric studies that have shown asymmetric temporal lobe atrophy, with particularly severe amygdala atrophy and an anterior-posterior gradient of atrophy, in SD patients (Chan et al., 2001b; Galton et al., 2001a), yet relatively symmetrical atrophy in patients with fvFTD (Boccardi et al., 2002; Rosen et al., 2002c).

The major strength of this study is the pathological confirmation of disease in all cases. However, a limitation of using a pathologically defined patient group is that the study may be biased towards cases which were difficult to diagnose during life. Pathological confirmation is most likely to be sought from either biopsy or post-mortem in these unusual cases. Therefore, the study's applicability to more routine cases may be limited. Another limitation which all studies of this type encounter is that of accurately matching AD and FTLD patients for disease severity (as discussed in chapter 7). Although the MMSE has been useful as a measure of disease severity in AD (Fox et al., 1999a), it provides a poor measure in FTLD. It is particularly biased towards the episodic memory deficits found in AD patients and is insensitive to the behavioural dysfunction observed in FTLD patients. It is also much influenced by language dysfunction, and so is often disproportionately low in patients with SD and PNFA. The MMSE score was higher in the FTLD group than the AD group in this study, probably reflecting the predominance of the behavioural, or frontal, variant of FTLD. Owing to this potential problem we also assessed the disease duration of all patients. Both the AD and FTLD groups had similar mean disease duration of approximately three years.

The patient groups were also relatively small in this study, especially in the FTLD subgroups. Therefore more subtle differences that may exist in hippocampal and amygdala atrophy between AD and FTLD, and between the pathological and clinical subgroups of FTLD, may not have been detected. One additional limitation is the possible circularity introduced into the clinical diagnosis of the FTLD subgroups since the MRI scan is routinely used as a guide to clinical assessment and diagnosis.

We attempted to reduce this potential effect by choosing the earliest scan available and accepting the last clinical assessment prior to death.

8.5. Conclusion

This chapter has shown that within three years of symptom onset both the hippocampus and amygdala are significantly reduced in volume in pathologically confirmed cases of AD and FTLD compared to controls, with the greatest loss shown in the FTLD subjects. This confirms that hippocampal atrophy is not specific to AD, and that in actual fact severe hippocampal atrophy suggests pathological FTLD rather than AD. Both structures provide good discrimination of disease groups from controls, and from each other. In addition, there was a suggestion that atrophy of the amygdala (more atrophic in FTLD) may provide the best discrimination between AD and FTLD groups. No differential patterns of atrophy were observed when comparing measures across pathological subgroups; however the syndromic variants of FTLD did show differences in asymmetry and the relative patterns of amygdala and hippocampal atrophy. This study may have important implications on the interpretation of visual assessments of hippocampal and amygdala atrophy on MRI.

9. MRI correlates of FTLD pathology

9.1. Introduction

This thesis has so far concentrated on examining the patterns of atrophy in the clinical syndromes of FTLD. However, pathology provides the only definitive diagnosis of FTLD. Unfortunately the pathological subtypes of FTLD are highly heterogeneous and do not map neatly onto the clinical syndromes (see chapter 1), making it difficult to predict FTLD pathology during life. The identification of reliable *in vivo* predictors of tissue pathology would be very valuable for the development, evaluation and monitoring of disease-modifying therapies in FTLD. Volumetric brain MRI can reliably distinguish the clinical syndromes of FTLD from other neurodegenerative disorders based on patterns of regional atrophy, however the role of MRI techniques in the identification of tissue pathology in FTLD has not been established and remains contentious (Bird et al., 1999; Kertesz et al., 2000b; Kril and Halliday, 2004).

The aim of this chapter was to evaluate the potential of brain MRI to predict FTLD pathology. The patterns of atrophy on MRI were assessed firstly, in tau-positive and tau-negative cases of FTLD, and second, in the specific pathological substrates of FTLD. In both studies the patterns of atrophy were examined retrospectively in cases of FTLD ascertained on pathological grounds.

9.2. Correlates of tau immunohistochemistry

9.2.1. Introduction

Tau is a microtubule-associated protein that has been implicated in the pathogenesis of many sporadic and hereditary neurodegenerative diseases. In the normal brain, alternative splicing from a gene on chromosome 17q21 produces six different isoforms of tau. A number of mutations in the tau gene on chromosome 17 have been identified in families with FTLD (Hutton et al., 1998; Petersen, 2001; Rosso and van Swieten, 2002; Schott et al., 2002; Cummings, 2003). FTLD can be divided into those with (tau-positive), and without (tau-negative), tau-positive inclusions. It is possible that a different neurobiological process underlies the neurodegeneration in each of these forms of the disease, and consequently the two variants may show different patterns of progression. There is a suggestion that patients with tau-positive pathology have a slower rate of progression than those without (Hodges et al., 2003; Roberson et al., 2005). However, post mortem studies have not established patterns of brain atrophy that reliably distinguish diseases with and without tau pathology (Mann and South, 1993; Broe et al., 2003; Kril and Halliday, 2004). Pathological cases series are likely collectively to represent a more advanced stage of disease; brain imaging during life might detect specific macroscopic correlates of tau dysfunction at an earlier stage of disease.

In this study, the MRI phenotypes of tau-positive and tau-negative patients were compared using VBM: an unbiased statistical methodology that has already been shown as a useful tool in the identification of characteristic patterns of brain atrophy in the clinical subtypes of FTLD (see chapter 4).

9.2.2. Methods

9.2.2.1. Subjects

From a series of cases of dementia that had undergone post-mortem examination or *in vivo* brain biopsy at the Institute of Neurology, London or the Institute of Psychiatry, King's College London between 1990 and 2003, we identified those with pathologically confirmed FTLD who had had at least one volumetric brain MRI study. For patients with more than one MRI study, the first was used. One additional case without pathological confirmation was included: this patient had a recognized mutation in exon10 of the tau gene (tau exon10^{+16}), and the diagnosis was pathologically confirmed in a sibling. Seventeen patients were identified, and were diagnosed clinically as having fvFTD (13 cases), SD (three cases) or PNFA (one case) according to current consensus criteria (Neary et al., 1998) (table 9-1).

9.2.2.2. Neuopathological procedure

The neuropathological procedures were as described in chapter 8. Pathological diagnosis was based on consensus criteria (McKhann et al., 2001). In patients with tau pathology and an autosomal dominant pedigree, the tau gene was sequenced and screened for known mutations. Two pathological subgroups were defined: a) "tau-positive" = patients with tau inclusions (nine cases), consisting of four cases of familial FTLD with tau exon 10^{+16} mutations (tau exon 10^{+16}) and five cases of sporadic PiD; b) "tau-negative" = patients with ubiquitin-positive, tau-negative inclusions (FTLD-U, eight cases). Characteristics of the tau-positive and tau-negative subgroups are summarised in table 9-1. There was no significant difference in disease duration or clinical severity (as indexed by MMSE and CDR) between the tau-

positive and tau-negative groups; although the mean age of patients in the tau-negative subgroup was significantly older than the tau-positive subgroup (p=0.02).

Table 9-1: Characteristics of tau-positive and tau-negative groups

	Tau-positive (n=9)	Tau-negative (n=8)
Gender (M:F)	5:4	6:2
Age (yrs)	51.8 ± 8.7	62.7 ± 6.8†
Handedness (R:L)	7:1*	7:0*
Duration of symptoms (yrs)	4.0 (2.1)	3.9 (2.3)
MMSE (/30)	21.2 (4.5)	22.0 (5.5)
CDR	1.4 (0.2)	1.2 (0.5)

*Values refer to mean (standard deviation) at time of brain MRI. * Handedness information was not available for all subjects. † $p<0.05$ (Mann-Whitney U test)*

9.2.2.3. Image analysis

In all 17 patients and in 20 healthy age- and sex-matched controls, T1-weighted volumetric MR scans were acquired using the standard imaging protocol described in Appendix 3. Distributions of brain atrophy in the tau-positive and tau-negative groups were compared with the control group using VBM; the various processing steps have been described in detail in chapter 3. All images were first normalised to a customised template. This customised template was based on a mean brain image derived from a group of 10 normal controls and 10 patients with a neurodegenerative disease (5 AD, 5 FTLD). None of these patients were included in the study, and all

were age- and gender- matched to the study cohort and acquired on the same MR scanner. The mean image was normalised to a standard stereotactic space defined by the Montreal Neurological Institute (MNI) standard brain (Mazziotta et al., 1995) and spatially smoothed using an isotropic Gaussian kernel of 8mm FWHM. Each subject's normalised brain image was segmented into grey matter, white matter and cerebrospinal fluid. Each grey matter image was masked with a brain region to exclude all non-brain voxels; brain segmentations were performed using a semi-automated technique based on MIDAS image analysis software. Masked grey matter images were modulated and smoothed with an isotropic Gaussian kernel of 8mm FWHM. Regionally specific differences in grey matter volume between the tau-positive and tau-negative subgroups and between each pathological subgroup and controls were assessed using a single subject conditions and covariates model; age and gender were included in the model as nuisance variables. Volume changes in the tau-positive and tau-negative subgroups relative to the control group and between the two pathological subgroups were assessed at every brain voxel by estimating the t score at a significance threshold of $p < 0.05$ corrected for multiple comparisons (FWE) across the entire brain volume according to Gaussian random field theory.

In every subject, the whole-brain volume and TIV were measured from the raw T1-weighted MRI volume using MIDAS image-analysis software as described in chapter 3. Whole brain volume was measured using the protocol described in Appendix 5. To estimate TIV, each volume was registered to the standard MNI template and every 10^{th} axial slice was measured using a fixed threshold (30% of mean brain signal intensity) to outline the outer border of dura, with linear interpolation between slices (see protocol in Appendix 5 (Whitwell et al., 2001)). Segmentations were manually

checked and edited to ensure accuracy. Whole-brain volumes were normalised to TIV and the mean normalised whole-brain volumes in the tau-positive and tau-negative groups were compared in a one-way analysis of variance.

9.2.3. Results

Both the pathological subgroups had significant and extensive cortical volume loss compared with healthy controls (figure 9.1): in both the tau-positive and tau-negative cases, atrophy involved predominantly frontal and temporal cortices and was somewhat more pronounced in the right hemisphere. Areas of atrophy that were common to both tau-positive and tau-negative cases clustered in the anterior temporal lobes, frontal operculae and frontal convexities bilaterally. The locations of maximal volume loss within each of these brain regions in the tau-positive and tau-negative subgroups are presented in table 9-2. No brain regions were involved exclusively in the tau-positive or tau-negative subgroup. However, inspection of figure 9.1 and table 9-2 suggests differences in the distribution of atrophy within the common affected regions between the tau-positive and tau-negative subgroups: for example, atrophy was relatively more severe in the right anterior temporal lobe and bilateral prefrontal regions in the tau-positive cases, and relatively more severe in the left posterior temporal lobe in the tau-negative cases. A direct comparison of the tau-positive and tau-negative cases yielded no significant differences in regional grey matter volume between the two subgroups (threshold $p < 0.05$ corrected). Mean TIV-normalised whole-brain volumes did not differ significantly between the tau-positive and tau-negative subgroups (threshold $p < 0.05$).

Figure 9.1: Patterns of grey matter atrophy in the tau-positive and tau-negative groups of FTLD ($p<0.0001$, uncorrected)

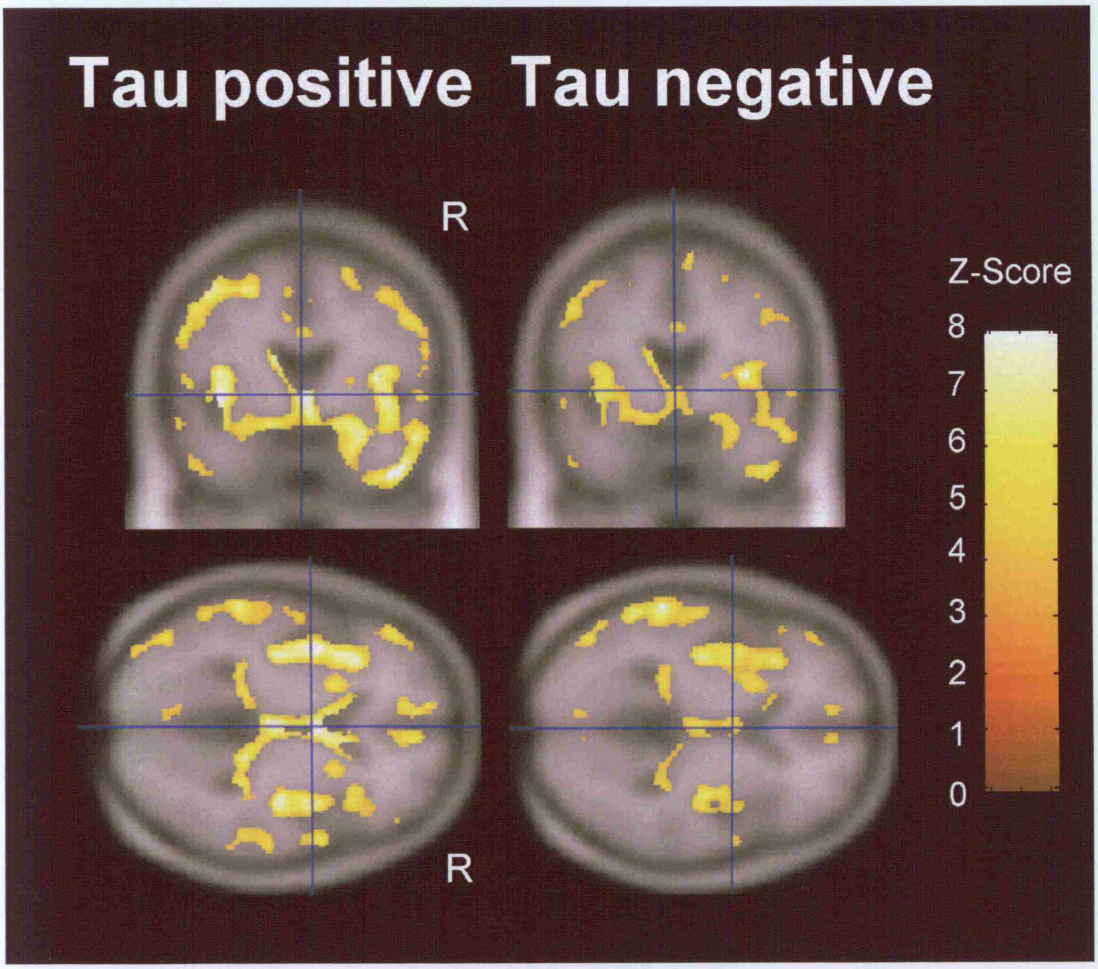

Table 9-2: Locations of maximal volume loss in tau-positive and tau-negative groups. Data are derived from comparisons of each of the two FTLD subgroups with the healthy control subjects. Voxel coordinates are in mm after transformation into standard MNI stereotactic space. Only those local maxima exceeding a stringent statistical threshold of $p<0.001$ corrected for multiple comparisons across the entire brain volume are shown.

Region	**Side**	**Coordinates of maximal volume loss (mm)**			**Z score**
		x	**y**	**z**	
Tau-positive					
Premotor	R	57	-9	38	6.7
Inferior anterior temporal	R	44	7	-42	6.6
Orbitofrontal	R	6	4	-9	6.5
Frontal operculum	L	-42	3	-3	6.2
Frontal operculum	R	37	-2	9	6.1
Medial frontal	R	5	25	44	6.1
Lateral anterior temporal	R	54	8	-25	5.9
Hippocampus	R	34	-13	-16	5.8
Post-central gyrus	L	-60	-24	37	5.8
Orbitofrontal	L	-39	34	-13	5.8
Tau-negative					
Frontal operculum	R	36	-1	9	6.3
Posterior superior temporal	L	-63	-37	0	5.9
Post-central	L	-58	-55	33	5.9

9.2.4. Discussion

This work suggests that patterns of frontotemporal atrophy do not predict the presence or absence of tau pathology, and conversely, that different immunohistochemical profiles are associated with similar patterns of regional vulnerability to neuronal loss in FTLD. These findings support the view that the topography of atrophy rather than immunohistochemistry determines phenotype in FTLD (Petersen, 2001), and emphasise the pathological and genetic heterogeneity of these diseases. The results are consistent with pathological case series that have failed to identify specific macroscopic correlates of tau pathology (Mann and South, 1993; Broe et al., 2003). However, the apparent lack of correlation between tau pathology and the distribution of atrophy on brain imaging should be interpreted cautiously. The number of patients in each of the pathological subgroups here was relatively small, and the study may therefore have lacked sensitivity to detect subtle differences in the cross-sectional profile of atrophy that might emerge in larger populations.

The present data (figure 9.1 and table 9.2) do suggest differences in the profile of frontotemporal atrophy between tau-positive and tau-negative subgroups, however these differences did not attain statistical significance. Even if such differences are substantiated in larger cohorts, they are unlikely to be useful in predicting the pathological diagnosis in the individual patient with an established clinical FTLD syndrome. All of the patients in this study fulfilled consensus clinical criteria for the diagnosis of FTLD (Neary et al., 1998); it remains possible that pathologically determined differences in the profile of frontotemporal atrophy may be present earlier in the course of these diseases (possibly preceding the onset of clinical symptoms), with convergent involvement of cortical regions as the pathological process becomes

more widely distributed. In AD, it is known that the pattern of regional atrophy may shift with advancing disease (Braak and Braak, 1996; Scahill et al., 2002), however little information is presently available concerning the evolution of atrophy in FTLD (this issue is addressed in chapter 11). The prospect of disease-modifying therapies in the neurodegenerative diseases (Rosso and van Swieten, 2002) means that the detection of clinico-radiological correlations would have both maximal specificity and maximal clinical value early in the course of the disease.

It is important to keep in mind that FTLD is highly heterogeneous clinically as well as pathologically, and certain clinical phenotypes such as PNFA are under-represented in the present sample: specific radiological and pathological correlations may exist for clinically defined subpopulations within the FTLD spectrum, though not for the group considered collectively. In addition, both the tau-positive and tau-negative groups are pathologically heterogeneous, consisting of a number of specific pathological substrates. It may be these pathological substrates, rather than the tau immunohistochemistry that determines the pattern and progression of atrophy in FTLD. An uncertain proportion of cases classified as tau-negative using currently available pathological and genetic criteria may nevertheless have tau dysfunction, which might produce a similar pattern of tissue destruction (Rosso and van Swieten, 2002). The rightward asymmetric distribution of anterior temporal lobe involvement in both subgroups here might appear somewhat at variance with previous studies describing a leftward asymmetry of temporal atrophy (Chan et al., 2001b; Galton et al., 2001a; Boccardi et al., 2003): this difference may reflect the relative preponderance of behavioural and personality disturbance (the frontotemporal dementia syndrome) in the majority (13/17) of cases in the present cohort. In contrast

to primary impairments of language (PNFA) or semantic memory (SD), which are associated with selective involvement of frontotemporal regions in the dominant hemisphere (Gorno-Tempini et al., 2004a), frontal behavioural presentations are frequently associated with non-dominant frontotemporal atrophy (Rosen et al., 2002a; Liu et al., 2004).

It remains possible that differences between pathological subgroups may be detected using imaging parameters other than the cross-sectional extent or severity of volume loss: for example, different rates of global or regional brain atrophy (Fox and Schott, 2004) or by using different imaging modalities. The present cross-sectional study detected no significant differences in whole-brain volume between tau-positive and tau-negative cases after a similar duration of clinical disease. However, the direct demonstration of differential rates of atrophy would require the prospective analysis of serial volumetric MR images registered into a common stereotactic space; moreover, differential rates of atrophy might manifest at the level of particular brain regions rather than globally (Scahill et al., 2002). The present findings underline the need for further prospective studies of genetically defined 'at-risk' FTLD populations.

9.3. Correlates of specific tissue pathology in FTLD

9.3.1. Introduction

The previous section suggested that patterns of atrophy on MRI are not useful in differentiating tau-positive and tau-negative cases of FTLD. However, both these groups are pathologically heterogeneous. The tau-positive group includes four different forms of tauopathy: PiD, PSP, CBD, and FTDP-17 (see chapter 1 for details). The tau negative group includes one form with tau-negative, ubiquitin positive inclusions without MND (FTLD-U), one form with tau-negative, ubiquitin positive inclusions with MND and one form with neither tau-positive nor ubiquitin-positive inclusions. These subtypes are defined based on the immunohistochemical characteristics and patterns of neuronal loss.

Recent clinicopathological studies have identified certain clinical predictors of specific tissue pathology in FTLD (Hodges et al., 2004; Kertesz et al., 2005): patients fulfilling clinical criteria for CBD were likely to show CBD pathology, patients with FTLD and clinical features of MND are likely to have ubiquitin-positive pathology, and patients with PNFA tended to have tau positive pathology at postmortem. However, tissue pathology in the important clinical variants fvFTD and SD was generally unpredictable, suggesting that clinical classification alone would not be sufficiently reliable to guide disease-modifying therapies targeted to specific pathological substrates across the FTLD spectrum. Volumetric brain MRI can fairly reliably distinguish Alzheimer and non-Alzheimer dementias based on patterns of regional atrophy, however the role of MRI techniques in the identification of specific tissue pathologies in FTLD has not been established and remains both ambitious and contentious (Bird et al., 1999; Kertesz et al., 2000b; Kril and Halliday, 2004). Whilst

the previous chapter found no differences between pathological subgroups, it was limited to the assessment of only the hippocampus and amygdala. Global patterns throughout the whole brain may be more informative.

The aim of this study was to evaluate the potential of brain MRI to predict the specific pathological substrates of FTLD. Different pathological subgroups were compared using two independent MRI analyses: the unbiased and automated technique of VBM and blinded visual assessment of the pattern of regional atrophy on each MRI scan by an experienced neuroradiologist.

9.3.2. Methods

9.3.2.1. Subjects

Cases were obtained from a series of cases of dementia that had undergone post-mortem examination or in vivo brain biopsy at the Institute of Neurology, London or the Institute of Psychiatry, King's College London between 1990 and 2004. Twenty-one cases of FTLD were identified with at least one volumetric MRI and divided on the basis of pathological and genetic findings into the following groups: FTLD-U (n=9), PiD (n=7), and familial FTLD with tau exon 10^{+16} mutations (tau exon 10^{+16}) (n=5). The number of cases meeting pathological criteria for CBD and DLDH was insufficient to support group analyses and were therefore not included. No case had clinical evidence of MND. A family history of dementia was present in all tau exon 10^{+16} cases and three FTLD-U cases. Two cases without pathological confirmation were included: each of these patients had a recognized mutation in exon 10 of the tau gene (exon10^{+16}), and the diagnosis was pathologically confirmed in a sibling. Medical records were reviewed and the clinical presentation, disease duration, MMSE

score and CDR at the time of the MRI study were noted. CDR was established retrospectively from information given in the records. Clinical classification was based on consensus criteria for fvFTD, SD and PNFA (Neary et al., 1998). The cohort was age and gender-matched to a group of 20 healthy controls. Age, MMSE, CDR, disease duration and time to death, were compared between groups using the Mann Whitney U test, and gender ratios were compared using the Fisher's exact test.

9.3.2.2. Neuropathological procedure

The neuropathological procedures were as described in chapter 8. Pathological diagnosis was based upon consensus criteria (McKhann et al., 2001). The diagnosis of FTLD-U was based on the presence of ubiquitin positive, tau and alpha-synuclein negative, abnormal neurites and neuronal, intra-cytoplasmic inclusions in frontotemporal cortices or the hippocampal dentate fascia. None of the cases classified as FTLD-U in this series had clinical or pathological characteristics of motor neuron disease. The diagnosis of PiD was based upon the findings of silver, tau and ubiquitin positive, intraneuronal Pick bodies in frontal and temporal cortices and subcortical grey matter structures including the amygdala, basal ganglia and brainstem nuclei. Cases in the tau exon 10^{+16} group all had a positive family history and tau exon 10^{+16} C-T (cytosine to thymine) splice site mutations (OMIM 157140.0006 [MAPT, IVS10, G-A, +1]). These cases were included in a previously published clinicopathological series (Janssen et al., 2002; Lantos et al., 2002).

9.3.2.3. VBM analysis

The standard imaging protocol described in Appendix 4 was used for acquisition of T1-weighted images. An optimized method of VBM was used (Good et al., 2001a).

All study images were normalized to the customized template described in the previous study. Each normalized image was segmented into grey matter, white matter and cerebrospinal fluid. Each grey matter image was masked with a brain region to exclude all non-brain voxels; brain segmentations were performed using a semi-automated technique based on MIDAS image analysis software as described previously. Grey matter, white matter and CSF images were modulated and smoothed with an isotropic Gaussian kernel of 8mm FWHM. The smoothed images were analysed using a single subject condition and covariate model that incorporated age and gender as nuisance variables. MMSE score was also included as a nuisance variable to correct for differences in disease severity between the pathological subgroups.

Regional grey matter volumes were compared between pathological subgroups and between each pathological subgroup and controls. Grey matter volume differences were assessed both at an uncorrected statistical threshold ($p<0.0001$) and after correction for multiple comparisons over the whole brain volume ($p<0.05$). Masking procedures were used to identify regions of grey matter atrophy that were common to all pathological subgroups and regions that were unique to each subgroup; these procedures applied Boolean algebra criteria to every voxel in the thresholded statistical parametric map for each contrast. Inclusive masking was used to identify voxels at which grey matter volume loss occurred in every FTLD subgroup relative to controls; exclusive masking was used to identify voxels at which volume loss occurred only in a particular FTLD subgroup relative to controls.

9.3.2.4. Visual MRI assessments

Each MRI scan was graded for regional atrophy by an experienced neuroradiologist, blinded to the pathological diagnosis and to clinical information other than age. Brain regions assessed included the entire temporal lobe, the hippocampus, amygdala, and the frontal, parietal and occipital lobes. In each case, regional brain atrophy was graded numerically as absent (0), mild (1), moderate (2), or severe (3) and normalised for the average atrophy score (corrected score = rating for that region - average rating across all regions for that subject). Pathological subgroups were compared using the Mann-Whitney U test, and corrected atrophy scores were compared between hemispheres using the Wilcoxon signed rank test.

9.3.3. Results

9.3.3.1. Patient characteristics

There were no significant differences in age or gender distribution between any of the pathological subgroups and the control group (table 9-3). All the pathological subgroups had significantly lower MMSE scores than the control group ($p<0.03$), and the PiD group had significantly lower MMSE scores ($p<0.02$) than the tau exon 10^{+16} group. There were no significant differences in disease duration between the patient groups. The majority of patients had a clinical diagnosis of fvFTD, approximately equally distributed among the pathological subgroups; three of the four patients with SD had FTLD-U and the single patient with PNFA had PiD on pathological examination (table 9-3).

Table 9-3: Patient characteristics of control subjects and patients at MRI

Subject characteristics	Controls (n=20)	Pathological subgroup		
		FTLD-U (n=9)	PiD (n=7)	tau exon 10^{+16} (n=5)
Subjects: M:F (% total)	11:9 (55)	7:2 (78)	4:3 (57)	3:2 (60)
Handedness Right: Left	NA	8: 0 *	5: 1 *	5: 0
Age (yrs): mean (StDev)	55.7 (12.3)	60.8 (8.5)	51.6 (11.7)	54.9 (4.9)
MMSE (/30): mean (StDev)	28.8 (1.4)	22.8 †† (5.6)	16.5 †† ‡ (5.6)	26.8 † (2.2)
CDR (0.5 - 3) mean (StDev)	NA	1.1 (0.5)	1.5 (0.6)	0.9 (0.2)
Disease duration (yrs): mean (StDev)	NA	3.8 (2.1)	3.2 (1.4)	4.9 (3.0)
Time to death (yrs): mean (StDev)	NA	4.8 (2.3)	3.2 (2.3)	5.3 (0.9)
Clinical diagnosis: No. of subjects				
fvFTD	NA	6	5	5
SD	NA	3	1	0
PNFA	NA	0	1	0

*† $p<0.05$ †† $p<0.01$ compared with controls (Mann Whitney U test); ‡ $p<0.05$ compared with tau exon 10^{+16} (Mann Whitney U test). * Handedness information was not available for all subjects.*

9.3.3.2. VBM analysis

Compared with controls, the FTLD-U group showed cortical grey matter atrophy involving frontal and temporal regions, more severe in the left hemisphere; the PiD group showed severe and extensive bifrontal atrophy, with milder atrophy of the temporal lobes; and the tau exon 10^{+16} group showed rightward-asymmetric atrophy involving the anterior and medial temporal lobes and orbitofrontal cortex (see figure 9.2). Regions surviving correction for multiple comparisons across the entire brain volume in each subgroup are shown in table 9-4; only local maxima exceeding a stringent statistical threshold ($p<0.001$ corrected) are presented. Atrophy was most marked in the insula and left temporal lobe in FTLD-U; in bilateral frontal regions in PiD; and in the right medial temporal region in tau exon 10^{+16}. Compared with controls, very few regions of white matter atrophy reached significance in any of the groups (figure 9.3). White matter atrophy was observed in the right temporal lobe in FTLD-U, and in frontal regions in PiD. All three groups showed CSF expansion bilaterally in the perisylvian fissures compared to controls, with some ventricular expansion in the PiD group (figure 9.4).

Regions of grey matter atrophy common to all FTLD subgroups and regions that were unique to each subgroup compared with controls are shown in figure 9.5. All three pathological subgroups showed atrophy involving middle and inferior temporal gyri, medial temporal lobes, insula, orbitofrontal cortex and sub-fornicial regions (figure 9.5, yellow). Atrophy particular to the FTLD-U group involved the orbitofrontal cortex, posterior superior temporal lobe and posterior fusiform gyri bilaterally; atrophy was more severe in the left hemisphere (figure 9.5, green). Areas of significant atrophy particular to the PiD group predominantly involved the

dorsolateral frontal regions bilaterally (figure 9.5, blue). Regions of significant loss "unique" to the tau exon 10^{+16} group predominantly involved the right medial temporal lobe (figure 9.5, red). On direct statistical comparison between pathological subgroups (threshold $p<0.0001$ uncorrected), the PiD group showed significantly more atrophy in bilateral frontal regions than the FTLD-U and tau exon 10^{+16} groups (figure 9.6), and the tau exon 10^{+16} group showed significantly more atrophy in the right medial temporal lobe than the FTLD-U and PiD groups (figure 9.7); differences between the FTLD-U group and the other pathological subgroups did not reach significance.

Figure 9.2: Statistical parametric maps of grey matter atrophy in FTLD pathological subgroups compared to controls ($p<0.0001$, uncorrected).

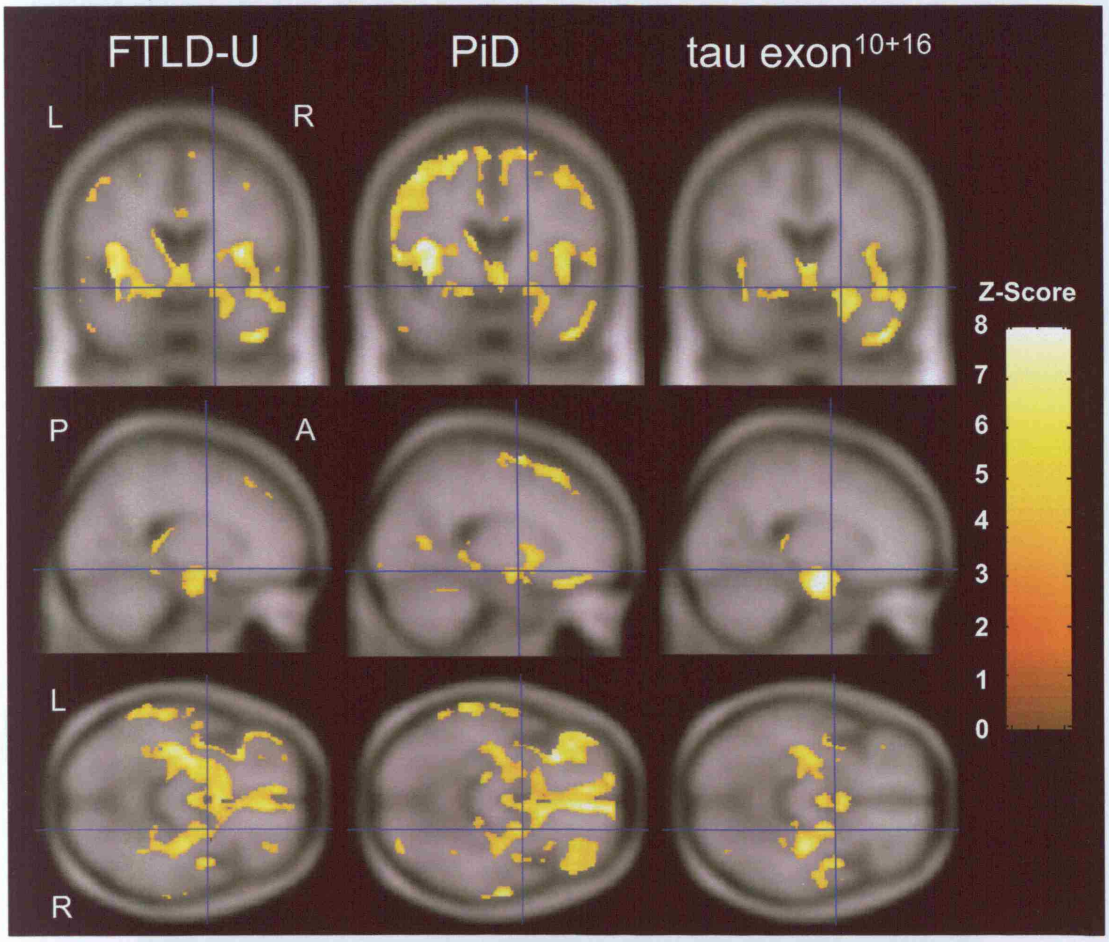

Figure 9.3: Statistical parametric maps of white matter loss in FTLD pathological subgroups (FTLD-U and PiD) compared to controls ($p<0.0001$, uncorrected). No regions of white matter atrophy reached statistical significance in the tau exon^{10+16} group (images not shown).

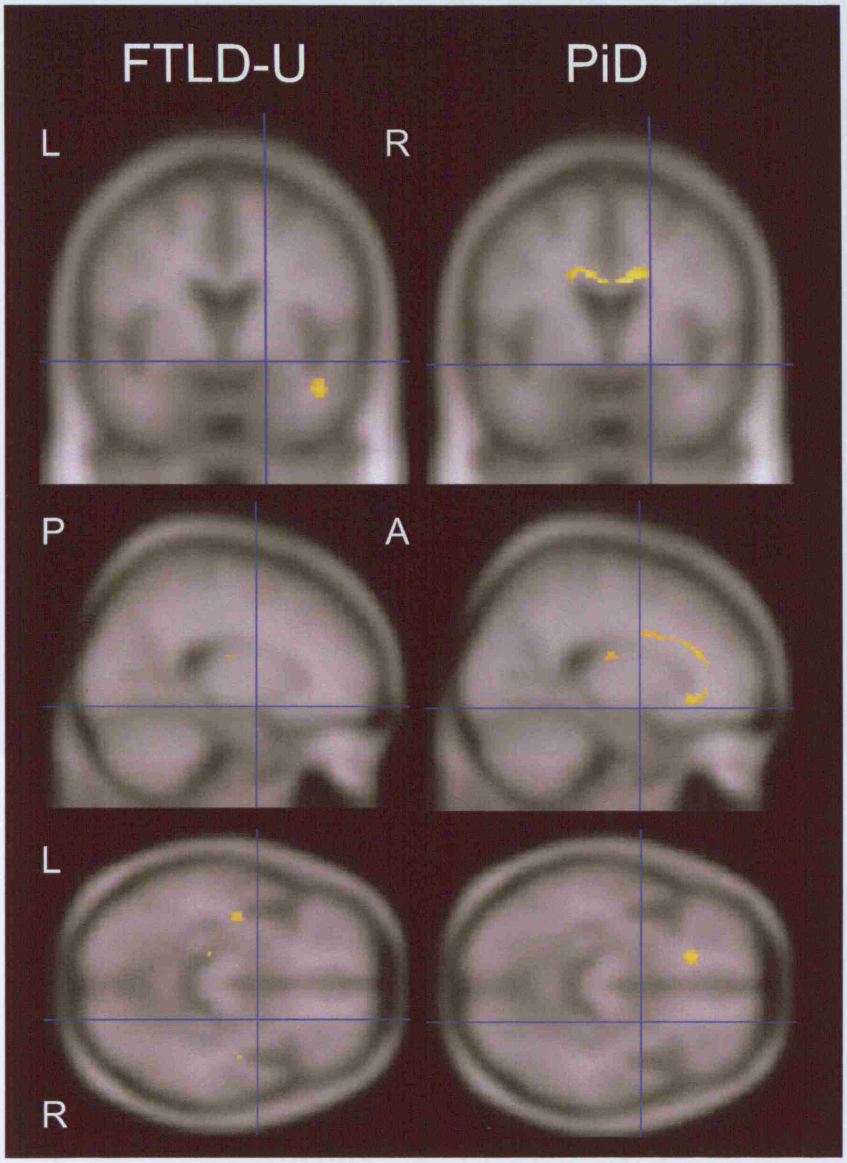

Figure 9.4: Statistical parametric maps of CSF expansion in FTLD pathological subgroups compared to controls ($p<0.0001$, uncorrected).

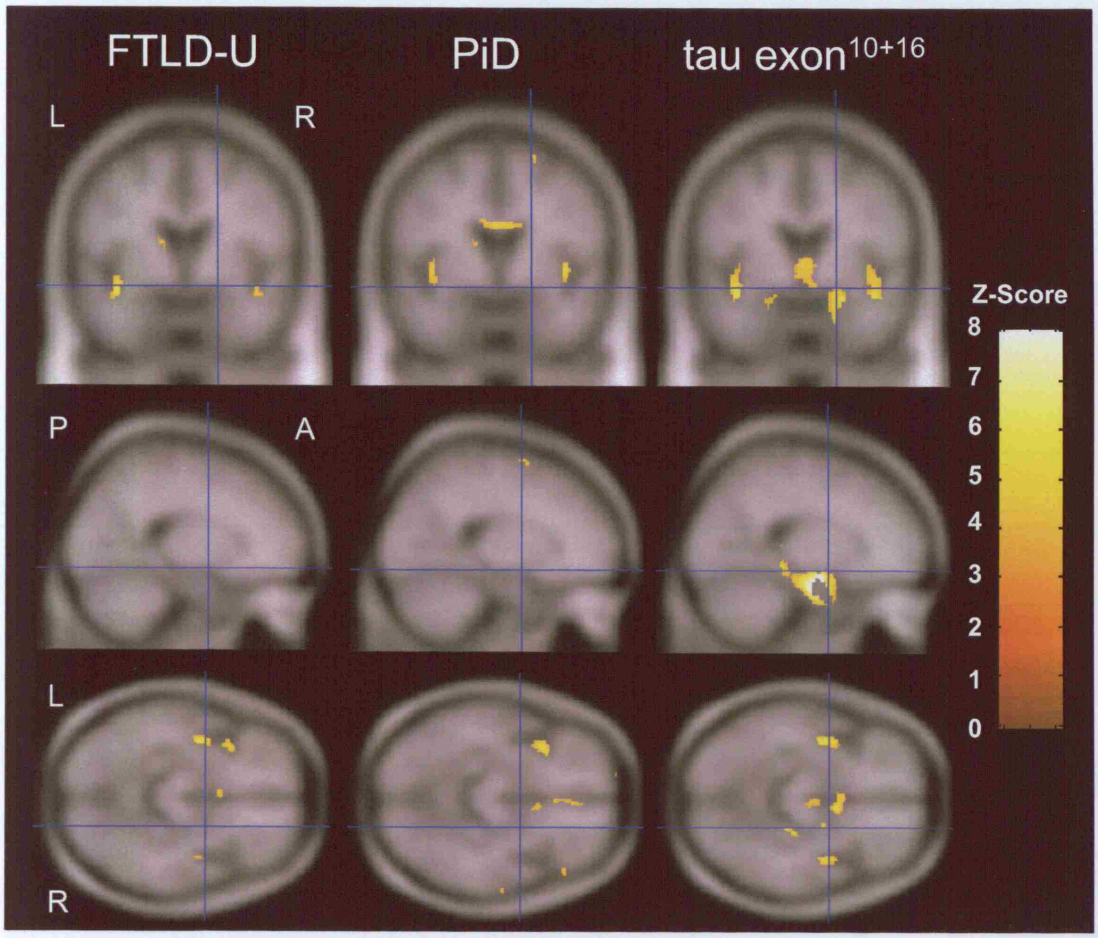

Table 9-4: Regions of grey matter atrophy in FTLD-U, PiD and tau exon 10^{+16} relative to controls. Voxel coordinates are in mm after transformation into standard MNI stereotactic space. Only local maxima exceeding a stringent statistical threshold ($p < 0.001$ corrected for multiple comparisons across the entire brain volume) are presented. The uncus includes the amygdala and medial temporal cortex overlying the amygdala.

Region	**Side**	**Coordinates**			**Z score**
		x	**y**	**z**	
FTLD-U					
Posterior insula	R	36	-2	9	6.30
Posterior middle temporal gyrus	L	-58	-28	-6	6.06
Anterior insula	L	-34	22	-4	6.03
PiD					
Dorsolateral frontal atrophy	L	-20	22	58	7.09
Anterior insula	L	-32	20	-3	6.76
Ventromedial frontal atrophy	L	-10	48	2	6.51
Anterior cingulate	R	6	21	46	6.44
Posterior insula	R	36	-15	4	6.00
Dorsolateral frontal atrophy	R	57	-10	38	5.93
tau exon 10^{+16}					
Medial temporal (uncus / hippocampus)	R	21	-10	-24	6.34
Inferior temporal / fusiform gyri	R	33	9	-44	5.91

Figure 9.5: Statistical parametric maps of grey matter atrophy in FTLD pathological subgroups compared to controls. Regions involved only in a particular subgroup and regions involved in all subgroups are shown on coronal sections of the mean customized template brain (MNI stereotactic y coordinate in mm) through the anterior commissure (y = 0), the temporo-parietal junction (y = -40), and the anterior temporal and frontal lobes (y = 15) (p<0.0001 uncorrected).

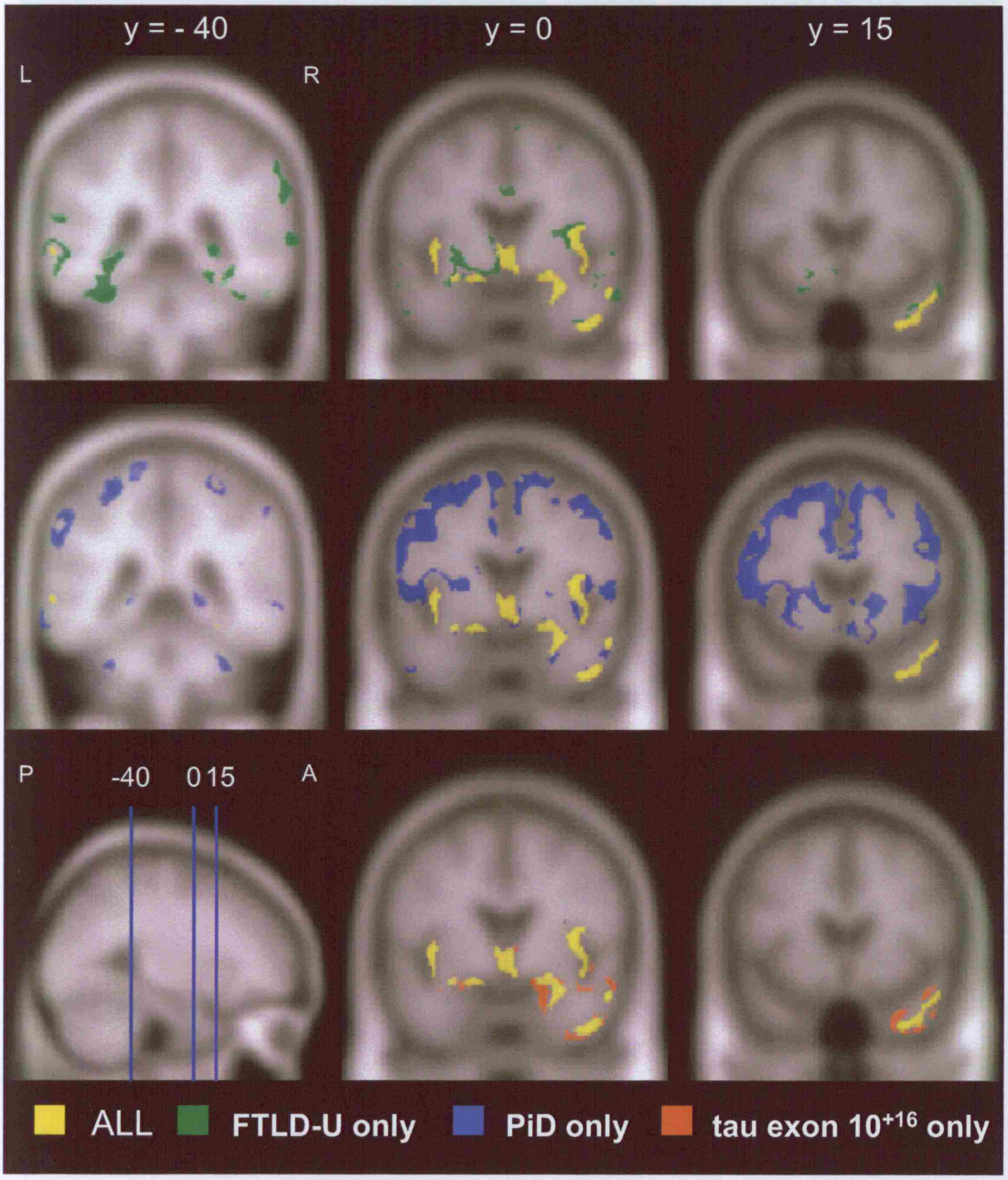

Figure 9.6: Statistical parametric maps of grey matter atrophy in PiD compared to both FTLD-U and tau exon10+16 groups ($p<0.001$, uncorrected).

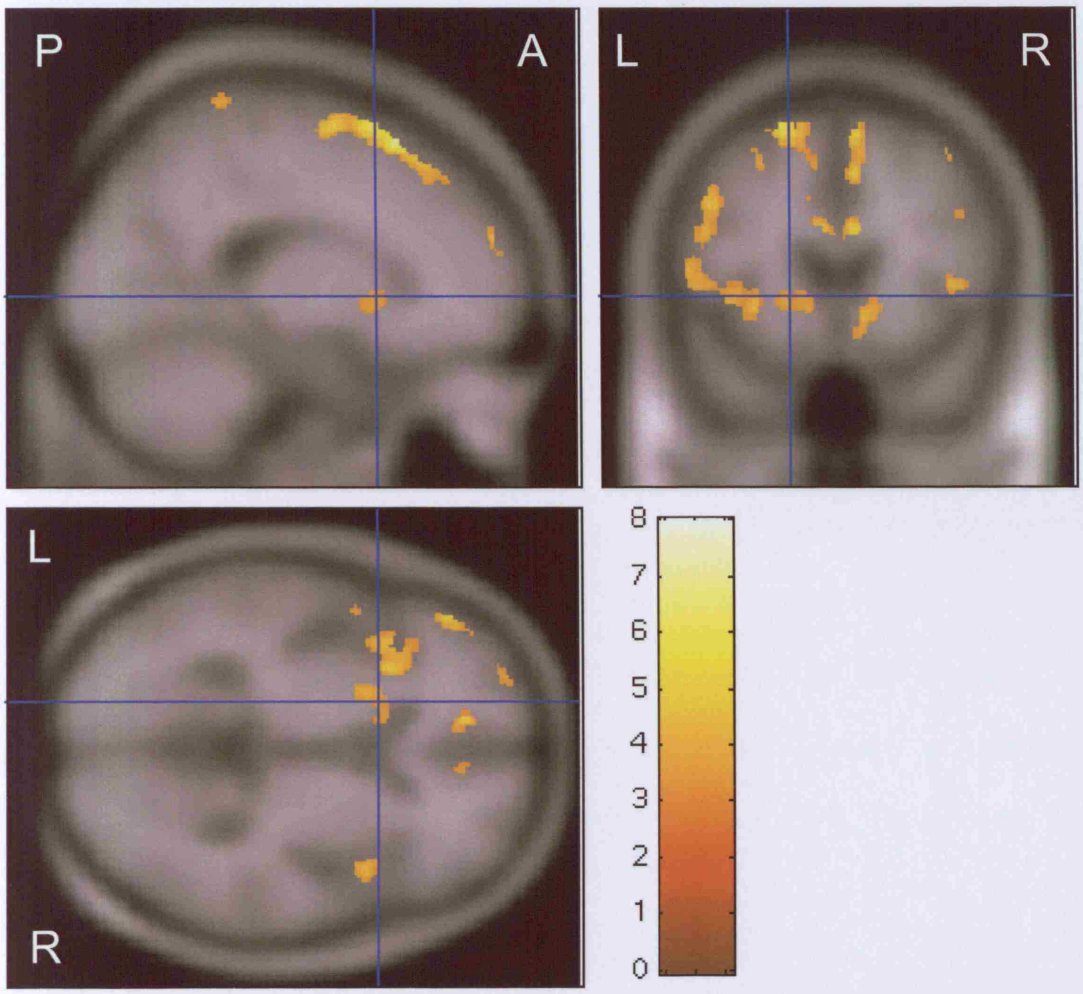

Figure 9.7: Statistical parametric maps of grey matter atrophy in tau exon10+16 compared to both FTLD-U and PiD groups ($p<0.001$, uncorrected).

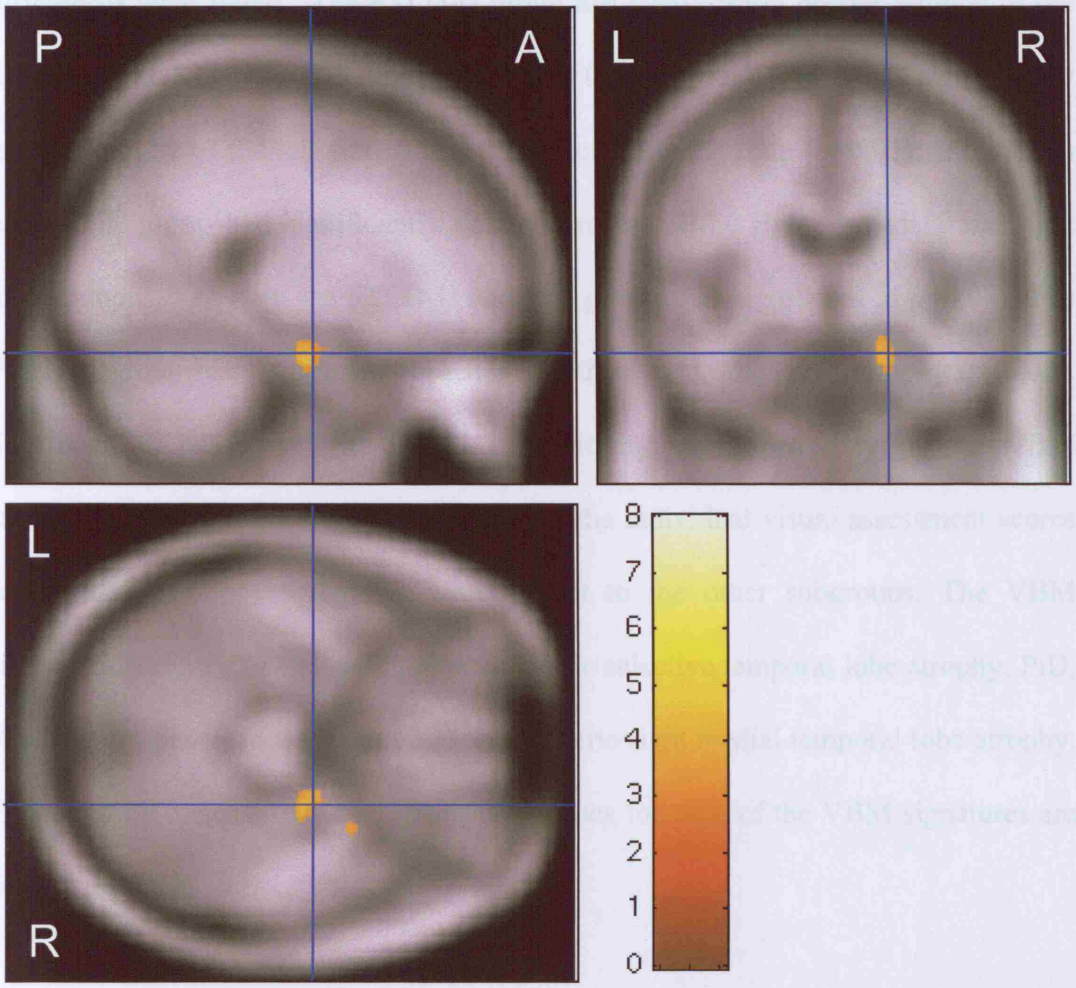

9.3.3.3. Visual MRI assessments

The results of visual assessments of atrophy are shown in figure 9.8. Despite variation in the distribution of atrophy at the individual level, significant inter-group differences were found. The FTLD-U group had significantly greater atrophy of the left temporal lobe than the PiD group (p=0.04); the PiD group had significantly greater atrophy of the left frontal lobe than the FTLD-U group (p=0.03); and the tau exon 10^{+16} group had significantly greater atrophy of the right amygdala and right hippocampus than both the FTLD-U and PiD groups (all significant at p=0.04). The FTLD-U group had significantly greater left, than right, amygdala atrophy (p=0.02). The positive predictive value (PPV), sensitivity, and specificity of the VBM signatures of pathology were estimated from the individual visual assessment scores for each pathological subgroup with respect to the other subgroups. The VBM signatures were: FTLD-U, leftward-asymmetric selective temporal lobe atrophy; PiD, bifrontal atrophy; and tau exon 10^{+16}, asymmetric right medial temporal lobe atrophy. Estimated PPV, sensitivity and specificity values for each of the VBM signatures are presented in table 9-5.

*Figure 9.8: Histograms showing mean (standard error) corrected scores for visual assessments of atrophy in FTLD patients. † FTLD-U > PiD ($p<0.04$); ‡ PiD > FTLD-U ($p<0.03$); * tau exon 10^{+16} > PiD and FTLD-U (all significant at $p<0.04$)*

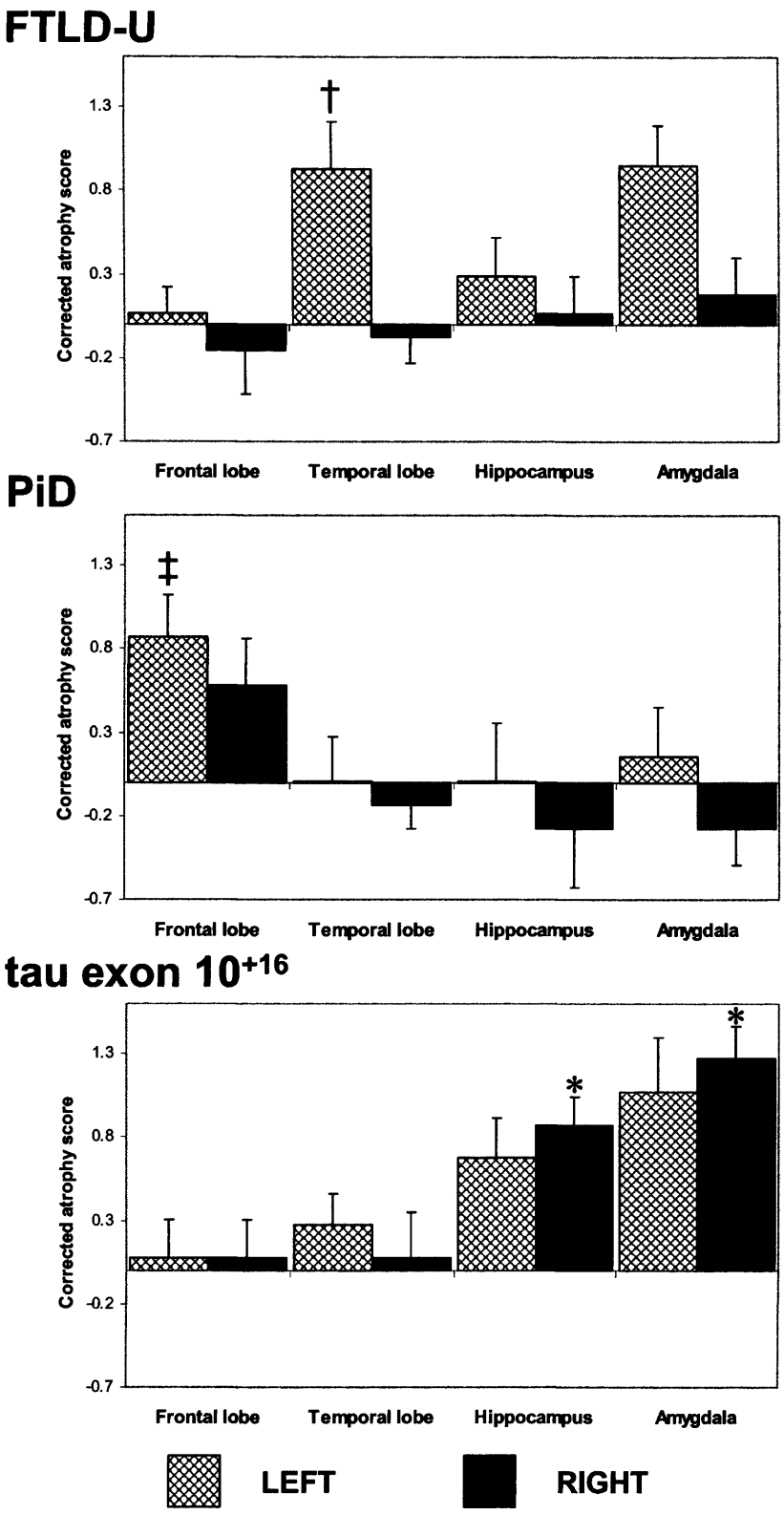

Table 9-5: The positive predictive value (PPV), sensitivity, and specificity of VBM signatures of pathology were estimated from the individual visual assessment scores for each pathological subgroup with respect to the other subgroups.

	Characteristics of MRI signatures of pathology based on visual assessment scores					
	FTLD-U (n = 9)		**PiD (n = 7)**		**tau exon 10^{+16} (n = 5)**	
	No.	%	No.	%	No.	%
PPV	6/8	75	4/6	67	1/2	50
Sensitivity	6/9	67	4/7	57	1/5	20
Specificity	10/12	83	12/14	86	15/16	94

9.3.4. Discussion

This study has analysed MRI patterns of brain atrophy in pathologically defined FTLD subgroups using the parallel, unbiased techniques of VBM and blinded visual assessment. The findings demonstrate that certain brain regions, including the insula, orbitofrontal cortex and temporal lobe, are in general involved across FTLD pathological subgroups when compared with age matched controls. In addition, we have identified profiles of atrophy that differ between subgroups and can be considered as constituting approximate signatures of specific tissue pathology in FTLD. FTLD-U was associated with predominant temporal lobe atrophy, more severe in the left hemisphere, whereas PiD was associated with a more severe pattern of bilateral frontal atrophy, and tau exon 10^{+16} was associated with a more focal pattern of atrophy involving the medial temporal lobe.

Macroscopic examination of the brains of FTLD patients at necropsy has shown predominantly frontal and temporal, and less commonly, parietal atrophy (Dickson, 2001; Lantos et al., 2002). Patterns of regional synaptic loss have been shown to correlate with neuropsychological and behavioural deficits in FTLD (Lipton et al., 2001), however the macro-anatomical correlates of histopathologically or immunohistochemically defined FTLD subgroups are heterogeneous (Mann et al., 1993; Brun, 1994; Hodges et al., 2004; Kril and Halliday, 2004). Necropsy descriptions of asymmetric temporal lobe atrophy in FTLD-U (Kertesz et al., 2000b), severe frontal atrophy in PiD (Brun, 1994) and severe medial temporal lobe atrophy in tau exon 10^{+16} (Lantos et al., 2002) are consistent with the present MRI findings. However, histopathological changes involving the amygdala have been reported as severe in PiD (Dickson, 2001), whereas in the present study radiological involvement

(atrophy) of the amygdala was more severe in FTLD-U than PiD. In a previous histopathological study of tau exon 10^{+16} cases, changes were widespread and, in contrast to our findings, showed no particular predilection for the medial temporal lobe (Lantos et al., 2002). These apparent discrepancies may indicate that the microscopic distribution of tissue pathology does not translate directly to macroscopic volume loss; alternatively, they may reflect the comparison of different disease stages between studies or other sources of between-subject heterogeneity. By the time patients come to necropsy, atrophy is likely to be more widespread and group differences that may have existed at an earlier stage of disease may have been obscured. Macro-anatomical (atrophy) patterns that distinguish FTLD subgroups may be more likely to be derived from imaging than from necropsy studies. Ideally, imaging measures of regional atrophy in FTLD should be directly correlated with quantitative pathological measures of regional tissue loss (Lipton et al., 2001; Kril and Halliday, 2004) and other indices of regional disease involvement (for example, density of inclusions) at necropsy. Such quantitative pathological correlation was not available for the cases included in the present study, but represents a clear direction for future work.

As described in chapter 5, the clinically defined subgroups of FTLD have distinctive patterns of atrophy: fvFTD is typically associated with frontal atrophy, SD with focal left anterior temporal atrophy and PNFA with left perisylvian and inferior frontal atrophy. The distribution of clinical phenotypes in this study (table 9-3) is likely to reflect the clinical spectrum of the respective pathological substrates. For example, the pattern of left temporal atrophy in FTLD-U is consistent with emerging evidence that FTLD-U may be the typical pathology of SD (Rossor et al., 2000; Davies et al.,

2005). Cases in our study were selected on pathological rather than clinical grounds: the MRI signatures we have identified are therefore contingent on specific tissue pathologies rather than their clinical associations. Recent studies have demonstrated that clinicopathological correlations in FTLD are imprecise (Hodges et al., 2004; Kertesz et al., 2005; Josephs et al., 2006b), while the correlation between clinical and radiological findings is itself often difficult. The present study therefore provides complementary information that could be used to predict tissue pathology where this is not possible on clinical grounds alone (for example, in patients presenting with fvFTD).

The present findings were obtained from a relatively small group of well-characterized cases, and may not generalize to more heterogeneous cohorts; the findings need to be validated prospectively in larger populations. It is unclear whether the patterns of atrophy found in the tau exon 10^{+16} group would also be associated with other tau mutations, given the substantial clinical and pathological heterogeneity of familial FTLD (Bird et al., 1999; Lantos et al., 2002). One confound of these between-group comparisons is the difficulty in assessing disease severity and duration reliably in FTLD; as discussed previously MMSE is particularly sensitive to language deficits and CDR to memory impairment, while behavioural change is difficult to quantify. The technique of VBM itself has several potential limitations in atrophic brains that will be discussed further in the overall discussion.

Despite these caveats, independent blinded visual assessment of atrophy supported the findings on VBM, although the convergence between the two methods of evaluation varied depending on the pathological subgroup. In the small groups studied here, on

visual rating, the VBM criterion of leftward-asymmetric temporal lobe atrophy reliably predicted FTLD-U; bifrontal atrophy had relatively high sensitivity and specificity (but poor PPV) for PiD; and the VBM criterion of rightward-asymmetric medial temporal atrophy had poor sensitivity and PPV for tau exon 10^{+16}. On inspection of figure 9.8, medial temporal atrophy was clearly bilateral on visual rating in tau exon 10^{+16}, with only a weak trend for rightward-asymmetry. This apparent discrepancy between VBM and visual rating methods may reflect a wider individual variation in left than right medial temporal volume loss. Due to the small numbers in each pathological subgroup, caution is needed in extrapolating these findings to larger populations. A further issue concerns the usefulness of these findings in distinguishing FTLD from other causes of dementia, in particular AD: available evidence supports distinct MRI profiles in AD and FTLD, however this issue was not addressed directly in the present study. Nevertheless, the present findings suggest that certain radiological patterns may assist in predicting pathological diagnosis in the individual patient with FTLD. These findings might be especially valuable if used in conjunction with clinical indices (Hodges et al., 2004), for example in guiding recruitment to clinical trials.

9.4. Conclusion

The findings of this chapter suggest that MRI signatures of tissue pathology in FTLD may be identified at the time of clinical presentation. Whilst, there were no significant differences overall in the patterns of atrophy between tau-positive and tau-negative cases, there were MRI signatures of the specific pathological substrates of FTLD. Predominant left temporal lobe atrophy suggests FTLD-U; severe bilateral frontal lobe atrophy suggests PiD; and relatively focal right medial temporal lobe atrophy suggests tau exon 10^{+16}. Certain brain regions (such as the right inferior temporal lobe, orbitofrontal cortex or insula) are involved across FTLD subgroups, and are therefore characteristic of FTLD as a whole and of little value in discriminating between histological substrates. The overlap between individuals and between histopathological subgroups in FTLD suggests that MRI findings should be interpreted in conjunction with clinical indices and other biomarkers in order to improve predictive power and diagnostic usefulness in the individual case. The identification of MRI signatures of specific FTD pathologies at the population level may have important implications for the design and analysis of clinical trials.

10. Stability in Longitudinal Scanning

10.1. Introduction

The previous chapters have all concentrated on cross-sectional patterns of regional change in FTLD. However, cross-sectional measures may be confounded by the large amount of variation in brain volumes between individuals. Longitudinal studies which measure change over time in an individual's cerebral volume, use the subjects as their own control, and thereby largely avoid the problem of wide inter-individual variation in brain volume. MR based measures of rates of atrophy from serial imaging have been proposed as diagnostic markers and, more recently, as surrogate markers of disease progression for therapeutic trials in diseases such as AD and multiple sclerosis (Losseff et al., 1996; Jack et al., 1998; Fox et al., 1999a; Simon et al., 1999). However, because rates of change in brain volumes may be relatively small, even in diseases such as AD (Fox et al., 1999b) these longitudinal studies are very sensitive to subtle differences in acquisition.

There are several sources of error that may be introduced to the measurement of volume change derived from an individual's serial scans. These include differences in the amount of movement artefact, alterations in magnetic field inhomogeneity (Styner et al., 2000), machine-dependent scan-to-scan variation in MR image intensity scale (Nyul and Udupa, 1999) and, importantly, voxel size variations due to drifts in scanner calibration or fluctuation in the performance of scanner gradients. The latter may not be obvious on simple inspection but may lead to artefactual changes in the measured volumes of cerebral structures. Freeborough *et al* confirmed that significant inconsistencies in voxel size exist between serial images even on modern

machines, with voxel changes producing an apparent artefactual "stretching" of the brain and cranium (with apparent volume changes of up to 3%) even over short intervals (Freeborough et al., 1996). These resulting intra-individual variations in cerebral volume are under-recognised and are an important potential source of error in progression studies or therapeutic trials. Errors related to drifts in voxel size become more relevant as other sources of artefact (movement artefact, inhomogeneity e.t.c.) are reduced.

Test objects (phantoms) could theoretically be used to correct for these voxel size fluctuations. They can be serially scanned, and relative scanner fluctuations detected either from measurements of the dimensions of the phantom, or from scaling factors provided by registering (positionally matching) the serially acquired phantom images (Lemieux and Barker, 1998). However, the accuracy of the correction depends on the precision to which the test object can be measured, and unless a phantom is scanned concurrently with each acquisition it is not possible to adjust for drift in voxel size on a scan-by-scan basis. The aim of this chapter was to assess two methods that could allow correction for voxel drift on a scan-by-scan basis: firstly, the manual measurement of TIV, and secondly the use of 9dof registration. Both techniques were assessed in control subjects that should be fairly stable over time, and in AD subjects, in which the rates and patterns of longitudinal change have been well established (Fox and Freeborough, 1997), in order to check that the techniques were not confounded by real atrophy. The techniques examined and validated in this chapter could then be applied to the longitudinal analysis of the less well-characterised FTLD patients.

10.2. Intracranial volume normalisation

10.2.1. Introduction

Total intracranial volume can be defined as the volume within the cranium including brain, meninges and cerebrospinal fluid. Measuring TIV allows whole brain and regional volumetric measures to be normalised for head size cross-sectionally. It can be hypothesised that it can also be used to control for variations in voxel size over time. This hypothesis assumes that 1) the TIV is not altered by the disease process; and 2) total or regional brain volumes are more comparable when normalised for TIV. In degenerative diseases, where the whole brain is subject to atrophy, the TIV may provide the best available estimate of premorbid brain volume.

Generally, T2-weighted images have been used to measure TIV (Phillips et al., 1998; Miki et al., 1999; Jenkins et al., 2000) because the high signal of CSF on T2 makes identification of the TIV surface relatively easy (see chapter 2). In some studies simple estimates of size which correlate with the TIV (e.g. intracranial width or cross-sectional area) have been used (van der Knaap et al., 1992; Laakso et al., 2000). However, width or cross-sectional area measures cannot account satisfactorily for the great difference between individuals in head shape, and measurement reproducibility is dependent upon choice of position and plane of view. The TIV measure should ideally be performed on the same acquisition as that used to calculate the brain volumes as this will minimise scanning time and ensure that brain and TIV measures are affected systematically (similarly) by any scan acquisition factors. In contemporary structural imaging this usually means measuring TIV from a T1-weighted volumetric image. It will also allow retrospective normalisation of brain volume in patients lacking a T2-weighted image. The TIV may be used to normalise

volumes either by simple division, as in this study, or by using the covariance method (Jack et al., 1989).

This study aimed to a) demonstrate that TIV normalisation of cross-sectional brain volumes can reduce individual variation, then b) develop a TIV measured on a T1-weighted image and validate it against the existing T2-weighted TIV. It also aimed to assess fluctuations in intra-individual structural volumes in serial images that could be caused by scanner acquisition differences, and show that normalisation of every image using a T1-weighted TIV can reduce these differences.

10.2.2. Methods

10.2.2.1. Subjects

Fifty-five healthy control subjects (twenty-four male and 31 female) with an age range of 23-83 years underwent cross-sectional MRI measurements. These clinically normal individuals were recruited from the spouses of patients and normal volunteers. They had no complaints of cognitive impairment and had a MMSE score of ≥27/30. History of stroke, dementia or other overt cerebral pathology were exclusion criteria, but otherwise the subjects were unselected. Ten patients with probable AD, according to the NINCDS-ADRDA criteria (McKhann et al., 1984), underwent identical MR measurements on serial imaging, five had inter-scan intervals of one year (mean MMSE score decreased from 22.4 ± 5.3 to 17.0 ± 6.7 over this period), and five had intervals of only 2-4 weeks (mean MMSE 17.2 ± 2.8 on baseline). These were analysed alongside ten healthy controls with three serial images. In addition two individuals at risk of familial AD had serial MR imaging with over eight scans spanning at least seven years. One individual remains well and has subsequently been

shown not to carry a pathogenic mutation while the other has become clinically affected with AD.

10.2.2.2. Image analysis

T1-weighted volumetric MR images were acquired using the standard protocol described in Appendix 4. Each image had 124 coronal slices with a slice thickness of 1.5mm. T2-weighted dual-echo MR images were acquired with a 240mm field of view and a 256*192 matrix, resulting in 44 5mm slices with 2.5mm interslice spacing. All measurements were performed using MIDAS image analysis software (Freeborough et al., 1997). All segmentations used intensity thresholding with thresholds set empirically as fixed fractions of mean brain intensity or intracranial intensity. This approach requires consistency in image acquisition and will be affected by acquisition problems such as movement artefact and, or, RF-inhomogeneity ("shading") artefact. All scans analysed for this study were relatively free of such artefacts. A number of methods exist for post-acquisition correction of inhomogeneity artefact but these were not used in this study (Sled et al., 1998). Scans with very large movement artefact problems were excluded. All measurements were performed blind to subject details and the results of any other measurements.

10.2.2.3. Brain Segmentation

Whole brain volumes were obtained from the T1-weighted volumetric imaging using a semi-automated iterative 3D morphological technique which has been described in Appendix 5. This technique includes a consistent CSF-brain intensity threshold set at 60% of mean brain intensity. Every slice between the inferior limit of segmentation, set at the lowest point of the cerebellum, and the superior point of the cortex were

measured. Brain segmentations were performed on all controls and AD patients and manually checked and edited to ensure accuracy.

10.2.2.4. TIV measured on T2-weighted images

This measure of TIV uses the T2-weighted images and has been described in detail previously (Jenkins et al., 2000). The inner boundary of the calvarium is outlined using a semi-automatic grey level thresholding technique with a standard threshold set to 60% of the mean intracranial signal intensity (figure 10.1). The inferior limit of segmentation is set as the lowest slice in which cerebellar tissue is present. T2-weighted TIVs were measured in the normal control group, and in five AD patients, at a single time point.

10.2.2.5. TIV measured on T1-weighted images

The TIV was measured from T1-volumetric images put into the orientation defined by the MNI 305 brain average (Mazziotta et al., 1995) using three dimensional registration. The method used for delineating the TIV is analogous to that described above, except the semi-automatic grey level thresholding technique was set at a standard threshold of 33% of the mean intracranial signal intensity to outline the outer border of dura (see Appendix 5, figure 10.2a), this reflects the different contrast in the T1-weighted image as compared to the T2-weighted image. Every 10^{th} axial slice was segmented with the inferior border set as the lowest slice in which cerebellar tissue was present (figure 10.2b). Linear interpolation of areas was used to obtain an estimate of the TIV from the segmented slices. This method is supported by Eritaia *et al* who evaluated various sampling strategies used to measure a TIV from T1-weighted images and concluded that the TIV can be confidently traced using a 1-in-10

slice strategy without significant loss of accuracy (Eritaia et al., 2000). The T1-weighted TIVs were initially measured on two serial scans from a group of five AD patients and five controls, to compare to the T2-weighted TIVs and to look for variability over serial scans. T1-weighted TIVs and brain volumes were then measured on multiple serial images of five AD patients with short scan intervals, ten controls and the two individuals at risk of FAD.

10.2.2.6. Reproducibility

To evaluate the intra-rater reproducibility the brain and TIV measurements were repeated twice, at least a week apart, on ten randomly selected subjects. The inter-rater reproducibilities were assessed by two investigators, blinded to patient details, measuring TIVs and brain volumes on five randomly selected subjects.

10.2.2.7. Statistics

Data were analysed using Microsoft Excel 95 (Microsoft Corporation 1995) and Stata version 6.0 (Stata Corporation 1999). Paired t-tests were used to test for evidence of systematic differences in mean volumes between the different measuring techniques. Regression analyses were used to look at the effect of age and sex on TIV, brain volume, and normalised brain volume. Plots of standardised residuals were examined which indicated that the linear assumptions with age were appropriate. Pearson's correlation coefficients were used to measure the extent of linear association between two variables. Pitman's and Wilcoxon's signed rank tests were used to analyse variability reductions after normalisation.

Figure 10.1: Total intracranial region shown on a T2-weighted image

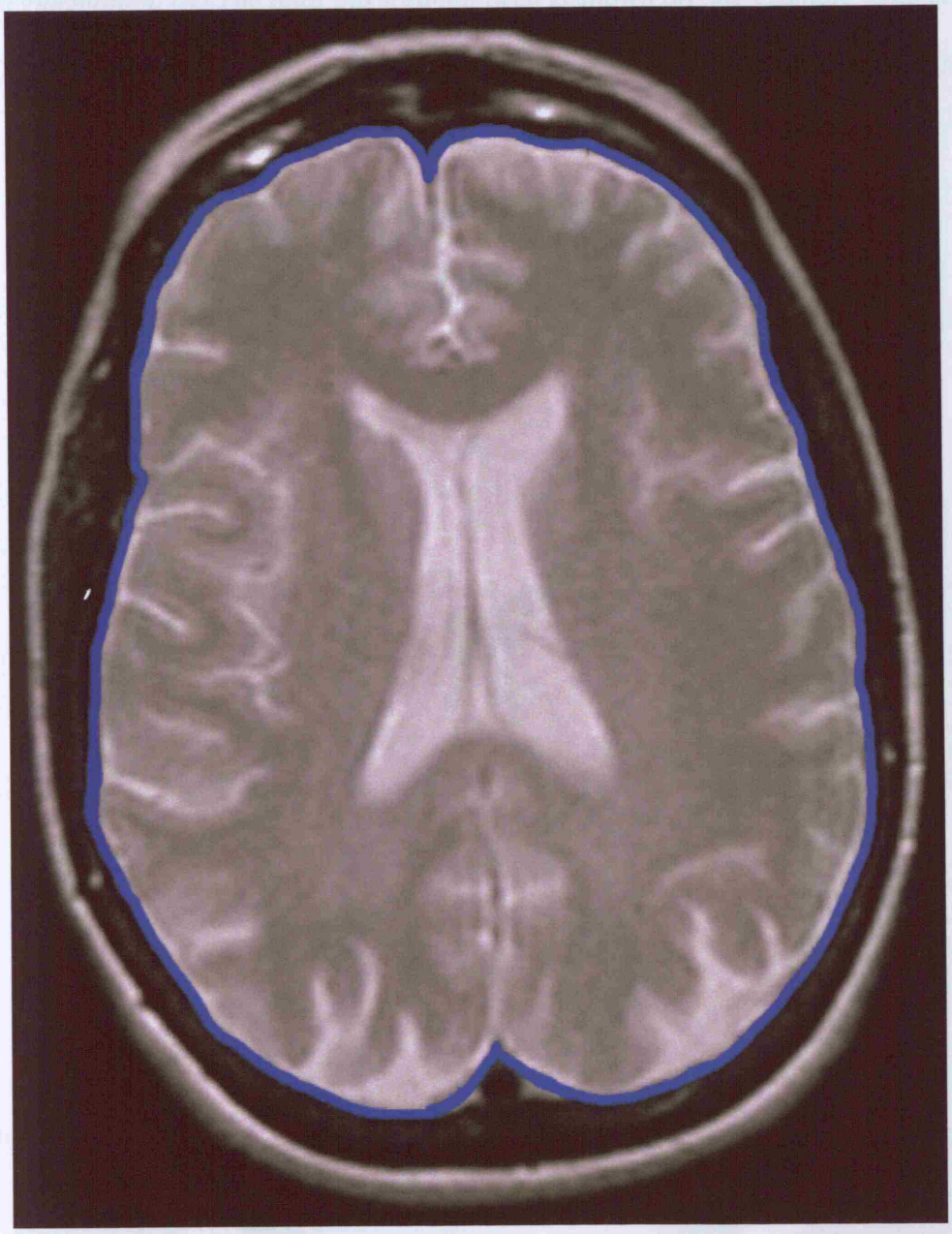

Figure 10.2: TIV shown on a T1-weighted image. The intensity windowing is as used for segmentation. (A) The total intracranial area is shown on one example axial slice. (B) The axial slices used to sample the total intracranial volume are marked on the sagittal view.

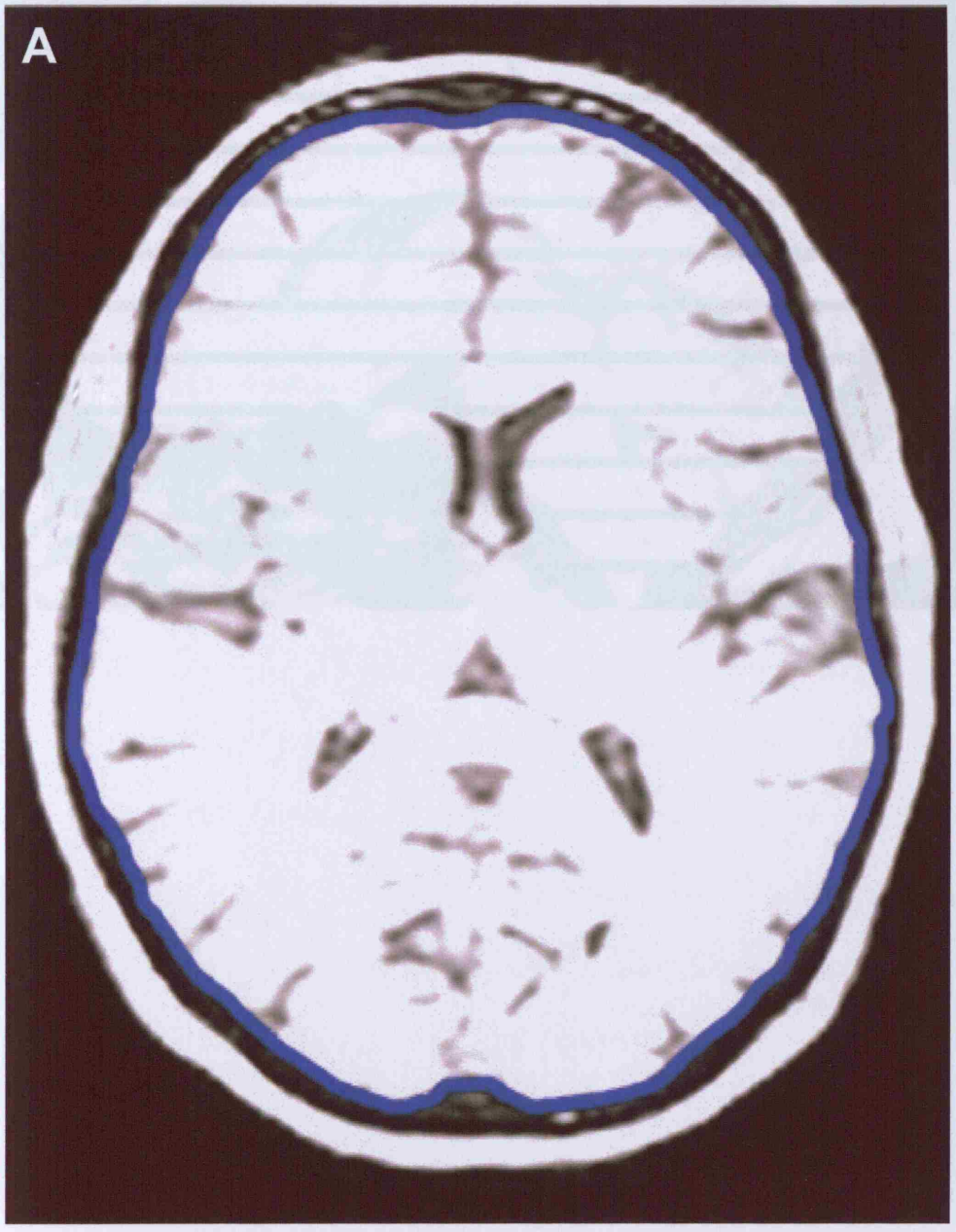

Continued….

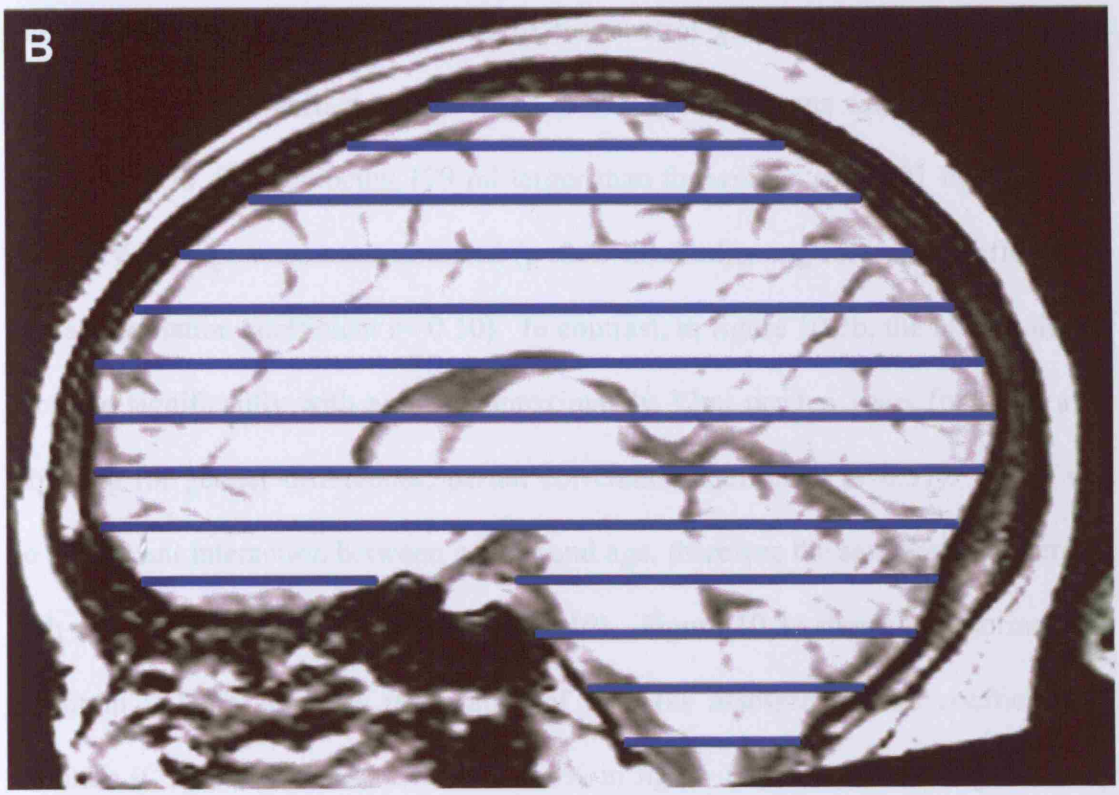

10.2.3. Results

10.2.3.1. Cross-sectional TIV normalisation

The T2-weighted TIV measurements of the control group are displayed in figure 10.3a. There were significant differences in TIV measurements according to gender, with mean TIV for men being 179 ml larger than for women ($p<0.001$ by unpaired t test). TIV and age were not associated ($p=0.49$ after adjusting for gender differences, partial correlation coefficient $r=-0.10$). In contrast, in figure 10.3b, the brain volumes decrease significantly with age by approximately 32ml per ten years ($p<0.001$ after adjusting for gender differences, partial correlation coefficient $r=-0.51$). There was no significant interaction between gender and age, therefore the same rate of decrease with age was taken for both genders ($p=0.10$). Figure 10.3c shows that normalising the brain volumes reduces the scatter of data (as assessed by the coefficient of variation (CV) which decreases from 10.0% in figure 10.3b to 6.0% in figure 10.3c, $p<0.001$ by Pitman's test). A reduction in gender differences can also be observed when the brain volumes are normalised (figure 10.4). The mean male brain volumes (mean ± standard deviation =1262 ± 113ml) are 12% larger, on average, than the females (1123± 810ml), but the normalised volumes are very similar (male 0.84 ± 0.05, female 0.85 ± 0.05, $p=0.57$ by unpaired t-test). This remains statistically insignificant after adjusting for age ($p=0.37$ by unpaired t-test).

Figure 10.3: The relationship between (a) TIV and age, (b) brain volume and age, and (c) normalised brain volume and age, in normal controls.

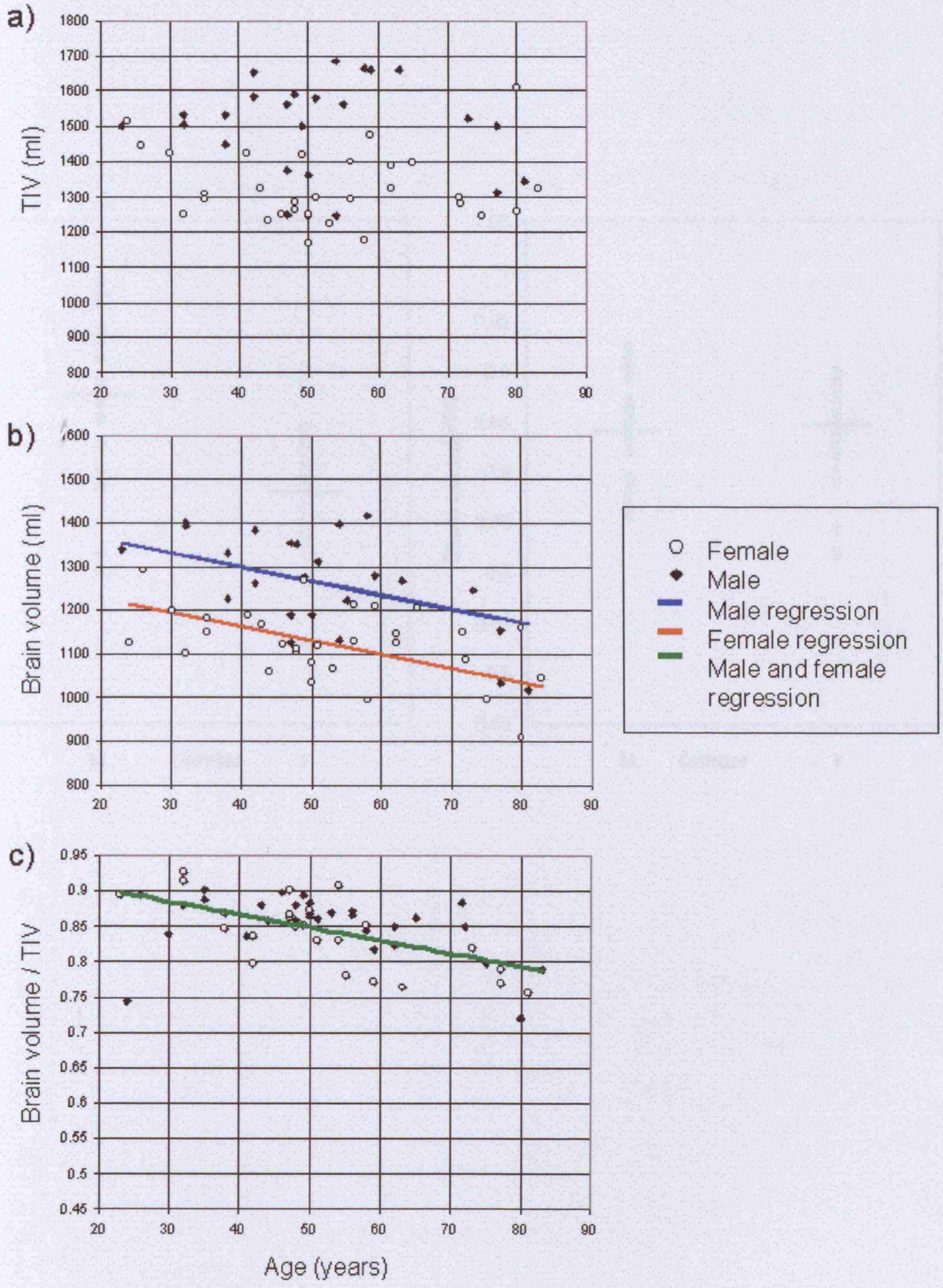

Figure 10.4: Brain volumes and normalised brain volumes in male (M) and female (F) controls with group averages marked, demonstrating a reduction in gender differences after TIV normalisation.

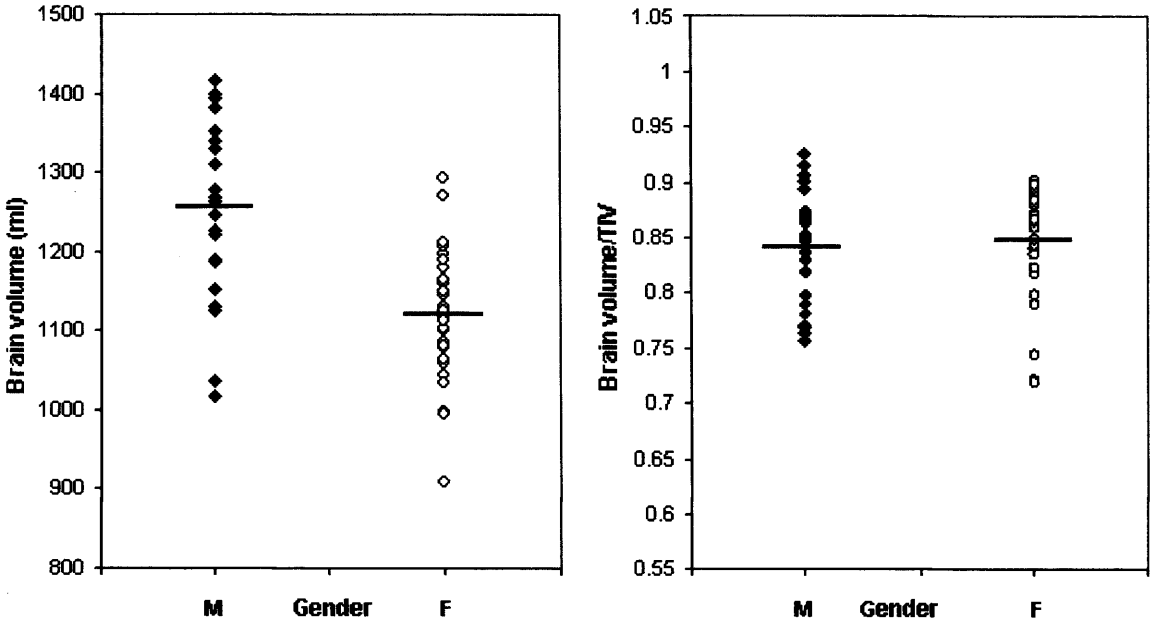

10.2.3.2. Validation - T1 v T2-weighted TIV

Figure 10.5 shows the relationship between the TIV as measured from T2-weighted imaging compared to T1-weighted imaging. The mean TIV volumes are 1382 ± 144ml when measured on T1-weighted images compared with 1374 ± 150ml when measured on T2-weighted images ($p=0.16$ by paired t test). The measures are in close agreement in absolute terms (0.93 ± 0.65% mean absolute percentage difference [MAPD]) and are highly correlated ($R=0.99$, $p<0.001$).

Figure 10.5: Comparison of TIV measurements from T1 and T2-weighted MRI in five controls and five AD patients.

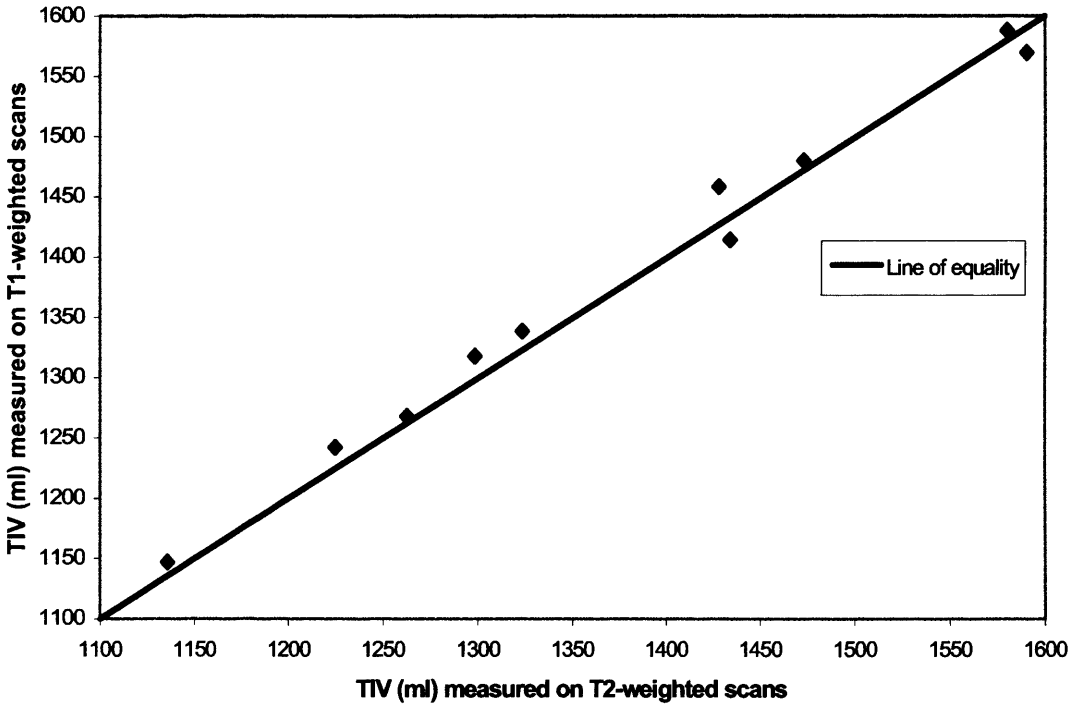

10.2.3.3. Reproducibility

The intra- and inter-rater variabilities are displayed in table 10-1. The TIV measured on T1-weighted images has a lower variability (0.23 ± 0.17% MAPD on repeated measures) than the TIV measured on T2-weighted images (0.99 ± 0.38% MAPD on repeated measures, p=0.007 by unpaired t-test). The coefficients of variation are similarly significantly different (p=0.003 by unpaired t-test).

Table 10-1: Reproducibilities and operator times

		Intra-rater variability (n=10)				Inter-rater variability (n=5)			
Measurement	**Operator time (mins)**	**MAPD**	**Range**	**CV%**	**Range**	**MAPD**	**Range**	**CV%**	**Range**
T1-weighted TIV	20	0.23	0.05-0.62	0.16	0.04-0.44	0.88	0.35-1.54	0.62	0.25-1.09
T2-weighted TIV	15	0.99	0.47-1.36	1.20	0.60-2.00	0.92	0.61-1.20	0.65	0.43-0.84
Brain volumes	10	0.36	0.05-0.69	0.25	0.04-0.49	0.42	0.11-0.77	0.30	0.07-0.55

* MAPD; Mean absolute percentage difference, CV%; Coefficient of variation expressed as a percentage.

10.2.3.4. Longitudinal TIV normalisation

There were no systematic shifts between the two serial TIVs measured from T1-weighted imaging (p=0.55 by paired t-test, figure 10.6). However, small but measurable variations did exist over time with a 0.69 ± 0.39% MAPD between the pairs of scans (compared with the intra-rater variability of 0.23 ± 0.17% MAPD). This variation is demonstrated in the T1-weighted TIVs of an at risk patient who remained well with eight scans over a period of eight years (figure 10.7a). Accurately measured brain volumes of the control also fluctuated over time (figure 10.7a). The brain and TIV fluctuations are highly correlated (R=0.88, p=0.004). The intra-individual variation in these measures is decreased when the brain volumes are normalised; the CV decreased from 1.0% to 0.5% (figure 10.7c). The fluctuations in brain volume of an initially asymptomatic subject who became clinically affected with AD are also reduced after TIV normalisation. Over a period of seven years the TIV fluctuations match those of the brain volume (figure 10.7b). Once normalised for TIV, brain volumes show a smooth decrease over time (figure 10.7c). Similar correlated fluctuations and reduction in intra-individual variation after normalisation were observed in ten controls and five AD patients with short interval serial scans (total CV decreased from 1.3% to 0.5%, p=0.002 by Wilcoxon signed rank test).

Figure 10.6: Serial T1-weighted TIV measurements in five controls and five AD patients

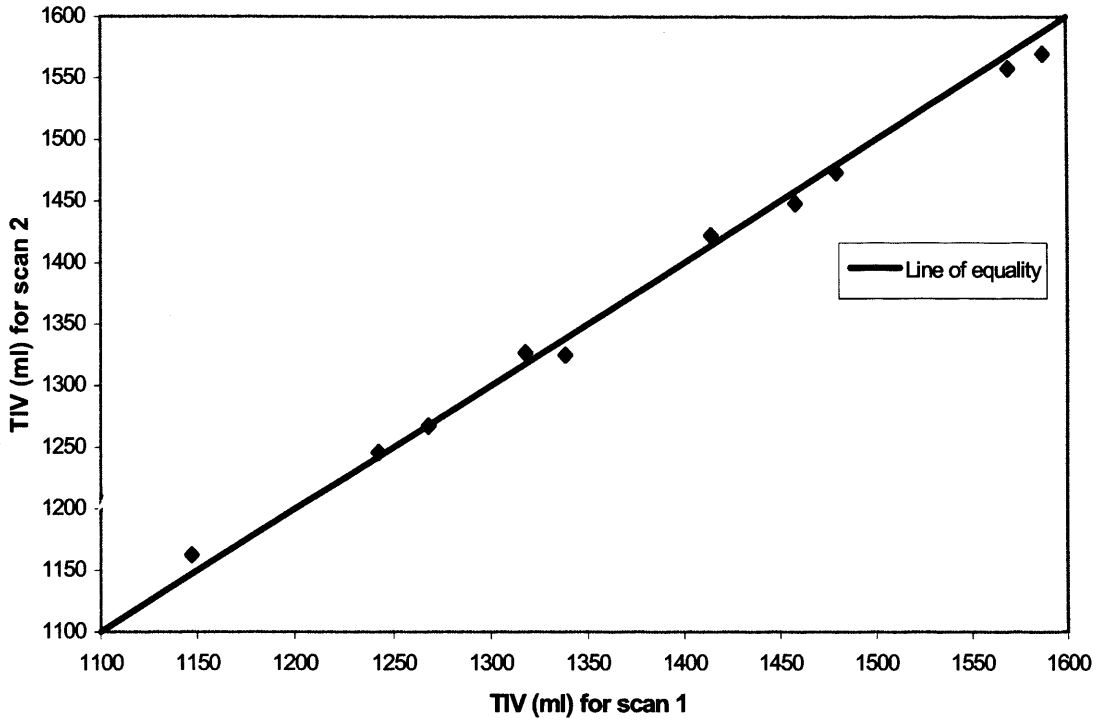

Figure 10.7: Serial TIV and brain volumes in (a) an at-risk patient who remained well, and (b) an at-risk patient who became clinically affected with AD, compared with, (c) normalised brain volumes from serial scans in both the at-risk patients.

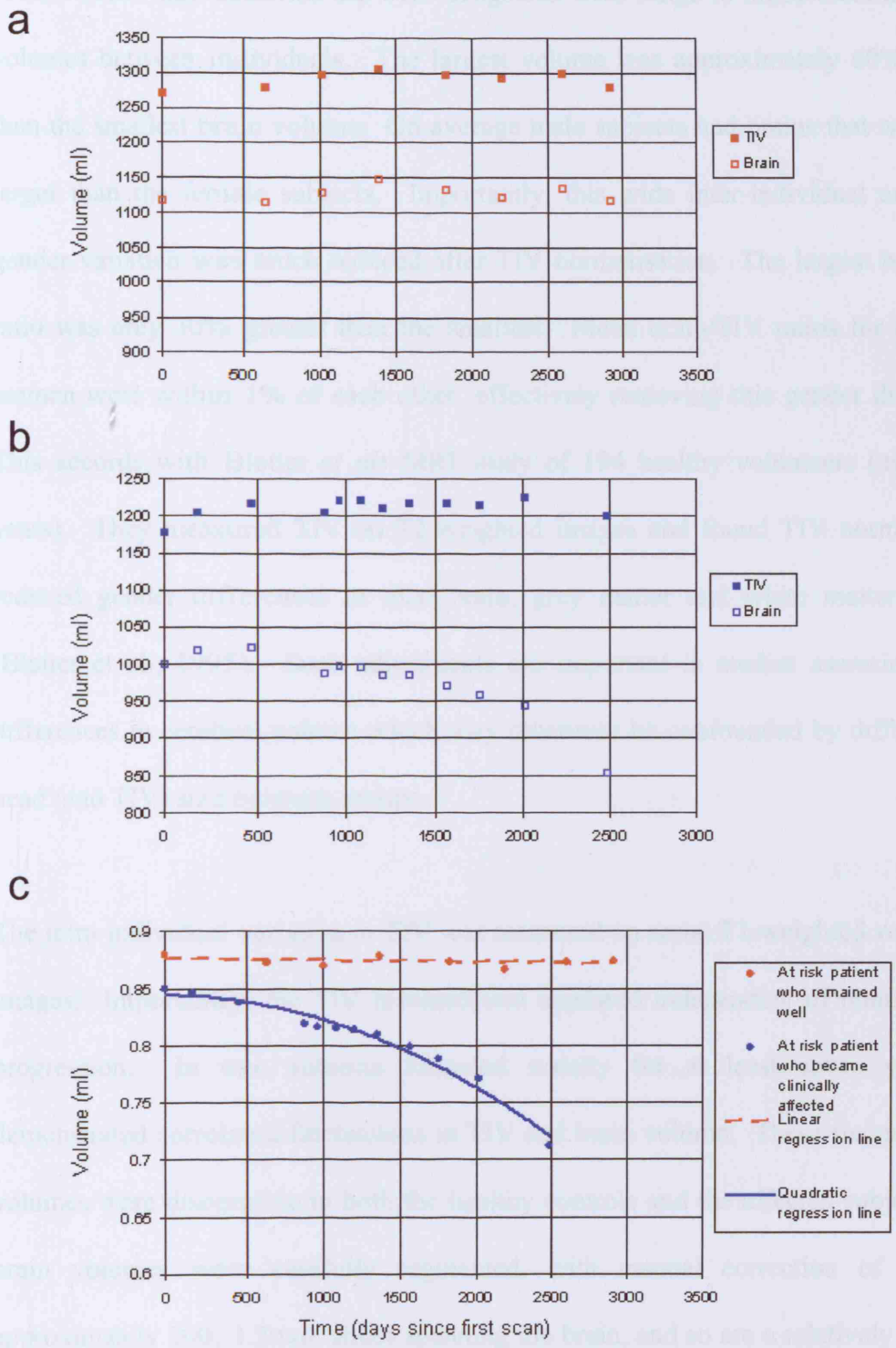

10.2.4. Discussion

The total intracranial volume measurements in controls were relatively stable across the age range (23-83 years) studied, consistent with previous studies (Matsumae et al., 1996). Our study confirms the well-recognised wide range in intracranial and brain volumes between individuals. The largest volume was approximately 60% greater than the smallest brain volume. On average male subjects had brains that were 12% larger than the female subjects. Importantly, this wide inter-individual and inter-gender variation was much reduced after TIV normalisation. The largest brain/TIV ratio was only 30% greater than the smallest. Mean brain/TIV ratios for men and women were within 1% of each other, effectively removing this gender difference. This accords with Blatter *et als* MRI study of 194 healthy volunteers (age 36-45 years). They measured TIV on T2-weighted images and found TIV normalisation reduced gender differences in total brain, grey matter and white matter volume (Blatter et al., 1995). Such adjustments are important in studies assessing group differences in cerebral volume which may otherwise be confounded by difference in head (and TIV) size between groups.

The intra-individual variation in TIV was measured on serial T1-weighted volumetric images. Importantly, the TIV measurement appeared independent of brain atrophy progression. In two subjects followed serially for at least seven years we demonstrated correlated fluctuations in TIV and brain volume. These fluctuations in volumes were discernible in both the healthy controls and the affected subjects. The brain volumes were carefully segmented, with manual correction of each of approximately 100, 1.5mm, slices spanning the brain, and so are a relatively accurate measure of the brain volume represented by the scan acquisition. Therefore some of

the correlated fluctuation can be attributed to changes or "drifts" in the true voxel dimensions between scans (Freeborough et al., 1996). The TIV measurements matched this pattern because the voxel distortions affect brain and skull similarly. Therefore, the TIV can be used to normalise the brain volumes, revealing a smooth decrease in brain volume in the clinically affected at risk patient and a relatively constant brain volume, with less variation, in the at risk patient who remained well.

It is not common practice to measure a TIV on every volumetric acquisition, although we have demonstrated why it is potentially important. Unfortunately longitudinal correction does increase the amount of measurements performed in a study, the method was simple to apply but does create a penalty in terms of operator time. A quicker automated procedure would be ideal. Rudick *et al* have developed the brain parenchymal fraction (BPF), calculated as a ratio of brain parenchymal volume to total volume contained within the brain surface contour, as an automated normalised measure of atrophy (Rudick et al., 1999). This BPF will be relatively independent of voxel scaling distortions and will normalise longitudinally in much the same way as our brain/TIV measure. However, the BPF may underestimate atrophy progression as not all 'sulcal' (extracerebral) CSF is included in the measure. This may be particularly important in diseases where sulcal CSF increases are considerable e.g. AD. Another automated method has been utilised by Yasuda *et al* who measured TIV using a fully automated algorithm to detect the outer surface of dura on every slice of coronal T1-weighted images (Yasuda et al., 1998). This should allow a similar longitudinal normalisation if measured on every serial image.

A T1-weighted TIV can be used to normalise other regions of interest within the brain, e.g. amygdala (van Elst et al., 2000). TIV-based correction of hippocampal volumes have been shown to reduce between-individual variation (Free et al., 1995). Similarly, the TIV measurements may prove useful in serial studies of hippocampal atrophy using the TIV to reduce the confounding effects of voxel size changes.

10.2.5. Conclusion

This study has evaluated the application of TIV normalisation of brain volumes measured from the same volumetric T1-weighted image. TIV correction can be used cross-sectionally, to reduce inter-individual variation, and longitudinally, to adjust for subtle scan distortions affecting measurements of change in the individual. This is likely to become increasingly important as serial imaging measures of atrophy are used as surrogate markers of disease progression in therapeutic trials.

10.3. Nine degrees-of-freedom registration

10.3.1. Introduction

The previous study demonstrated that TIV, an estimate of premorbid brain volume which is unaffected by neurodegeneration (Jenkins et al., 2000), can be calculated on every scan acquired, and can be used to help correct for voxel size drift as the skull provides an invariant structure which acts as a natural 'test object'. Skull or TIV-based correction can also increase the sensitivity of registration to detect brain atrophy accurately (Freeborough et al., 1996). TIV measures are, however, only semi-automated and are operator intensive. In multi-centre clinical trials it is clearly advantageous to use a technique that is automated, fast, and as unbiased as possible. It can be hypothesised that an automated 9-degrees-of-freedom registration would compensate for variations in voxel size between pairs of scans without scaling away real atrophy. The 9dof registration process combines a 6dof rigid registration (3 translations and 3 rotations), which matches the position and orientation of two brain volumes acquired from serial scans to a sub-voxel degree of accuracy, with an additional 3 scaling parameters (spatial scaling factors in three dimensions: x,y,z) to correct differences in voxel size (Woods et al., 1992; Woods et al., 1993). The hypothesis was based on observations of serial registered imaging in AD where, despite significant atrophy (e.g. 2-3% per year), 9dof registration did not appear to stretch scans to remove atrophy. The theoretical explanation for this was that the brains' inherently complex shape (including its gyral foldings and central ventricles), atrophies in a way that cannot be corrected for by a linear scaling and therefore scans could be matched using a 9dof registration without, "registering away" atrophy.

No previous studies have compared the relative merits of 9dof registration and TIV normalisation in correcting for longitudinal fluctuations in voxel size. In this study, we used artificially scaled scans from both control and AD subjects to: 1) assess the ability of the 9dof registration to recover scaling changes; 2) investigate the hypothesis that the scaling correction in the 9dof registration algorithm does not alter atrophy rates obtained from an automated atrophy quantification; and 3) compare the accuracy of the 9dof registration scaling correction compared to normalisation using TIV. These two methods were then assessed in cohorts of patients with AD and controls scanned longitudinally over a variety of intervals ranging from two weeks to six months.

10.3.2. Methods

10.3.2.1. Subjects

Eighty-one scans from 23 subjects (11 healthy controls and 12 patients with mild-to-moderate probable sporadic AD (McKhann et al., 1984)) taking part in the MIRIAD longitudinal imaging study (see chapter 3) were included. All subjects had short interval serial volumetric imaging obtained using the MIRIAD protocol described in Appendix 4; eight subjects had two scans; six had three scans; seven had four scans; and two had five scans. The scan intervals ranged from 10 to 182 days. In addition nine AD patients had a further serial scan one year from baseline.

10.3.2.2. Phantom acquisition and data analysis

The scanner quality assurance (QA) consists of a structured programme in which all quantitative measurements are monitored by imaging suitable phantoms. This program is supplemented by regular imaging of normal control subjects.

To assess geometric distortion, the QA programme consists of scanning a cylindrical phantom (test object 2) from the Eurospin II Magnetic Resonance Quality Assurance Test Objects kit (Diagnostic Sonar Ltd, UK) using a scan sequence comparable to that previously described (inversion recovery prepared fast gradient echo). Geometric distortion is determined by transferring the image data to a Sun workstation (Sun Microsystems, Mountain View, CA, USA) and comparing the test object dimensions to a "reference" image. This is facilitated by the use of a locally written image registration programme, MRreg. The post processing and analysis has been described in detail elsewhere (Lemieux and Barker, 1998). The degree of geometric distortion in the x, y and z axis, as compared with the reference scan, is expressed as a correction factor which would be necessary to normalise the image dimensions.

10.3.2.3. Image processing

All measurements were performed using the MIDAS image analysis software package. Whole brain volumes were delineated using the semi-automated, iterative 3D morphological technique described in Appendix 5. Serial scans were positionally matched to the baseline image using a 9dof registration (Woods et al., 1992; Woods et al., 1993; Freeborough et al., 1996). The registration is driven by the optimisation of a cost function based on the ratio of the voxel signal intensities of the two images; the complex structure of the brain enables the calculation of the optimal rigid body rotations, translations and scalings necessary to optimise the cost function, resulting in one brain being accurately matched to the other. The scaling parameters within this algorithm define the voxel 'stretch' necessary to match image sizes, thereby

accounting for any differences in voxel sizes. TIV was measured on T1-weighted images using a previously described and validated technique (Whitwell et al., 2001).

10.3.2.4. Recovering artificial scaling changes using 9dof registration

The baseline scans, along with the outlined brain regions, for ten of the control subjects were artificially scaled (stretched) in the x, y and z dimensions. The same scalings were applied in each dimension: 0.5, 1.0, 1.5 and 2%. These artificial scalings resulted in a total volume change of 1.5, 3.0, 4.6 and 6.1% per scan respectively. A 9dof registration was used to register the scaled brains back onto the original baseline brain. The volume scaling factor (the product of the 3 linear scaling factors in 3 different dimensions, xyz) for each of these intervals was calculated from the 9dof registration.

10.3.2.5. Comparison of atrophy quantification in Alzheimer's disease using scan pairs with and without scaling change

Nine patients with AD had one-year scans. These scans, as well as the outlined brain regions, were artificially scaled by 1.0% in each of the x, y and z dimensions, resulting in a total volume change of 3.0%. The resultant 'scaled' one year scans were then registered to the relevant baseline scan. Global brain atrophy was calculated from the registered scans using a previously validated automated tool, the BBSI (Freeborough and Fox, 1997). Atrophy rates derived from the original and scaled one-year to baseline scans were compared.

10.3.2.6. Comparison of TIV and registration using artificially scaled scans

As in section 11.3.2.4, the baseline scans, along with the brain regions, for ten of the control subjects were artificially scaled in the x, y and z dimensions by 1.5%, resulting in a volume change of 4.6%. TIV was measured on the baseline scans and the artificially scaled scans. The TIV ratio (ratio of the TIV of each serial scan to baseline TIV) was calculated and compared to the volume scaling factor generated from the 9dof registration.

10.3.2.7. Comparison of TIV and registration using serial scans from AD and control subjects

Serial scans (excluding the one year scans i.e. a total of 49 scan pairs) for each of the 23 subjects were compared to baseline. TIV was measured on all scans. Each serial scan was registered (9dof) to the baseline scan.

10.3.2.8. Statistical analysis

The TIV ratios and volume scaling factors were compared using the Wilcoxon signed rank test. Pitman's test was applied to test for differences in standard deviation between groups. The scaling factors generated from the serial scans from AD and control subjects clearly separated into three distinct groups. In order to compare the variability of the TIV and scaling factors for the entire group, it was necessary to normalize the values from the three groups. Thus, for each of the three groups, the standard deviations of the scaling factors and TIV ratios were divided by the relevant group-specific mean. Pitman's test was then performed on this variable with all data points included in the analysis.

10.3.3. Results

10.3.3.1. Recovering artificial scalings using 9dof registration

Figure 10.8 demonstrates that volume scaling factors generated from the 9dof registration were highly correlated to the known (artificial) volume scaling change ($R=1.00$, $p<0.001$). There was almost complete recovery of the imposed artificial changes; the mean difference between the volume scaling factors (xyz) from the registration and the known induced scaling changes (xyz) was very small: at an artificial volume change of 1.5%, the mean obtained volume change was 1.4%, mean squared error (MSE) 0.016; at 3.0%, the mean obtained was 3.1%, MSE 0.016; at 4.6%, the mean obtained was 4.6%, MSE 0.004; and at 6.1% the mean obtained was 6.2%, MSE 0.007.

Figure 10.8: The volume scaling factor (xyz) generated from each of the 9dof registrations, for each of the ten control subjects, is plotted against the known (artificial) scaling factor.

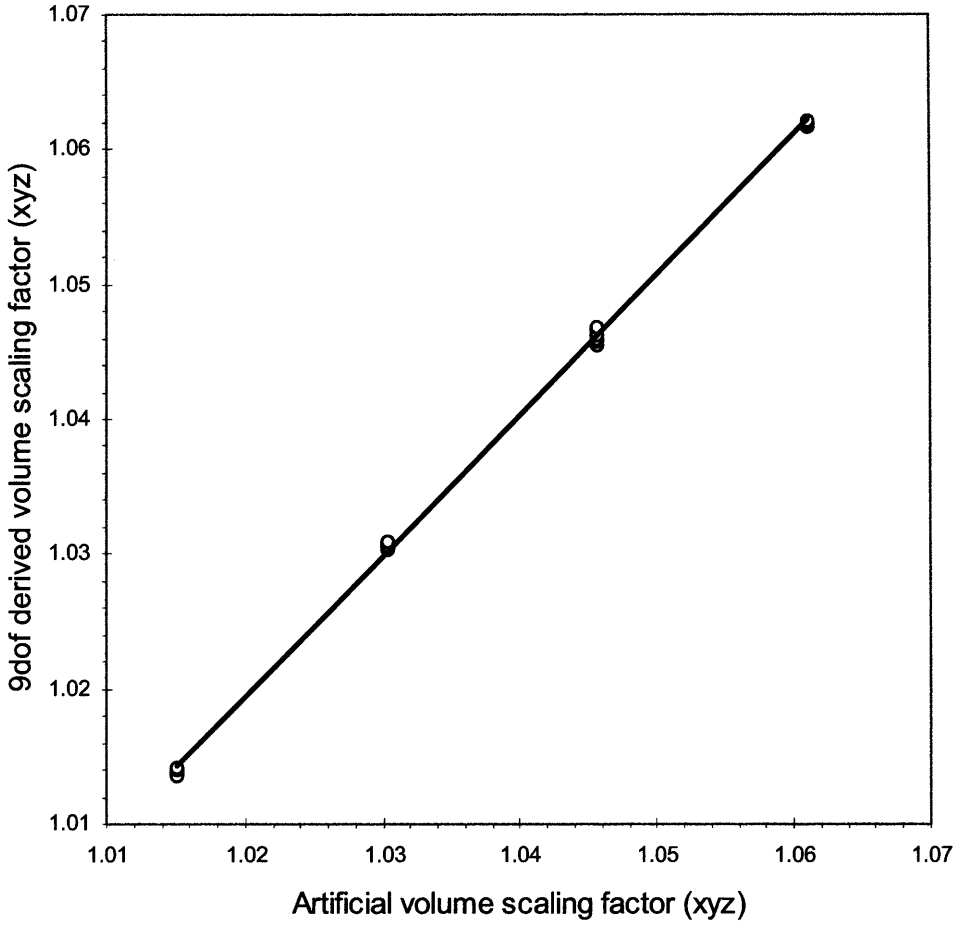

10.3.3.2. Comparison of atrophy quantification in Alzheimer's disease using scan pairs with and without scaling change

The mean loss of brain volume over a one-year interval in nine of the AD patients was 20.4 ± 9.6mls. Artificially scaling the repeat scans by 3.0% and then using a 9dof registration to correct for this change resulted in a very similar calculated mean volume loss of 19.4 ± 9.7mls.

10.3.3.3. Comparison of TIV and registration using artificially scaled scans

At an artificial scaling factor of 4.6% (1.5% in each dimension) there was no significant difference between the 9dof registration derived volume scaling factors (1.0461 ± 0.0004) and TIV ratio (1.0433 ± 0.0042; p=0.06). However the variance of the 9dof-derived volume scaling factors was significantly less than that of the TIV ratio ($p<0.001$, figure 10.9).

Figure 10.9: The volume scaling factors for both TIV correction (TIV2/TIV1) and 9dof registration (xyz) on ten control scans after an artificial scaling change of 4.6% (1.5% in each dimension) are shown. The known (artificial) volume scaling factor is indicated by a dashed line.

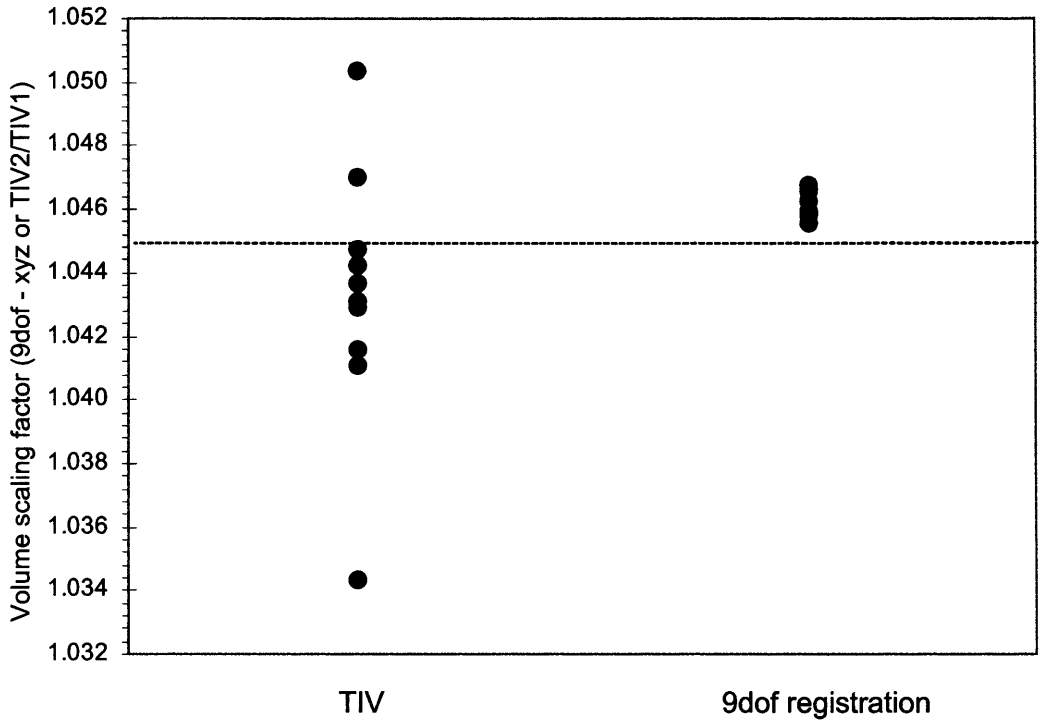

10.3.3.4. Comparison of TIV and registration using serial scans from AD and control subjects

The TIV ratio and 9dof derived volume scaling factors were highly correlated ($R=0.98$, $p<0.001$, figure 10.10) with a mean difference of –0.0009. When the variability of the two methods was compared, the estimated standard deviation of the scaling factors was significantly less (by approximately one third) than that of the TIV ratios ($p<0.001$, figure 10.10).

Figure 10.10: The relationship between the 9dof registration volume scaling factor (xyz) and the TIV ratio (the ratio of the TIV of the serial scans to baseline TIV, i.e. TIV2/TIV1) for each scan pair (n=49).

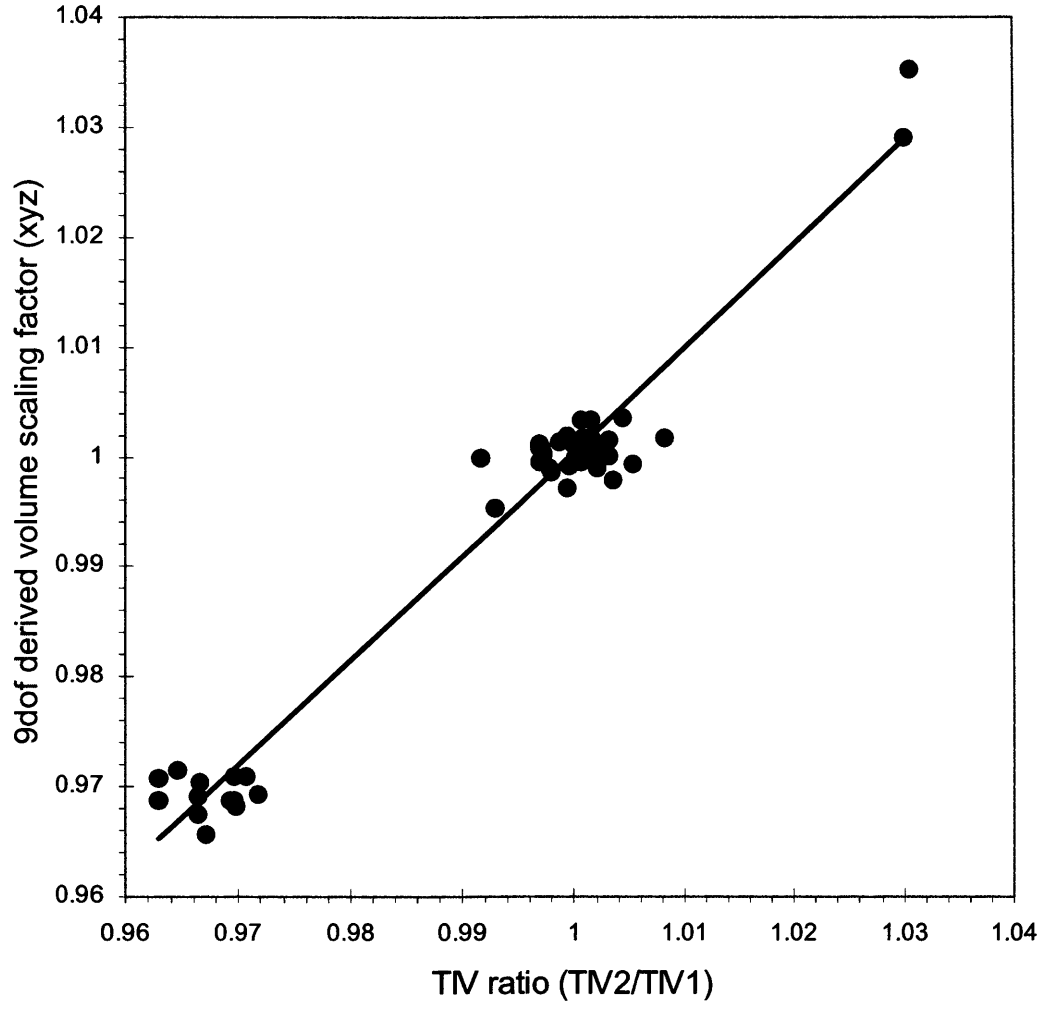

The total voxel size drifts, determined by both the volume scaling factors and TIV ratios, were not normally distributed, but surprisingly fell into three distinct groups (figure 10.10): those with volume change of approximately 1 (>0.99, <1.01, n=34), and two smaller groups with volume changes around 0.97 (>0.96, <0.98, n=13) or 1.03 (>1.02, <1.04 n=2). When the volume scaling factors were plotted against the period over which the scans were acquired (figure 10.11) it was possible to identify

two time points at which systematic changes had occurred. The first (labelled A on figure 10.11) occurred between the 23rd and 27th of September 2000, and resulted in scaling increases of approximately 3%, implying a concurrent increase in voxel size by this amount. The second (labelled B) occurred between the 26th of October and 1st of November 2000 and resulted in a decrease of scaling factors (and therefore voxel size) by approximately 3%, i.e. correcting the original shift. It is notable that all scans encompassing only one of these time points have scaling factors of approximately +3% or -3%, whereas all scan pairs encompassing neither or both of these times have scaling factors approaching unity. The phantom quality assessment (QA) from the scanner is also shown in figure 10.11, and demonstrates the same fluctuations in voxel size implied by our results. Significant shifts in voxel size occurred only in the x and y dimensions; the z (antero-posterior) dimension remained unchanged. The x (± 1.5%) and y (± 1.5%) dimension changes account for the volume changes of ± 3%. These results mirror the time course and magnitude of the changes suggested by the TIV or scaling changes.

Figure 10.11: Correction factors from the scanner QA (upper panel) and the volume scaling factors from the 9dof registration (lower panel) are plotted against time. Correction factors are plotted for the x (x), y (●) and z dimensions (○) and represent the degree (%) of geometric distortion required to normalise the image dimensions to a reference scan. Each scan pair (n=49) is associated with a scaling; both time points (baseline and repeat) are assigned this value and plotted with a line joining them.

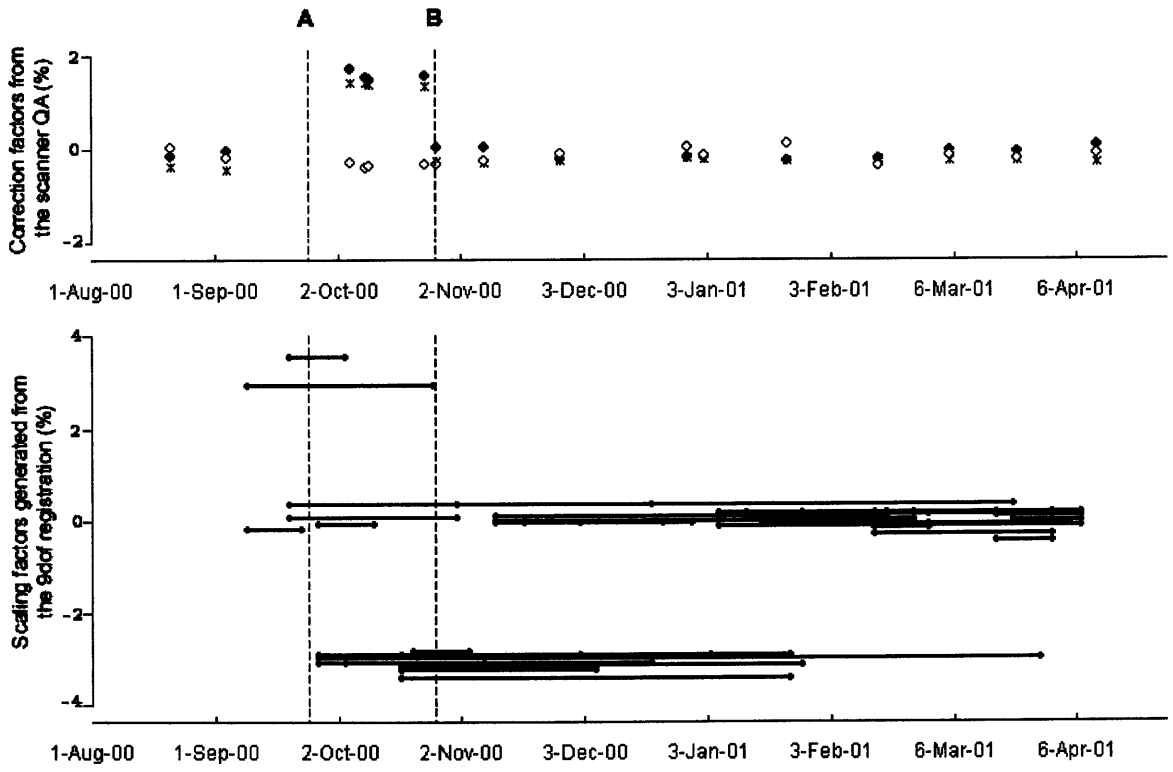

10.3.4. Discussion

Scanner related changes can significantly alter volume measurements made from serial MRI scans. These changes may be of the same order of magnitude as volume change due to neurodegeneration over a one-year period. This study has demonstrated that scaling factors automatically generated from a 9dof registration can correct for these fluctuations in voxel size as well, or better, than TIV measurements in longitudinal MRI studies.

The experiments using artificially scaled voxel sizes showed that the 9dof registration can recover substantial scaling changes (ranging from 1.5 to 6.1%), whilst preserving the true atrophy occurring between two serial scans. Previous studies have established that measures of TIV are unaffected by brain atrophy (Jenkins et al., 2000; Whitwell et al., 2001), this is unsurprising given that the measure is based on the invariant skull boundary. By contrast the use of a 9dof registration to correct for voxel size drift might theoretically affect measures of atrophy; in particular 9dof registration might "remove atrophy". These results suggest that, as with measures of TIV, the scaling factors generated by 9dof registration are not influenced by ongoing atrophy in AD. This is likely to be because brain atrophy in neurodegeneration involves complex, non-linear changes with ventricles enlarging outwards and individual sulci selectively enlarging inwards – changes that cannot be matched by the application of simple linear scalings (Freeborough and Fox, 1998; Scahill et al., 2002).

The 9dof registration corrects for drifts in voxel size at least as well as TIV correction. The smaller variance in the registration scaling factors in both the artificial

and 'real' situation provides evidence to suggest that the 9dof registration may in fact be the more precise of the two methods. This may be due to the degree of operator error inherent in a semi-automated TIV measurement; TIV may also be affected by inadequate head coverage or changes in chemical shift. Furthermore, TIV measurement is time consuming, taking on average 20 minutes per scan. Whilst accuracy of TIV correction might be improved by performing more measurements per scan (Eritaia et al., 2000), this would come at increased loss in terms of operator time. By contrast, 9dof registration is an automated technique, not significantly increasing post-processing time, less reliant on segmentation quality, affected neither by operator bias nor error, and utilizing the entire brain volume.

During the course of the study, as a consequence of acquiring multiple scans at different, short intervals, the timing of two systematic changes resulting in voxel size shifts of approximately 3% were identified. As the annual rate of whole brain atrophy in AD is of the order of 2-3% (Fox and Freeborough, 1997), it is clear that such changes, if uncorrected, would seriously compromise the use of serial scanning to determine volume change (and consequently atrophy of whole brain or regional measures such as the hippocampus) as outcome measures in clinical trials of neurodegenerative diseases. The use of either 9dof registration or correction for TIV was successfully able to correct for these changes. The scanner log demonstrated that the initial increase in voxel size occurred following a routine service on the 27th September 2000 by an engineer who did not regularly work on this scanner. The subsequent reduction of voxel size (i.e. correction to baseline) occurred at the next routine service on the 27th October 2000, this time carried out by the regular engineer. Whilst neither engineer noted any specific scanner problems, the scanner

radiographers identified a fluctuation in QA after the first service and informed the regular engineer before the second service. It is important to note that this problem is unlikely to be unique to this particular scanner; drifts in voxel size, and the potential for miscalibration are generic problems affecting all MRI scanners. Although this shift in voxel size was demonstrated in the weekly QA phantom scan, it would not have been possible to correct each individual scan accurately on this basis. Either the scans would have to have been discarded or the patient recalled. As MRI-based measures of atrophy are increasingly used in multi-centre trials, there are clear advantages in using a post-processing method to allow retrospective correction both for drift in voxel size and for the possibility of scanner miscalibration, thus allowing a higher proportion of acquired scans to be included in the analysis.

10.3.5. Conclusion

Stability of MR acquisition is fundamental to the accurate measurement of cerebral atrophy rates. In trials in which brain atrophy is an outcome measure, the potential for acquisition instability needs to be recognised and minimised. Routine scanner services may introduce significant acquisition changes and whilst quality assurance is an essential component of all serial MRI studies (Leary et al., 1999) post-acquisition correction methods are likely to be critical to the success of MR-based outcome measures in multi-centre studies. This study has shown that 9dof registration can correct for voxel drifts without altering atrophy measures. The 9dof scaling correction was validated against the artificial known scalings and against manual TIV measures. 9dof registration is unbiased, automated, quicker and less variable than correction factors based on manual measures of TIV. TIV measurement is likely to remain a useful technique in correcting for inter-individual differences in cross-

sectional studies. As either method can correct for voxel drift without affecting measures of atrophy, these results suggest that 9dof may be the superior method for longitudinal studies.

11. Rates of whole brain atrophy in FTLD

11.1. Introduction

The majority of MRI studies in FTLD have been cross-sectional. Studies have applied automated whole brain analysis techniques as well as manual regional measurements in an attempt to characterise the patterns of atrophy in FTLD. They have demonstrated a focal pattern of atrophy, affecting both the frontal and temporal lobes, and highlighted differences between the different syndromic variants of FTLD. However, the diagnostic utility of cross-sectional measures is limited by the large variability present between individuals. In addition, regional measures are time consuming and limited by measurement error. As discussed in chapter 10, looking at changes within an individual reduces the problem of inter-individual variation in brain volume. It also permits the assessment of disease progression over time. Registering serial MRI from the same individual increases the reliability of longitudinal measures. Registration positionally matches scans to within subvoxel accuracy and permits even small volume changes to be detected by image subtraction. As discussed in the previous chapter it can also incorporate scaling factors to correct for fluctuations in voxel dimension over time. Brain volume changes can be calculated from registered scans using the BBSI (Freeborough and Fox, 1997). This provides an automated, quick and reproducible method for measuring volume change over time. Rates of atrophy have already been proposed as markers of disease progression in AD and have been used as outcome measures in clinical trials in AD and MCI (Fox et al., 2005; Schott et al., 2005).

Rates of whole brain and hippocampal atrophy have been shown to be significantly greater in AD than controls, to correlate with cognitive decline (Fox et al., 1999a), and to predict conversion from MCI to AD (Jack et al., 2000; Grundman et al., 2002). A much more limited number of MRI and post-mortem studies in FTLD have reported progression of atrophy over time and with disease severity (Graff-Radford et al., 1990; Rosen et al., 2002d; Broe et al., 2003; Hodges et al., 2003). Only one previous MRI study has systematically assessed rates of atrophy in an FTLD cohort. Chan et al (2001) found a mean rate of whole brain atrophy of approximately 3.2% per year, with a rate of 3.7% in the frontal variants of FTLD and 2.5% in the temporal variants (Chan et al., 2001a). They did not, however, assess rates of atrophy in patients with PNFA (they only had one patient with PNFA). The different syndromic variants of FTLD may show different rates of whole brain atrophy and so should be considered separately.

The aim of this chapter was to assess and compare the rates of whole brain atrophy in all three of the syndromic variants of FTLD using registration of serial scans and automated quantification using the BBSI. A secondary aim was to increase the statistical power of the study by selecting the largest possible group of FTLD patients and by performing a rigorous quality assessment of each registration prior to analysis.

11.2. Methods

11.2.1. Subjects

Patients were recruited from the Specialist Cognitive Disorders Clinic (see chapter 3). All patients that had been given a diagnosis of FTLD and had at least two serial MRI scans were identified (n=105). For patients with more than two MRI scans, the longest interval was used. Medical records were reviewed and the clinical presentation, disease duration, and MMSE score at the time of the baseline MRI scan were noted. Disease duration was defined as the time from first symptom onset to baseline MRI. Clinical classification was based on consensus criteria for fvFTD, SD and PNFA (Neary et al., 1998).

11.2.2. Image analysis

The standard imaging protocol described in Appendix 4 was used for acquisition of T1-weighted images. Whole brain and TIV segmentations were performed on all scans using the protocols described in Appendix 5. All serial scans were registered using a 9dof registration described in chapter 3. A differential bias correction (DBC) was applied to all scan pairs during registration in order to correct for differences in intensity inhomogeneity over time (see chapter 3). All registrations were then assessed for quality and consistency of acquisition. Registrations were rejected either due to poor quality scans, changes in acquisition or poor quality registration. Rates of global brain change were calculated using the BBSI (see chapter 3).

11.2.3. Statistics

Data were analysed using STATA. Brain volumes were assessed and standardised to TIV volume using the following equation:

$$sbv = bv - \beta(TIV - meanTIV)$$

sbv = standardised brain volume, bv = brain volume, β = regression coefficient of brain volume on TIV in controls, meanTIV = mean TIV in the control group.

Rates of whole brain atrophy were calculated using the BBSI. Rates are given in percentage of baseline brain volume change per year. Age, MMSE, disease duration, brain volumes, intervals and rates of change were compared between groups using the Mann Whitney U test. Gender ratios were compared using the Fisher's exact test. Regression models were applied to investigate the effects of brain volume, MMSE and disease duration on rate of atrophy.

11.3. Results

11.3.1. Patient characteristics

After detailed assessments of both clinical information and brain registration quality for each subject, almost 50% (n=49) of the original patient group (n=105) were rejected from the study. The reasons were as follows:

- Serial scans were performed on different scanners or across scanner upgrades (n=7)
- Poor quality scans (movement n=14, poor contrast n=4, other n=4)
- Incomplete scans (n=2)
- Patients did not fulfil consensus criteria for FTLD at follow-up, or had a non-FTLD pathology at post-mortem (n=14)
- Insufficient clinical information (n=3)

Therefore, a total of 56 patients with FTLD were included in the study (32 fvFTD, 13 SD, 11 PNFA). The cohort was age, gender and scanner-matched to 15 healthy

controls that each had two serial MRI. The control subjects were typical of normal ageing and had no complaints of cognitive impairment or behavioural problems. Exclusion criteria included a history of stroke or dementia. The clinical characteristics of this group and the control subjects at baseline are shown in table 11-1. Post-mortem confirmation was obtained in six of the FTLD patients (three FTLD-U, and three tau-positive with a tau exon^{10+16} mutation). In addition, recognized tau mutations were present in a further two FTLD patients. There was no significant difference between the ages of the control subjects and the patients with FTLD, or between the control subjects and any of the clinical subtypes of FTLD. Gender distributions were similar in the control subjects and FTLD patients, however the fvFTD group had a disproportionately large number of men (n=28), compared to women (n=5). The MMSE was significantly lower in all FTLD subgroups compared to controls ($p<0.01$ in all), yet there were no significant differences between any of the FTLD subgroups. There were no significant differences in disease duration, or scan interval between any of the groups.

Table 11-1: Patient characteristics.

	Controls (n=15)	FTLD (n=56)	fvFTD (n=32)	PNFA (n=11)	SD (n=13)
Gender (M:F)	10:5	40:16	27:5‡	6:5	6:7
Age (yrs)	60.6 (12.7)	60.7 (7.0)	59.2 (6.6)	63.7 (7.1)	62.1 (7.2)
MMSE (/30)	29.2 (0.9)	22.6** (6.6)	23.5** (6.0)	22.8** (7.9)	20.0** (6.9)
Duration (yrs)	N/A	5.0 (2.5)	5.1 (2.8)	5.1 (2.4)	4.7 (1.8)
Interval (days)	548 (396)	697 (338)	717 (357.4)	624 (217)	710 (386)

*Results are expressed as mean (standard deviation); * Significantly different controls (* <0.05, **<0.01); ‡ Significantly different SD (‡<0.05, ‡‡<0.01)*

11.3.2. Image analysis

Table 11-2 shows the mean TIV-corrected brain volumes at baseline and repeat time-points, and the rates of atrophy calculated from the BBSI in the FTLD and control subjects. The volume of brain loss calculated from the BBSI has been plotted against the difference in manual brain volumes between baseline and repeat time-points for the FTLD patients in figure 11.1. This demonstrates a good correlation between the two measures, although BBSI tends to underestimate the amount of brain loss compared to that calculated directly from the brain volumes.

TIV-corrected brain volumes were significantly smaller in the FTLD group than the control group at both baseline ($p<0.003$) and repeat ($p<0.001$) time-points (table 11-2). The smallest brain volumes were observed in the SD and PNFA groups. The rates of atrophy calculated from the BBSI were significantly larger in all FTLD subgroups compared with controls (fvFTD $p<0.0004$, SD $p<0.0001$, PNFA $p<0.0001$), with the greatest rates of atrophy observed in the SD ($1.9 \pm 0.7\%$ per year) and PNFA ($2.2 \pm 1.4\%$ per year) groups. There were no significant differences in rates of atrophy between the FTLD subgroups.

Table 11-2: TIV-corrected brain volumes and rates of atrophy (calculated from BBSI)

	C (n=15)	FTLD (n=56)	fvFTD (n=32)	PNFA (n=11)	SD (n=13)
Baseline brain volume (ml)	1154 (102)	1100** (66)	1116 (73)	1062** (47)	1093** (48)
Repeat brain volume (ml)	1153 (103)	1057** (80)	1076* (91)	1011** (56)	1047** (46)
Rate of atrophy (BBSI) (%/yr)	0.2 (0.3)	1.7** (1.3)	1.5** (1.3)	2.2** (1.4)	1.9** (0.7)

*Results are expressed as mean (standard deviation); * Significantly different controls (* <0.05, **<0.01)*

Figure 11.1: Scatter-plot showing the relationship between brain volume loss measured from the BBSI and the manual difference in brain volume between baseline and repeat scans for the FTLD subjects (n=56)

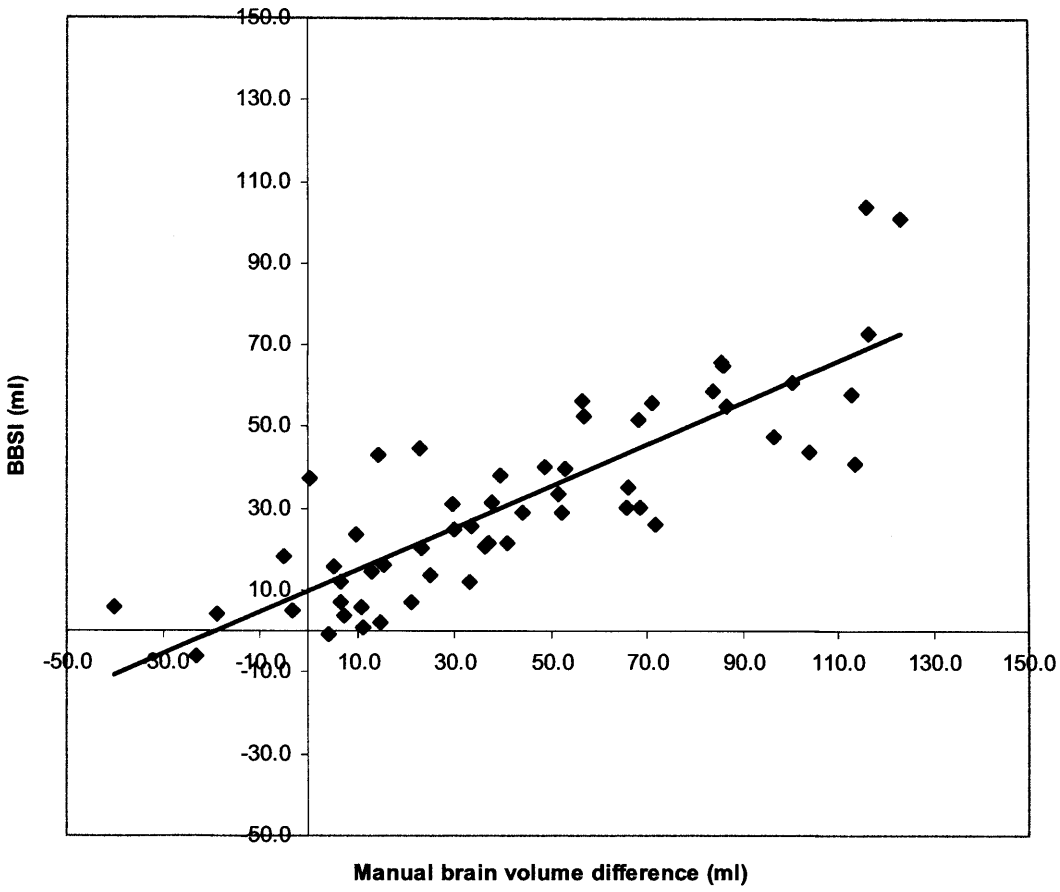

The rates of atrophy (measured from BBSI) in each subject are plotted in figure 11.2. It is clear that while there is a large degree of overlap in the rates of atrophy in each of the three FTLD subgroups, the fvFTD and PNFA groups show a wider range of atrophy rates than the SD group. The rates of atrophy in the SD and PNFA group almost completely separate from those observed in the control subjects, however approximately 30% of the fvFTD group showed rates of atrophy no greater than the control group. It is possible to identify a group of 12 clinically diagnosed fvFTD subjects which have a rate of atrophy that both overlaps with the control group, and is less than that observed in any of the SD or PNFA patients (less than 0.6% per year, marked in red on figure 11.2). Table 11-3 shows the characteristics of this group of patients compared to the rest of the fvFTD group. The group of patients with low rates of atrophy had a significantly higher mean MMSE score than the rest of the cohort ($p=0.006$); in fact it was no different to that observed in the control group ($p=0.08$). The baseline and repeat brain volumes of the patients with a low rate of atrophy were not statistically different from that of the control group ($p=0.8$, $p=0.9$). The rate of change in the fvFTD group, once the patients with low rates of atrophy were removed, increased to 2.3% (1.1%) per year, which is similar to that observed in the SD and PNFA groups.

Figures 11.3 to 11.5 show some example BBSI colour overlays from the FTLD subjects. It highlights the variability present in each of the syndromic groups and shows an example of a patient with fvFTD that showed a low rate of brain atrophy over an interval of 17 months (figure 11.3).

Figure 11.2: Scatter-plots showing rates of whole brain atrophy (measured from BBSI) in the FTLD subgroups and healthy controls. The twelve fvFTD patients with low rates of atrophy have been highlighted in red on figure 11.2B.

A

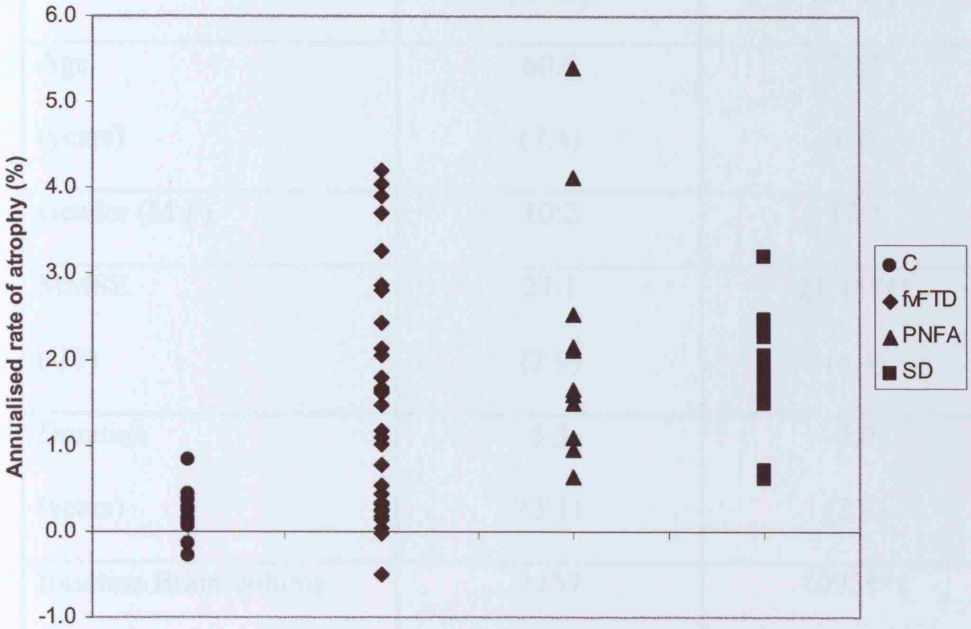

B

Table 11-3: Clinical characteristics and brain volume data for the fvFTD patients. The cohort has been divided into those patients identified with a low rate of atrophy, and then the rest of the fvFTD cohort that had 'higher' rates of atrophy.

	Low rate group (n=12)	**High rate group (n=20)**
Age (years)	60.6 (7.4)	58.3 (6.0)
Gender (M:F)	10:2	17:3
MMSE (/30)	27.1 (2.9)	21.4**†† (6.4)
Duration (years)	5.3 (3.1)	5.0 (2.8)
Baseline Brain volume (ml)	1157 (74)	1092**† (63)
Repeat Brain volume (ml)	1153 (78)	1030**†† (62)
Interval (days)	813.8 (408.0)	659.2 (320.3)
Rate of atrophy (%)	0.2 (0.3)	2.3**†† (1.1)

*Results are expressed in mean (standard deviation); * Significantly different from controls (* <0.05, **<0.01); † Significantly different between low and high rate fvFTD (†<0.05, ††<0.01)*

Figure 11.3: BBSI colour overlay showing regions of atrophy in two patients with fvFTD. The subject on the left showed almost no brain atrophy over time. In contrast, the patient on the right shows significant expansion of the ventricles and tissue loss around both temporal lobes and the orbitofrontal region.

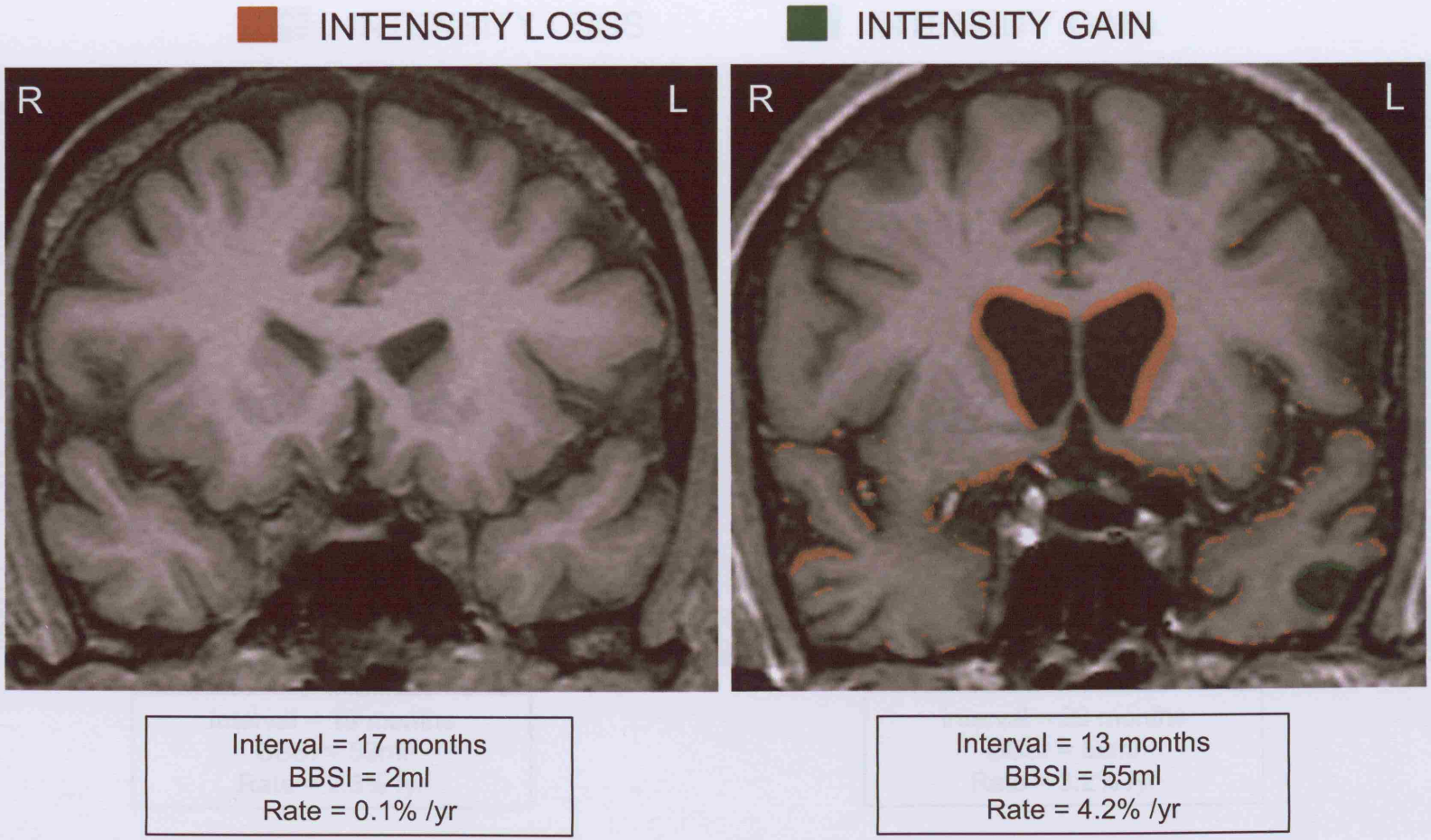

Figure 11.4: BBSI colour overlay showing regions of atrophy in two patients with SD. Both subjects show expansion of the ventricles and asymmetric tissue loss affecting predominantly the right temporal lobe and left frontal gyri between the baseline and repeat scan. The left temporal lobe is already highly atrophic at baseline in both subjects.

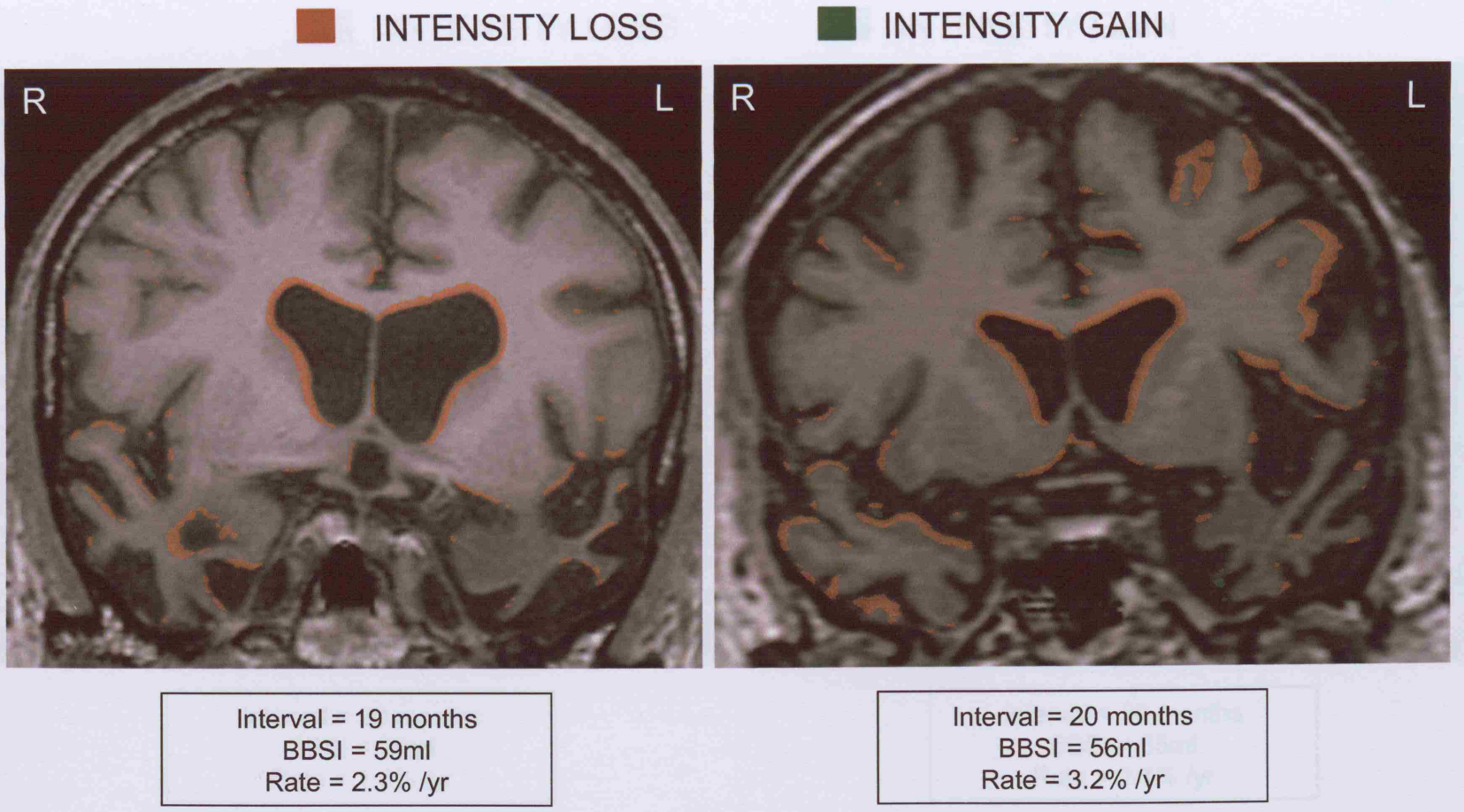

Figure 11.5: BBSI colour overlay showing regions of atrophy in two patients with PNFA. The subject on the right shows a severe pattern of left-ward asymmetric atrophy, involving the frontal and temporal lobes. The subject on the left has a shorter interval but still demonstrates expansion of the ventricles and atrophy of the frontal and temporal lobes.

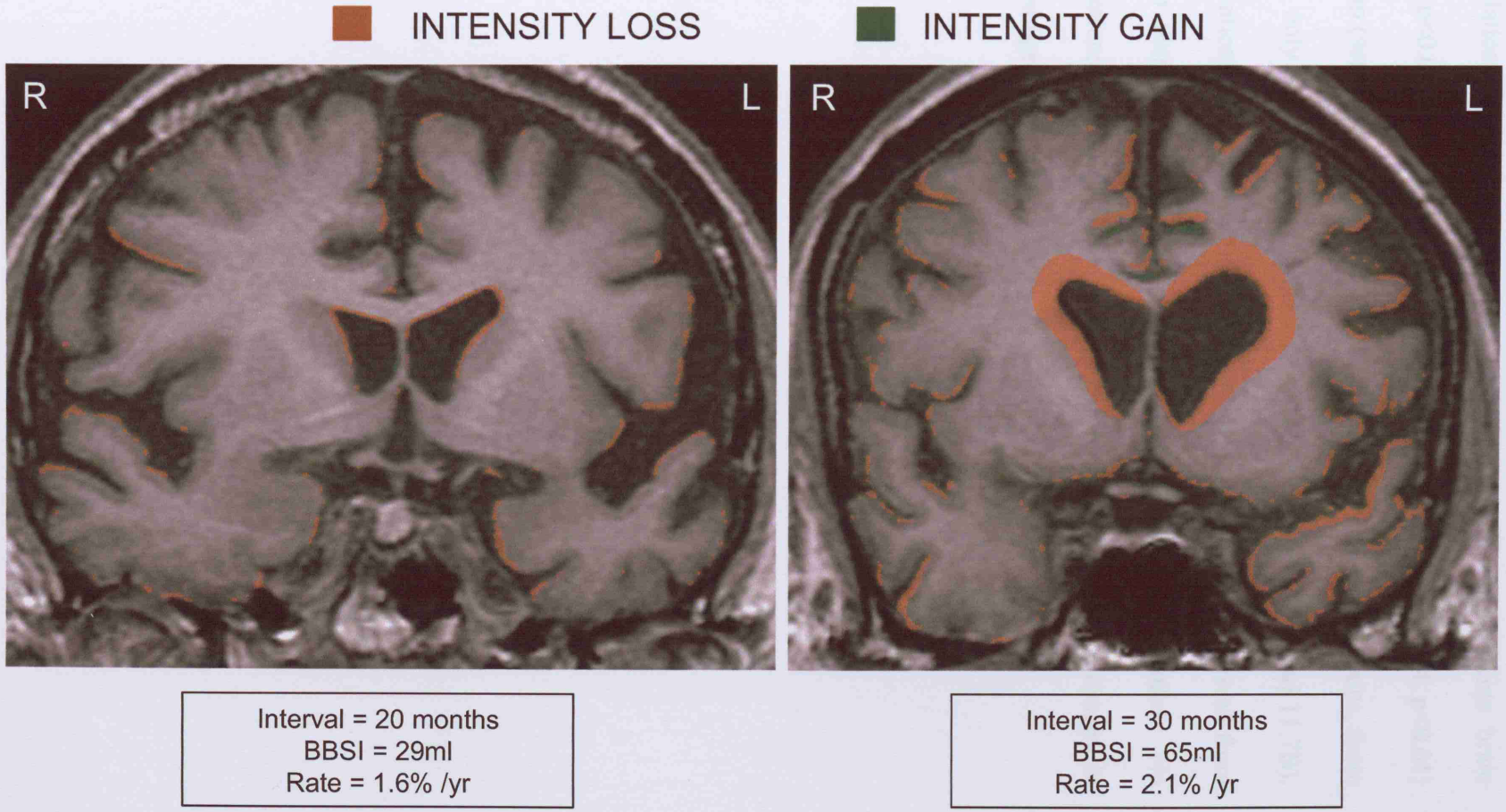

11.3.3. Regression analysis

Significant correlations were found between rate of atrophy and baseline brain volume ($R=0.41$, $p<0.01$), and between rate of atrophy and MMSE ($R=0.34$, $p<0.01$) in the FTLD group (see figure 11.6A and 11.7A). Within the FTLD subgroups, these correlations were only significant in the fvFTD group (see figure 11.6B and 11.7B). However, if the patients identified as having a low rate of atrophy are removed from the fvFTD group then neither of these relationships maintains significance. No significant correlations were found between disease duration and rate of atrophy in any of the FTLD subgroups.

Figure 11.6: Rate of atrophy (%/yr) calculated from the BBSI plotted against brain volume for A) the FTLD group, and B) the fvFTD group. The subjects identified as having particularly low rates of atrophy are marked in red on B.

A

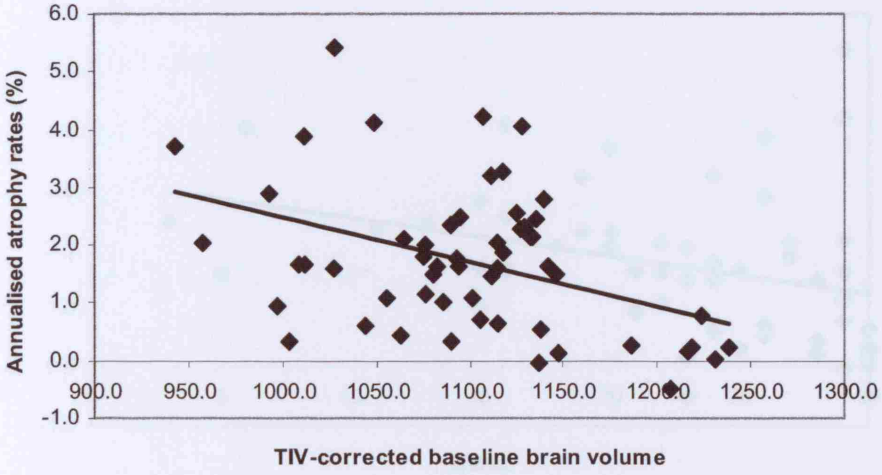

B

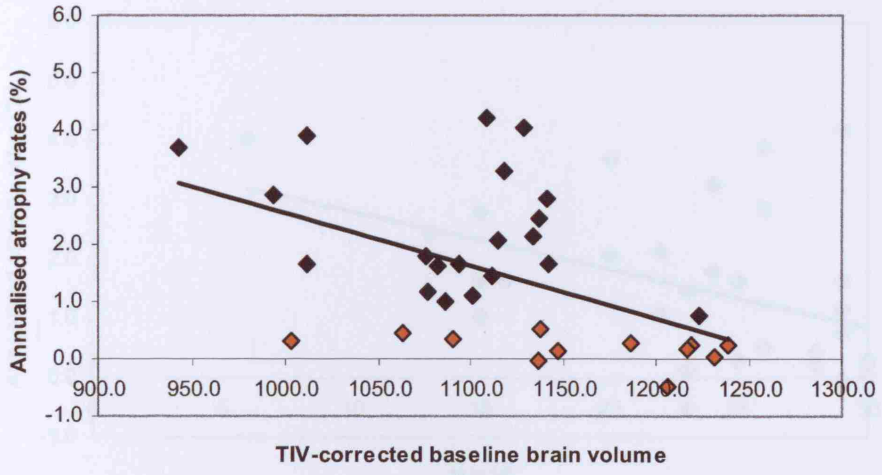

Figure 11.7: Rate of atrophy (%/yr) calculated from the BBSI plotted against MMSE for A) the FTLD group, and B) the fvFTD group. The subjects identified as having particularly low rates of atrophy are marked in red on B.

A

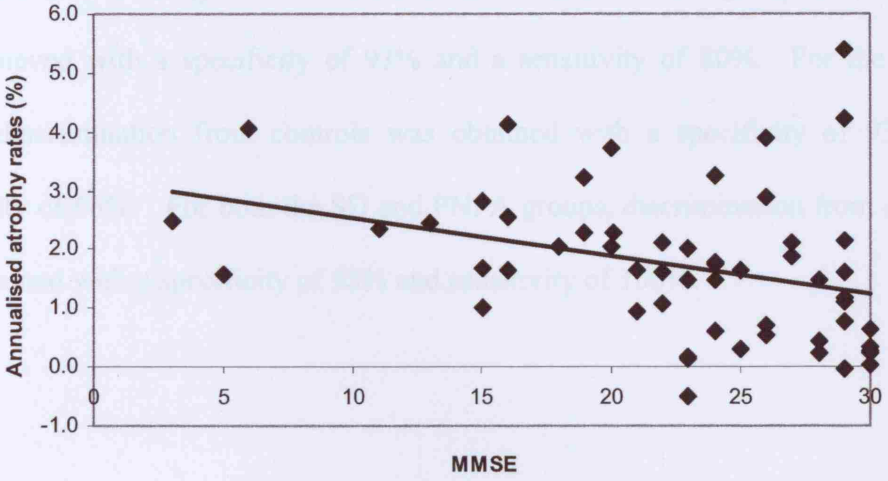

B

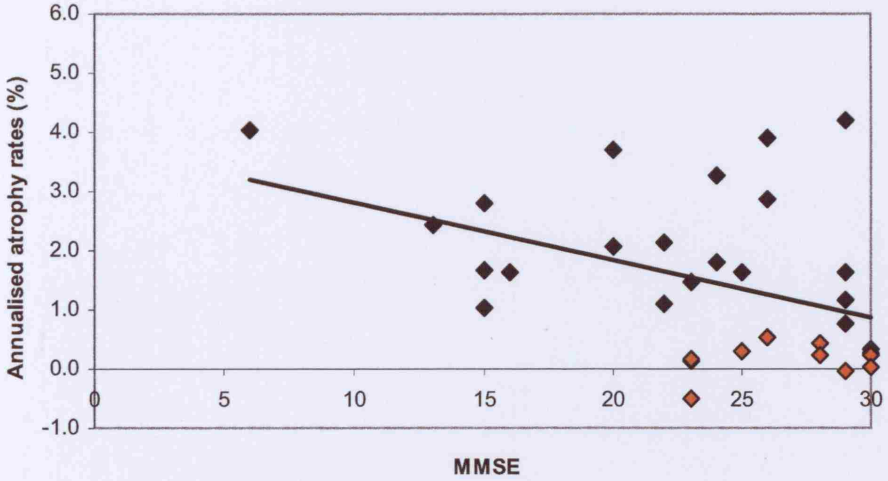

11.3.4. Discriminate analysis

The value of the measurement of rate of whole-brain atrophy as a variable to discriminate between control subjects and FTLD patients was determined by calculation of sensitivity and specificity. The receiver operator characteristic (ROC) curves are shown in figure 11.8. Discrimination of the FTLD group from controls was achieved with a specificity of 93% and a sensitivity of 80%. For the fvFTD group, discrimination from controls was obtained with a specificity of 93% and sensitivity of 66%. For both the SD and PNFA groups, discrimination from controls was obtained with a specificity of 93% and sensitivity of 100%.

Figure 11.8: Receiver operator characteristic (ROC) curves illustrating the ability of rates of atrophy to discriminate between healthy controls and A) FTLD, B) fvFTD, C) SD and D) PNFA (NB clinically diagnosed)

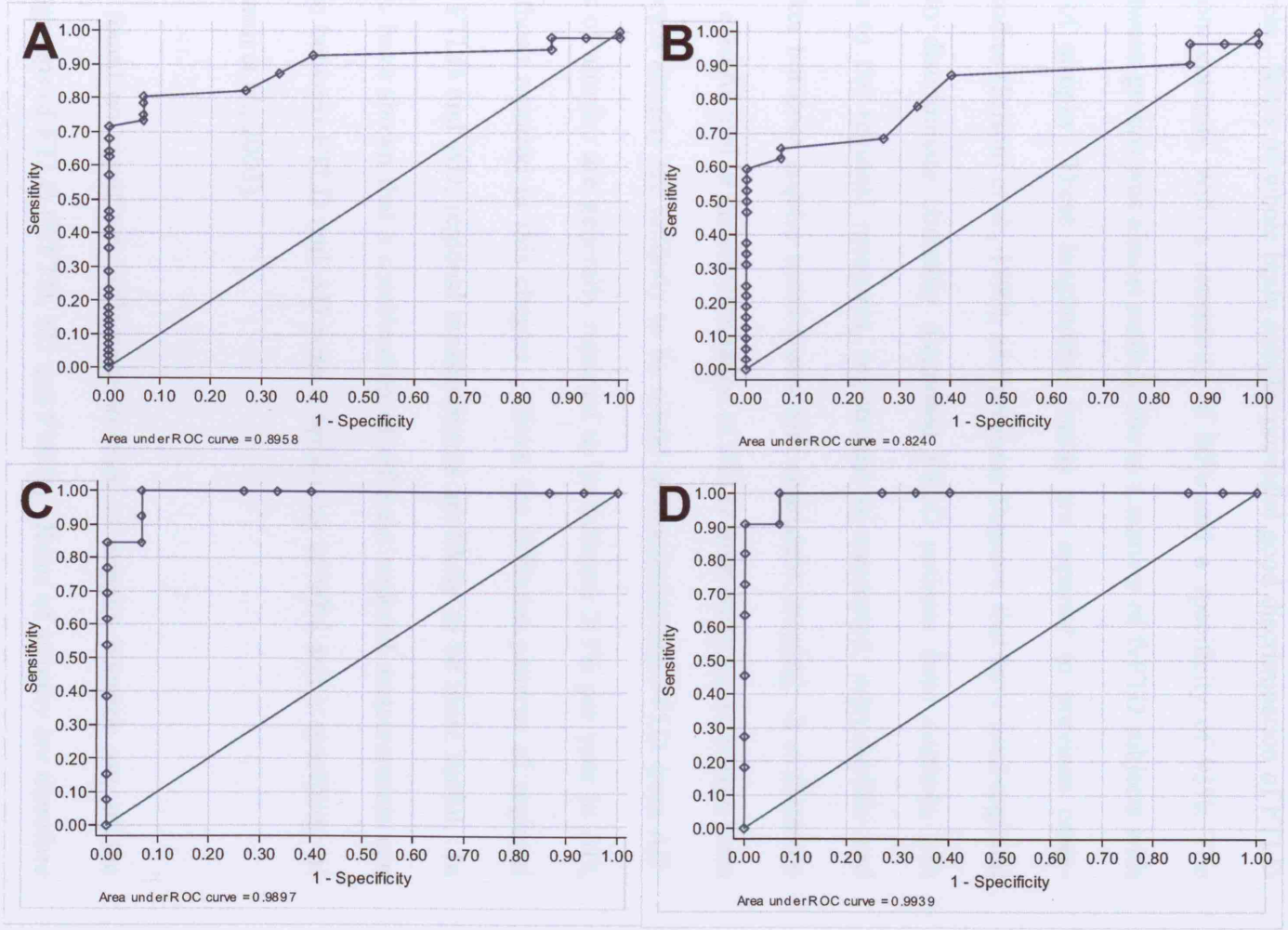

11.4. Discussion

This chapter analysed rates of atrophy in FTLD subjects compared to healthy controls. The mean rate of whole brain atrophy observed in the FTLD group was 1.7% per year. Rates of whole brain atrophy provided good discrimination of FTLD subjects from controls, with a sensitivity of 80% and a specificity of 93%. The overlap between groups was almost entirely due to a number of fvFTD subjects with low rates of atrophy. These longitudinal results are superior to previous cross-sectional studies (Frisoni et al., 1999), and previous chapters, that have used regional measures to discriminate clinically diagnosed FTLD patients from controls. In comparison to the regional measures, registration is automated, reproducible and much quicker but does require serial scans with consistent imaging. It is therefore likely to be a useful tool in the discrimination of FTLD from controls. However, rates of whole brain atrophy are unlikely to be useful in discriminating FTLD from AD. Mean rates of atrophy are generally reported to be between 2-3% per year in AD, similar to those reported in this chapter. Given the different patterns of regional atrophy in FTLD and AD, regional measurements are likely to be more useful. In fact, studies have shown that a combination of different regional measurements can discriminate between FTLD and AD with a sensitivity of 90% and a specificity of 93% (Boccardi et al., 2003).

This study found no significant difference in rates of atrophy between any of the clinical subgroups of FTLD (fvFTD, SD and PNFA). Rates of atrophy are therefore unlikely to be useful in discriminating the syndromic variants of FTLD. A large degree of variability was observed in the fvFTD group. Despite the fact that all fvFTD patients fulfilled consensus criteria, a number of subjects showed a rate of

atrophy consistent with that of a healthy control (n=12). This limited the discrimination of the fvFTD patients from controls, and gave a sensitivity of only 66% for a specificity of 93%. These subjects had a similar mean MMSE score, brain volume and rate of atrophy to the control subjects, although they had the same disease duration as the rest of the fvFTD group. It is unclear why this group of fvFTD patients are showing such low rates of atrophy, and it definitely warrants further study. It will be important to know whether these patients are progressing clinically; if so it would suggest that damage is occurring to the cells but not resulting in cell death (hence atrophy). Only longer (ongoing) follow-up will show whether these individuals do deteriorate cognitively. If these subjects are removed from the fvFTD group then the mean rates of atrophy increase from 1.5% to 2.3% per year.

In comparison, the rates of atrophy in the PNFA and SD group showed almost no overlap with the control subjects. Both groups can be discriminated from the control subjects with a sensitivity of 100% and a specificity of 93%. The PNFA group had a mean rate of atrophy of 2.2% but also had a large degree of variability, with the rates of atrophy ranging from 0.6-5.4% per year. In contrast, the SD group showed more homogenous rates of atrophy, with a mean of 1.9%, and a range of 0.6-3.2% per year. These rates are similar to those found in the temporal variant of FTLD group in the study by Chan et al (2001). Variability within the groups may reflect the heterogeneous pathological substrates that can underlie all three of the syndromic variants of FTLD (Hodges et al., 2004), since chapter 9 suggested that the different pathological substrates of FTLD may show differing patterns of regional atrophy. Alternatively it may reflect the variability in the regional distributions of atrophy within each syndromic group (highlighted in figures 11.3 to 11.5). Chan et al (2001)

demonstrated differences in the regional distribution of BBSI in the frontal and temporal variants of FTLD (Chan et al., 2001a). A whole-brain atrophy rate cannot provide information on such regional differences in tissue loss. The regional patterns of atrophy in all three of the syndromic variants will be investigated further in chapter 13.

There was a suggestion from the data that the rate of atrophy in the FTLD group correlated with both baseline brain volume and MMSE. However this correlation appeared to be driven by the subjects that showed a low rate of brain atrophy in the fvFTD group; these subjects had large brain volumes and MMSE scores. As discussed in previous chapters the MMSE does not provide a very sensitive measure of disease severity in FTLD and would be disproportionately affected in the language variants (PNFA and SD).

A limitation of this study is the lack of pathological confirmation of diagnosis. This is particularly important in the fvFTD cases where clinical progression is slow or unclear. Recent studies suggest that only between 63 and 79% of pathologically confirmed FTLD cases are correctly classified clinically using consensus criteria (Rosen et al., 2002b; Knopman et al., 2005). This introduces uncertainty into the clinical diagnoses. In addition, it is likely that the subjects that show very slow clinical progression and low rates of atrophy are the most difficult to diagnose, perhaps overlapping with vascular and psychiatric pathology, and they may tend to not come to post-mortem. Pathological confirmation was only obtained in six cases and none of these subjects showed low rates of atrophy.

This study also highlights some of the problems associated with longitudinal scanning of subjects with FTLD. A large number of patients had serial imaging (n=105) but approximately 20% of these had to be rejected due to poor quality scans. The most common problem was movement in the scanner which is a particular issue in the more severely affected patients. In addition, those cases with the most severe patterns of atrophy often have conformational changes in the brain which can not be well matched with a rigid body registration. The reported rates of atrophy may, therefore, be underestimated, because the largest volume loss over time should occur in the rapidly progressing subjects. Nonetheless the rates of change were consistent with the manual cross-sectional measurements of brain volume. Serial scans that were performed on different scanners or across scanner upgrades also resulted in a lot of patients being rejected from the study. In all cases differences in quality between the two scans rendered the data unusable. This emphasises the need for well-controlled serial studies in FTLD.

11.5. Conclusion

Atrophy rates calculated from the BBSI are useful in differentiating FTLD from healthy controls, especially the SD and PNFA variants. If the clinical diagnoses are correct then they are not useful in differentiating the clinical subgroups of FTLD and variability in rates of atrophy limits the diagnostic utility in the fvFTD group. However, this study does highlight an interesting group of fvFTD patients that show low rates of brain atrophy and warrant further study. Follow-up will show whether or not these subjects have different clinical outcomes or different (or no) pathological substrate for their symptoms. Rates of atrophy may still prove to be sensitive markers of disease progression in FTLD and may prove useful in future clinical trials.

12. Change in rates of brain atrophy over time in FTLD

12.1. Introduction

The previous chapter demonstrated rates of whole brain atrophy of approximately 2% per year in patients with FTLD. However, a significant amount of heterogeneity was observed in the FTLD cohort. It is possible that the rate of atrophy may change during progression of the disease. Previous work has shown that rates of atrophy accelerate over time in early AD (Chan et al., 2003). At the time when patients are judged to have mild dementia (MMSE = 23), the mean yearly loss of brain volume is 2.8%, having risen by 0.32% per year (table 12-1). Figure 12.1 illustrates the change in rates of brain atrophy over time in 12 patients with AD.

The extent to which atrophy rates change over time in FTLD is not known. Understanding the natural progression of the disease will be important for the assessment of future disease modifying treatments. Therefore, this study aimed to assess changes in atrophy rates over time in subjects with FTLD.

Table 12-1: Estimated mean (95% CI) annual rates according to time (relative to the time when the MMSE score was 23/30) and according to method of measurement of atrophy (Chan et al., 2003)

Time (in years) from MMSE = 23/30	Brain atrophy rate (%/year) as derived from TIV corrected brain volume measurements (95% CI)	Brain atrophy rate (%/year) as derived using BBSI measurements (95% CI)
-2	2.17 (1.58 - 2.75)	1.60 (1.23 - 1.96)
-1	2.49 (1.97 - 3.00)	1.90 (1.59 - 2.21)
0	2.80 (2.32 – 3.29)	2.21 (1.91 - 2.50)
+1	3.12 (2.60 - 3.64)	2.51 (2.18 - 2.84)

Figure 12.1: Change in rates of brain atrophy over time, as determined by serial measurements of total brain volume in 12 patients with AD, represented as a proportion of TIV. Patients are individually colour-coded. Time is plotted relative to the time (t=0) when a score of 23 out of 30 was obtained on MMSE. The y-axis scale is logarithmic (Chan et al., 2003).

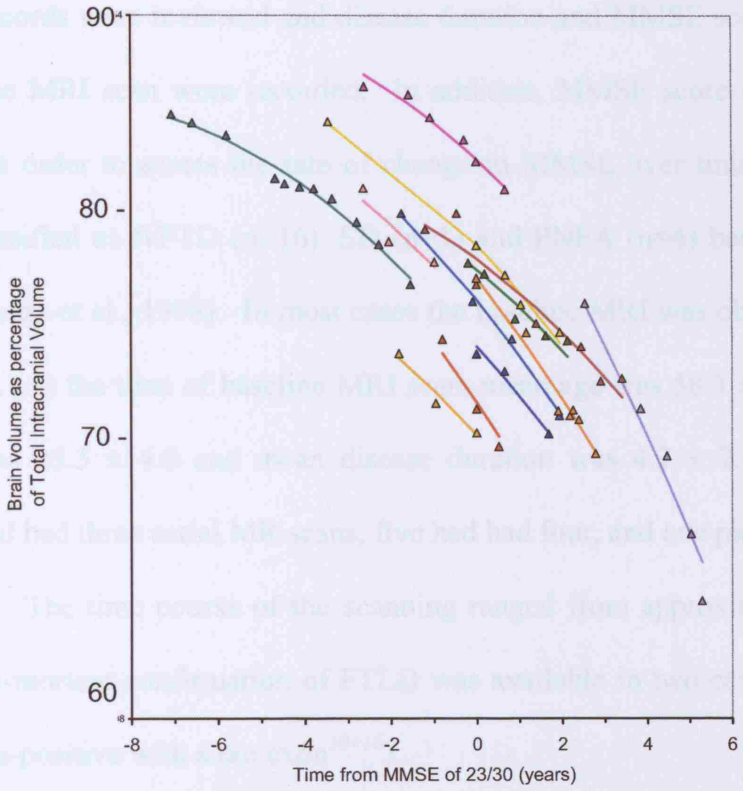

12.2. Methods

12.2.1. Subjects

Twenty-one patients (16 male and 5 female) with clinically diagnosed FTLD (Neary et al., 1998) and at least three serial MRI scans were recruited retrospectively from the Specialist Cognitive Disorders Clinic. These subjects were selected from the 56 FTLD subjects identified in the previous chapter as having adequate serial imaging. Medical records were reviewed and disease duration and MMSE score at the time of the baseline MRI scan were recorded. In addition, MMSE score at final scan was recorded in order to assess the rate of change in MMSE over time. Subjects were further classified as fvFTD (n=16), SD (n=1) and PNFA (n=4) based on consensus criteria (Neary et al., 1998). In most cases the baseline MRI was obtained at the first clinic visit. At the time of baseline MRI scan, mean age was 58.3 ± 6.9 years, mean MMSE was 25.3 ± 4.6 and mean disease duration was 4.2 ± 2.4 years. Fifteen patients had had three serial MR scans, five had had four, and one patient had had five MR scans. The time course of the scanning ranged from approximately one to six years. Post-mortem confirmation of FTLD was available in two cases (one FTLD-U and one tau-positive with a tau exon^{10+16}).

12.2.2. Image analysis

All MR images were acquired using the protocol described in Appendix 4. Brain volumes were measured on every scan using a semi-automated iterative 3D morphological technique (see Appendix 5). TIV was measured on all baseline scans in order to correct for inter-individual differences in head size (Whitwell et al., 2001). Each consecutive scan pair was positionally matched using nine degrees-of-freedom

rigid-body registration and volume changes were calculated using the BBSI (see chapter 3). All serial scans were performed on the same scanner.

For all scan–pairs for each individual, percentage change in brain volume was calculated as change in volume (BBSI) relative to volume at the earlier of the two scans expressed on a logarithmic scale. These repeated measures were analysed using an extension of a previously validated linear mixed modelling framework (Frost et al., 2004). This relates a change in brain volume to the subject-specific atrophy rate and time interval between scans, plus within-subject variability. Quadratic terms were introduced to test for departures from linearity (Chan et al., 2003). Interaction terms were introduced to investigate the relationship between atrophy rate and disease duration at baseline, age at baseline, gender, MMSE at baseline, and baseline brain volume corrected for TIV.

12.3. Results

Figure 12.2 shows the changes in brain volume over time in all FTLD subjects. The mean rate of atrophy was estimated to be 1.6% per year (95% confidence interval (CI) 0.9-2.3% per year) in the whole cohort. There was statistically significant hetereogeneity in rates between subjects ($p<0.001$) with the standard deviation estimated as 1.4% per year (CI 1.1 – 2.2% per year).

There was no evidence for acceleration in atrophy over time in the whole cohort ($p=0.57$). In addition, there was no evidence that the slope varied with age, MMSE or gender. However, there was evidence in multiple regression analyses that the slope varied with both disease duration and baseline brain volume. Patients with longer

disease duration had a lower rate of atrophy, i.e. for every year since disease onset the rate of atrophy was estimated to decrease by 0.32% per year ($p<0.01$), and patients with a larger baseline brain volume had a lower rate of atrophy, i.e. for every 100ml decrease in baseline brain volume the rate of atrophy increased by 1.27% per year ($p<0.001$). The fvFTD group had a significantly ($p=0.03$) lower rate of atrophy (1.2% per year, CI 0.5-2.0%) compared to the PNFA subjects (3.1% per year, CI 1.5-4.6%).

However, from inspection of figure 12.2 it is clear that a number of subjects did not exhibit atrophy over the period of the study (marked in red). Those subjects with a rate of atrophy less than 0.6% per year ($n=6$) (figure 12.2, upper group), similar to controls (miriad), were removed from a secondary analysis of the data. The cut-off of 0.6% was applied from chapter 11. The characteristics of these patients compared to the rest of the cohort are shown in table 12.2. The mean rate of atrophy was now estimated to be 2.2% per year (CI 1.4-3.0%) with the between subject standard deviation reduced to 1.3% per year. There was still statistically significant heterogeneity in rates between subjects ($p<0.01$). As before, there was no significant evidence for acceleration in rates over time. There was no evidence that the slope varied with age, MMSE, gender, or clinical group. However, there was still evidence in multiple regression analyses that the slope varied with both disease duration and baseline brain volume.

Figure 12.2: Change in rates of brain atrophy over time in 21 subjects with FTLD. Those subjects with a fitted slope of less than 0.6% per year are shown in red. The baseline brain volume corrected for TIV is plotted at baseline for each subject, and then each subsequent point shows the reduction in BBSI (ml) over the specific interval. The serial data from one subject crossed a scanner upgrade: this interval is represented as a dotted line to indicate that a reliable BBSI cannot be calculated. The first post-upgrade data point shows the TIV-corrected brain volume at this date.

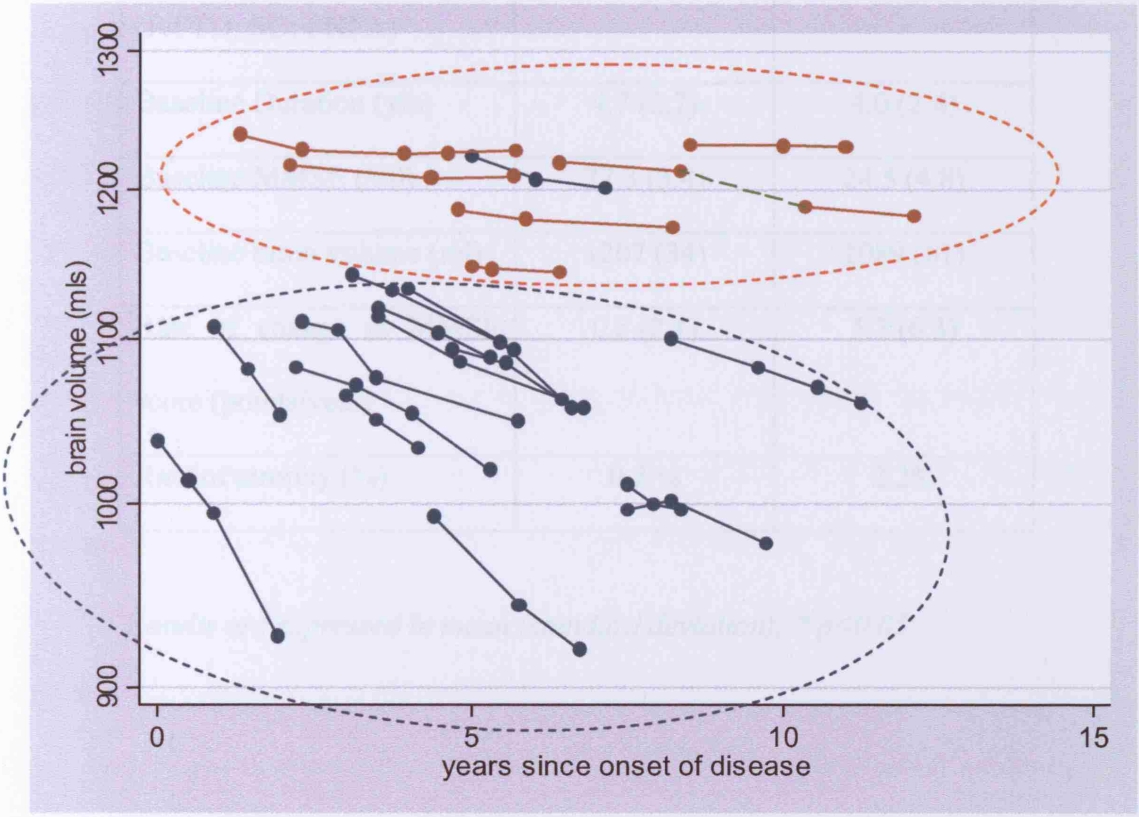

Table 12-2: Patient characteristics for subjects showing a low rate of atrophy versus the rest of the cohort.

	Low rate group (n=6)	**High rate group** (n=15)
Gender (M:F)	6 : 0	10 : 5
Age	56.1 (6.9)	59.2 (6.9)
Clinical diagnosis (fvFTD: SD: PNFA)	6 : 0 : 0	10 : 1 : 4
Baseline Duration (yrs)	4.7 (2.7)	4.0 (2.4)
Baseline MMSE (/30)	27.3 (3.4)	24.5 (4.8)
Baseline brain volume (ml)	1207 (34)	1089 (61)
Rate of change in MMSE score (points/year)	0.8 (2.1)	5.7 (6.3)
Rate of atrophy (%)	0.2 %	2.2%

*Results are expressed in mean (standard deviation); * $p<0.05$*

12.4. Discussion

This chapter assessed the change in rates of atrophy over time in subjects with FTLD. It demonstrates firstly that a significant amount of heterogeneity exists in the rates of atrophy, and second that there may be two separate populations of FTLD patients. The majority of patients showed progressive atrophy, with an annualised brain volume loss of 2.2% per year, however a subgroup of patients had no whole brain atrophy over the entire period of study (less than 0.6% per year), similar to controls. These subjects represent a subset of the subjects identified in the previous chapter with a low rate of atrophy. These results extend those findings by demonstrating that subjects can remain stable for over 5 years, and perhaps for as long as 10 years (based on disease duration). In addition, the subjects with a low rate of atrophy also had a low rate of change in MMSE score over time (only 0.8 points change per year compared to 5.7 in the rest of the cohort); suggesting a low rate of clinical progression. This is a finding that is likely to have implications for future clinical trials. Including subjects that do not atrophy or progress clinically over time could reduce the ability to detect treatment effects. It will be important to determine whether these patients have FTLD at post-mortem, and also whether these patients progress clinically at future follow-up. It is likely that a number of years of follow-up would be required to assess the outcome of these patients. Unfortunately, pathological confirmation was not available in any of these patients; however they all fulfilled established clinical criteria for FTLD.

There was no evidence for accelerating atrophy over time within the FTLD subjects. In fact, the mean slope was approximately linear. This is consistent with a study looking at gross atrophy at post-mortem in FTLD (Broe et al., 2003) that found a

linear rate of change over the first five years from diagnosis. However, it contrasts with the results from subjects with AD, in which the rate of atrophy appears to accelerate over time (Chan et al., 2003). The study looking at AD investigated clinically early cases, with some patients presymptomatic at the time of first scan. None of the FTLD subjects in this study were scanned before the onset of symptoms; therefore it remains possible that the rates of atrophy do accelerate in the very earliest stages of the disease. It is also possible that while the rates of whole brain atrophy are not accelerating over time, there may be changes in the rates of atrophy of regional structures.

Whilst this study has the strength that each subject was followed serially using at least three MRI, one concern is that these inclusion criteria may introduce bias into the results. Subjects that can tolerate multiple serial MRI are likely to be the least severe cases clinically. The more severe cases, that are likely to have the largest volume loss over time, are more likely to drop out at an early stage or not achieve adequate imaging. This may explain why the patients with longer disease duration appeared to have lower rates of atrophy, and why the mean rate of atrophy from the whole group was lower than has been previously reported (Chan et al., 2001a). In addition, FTLD patients are notoriously difficult to match according to disease severity. Whilst the MMSE has been used to align changes in atrophy rate in AD (see figure 12.1), the MMSE, as discussed previously, is a poor measure of severity in FTLD. The rates of atrophy in this study have been plotted according to disease duration, but due to the imprecise nature of this assessment the statistics for this chapter were performed without correction for disease severity.

12.5. Conclusion

This study highlights the variability present in longitudinal rates of atrophy in FTLD and demonstrates that some patients with FTLD (especially fvFTD) may remain stable, with no significant brain atrophy, for over five years. It will be important to follow these patients over time and obtain a post-mortem to confirm diagnosis. It also suggests that patients with FTLD undergo cerebral atrophy at an approximately linear rate from the time of diagnosis.

13. Longitudinal patterns of regional atrophy in FTLD

13.1. Introduction

Chapter 11 assessed rates of global atrophy in FTLD and demonstrated very similar rates of global atrophy in all three syndromic variants of FTLD. However, rates of regional atrophy may perhaps be more diagnostically useful and provide a marker of disease progression in these very focal FTLD disorders. Increased rates of regional atrophy have been reported in AD patients compared to healthy controls (Jack et al., 1998; Fox et al., 2000), and have been detected prior to the onset of symptoms (Fox et al., 1996a; Scahill et al., 2002). Moreover, these increased rates of atrophy have been shown to correlate to clinical decline (Jack et al., 2000) and have been used as outcome measures in therapeutic trials in AD (Jack et al., 2003). Identification of the regional patterns of longitudinal change in FTLD may similarly provide markers of disease progression for future therapeutic trials.

Detection of small amounts of regional change remains difficult with manual volumetric measurements. They are time intensive and subject to operator bias and error. Ideally, an automated, unbiased technique that does not involve a priori assumptions concerning which structures to assess would be applied. The previous chapters used rigid body registration to positionally match the repeat scans onto baseline. This treats the brain as a rigid body, matching the brain as a whole and quantifying whole-brain atrophy. However, because of structural readjustment, the sites of tissue loss cannot accurately be determined. Fluid registration is a non-linear registration technique (see chapter 3) that can track local cerebral losses and deformations. The repeat scan is matched to baseline using a series of voxel-level

deformation fields that are based on the constraints of a viscous fluid model. Jacobian determinants can then be calculated from these deformation fields and used to quantify change at the voxel level. This technique has been validated in both AD and control subjects (Freeborough and Fox, 1998), and used to demonstrate presymptomatic change in individuals at genetic risk of AD (Fox et al., 2001) and FTLD (Janssen et al., 2005).

The aim of this chapter was to assess the regional patterns of longitudinal change in patients with different syndromic variants of FTLD. A traditional VBM approach was used to compare controls and disease subjects at baseline and repeat time-points (see chapter 5). Direct longitudinal analyses were then performed firstly using VBM to compare the baseline and repeat assessments (this method has previously been applied to study change over time in normal ageing (Tisserand et al., 2004)), and secondly using fluid registration to examine directly the longitudinal patterns of regional change in each individual. To determine which changes are truly disease-specific SPM was used to perform robust group statistical comparisons using the Jacobian determinants (a measure of contraction/expansion required at each voxel to match the serial imaging) from the fluid registrations (Scahill et al., 2002).

13.2. Methods

13.2.1. Subjects

Forty-six patients were recruited from the Specialist Cognitive Disorders Clinic (see chapter 3). All subjects fulfilled clinical criteria for FTLD (Neary et al., 1998); 29 were subsequently diagnosed with fvFTD, ten with SD and seven with PNFA. Serial T1-weighted MR scans were acquired for all patients. The patient groups were

compared with an age and sex-matched group of fifteen cognitively intact controls who had undergone serial imaging. Post mortem examination was available in three cases (one case with FTLD-U, and two cases with tau-positive pathology with mutations in tau exon^{10+16}). Subject details are shown in table 13-1.

Table 13-1: Patient characteristics

	Controls (n=15)	FTLD (n=46)	fvFTD (n=29)	SD (n=10)	PNFA (n=7)
Gender (M:F)	9:6	33:13	24:5	5:5	4:3
Age (yrs)	62.4 (13.2)	62.6 (6.8)	61.2 (6.5)	64.6 (7.5)	65.6 (5.7)
Baseline MMSE	NA	22.1 (7.4)	24.6 (4.6)	21.4 (6.2)	11.7 (10.9)
Repeat MMSE	NA	19.6 (8.1)	22.3 (5.9)	14.3 (8.1)	12.2 (10.4)
Interval (days)	487 (361)	501 (293)	465 (256)	689 (401)	382 (127)
Disease duration (yrs)	NA	5.0 (2.9)	5.1 (3.1)	3.8 (1.4)	5.8 (3.3)

Results given as mean (sandard deviation)

13.2.2. MRI Acquisition and MIDAS pre-processing

T1-weighted volumetric images were acquired using the standard protocol described in Appendix 4. Each brain was outlined using a semi-automated technique described in Appendix 5 using MIDAS image analysis software (Freeborough et al., 1997). A nine degrees-of-freedom registration was performed to align accurately the repeat scan onto the baseline image (see chapter 3). A viscous fluid model was then applied to the rigidly-aligned repeat scan and used to compute a deformation field throughout the image at the voxel level (see chapter 3). This model gives an estimate of the volume change occurring at each voxel within the image. The Jacobian determinants from the deformation field can be colour-coded and visualised by overlaying them on the original scan. This is referred to hereafter as a Jacobian value. To examine the change within individuals over time, logs of the Jacobian values for each voxel within the image were analysed. Two images were created for each patient; one for voxel expansion (Jacobian values ≥ 1), and one for voxel contraction (Jacobian values < 1). This separation was performed to prevent cancellation errors during smoothing (e.g. expanding areas such as CSF being adjacent to contracting areas of brain such as hippocampus). The jacobians could also have been separated into brain or non brain regions, or even grey matter, white matter and CSF using the SPM segmentations. However these methods still have the inherent problem that segmentation errors could result in cancellation affects around the brain-csf boundaries. Recent work has suggested that splitting the jacobains by expansion and contraction is more sensitive (Scahill, 2003).

13.2.3. SPM pre-processing

The baseline, repeat and Jacobian images were transferred to SPM99 (Wellcome Department of Cognitive Neurology, London), running in MATLAB 6 (Mathworks Incorporated, Sherbourn, Massachusetts), for analysis. In order to optimise normalization a customized template was generated from a group of 10 normal controls, four patients with fvFTD, three patients with SD and three patients with PNFA. These groups did not include subjects involved in the study and were age and gender matched to the study subjects.

Each image (baseline and repeat) was normalised to the customised template using the default SPM parameters (see chapter 3) and then segmented into grey matter, white matter and CSF. Each grey matter image was masked with a MIDAS brain segmentation to exclude all non-brain voxels. Grey matter, white matter and CSF images were then modulated and smoothed with an isotropic Gaussian kernel of 8mm FWHM.

The contraction and expansion images were transformed into standard space by applying the normalization parameters generated by the spatial normalization of the baseline images. They were convolved with a mask to exclude scalp, and smoothed with an isotropic Gaussian kernel of 8mm FWHM. An explicit mask was used to ensure that all brain voxels were included in the analysis.

13.2.4. Statistical analysis

Cross-sectional VBM analysis

A single subject condition and covariate model was used to compare controls to each of the FTLD groups at both baseline and repeat assessments using:

a) Grey matter

b) White matter

c) CSF

Exclusive masking procedures were used to identify regions of atrophy present on the repeat analysis that were not present in the baseline analysis; these procedures applied Boolean criteria to every voxel in the thresholded statistical parametric map for each contrast. Results are displayed showing the cross-sectional baseline patterns of atrophy in yellow and the regions of atrophy present only on the repeat analysis in red.

Longitudinal VBM analysis

A paired t-test model was used to compare the repeat scans directly to the baseline scans in each FTLD group and the control group using:

a) Grey matter

b) White matter

c) CSF

Longitudinal fluid analysis

A single subject condition and covariate model was used to compare controls to each of the FTLD groups using

a) Fluid contraction images

b) Fluid expansion images

Age and gender were included as nuisance variables, with time interval between scans used as a covariate in the longitudinal analyses. Results were assessed both at an uncorrected statistical threshold ($p<0.001$) and after correction for multiple comparisons over the whole brain volume ($p<0.05$).

13.3. Results

13.3.1. Controls

The repeat scans were compared directly to the baseline in the control group (figure 13.1). Very little change was observed over time in the grey matter and CSF comparisons. The white matter analysis showed diffuse change, predominantly focused around the lateral ventricles and in the left temporal lobe ($p<0.001$, uncorrected). No regions (of change over time) survived correction for multiple comparisons ($p<0.05$).

13.3.2. FTLD

13.3.2.1. Grey matter

The FTLD group as a whole showed a widespread pattern of frontal and temporal, and also parietal, grey matter atrophy at baseline compared to controls (figure 13.2). The pattern of atrophy was more widespread on the repeat analysis but involved the same regions as at baseline (figure 13.2). Directly comparing the grey matter at repeat assessment with the baseline showed grey matter loss over time predominantly in the temporal lobes over time, including the medial and superior temporal gyri. Grey matter differences were also found in the frontal lobe, predominantly on the left, and the parietal lobe (figure 13.2). Apparent losses were also shown around the

ventricles and the sylvian fissures. Areas that survived the correction for multiple comparisons were found in the left perisylvian region ($p<0.05$).

13.3.2.2. White matter

At baseline, white matter loss was found in the left temporal lobe, frontal midline, orbitofrontal cortex, and bilaterally in the lateral ventricles, compared to controls (figure 13.3). The repeat analysis showed a more widespread pattern of atrophy in all the above regions, and in addition showed a small amount of white matter atrophy in the right temporal lobe, compared to controls (figure 13.3). When compared directly to baseline, the repeat analysis showed white matter loss bilaterally in the temporal lobes and lateral ventricles over the study period (figure 13.3).

13.3.2.3. CSF

The CSF baseline analysis showed significantly more CSF in the lateral and third ventricles, the collateral sulci, inferior temporal sulci and the left perisylvian fissure compared to controls (figure 13.4). The repeat analysis showed greater CSF expansion in all the above regions compared to controls (figure 13.4). The direct comparison showed a widespread pattern of increased CSF spaces over time. CSF differences were found bilaterally in the lateral and third ventricles, the perisylvian fissures and the temporal horns. All these regions survived the correction for multiple comparisons at $p<0.05$. There were also widespread CSF differences in frontal, temporal and parietal sulci (uncorrected, $p<0.001$) which did not survive correction for multiple comparisons.

13.3.2.4. Fluid analysis

The fluid contraction analysis showed patterns of increased rates of volume loss (atrophy) in frontal, temporal and parietal regions compared to controls (figure 13.5). This preferentially involved both temporal lobes, including the temporal stem, and the middle and inferior frontal gyri, predominantly on the left. Increased rates of change were also observed bilaterally in the posterior cingulate, with the greatest rates of change on the left, and to a lesser extent the parietal lobe, predominantly on the right. No regions survived the correction for multiple comparisons ($p<0.05$).

The fluid expansion analysis revealed very significant expansion of the lateral and third ventricles, bilaterally, in the FTLD group compared to controls (figure 13.5).

Figure 13.1: Statistical parametric maps showing regions of grey matter, white matter and CSF change at repeat assessment compared to baseline in healthy controls (uncorrected, p<0.001).

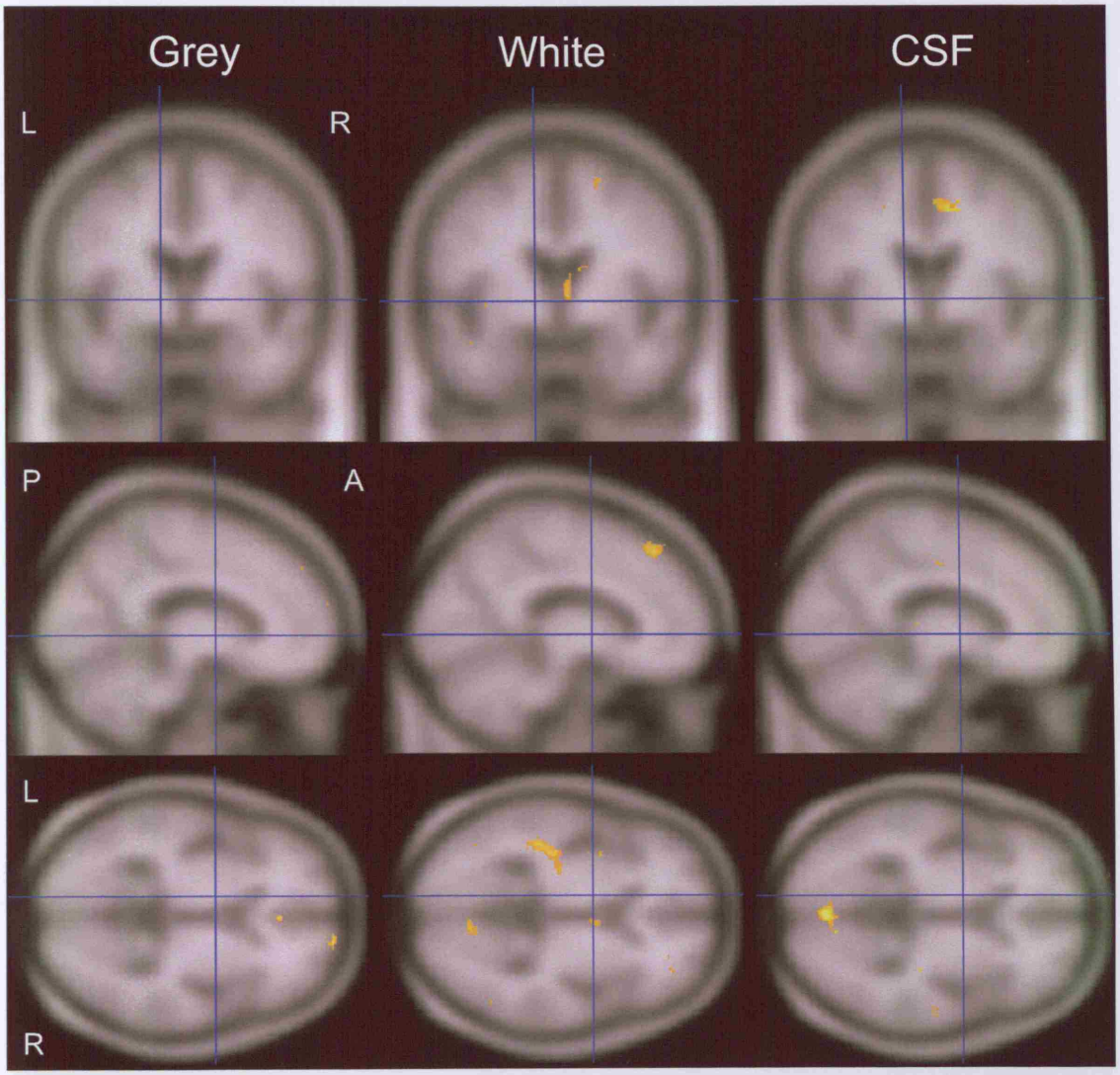

Figure 13.2: Statistical parametric maps showing regions of grey matter atrophy in FTLD compared to controls at baseline (C-B) and repeat (C-R) assessments, and regions of grey matter atrophy in FTLD at repeat assessment compared to baseline (B-R) (uncorrected, p<0.001).

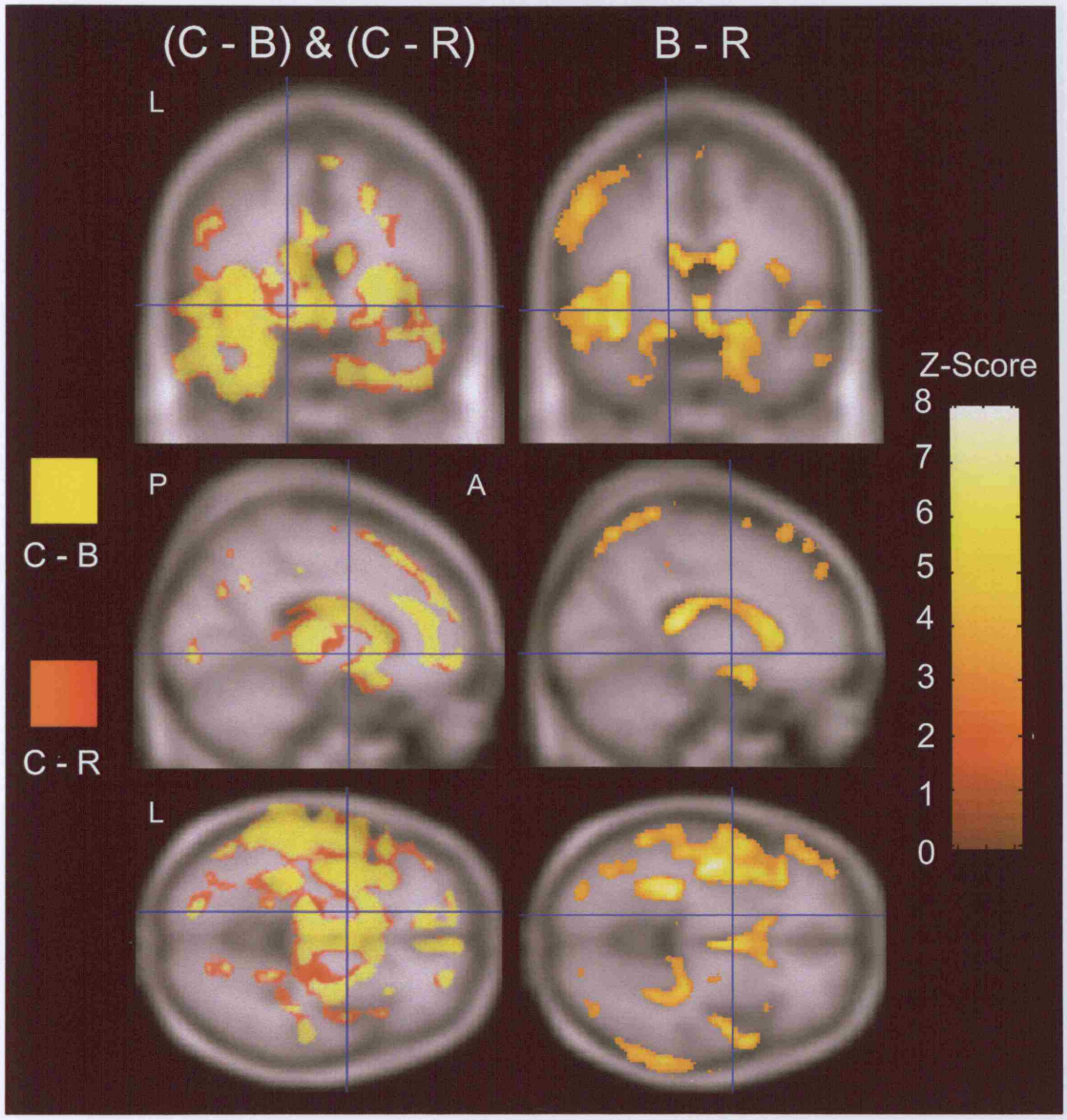

Figure 13.3: Statistical parametric maps showing regions of white matter loss in FTLD compared to controls at baseline (C-B) and repeat (C-R) assessments, and regions of white matter atrophy at repeat assessment compared to baseline (B-R) (uncorrected, $p<0.001$).

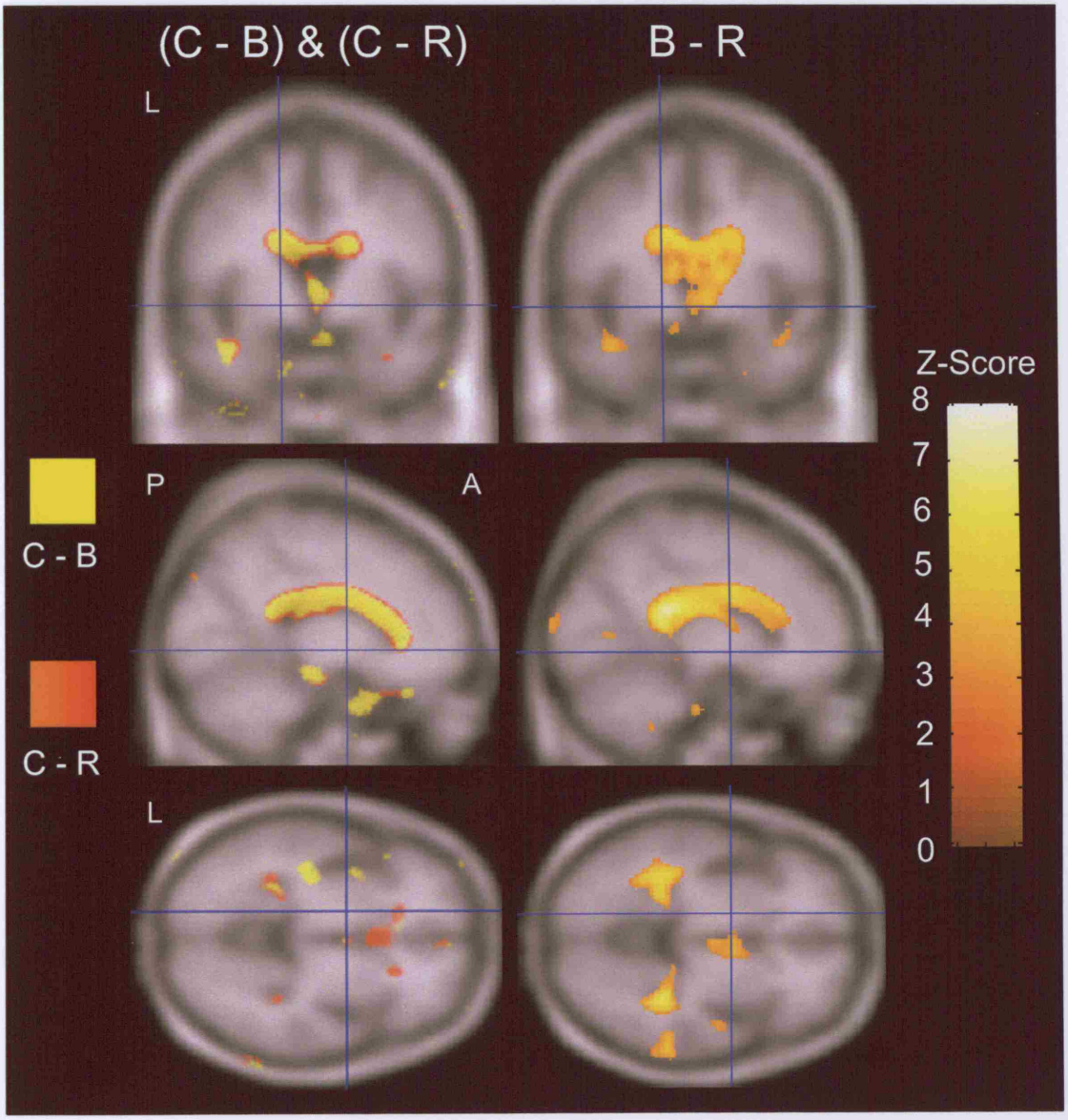

Figure 13.4: Statistical parametric maps showing regions of CSF increase in FTLD compared to controls at baseline (C-B) and repeat (C-R) assessments, and regions of CSF increase at repeat assessment compared to baseline (B-R) (uncorrected, $p<0.001$).

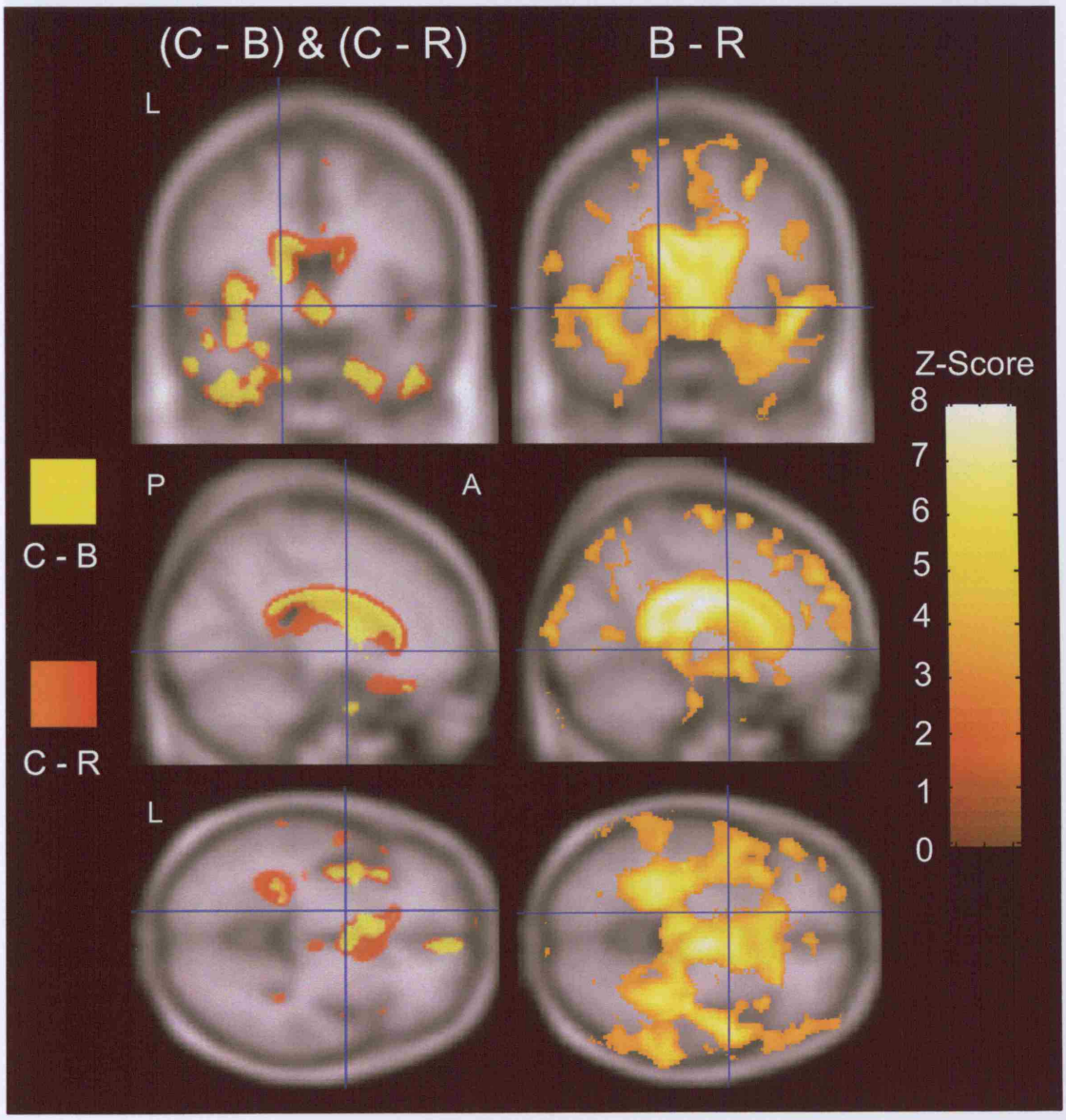

Figure 13.5: Statistical parametric maps showing regions of significant fluid contraction and expansion in FTLD compared to controls (uncorrected, p<0.001).

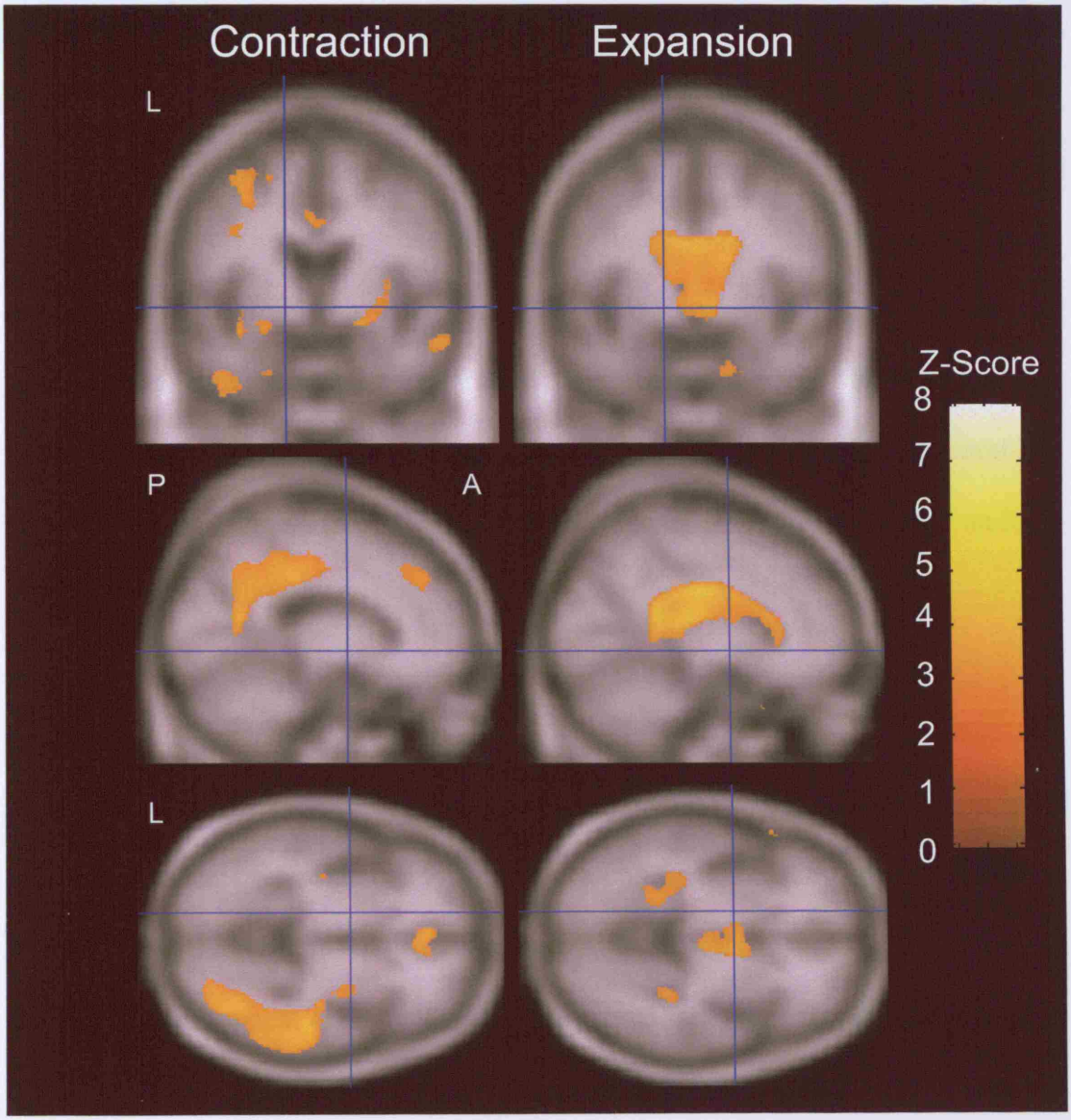

13.3.3. fvFTD

13.3.3.1. Grey matter

Compared to controls, the baseline grey matter analysis in the fvFTD group showed bilateral atrophy of the frontal and temporal lobes, but also some losses in the parietal lobes. The repeat analysis showed a more extensive pattern of grey matter atrophy, but again involving similar regions to baseline (figure 13.6). Directly comparing the grey matter at baseline with the repeat assessment showed significant atrophy over time in the hippocampus bilaterally, the left insula and the perisylvian region. In addition, grey matter differences were found in the frontal lobes and the lateral and third ventricles (figure 13.6). No regions survived the correction for multiple comparisons ($p<0.05$).

13.3.3.2. White matter

Very little white matter loss was observed in the fvFTD group. At both baseline and repeat assessments white matter losses were found predominantly around the lateral ventricles and the orbitofrontal cortex compared to controls (figure 13.7). Comparing the baseline and repeat assessments showed a small amount of white matter change over time in the left temporal lobe and the lateral ventricles (figure 13.7). No regions survived the correction for multiple comparisons ($p<0.05$).

13.3.3.3. CSF

Very little CSF enlargement was present at baseline compared to controls (figure 13.8). At the repeat assessment increased CSF was found in the lateral and third ventricles, the left perisylvian fissure and the right collateral sulcus compared to controls (figure 13.8). Comparing the baseline and repeat assessments showed

increased CSF in the lateral and third ventricles, the perisylvian fissure and the temporal horns bilaterally over time (figure 13.8). No regions survived the correction for multiple comparisons ($p<0.05$).

13.3.3.4. Fluid analysis

The only region that showed significantly increased rates of volume loss on the fluid analysis was the posterior cingulate, bilaterally (figure 13.9). The fluid expansion analysis revealed small regions of significant expansion in the lateral ventricles compared to controls (figure 13.9). No regions survived the correction for multiple comparisons ($p<0.05$).

Figure 13.10 shows voxel-compression maps for two fvFTD subjects. It demonstrates the variability present in the fvFTD group: the case on the left shows mild diffuse atrophy, yet the case on the right shows a more focal pattern of atrophy affecting the temporal lobes, and more severe expansion of the ventricles.

Figure 13.6: Statistical parametric maps showing regions of grey matter atrophy in fvFTD compared to controls at baseline (C-B) and repeat (C-R) assessments, and regions of grey matter atrophy at repeat assessment compared to baseline (B-R) (uncorrected, $p<0.001$).

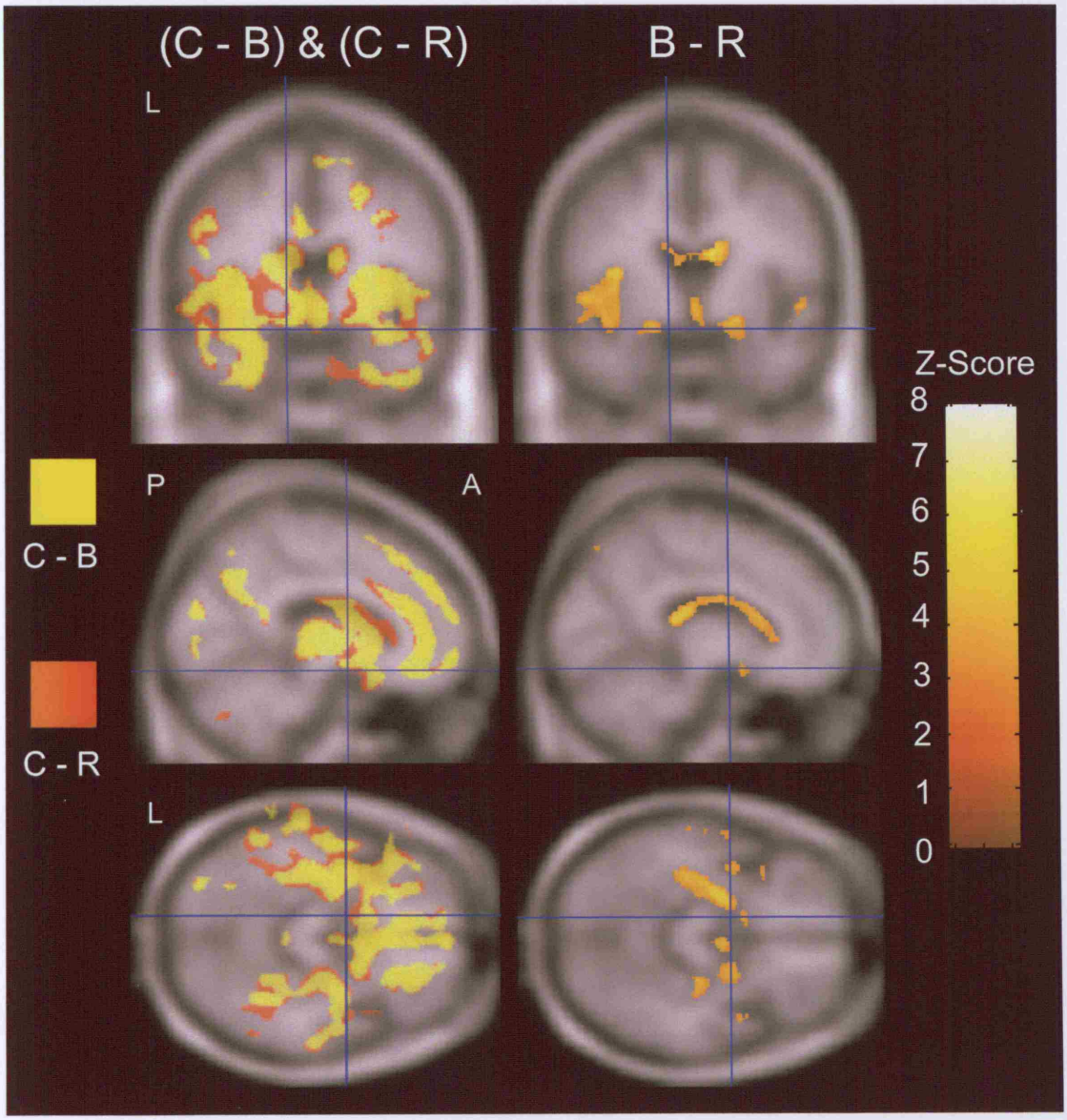

Figure 13.7: Statistical parametric maps showing regions of white matter loss in fvFTD compared to controls at baseline (C-B) and repeat (C-R) assessments, and regions of white matter atrophy at repeat assessment compared to baseline (B-R) (uncorrected, p<0.001).

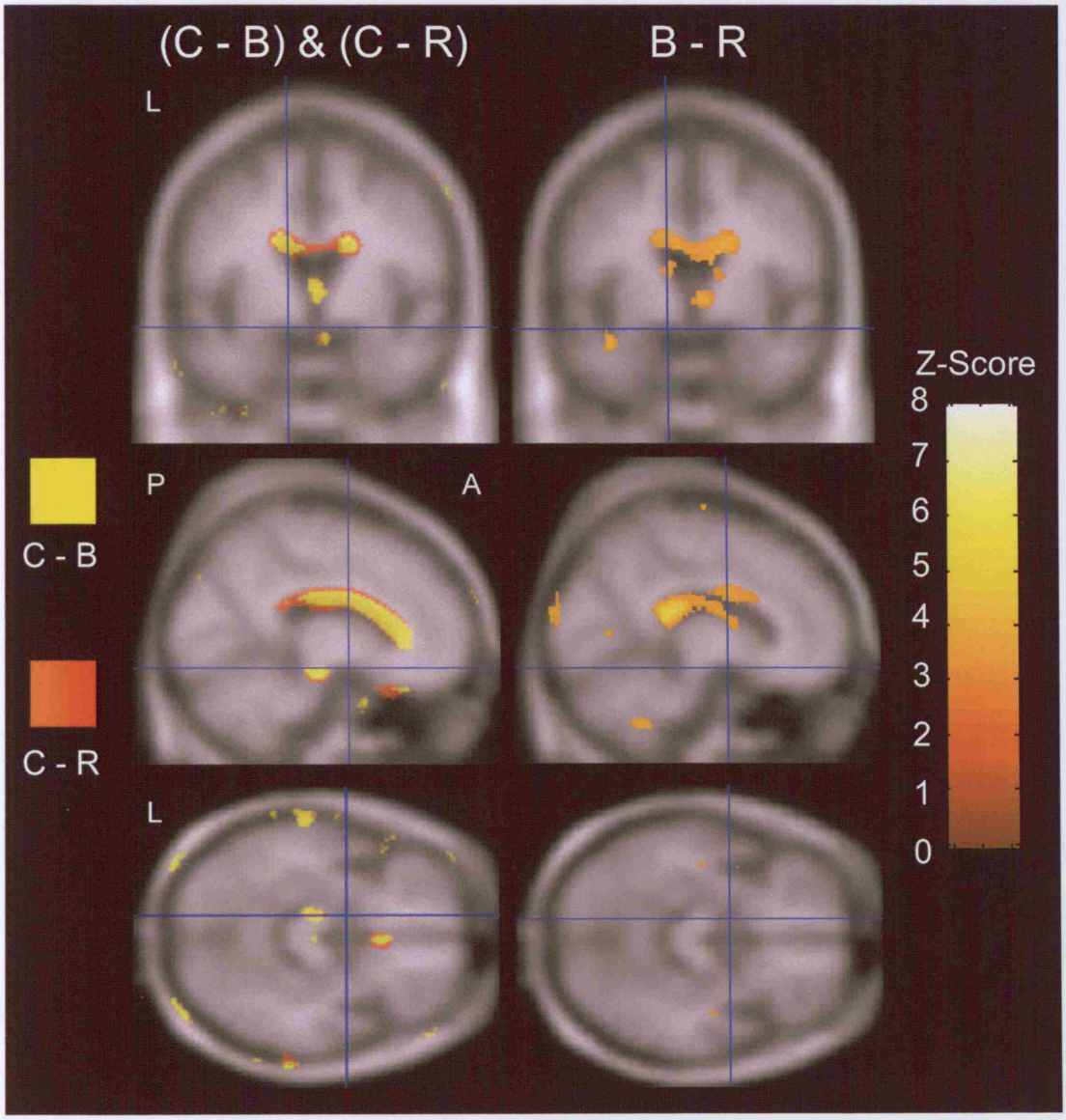

Figure 13.8: Statistical parametric maps showing regions of CSF increase in fvFTD compared to controls at baseline (C-B) and repeat (C-R) assessments, and regions of CSF increase at repeat assessment compared to baseline (B-R) (uncorrected, $p<0.001$).

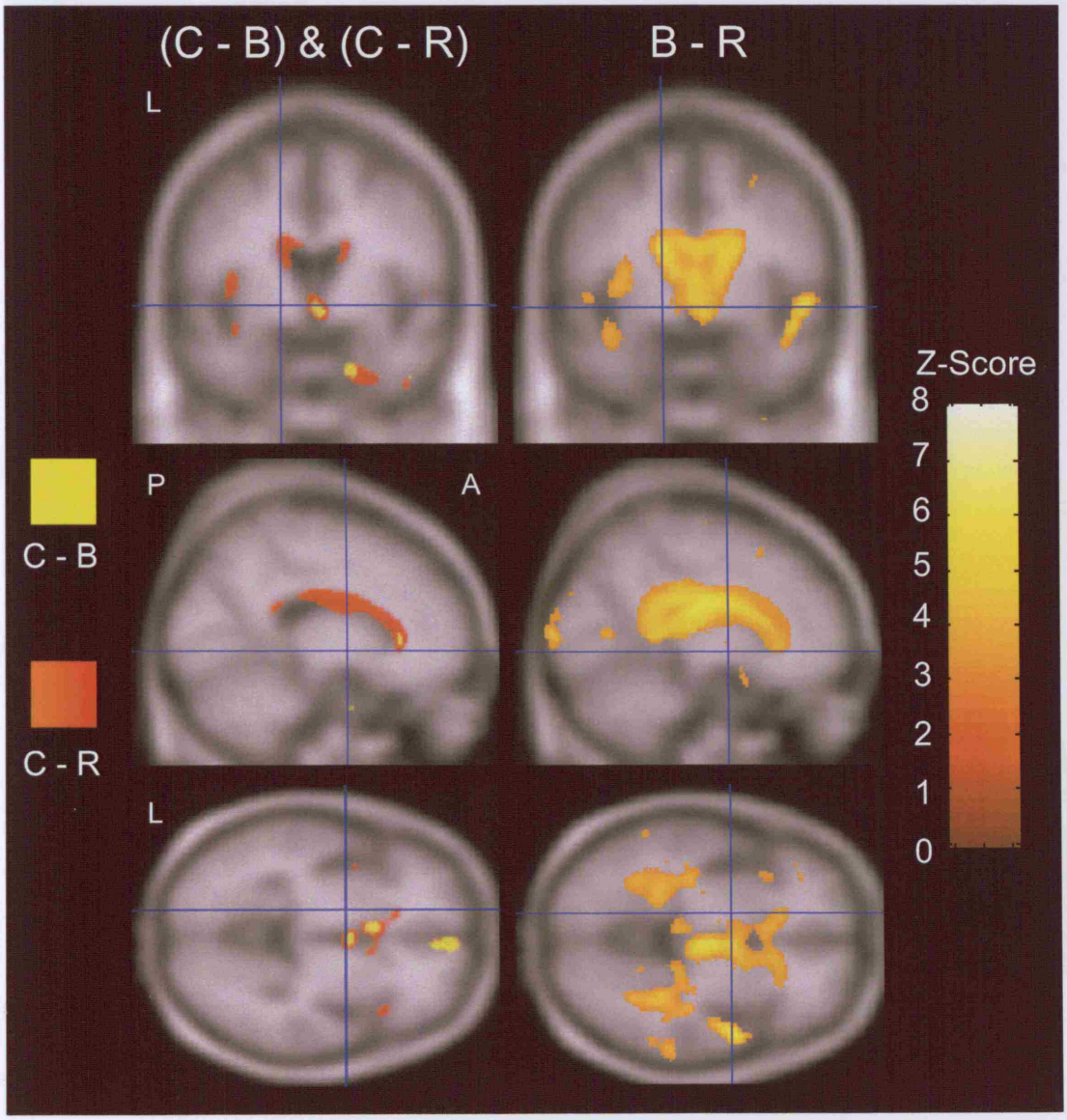

Figure 13.9: Statistical parametric maps showing regions of significant fluid contraction and expansion in fvFTD compared to controls (uncorrected, p<0.001).

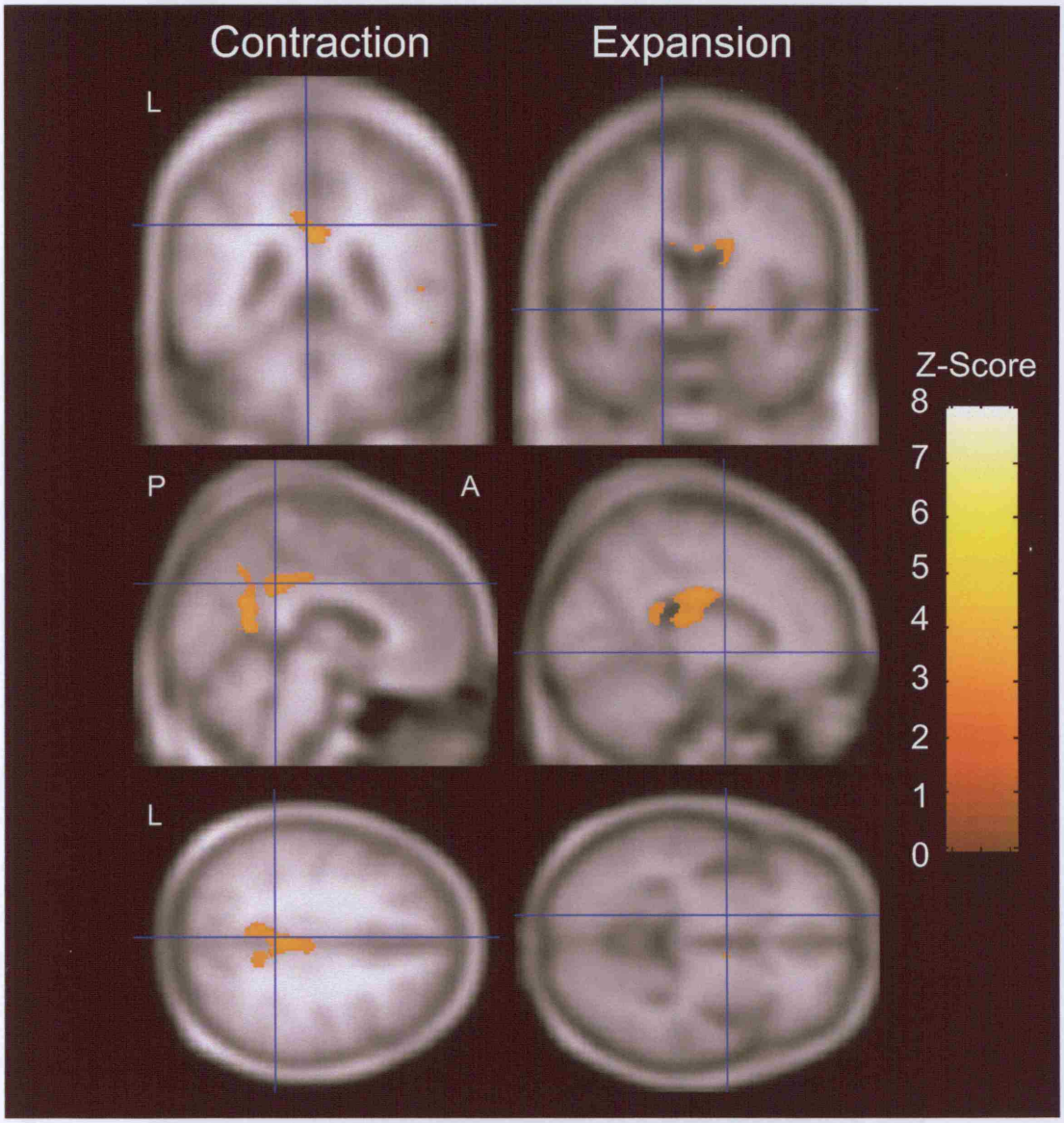

Figure 13.10: Voxel-compression maps showing change over approximately 12 months in two patients with fvFTD.

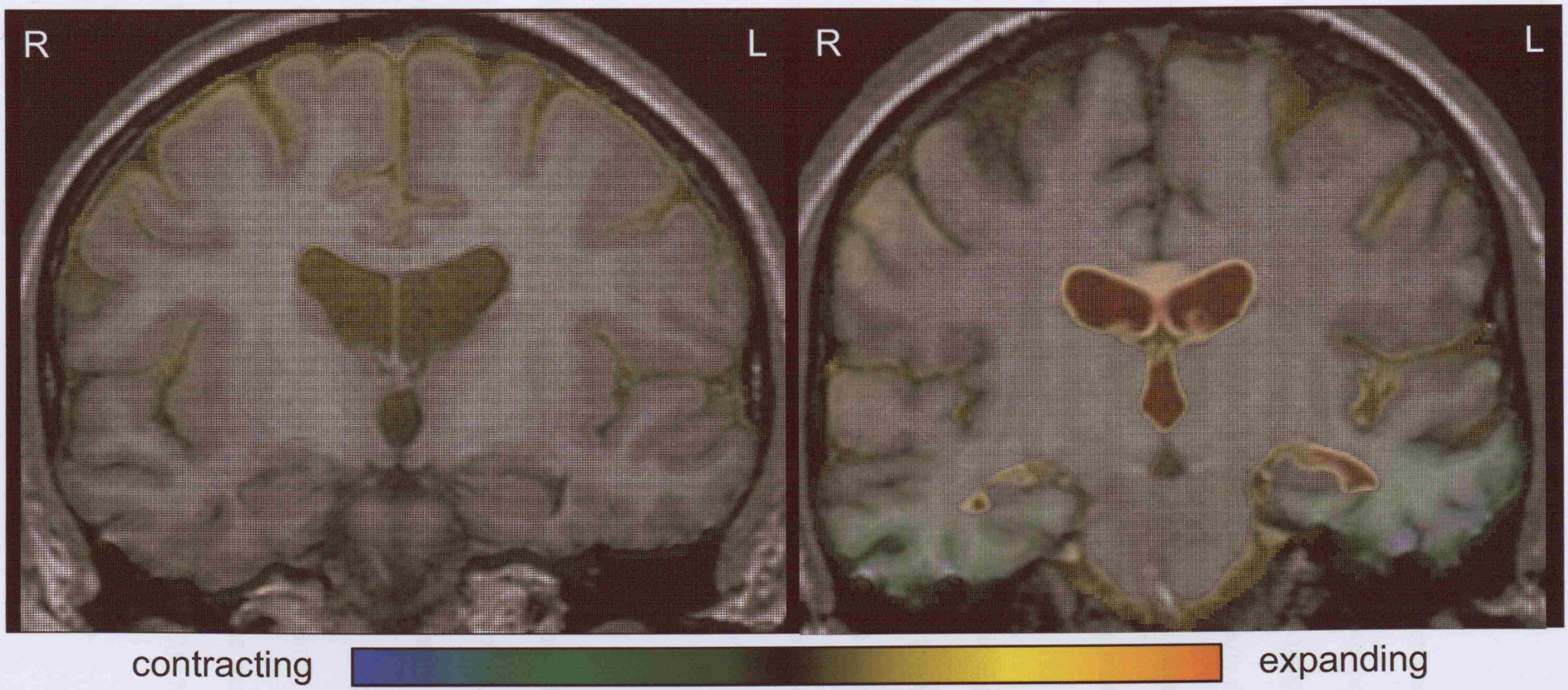

13.3.4. SD

13.3.4.1. Grey matter

The baseline analysis showed severe grey matter atrophy of the left temporal lobe in the SD patients compared to controls. This was widespread including the temporal pole, inferior, middle and superior temporal gyri, and the medial temporal lobe. There was also some involvement of the right temporal lobe, particularly the inferior temporal gyrus, and the left inferior frontal lobe and left parietal lobe (figure 13.11). Atrophy in each of these regions was more extensive on the repeat analysis, particularly in the right temporal lobe, compared to controls (figure 13.11). When the repeat scans were compared directly to baseline, the repeat analysis showed grey matter atrophy bilaterally, but more severe on the left, in the superior temporal gyrus, the amygdala and the frontal lobes. Grey matter loss was also found bilaterally, but more severe on the right, in the hippocampus, and the posterior temporal lobe (figure 13.11). No regions survived the correction for multiple comparisons ($p<0.05$).

13.3.4.2. White matter

The baseline analysis showed significant white matter atrophy of the left temporal lobe, the frontal midline, the orbitofrontal cortex and the lateral ventricles, in the SD group compared to controls. The repeat analysis showed more widespread atrophy of these regions, but in addition showed involvement of the right temporal lobe, compared to controls (figure 13.12). The only regions of white matter atrophy to reach significance on the repeat assessment when compared to baseline were found in the right temporal lobe and the posterior ventricles (figure 13.12). No regions survived the correction for multiple comparisons ($p<0.05$).

13.3.4.3. CSF

The baseline CSF analysis showed increased CSF in the lateral and third ventricles, left temporal sulci, and the inferior right temporal sulci compared to controls. The repeat analysis showed a more extensive pattern of increased CSF compared to controls (figure 13.13). Comparing the CSF at baseline and repeat assessment showed CSF differences in the left lateral ventricle, the perisylvian fissure, greater on the right, the right temporal horn, and the right inferior and middle temporal sulci. Some increased CSF was also observed around the frontal lobes. No regions survived the correction for multiple comparisons ($p<0.05$).

13.3.4.4. Fluid analysis

The fluid contraction analysis showed increased rates of atrophy in both temporal lobes. On the left the focus of progression was in the posterior temporal lobe, whereas on the right it was focused on the anterior temporal lobe. There was also significant atrophy of the inferior frontal lobes, greater on the left, as well as in deep structures including the basal ganglia (figure 13.14). The right infero-lateral temporal gyrus ($z=6.42$) survived the correction for multiple comparisons ($p<0.05$). The fluid expansion analysis revealed significant expansion of the lateral and third ventricles, the parahippocampal spaces and the perisylvian fissures (figure 13.14).

The voxel-compression maps in figure 13.15 show the patterns of expansion and contraction in two subjects with SD. Both cases show atrophy of frontal and temporal lobes, although it appears to be more severe in the temporal lobes, especially on the right. CSF expansion is present in the ventricles and in the CSF spaces around the brain.

Figure 13.11: Statistical parametric maps showing regions of grey matter atrophy in SD compared to controls at baseline (C-B) and repeat (C-R) assessments, and regions of grey matter atrophy at repeat assessment compared to baseline (B-R) (uncorrected, p<0.001).

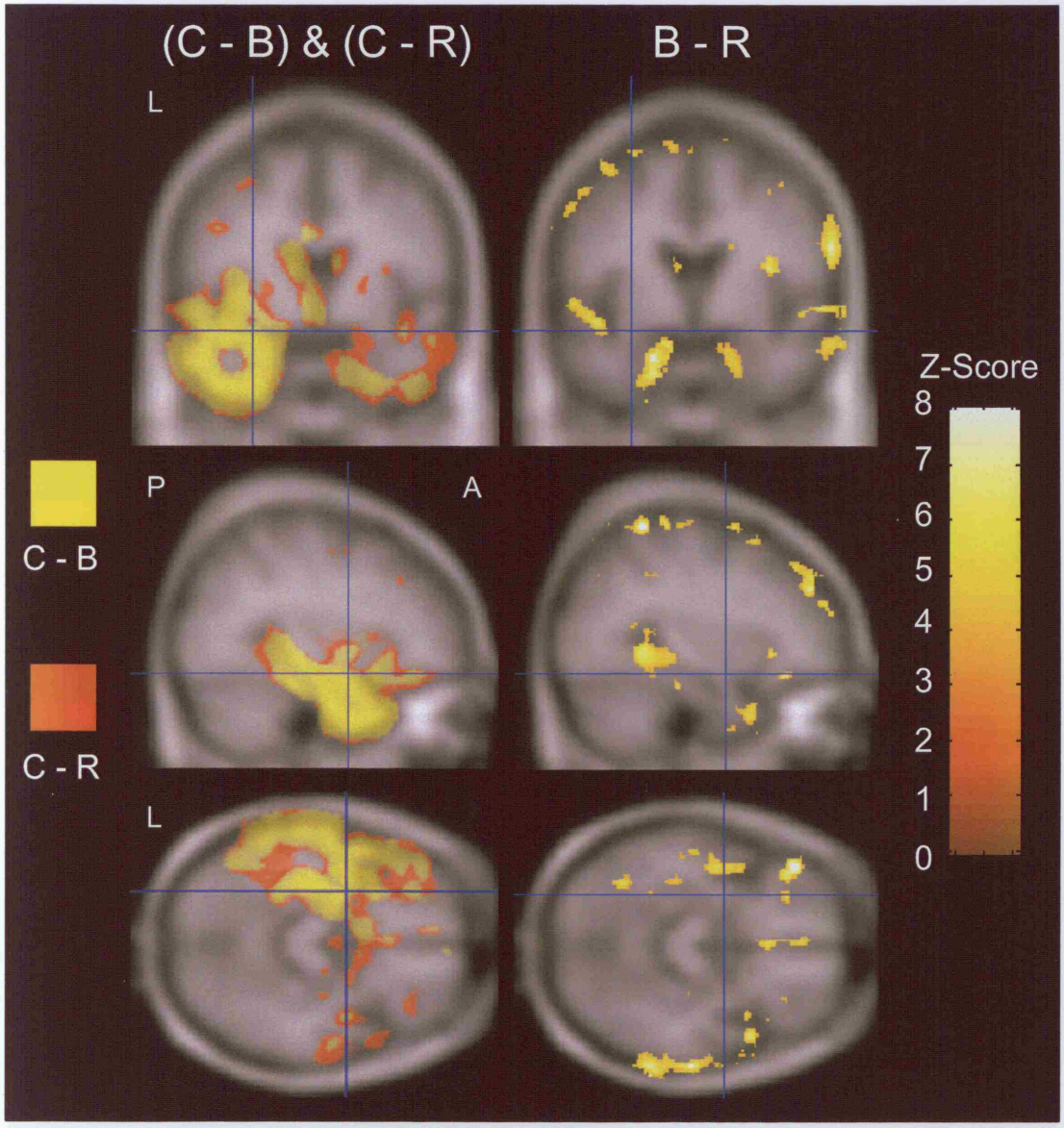

Figure 13.13: Statistical parametric maps showing regions of CSF increase in SD compared to controls at baseline (C-B) and repeat (C-R) assessments, and regions of CSF increase at repeat assessment compared to baseline (B-R) (uncorrected, $p<0.001$).

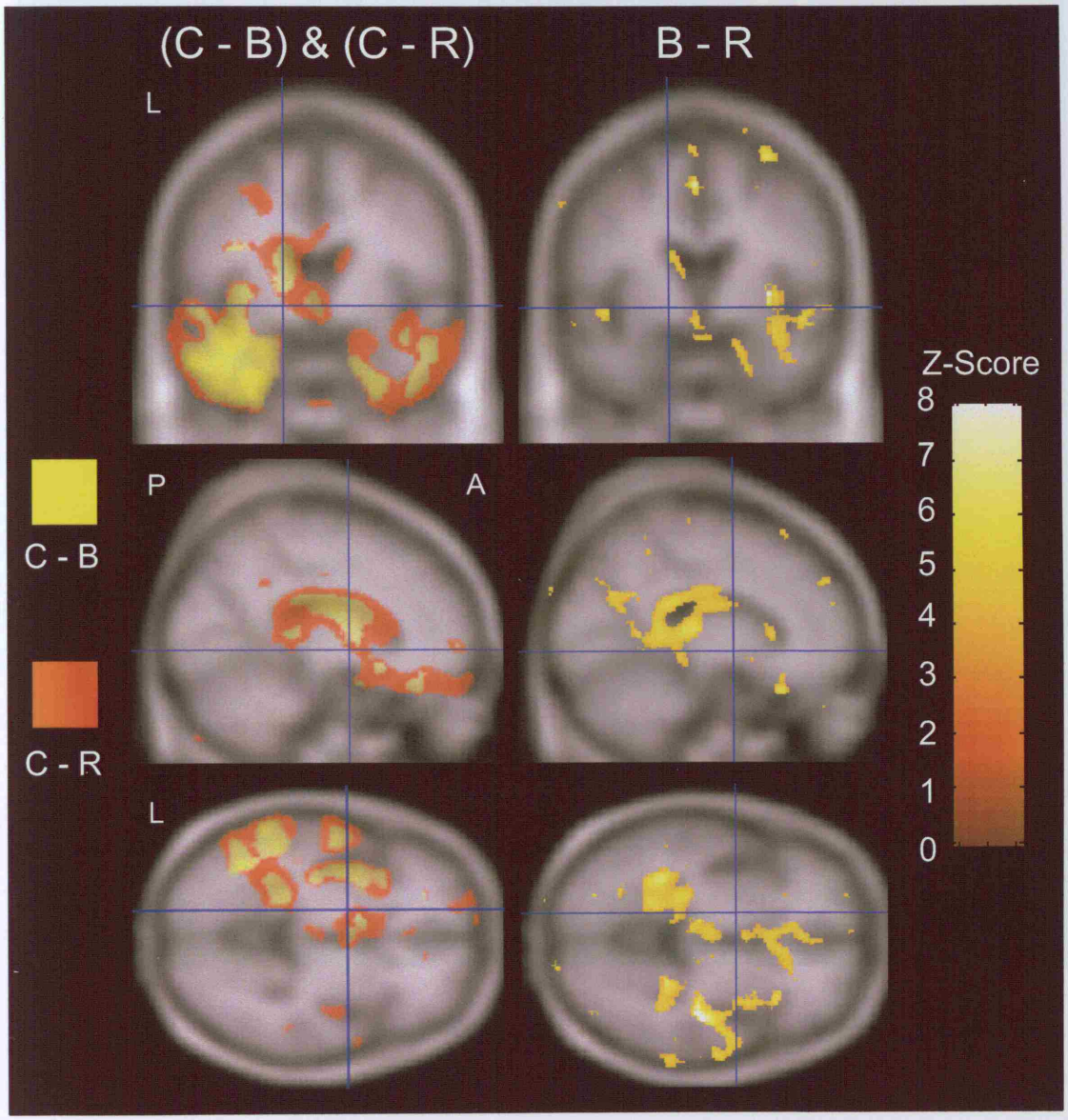

Figure 13.14: Statistical parametric maps showing regions of significant fluid contraction and expansion in SD compared to controls (uncorrected, p<0.001).

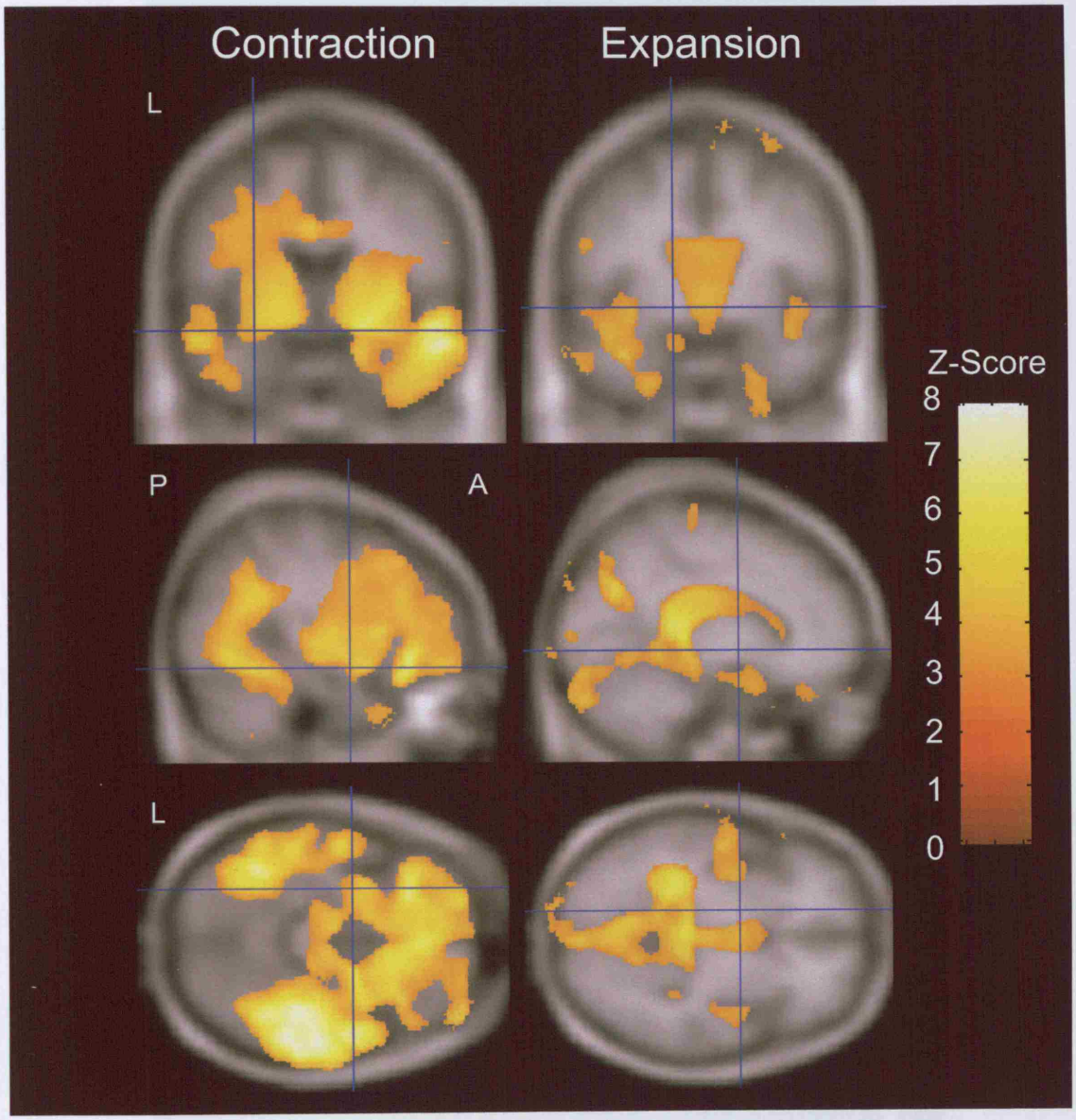

Figure 13.15: Voxel-compression maps showing change over approximately 20 months in two patients with SD.

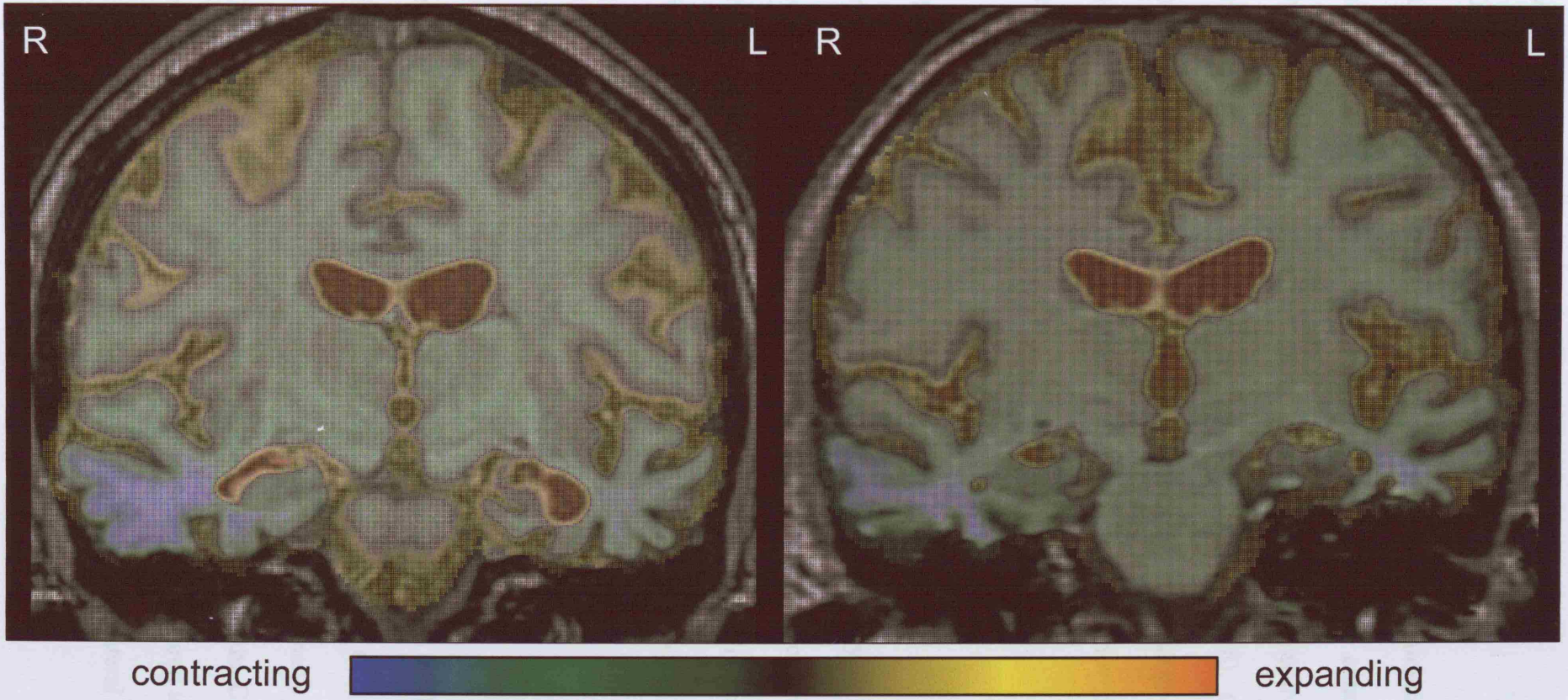

13.3.5. PNFA

13.3.5.1. Grey matter

The PNFA group showed a strikingly asymmetric pattern of left inferior frontal, temporal and insula grey matter atrophy at baseline compared with controls. The repeat analysis showed more extensive atrophy in the left hemisphere, with very little progression in the right hemisphere, compared to controls (figure 13.16). Comparing the grey matter at baseline and repeat assessment showed very little change over time, with just a few regions of atrophy scattered around the left inferior frontal and temporal regions (figure 13.16).

13.3.5.2. White matter

The baseline analysis showed small amounts of white matter atrophy in the frontal midline and the lateral ventricles in the PNFA group compared to controls (figure 13.17). The repeat analysis showed a very similar pattern of atrophy compared to controls (figure 13.17). Almost no regions reached significance when the repeat assessment was compared directly to baseline (figure 13.17).

13.3.5.3. CSF

The baseline CSF analysis showed increased CSF predominantly in the lateral and third ventricles, and in the left inferior, middle and superior temporal sulci compared to controls (figure 13.18). The repeat analysis showed a more extensive pattern of increased CSF in the same regions as at baseline, but also involving the CSF around the anterior frontal lobes, compared to controls (figure 13.18). Compared to baseline, the repeat analysis showed increased CSF predominantly in the lateral ventricles

bilaterally, the left perisylvian region, and the left temporal horn over time (figure 13.18).

13.3.5.4. Fluid analysis

The fluid contraction analysis showed predominantly left-sided regions of increased volume loss, including the middle and superior frontal gyri, the parahippocampal gyrus, and a region adjacent to the most medial extent of the left sylvian fissure. Increased rates of atrophy were also observed in the right posterior temporal lobe (figure 13.19). A region of apparent increased rates of atrophy was also found in the cerebellum. The fluid expansion analysis revealed significant expansion of the lateral ventricles (figure 13.19).

The voxel-compression maps in figure 13.20 show the patterns of expansion and contraction in two subjects with PNFA. Both cases show left-sided atrophy of the frontal and temporal lobes, with CSF expansion in the ventricles.

Figure 13.16: Statistical parametric maps showing regions of grey matter atrophy in PNFA compared to controls at baseline (C-B) and repeat (C-R) assessments, and regions of grey matter atrophy at repeat assessment compared to baseline (B-R) (uncorrected, p<0.001).

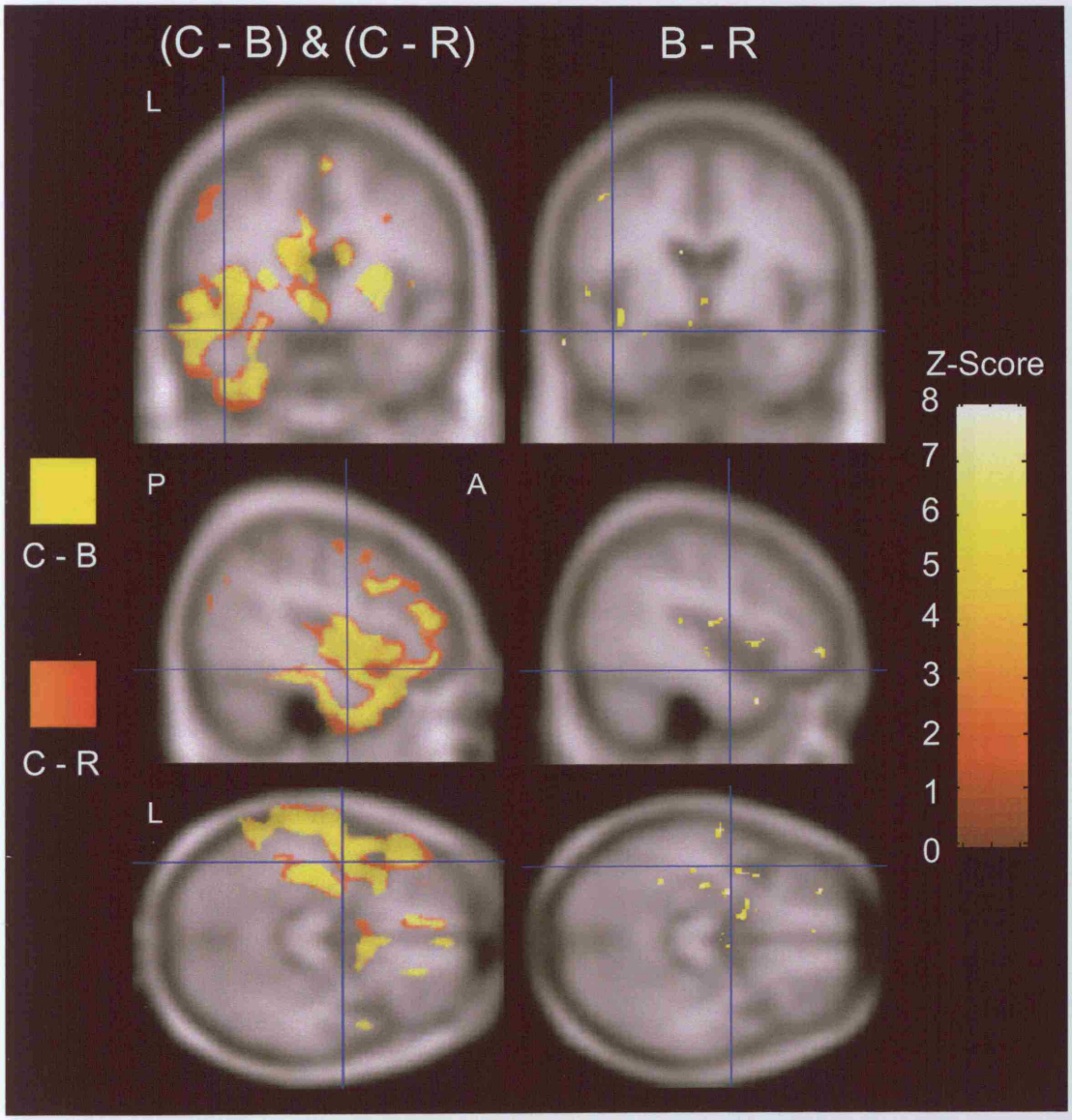

Figure 13.17: Statistical parametric maps showing regions of white matter loss in PNFA compared to controls at baseline (C-B) and repeat (C-R) assessments, and regions of white matter atrophy at repeat assessment compared to baseline (B-R) (uncorrected, p<0.001).

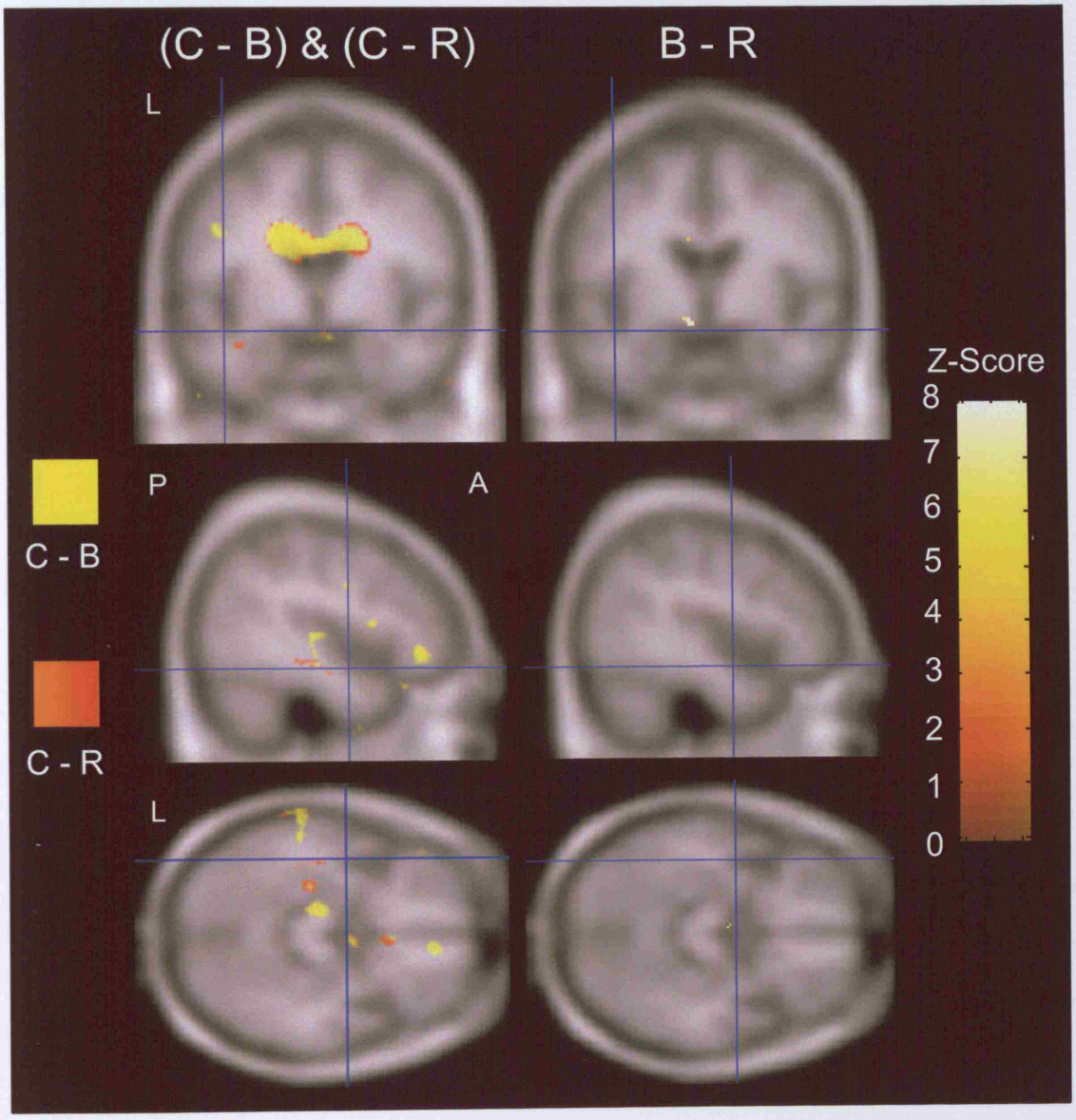

Figure 13.18: Statistical parametric maps showing regions of CSF increase in PNFA compared to controls at baseline (C-B) and repeat (C-R) assessments, and regions of CSF increase at repeat assessment compared to baseline (B-R) (uncorrected, $p<0.001$).

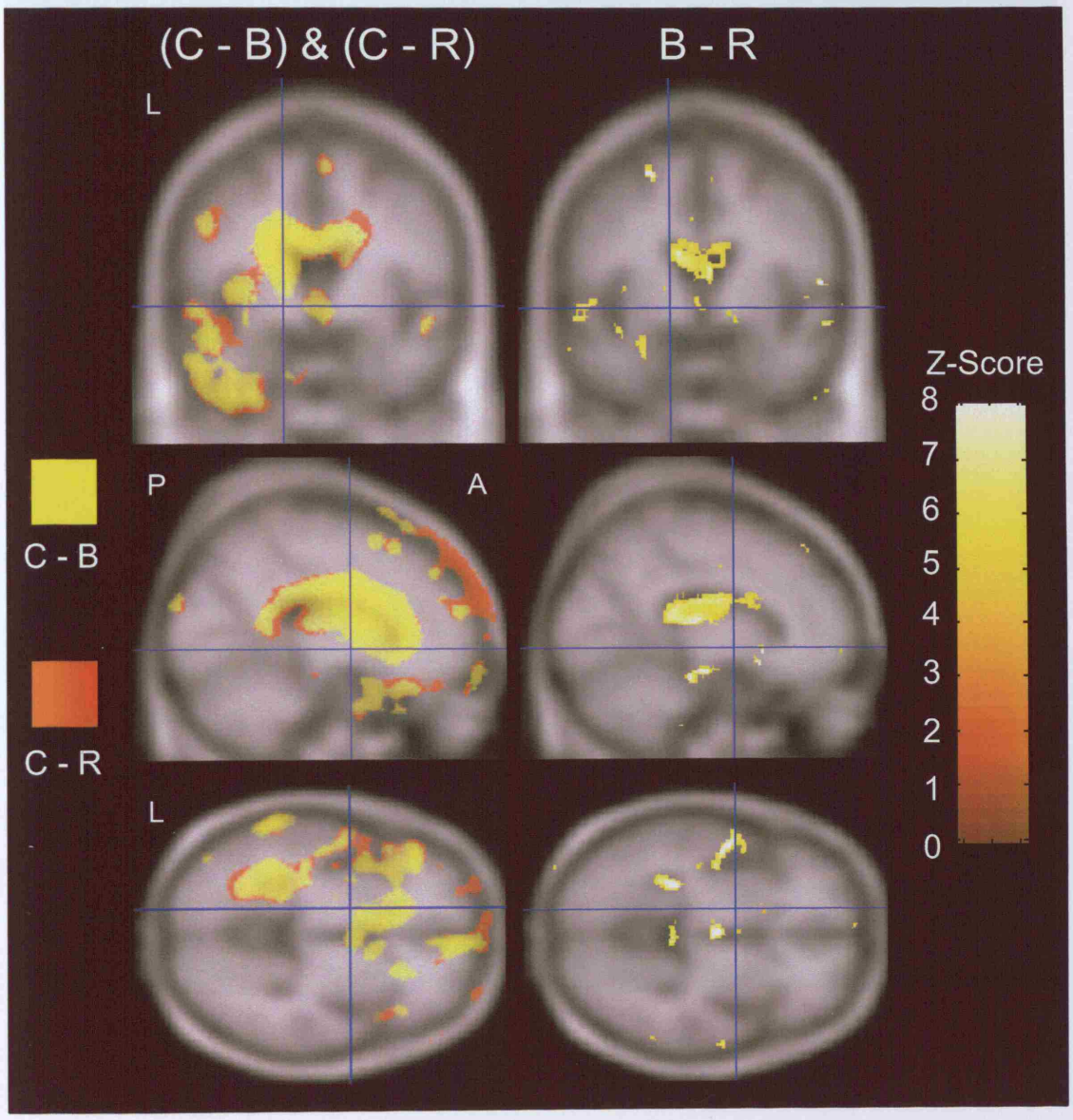

Figure 13.19: Statistical parametric maps showing regions of significant fluid contraction and expansion in PNFA compared to controls (uncorrected, p<0.001).

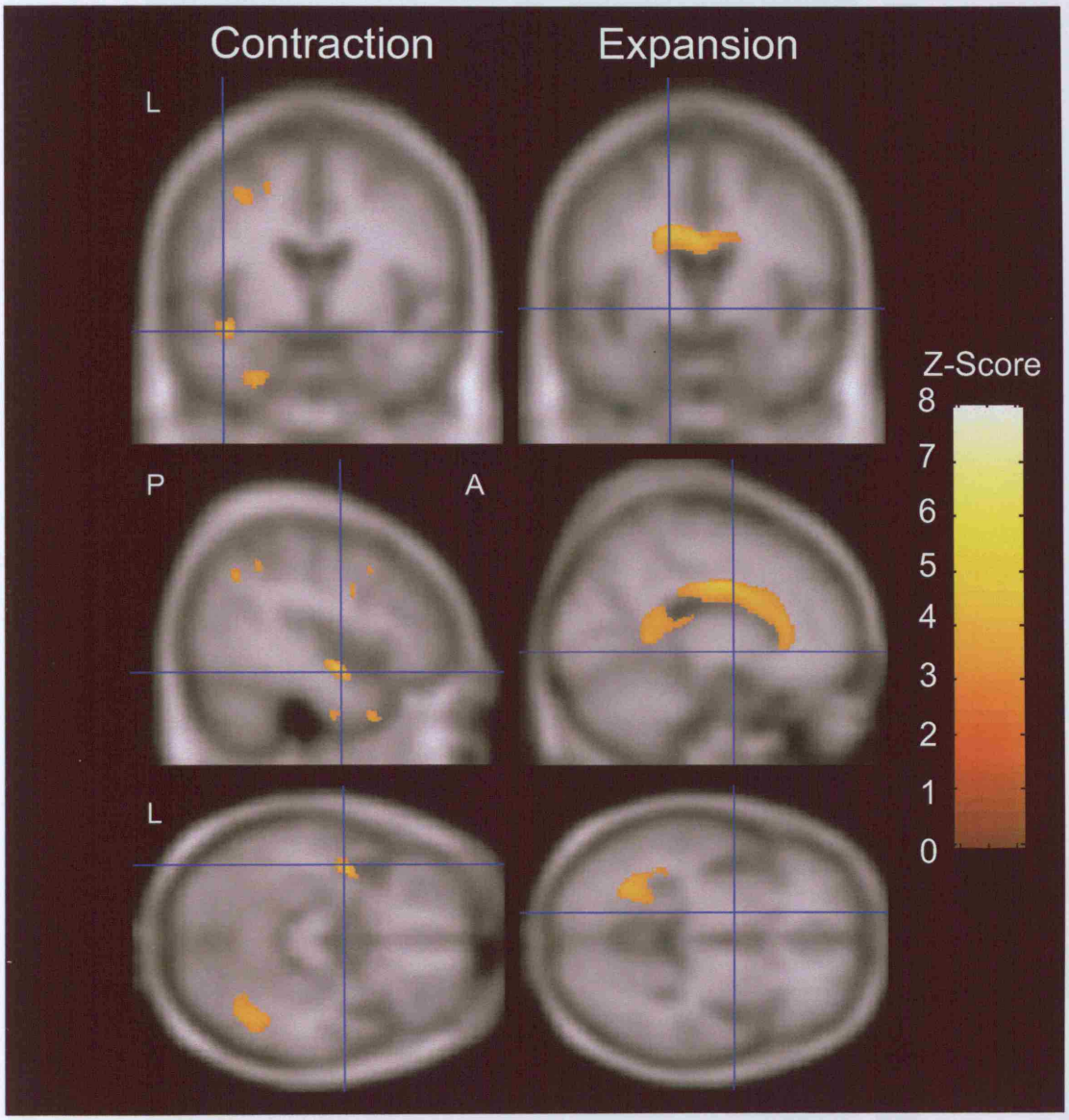

Figure 13.20: Voxel-compression maps showing change over approximately 15 months in two patients with PNFA

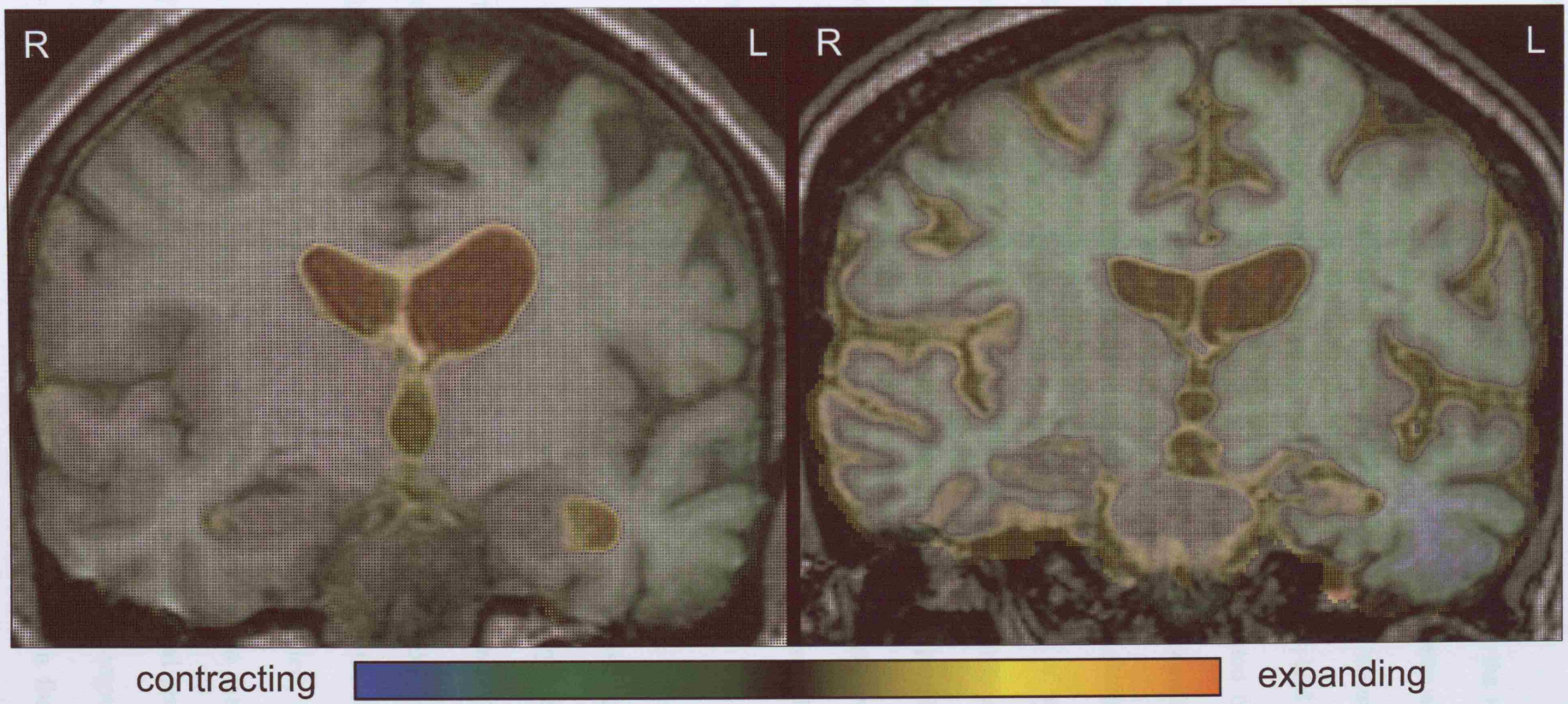

13.4. Discussion

This study has used three automated unbiased techniques to examine the longitudinal patterns of regional change in FTLD. Firstly, the cross-sectional patterns of atrophy at baseline and repeat assessments were analyzed and compared, second a direct VBM analysis was performed between the baseline and repeat scans, and third, SPM was used to compare patterns of contraction and expansion generated from a fluid registration. Regional progression was observed in the FTLD group as a whole, and in each syndromic variant, over the course of the study. Grey matter atrophy was not restricted to the frontal and temporal lobes, with increased rates of atrophy also observed even in the right parietal lobe in the FTLD group. Very little white matter progression was observed over the period of study. The CSF expansion analysis demonstrated significant enlargement of the ventricles over the period of study. Expansion of CSF spaces, a concomitant of total brain volume loss, illustrates the increased rates of whole brain atrophy in the FTLD patients.

The three syndromic variants displayed different patterns of regional change over time. The cross-sectional analyses in the fvFTD patients showed grey matter atrophy in frontal, temporal and parietal regions over the study period. This is consistent with previous studies (Rosen et al., 2002c), although showed significantly more temporal lobe atrophy than observed in chapter 5. The differences between the two chapters are likely to be because of the different number of subjects studied; this chapter included a larger patient group and so may have had more power to detect regional patterns of change. The longitudinal VBM analysis showed bilateral progression of atrophy in predominantly temporal regions, especially the hippocampus, however very little change reached statistical significance in the contraction fluid analysis.

This could suggest that the rates of progression were too slow to be detected or perhaps reflect the large amount of variation between subjects that was observed in the fluid registrations (see figure 13.10). Rates of whole brain atrophy have also been shown to be more variable in fvFTD patients than in the other variants of FTLD (chapter 11, (Chan et al., 2001a)). Anatomical variability between individuals may reduce the sensitivity of the statistical technique to detect significant group differences. The posterior cingulate was the only region to reach significance in the fluid contraction analysis. This result is somewhat surprising since the posterior cingulate is generally considered to be more heavily involved in AD than FTLD (Salmon et al., 1997; Boxer et al., 2003; Nestor et al., 2003c; Nestor et al., 2003b; Bonte et al., 2004). It is thought to play a role in memory function perhaps by connecting the prefrontal areas that implement retrieval strategies for episodic memory and the hippocampus (Nestor et al., 2003c; Nestor et al., 2003b). Posterior cingulate atrophy was absent at baseline in the fvFTD subjects, consistent with a lack of early memory impairment in fvFTD, but it is possible that change in the posterior cingulate over time reflects increasing deficits in both memory and spatial navigation that can occur during the disease course of fvFTD patients. Metabolic changes have been observed in this region in fvFTD (Varrone et al., 2002; Kizu et al., 2004). However, it is also possible that the posterior cingulate atrophy reflects the fact that some of the fvFTD subjects may have AD on pathology.

The SD patients showed increased rates of atrophy predominantly in the posterior left temporal lobe and inferior left frontal regions but also apparent progession of atrophy in the right temporal lobe. At baseline, the most severe grey and white matter atrophy involved the left temporal lobe, consistent with previous chapters. Our results

therefore suggest that the disease spreads from a focus in the anterior left temporal lobe both anteriorly and posteriorly in the left hemisphere and progressively involves the right temporal lobe. These results concur with the findings of chapter 5 where right temporal lobe involvement was shown to be greater in subjects that were more clinically severe (based on the Oldfield). In addition, post-mortem studies have found that at death cases often have symmetrical temporal lobe atrophy (Harasty et al., 1996) and single case reports have similarly shown progressive involvement of the right temporal lobe (Rosen et al., 2002d). Apparent increased rates of atrophy were also observed in the basal ganglia in the SD patients. This finding is consistent with post-mortem and imaging reports of basal ganglia involvement in fvFTD and PPA (Mann and South, 1993; Fukui and Kertesz, 2000; Broe et al., 2003).

The PNFA patients showed increased rates of atrophy predominantly in the left perisylvian region, similar to regions of atrophy reported in cross-sectional studies (Abe et al., 1997). The relatively focal distribution of atrophy and limited progression could reflect the slow gradual clinical progression characteristic of PNFA, with the relative preservation of cognitive functions other than language until later in the disease course (Mesulam, 1982; Weintraub et al., 1990). Some PNFA cases still show a predominantly left-sided pattern of gross atrophy at post-mortem (Turner et al., 1996). It is likely that the significant regions of contraction observed in the cerebellum of the PNFA group are artefactual; the shape and position of the cerebellum make it particularly vulnerable to differences in intensity inhomogeneity (see chapter 3).

The increased rates of atrophy and ventricular expansion predicted from the three analyses were generally consistent. However, there were discrepancies and differences in the localization of change, which could be due to the differences in the techniques. The cross-sectional VBM analysis does not provide a direct statistical comparison of change over time, but relies on a subjective assessment of statistical maps at each time point. This is limited by inaccuracies in matching between different time-points (Shen and Davatzikos, 2004) and also by inaccuracies in the segmentation step of VBM. As discussed in chapter 5 the misclassification of tissue is especially likely in atrophic brains. Comparing the repeat assessment to baseline using VBM generally showed a pattern of change consistent with that expected from the cross-sectional analysis; however this technique allows a direct longitudinal assessment of change over time. Paired t-tests use serial information from each individual, rather than performing independent group analyses, and so provide more statistical power. However, this technique is subject to the inaccuracies and variability introduced by segmentation and spatial normalisation at both time-points. The baseline and repeat scans are both independently normalized to a customised template generated using the baseline images. Therefore, it is also possible that a systematic bias in normalization accuracy could occur between the baseline and the more severely atrophic repeat images.

In contrast, the fluid analysis performs a direct longitudinal comparison using voxel compression maps generated from an automated fluid registration of each subject. This technique is not subject to segmentation errors, and only requires one spatial normalization procedure, thereby reducing the potential noise. In addition, rates of change are generally associated with lower variability than the assessment of regional

volumes and would therefore provide more power for detecting regional change. Recent work in AD suggests that the combination of fluid registration and group statistics using SPM provides a sensitive tool for detecting longitudinal change in AD (Scahill et al., 2002), and is more powerful than a direct SPM comparison of serial grey matter images (Scahill, 2003). This study demonstrates that this technique may also provide insights into disease progression in FTLD.

13.5. Conclusion

This study used three unbiased techniques to examine the longitudinal patterns of regional change in FTLD. A cross-sectional analysis was performed at both baseline and repeat time-points, and then two longitudinal analyses were performed firstly by comparing the baseline and repeat image using VBM and secondly by using fluid registration to assess the direct patterns of regional change. Progression of atrophy was present in all of the FTLD subgroups over the period of study, although it varied in distribution and severity. The fvFTD group showed a subtle pattern of regional progression, with a lot of variability between individuals. The SD patients showed severe patterns of regional progression spreading from a focus in the anterior left temporal lobe both anteriorly and posteriorly in the left hemisphere and progressively involving the right temporal lobe. In contrast, the PNFA group showed less significant rates of regional atrophy and progression was restricted to the left hemisphere, particularly the left perisylvian region. The three methods of analysis were generally consistent. However, the fluid analysis provides a direct comparison of change over time and is less subject to the segmentation errors that are potentially present in the VBM analyses. This technique provides an insight into disease

evolution in these disorders and may be useful as a method of tracking progression in clinical trials.

Overall Discussion

This thesis has used a number of different MRI techniques to examine the cross-sectional and longitudinal patterns of atrophy in patients with FTLD. A number of chapters confirmed previous reports of focal frontal and temporal lobe atrophy in FTLD patients, but also demonstrated involvement of the parietal lobe. An anterior-posterior gradient of atrophy was a common feature of FTLD; present in approximately 50% of subjects and more common than in other neurodegenerative diseases. In addition, asymmetries in the patterns of atrophy were identified in approximately half of the FTLD subjects.

It was clear throughout the thesis that the different syndromic variants of FTLD showed different, yet overlapping, patterns of atrophy. The most striking patterns were observed in the SD patients where the atrophy was focused on the temporal lobes, particularly on the left. The techniques of visual rating (chapter 4) and VBM (chapter 5) all suggested that the focus of atrophy lies in the anterior temporal lobe (pole), the fusiform gyrus, parahippocampal gyrus and the inferior temporal gyrus. One can speculate therefore that these regions may play a key role in semantic dementia. Severe atrophy was also noted in the amygdala, hippocampus, and entorhinal cortex, with a relative sparing of the superior temporal gyrus.

PNFA is the other language variant of FTLD and whilst it also shows left hemisphere dominance the patterns of atrophy are different from those observed in SD. The focus of the disease appears to be in the perisylvian region, with specific involvement of the inferior frontal lobes, superior temporal gyrus and insula. Widespread left frontal

lobe changes were also quite common. Interestingly a number of features were observed that suggest considerable overlap between PNFA and CBD. Namely, the involvement of the putamen identified by VBM in chapter 5 and also the parietal lobe atrophy observed in chapter 4. Both these regions have been shown to be involved in CBD. Previous studies have shown that PNFA cases often turn out to have CBD on pathology (Kertesz et al., 1999), and in this thesis a number of PNFA subjects showed clinical features of CBD later in the disease course. These results may help support the notion that CBD should be considered part of the FTLD spectrum (or Pick complex).

In contrast to the language variants of FTLD the fvFTD patients showed a much more symmetric pattern of atrophy. Frontal and temporal regions were both involved, although the brunt of the atrophy appeared to be in the frontal lobes, including both orbitofrontal and dorsolateral gyri. Atrophy of these frontal regions may explain the severe behavioural deficits present in these fvFTD subjects (as shown in chapter 5).

A number of regions (the insula, orbitofrontal cortex and anterior cingulate) were also found to be involved across all three syndromic groups. In addition, chapter five demonstrated that behavioural abnormalities were present in all three groups: the most common features included obsessive and ritualistic behaviours which were present in approximately 50% of the SD and PNFA patients and 70% of the fvFTD patients. We can therefore postulate that these common regions may contribute to these shared behavioural features. Chapter 6 looked into this hypothesis in more detail and examined the brain atrophy correlates of one of those features: changes in "eating" behaviour in FTLD subjects. Whilst the number of subjects in this chapter was small

a clear association was demonstrated between a preference for sweet foods and atrophy of the orbitofrontal cortex, amygdala and insula. The patterns of atrophy in FTLD therefore appear to have a strong functional consequence. Studying behavioural dysfunction in patients with FTLD may provide important information concerning the neuroanatomical basis of behavioural changes.

The diagnostic utility of regional temporal lobe volumetric measurements was also examined. Significant differences were found in cross-sectional amygdala volumes between AD subjects and individuals with FTLD. Amygdala atrophy was present in all three syndromic variants of FTLD, although was most severe in the subjects with SD. The diagnostic utility of the amygdala and hippocampus in pathologically confirmed (hence definite) cases of FTLD and AD was then assessed. Both structures were more severely affected in FTLD than AD, which contradicts previous opinion that the hippocampus is an excellent diagnostic marker of AD. Furthermore, the right amygdala could differentiate FTLD and AD with a specificity of 80% and a sensitivity of 88% which suggests that assessments of the amygdala may be useful in the differential diagnosis of FTLD.

The syndromic variants of FTLD therefore seem to have relatively well defined patterns of atrophy, although there is still considerable overlap at the individual level. Pathology provides the only definitive diagnosis of FTLD, but unfortunately the pathological subtypes of FTLD are highly heterogeneous and do not map neatly onto the clinical syndromes. This makes it very difficult to predict pathology in FTLD. This thesis used VBM to evaluate the potential of brain MRI to predict the pathological subtypes of FTLD. Potential signatures of brain pathology were

identified: severe bilateral frontal lobe atrophy suggested PiD, predominant left temporal lobe atrophy suggested FTLD-U, and medial temporal atrophy was observed in tau exon 10^{+16}. This suggests that the pathological process may be directly influencing the patterns of regional degeneration, and that MRI may be useful in the prediction of the underlying pathology. This may be especially important in the diagnosis of fvFTD patients in which the pathology and the patterns of atrophy are typically heterogeneous. However, it is less likely to be useful in predicting the biochemical basis of the disease since no differences were observed at least between tau positive and tau negative cases. The fact that MRI may help predict pathology is a controversial and important concept that should be validated in larger subject groups.

Change in the brain over time was also assessed in the FTLD patients. Rates of whole brain atrophy were calculated using the BBSI and found to be approximately 2% per year, which is very similar to the rates commonly found in AD patients (Fox and Freeborough, 1997). Patients were tracked over time (for up to 5 years in some cases) and the rates of atrophy were shown to be approximately constant from the time of diagnosis. In addition, there was no significant difference in the rate of atrophy between the clinical syndromes of FTLD, although greater variability in rates was observed in the fvFTD group. In fact some of the fvFTD patients showed almost no global atrophy over time, and also showed very little clinical progression as measured by the MMSE. It will be important to identify whether these patients show future clinical deterioration and also whether they have FTLD at post-mortem. The assessment of fluidly registered serial images provided more useful information concerning differences between the syndromic variants since it looks specifically at patterns of regional change over time. The SD patients showed a very interesting

pattern with progression from the initial focus in the left temporal lobe spreading both anteriorly and posteriorly in the left hemisphere, and also over to the right temporal lobe. In contrast, the PNFA patients showed less significant patterns of change and the increased volume loss was restricted to the left hemisphere for longer; with progression observed in the perisylvian region and the frontal lobes compared to controls. The fvFTD patients showed very little change over time on the fluid analysis but a direct VBM comparison suggested bilateral progression in predominantly temporal lobe regions, especially the hippocampus. The lack of significance on the fluid analysis may well reflect the variability observed in the fvFTD cohort, and could be influenced by the subjects that show very low rates of global atrophy. Therefore, not only do the different syndromic variants have different cross-sectional patterns of atrophy but they also show different patterns of regional change over time. This has important implications for any future clinical trials that aim to slow progression of the disease over time.

Methodological issues

A number of different techniques were applied to the study of FTLD in this thesis. These techniques ranged from simple visual assessments to more detailed volumetric measurements and automated techniques such as VBM. Whilst they provided complementary information about the disease process they each had their own limitations.

Visual ratings of regional atrophy were applied in chapter 4. These ratings were relatively quick to perform and provided a nice overview of the patterns of atrophy occurring in FTLD. However, visual assessments are highly subjective and may

therefore have poor inter-observer reliability. The assessments in this thesis were all performed by one experienced rater so we were unable to assess inter-rater reliability. However, the intra-rater reliability was good. There was also evidence from chapter 4 that visual ratings may not be equally reliable across brain regions. Parietal lobe atrophy assessments in particular were not very reproducible. This has potentially important implications for the interpretation of reports of parietal atrophy in routine clinical reporting. This thesis did not attempt to assess the diagnostic utility of visual assessments although recent studies have shown that they can be useful (Likeman et al., 2005). A quick, easy to apply, visual rating scheme can be very useful to the clinician, and the results of chapter 4 would suggest that assessing patterns of atrophy across the whole brain may be diagnostically useful in FTLD. A number of previous studies have concentrated solely on the temporal lobes (Scheltens et al., 1995).

Volumetric measurements allow a more detailed and quantitative assessment of specific structures. The results are closely related to the scan appearance, relatively easy to interpret and can provide valuable information about the disease process. However, volumetric measurements are dependent upon the use of experienced operators and require a priori decisions concerning which structures to assess. While the measurements of the amygdala and hippocampus in chapters 7 and 8 provided useful information about the involvement of these structures in the disease they do not tell us anything about what is happening in the rest of the brain. The measurements are also extremely labour-intensive with amygdala measurements taking approximately 45 minutes per structure. It is therefore not always feasible to perform such measurements in a clinical setting or in large clinical trials. In addition, measurement errors can reduce sensitivity, particularly in small structures such as the

hippocampus. Subjective decisions are also required concerning the placement of boundaries which make it particularly difficult to compare results across different institutions. Despite these limitations the amygdala and hippocampal measurements performed in this thesis provided good sensitivity and specificity for pathologically confirmed FTLD. While it is unlikely that measurements in a single subject could be diagnostic due to the large degree of variability across subjects, considering the size of these structures as part of the radiological and clinical assessment may be diagnosically helpful.

The technique of VBM is automated, unbiased and does not require any a priori hypotheses concerning which structures to assess. It looks at patterns of atrophy across the whole brain. It was applied throughout this thesis in order to examine group differences in patterns of atrophy. It is not as operator intensive as manual measurements, and does not require subjective decisions, although it is highly computer-intensive. However, this technique is greatly affected by variability. Variability among individuals both due to heterogeneity within the sample and errors introduced by the pre-processing steps reduce sensitivity for the detection of group differences. For example, VBM is critically dependent on the accuracy of the normalisation procedure. Mis-registration can result in errors in both segmentation and the final voxel level statistical comparisons (Bookstein, 2001). This is a particular problem in subjects with a large degree of cerebral atrophy since they may not register well to the standard MNI template that consists of young healthy controls. To reduce a systematic bias in registration accuracy between disease and controls subjects customised templates were applied throughout the thesis consisting of both FTLD and controls subjects. The segmentation step provides an additional potential

source of error: the misclassification of tissue is especially likely in atrophic brains, both because there is greater potential for partial volume effects between grey matter and CSF, and because tissue pathology may be associated with reduced grey/white matter contrast (Good et al., 2002). Errors in segmentation can also occur due to displacement of tissues. If the interfaces between compartments move due to mass effect or volume loss, the changes can be reflected in both compartments (Good et al., 2002). This is a particular problem in cases with ventricular enlargement, where VBM often shows changes in the CSF and white matter compartments. This misclassification of the ventricular boundary was observed throughout this thesis. In addition, spatial smoothing reduces anatomical resolution, involving a trade-off between the sensitivity to detect atrophy and the specificity of region localization. The power of VBM to detect group differences is also highly dependent on the sample size. The statistical thresholds applied are relatively arbitrary and may depend on the sample size and the degree of smoothing. It is therefore important to realise that if VBM fails to detect a difference at a given statistical threshold it may be due to the lack of power and not necessarily the lack of any morphological difference. It is therefore important to be cautious in the interpretation of VBM. However, despite these problems chapter 9 compared the results of a VBM analysis to visual ratings of atrophy and found that they were highly concordant.

The patterns of atrophy identified by VBM in FTLD (chapter 5) were also generally concordant with patterns of change reported in functional imaging studies using PET and SPECT, although a comparison of this nature was not the aim of this thesis. These functional techniques measure neural activity using glucose metabolism or cerebral blood flow as surrogate markers. One study did directly compare PET and

VBM in subjects with PNFA and found a considerable difference between the techniques, with the VBM analysis identifying far fewer significant voxels (Nestor et al., 2003a). These results suggest a greater sensitivity of physiological compared to anatomical measures. Studies in AD have suggested that a combination of both VBM and PET will yield a higher diagnostic accuracy (Kawachi et al., 2006). The relationship between structural and metabolic deficits in FTLD should be investigated in more detail in future studies.

All the above techniques are cross-sectional which have the added disadvantage that small brain changes tend to be masked by large variation between individuals. Longitudinal studies use serial scans to measure changes over time in a single individual, and thereby largely avoid the problem of inter-individual variation in brain volume. A number of serial techniques were applied in this thesis. Rates of whole brain atrophy in FTLD were calculated using the BBSI. This is a well-validated, automated and unbiased technique that looks for change across the whole brain boundary. It is relatively robust to operator error and applies three scaling factors which allow the correction of voxel drift over time. This correction was validated against the manual TIV gold standard in chapter 10. The boundary shift technique can also be applied to measures rates of change in regional volumes, such as the ventricles or hippocampus (Barnes et al., 2004; Schott et al., 2005). Semi-automated regional BSI measures reduce operator time and error compared to manual measurements (Barnes et al., 2004), although some studies have suggested that they may not be as sensitive to detect disease progression (Ezekiel et al., 2004).

The disadvantage of the BBSI is that because of structural readjustment, the site of tissue loss cannot accurately be determined. Fluid registration is a non-linear registration technique that can track cerebral losses and deformations. It was used in this thesis to localise regional volume change within FTLD subjects over time. Such localisation is difficult to validate precisely, nevertheless, voxel compression maps (VCM) generated by fluid registration show patterns of regional atrophy that are consistent with previous case studies and post mortem data. However, these provide a qualitative, rather than a quantitative assessment, and consequently interpretation can be subjective. There are also a number of problems that can affect the quality of the fluid results. One such problem concerns when to terminate the registration. One could either set the registration to terminate if the change in the cost function is less than a set value (see chapter three), or it could simply be set to run for a limited number of iterations. The later technique was applied in this thesis but this has the inherent limitation that in some cases, especially in those with severe cerebral atrophy, the registration may not have 'reached' the maximum possible deformation. In an attempt to minimise the effects of this limitation all registrations were visually assessed. However, it is still possible that in some cases further iterations could have improved the deformation. The fluid registration is also relatively sensitive to intensity inhomogeneities and scan artefacts, such as susceptibility artefact or movement artifact. Again, visual assessment of all scan pairs and compression maps were performed to minimise errors. There are many other non-linear registration techniques which have been applied to assess regional volume loss over time. These registrations tend to vary in the type of regularisation, i.e. how the registration is constrained. One example is tensor-based morphometry which uses an elastic constraint (Leow et al., 2006). The advantage of the fluid registration is that the fluid

constraint favours smooth deformations, however to my knowledge no studies have directly compared these techniques. It is however likely that all non-linear techniques will be sensitive to the limitations of scan quality and stability over time.

In this thesis in order to generate quantitative group results from the fluid registrations robust group statistics were performed on these fluid generated VCMs using SPM. This technique was then compared to the direct assessment of grey matter changes over time using VBM. Results from the two techniques were comparable; however the direct technique is subject to the inaccuracies and variability introduced by the segmentation and normalisation at both time-points. SPM analysis of contraction and expansion measures generated by fluid registration does not rely on segmentation. However, the fluid registration is driven by tissue contrast and intensity, so changes in signal characteristics due to disease progression may affect the Jacobian values. Fluid registration is also a relatively recent technique which will most certainly undergo further refinement in the future. Nevertheless, this technique was previously applied to subjects with AD (Scahill et al., 2002), and this thesis has shown that it has potential to provide insights into the disease progression in FTLD and may prove useful for tracking disease progression in future clinical trials.

Limitations

This thesis has highlighted two major difficulties in the study of patients with FTLD. First, it was very difficult to obtain good serial MRI data. Chapter 11 showed that 20% of subjects that had had serial MRI had to be rejected due to poor quality scans. The most common problem was subjects moving in the scanner. This is most likely

to be a problem in the more clinically severe subjects. In addition, those cases with the most severe patterns of atrophy often have conformational changes in the brain that can not be well matched by a rigid body registration and may not, for example, register well to a common VBM template. This thesis may therefore be biased towards the less severe cases of FTLD that can still provide adequate imaging.

Second, it was very difficult to adequately match patients with FTLD and AD for clinical severity. The MMSE is typically used to assess disease severity in AD, but is particularly sensitive to language deficits, and therefore will be disproportionately low in the language variants of FTLD. The CDR provides a more functional scale but is particularly sensitive to memory impairment and so still may not provide a reliable assessment of impairment across diseases such as AD and FTLD. In addition, neither the MMSE nor the CDR account for the behavioural dysfunction that is an early feature of FTLD. Owing to this problem disease duration was recorded throughout this thesis. However, this is also an unreliable measure given the reliance on accurate patient/carer accounts. This problem not only means that it is difficult to match specific patient groups, but also that it is difficult to compare results across studies. The field of FTLD research is in need of a well validated and specifically designed severity scale(s).

Summary

This thesis has demonstrated the importance of volumetric MRI in the study of FTLD. It has provided information that complements the existing literature concerning patterns of regional atrophy in the different syndromic variants of FTLD and showed

that the patterns of atrophy on MRI can be useful in the differential diagnosis of FTLD. It has demonstrated that the behavioural dysfunction in FTLD patients has a strong structural basis which has important implications in the study of human behaviour. Serial data has also been analysed and has provided novel information concerning the patterns of regional progression in FTLD. Each of the syndromic variants has characteristic patterns of both cross-sectional and longitudinal atrophy. In addition, this thesis has suggested for the first time that MRI may be useful in the prediction of the pathological subtypes of FTLD. This is an important finding that has major consequences for the design of future disease modifying treatment trials in FTLD.

A number of different techniques were applied and assessed in this thesis. Visual assessments, volumetric measurements and the automated technique of VBM all provided complementary information in the cross-sectional studies. The choice of technique will depend upon the question being asked and the trade-off between accuracy, subjectivity and processing time. In addition, this thesis assessed various techniques for the analysis of longitudinal patterns of atrophy in FTLD. It highlighted the importance of correcting for drift in voxel dimension over time in longitudinal studies and showed that the combination of fluid registration and SPM may be useful in the study of regional patterns of change in FTLD. Automated techniques are likely to play an important role in the future of FTLD research, although it is important to be cautious in the interpretation of such automated techniques. This thesis also highlighted some of the difficulties in the study of FTLD and emphasized the need for more well controlled prospective serial MRI studies in FTLD.

Acknowledgements

I would firstly like to thank all the patients and their families for agreeing to take part in these studies, without them none of this work would have been possible. In addition I would like to give special thanks to my supervisors, Professor Nick Fox and Professor Martin Rossor, for their help, support and guidance throughout my PhD.

A number of other people have contributed to this thesis that I would like to thank: Dr Liz Sampson, Dr John Schott, Dr Alison Godbolt, Dr Nick fox and Professor Martin Rossor for recruiting and assessing the patients studied in this thesis; Dr John Stevens for performing the visual assessments of atrophy and for his guidance; Professor Elizabeth Warrington and Susie Henley for performing and assessing the neuropsychological data; Dr Jason Warren for his supervision and VBM advice; Dr Chris Frost and Hilary Watt for their statistical expertise; and Dr Keith Josephs, Dr Tamas Revesz, Dr Janice Holton and Professor Safa Al-Sarraj for pathological analyses.

In addition I would like to thank everyone at the Dementia Research Centre for their support. I would especially like to thank Keith Josephs, Valerie Anderson, Emma Lewis, Shona Price, Jo Barnes, Susie Henley and Rachael Scahill for their never-ending help, support and friendship.

This thesis was supported by a project grant awarded by the Clinical Research and Development Committee from the Special trustees of UCLH and NHNN. Ethics

committee approval was granted by the National hospital for Neurology and Neurosurgery and Institute of Neurology joint research ethics committee.

Publications

Published peer-reviewed papers based on results described in this thesis are detailed below. Publications have been ordered according to chapter, and specific contributions have been discussed.

Chapter 7

A volumetric Magnetic Resonance Imaging Study of the Amygdala in Frontotemporal Lobar Degeneration and Alzheimer's disease.

Jennifer L Whitwell, Elizabeth L Sampson, Hilary C Watt, Richard J Harvey, Martin N Rossor, Nick C Fox

Dementia Geriatric Cognitive Disorders 2005; 20(4): 238-44 (Whitwell et al., 2005b)

Patients were recruited and assessed by Elizabeth Sampson, Richard Harvey, Nick Fox and Martin Rossor. All volumetric measurements were performed by myself. Statistical analysis was performed by Hilary Watt. The paper was drafted by myself, and revised by Elizabeth Sampson, Richard Harvey, Nick Fox and Martin Rossor.

Chapter 8

Measurements of the amygdala and hippocampus in pathologically confirmed Alzheimer's disease and frontotemporal lobar degeneration.

Josephine Barnes, **Jennifer L Whitwell**, Chris Frost, Keith Josephs, Martin Rossor, Nick C Fox

Archives of Neurology In Press

Patients were recruited and assessed by Nick Fox and Martin Rossor. Original post-mortems were performed by Tamas Revesz. All pathological diagnoses were reanalysed by Keith Josephs. Hippocampal measurements were performed by Josephine Barnes and amygdala measurements were performed by myself. Statistical analysis was performed by Chris Frost. The paper was drafted by myself, Josephine Barnes, and Keith Josephs, and revised by Nick Fox and Martin Rossor.

Chapter 9

Voxel-based Morphometry in Tau-positive and Tau-negative Frontotemporal lobar degenerations

Jennifer L. Whitwell, Jason D. Warren, Keith A. Josephs, Alison K. Godbolt, Tamas Revesz, Nick C. Fox, Martin N. Rossor

Neurodegenerative Diseases 2004;1:225–230. (Whitwell et al., 2004c)

Patients were recruited and assessed by Nick Fox and Martin Rossor. Original post-mortems were performed by Tamas Revesz. All pathological diagnoses were reanalysed by Keith Josephs. All VBM analysis was performed by myself. The paper was drafted by myself and Jason Warren, and revised by Keith Josephs, Nick Fox and Martin Rossor.

Magnetic Resonance Imaging Signatures of Tissue Pathology in Frontotemporal Dementia

Jennifer L Whitwell, Keith A Josephs, Martin N Rossor, John M Stevens, Tamas Revesz, Janice L Holton, Safa Al-Sarraj, Alison K Godbolt, Nick C Fox, Jason D Warren

Archives of Neurology 2005; 62: 1402-1408 (Whitwell et al., 2005a)

Patients were recruited and assessed by Alison Godbolt, Nick Fox and Martin Rossor. Original post-mortems were performed by Tamas Revesz, Janice Holton and Safa Al-Sarraj. All pathological diagnoses were reanalysed by Keith Josephs. All VBM analysis was performed by myself. All visual assessments of atrophy were performed by John Stevens. The paper was drafted by myself and Jason Warren, and revised by Keith Josephs, Nick Fox and Martin Rossor.

Chapter 10

Normalization of Cerebral Volumes using Intracranial Volume: Implications for Longitudinal Quantitative MR Imaging

Jennifer L. Whitwell, William R. Crum, Hilary C. Watt, Nick C. Fox

Am J Neuroradiol 2001 22: 1483-1489 (Whitwell et al., 2001)

Patients were recruited and assessed by Nick Fox. All volumetric measurements were performed by myself. Statistical analysis was performed by Hilary Watt. The paper was drafted by myself and William Crum, and revised by Nick Fox.

Using nine degrees-of-freedom registration to correct for changes in voxel size in serial MRI studies

Jennifer L. Whitwell BA, Jonathan M. Schott MRCP, Emma Lewis PhD,David G. MacManus MSc, Nick C. Fox MD

Magnetic Resonance Imaging 2004: 22: 993-999. (Whitwell et al., 2004b)

Patients were recruited and assessed by Jonathan Schott and Nick Fox. All volumetric measurements were performed by myself. Artificial scalings were performed by Emma Lewis. Phantom QC data was performed by Dave MacManus. The paper was drafted by myself and Jonathan Schott, and revised by Emma Lewis and Nick Fox.

Chapter 13

Longitudinal patterns of regional change on volumetric MRI in frontotemporal lobar degeneration.

Jennifer L Whitwell BA, Valerie M Anderson BSc, Rachael I Scahill PhD, Martin N Rossor MD, Nick C Fox MD

Dementia Geriatric Cognitive Disorders 2004;17(4):307-310. (Whitwell et al., 2004a)

Patients were recruited and assessed by Nick Fox and Martin Rossor. All fluid and VBM analyses were performed by myself and Valerie Anderson. The paper was drafted by myself, and revised by Valerie Anderson, Rachael Scahill, Nick Fox and Martin Rossor.

Appendix 7

Patterns of Temporal Lobe atrophy in Semantic Dementia and Alzheimer's disease

Chan DC, Fox NC, Scahill RI, Crum WR, **Whitwell JL**, Leschziner G, Rossor A, Stevens J, Cipolotti L, Rossor M.

Ann Neurol 2001;49: 433-442 (Chan et al., 2001b)

Patients were recruited and assessed by Nick Fox and Martin Rossor. Volumetric measurements were performed by Dennis Chan (entorhinal cortex), myself (amygdala), Rachael Scahill (hippocampi), Alex Rossor (temporal lobe regions) and Guy Leschziner (temporal lobe regions). John Stevens was responsible for reviewing the scans, and Lisa Cipolotti for the neuropsychological assessments. Bill Crum provided technical support. The paper was drafted by Dennis Chan, Nick Fox, Lisa Cipolotti and myself, and revised by Martin Rossor.

Appendix 1: Diagnostic criteria for FTLD

This appendix details diagnostic criteria for FTLD as defined both by Neary et al (1998) and the Lund-Manchester group in 1994. The criteria by Neary et al (1998) were applied throughout this thesis.

Frontotemporal lobar degeneration

Criteria given by Neary *et al (Neary et al., 1998)*

Clinical diagnostic features of **FTD**

Core diagnostic features

- Insidious onset and gradual progression
- Early decline in social interpersonal conduct
- Early impairment in regulation of personal conduct
- Early emotional blunting
- Early loss of insight

Supportive diagnostic features

- Behavioural disorder
    - Decline in personal hygiene and grooming
    - Mental rigidity and inflexibility
    - Distractibility and impersistence
    - Hyperorality and dietary changes
    - Perseverative and stereotyped behaviour
    - Utilization behaviour

- Speech and Language
    - Altered speech output
    - Aspontaneity and economy of speech
    - Press of speech
    - Stereotypy of speech
    - Echolalia
    - Perseveration
    - Mutism
- Physical signs
    - Early primitive reflexes
    - Early incontinence
    - Akinesia, rigidity, and tremor
    - Low and labile blood pressure
- Investigations
    - Neuropsychology: significant impairment on frontal lobe tests in the absence of severe amnesia, aphasia, or perceptuospatial disorder
    - Electroencephalography: normal on conventional EEG despite clinically evident dementia
    - Brain imaging (structural and/or functional): predominant frontal and/or anterior temporal abnormality

Clinical diagnostic features of **PNFA**

Core diagnostic features

- Insidious onset and gradual progression
- Nonfluent spontaneous speech with at least one of the following: agrammatism, phonemic paraphasias, anomia

Supportive diagnostic features

- Speech and language
    - Stuttering or oral apraxia
    - Impaired repetition
    - Alexia, agraphia
    - Early preservation of word meaning
    - Late mutism
- Behaviour
    - Early preservation of social skills
    - Late behavioural changes similar to FTD
- Physical signs: late contralateral primitive reflexes, akinesia, rigidity, and tremor
- Investigations
    - Neuropsychology: nonfluent aphasia in the absence of severe amnesia or perceptuospatial disorder
    - Electroencephalography: normal or minor asymmetric slowing
    - Brain imaging (structural and/or functional): asymmetric abnormality predominantly affecting dominant (usually left) hemisphere

Clinical diagnostic features of **SD**

Core diagnostic features

- Insidious onset and gradual progression
- Language disorder characterised by
    - Progressive, fluent, empty spontaneous speech
    - Loss of word meaning, manifest by impaired naming and comprehension
    - Semantic paraphasias and/or
- Perceptual disorder characterised by
    - Prosopagnosia: impaired recognition of identity of familiar faces and/or
    - Associative agnosia: impaired recognition of object identity
- Preserved perceptual matching and drawing reproduction
- Preserved single-word repetition
- Preserved ability to read aloud and write to dictation orthographically regular words

Supportive features

- Speech and language
    - Press of speech
    - Idiosyncratic word usage
    - Absence of phonemic paraphasias
    - Surface dyslexia and dysgraphia
    - Preserved calculation
- Behaviour

    - Loss of sympathy and empathy
    - Narrowed preoccupations
    - Parsimony
- Physical signs
    - Absent or late primitive reflexes
    - Akinesia, rigidity, and tremor
- Neuropsychology
    - Profound semantic loss, manifest in failure of word comprehension and naming and/or face and object recognition
    - Preserved phonology and syntax, and elementary perceptual processing, spatial skills, and day-to-day memorising
- Electroencephalography: normal
- Brain imaging (structural and/or functional): predominant anterior temporal abnormality (symmetric or asymmetric)

Features common to clinical syndromes of **FTLD**

Supportive features

- Onset before age 65 years: positive family history of similar disorder in first degree relative
- Bulbar palsy, muscular weakness and wasting, fasiculations

Diagnostic exclusion criteria

- Historical and clinical
    - Abrupt onset with ictal events

  - Head trauma related to onset
  - Early, severe amnesia
  - Spatial disorientation
  - Logoclonic, festinant speech with loss of train of thought
  - Myoclonus
  - Corticospinal weakness
  - Cerebellar ataxia
  - Choreoathetosis
- Investigations
  - Brain imaging: predominant postcentral structural or functional deficit; multifocal lesions on CT or MRI
  - Laboratory tests indicating brain involvement of metabolic or inflammatory disorder

Relative diagnostic exclusion features

- Typical history of chronic alcoholism
- Sustained hypertension
- History of vascular disease

Frontotemporal dementia

Criteria given by Lund and Manchester Criteria (Brun, 1994)

Core diagnostic features

- Behavioural disorder
  - Insidious onset and slow progression

- Early loss of personal awareness
- Early loss of social awareness
- Early signs of disinhibition
- Mental rigidity and inflexibility
- Hyperorality
- Stereotyped and preservative behaviour
- Utilisation behaviour
- Distractibility. Impulsivity, and impersistence
- Early loss of insight into the fact that the altered condition is due to a pathological change of own mental state

- Affective symptoms
  - Depression, anxiety, excessive sentimentality, suicidal, delusion
  - Hypochondriasis, bizarre somatic preoccupation
  - Emotional unconcern
  - Amimia
- Speech disorder
  - Progressive reduction of speech
  - Stereotypy of speech
  - Echolalia and perseveration
  - Late mutism
  - Spatial orientation and praxis preserved
- Physical signs
  - Early primitive reflexes
  - Early incontinence
  - Late akinesia, rigidity, tremor

  - Low and labile blood pressure
- Investigations
  - Normal EEG despite clinically evident dementia
  - Brain Imaging: predominant frontal anterior temporal abnormality, or both
  - Neuropsychology (profound failure on frontal lobe tests in the absence of severe amnesia, or perceptual spatial disorder)

Supportive diagnostic features

- Onset before 65
- Positive family history of similar disorder in a first degree relative
- Bulbar palsy, muscular weakness and wasting, fasiculations

Diagnostic Exclusion Features

- Abrupt onset with ictal events
- Head trauma related to onset
- Early severe amnesia
- Early spatial disorientation
- Early severe apraxia
- Logoclonic speech with rapid loss of train of thought
- Myoclonus
- Cortical bulbar and spinal deficits
- Cerebellar ataxia
- Choreo-athetosis
- Early, severe, pathological EEG

- Brain imaging (predominantly post-central structural or functional deficit, Multifocal cerebral lesions on CT or MRI)
- Labortatory tests indicating brain involvement or inflammatory disorder

Relative diagnostic exclusion features

- Typical history of chronic alcoholism
- Sustained hypertension
- History of vascular dementia

Appendix 2: Diagnostic criteria for AD

Criteria given by the National Institute of Neurological and Communicative Disorders and the Alzheimer's Disease and Related Disorders Association (NINCDS-ADRDA) (McKhann et al., 1984):

Probable Alzheimer's disease

The diagnosis of PROBABLE Alzheimer's disease is supported by:

- Dementia established by clinical examination and documented by the Mini-Mental Test; Blessed Dementia Scale, or some similar examination, and confirmed by neuropsychological tests
- Deficits in two or more areas of cognition
- Progressive worsening of memory and other cognitive functions
- No disturbance of consciousness
- Onset between ages 40 and 90, most often after age 65
- Absence of systemic disorders or other brain diseases that in and of themselves could account for the progressive deficits in memory and cognition

The diagnosis of PROBABLE Alzheimer's disease is supported by:

- Progressive deterioration of specific cognitive functions such as language (aphasia), motor skills (apraxia), and perceptions (agnosia)
- Impaired activities of daily living and altered patterns of behaviour

- Family history of similar disorders, particularly if confirmed neuropathologically
- Normal lumbar puncture as evaluated by standard techniques
- Normal pattern or non-specific changes in EEG, such as increased slow-wave activity
- Evidence of cerebral atrophy on CT with progression documented by serial observation

Other clinical features consistent with the diagnosis of PROBABLE Alzheimer's disease:

- Plateaus in the course of progression of the illness
- Associated symptoms of depression, insomnia, incontinence, delusions, illusions, hallucinations, catastrophic verbal, emotional, or physical outbursts, sexual disorders, and weight loss
- Other neurologic abnormalities in some patients, especially with more advanced disease and including motor signs such as increased muscle tone, myoclonus, or gait disorder
- Seizures in advanced disease
- CT normal for age

Features that make the diagnosis of PROBABLE Alzheimer's disease uncertain or unlikely:

- Sudden, apoplectic onset

- Focal neurologic findings such as hemiparesis, sensory loss, visual field deficits, and incoordination early in the course of the illness
- Seizures or gait disturbances at the onset or very early in the course of the illness

Probable Alzheimer's disease if:

- all criteria I are answered with "yes"

Possible Alzheimer's disease

- may be made on the basis of the dementia syndrome, in the absence of other neurologic, psychiatric, or systemic disorders sufficient to cause dementia, in the presence of variations in the onset, in the presentation, or in the clinical course
- may be made in the presence of a second systemic or brain disorder sufficient to produce dementia, which is not considered to be the cause of the dementia
- should be used in research studies when a single, gradually progressive severe cognitive deficit is identified in the absence of other identifiable cause

Possible Alzheimer's disease if:

- criteria above are appropriate

Definite Alzheimer's disease

Definite AD refers to histopathologically confirmed disease. The methods by which pathologists should make this diagnosis are described in Mirra *et al* (Mirra *et al*, 1991; Mirra *et al*, 1993). Histopathological methods (and AD criteria) are imperfect

and continue to be refined but in essence depend on demonstrating sufficient age-related densities of neurofibrillary tangles and amyloid plaques.

Appendix 3: Clinical assessment scales

The following pages show the mini-mental status examination (MMSE) (Folstein et al., 1975), clinical dementia rating (CDR) (Hughes et al., 1982), and the Manchester and Oxford Univerisities scale for the psychopathological assessment of dementia (MOUSEPAD) (Allen et al., 1996). All three of these clinical assessments were used in this thesis.

CDR

Clinical Dementia Rating Scale

CDR

Category	Healthy CDR 0	Questionable dementia CDR 0.5	Mild dementia CDR 1	Moderate dementia CDR 2	Severe dementia CDR 3
Memory	No memory loss or slight inconstant forgetfulness	Mild consistent forgetfulness; partial recollection of events; 'benign' forgetfulness	Moderate memory loss, more marked for recent events; defect interferes with everyday activities	Severe memory loss; only highly learned material retained; new material rapidly lost	Severe memory loss; only fragments remain
Orientation	Fully oriented		Some difficulty with time relationships; oriented for place and person at examination but may have geographic disorientation	Usually disoriented in time, often to place	Orientation to person only
Judgment + problem solving	Solves every day problems well; judgment good in relation to past performance	Only doubtful impairment in solving problems, similarities, differences	Moderate difficulty in handling complex problems; social judgment usually maintained	Severely impaired in handling problems, similarities, differences; social judgment usually impaired	Unable to make judgments or solve problems
Community affairs	Independent function at usual level in job, shopping, business and financial affairs, volunteer and social groups	Only doubtful or mild impairment, if any, in these activities	Unable to function independently at these activities though may still be engaged in some; may still appear normal to casual inspection	No pretence of independent function outside home	
Home + hobbies	Life at home, hobbies, intellectual interests well maintained	Life at home, hobbies, intellectual interests well maintained or only slightly impaired	Mild but definite impairment of function at home; more difficult chores abandoned; more complicated hobbies and interests abandoned	Only simple chores preserved; very restricted interests, poorly sustained	No significant function in home outside of own room
Personal care	Fully capable of self care		Needs occasional prompting	Requires assistance in dressing, hygiene, keeping of personal effects	Requires much help with personal care; often incontinent
Score using box overleaf. Score as 0, 0.5, 1, 2, 3 only if impairement is due to cognitive loss.					

Hughes CP *et al*, *Br J Psychiatry* 1982; 140: 566-572.
Reprinted by permission.

Clinical Dementia Rating Scale cont'd

CDR

ASSIGNING THE CLINICAL DEMENTIA RATING

There are two methods of combining the domain scores to give the overall CDR. The domain scores can either be summed to give the CDR-SB (Sum of Boxes) score, or an algorithm can be used as follows:

The global CDR score is derived from the scores in each of the six categories. Memory (M) is considered the primary category and all others are secondary. CDR = M if at least three secondary categories are given the same score as memory. Whenever three or more secondary categories are given a score greater or less than the memory score, CDR equals the score of the majority of secondary categories that are on whichever side of M has the greatest number of secondary categories. If there are ties in the secondary categories on one side of M, the CDR score closest to M is chosen.

When M = 0.5, CDR = 1 if at least three of the other categories are scored one or greater. If M = 0.5, CDR cannot be 0; it can only be 0.5 or 1. If M = 0, CDR = 0 unless there is questionable impairment in two or more secondary categories, in which case CDR = 0.5.

Score	0	0.5	1	2	3
M					
O					
JPS					
C					
HH					
PC					

Mark in only one box for each category. To assign the CDR, see grids on the right. Shaded areas indicate defined range within which the scores of individual subjects must fall to be assigned a given CDR.

Clinical Dementia Rating ☐

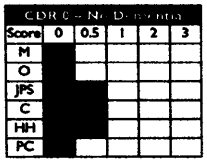

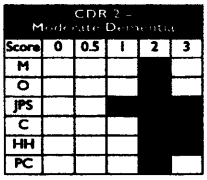

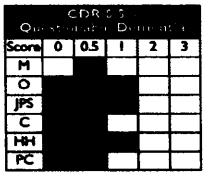

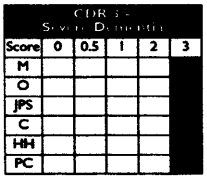

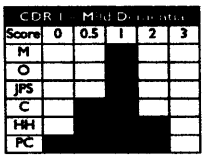

MMSE

Mini Mental State Examination MMSE

Code: 1 = correct
0 = incorrect

1. Orientation

What is the year we are in?	☐
What season is it?	☐
What is today's date?	☐
What day of the week is it today?	☐
What month are we in?	☐
What county are we in?	☐
What country are we in?	☐
What town are we in?	☐
Can you tell me the name of this place?	☐
What floor of the building are we on?	☐

2. Registration

Ask the subject if you may test his memory. Then say the names of 3 unrelated objects, clearly and slowly, about one second for each, "lemon, key, ball". After you have said all 3, ask him to repeat them. This first repetition determines his score (0-3) but keep saying them until he can repeat all 3, up to 5 trials. If he does not eventually learn all 3, recall cannot be meaningfully tested.

Score 0-3 ☐

3. Attention and Calculation

Ask the subject to begin with 100 and subtract 7 from 100 and keep subtracting 7. Stop after 5 subtractions (93,86,79,72,65). Score the total number of correct answers. Ask the subject to spell the word "world" backwards. The score is the number of letters in correct order.
(e.g., dlrow = 5, dlorw = 3). The highest score will be recorded.

Score 0-5 ☐

4. Recall

Ask the subject if he can recall the 3 words you previously asked him to remember.

Score 0-3 ☐

Mini Mental State Examination cont'd

MMSE

5. Naming
a. Show the subject a wristwatch and ask him what it is.
b. Repeat for a pencil.

Score 0-2 ☐

6. Repetition
Ask the subject to repeat this sentence after you -
"No Ifs, Ands, or Buts". Allow only one trial.

Score 0-1 ☐

7 3-Stage Command
Have the subject follow this command -
"Take a paper in your hand, fold it in half, and put in on the floor".
Score one point for each part correctly executed.

Score 0-3 ☐

8. Reacting
On a blank piece of paper print the sentence "Close your eyes"
in letters large enough for the subject to see clearly.
Ask him to read it and do what it says.
Score one point only if he actually closes his eyes.

Score 0-1 ☐

9. Writing
Give the subject a blank piece of paper and ask him to write a
sentence for you. Do not dictate a sentence, it is to be written
spontaneously. It must contain a subject and a verb and be
sensible. Correct grammar and punctuation are not necessary.

Score 0-1 ☐

10. Copying
On a clean piece of paper, draw intersecting pentagons, ask him to copy it exactly as it is.
All 10 angles must be present and 2 must intersect to score one point.
Tremor and rotation are ignored.

Score 0-1 ☐

Total Score ☐
(maximum 30)

_____
Rater's Initials

"Mini Mental State: A Practical Method for Grading the Cognitive State of Patients for the Clinician". *Journal of Psychiatric Research* 1975; **12(3)**: 189-198.

Mini Mental State Examination cont'd

MMSE

Tools Needed for MMSE

5 NAMING

Wristwatch, pencil.

3-STAGE COMMAND

Sheet of paper.

8 REACTING

Blank piece of paper with "close your eyes" printed on it.

9 WRITING

Blank piece of paper.

10 COPYING

A clean piece of paper with intersecting pentagons drawn on it.

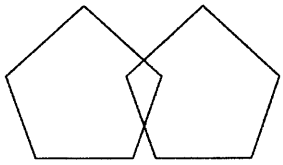

Manchester and Oxford Universities Scale for the Psychopathological Assessment of Dementia cont'd

MOUSEPAD

DESCRIPTIVE PSYCHOPATHOLOGY OF DEMENTIA

Name _____ Date _____

No. _____ Informant _____

First, establish the duration of the dementia syndrome in months: How long ago was the first symptom you noticed? (Cases referred to are 'she'/'her' purely for convenience.)

☐ months

RATE AS FOLLOWS

This rating scale can rate symptoms and behaviours which are currently occurring and also those which have existed at some point since the onset of dementia.

0: absent
1: mild – that the symptom is apparent infrequently (less than once a week)
2: moderate – that the symptom is present frequently (one day a week or more but less than four out of seven days)
3: severe – that the symptom is present at least four times a week
8: not applicable or not asked
9: interviewee does not know

DELUSIONS

(These beliefs should be held firmly, be false (as far as can be ascertained), last for more than seven days and occur in the absence of acute physical illness). The false beliefs should be rated even if they could be accounted for in terms of memory impairment. (Do not rate "misidentifications" here – see below.)

	Yes/No	Severity	Months from onset	Duration in months	In last month? Y/N	Convince otherwise	Score
Has she ever said: she is being watched or spied upon?							
her food or drink is being poisoned?							
she is being followed?							
her possessions are being hidden?							
her possessions are being stolen?							
her house is not her own home?							
her spouse is having an affair?							
she is involved in an amorous affair?							
she is about to be abandoned by her family?							
someone else is in the house?							

Manchester and Oxford Universities Scale for the Psychopathological Assessment of Dementia cont'd

MOUSEPAD

HALLUCINATIONS

Rate as follows

This rating scale can rate symptoms and behaviours which are currently occurring and also those which have existed at some point since the onset of dementia.

0: absent

1: mild – that the symptom is apparent infrequently (less than once a week)

2: moderate – that the symptom is present frequently (one day a week or more but less than four out of seven days)

3: severe – that the symptom is present at least four times a week

8: not applicable or not asked

9: interviewee does not know

(These experiences can be considered present if the patient has spontaneously complained of the phenomenon or if there is evidence that she has been seen interacting with an apparently false perception. They must have occurred in the absence of acute physical illness and have lasted for more than seven days. NB. Do not rate here patients talking to mirror image, to photographs or to television – these should be rated under misidentifications.)

	Yes/No	Severity	Months from onset	Duration in months	In last month? Y/N	Score
Has she heard voices or other sounds where there have been none apparent? *If so, have they been:*						
voices from known persons						
from unknown persons						
does she appear to understand the voices? Yes/No						
music						
animals						
other noises						
Has she seen things where there have been none apparent? *If so, have they been:*						
people known persons						
unknown persons						
dwarf-life figures						
children						
animals						
other						
Has the patient reported strange smells when none have been apparent?						
Has the patient reported strange sensations in her body?						
Has the patient reported an unusual taste in her food or drink?						

Manchester and Oxford Universities Scale for the Psychopathological Assessment of Dementia cont'd

MOUSEPAD

MISIDENTIFICATIONS

Rate as follows

This rating scale can rate symptoms and behaviours which are currently occurring and also those which have existed at some point since the onset of dementia.

0: absent

1: mild – that the symptom is apparent infrequently (less than once a week)

2: moderate – that the symptom is present frequently (one day a week or more but less than four out of seven days)

3: severe – that the symptom is present at least four times a week

8: not applicable or not asked

9: interviewee does not know

(These experiences must have lasted for at least seven days and have occurred in the absence of acute physical illness.)

	Yes/No	Severity	Months from onset	Duration in months	In last month? Y/N	Score
Has she acted unusually when seeing herself in the mirror? *If so, has she:*						
claimed that her mirror image is not her own self?						
spent time conversing with her own image?						
Has she ever apparently believed: that a close relative or carer is not who they claim to be?						
that they have been replaced by an impostor?						
that TV images or photographs are real events?						
that she is infested with small animals?						

REDUPLICATIONS

(These experiences must have lasted for at least seven days and have occurred in the absence of acute physical illness.)

	Yes/No	Severity	Months from onset	Duration in months	In last month? Y/N	Score
Has she ever said that things have been reduplicated (e.g. that there are two of anyone or anything in existence) *If so, what?*						
Spouses or carers						
Houses or other inanimate objects						
Animate objects (pets etc.)						

Manchester and Oxford Universities Scale for the Psychopathological Assessment of Dementia cont'd

MOUSEPAD

BEHAVIOURAL CHANGES IN DEMENTIA

Frequency rating scale (to be used for those items which do not include a specific rating scale):

0: absent

1: mild – that the behaviour is apparent occasionally (once a week or less often)

2: moderate – that the behaviour is present more often than once a week but less than four days/nights a week

3: severe – that the behaviour is present most days/nights (at least four out of seven days)

8: not applicable or not asked

9: not known

Note any physical problems which might significantly alter ratings (e.g. arthritis might affect her walking around). If physical problem makes rating inappropriate rate 8 and explain.

WALKING

	Yes/No	Severity	Months from onset	Duration in months	In last month? Y/N	Score
Does she walk around more often than she used to just before the memory problems started? *If yes then rate:*						
1: mild: sits most days for more than 15 minutes at a time, awake						
2: severe: will not sit, most days, for as long as 15 minutes at a time, awake						
Does she follow you (or anyone else) around?						
0: follows others around less than 30 minutes each day						
1: follows others around, most days, for more than 30 minutes but less than 2 hours						
2: follows others around for more than 2 hours most days						
Does she wander out of the house or home (beyond the garden)?						
0: absent or occasional only (less than 1 hour on a typical day)						
1: for less than 3 hours most days						
2: for more than 3 hours most days						
Does she wander at night (i.e. after she has gone to bed)?						
Has she wandered away from home and had to be brought back home?						

Manchester and Oxford Universities Scale for the Psychopathological Assessment of Dementia cont'd

MOUSEPAD

EATING

Has her weight changed since onset of problems? No ☐ Clearly gained ☐ Clearly lost ☐						
	Yes/No	Severity	Months from onset	Duration in months	In last month? Y/N	Score
Does she eat more than just before the onset of problems than she used to?						
1: eats a little more						
2: eats half as much again, or more						
Does she eat more quickly than just before the onset of problems than she used to?						
1: eats a little more quickly						
2: eats much more quickly						
Have you ever had to limit how much she eats because otherwise she would try to eat too much?						
1: on a few occasions only						
2: need to control intake much of the time						
Does she eat more sweet things than she used to? (More of a sweet tooth) Yes/No						

SLEEP

	Yes/No	Severity	Months from onset	Duration in months	In last month? Y/N	Score
Is she restless/wakeful during the night?						
Does she confuse night and day?						
Does she 'doze' during the day, more than she did before the onset of her problems?						

Manchester and Oxford Universities Scale for the Psychopathological Assessment of Dementia cont'd

MOUSEPAD

SEXUAL BEHAVIOUR

	Yes/No	Severity	Months from onset	Duration in months	In last month? Y/N	Score
Does she talk inappropriately about sex?						
Does she act in a sexually disinhibited manner?						

AGGRESSION

	Yes/No	Severity	Months from onset	Duration in months	In last month? Y/N	Score
Has she been physically or verbally aggressive since onset of memory problems (*more* aggressive than before onset of dementia)? Yes ☐ No ☐						
If yes, under what circumstances?						
While she was being cared for (e.g. washing, dressing)? Yes ☐ No ☐						
Unprovoked or impatient? Yes ☐ No ☐						
In response to hallucinations or mistaken ideas you were going to harm her? Yes ☐ No ☐						
Is the aggression: physical – against other people?						
– against objects?						
verbal						
Does she have outburst of: laughing						
crying						

OTHER TYPES OF BEHAVIOUR IN THE LAST MONTH

Does she move objects and hide them, or put them in strange places?	Yes ☐ No ☐
Does she mislay things?	Yes ☐ No ☐

Allen N.H.P., *et al. Br J Psychiatry* 1996; **169**: 293-307. Reprinted by permission.

Appendix 4: Image Acquisition protocols

Standard imaging protocol

Scans were performed by the staff at St Mary's Hospital, Paddington and the Queen Square Imaging Centre. Acquisition parameters were: time to repeat, 35ms; time to echo, 5ms; flip angle 35°, field of view 24x24 cm, and matrix size 256*128.

MIRIAD protocol

Scans were acquired by Dave MacManus of the NMR group, Queen Square. The following parameters were used for acquisition: time to repeat, 15ms; time to echo, 5.4ms; flip angle 15°, field of view 24x24 cm, matrix size 256*256, producing 124 contiguous 1.5mm slices.

Appendix 5: Regional segmentation protocols

Whole brain (Appendix Figure 5-1)

Whole brain segmentation was performed using a protocol described in detail by Freeborough *et al* 1997 (Freeborough et al., 1997). This is a semi-automated algorithm which identifies voxels within the brain using interactive thresholding. Upper and lower intensity thresholds are set with the aim of outlining the brain as accurately as possible and to prevent connection to the dura (Appendix figure 5-1A). The lower level of the brain segmentation is then defined as the bottom slice of the cerebellum (Appendix figure 5-1B). Brain tissue is then isolated from the surrounding tissue such as scalp and dura using a series of erosions (Appendix figure 5-1C) and dilations (Appendix figure 5-1D). Manual editing is then performed if necessary using MIDAS image analysis tools. Inter-rater reproducibility was 0.42% and intra-rater reproducibility was 0.36%.

TIV (see Chapter 10)

The TIV measure employed in this thesis uses T1-volumetric images put into the orientation defined by the Montreal Neurological Institute 305 brain average (Mazziotta et al., 1995) using three dimensional registration. The semi-automatic grey level thresholding technique was set at a standard threshold of 33% of the mean intracranial signal intensity to outline the outer border of dura. Every 10^{th} axial slice was segmented with the inferior border set as the lowest slice in which cerebellar tissue was present (see chapter 10). Linear interpolation of areas was used to obtain an estimate of the TIV from the segmented slices (Whitwell et al., 2001).

The hippocampus (Appendix Figure 5-2)

The hippocampus was defined as including the hippocampus proper, the subiculum and the alveus. Measurements were taken from coronal slices from the posterior to anterior boundaries using a standard neuroanatomical atlas (Duvernoy, 1998). The posterior limit of the HF was defined as the coronal slice where the longest length of the crus of the fornix was seen (Watson et al., 1992). The hippocampus was bounded superiorly, medially and laterally by CSF and inferiorly by the white matter of the subiculum. The head of the hippocampus was delineated from the amygdala by inclusion of the alveus, which was best seen as a band of high signal intensity on the sagittal sections. A consistent threshold of 70% of mean brain intensity was applied to exclude CSF voxels that have a lower intensity. This measurement method excludes the hippocampal tail in order to achieve satisfactory reproducibility of segmentation, as recommended by Watson et al (Watson et al., 1992). Reproducibility error was 3%

The amygdala (Appendix Figure 5-3)

The rostral limit corresponds to the rostral extreme of the temporal stem. Caudally the amygdala was defined using the border with the lateral ventricle and the alveus, ending when the alveus disappears. Superiorly the boundary was set anteriorly by a line connecting the inferior point of the lateral fissure to the lateralmost point of the paramedian cisternae, and posteriorly by the superior and lateral borders of the optic tract. Inferolaterally the amygdala were bounded by white matter and medially by the ambient cistern. Reproducibility error was 4%. A consistent threshold of 70% of mean brain intensity was applied to exclude CSF voxels that have a lower intensity.

Appendix Figure 5-1: Steps involved in brain segmentation: A) setting intensity thresholds, B) lower cut-off, C) erosions, and D) dilations

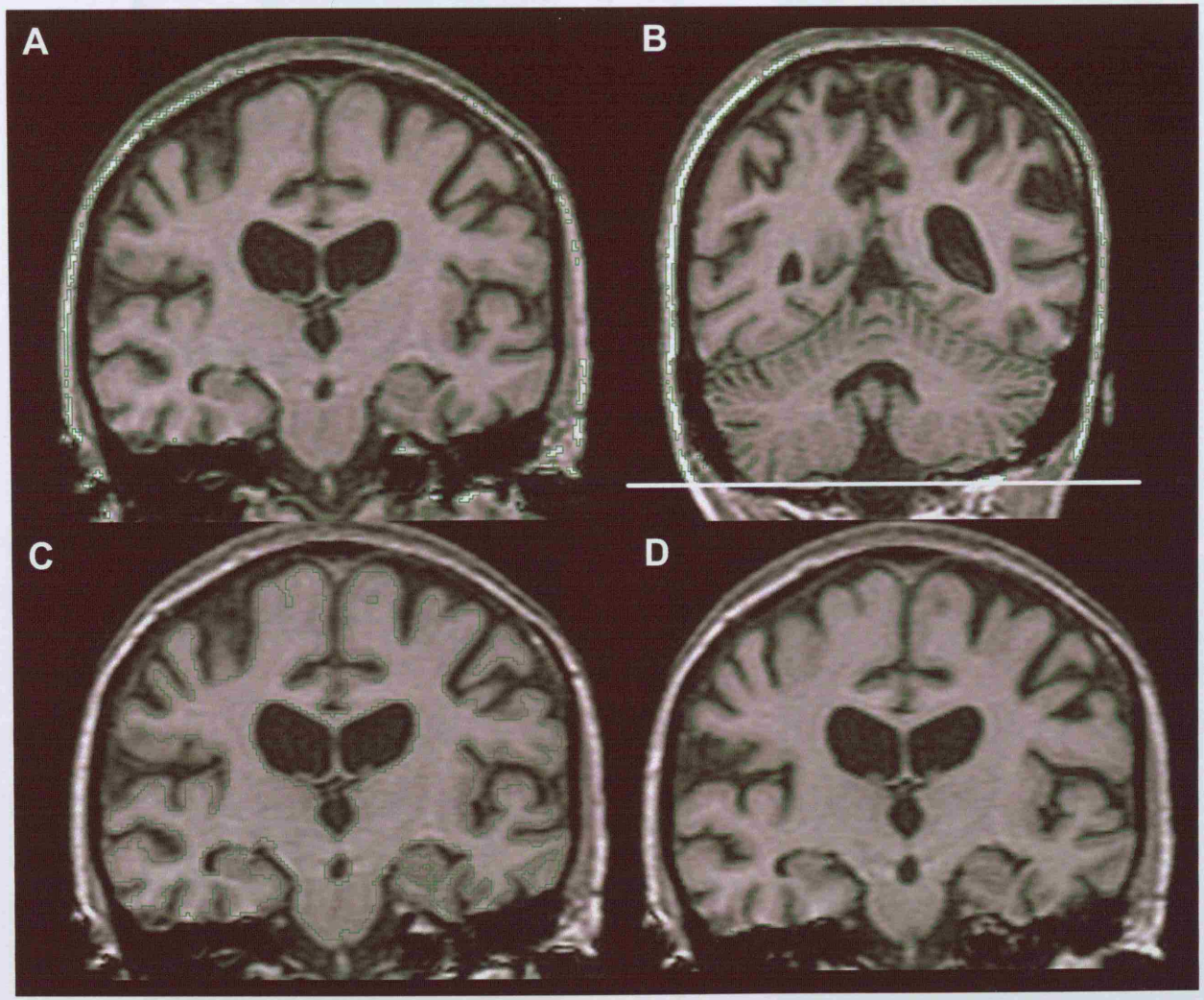

Appendix Figure 5-2: An example hippocampal segmentation shown in both sagittal and coronal views

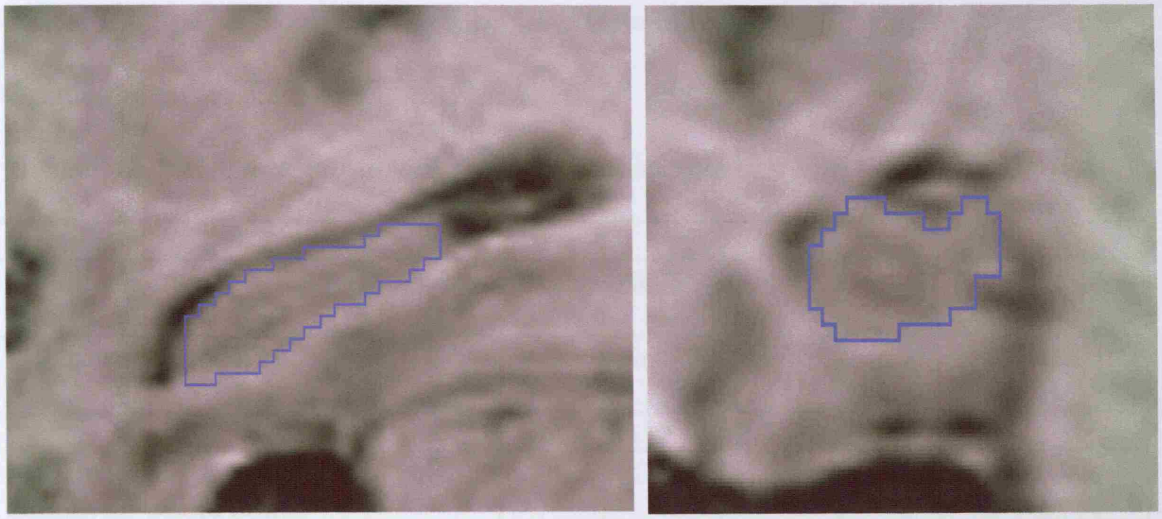

Appendix Figure 5-3: An example amygdala segmentation shown in both sagittal and coronal views

Appendix 6: Chapter 4 radiology questionnaire

Radiology questionnaire

Patient ID ..... Date of review .....

Diagnosis ..... Age .....

To note: A > P = Anterior atrophy > Posterior atrophy

Question							
Is cortical atrophy present?		Yes ☐	No ☐				
Is the atrophy focal?		Yes ☐	No ☐				
		None	A > P	P > A			
Is there an A-P gradient of atrophy in whole brain?		☐	☐	☐			
If focal, which parts are affected?	Normal	Mild	Mod	Severe	None	L > R	R > L
Left frontal lobe	☐	☐	☐	☐			
~ orbitofrontal	☐	☐	☐	☐			
~ dorsolateral	☐	☐	☐	☐			
Right frontal lobe	☐	☐	☐	☐			
~ orbitofrontal	☐	☐	☐	☐			
~ dorsolateral	☐	☐	☐	☐			
Frontal lobe asymmetry?					☐	☐	☐
Left occipital lobe	☐	☐	☐	☐			
Right occipital lobe	☐	☐	☐	☐			
Occipital lobe asymmetry?					☐	☐	☐
Left parietal lobe	☐	☐	☐	☐			
Right parietal lobe	☐	☐	☐	☐			
Parietal lobe asymmetry?					☐	☐	☐
Left temporal lobe	☐	☐	☐	☐			
~ superior temporal gyrus	☐	☐	☐	☐			
~ inferior temporal gyrus	☐	☐	☐	☐			
~ fusiform gyrus	☐	☐	☐	☐			
~ parahippocampal gyrus	☐	☐	☐	☐			

	Normal	Mild	Mod	Severe	None	L > R	R > L
Right temporal lobe	☐	☐	☐	☐			
~ superior temporal gyrus	☐	☐	☐	☐			
~ inferior temporal gyrus	☐	☐	☐	☐			
~ fusiform gyrus	☐	☐	☐	☐			
~ parahippocampal gyrus	☐	☐	☐	☐			
Temporal lobe asymmetry?					☐	☐	☐
Left hippocampus	☐	☐	☐	☐			
Right hippocampus	☐	☐	☐	☐			
Hippocampal asymmetry?					☐	☐	☐
Left amygdala	☐	☐	☐	☐			
Right amygdala	☐	☐	☐	☐			
Amygdala asymmetry?					☐	☐	☐
Ventricles	☐	☐	☐	☐			
Ventricular asymmetry?					☐	☐	☐
Cerebellum	☐	☐	☐	☐			
Cerebellar asymmetry?					☐	☐	☐
Vascular load	☐	☐	☐	☐			
Vascular asymmetry?					☐	☐	☐

Overall severity of tissue loss	☐	☐	☐	☐

Appendix 7: Patterns of temporal lobe atrophy in SD and AD (study by Chan et al 2001)

Introduction

Alzheimer's disease (AD) and frontotemporal degeneration (FTD) are neurodegenerative diseases characterized by the insidious onset and gradual progression of cognitive impairment. Patients with AD typically present with episodic memory impairment, with disease progression leading to global cognitive impairment. Neuroimaging reveals medial temporal lobe atrophy in early stages of the disease(de Leon et al., 1989; Killiany et al., 1993; Fox et al., 1996a; Juottonen et al., 1998), while generalized temporal lobe and global cerebral atrophy are characteristic of advanced AD.

By contrast, FTD is characterized by focal cognitive deficits which are associated with focal cortical atrophy. Three main syndromic variants exist(Neary et al., 1998): frontotemporal dementia, primary progressive aphasia and semantic dementia (SD), the last of which was characterized by Snowden and colleagues(Snowden, 1989). Typically SD patients present with an impairment of naming and a loss of word meaning. Speech is fluent, with normal articulation, prosody and relative preservation of syntax. Often, but not always (Cipolotti and Warrington, 1995), these patients exhibit surface dyslexia and dysgraphia. Impaired face and object recognition may be present in the absence of visuoperceptual deficits (Hodges et al., 1992).

Semantic memory impairment, in the context of preserved episodic memory, was initially described by Warrington (Warrington, 1975) and is a key aspect of the

diagnostic differentiation between SD and AD. However, differentiation can prove difficult, particularly in the early stages of the diseases, and supportive imaging is important in establishing the diagnosis. The small number of studies that have investigated cerebral atrophy in SD were based primarily on visual MRI assessment involving small numbers of subjects. These studies have reported focal temporal lobe atrophy which was usually bilateral and often asymmetrical, with greater left-sided atrophy, although in a few instances the atrophy was noted to be unilateral(Tyrrell et al., 1990). Functional imaging studies have shown hypometabolism in the left inferolateral temporal lobe(Cardebat et al., 1996), although Mummery and co-workers also noted reduced activity of the left posterior inferior temporal gyrus accompanied by any associated regional atrophy(Mummery et al., 1999). More recently, a study using voxel-based morphometry demonstrated that atrophy in SD was primarily confined to the temporal lobes, with significant atrophy of the left temporal pole, amygdala, MITG and the anterior fusiform gyrus(Mummery et al., 2000). No significant atrophy was observed in the hippocampus or entorhinal cortex.

This study aimed to examine in greater detail the pattern of atrophy in SD, and to identify regions within the temporal lobe that are associated with semantic memory function by comparing the volumes of temporal lobe regions in SD patients with those of AD patients and with control subjects.

Methods

Subjects

Patients were recruited from the Specialist Cognitive Disorders Clinic (see chapter 3). The two patient groups consisted of 10 patients (6 male, 4 female) with probable AD and 10 patients (6 male, 4 female) with SD. The diagnosis of FTLD or AD was made on clinical grounds and imaging was used to exclude space-occupying lesions, vascular disease and other pathologies. The 10 SD patients were then selected from the FTLD patients on the basis of neuropsychological findings without further reference to neuroimaging data. Similarly, the AD subjects were given a clinical diagnosis, which was supplemented only by the demonstration on neuropsychological testing of deficits in multiple cognitive domains. The AD and SD patients were considered to be representative of each disease and were not chosen to be at the extremes of their respective diagnostic criteria.

The diagnosis of probable AD was made according to NINCDS-ADRDA criteria (McKhann et al., 1984). All AD patients presented with cognitive impairment primarily affecting episodic memory. All had histories of progressive cognitive decline and were chosen such that they matched the SD cases in terms of full scale IQ. The SD patients presented with progressive loss of vocabulary affecting expressive and receptive language in the context of fluent speech production. All fulfilled accepted criteria for the diagnosis of SD (Neary et al., 1998). A control group of 10 subjects (5 male, 5 female) consisted of age-matched individuals with normal cognitive function and no history of neurological disorder.

Neuropsychological Assessment

Neuropsychological assessments were performed around the time of the MRI scans. The tests administered were the shortened Wechsler Adult Intelligence Scale Revised

(Wechsler, 1981), the Incomplete Letters (IL) visuoperceptual subtest of the Visual Object & Space Perception Battery (Warrington and James, 1991), the National Adult Reading Test (NART) (Nelsen, 1982), the Graded Difficulty Spelling test (GDS) (Baxter and Warrington, 1994), the Graded Difficulty Naming Test (GNT) (McKenna and Warrington, 1983), the Oldfield picture naming test (Old) (Oldfield and Wingfield, 1965), the Recognition Memory Tests (RMT) (Warrington, 1984) and the Short Recognition Memory Test (Warrington, 1996).

Structural MRI

The standard imaging protocol described in Appendix 4 was used for acquisition of T1-weighted images. The MIDAS image analysis tools (see chapter 3) were used for brain region segmentation. Regions were outlined using a mouse-driven cursor. All measurements were performed by raters blinded to the clinical diagnosis. Each image was presented in random order, once conventionally and once flipped across a plane parallel to the mid-sagittal plane. Structures were outlined on the right of each presented image, thus ensuring blinding to structure laterality. All measurements were normalised to the total intracranial volume (TIV), to compensate for differences in head size (Whitwell et al., 2001), and all volumes are therefore expressed as fractions of the TIV. The techniques for measuring TIV, whole brain volume, hippocampus and amygdala are detailed in Appendix 5. The techniques for measuring all other structures are given below. Measurement reproducibility was tested by undertaking a comparison of six repeated blinded measurements performed for each structure. Reproducibility error is expressed below in terms of the mean absolute difference between repeated measurements.

The temporal lobe

The boundary between the temporal lobe and the remainder of the brain was defined by drawing a line across the temporal stem from the inferomedial extreme of the Sylvian fissure to the most superior point of the temporal lobe on the medial side of the stem. The posterior limit was defined as the longest length of the fornix where it is not obstructed by the thalamus. The anterior limit is defined as the last slice in which temporal lobe is present. Reproducibility error was 3%.

The parahippocampal gyrus

The PHG was measured along its length corresponding to the rostrocaudal length of the hippocampus. The white matter layer was included in these measurements. The superomedial border was the interface between the white matter layer and the overlying hippocampus, and superolaterally the boundary was the junction of the white matter layer with the inferior edge of the choroid fissure. Inferomedially the gyrus was bounded by the ambient cistern and inferolaterally by the collateral sulcus. Reproducibility error was 6%.

The entorhinal cortex

EC segmentation was undertaken using a modified version of the protocol of Insausti and colleagues (Insausti et al., 1998). White matter was not included in this measurement. Rostrally the EC extended as far as the rostral extreme of the sulcus semiannularis and caudally as far as the caudal end of the gyrus infralimbicus. Superiorly the EC was bounded by the white matter separating it from the amygdala (rostrally) and the hippocampus (caudally). Inferomedially the EC was bounded by the ambient cistern and laterally the EC was measured as far as the medial lip of the

collateral sulcus. The portion of the EC that extended along the medial bank of the collateral sulcus was not included because of the inter-individual variation in the position of the lateral border of the EC. Reproducibility error was 5%.

The superior temporal gyrus

The STG was bounded superiorly by the Sylvian fissure and inferiorly by the superior temporal sulcus. The posterior limit was defined as the longest length of the fornix where it is not obstructed by the thalamus. Reproducibility error was 5%.

The middle and inferior temporal gyri (MITG)

The MITG were bounded superolaterally by the superior temporal sulcus and inferomedially by the lateral occipitotemporal sulcus. The posterior limit was defined as the longest length of the fornix where it is not obstructed by the thalamus. The middle and inferior temporal gyri were measured together because the border between the two gyri is often indistinct. Reproducibility error was 5%.

The fusiform gyrus

The fusiform gyrus was bounded superolaterally by the lateral occipitotemporal sulcus and inferomedially by the collateral sulcus. The posterior limit was defined as the longest length of the fornix where it is not obstructed by the thalamus. Reproducibility error was 5%.

Appendix Figure 7-1: A coronal section through the brain of a control subject, at the level of the amygdalohippocampal junction. The left temporal lobe (inset, magnified), is used to highlight the segmentation of individual structures.

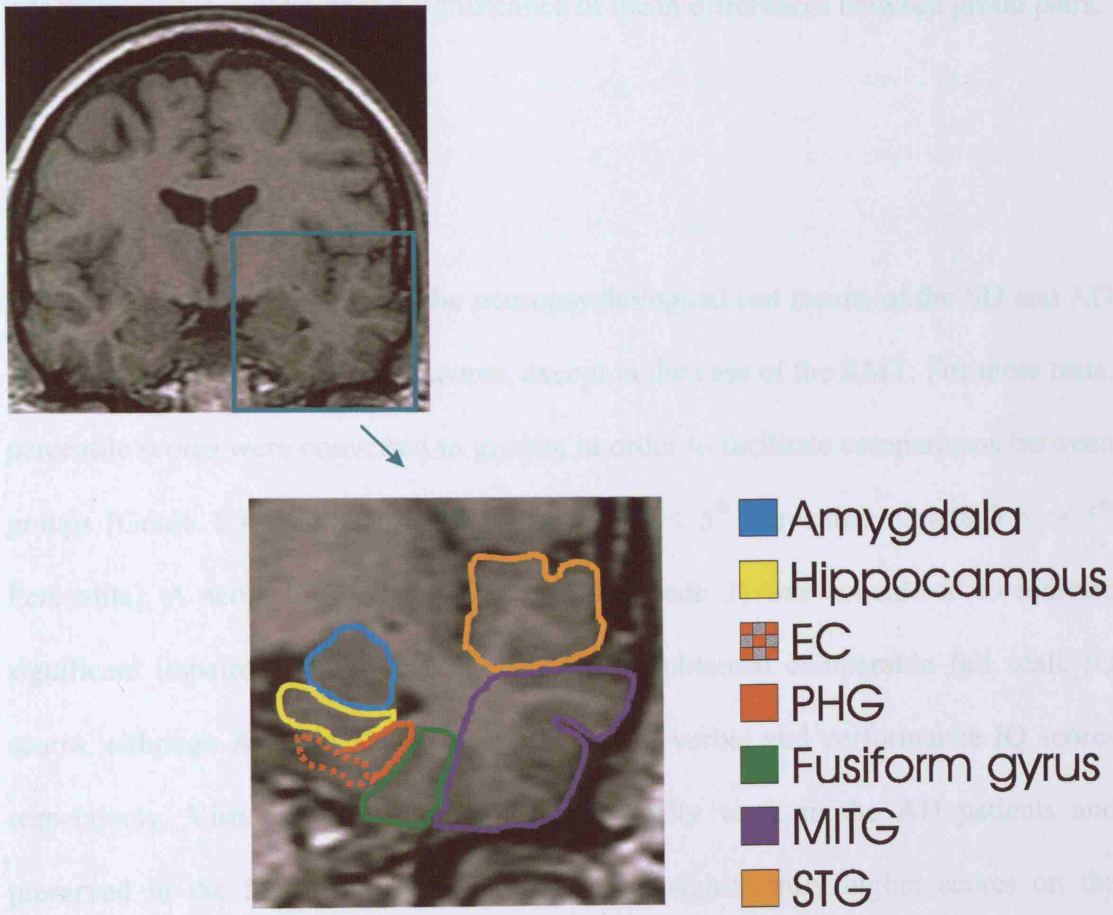

Statistical analysis

SPSS version 8.0 (SPSS Inc., Chicago, Illinois, USA) was used for statistical calculations. Analysis of variance (ANOVA) between the three subject groups was performed for each measured structural variable. In addition, Tukey posthoc analysis was employed to determine the significance of mean differences between group pairs.

Results

Neuropsychological Results

Appendix table 7-1 summarises the neuropsychological test results of the SD and AD groups in terms of mean correct scores, except in the case of the RMT. For these tests, percentile scores were converted to grades, in order to facilitate comparisons between groups [Grade 1 = < 1^{st} percentile, Grade 2 = < 5^{th} Percentile, Grade 3 = > 5^{th} Percentile]. A score below the 5^{th} percentile (grade 2) was considered to indicate significant impairment. The two patient groups obtained comparable full scale IQ scores, although AD and SD patients had higher verbal and performance IQ scores respectively. Visuoperceptual skills were generally weak in the AD patients and preserved in the SD patients. AD patients had significantly higher scores on the NART than the SD group, reflecting the higher incidence of surface dyslexia in SD. Similarly, SD patients performed significantly worse on the graded difficulty spelling test, in keeping with the higher incidence of surface dysgraphia. Auditory short term memory was assessed by the forward digit span and was well preserved in both patient groups.

All SD patients had severe word finding difficulties. All scored zero on the GNT and scored very poorly on the Oldfield picture naming test. By contrast, the majority of

the AD patients had relatively spared nominal skills. All SD patients also presented with very severe deficits of word comprehension.

The RMT scores revealed differences between the two patient groups. All AD patients were impaired, with global impairment in 6 out of 10 patients, and impairment was generally severe, with scores predominantly between the 1st and 5th percentiles of performance (grades 1-2) on both verbal and visual subtests. In contrast, only 3/10 SD patients revealed deficits on both subtests, with 5/10 impaired only on the verbal subtest. The SD patients were less severely impaired than the AD patients, with test scores predominantly at the 5th percentile (grade 2) for the RMT words subtest and above the 5th percentile for the RMT faces subtest.

Appendix Table 7-1: Neuropsychological test scores.

	SD		AD	
	Mean	*StDev*	*Mean*	*StDev*
VIQ	81.6	11.5	90	12.7
PIQ	98.1	10.1	83.4	14.8
FSIQ	89.8	7.9	86.4	12.8
IL	19.6	0.5	17.4	2.9
NART	18.1	14.9	31.1	14.3
GDS	8.0	7.6	17.3	11.9
GNT	0	0	19.5	8.9
Old	5.0	4.0	19.0	0.0
Dspan fwd	6.4	1.4	5.7	0.5
RMW*	1.9	0.6	1.4	0.5
RMF*	2.9	1.3	2.0	0.8

*Test scores for SD and AD patients, presented as means and standard deviations (StDev) across groups. *Mean RMT scores presented as grades (see text).*

VIQ = verbal IQ; PIQ = performance IQ; FSIQ = full scale IQ; Dspan fwd = digit span forwards; RMW = recognition memory for words; RMF = recognition memory for faces. See text for other abbreviations.

Patient characteristics

There was no significant difference in gender distribution or handedness (Appendix table 7-2). ANOVA did not reveal any significant group differences in age ($p = 0.42$) and posthoc analysis did not reveal any significant differences between group pairs, including AD and SD. Both the SD and AD groups had significantly lower MMSE scores than controls ($p<0.001$).

Appendix Table 7-2: Patient characteristics

	Control	SD	AD
Gender (M:F)	5:5	6:4	6:4
Handedness (right:left)	9:1	9:1	9:1
Age (yrs)	60 (6)	63 (6)	60 (8)
MMSE (/30)	29.8 (0.4)	21.8 (4.9)	21.2 (5.0)

Age and MMSE are expressed as mean (standard deviation))

Volumetric results

Appendix Figure 7.2 compares left temporal lobe structures in a control subject, an SD patient, and an AD patient. ANOVA calculations (summarised in Appendix table 7-3) showed that there were significant differences in the volumes of the structural variables across the three groups. Posthoc analysis revealed that, for all regional structures measured, there was a significant difference between the SD and control groups whereas for the global measures, there was a significant difference in ventricular volume between groups but not for whole brain volumes. There was no significant difference in either of the two global measures between the SD and AD

groups. With regard to the SD and AD groups, all left-sided temporal lobe measures were significantly different, in contrast with the right-sided measures, of which only the amygdala and STG were significantly different.

In order to estimate the degree of atrophy of individual structures in SD and AD, the mean volumes for each structure were compared with the control mean volumes. The left EC was by far the most severely atrophied structure in SD (21% of control volume), with the left amygdala reduced to 40% of control volume and the left MITG and fusiform gyrus both reduced by approximately 50%. There was a marked asymmetry in the distribution of atrophy in the temporal lobe, with greater left-sided atrophy noted for all structures. By comparison, AD was associated with symmetrical atrophy of the EC, the amygdala and the hippocampus, with the former being most severely atrophied.

Appendix Figure 7-2: Coronal sections through the left temporal lobes of three subjects (left to right: control; SD; AD), at the level of the amygdalohippocampal junction. Note the atrophy of all *temporal lobe structures in SD at this anterior level, and the medial temporal lobe atrophy in AD.*

Appendix Table 7-3: Volumes of measured brain regions

	Control	SD	AD	ANOVA	% SD /CON	% AD /CON
TIV (mm^3)	1427400 (182600)	1368200 (148200)	1410600 (182200)	0.62		
Whole brain	83.7 (4.1)	77.8 (4.5)	77.9 (3.2)	$0.003^{1\dagger 2\dagger}$	93.0	93.1
Ventricles	1.32 (0.59)	2.64 (0.90)	3.04 (1.69)	$0.007^{1*2\dagger}$	203.0	230.3
L amygdala	0.121 (0.013)	0.050 (0.011)	0.096 (0.016)	$< 0.001^{1\ddagger 2\dagger 3\ddagger}$	41.3	79.3
R amygdala	0.132 (0.017)	0.076 (0.013)	0.105 (0.017)	$< 0.001^{1\ddagger 2\dagger 3\dagger}$	57.6	79.5
L hippocampus	0.19 (0.02)	0.12 (0.03)	0.15 (0.02)	$< 0.001^{1\ddagger 2\dagger 3*}$	63.2	78.9
R hippocampus	0.24 (0.03)	0.20 (0.03)	0.20 (0.04)	0.020^{1*2*}	83.3	83.3
L EC	0.024 (0.005)	0.005 (0.003)	0.017 (0.004)	$< 0.001^{1\ddagger 2\dagger 3\ddagger}$	20.8	70.8
R EC	0.025 (0.007)	0.010 (0.005)	0.015 (0.006)	$< 0.001^{1\ddagger 2\dagger}$	40.0	60.0
L temporal lobe	4.90 (0.31)	2.67 (0.61)	4.39 (0.57)	$< 0.001^{1\ddagger 3\ddagger}$	55.3	89.6
R temporal	5.03	3.76	4.53	$< 0.001^{1\ddagger 3\dagger}$	76.1	90.1

lobe	(0.22)	(0.63)	(0.53)			
L PHG	0.21 (0.05)	0.13 (0.04)	0.19 (0.05)	$0.001^{1‡3*}$	62.2	91.2
R PHG	0.25 (0.04)	0.18 (0.03)	0.18 (0.04)	$< 0.001^{1†2†}$	76.5	88.2
L fusiform gyrus	0.29 (0.06)	0.14 (0.04)	0.34 (0.11)	$< 0.001^{1†3‡}$	51.7	117.2
R fusiform gyrus	0.38 (0.09)	0.27 (0.10)	0.36 (0.08)	0.020^{1*}	71.1	94.7
L MITG	1.78 (0.12)	0.82 (0.25)	1.53 (0.32)	$< 0.001^{1‡3‡}$	46.6	86.0
R MITG	1.77 (0.12)	1.30 (0.30)	1.51 (0.20)	$< 0.001^{1‡2*}$	74.6	85.3
L STG	1.41 (0.15)	0.90 (0.22)	1.34 (0.16)	$< 0.001^{1‡3‡}$	64.5	95.0
R STG	1.53 (0.16)	1.22 (0.19)	1.50 (0.18)	$0.001^{1†3†}$	81.0	98.0

All measurement values are expressed as percentages of the total intracranial volume.

*Posthoc analysis: [1]probability of difference between control and SD; [2]probability of difference between control and AD; [3]probability of difference between SD and AD. *p < 0.05; †p < 0.01; ‡p < 0.001; % SD/CON = mean standard deviation volume as fraction of mean control volume; % AD/CON = mean AD volume as fraction of mean control volume; L = left; R = right. EC = entorhinal cortex; PHG =*

parahippocampal gyrus; MITG = middle and inferior temporal gyri; STG = superior temporal gyrus.

The volumes for selected structures are plotted in Appendix figure 7.3. The asymmetrical atrophy of temporal lobe structures in SD is shown, in contrast to the symmetrical atrophy observed in AD. These graphs also highlight the hippocampal damage and the severe atrophy of the amygdala and EC in SD, as well as the lesser degree of atrophy of all medial temporal structures in AD, with relative preservation of other temporal gyri including the MITG.

Appendix Figure 7-3: Volumes of individual structures as plotted for each group. All volumes are expressed as percentages of TIV.

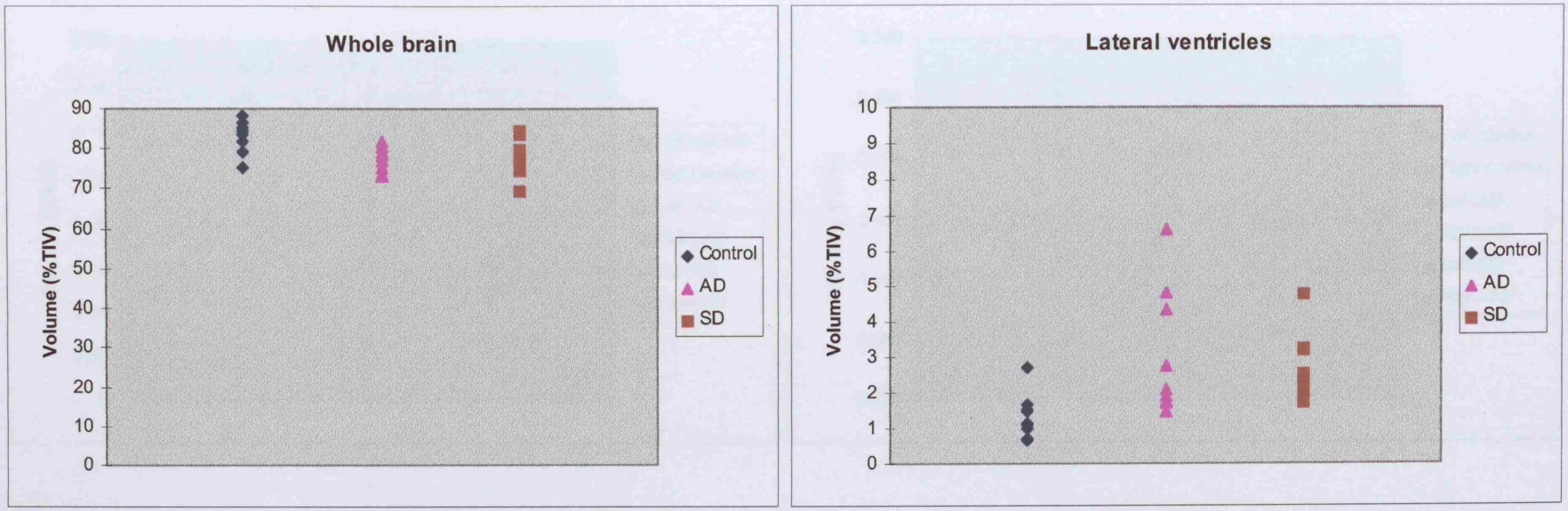

Continued…

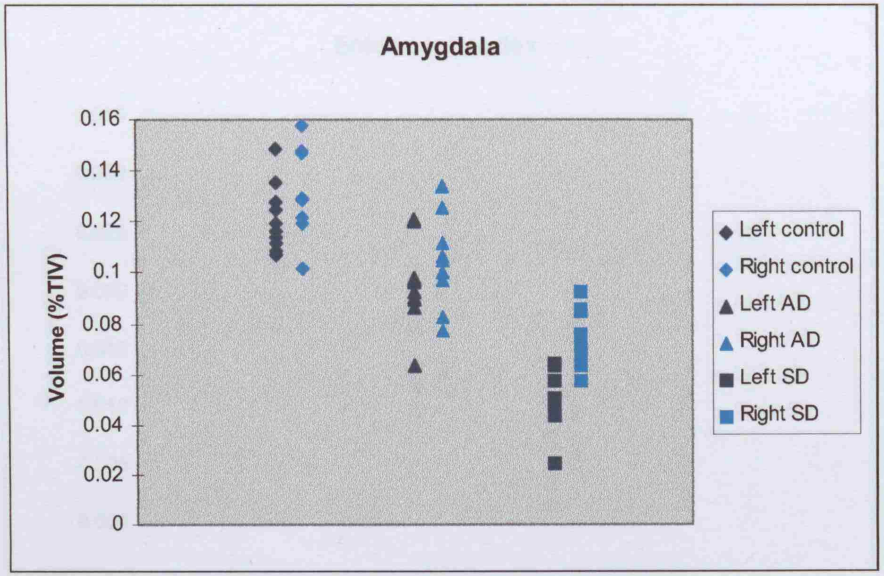
Amygdala
Volume (%TIV)
0.16
0.14
0.12
0.1
0.08
0.06
0.04
0.02
0
Left control
Right control
Left AD
Right AD
Left SD
Right SD

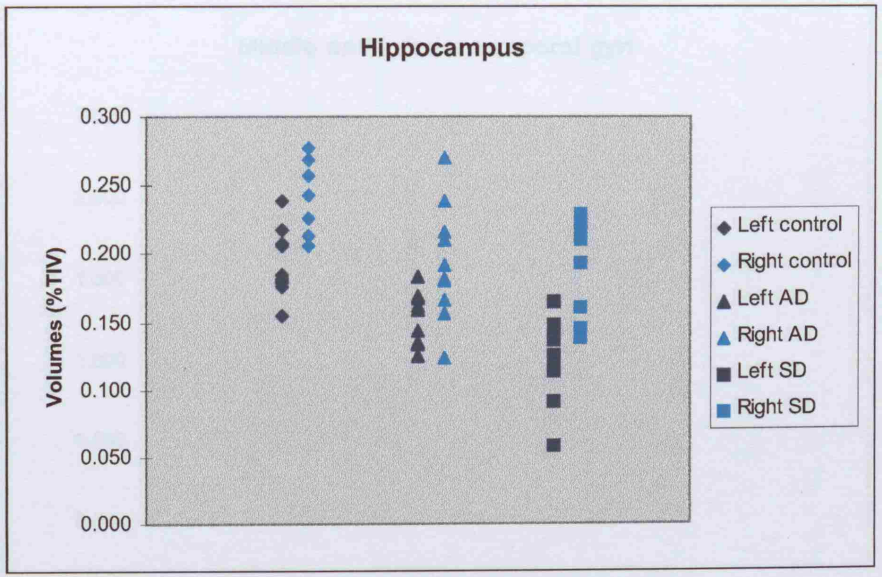
Hippocampus
Volumes (%TIV)
0.300
0.250
0.200
0.150
0.100
0.050
0.000
Left control
Right control
Left AD
Right AD
Left SD
Right SD

Continued…

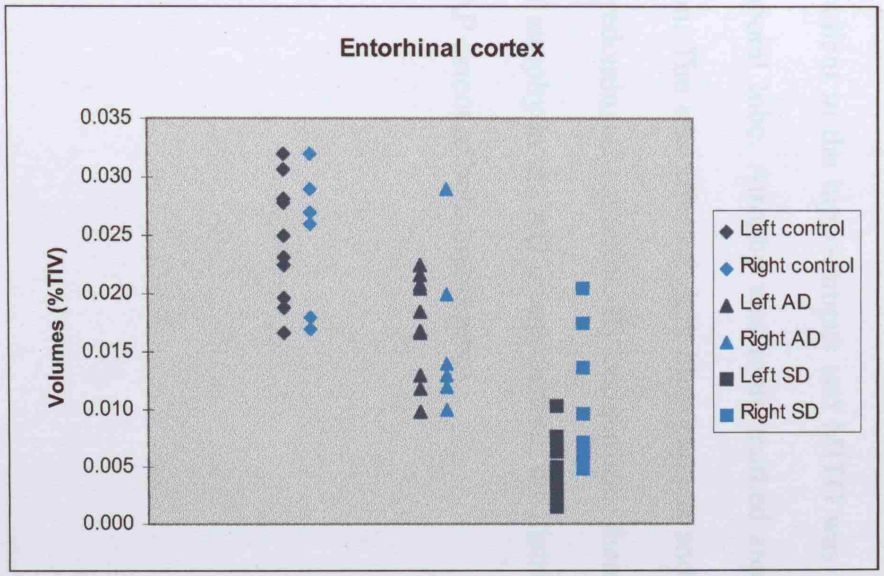
Entorhinal cortex
Volumes (%TIV)
0.035
0.030
0.025
0.020
0.015
0.010
0.005
0.000
Left control
Right control
Left AD
Right AD
Left SD
Right SD

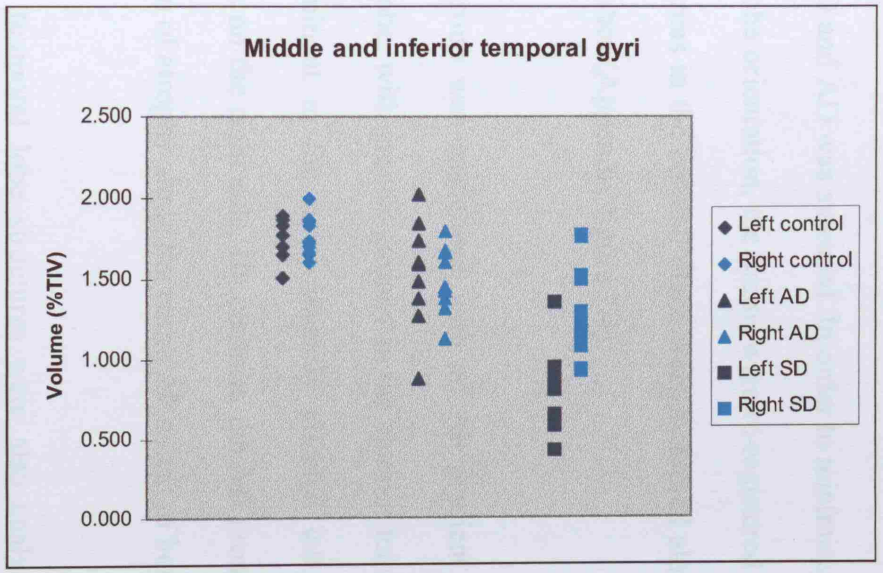
Middle and inferior temporal gyri
Volume (%TIV)
2.500
2.000
1.500
1.000
0.500
0.000
Left control
Right control
Left AD
Right AD
Left SD
Right SD

The distribution of atrophy along the anteroposterior (AP) length of the temporal lobes in SD and AD was assessed. In order to minimise inter-individual differences in temporal lobe orientation, the brains were re-registered into standard space and cross-sectional areas in the coronal plane were measured along the entire AP length of the temporal lobes (Appendix figure 7.4).

The SD group was associated with an AP gradient of atrophy across the whole temporal lobe, with greater atrophy in the anterior temporal lobes. This gradient was more prominent in the more severely affected left temporal lobe but was also discernible on the right side. By contrast, the AD group was associated with an even distribution of atrophy along the entire AP extent of both temporal lobes.

Individual temporal lobe structures were also analysed. In SD patients, the AP atrophy gradient in the hippocampus and MITG was similar to that observed in the whole temporal lobe. Atrophy was more marked anteriorly, with relative posterior preservation. The less affected right hippocampus and MITG also displayed atrophy that was predominantly anterior. By comparison, there was little evidence of an AP gradient of atrophy in the AD group: instead, the distribution of atrophy was uniform along the AP extent of both hippocampi.

Apendix Figure 7-4: Mean cross-sectional areas through the rostrocaudal extents of the temporal lobes and selected structures. All areas are corrected for TIV (unit of measurement: area mm^2/TIV $mm^3 \times 10^6$).

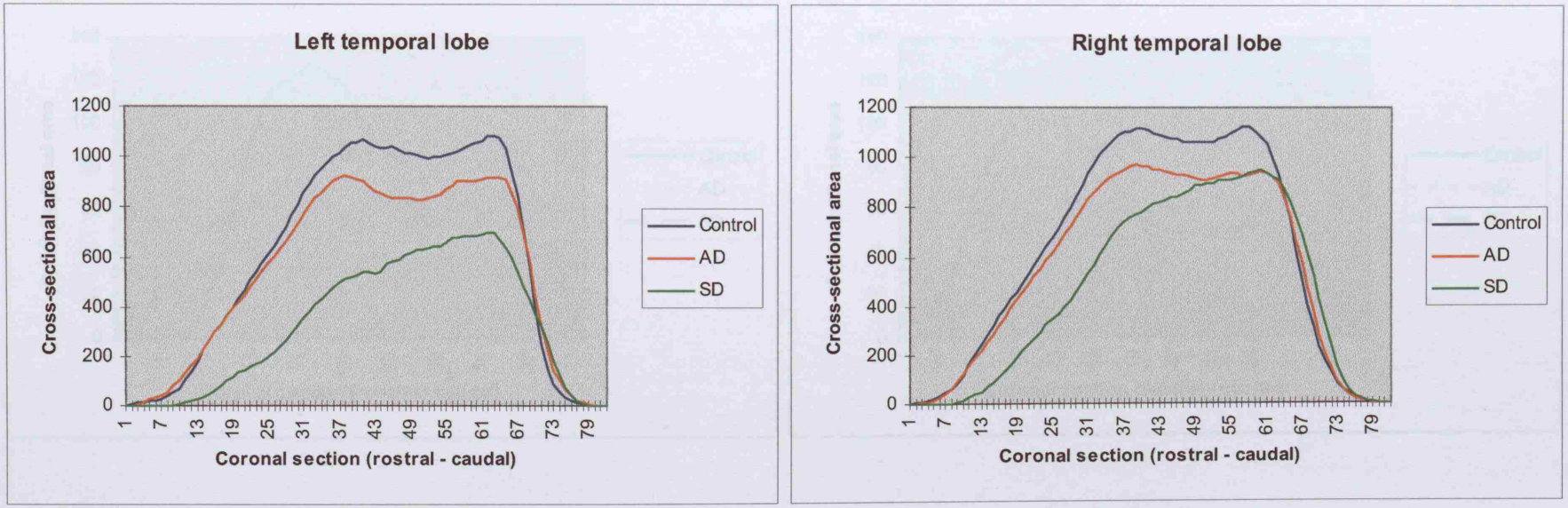

Continued…

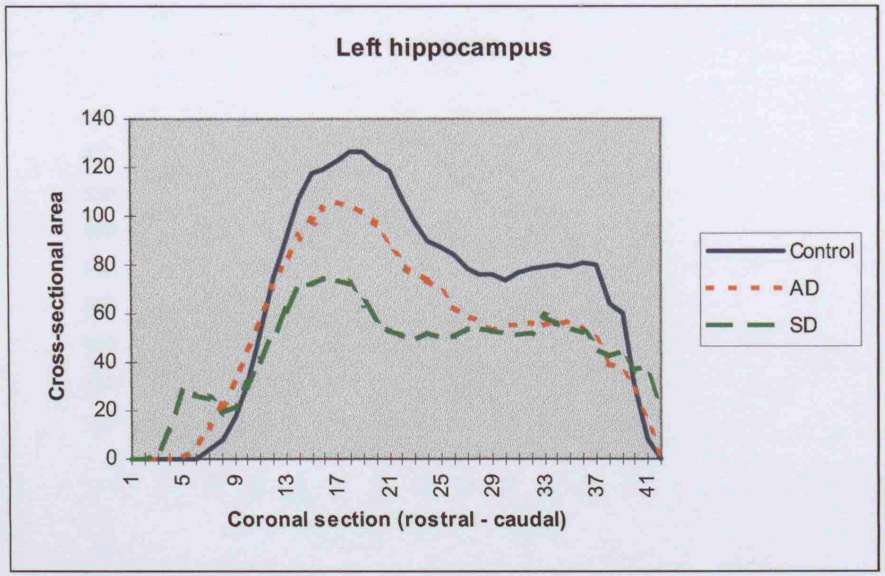
Left hippocampus
Cross-sectional area
140
120
100
80
60
40
20
0
1
5
9
13
17
21
25
29
33
37
41
Coronal section (rostral - caudal)
Control
AD
SD

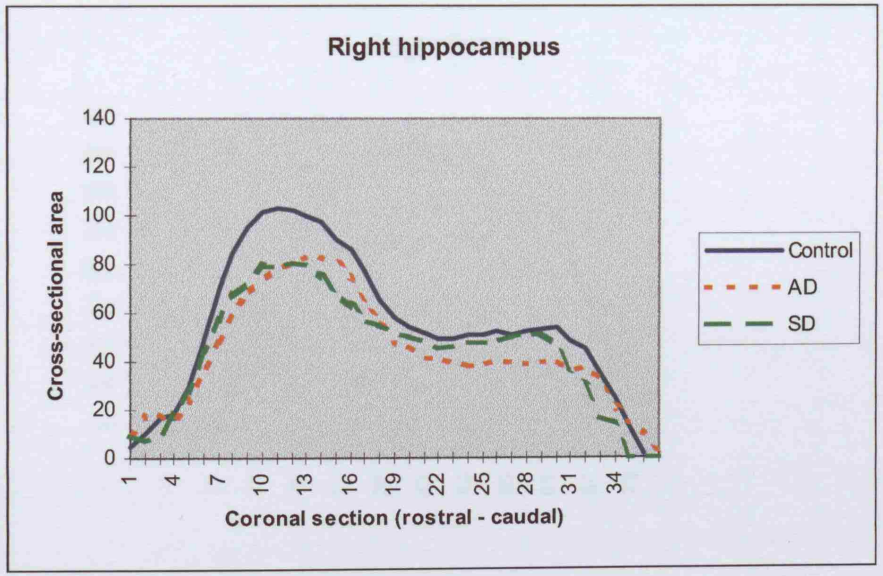
Right hippocampus
Cross-sectional area
140
120
100
80
60
40
20
0
1
4
7
10
13
16
19
22
25
28
31
34
Coronal section (rostral - caudal)
Control
AD
SD

Continued…

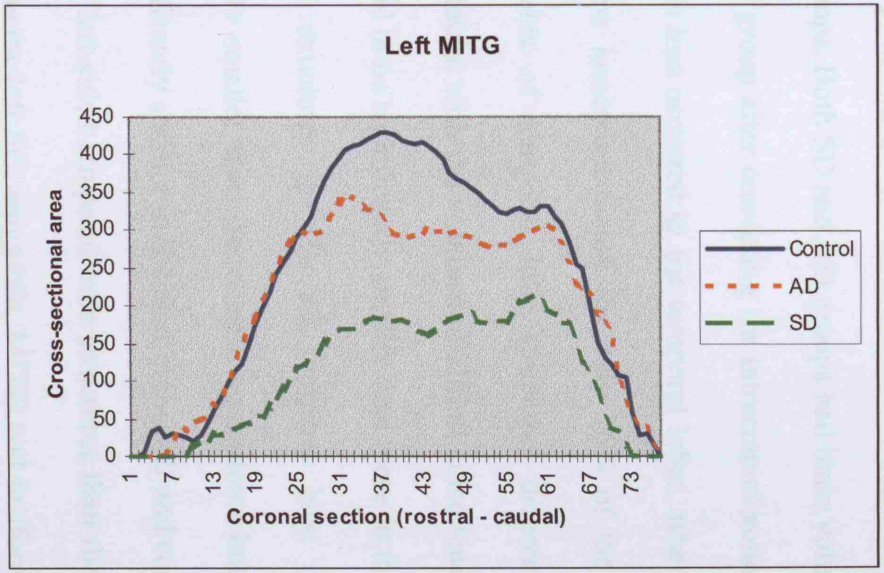
Left MITG
Cross-sectional area
450
400
350
300
250
200
150
100
50
0
1
7
13
19
25
31
37
43
49
55
61
67
73
Coronal section (rostral - caudal)
Control
AD
SD

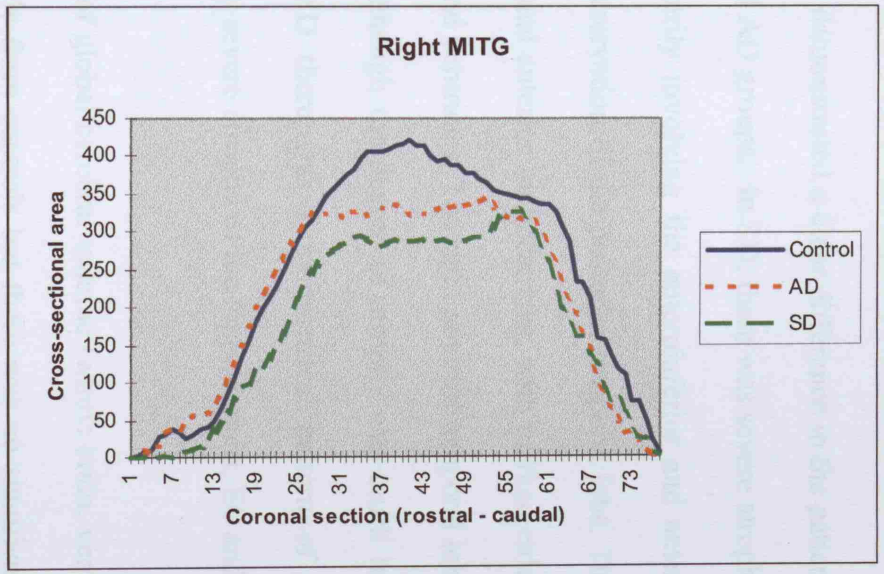
Right MITG
Cross-sectional area
450
400
350
300
250
200
150
100
50
0
1
7
13
19
25
31
37
43
49
55
61
67
73
Coronal section (rostral - caudal)
Control
AD
SD

Discussion

This study demonstrated a clear difference in the pattern of cerebral atrophy between the SD and AD groups. In SD, there was severe atrophy of the left anterior temporal lobe, primarily involving the anteroinferior and anteromedial temporal lobe, with relative preservation of the posterior temporal lobe. There was severe atrophy of the amygdala and anterior hippocampus, with marked enlargement of the temporal horn of the lateral ventricles. The right anterior temporal lobe revealed a similar pattern of atrophy, although the degree of atrophy was much less prominent than on the left side. In AD there was a symmetrical pattern of temporal lobe atrophy, with particularly severe atrophy of the hippocampus, EC and amygdala.

Measures of global cerebral volume (whole brain, ventricles) in SD and AD differed significantly from controls but there was no significant difference between the two disease groups. Both SD and AD groups had brain volumes that were 7% smaller than the control group after correcting for intracranial volume. However, in the SD group 60% of this loss occurred in the temporal lobes, whereas in the AD group temporal lobe volume losses accounted for only 16% of the global cerebral volume loss. Measurements of temporal lobe structures demonstrated significant differences between groups, with the volumes of all left-sided temporal lobe structures in the SD group found to be significantly smaller than those in the AD or control groups. Of the right-sided structures in SD, all temporal lobe structures were found to be significantly smaller than the control equivalents but only the amygdala and STG were significantly smaller in SD than in the AD and control groups. There was greater atrophy of left-sided temporal lobe structures than the right-sided equivalents in SD and of these the left EC, amygdala, MITG and fusiform gyrus were the most severely

affected structures. In AD the medial temporal lobe structures were symmetrically atrophied, with greatest atrophy of the EC and a similar degree of atrophy of the amygdala and hippocampus.

The difference between SD and AD in the distribution of atrophy within the temporal lobe was assessed by plotting the cross-sectional areas along the anteroposterior lengths of both temporal lobes. These area plots showed that SD was associated with a gradient of atrophy along the AP axis, with progressively more atrophy towards the anterior end of the temporal lobe. Although this gradient was more prominent in the more severely affected left temporal lobe, it was also detectable on the right side. Further analysis of individual structures such as the hippocampus and the MITG revealed the existence of similar AP atrophy gradients and these AP gradients were also more marked on the left side. These findings contrasted with those observed in AD, in which there was even distribution of atrophy along the AP extent of the whole temporal lobe as well as individual temporal lobe structures. In keeping with the results of volumetric analysis, there were no obvious interhemispheric differences.

Previous studies have suggested that focal anterior temporal lobe atrophy was a feature of SD, with severe atrophy of the temporal pole and the MITG (Hodges and Patterson, 1996; Snowden et al., 1996). The current data confirm that there is a marked interhemispheric asymmetry in the pattern of atrophy, with more prominent left-sided atrophy. Importantly, however, these results indicate that atrophy in SD is not confined to the inferior portion of the anterior temporal lobe, but that there is also marked atrophy of cortical and subcortical anterior medial temporal lobe structures as well as a lesser degree of atrophy affecting the anterior STG.

Mummery and colleagues (Mummery et al., 2000) did not find significant atrophy of the hippocampus or EC in SD. This probably reflects the lack of resolution of the VBM technique used in their study, or possibly differences in the patient groups used. Visual inspection of the MRI scans of all the SD patients in this study confirmed clear involvement of the anterior left hippocampus (see Appendix figure 7.2). The results are more in keeping with those obtained by Frisoni et al (1999) and Galton et al (2001), in which hippocampal atrophy was associated with FTLD and SD (Frisoni et al., 1999; Galton et al., 2001a).

In the AD group, temporal lobe atrophy was most severe for the EC, hippocampus and amygdala, with the volume reductions of 20-30% in keeping with that observed in previous studies of patients with mild to moderate AD (Seab et al., 1988; Kesslak et al., 1991; Jack et al., 1992; Killiany et al., 1993; Lehericy et al., 1994). The demonstration that the EC is more severely atrophied than the hippocampus in AD parallels the findings of Juottonen and colleagues (Juottonen et al., 1999), and the results are also in keeping with their observation that the EC measurements had slightly poorer reproducibility and greater variance than the hippocampal measurements. Different opinions exist as to the relative utility of EC volumetric measurements in very early AD (Killiany et al., 2000; Xu et al., 2000), but in this study of moderately affected AD and SD patients hippocampal and EC measurements were found to be of similar diagnostic utility.

A number of anterior temporal lobe regions were found to be atrophied in SD. Hence, in terms of identifying the locus of semantic memory, two main possibilities might be

considered. The first is that semantic memory is subserved by a network of anterior temporal regions, disruption of which causes semantic memory impairment. The second possibility is that there exists within the anterior temporal lobe individual region(s) that are critical to semantic memory function, and that damage to these region(s) gives rise to impairment.

The most severely damaged temporal lobe regions in the SD group were the left amygdala, EC, anterior fusiform gyrus and anterior MITG. The functions of the amygdala (Morris et al., 1998), EC (Squire and Zola-Morgan, 1991) and fusiform gyrus (Meadows, 1974) have been widely investigated and are not believed to be associated directly with semantic memory. The left MITG was atrophied (≥3 S.D. below the control mean) in every SD patient (see Appendix figure 7.3). Consequently it is tempting to speculate that the left anterior MITG may play a key role in semantic dementia, either in terms of individual function or as a key part of a functional network. It will be interesting to see if this observation is replicated in other studies, particularly those involving very early SD cases. Recent VBM studies have demonstrated correlations between semantic memory and the anterior temporal lobe, however the limitations of VBM prevent more precise localisation (see chapter 3) (Mummery et al., 2000; Williams et al., 2005).

As expected, all AD patients showed impairment of recognition memory, with global deficits and severe impairment in the majority of cases. This was associated with bilateral atrophy of the hippocampus and EC, and as such these data are in accordance with the postulated roles of these regions in episodic memory (Squire and Zola-Morgan, 1991).

In the SD group the predominantly left-sided temporal lobe atrophy was associated with a greater impairment of verbal (relative to visual) recognition memory, in keeping with the view that verbal and visual memory are subserved by left- and right-sided temporal lobe structures respectively (Smith and Milner, 1981; Frisk and Milner, 1990). Despite the severe atrophy of the left EC and the left anterior hippocampus in all SD patients, the SD patients were not found to have a greater impairment of verbal recognition memory than the AD patients. This observation raises the interesting possibility that the relative sparing of recognition memory in early SD cases (Graham et al., 2000) may be due to the relative preservation of the posterior hippocampus. This possibility is supported by the observation that the SD group had relatively preserved visual recognition memory with a mean test score above the defective range, despite the fact that the right anterior hippocampus in the SD group was as atrophied as in the AD group. A study by Galton et al (2001) similarly found hippocampal atrophy in SD patients, but hypothesised that episodic memory function may be maintained by the right hippocampus (Galton et al., 2001a). However, in both studies the right hippocampus in the SD patients was found to be at least as atrophied as in the AD patients. They also suggested that frontal lobe dysfunction in the AD patients may exacerbate the memory problem in AD. This argument, though, is weakened by the knowledge that the frontal lobes are frequently affected in SD, as demonstrated in chapter 5. It is likely however, that episodic memory impairment in AD may be contributed to by damage to other limbic areas that are heavily involved in AD, such as the posterior cingulate (Nestor et al., 2003c).

Conclusion

Semantic dementia and AD are associated with very different patterns of temporal lobe atrophy. These differences are usually obvious on visual inspection of MRI scans and may help to support a clinical diagnosis. In SD, temporal lobe atrophy is primarily anterior in location and is asymmetrical, with greater left-sided involvement. The atrophy in AD is symmetrical and principally affects the medial temporal lobe structures. Importantly, the medial temporal structures are also severely affected in SD, with marked destruction of the amygdala, entorhinal cortex and anterior hippocampus.

Glossary

AD	Alzheimer's disease
ALS	Amyotrophic lateral sclerosis
AP	Anteroposterior
APOE	Apolipoprotein gene
APP	Amyloid Precursor Protein
BBSI	Brain Boundary Shift Integral
BPF	Brain Parenchymal Fraction
CBD	Corticobasal degeneration
CBS	Corticobasal Syndrome
CDR	Clinical Dementia Rating
CJD	Creutzfeldt-Jacob Disease
CSF	Cerebrospinal fluid
CT	Computed Tomography
CV	Coefficient of Variation
DCTs	Discrete Cosine Transforms
DLB	Dementia with Lewy Bodies
DLDH	Dementia Lacking Distinctive Histology
dof	Degrees of Freedom
Dspan Fwd	Digit Span Forward
EEG	Electroencephalogram
FAD	Familial Alzheimer's disease
FDR	False Discovery Rate correction for multiple comparisons
FWE	Family-wise Error correction for multiple comparisons
FG	Fusiform gyrus

FL	Frontal lobe
fMRI	Functional Magnetic Resonance Imaging
FSIQ	Full Scale IQ
FTD	Frontotemporal dementia (Lund Manchester Criteria)
FTDP-17	FTD with Parkinsonism that is chromosome 17-linked
FTLD	Frontotemporal lobar degeneration (Neary Criteria)
FTLD-MND	FTLD with tau-negative, ubiquitin positive inclusions with motor neuron disease
FTLD-U	FTLD with tau-negative, ubiquitin positive inclusions without motor neuron disease
fvFTD	Frontal/behavioural variant Frontotemporal dementia
FWHM	Full Width Half Maximum
GDS	Graded Difficulty Spelling Test
GNT	Graded Naming Test
HMG	Homophone Meaning Generation
IL	Incomplete Letters
ITG	Inferior temporal gyrus
MAPD	Mean Absolute Percentage Difference
MCI	Mild Cognitive Impairment
MIDAS	Medical Information Display and Analysis System
MIRIAD	Minimal Interval Resonance Imaging in AD
MMSE	Mini-mental status examination
MND	Motor Neuron Disease
MNI	Montreal Neurologic Institute

MOUSEPAD	Manchester and Oxford Universities Scale for the Psychopathological Assessment of Dementia
MRI	Magnetic Resonance Imaging
MSE	Mean Squared Error
MTG	Middle Temporal gyrus
NART	National Adult Reading Test
NIBD	Neurofilament Inclusion Body Disease
NPI	Neuropsychiatric Inventory
OFC	Orbitofrontal cortex
OL	Occipital Lobe
Oldfield	Oldfield naming test
PD	Proton Density
PET	Positron Emission Tomography
PG	Parahippocampal gyrus
PiD	Pick's Disease
PIQ	Performance IQ
PL	Parietal lobe
PNFA	Progressive non-fluent aphasia
PPA	Primary Progressive Aphasia
PPV	Positive Predictive Value
PS1	Presenilin 1
PS2	Presenilin 2
PSP	Progressive Supranuclear Palsy
QA	Quality Assurance
RF	Radiofrequency

RIU	Ratio Image Uniformity
RMF	Recognition Memory Test for Faces
RMW	Recognition Memory Test for Words
ROC	Receiver Operator Characteristic
ROI	Region of Interest
SAD	Sporadic Alzheimer's disease
SD	Semantic Dementia
SNR	Signal-to-noise ratio
SPECT	Single Photon Emission Computed Tomography
SPM	Statistical Parametric Mapping
StDev	Standard Deviation
STG	Superior Temporal gyrus
tau exon10^{+16}	FTLD with mutation in exon10 of the tau gene
TBM	Tensor-Based Morphometry
TE	Time to echo i.e. time between transmission of RF pulse and collection of signal
TIV	Total Intracranial Volume
TL	Temporal lobe
TR	Time to repeat i.e. time between RF pulses
VaD	Vascular Dementia
VBM	Voxel-Based Morphometry
VCM	Voxel Compression Map
VIQ	Verbal IQ
WAIS	Wechsler Adult Intelligence Scale

Reference List

Aarsland D, Litvan I, Larsen JP. Neuropsychiatric symptoms of patients with progressive supranuclear palsy and Parkinson's disease. J Neuropsychiatry Clin Neurosci 2001; 13: 42-9.

Abe K, Ukita H, Yanagihara T. Imaging in primary progressive aphasia. Neuroradiology 1997; 39: 556-9.

Adolphs R, Tranel D, Damasio H, et al. Impaired recognition of emotion in facial expressions following bilateral damage to the human amygdala. Nature 1994; 372: 669-72.

Allen NH, Gordon S, Hope T, et al. Manchester and Oxford Universities Scale for the Psychopathological Assessment of Dementia (MOUSEPAD). Br J Psychiatry 1996; 169: 293-307.

Alzheimer A. Uber eigenartige Krankheitsfalle des spateren Alters. Zeitscrift fur die Gesamte Neurologie und Psychiatrie 1911; 4: 356-385.

American Pyschiatric Association. Diagnostic and Statistical Manual of Mental Disorders (4th Ed) (DSM IV). Washington DC: American Psychiatric Association, 1994.

Ames D, Cummings JL, Wirshing WC, et al. Repetitive and compulsive behavior in frontal lobe degenerations. J Neuropsychiatry Clin Neurosci 1994; 6: 100-13.

Arai H, Morikawa Y, Higuchi M, et al. Cerebrospinal fluid tau levels in neurodegenerative diseases with distinct tau-related pathology. Biochem Biophys Res Commun 1997; 236: 262-4.

Arnold JB, Liow JS, Schaper KA, et al. Qualitative and quantitative evaluation of six algorithms for correcting intensity nonuniformity effects. Neuroimage 2001; 13: 931-43.

Ashburner J, Friston KJ. Voxel-based morphometry--the methods. Neuroimage 2000; 11: 805-21.

Ashburner J, Good CD. Spatial registration of images. In: Tofts P, editor. Quantitative MRI of the Brain: Measuring Changes Caused by Disease: John Wiley and Sons, Inc, 2003.

Augustine JR. Circuitry and functional aspects of the insular lobe in primates including humans. Brain Res Brain Res Rev 1996; 22: 229-44.

Bak TH, Hodges JR. Cognition, language and behaviour in motor neurone disease: evidence of frontotemporal dysfunction. Dement Geriatr Cogn Disord 1999; 10 Suppl 1: 29-32.

Bak TH, Hodges JR. Motor neurone disease, dementia and aphasia: coincidence, co-occurrence or continuum? J Neurol 2001; 248: 260-70.

Ballard CG. Advances in the treatment of Alzheimer's disease: benefits of dual cholinesterase inhibition. Eur Neurol 2002; 47: 64-70.

Barnes J, Scahill RI, Boyes RG, et al. Differentiating AD from aging using semiautomated measurement of hippocampal atrophy rates. Neuroimage 2004; 23: 574-81.

Baron JC, Chetelat G, Desgranges B, et al. In vivo mapping of gray matter loss with voxel-based morphometry in mild Alzheimer's disease. Neuroimage 2001; 14: 298-309.

Bathgate D, Snowden JS, Varma A, et al. Behaviour in frontotemporal dementia, Alzheimer's disease and vascular dementia. Acta Neurol Scand 2001; 103: 367-78.

Baxter DM, Warrington EK. Measuring dysgraphia: A graded-difficulty spelling test. Behavioural Neurology 1994; 7: 107-116.

Bechara A, Damasio H, Damasio AR. Emotion, decision making and the orbitofrontal cortex. Cereb Cortex 2000; 10: 295-307.

Berlin HA, Rolls ET, Kischka U. Impulsivity, time perception, emotion and reinforcement sensitivity in patients with orbitofrontal cortex lesions. Brain 2004; 127: 1108-26.

Bird T, Knopman D, VanSwieten J, et al. Epidemiology and genetics of frontotemporal dementia/Pick's disease. Ann Neurol 2003; 54 Suppl 5: S29-31.

Bird TD, Nochlin D, Poorkaj P, et al. A clinical pathological comparison of three families with frontotemporal dementia and identical mutations in the tau gene (P301L). Brain 1999; 122 (Pt 4): 741-56.

Black SE. The search for diagnostic and progression markers in AD: so near but still too far? Neurology 1999; 52: 1533-4.

Blatter DD, Bigler ED, Gale SD, et al. Quantitative volumetric analysis of brain MR: normative database spanning 5 decades of life. AJNR Am J Neuroradiol 1995; 16: 241-51.

Boccardi M, Pennanen C, Laakso MP, et al. Amygdaloid atrophy in frontotemporal dementia and Alzheimer's disease. Neurosci Lett 2002; 335: 139-43.

Boccardi M, Laakso MP, Bresciani L, et al. The MRI pattern of frontal and temporal brain atrophy in fronto-temporal dementia. Neurobiol Aging 2003; 24: 95-103.

Boccardi M, Sabattoli F, Laakso MP, et al. Frontotemporal dementia as a neural system disease. Neurobiol Aging 2005; 26: 37-44.

Boeve BF, Lang AE, Litvan I. Corticobasal degeneration and its relationship to progressive supranuclear palsy and frontotemporal dementia. Ann Neurol 2003; 54 Suppl 5: S15-9.

Bonte FJ, Harris TS, Roney CA, et al. Differential diagnosis between Alzheimer's and frontotemporal disease by the posterior cingulate sign. J Nucl Med 2004; 45: 771-4.

Bookstein FL. "Voxel-based morphometry" should not be used with imperfectly registered images. Neuroimage 2001; 14: 1454-62.

Boxer AL, Rankin KP, Miller BL, et al. Cinguloparietal atrophy distinguishes Alzheimer disease from semantic dementia. Archives of Neurology 2003; 60: 949-56.

Bozeat S, Gregory CA, Ralph MA, et al. Which neuropsychiatric and behavioural features distinguish frontal and temporal variants of frontotemporal dementia from Alzheimer's disease? J Neurol Neurosurg Psychiatry 2000; 69: 178-86.

Braak H, Braak E. Evolution of the neuropathology of Alzheimer's disease. Acta Neurol Scand Suppl 1996; 165: 3-12.

Broe M, Hodges JR, Schofield E, et al. Staging disease severity in pathologically confirmed cases of frontotemporal dementia. Neurology 2003; 60: 1005-11.

Brown J, Ashworth A, Gydesen S, et al. Familial non-specific dementia maps to chromosome 3. Hum Mol Genet 1995; 4: 1625-8.

Brun A. Clinical and neuropathological criteria for frontotemporal dementia. The Lund and Manchester Groups. J Neurol Neurosurg Psychiatry 1994; 57: 416-8.

Burns A, Jacoby R, Levy R. Psychiatric phenomena in Alzheimer's disease. IV: Disorders of behaviour. Br J Psychiatry 1990; 157: 86-94.

Burton EJ, Karas G, Paling SM, et al. Patterns of cerebral atrophy in dementia with Lewy bodies using voxel-based morphometry. Neuroimage 2002; 17: 618-30.

Cairns NJ, Perry RH, Jaros E, et al. Patients with a novel neurofilamentopathy: dementia with neurofilament inclusions. Neurosci Lett 2003; 341: 177-80.

Cairns NJ, Zhukareva V, Uryu K, et al. alpha-internexin is present in the pathological inclusions of neuronal intermediate filament inclusion disease. Am J Pathol 2004; 164: 2153-61.

Callen DJ, Black SE, Gao F, et al. Beyond the hippocampus: MRI volumetry confirms widespread limbic atrophy in AD. Neurology 2001; 57: 1669-74.

Cannon A, Baker M, Boeve B, et al. CHMP2B mutations are not a common cause of frontotemporal lobar degeneration. Neurosci Lett 2006; 398: 83-4.

Cardebat D, Demonet JF, Celsis P, et al. Living/non-living dissociation in a case of semantic dementia: a SPECT activation study. Neuropsychologia 1996; 34: 1175-9.

Caselli RJ, Jack CR, Jr., Petersen RC, et al. Asymmetric cortical degenerative syndromes: clinical and radiologic correlations. Neurology 1992; 42: 1462-8.

Chan D, Fox NC, Jenkins R, et al. Rates of global and regional cerebral atrophy in AD and frontotemporal dementia. Neurology 2001a; 57: 1756-63.

Chan D, Fox NC, Scahill RI, et al. Patterns of temporal lobe atrophy in semantic dementia and Alzheimer's disease.[see comment]. Annals of Neurology 2001b; 49: 433-42.

Chan D, Janssen JC, Whitwell JL, et al. Change in rates of cerebral atrophy over time in early-onset Alzheimer's disease: longitudinal MRI study. Lancet 2003; 362: 1121-2.

Chan D, Walters RJ, Sampson EL, et al. EEG abnormalities in frontotemporal lobar degeneration. Neurology 2004; 62: 1628-30.

Chawluk JB, Mesulam MM, Hurtig H, et al. Slowly progressive aphasia without generalized dementia: studies with positron emission tomography. Ann Neurol 1986; 19: 68-74.

Chow TW, Miller BL, Hayashi VN, et al. Inheritance of frontotemporal dementia. Arch Neurol 1999; 56: 817-22.

Christensen GE, Rabbitt RD, Miller MI. Deformable Templates Using Large Deformation Kinematics. IEEE Trans Image Proc 1996; 5: 1435-47.

Cipolotti L, Warrington EK. Semantic memory and reading abilities: a case report. J Int Neuropsychol Soc 1995; 1: 104-10.

Convit A, de Leon MJ, Golomb J, et al. Hippocampal atrophy in early Alzheimer's disease: anatomic specificity and validation. Psychiatr Q 1993; 64: 371-87.

Convit A, De Leon MJ, Tarshish C, et al. Specific hippocampal volume reductions in individuals at risk for Alzheimer's disease. Neurobiol Aging 1997; 18: 131-8.

Critchley HD, Elliott R, Mathias CJ, et al. Neural activity relating to generation and representation of galvanic skin conductance responses: a functional magnetic resonance imaging study. J Neurosci 2000; 20: 3033-40.

Crum WR, Scahill RI, Fox NC. Automated hippocampal segmentation by regional fluid registration of serial MRI: validation and application in Alzheimer's disease. Neuroimage 2001; 13: 847-55.

Cuenod CA, Denys A, Michot JL, et al. Amygdala atrophy in Alzheimer's disease. An in vivo magnetic resonance imaging study. Arch Neurol 1993; 50: 941-5.

Cullen P, Abid F, Patel A, et al. Eating disorders in dementia. Int J Geriatr Psychiatry 1997; 12: 559-62.

Cummings JL, Duchen LW. Kluver-Bucy syndrome in Pick disease: clinical and pathologic correlations. Neurology 1981; 31: 1415-22.

Cummings JL, Mega M, Gray K, et al. The Neuropsychiatric Inventory: comprehensive assessment of psychopathology in dementia. Neurology 1994; 44: 2308-14.

Cummings JL. Toward a molecular neuropsychiatry of neurodegenerative diseases. Ann Neurol 2003; 54: 147-54.

Damasio AR. The somatic marker hypothesis and the possible functions of the prefrontal cortex. Philos Trans R Soc Lond B Biol Sci 1996; 351: 1413-20.

Davatzikos C, Genc A, Xu D, et al. Voxel-based morphometry using the RAVENS maps: methods and validation using simulated longitudinal atrophy. Neuroimage 2001a; 14: 1361-9.

Davatzikos C, Li HH, Herskovits E, et al. Accuracy and sensitivity of detection of activation foci in the brain via statistical parametric mapping: a study using a PET simulator. Neuroimage 2001b; 13: 176-84.

Davies RR, Hodges JR, Kril JJ, et al. The pathological basis of semantic dementia. Brain 2005; 128: 1984-95.

Davis PC, Gray L, Albert M, et al. The Consortium to Establish a Registry for Alzheimer's Disease (CERAD). Part III. Reliability of a standardized MRI evaluation of Alzheimer's disease. Neurology 1992; 42: 1676-80.

de Leon MJ, George AE, Stylopoulos LA, et al. Early marker for Alzheimer's disease: the atrophic hippocampus. Lancet 1989; 2: 672-3.

Deakin JB, Rahman S, Nestor PJ, et al. Paroxetine does not improve symptoms and impairs cognition in frontotemporal dementia: a double-blind randomized controlled trial. Psychopharmacology (Berl) 2004; 172: 400-8.

Dermaut B, Kumar-Singh S, Engelborghs S, et al. A novel presenilin 1 mutation associated with Pick's disease but not beta-amyloid plaques. Ann Neurol 2004; 55: 617-26.

Dickson DW. Neuropathologic differentiation of progressive supranuclear palsy and corticobasal degeneration. J Neurol 1999; 246 Suppl 2: II6-15.

Dickson DW. Neuropathology of Pick's disease. Neurology 2001; 56: S16-20.

Dickson DW, Bergeron C, Chin SS, et al. Office of Rare Diseases neuropathologic criteria for corticobasal degeneration. J Neuropathol Exp Neurol 2002; 61: 935-46.

Diehl J, Grimmer T, Drzezga A, et al. Cerebral metabolic patterns at early stages of frontotemporal dementia and semantic dementia. A PET study. Neurobiol Aging 2004; 25: 1051-6.

Dronkers NF. A new brain region for coordinating speech articulation. Nature 1996; 384: 159-61.

Duvernoy HM. The Human Hippocampus. Heidelberg: Springer-Verlag, 1998.

Edwards-Lee T, Miller BL, Benson DF, et al. The temporal variant of frontotemporal dementia. Brain 1997; 120 (Pt 6): 1027-40.

Eritaia J, Wood SJ, Stuart GW, et al. An optimized method for estimating intracranial volume from magnetic resonance images. Magn Reson Med 2000; 44: 973-7.

Eslinger PJ, Damasio AR. Severe disturbance of higher cognition after bilateral frontal lobe ablation: patient EVR. Neurology 1985; 35: 1731-41.

Evans DW, Lewis MD, Iobst E. The role of the orbitofrontal cortex in normally developing compulsive-like behaviors and obsessive-compulsive disorder. Brain Cogn 2004; 55: 220-34.

Evans JJ, Heggs AJ, Antoun N, et al. Progressive prosopagnosia associated with selective right temporal lobe atrophy. A new syndrome? Brain 1995; 118 (Pt 1): 1-13.

Ezekiel F, Chao L, Kornak J, et al. Comparisons between global and focal brain atrophy rates in normal aging and Alzheimer disease: Boundary Shift Integral versus tracing of the entorhinal cortex and hippocampus. Alzheimer Dis Assoc Disord 2004; 18: 196-201.

Folstein MF, Folstein SE, McHugh PR. "Mini-mental state". A practical method for grading the cognitive state of patients for the clinician. J Psychiatr Res 1975; 12: 189-98.

Foster NL, Wilhelmsen K, Sima AA, et al. Frontotemporal dementia and parkinsonism linked to chromosome 17: a consensus conference. Conference Participants. Ann Neurol 1997; 41: 706-15.

Fox NC, Warrington EK, Freeborough PA, et al. Presymptomatic hippocampal atrophy in Alzheimer's disease. A longitudinal MRI study. Brain 1996a; 119 (Pt 6): 2001-7.

Fox NC, Freeborough PA, Rossor MN. Visualisation and quantification of rates of atrophy in Alzheimer's disease. Lancet 1996b; 348: 94-7.

Fox NC, Freeborough PA. Brain atrophy progression measured from registered serial MRI: validation and application to Alzheimer's disease. J Magn Reson Imaging 1997; 7: 1069-75.

Fox NC, Scahill RI, Crum WR, et al. Correlation between rates of brain atrophy and cognitive decline in AD. Neurology 1999a; 52: 1687-9.

Fox NC, Warrington EK, Rossor MN. Serial magnetic resonance imaging of cerebral atrophy in preclinical Alzheimer's disease. Lancet 1999b; 353: 2125.

Fox NC, Cousens S, Scahill R, et al. Using serial registered brain magnetic resonance imaging to measure disease progression in Alzheimer disease: power calculations and estimates of sample size to detect treatment effects. Arch Neurol 2000; 57: 339-44.

Fox NC, Crum WR, Scahill RI, et al. Imaging of onset and progression of Alzheimer's disease with voxel-compression mapping of serial magnetic resonance images. Lancet 2001; 358: 201-5.

Fox NC, Schott JM. Imaging cerebral atrophy: normal ageing to Alzheimer's disease. Lancet 2004; 363: 392-4.

Fox NC, Black RS, Gilman S, et al. Effects of A{beta} immunization (AN1792) on MRI measures of cerebral volume in Alzheimer disease. Neurology 2005.

Free SL, Bergin PS, Fish DR, et al. Methods for normalization of hippocampal volumes measured with MR. AJNR Am J Neuroradiol 1995; 16: 637-43.

Freeborough PA, Woods RP, Fox NC. Accurate registration of serial 3D MR brain images and its application to visualizing change in neurodegenerative disorders. J Comput Assist Tomogr 1996; 20: 1012-22.

Freeborough PA, Fox NC, Kitney RI. Interactive algorithms for the segmentation and quantitation of 3-D MRI brain scans. Comput Methods Programs Biomed 1997; 53: 15-25.

Freeborough PA, Fox NC. The boundary shift integral: an accurate and robust measure of cerebral volume changes from registered repeat MRI. IEEE Trans Med Imaging 1997; 16: 623-9.

Freeborough PA, Fox NC. Modeling brain deformations in Alzheimer disease by fluid registration of serial 3D MR images. J Comput Assist Tomogr 1998; 22: 838-43.

Frisk V, Milner B. The role of the left hippocampal region in the acquisition and retention of story content. Neuropsychologia 1990; 28: 349-59.

Frisoni GB, Beltramello A, Weiss C, et al. Usefulness of simple measures of temporal lobe atrophy in probable Alzheimer's disease. Dementia 1996a; 7: 15-22.

Frisoni GB, Beltramello A, Weiss C, et al. Linear measures of atrophy in mild Alzheimer disease. AJNR Am J Neuroradiol 1996b; 17: 913-23.

Frisoni GB, Beltramello A, Geroldi C, et al. Brain atrophy in frontotemporal dementia. J Neurol Neurosurg Psychiatry 1996c; 61: 157-65.

Frisoni GB, Laakso MP, Beltramello A, et al. Hippocampal and entorhinal cortex atrophy in frontotemporal dementia and Alzheimer's disease. Neurology 1999; 52: 91-100.

Friston KJ, Holmes AP, Worsley KJ, et al. Statistical Parametric Maps in Functional Imaging: A General Linear Approach. Hum Brain Mapp 1995; 2: 189-210.

Frost C, Kenward MG, Fox NC. The analysis of repeated 'direct' measures of change illustrated with an application in longitudinal imaging. Stat Med 2004; 23: 3275-86.

Fukui T, Kertesz A. Volumetric study of lobar atrophy in Pick complex and Alzheimer's disease. J Neurol Sci 2000; 174: 111-21.

Galasko D, Hansen LA, Katzman R, et al. Clinical-neuropathological correlations in Alzheimer's disease and related dementias. Arch Neurol 1994; 51: 888-95.

Galton CJ, Patterson K, Xuereb JH, et al. Atypical and typical presentations of Alzheimer's disease: a clinical, neuropsychological, neuroimaging and pathological study of 13 cases. Brain 2000; 123 Pt 3: 484-98.

Galton CJ, Patterson K, Graham K, et al. Differing patterns of temporal atrophy in Alzheimer's disease and semantic dementia. Neurology 2001a; 57: 216-25.

Galton CJ, Gomez-Anson B, Antoun N, et al. Temporal lobe rating scale: application to Alzheimer's disease and frontotemporal dementia. J Neurol Neurosurg Psychiatry 2001b; 70: 165-73.

Garrard P, Perry R, Hodges JR. Disorders of semantic memory. J Neurol Neurosurg Psychiatry 1997; 62: 431-5.

Garraux G, Salmon E, Degueldre C, et al. Comparison of impaired subcortico-frontal metabolic networks in normal aging, subcortico-frontal dementia, and cortical frontal dementia. Neuroimage 1999; 10: 149-62.

Gibb WR, Luthert PJ, Marsden CD. Corticobasal degeneration. Brain 1989; 112 (Pt 5): 1171-92.

Gilman S, Koller M, Black RS, et al. Clinical effects of A{beta} immunization (AN1792) in patients with AD in an interrupted trial. Neurology 2005.

Gitelman DR, Ashburner J, Friston KJ, et al. Voxel-based morphometry of herpes simplex encephalitis. Neuroimage 2001; 13: 623-31.

Goate A, Chartier-Harlin MC, Mullan M, et al. Segregation of a missense mutation in the amyloid precursor protein gene with familial Alzheimer's disease. Nature 1991; 349: 704-6.

Godbolt AK, Josephs KA, Revesz T, et al. Sporadic and familial dementia with ubiquitin-positive tau-negative inclusions: clinical features of one histopathological abnormality underlying frontotemporal lobar degeneration. Arch Neurol 2005; 62: 1097-101.

Good CD, Johnsrude IS, Ashburner J, et al. A voxel-based morphometric study of ageing in 465 normal adult human brains. Neuroimage 2001a; 14: 21-36.

Good CD, Ashburner J, Frackowiak RS. Computational neuroanatomy: new perspectives for neuroradiology. Rev Neurol (Paris) 2001b; 157: 797-806.

Good CD, Scahill RI, Fox NC, et al. Automatic differentiation of anatomical patterns in the human brain: validation with studies of degenerative dementias. Neuroimage 2002; 17: 29-46.

Gorno-Tempini ML, Dronkers NF, Rankin KP, et al. Cognition and anatomy in three variants of primary progressive aphasia. Annals of Neurology 2004a; 55: 335-46.

Gorno-Tempini ML, Murray RC, Rankin KP, et al. Clinical, cognitive and anatomical evolution from nonfluent progressive aphasia to corticobasal syndrome: a case report. Neurocase 2004b; 10: 426-36.

Graff-Radford NR, Damasio AR, Hyman BT, et al. Progressive aphasia in a patient with Pick's disease: a neuropsychological, radiologic, and anatomic study. Neurology 1990; 40: 620-6.

Graham A, Davies R, Xuereb J, et al. Pathologically proven frontotemporal dementia presenting with severe amnesia. Brain 2005; 128: 597-605.

Graham KS, Simons JS, Pratt KH, et al. Insights from semantic dementia on the relationship between episodic and semantic memory. Neuropsychologia 2000; 38: 313-24.

Green J, Morris JC, Sandson J, et al. Progressive aphasia: a precursor of global dementia? Neurology 1990; 40: 423-9.

Gregory C, Lough S, Stone V, et al. Theory of mind in patients with frontal variant frontotemporal dementia and Alzheimer's disease: theoretical and practical implications. Brain 2002; 125: 752-64.

Groschel K, Hauser TK, Luft A, et al. Magnetic resonance imaging-based volumetry differentiates progressive supranuclear palsy from corticobasal degeneration. Neuroimage 2004; 21: 714-24.

Grossman M. Progressive aphasic syndromes: clinical and theoretical advances. Curr Opin Neurol 2002; 15: 409-13.

Grossman M, McMillan C, Moore P, et al. What's in a name: voxel-based morphometric analyses of MRI and naming difficulty in Alzheimer's disease, frontotemporal dementia and corticobasal degeneration. Brain 2004; 127: 628-49.

Grossman M, Farmer J, Leight S, et al. Cerebrospinal fluid profile in frontotemporal dementia and Alzheimer's disease. Ann Neurol 2005; 57: 721-9.

Grundman M, Sencakova D, Jack CR, Jr., et al. Brain MRI hippocampal volume and prediction of clinical status in a mild cognitive impairment trial. J Mol Neurosci 2002; 19: 23-7.

Gunter JL, Shiung MM, Manduca A, et al. Methodological considerations for measuring rates of brain atrophy. J Magn Reson Imaging 2003; 18: 16-24.

Gustafson L, Brun A, Passant U. Frontal lobe degeneration of non-Alzheimer type. Baillieres Clin Neurol 1992; 1: 559-82.

Harasty JA, Halliday GM, Code C, et al. Quantification of cortical atrophy in a case of progressive fluent aphasia. Brain 1996; 119 (Pt 1): 181-90.

Harvey RJ, Skelton-Robinson M, Rossor MN. The prevalence and causes of dementia in people under the age of 65 years. J Neurol Neurosurg Psychiatry 2003; 74: 1206-9.

Heutink P. Untangling tau-related dementia. Hum Mol Genet 2000; 9: 979-86.

Hodges JR, Patterson K, Oxbury S, et al. Semantic dementia. Progressive fluent aphasia with temporal lobe atrophy. Brain 1992; 115 (Pt 6): 1783-806.

Hodges JR, Patterson K. Nonfluent progressive aphasia and semantic dementia: a comparative neuropsychological study. J Int Neuropsychol Soc 1996; 2: 511-24.

Hodges JR, Patterson K, Ward R, et al. The differentiation of semantic dementia and frontal lobe dementia (temporal and frontal variants of frontotemporal dementia) from early Alzheimer's disease: a comparative neuropsychological study. Neuropsychology 1999; 13: 31-40.

Hodges JR. Frontotemporal dementia (Pick's disease): clinical features and assessment. Neurology 2001; 56: S6-10.

Hodges JR, Miller B. The neuropsychology of frontal variant frontotemporal dementia and semantic dementia. Introduction to the special topic papers: Part II. Neurocase 2001; 7: 113-21.

Hodges JR, Davies R, Xuereb J, et al. Survival in frontotemporal dementia. Neurology 2003; 61: 349-54.

Hodges JR, Davies RR, Xuereb JH, et al. Clinicopathological correlates in frontotemporal dementia. Ann Neurol 2004; 56: 399-406.

Holmes C. Genotype and phenotype in Alzheimer's disease. Br J Psychiatry 2002; 180: 131-4.

Hosler BA, Siddique T, Sapp PC, et al. Linkage of familial amyotrophic lateral sclerosis with frontotemporal dementia to chromosome 9q21-q22. Jama 2000; 284: 1664-9.

Hughes CP, Berg L, Danziger WL, et al. A new clinical scale for the staging of dementia. Br J Psychiatry 1982; 140: 566-72.

Hutton M, Lendon CL, Rizzu P, et al. Association of missense and 5'-splice-site mutations in tau with the inherited dementia FTDP-17. Nature 1998; 393: 702-5.

Ibach B, Koch H, Koller M, et al. Hospital admission circumstances and prevalence of frontotemporal lobar degeneration: a multicenter psychiatric state hospital study in Germany. Dement Geriatr Cogn Disord 2003; 16: 253-64.

Ikeda M, Tanabe H, Nakagawa Y, et al. MRI-based quantitative assessment of the hippocampal region in very mild to moderate Alzheimer's disease. Neuroradiology 1994; 36: 7-10.

Ikeda M, Brown J, Holland AJ, et al. Changes in appetite, food preference, and eating habits in frontotemporal dementia and Alzheimer's disease. J Neurol Neurosurg Psychiatry 2002; 73: 371-6.

Insausti R, Juottonen K, Soininen H, et al. MR volumetric analysis of the human entorhinal, perirhinal, and temporopolar cortices. AJNR Am J Neuroradiol 1998; 19: 659-71.

Jack CR, Jr., Twomey CK, Zinsmeister AR, et al. Anterior temporal lobes and hippocampal formations: normative volumetric measurements from MR images in young adults. Radiology 1989; 172: 549-54.

Jack CR, Jr., Petersen RC, O'Brien PC, et al. MR-based hippocampal volumetry in the diagnosis of Alzheimer's disease. Neurology 1992; 42: 183-8.

Jack CR, Jr., Petersen RC, Xu YC, et al. Medial temporal atrophy on MRI in normal aging and very mild Alzheimer's disease. Neurology 1997; 49: 786-94.

Jack CR, Jr., Petersen RC, Xu Y, et al. Rate of medial temporal lobe atrophy in typical aging and Alzheimer's disease. Neurology 1998; 51: 993-9.

Jack CR, Jr., Petersen RC, Xu Y, et al. Rates of hippocampal atrophy correlate with change in clinical status in aging and AD. Neurology 2000; 55: 484-89.

Jack CR, Jr., Slomkowski M, Gracon S, et al. MRI as a biomarker of disease progression in a therapeutic trial of milameline for AD. Neurology 2003; 60: 253-60.

Jack CR, Jr., Shiung MM, Gunter JL, et al. Comparison of different MRI brain atrophy rate measures with clinical disease progression in AD. Neurology 2004; 62: 591-600.

Jackson M, Lennox G, Lowe J. Motor neurone disease-inclusion dementia. Neurodegeneration 1996; 5: 339-50.

Janssen JC, Warrington EK, Morris HR, et al. Clinical features of frontotemporal dementia due to the intronic tau 10(+16) mutation. Neurology 2002; 58: 1161-8.

Janssen JC, Schott JM, Cipolotti L, et al. Mapping the onset and progression of atrophy in familial frontotemporal lobar degeneration. Journal of Neurology, Neurosurgery & Psychiatry 2005; 76: 162-8.

Jauss M, Herholz K, Kracht L, et al. Frontotemporal dementia: clinical, neuroimaging, and molecular biological findings in 6 patients. Eur Arch Psychiatry Clin Neurosci 2001; 251: 225-31.

Jenkins R, Fox NC, Rossor AM, et al. Intracranial volume and Alzheimer disease: evidence against the cerebral reserve hypothesis. Arch Neurol 2000; 57: 220-4.

Jeong Y, Cho SS, Park JM, et al. 18F-FDG PET findings in frontotemporal dementia: an SPM analysis of 29 patients. J Nucl Med 2005; 46: 233-9.

Johnson JK, Head E, Kim R, et al. Clinical and pathological evidence for a frontal variant of Alzheimer disease. Arch Neurol 1999; 56: 1233-9.

Johnson JK, Diehl J, Mendez MF, et al. Frontotemporal lobar degeneration: demographic characteristics of 353 patients. Arch Neurol 2005; 62: 925-30.

Josephs KA, Holton JL, Rossor MN, et al. Neurofilament inclusion body disease: a new proteinopathy? Brain 2003; 126: 2291-303.

Josephs KA, Tang-Wai DF, Edland SD, et al. Correlation between antemortem magnetic resonance imaging findings and pathologically confirmed corticobasal degeneration. Archives of Neurology 2004a; 61: 1881-4.

Josephs KA, Holton JL, Rossor MN, et al. Frontotemporal lobar degeneration and ubiquitin immunohistochemistry. Neuropathology & Applied Neurobiology 2004b; 30: 369-73.

Josephs KA, Jones AG, Dickson DW. Hippocampal sclerosis and ubiquitin-positive inclusions in dementia lacking distinctive histopathology. Dementia & Geriatric Cognitive Disorders 2004c; 17: 342-5.

Josephs KA, Knopman DS, Whitwell JL, et al. Survival in two variants of tau-negative frontotemporal lobar degeneration: FTLD-U vs FTLD-MND. Neurology 2005; 65: 645-7.

Josephs KA, Duffy JR, Strand EA, et al. Clinicopathological and imaging correlates of progressive aphasia and apraxia of speech. Brain 2006a.

Josephs KA, Petersen RC, Knopman DS, et al. Clinicopathologic analysis of frontotemporal and corticobasal degenerations and PSP. Neurology 2006b; 66: 41-8.

Juottonen K, Laakso MP, Insausti R, et al. Volumes of the entorhinal and perirhinal cortices in Alzheimer's disease. Neurobiol Aging 1998; 19: 15-22.

Juottonen K, Laakso MP, Partanen K, et al. Comparative MR analysis of the entorhinal cortex and hippocampus in diagnosing Alzheimer disease. AJNR Am J Neuroradiol 1999; 20: 139-44.

Kang DH, Kim JJ, Choi JS, et al. Volumetric investigation of the frontal-subcortical circuitry in patients with obsessive-compulsive disorder. J Neuropsychiatry Clin Neurosci 2004; 16: 342-9.

Kaufer DI, Miller BL, Itti L, et al. Midline cerebral morphometry distinguishes frontotemporal dementia and Alzheimer's disease. Neurology 1997; 48: 978-85.

Kawachi T, Ishii K, Sakamoto S, et al. Comparison of the diagnostic performance of FDG-PET and VBM-MRI in very mild Alzheimer's disease. Eur J Nucl Med Mol Imaging 2006.

Keller SS, Wieshmann UC, Mackay CE, et al. Voxel based morphometry of grey matter abnormalities in patients with medically intractable temporal lobe

epilepsy: effects of side of seizure onset and epilepsy duration. J Neurol Neurosurg Psychiatry 2002; 73: 648-55.

Kempler D, Metter EJ, Riege WH, et al. Slowly progressive aphasia: three cases with language, memory, CT and PET data. J Neurol Neurosurg Psychiatry 1990; 53: 987-93.

Kertesz A, Hudson L, Mackenzie IR, et al. The pathology and nosology of primary progressive aphasia. Neurology 1994; 44: 2065-72.

Kertesz A, Munoz D. Pick's disease, frontotemporal dementia, and Pick complex: emerging concepts. Arch Neurol 1998; 55: 302-4.

Kertesz A, Davidson W, Munoz DG. Clinical and pathological overlap between frontotemporal dementia, primary progressive aphasia and corticobasal degeneration: the Pick complex. Dement Geriatr Cogn Disord 1999; 10 Suppl 1: 46-9.

Kertesz A, Martinez-Lage P, Davidson W, et al. The corticobasal degeneration syndrome overlaps progressive aphasia and frontotemporal dementia. Neurology 2000a; 55: 1368-75.

Kertesz A, Kawarai T, Rogaeva E, et al. Familial frontotemporal dementia with ubiquitin-positive, tau-negative inclusions. Neurology 2000b; 54: 818-27.

Kertesz A. Pick Complex: an integrative approach to frontotemporal dementia: primary progressive aphasia, corticobasal degeneration, and progressive supranuclear palsy. Neurologist 2003; 9: 311-7.

Kertesz A, Hillis A, Munoz DG. Frontotemporal degeneration, Pick's disease, Pick complex, and Ravel. Ann Neurol 2003; 54 Suppl 5: S1-2.

Kertesz A, Munoz D. Relationship between frontotemporal dementia and corticobasal degeneration/progressive supranuclear palsy. Dement Geriatr Cogn Disord 2004; 17: 282-6.

Kertesz A, McMonagle P, Blair M, et al. The evolution and pathology of frontotemporal dementia. Brain 2005; 128: 1996-2005.

Kesslak JP, Nalcioglu O, Cotman CW. Quantification of magnetic resonance scans for hippocampal and parahippocampal atrophy in Alzheimer's disease. Neurology 1991; 41: 51-4.

Killiany RJ, Moss MB, Albert MS, et al. Temporal lobe regions on magnetic resonance imaging identify patients with early Alzheimer's disease. Arch Neurol 1993; 50: 949-54.

Killiany RJ, Gomez-Isla T, Moss M, et al. Use of structural magnetic resonance imaging to predict who will get Alzheimer's disease. Ann Neurol 2000; 47: 430-9.

Kitagaki H, Mori E, Hirono N, et al. Alteration of white matter MR signal intensity in frontotemporal dementia. AJNR Am J Neuroradiol 1997; 18: 367-78.

Kitagaki H, Mori E, Yamaji S, et al. Frontotemporal dementia and Alzheimer disease: evaluation of cortical atrophy with automated hemispheric surface display generated with MR images. Radiology 1998; 208: 431-9.

Kizu O, Yamada K, Ito H, et al. Posterior cingulate metabolic changes in frontotemporal lobar degeneration detected by magnetic resonance spectroscopy. Neuroradiology 2004; 46: 277-81.

Knibb JA, Xuereb JH, Patterson K, et al. Clinical and pathological characterization of progressive aphasia. Ann Neurol 2006; 59: 156-65.

Knopman DS, Mastri AR, Frey WH, 2nd, et al. Dementia lacking distinctive histologic features: a common non-Alzheimer degenerative dementia. Neurology 1990; 40: 251-6.

Knopman DS, Boeve BF, Parisi JE, et al. Antemortem diagnosis of frontotemporal lobar degeneration. Ann Neurol 2005; 57: 480-8.

Kovari E, Leuba G, Savioz A, et al. Familial frontotemporal dementia with ubiquitin inclusion bodies and without motor neuron disease. Acta Neuropathol (Berl) 2000; 100: 421-6.

Kramer JH, Jurik J, Sha SJ, et al. Distinctive neuropsychological patterns in frontotemporal dementia, semantic dementia, and Alzheimer disease. Cognitive & Behavioral Neurology 2003; 16: 211-8.

Kril JJ, Halliday GM. Clinicopathological staging of frontotemporal dementia severity: correlation with regional atrophy. Dement Geriatr Cogn Disord 2004; 17: 311-5.

Kringelbach ML, Rolls ET. The functional neuroanatomy of the human orbitofrontal cortex: evidence from neuroimaging and neuropsychology. Prog Neurobiol 2004; 72: 341-72.

Laakso MP, Partanen K, Lehtovirta M, et al. MRI of amygdala fails to diagnose early Alzheimer's disease. Neuroreport 1995a; 6: 2414-8.

Laakso MP, Soininen H, Partanen K, et al. Volumes of hippocampus, amygdala and frontal lobes in the MRI-based diagnosis of early Alzheimer's disease: correlation with memory functions. J Neural Transm Park Dis Dement Sect 1995b; 9: 73-86.

Laakso MP, Lehtovirta M, Partanen K, et al. Hippocampus in Alzheimer's disease: a 3-year follow-up MRI study. Biol Psychiatry 2000; 47: 557-61.

Lantos PL, Cairns NJ, Khan MN, et al. Neuropathologic variation in frontotemporal dementia due to the intronic tau 10(+16) mutation. Neurology 2002; 58: 1169-75.

Larsson E, Passant U, Sundgren PC, et al. Magnetic resonance imaging and histopathology in dementia, clinically of frontotemporal type. Dement Geriatr Cogn Disord 2000; 11: 123-34.

Larsson EM, Englund E, Sjobeck M, et al. MRI with diffusion tensor imaging post-mortem at 3.0 T in a patient with frontotemporal dementia. Dement Geriatr Cogn Disord 2004; 17: 316-9.

Leary SM, Parker GJ, Stevenson VL, et al. Reproducibility of magnetic resonance imaging measurements of spinal cord atrophy: the role of quality assurance. Magn Reson Imaging 1999; 17: 773-6.

Lehericy S, Baulac M, Chiras J, et al. Amygdalohippocampal MR volume measurements in the early stages of Alzheimer disease. AJNR Am J Neuroradiol 1994; 15: 929-37.

Lemieux L, Barker GJ. Measurement of small inter-scan fluctuations in voxel dimensions in magnetic resonance images using registration. Med Phys 1998; 25: 1049-54.

Leow AD, Klunder AD, Jack CR, Jr., et al. Longitudinal stability of MRI for mapping brain change using tensor-based morphometry. Neuroimage 2006.

Levy ML, Miller BL, Cummings JL, et al. Alzheimer disease and frontotemporal dementias. Behavioral distinctions. Arch Neurol 1996; 53: 687-90.

Lewis EB, Fox NC. Correction of differential intensity inhomogeneity in longitudinal MR images. Neuroimage 2004; 23: 75-83.

Likeman M, Anderson VM, Stevens JM, et al. Visual assessment of atrophy on magnetic resonance imaging in the diagnosis of pathologically confirmed young-onset dementias. Arch Neurol 2005; 62: 1410-5.

Lindau M, Almkvist O, Johansson SE, et al. Cognitive and behavioral differentiation of frontal lobe degeneration of the non-Alzheimer type and Alzheimer's disease. Dement Geriatr Cogn Disord 1998; 9: 205-13.

Lingford-Hughes AR, Davies SJ, McIver S, et al. Addiction. Br Med Bull 2003; 65: 209-22.

Lipton AM, Cullum CM, Satumtira S, et al. Contribution of asymmetric synapse loss to lateralizing clinical deficits in frontotemporal dementias. Arch Neurol 2001; 58: 1233-9.

Litvan I, Agid Y, Calne D, et al. Clinical research criteria for the diagnosis of progressive supranuclear palsy (Steele-Richardson-Olszewski syndrome): report of the NINDS-SPSP international workshop. Neurology 1996; 47: 1-9.

Liu W, Miller BL, Kramer JH, et al. Behavioral disorders in the frontal and temporal variants of frontotemporal dementia. Neurology 2004; 62: 742-8.

Lomen-Hoerth C, Anderson T, Miller B. The overlap of amyotrophic lateral sclerosis and frontotemporal dementia. Neurology 2002; 59: 1077-9.

Losseff NA, Wang L, Lai HM, et al. Progressive cerebral atrophy in multiple sclerosis. A serial MRI study. Brain 1996; 119 (Pt 6): 2009-19.

Lough S, Gregory C, Hodges JR. Dissociation of social cognition and executive function in frontal variant frontotemporal dementia. Neurocase 2001; 7: 123-30.

Maguire EA, Gadian DG, Johnsrude IS, et al. Navigation-related structural change in the hippocampi of taxi drivers. Proc Natl Acad Sci U S A 2000; 97: 4398-403.

Mann DM, South PW. The topographic distribution of brain atrophy in frontal lobe dementia. Acta Neuropathol (Berl) 1993; 85: 334-40.

Mann DM, South PW, Snowden JS, et al. Dementia of frontal lobe type: neuropathology and immunohistochemistry. J Neurol Neurosurg Psychiatry 1993; 56: 605-14.

Mataix-Cols D, Wooderson S, Lawrence N, et al. Distinct neural correlates of washing, checking, and hoarding symptom dimensions in obsessive-compulsive disorder. Arch Gen Psychiatry 2004; 61: 564-76.

Mathuranath PS, Nestor PJ, Berrios GE, et al. A brief cognitive test battery to differentiate Alzheimer's disease and frontotemporal dementia. Neurology 2000; 55: 1613-20.

Matsumae M, Kikinis R, Morocz IA, et al. Age-related changes in intracranial compartment volumes in normal adults assessed by magnetic resonance imaging. J Neurosurg 1996; 84: 982-91.

Mazziotta JC, Toga AW, Evans A, et al. A probabilistic atlas of the human brain: theory and rationale for its development. The International Consortium for Brain Mapping (ICBM). Neuroimage 1995; 2: 89-101.

McKeith I, Mintzer J, Aarsland D, et al. Dementia with Lewy bodies. Lancet Neurol 2004; 3: 19-28.

McKenna P, Warrington EK. The Graded Naming Test. Windsor: NFER-Nelson, 1983.

McKhann G, Drachman D, Folstein M, et al. Clinical diagnosis of Alzheimer's disease: report of the NINCDS-ADRDA Work Group under the auspices of Department of Health and Human Services Task Force on Alzheimer's Disease. Neurology 1984; 34: 939-44.

McKhann GM, Albert MS, Grossman M, et al. Clinical and pathological diagnosis of frontotemporal dementia: report of the Work Group on Frontotemporal Dementia and Pick's Disease. Arch Neurol 2001; 58: 1803-9.

Meadows JC. Disturbed perception of colours associated with localized cerebral lesions. Brain 1974; 97: 615-32.

Mendez MF, Selwood A, Mastri AR, et al. Pick's disease versus Alzheimer's disease: a comparison of clinical characteristics. Neurology 1993; 43: 289-92.

Mendez MF, Cherrier M, Perryman KM, et al. Frontotemporal dementia versus Alzheimer's disease: differential cognitive features. Neurology 1996; 47: 1189-94.

Mendez MF, Clark DG, Shapira JS, et al. Speech and language in progressive nonfluent aphasia compared with early Alzheimer's disease. Neurology 2003; 61: 1108-13.

Mesulam MM. Slowly progressive aphasia without generalized dementia. Ann Neurol 1982; 11: 592-8.

Mesulam MM, Weintraub S. Spectrum of primary progressive aphasia. Baillieres Clin Neurol 1992; 1: 583-609.

Mesulam MM. Primary progressive aphasia. Ann Neurol 2001; 49: 425-32.

Miki Y, Grossman RI, Udupa JK, et al. Differences between relapsing-remitting and chronic progressive multiple sclerosis as determined with quantitative MR imaging. Radiology 1999; 210: 769-74.

Miller BL, Chang L, Mena I, et al. Progressive right frontotemporal degeneration: clinical, neuropsychological and SPECT characteristics. Dementia 1993; 4: 204-13.

Miller BL, Darby AL, Swartz JR, et al. Dietary changes, compulsions and sexual behavior in frontotemporal degeneration. Dementia 1995; 6: 195-9.

Miller BL, Darby A, Benson DF, et al. Aggressive, socially disruptive and antisocial behaviour associated with fronto-temporal dementia. Br J Psychiatry 1997; 170: 150-4.

Miller BL, Gearhart R. Neuroimaging in the diagnosis of frontotemporal dementia. Dement Geriatr Cogn Disord 1999; 10 Suppl 1: 71-4.

Miller ER, 3rd, Pastor-Barriuso R, Dalal D, et al. Meta-analysis: high-dosage vitamin E supplementation may increase all-cause mortality. Ann Intern Med 2005; 142: 37-46.

Morita M, Al-Chalabi A, Andersen PM, et al. A locus on chromosome 9p confers susceptibility to ALS and frontotemporal dementia. Neurology 2006; 66: 839-44.

Morris JS, Ohman A, Dolan RJ. Conscious and unconscious emotional learning in the human amygdala. Nature 1998; 393: 467-70.

Mummery CJ, Patterson K, Wise RJ, et al. Disrupted temporal lobe connections in semantic dementia. Brain 1999; 122 (Pt 1): 61-73.

Mummery CJ, Patterson K, Price CJ, et al. A voxel-based morphometry study of semantic dementia: relationship between temporal lobe atrophy and semantic memory. Ann Neurol 2000; 47: 36-45.

Muzik O, Chugani DC, Juhasz C, et al. Statistical parametric mapping: assessment of application in children. Neuroimage 2000; 12: 538-49.

Neary D, Snowden JS, Gustafson L, et al. Frontotemporal lobar degeneration: a consensus on clinical diagnostic criteria. Neurology 1998; 51: 1546-54.

Neary D, Snowden JS, Mann DM. Classification and description of frontotemporal dementias. Ann N Y Acad Sci 2000; 920: 46-51.

Nelsen H. The National Adult Reading Test (NART): Test manual: The NFER-NELSON Publishing Company Ltd, 1982.

Nestor PJ, Graham KS, Bozeat S, et al. Memory consolidation and the hippocampus: further evidence from studies of autobiographical memory in semantic dementia and frontal variant frontotemporal dementia. Neuropsychologia 2002; 40: 633-54.

Nestor PJ, Graham NL, Fryer TD, et al. Progressive non-fluent aphasia is associated with hypometabolism centred on the left anterior insula. Brain 2003a; 126: 2406-18.

Nestor PJ, Fryer TD, Smielewski P, et al. Limbic hypometabolism in Alzheimer's disease and mild cognitive impairment. Ann Neurol 2003b; 54: 343-51.

Nestor PJ, Fryer TD, Ikeda M, et al. Retrosplenial cortex (BA 29/30) hypometabolism in mild cognitive impairment (prodromal Alzheimer's disease). Eur J Neurosci 2003c; 18: 2663-7.

Nyatsanza S, Shetty T, Gregory C, et al. A study of stereotypic behaviours in Alzheimer's disease and frontal and temporal variant frontotemporal dementia. J Neurol Neurosurg Psychiatry 2003; 74: 1398-402.

Nyul LG, Udupa JK. On standardizing the MR image intensity scale. Magn Reson Med 1999; 42: 1072-81.

O'Brien J, Ballard C. Drugs for Alzheimer's disease. British Medical Journal 2001; 323: 123-4.

O'Doherty J, Rolls ET, Francis S, et al. Representation of pleasant and aversive taste in the human brain. J Neurophysiol 2001; 85: 1315-21.

Ogai M, Iyo M, Mori N, et al. A right orbitofrontal region and OCD symptoms: a case report. Acta Psychiatr Scand 2005; 111: 74-6; discussion 76-7.

Oldfield RC, Wingfield A. Response latencies in naming objects. Q J Exp Psychol 1965; 17: 273-81.

Onari K, Spatz H. Anatomische Beitrage zur Lehre von der Pickschen umschriebene-Gosshirnrinden-Atrophie ('Picksche Krankheit'. Zeitscrift fur die Gesamte Neurologie und Psychiatrie 1926; 101: 470-511.

Pachana NA, Boone KB, Miller BL, et al. Comparison of neuropsychological functioning in Alzheimer's disease and frontotemporal dementia. J Int Neuropsychol Soc 1996; 2: 505-10.

Pasquier F. Early diagnosis of dementia: neuropsychology. J Neurol 1999; 246: 6-15.

Pasquier F, Fukui T, Sarazin M, et al. Laboratory investigations and treatment in frontotemporal dementia. Ann Neurol 2003; 54 Suppl 5: S32-5.

Paviour DC, Lees AJ, Josephs KA, et al. Frontotemporal lobar degeneration with ubiquitin-only-immunoreactive neuronal changes: broadening the clinical picture to include progressive supranuclear palsy. Brain 2004; 127: 2441-51.

Perry RJ, Hodges JR. Differentiating frontal and temporal variant frontotemporal dementia from Alzheimer's disease. Neurology 2000; 54: 2277-84.

Perry RJ, Rosen HR, Kramer JH, et al. Hemispheric dominance for emotions, empathy and social behaviour: evidence from right and left handers with frontotemporal dementia. Neurocase 2001; 7: 145-60.

Perry RJ, Miller BL. Behavior and treatment in frontotemporal dementia. Neurology 2001; 56: S46-51.

Petersen RC. Focal dementia syndromes: in search of the gold standard. Ann Neurol 2001; 49: 421-3.

Phillips MD, Grossman RI, Miki Y, et al. Comparison of T2 lesion volume and magnetization transfer ratio histogram analysis and of atrophy and measures of lesion burden in patients with multiple sclerosis. AJNR Am J Neuroradiol 1998; 19: 1055-60.

Pick A. Uber die Beziehungen der senilen Hirantropie zur aphasie. Prager Medizinishe Wochenscrift 1892; 17: 165-167.

Pick A. Uber Einen Weiteren Symptomenkomplex In Rahmen Der Dementia Senilis Bedingt Durch Umschirebene Starkere Hirnatrophie (gemischte Apraxie). Monatsschrift Fur Psychiatrie Und Neurologie 1906; 19: 97-108.

Piguet O, Brooks WS, Halliday GM, et al. Similar early clinical presentations in familial and non-familial frontotemporal dementia. J Neurol Neurosurg Psychiatry 2004; 75: 1743-5.

Poorkaj P, Grossman M, Steinbart E, et al. Frequency of tau gene mutations in familial and sporadic cases of non-Alzheimer dementia. Arch Neurol 2001; 58: 383-7.

Portet F, Cadilhac C, Touchon J, et al. Cognitive impairment in motor neuron disease with bulbar onset. Amyotroph Lateral Scler Other Motor Neuron Disord 2001; 2: 23-9.

Presti MF, Lewis MH. Striatal opioid peptide content in an animal model of spontaneous stereotypic behavior. Behav Brain Res 2005; 157: 363-8.

Price S, Paviour D, Scahill R, et al. Voxel-based morphometry detects patterns of atrophy that help differentiate progressive supranuclear palsy and Parkinson's disease. Neuroimage 2004; 23: 663-9.

Pujol J, Soriano-Mas C, Alonso P, et al. Mapping structural brain alterations in obsessive-compulsive disorder. Arch Gen Psychiatry 2004; 61: 720-30.

Rankin KP, Kramer JH, Mychack P, et al. Double dissociation of social functioning in frontotemporal dementia. Neurology 2003; 60: 266-71.

Rascovsky K, Salmon DP, Ho GJ, et al. Cognitive profiles differ in autopsy-confirmed frontotemporal dementia and AD. Neurology 2002; 58: 1801-8.

Ratnavalli E, Brayne C, Dawson K, et al. The prevalence of frontotemporal dementia. Neurology 2002; 58: 1615-21.

Rebeiz JJ, Kolodny EH, Richardson EP, Jr. Corticodentatonigral degeneration with neuronal achromasia. Arch Neurol 1968; 18: 20-33.

Reed LA, Wszolek ZK, Hutton M. Phenotypic correlations in FTDP-17. Neurobiol Aging 2001; 22: 89-107.

Riemenschneider M, Wagenpfeil S, Diehl J, et al. Tau and Abeta42 protein in CSF of patients with frontotemporal degeneration. Neurology 2002; 58: 1622-8.

Riley DE, Lang AE, Lewis A, et al. Cortical-basal ganglionic degeneration. Neurology 1990; 40: 1203-12.

Roberson ED, Hesse JH, Rose KD, et al. Frontotemporal dementia progresses to death faster than Alzheimer disease. Neurology 2005; 65: 719-25.

Rogaev EI, Sherrington R, Rogaeva EA, et al. Familial Alzheimer's disease in kindreds with missense mutations in a gene on chromosome 1 related to the Alzheimer's disease type 3 gene. Nature 1995; 376: 775-8.

Rolls ET, Hornak J, Wade D, et al. Emotion-related learning in patients with social and emotional changes associated with frontal lobe damage. J Neurol Neurosurg Psychiatry 1994; 57: 1518-24.

Rolls ET. The functions of the orbitofrontal cortex. Brain Cogn 2004; 55: 11-29.

Rombouts SA, Barkhof F, Witter MP, et al. Unbiased whole-brain analysis of gray matter loss in Alzheimer's disease. Neurosci Lett 2000; 285: 231-3.

Rosen HJ, Perry RJ, Murphy J, et al. Emotion comprehension in the temporal variant of frontotemporal dementia. Brain 2002a; 125: 2286-95.

Rosen HJ, Hartikainen KM, Jagust W, et al. Utility of clinical criteria in differentiating frontotemporal lobar degeneration (FTLD) from AD.[see comment]. Neurology 2002b; 58: 1608-15.

Rosen HJ, Gorno-Tempini ML, Goldman WP, et al. Patterns of brain atrophy in frontotemporal dementia and semantic dementia. Neurology 2002c; 58: 198-208.

Rosen HJ, Kramer JH, Gorno-Tempini ML, et al. Patterns of cerebral atrophy in primary progressive aphasia. American Journal of Geriatric Psychiatry 2002d; 10: 89-97.

Rosen HJ, Pace-Savitsky K, Perry RJ, et al. Recognition of emotion in the frontal and temporal variants of frontotemporal dementia. Dementia & Geriatric Cognitive Disorders 2004; 17: 277-81.

Rosso SM, van Swieten JC. New developments in frontotemporal dementia and parkinsonism linked to chromosome 17. Curr Opin Neurol 2002; 15: 423-8.

Rosso SM, Donker Kaat L, Baks T, et al. Frontotemporal dementia in The Netherlands: patient characteristics and prevalence estimates from a population-based study. Brain 2003; 126: 2016-22.

Rossor MN, Revesz T, Lantos PL, et al. Semantic dementia with ubiquitin-positive tau-negative inclusion bodies. Brain 2000; 123 (Pt 2): 267-76.

Rudick RA, Fisher E, Lee JC, et al. Use of the brain parenchymal fraction to measure whole brain atrophy in relapsing-remitting MS. Multiple Sclerosis Collaborative Research Group. Neurology 1999; 53: 1698-704.

Salmon E, Van der Linden MV, Franck G. Anterior cingulate and motor network metabolic impairment in progressive supranuclear palsy. Neuroimage 1997; 5: 173-8.

Scahill RI, Schott JM, Stevens JM, et al. Mapping the evolution of regional atrophy in Alzheimer's disease: unbiased analysis of fluid-registered serial MRI.[see comment]. Proceedings of the National Academy of Sciences of the United States of America 2002; 99: 4703-7.

Scahill RI, Frost C, Jenkins R, et al. A longitudinal study of brain volume changes in normal aging using serial registered magnetic resonance imaging. Archives of Neurology 2003; 60: 989-94.

Scahill RI. MRI in Alzheimer's disease and related disorders: the application of statistical tests of difference to serial and cross-sectional imaging to improve diagnosis and progression measurement. Institute of Neurology. London: Univeristy College London, 2003: 385.

Scheltens P, Launer LJ, Barkhof F, et al. Visual assessment of medial temporal lobe atrophy on magnetic resonance imaging: interobserver reliability. J Neurol 1995; 242: 557-60.

Schenk D, Barbour R, Dunn W, et al. Immunization with amyloid-beta attenuates Alzheimer-disease-like pathology in the PDAPP mouse. Nature 1999; 400: 173-7.

Schott JM, Fox NC, Rossor MN. Genetics of the dementias. J Neurol Neurosurg Psychiatry 2002; 73 Suppl 2: II27-31.

Schott JM. Short Interval Serial MRI Studies in Alzheimer's Disease and Normal Ageing. Institute of Neurology. London: University College London, 2004: 251.

Schott JM, Price SL, Frost C, et al. Measuring atrophy in Alzheimer disease: a serial MRI study over 6 and 12 months. Neurology 2005; 65: 119-24.

Seab JP, Jagust WJ, Wong ST, et al. Quantitative NMR measurements of hippocampal atrophy in Alzheimer's disease. Magn Reson Med 1988; 8: 200-8.

Seguin JR. Neurocognitive elements of antisocial behavior: Relevance of an orbitofrontal cortex account. Brain Cogn 2004; 55: 185-97.

Shen D, Davatzikos C. Measuring temporal morphological changes robustly in brain MR images via 4-dimensional template warping. Neuroimage 2004; 21: 1508-17.

Sherrington R, Rogaev EI, Liang Y, et al. Cloning of a gene bearing missense mutations in early-onset familial Alzheimer's disease. Nature 1995; 375: 754-60.

Short RA, Broderick DF, Patton A, et al. Different patterns of magnetic resonance imaging atrophy for frontotemporal lobar degeneration syndromes. Arch Neurol 2005; 62: 1106-10.

Simon JH, Jacobs LD, Campion MK, et al. A longitudinal study of brain atrophy in relapsing multiple sclerosis. The Multiple Sclerosis Collaborative Research Group (MSCRG). Neurology 1999; 53: 139-48.

Sinnatamby R, Antoun NA, Freer CE, et al. Neuroradiological findings in primary progressive aphasia: CT MRI and cerebral perfusion SPECT. Neuroradiology 1996; 38: 232-8.

Sjogren M, Gustafson L, Wikkelso C, et al. Frontotemporal dementia can be distinguished from Alzheimer's disease and subcortical white matter dementia

by an anterior-to-posterior rCBF-SPET ratio. Dement Geriatr Cogn Disord 2000a; 11: 275-85.

Sjogren M, Minthon L, Davidsson P, et al. CSF levels of tau, beta-amyloid(1-42) and GAP-43 in frontotemporal dementia, other types of dementia and normal aging. J Neural Transm 2000b; 107: 563-79.

Skibinski G, Parkinson NJ, Brown JM, et al. Mutations in the endosomal ESCRTIII-complex subunit CHMP2B in frontotemporal dementia. Nat Genet 2005; 37: 806-8.

Sled JG, Zijdenbos AP, Evans AC. A nonparametric method for automatic correction of intensity nonuniformity in MRI data. IEEE Trans Med Imaging 1998; 17: 87-97.

Small DM, Zatorre RJ, Dagher A, et al. Changes in brain activity related to eating chocolate: from pleasure to aversion. Brain 2001; 124: 1720-33.

Smith ML, Milner B. The role of the right hippocampus in the recall of spatial location. Neuropsychologia 1981; 19: 781-93.

Snowden JS. Semantic dementia: a form of circumscribed cerebral atrophy. Behavioural Neurology 1989; 2: 167-182.

Snowden JS, Neary D, Mann DM, et al. Progressive language disorder due to lobar atrophy. Ann Neurol 1992; 31: 174-83.

Snowden JS, Neary D, Mann D. Fronto-temporal lobar degeneration. Edinburgh: Churchill Livingstone, 1996.

Snowden JS, Bathgate D, Varma A, et al. Distinct behavioural profiles in frontotemporal dementia and semantic dementia. J Neurol Neurosurg Psychiatry 2001; 70: 323-32.

Snowden JS, Neary D, Mann DM. Frontotemporal dementia. Br J Psychiatry 2002; 180: 140-3.

Sonty SP, Mesulam MM, Thompson CK, et al. Primary progressive aphasia: PPA and the language network. Ann Neurol 2003; 53: 35-49.

Squire LR, Zola-Morgan S. The medial temporal lobe memory system. Science 1991; 253: 1380-6.

Starkstein SE, Migliorelli R, Teson A, et al. Specificity of changes in cerebral blood flow in patients with frontal lobe dementia. J Neurol Neurosurg Psychiatry 1994; 57: 790-6.

Stone VE, Baron-Cohen S, Knight RT. Frontal lobe contributions to theory of mind. J Cogn Neurosci 1998; 10: 640-56.

Strother SC, Anderson JR, Xu XL, et al. Quantitative comparisons of image registration techniques based on high-resolution MRI of the brain. J Comput Assist Tomogr 1994; 18: 954-62.

Studholme C, Cardenas V, Blumenfeld R, et al. Deformation tensor morphometry of semantic dementia with quantitative validation. Neuroimage 2004; 21: 1387-98.

Styner M, Brechbuhler C, Szekely G, et al. Parametric estimate of intensity inhomogeneities applied to MRI. IEEE Trans Med Imaging 2000; 19: 153-65.

Talairach J, Tournoux P. Co-planar Stereotaxic Atlas of the Human Brain. Stuttgart: Thieme Verlag, 1988.

Tataranni PA, DelParigi A. Functional neuroimaging: a new generation of human brain studies in obesity research. Obes Rev 2003; 4: 229-38.

Thieben MJ, Duggins AJ, Good CD, et al. The distribution of structural neuropathology in pre-clinical Huntington's disease. Brain 2002; 125: 1815-28.

Thompson SA, Patterson K, Hodges JR. Left/right asymmetry of atrophy in semantic dementia: behavioral-cognitive implications. Neurology 2003; 61: 1196-203.

Tisserand DJ, van Boxtel MP, Pruessner JC, et al. A voxel-based morphometric study to determine individual differences in gray matter density associated with age and cognitive change over time. Cereb Cortex 2004; 14: 966-73.

Tong R, Cox RW. Rotation of NMR images using the 2D chirp-z transform. Magn Reson Med 1999; 41: 253-6.

Tranel D, Hyman BT. Neuropsychological correlates of bilateral amygdala damage. Arch Neurol 1990; 47: 349-55.

Turner RS, Kenyon LC, Trojanowski JQ, et al. Clinical, neuroimaging, and pathologic features of progressive nonfluent aphasia. Ann Neurol 1996; 39: 166-73.

Tyrrell PJ, Warrington EK, Frackowiak RS, et al. Heterogeneity in progressive aphasia due to focal cortical atrophy. A clinical and PET study. Brain 1990; 113 (Pt 5): 1321-36.

van der Knaap MS, Bakker CJ, Faber JA, et al. Comparison of skull circumference and linear measurements with CSF volume MR measurements in hydrocephalus. J Comput Assist Tomogr 1992; 16: 737-43.

van Elst LT, Woermann FG, Lemieux L, et al. Affective aggression in patients with temporal lobe epilepsy: a quantitative MRI study of the amygdala. Brain 2000; 123 (Pt 2): 234-43.

Vance C, Al-Chalabi A, Ruddy D, et al. Familial amyotrophic lateral sclerosis with frontotemporal dementia is linked to a locus on chromosome 9p13.2-21.3. Brain 2006; 129: 868-76.

Vargha-Khadem F, Watkins KE, Price CJ, et al. Neural basis of an inherited speech and language disorder. Proc Natl Acad Sci U S A 1998; 95: 12695-700.

Varma AR, Snowden JS, Lloyd JJ, et al. Evaluation of the NINCDS-ADRDA criteria in the differentiation of Alzheimer's disease and frontotemporal dementia. J Neurol Neurosurg Psychiatry 1999; 66: 184-8.

Varma AR, Adams W, Lloyd JJ, et al. Diagnostic patterns of regional atrophy on MRI and regional cerebral blood flow change on SPECT in young onset patients with Alzheimer's disease, frontotemporal dementia and vascular dementia. Acta Neurol Scand 2002a; 105: 261-9.

Varma AR, Laitt R, Lloyd JJ, et al. Diagnostic value of high signal abnormalities on T2 weighted MRI in the differentiation of Alzheimer's, frontotemporal and vascular dementias. Acta Neurol Scand 2002b; 105: 355-64.

Varrone A, Pappata S, Caraco C, et al. Voxel-based comparison of rCBF SPET images in frontotemporal dementia and Alzheimer's disease highlights the involvement of different cortical networks. Eur J Nucl Med Mol Imaging 2002; 29: 1447-54.

Volkow ND, Fowler JS. Addiction, a disease of compulsion and drive: involvement of the orbitofrontal cortex. Cereb Cortex 2000; 10: 318-25.

Wahlund LO, Julin P, Lindqvist J, et al. Visual assessment of medical temporal lobe atrophy in demented and healthy control subjects: correlation with volumetry. Psychiatry Res 1999; 90: 193-9.

Wahlund LO, Julin P, Johansson SE, et al. Visual rating and volumetry of the medial temporal lobe on magnetic resonance imaging in dementia: a comparative study. J Neurol Neurosurg Psychiatry 2000; 69: 630-5.

Wang GJ, Volkow ND, Telang F, et al. Exposure to appetitive food stimuli markedly activates the human brain. Neuroimage 2004; 21: 1790-7.

Warrington EK. The selective impairment of semantic memory. Q J Exp Psychol 1975; 27: 635-57.

Warrington EK. Recognition Memory Test. Windsor: NFER-Nelson, 1984.

Warrington EK, James M. The visual object and space perception battery. Bury St Edmunds: Thames Valley Test Co, 1991.

Warrington EK. The Camden Memory Tests Manual. Hove: Psychology Press, 1996.

Watson C, Andermann F, Gloor P, et al. Anatomic basis of amygdaloid and hippocampal volume measurement by magnetic resonance imaging. Neurology 1992; 42: 1743-50.

Wechsler D. Manual for the Wechsler Adult Intelligence Scale. New York: Psychological Corporation, 1981.

Weintraub S, Rubin NP, Mesulam MM. Primary progressive aphasia. Longitudinal course, neuropsychological profile, and language features. Arch Neurol 1990; 47: 1329-35.

Westbury C, Bub D. Primary progressive aphasia: a review of 112 cases. Brain Lang 1997; 60: 381-406.

Whitwell JL, Crum WR, Watt HC, et al. Normalization of cerebral volumes by use of intracranial volume: implications for longitudinal quantitative MR imaging. Ajnr: American Journal of Neuroradiology 2001; 22: 1483-9.

Whitwell JL, Anderson VM, Scahill RI, et al. Longitudinal patterns of regional change on volumetric MRI in frontotemporal lobar degeneration. Dementia & Geriatric Cognitive Disorders 2004a; 17: 307-10.

Whitwell JL, Schott JM, Lewis EB, et al. Using nine degrees-of-freedom registration to correct for changes in voxel size in serial MRI studies. Magnetic Resonance Imaging 2004b; 22: 993-9.

Whitwell JL, Warren JD, Josephs KA, et al. Voxel-based morphometry in tau-positive and tau-negative frontotemporal lobar degenerations. Neurodegenerative diseases 2004c; 1: 225-230.

Whitwell JL, Josephs KA, Rossor MN, et al. Magnetic resonance imaging signatures of tissue pathology in frontotemporal dementia. Arch Neurol 2005a; 62: 1402-8.

Whitwell JL, Sampson EL, Watt HC, et al. A volumetric magnetic resonance imaging study of the amygdala in frontotemporal lobar degeneration and Alzheimer's disease. Dement Geriatr Cogn Disord 2005b; 20: 238-44.

Wilcock DM, Rojiani A, Rosenthal A, et al. Passive immunotherapy against Abeta in aged APP-transgenic mice reverses cognitive deficits and depletes parenchymal amyloid deposits in spite of increased vascular amyloid and microhemorrhage. J Neuroinflammation 2004; 1: 24.

Williams GB, Nestor PJ, Hodges JR. Neural correlates of semantic and behavioural deficits in frontotemporal dementia. Neuroimage 2005; 24: 1042-51.

Wisniewski T, Dowjat WK, Buxbaum JD, et al. A novel Polish presenilin-1 mutation (P117L) is associated with familial Alzheimer's disease and leads to death as early as the age of 28 years. Neuroreport 1998; 9: 217-21.

Woods RP, Cherry SR, Mazziotta JC. Rapid automated algorithm for aligning and reslicing PET images. J Comput Assist Tomogr 1992; 16: 620-33.

Woods RP, Mazziotta JC, Cherry SR. MRI-PET registration with automated algorithm. J Comput Assist Tomogr 1993; 17: 536-46.

Woods RP, Grafton ST, Watson JD, et al. Automated image registration: II. Intersubject validation of linear and nonlinear models. J Comput Assist Tomogr 1998a; 22: 153-65.

Woods RP, Grafton ST, Holmes CJ, et al. Automated image registration: I. General methods and intrasubject, intramodality validation. J Comput Assist Tomogr 1998b; 22: 139-52.

Wright P, He G, Shapira NA, et al. Disgust and the insula: fMRI responses to pictures of mutilation and contamination. Neuroreport 2004; 15: 2347-51.

Xu Y, Jack CR, Jr., O'Brien PC, et al. Usefulness of MRI measures of entorhinal cortex versus hippocampus in AD. Neurology 2000; 54: 1760-7.

Yamauchi H, Fukuyama H, Nagahama Y, et al. Comparison of the pattern of atrophy of the corpus callosum in frontotemporal dementia, progressive supranuclear palsy, and Alzheimer's disease. J Neurol Neurosurg Psychiatry 2000; 69: 623-9.

Yasuda M, Mori E, Kitagaki H, et al. Apolipoprotein E epsilon 4 allele and whole brain atrophy in late-onset Alzheimer's disease. Am J Psychiatry 1998; 155: 779-84.

Yener GG, Leuchter AF, Jenden D, et al. Quantitative EEG in frontotemporal dementia. Clin Electroencephalogr 1996; 27: 61-8.

Zahn R, Buechert M, Overmans J, et al. Mapping of temporal and parietal cortex in progressive nonfluent aphasia and Alzheimer's disease using chemical shift

imaging, voxel-based morphometry and positron emission tomography. Psychiatry Res 2005; 140: 115-31.